Advances in Intelligent Systems and Computing 591

Daniel N. Cassenti *Editor*

Advances in Human Factors in Simulation and Modeling

Proceedings of the AHFE 2017 International Conference on Human Factors in Simulation and Modeling, July 17–21, 2017, The Westin Bonaventure Hotel, Los Angeles, California, USA

Springer

Advances in Intelligent Systems and Computing

Volume 591

Series editor

Janusz Kacprzyk, Polish Academy of Sciences, Warsaw, Poland
e-mail: kacprzyk@ibspan.waw.pl

About this Series

The series "Advances in Intelligent Systems and Computing" contains publications on theory, applications, and design methods of Intelligent Systems and Intelligent Computing. Virtually all disciplines such as engineering, natural sciences, computer and information science, ICT, economics, business, e-commerce, environment, healthcare, life science are covered. The list of topics spans all the areas of modern intelligent systems and computing.

The publications within "Advances in Intelligent Systems and Computing" are primarily textbooks and proceedings of important conferences, symposia and congresses. They cover significant recent developments in the field, both of a foundational and applicable character. An important characteristic feature of the series is the short publication time and world-wide distribution. This permits a rapid and broad dissemination of research results.

Advisory Board

More information about this series at http://www.springer.com/series/11156

Daniel N. Cassenti
Editor

Advances in Human Factors in Simulation and Modeling

Proceedings of the AHFE 2017 International Conference on Human Factors in Simulation and Modeling, July 17–21, 2017, The Westin Bonaventure Hotel, Los Angeles, California, USA

Springer

Editor
Daniel N. Cassenti
RDRL-HRF-D
United States Army
Aberdeen Proving Ground, MD
USA

ISSN 2194-5357 ISSN 2194-5365 (electronic)
Advances in Intelligent Systems and Computing
ISBN 978-3-319-60590-6 ISBN 978-3-319-60591-3 (eBook)
DOI 10.1007/978-3-319-60591-3

Library of Congress Control Number: 2017943033

Printed on acid-free paper

This Springer imprint is published by Springer Nature
The registered company is Springer International Publishing AG
The registered company address is: Gewerbestrasse 11, 6330 Cham, Switzerland

Advances in Human Factors and Ergonomics 2017

AHFE 2017 Series Editors

Tareq Z. Ahram, Florida, USA
Waldemar Karwowski, Florida, USA

8th International Conference on Applied Human Factors and Ergonomics and the Affiliated Conferences

Proceedings of the AHFE 2017 International Conferences on Human Factors and Simulation and Digital Human Modeling and Applied Optimization, July 17–21, 2017, The Westin Bonaventure Hotel, Los Angeles, California, USA

Advances in Affective and Pleasurable Design	*WonJoon Chung and Cliff (Sungsoo) Shin*
Advances in Neuroergonomics and Cognitive Engineering	*Carryl Baldwin*
Advances in Design for Inclusion	*Giuseppe Di Bucchianico and Pete Kercher*
Advances in Ergonomics in Design	*Francisco Rebelo and Marcelo Soares*
Advances in Human Error, Reliability, Resilience, and Performance	*Ronald L. Boring*
Advances in Human Factors and Ergonomics in Healthcare and Medical Devices	*Vincent G. Duffy and Nancy Lightner*
Advances in Human Factors in Simulation and Modeling	*Daniel N. Cassenti*
Advances in Human Factors and System Interactions	*Isabel L. Nunes*
Advances in Human Factors in Cybersecurity	*Denise Nicholson*
Advances in Human Factors, Business Management and Leadership	*Jussi Kantola, Tibor Barath and Salman Nazir*
Advances in Human Factors in Robots and Unmanned Systems	*Jessie Chen*
Advances in Human Factors in Training, Education, and Learning Sciences	*Terence Andre*
Advances in Human Aspects of Transportation	*Neville A. Stanton*

(continued)

(continued)

Advances in Human Factors, Software, and Systems Engineering	*Tareq Z. Ahram and Waldemar Karwowski*
Advances in Human Factors in Energy: Oil, Gas, Nuclear and Electric Power Industries	*Paul Fechtelkotter and Michael Legatt*
Advances in Human Factors, Sustainable Urban Planning and Infrastructure	*Jerzy Charytonowicz*
Advances in the Human Side of Service Engineering	*Louis E. Freund and Wojciech Cellary*
Advances in Physical Ergonomics and Human Factors	*Ravindra Goonetilleke and Waldemar Karwowski*
Advances in Human Factors in Sports, Injury Prevention and Outdoor Recreation	*Tareq Z. Ahram*
Advances in Safety Management and Human Factors	*Pedro Arezes*
Advances in Social & Occupational Ergonomics	*Richard Goossens*
Advances in Ergonomics of Manufacturing: Managing the Enterprise of the Future	*Stefan Trzcielinski*
Advances in Usability and User Experience	*Tareq Ahram and Christianne Falcão*
Advances in Human Factors in Wearable Technologies and Game Design	*Tareq Ahram and Christianne Falcão*
Advances in Communication of Design	*Amic G. Ho*
Advances in Cross-Cultural Decision Making	*Mark Hoffman*

Preface

This volume is a compilation of cutting-edge research regarding how simulation and modeling supports human factors. The compilation of chapters is the result of efforts by the 8th International Conference on Applied Human Factors and Ergonomics (AHFE), which provides the organization for several affiliated conferences. Specifically, the chapters herein represent the 2nd International Conference on Human Factors and Simulation and the 6th International Conference on Digital Human Modeling and Applied Optimization.

Simulation can be thought of as technology that supports an approximation of real-world scenes and scenarios for a user. For example, a cockpit simulator represents how the inside of a cockpit is set up and will present a sensory experience to mimic flight. Simulations advance research by providing similar experiences to those scenarios that would otherwise be impractical to carry out in the real world for such reasons as monetary cost or safety concerns. Simulations can support numerous goals including training or practice on established skills.

Modeling is a somewhat different tool than simulation, though the two are often used interchangeably as they both imply estimation of real-world scenes or scenarios to bypass practical concerns. The difference in the context of this book is that modeling is not intended to provide a user with an experience, but rather to represent everything pertinent about the real world in computational algorithms, possibly including people and their psychological processing. Modeling may answer questions about large-scale scenarios that would be difficult to address otherwise, such as the effects of economic interventions or smaller scale scenarios such as the cognitive processing required to perform a task when it is otherwise undetectable by measurement devices.

The goal of the research herein is to bring awareness and attention to advances that human factors specialists can make in their field to address the design of programs of research, systems, policy, and devices. This book provides a plethora of avenues for human factors research that may be helped by simulation and modeling.

This book is divided into the following sections: (1) Human Factors and Automated Agents addresses how humans teaming with each other and with

technology; (2) Occupational Safety Simulators inspects workplace safety design and the important considerations necessary to the research; (3) Medical Simulation: Filling the Training Gap examines medical concerns that could help practitioners improve their craft; (4) Modeling and Simulation for the Extreme Environment considers how modeling and simulation can illuminate the effects of extreme environments on humans when it is impractical and unsafe to test these conditions in the real world; (5) Transportation Modeling and Simulation reviews research into transportation issues that arise in the real world through the use of modeling and simulation; (6) Advances in Computational Social Sciences regards large-scale relationships between people with a particular emphasis on how modeling can influence social policy; (7) User Experience Modeling discusses modeling research that considers the individual and how mental processing regarding different tasks unfolds; (8) Applied Digital Human Modeling and Simulation examines different aspects of humans including bodily and motion parameters that govern human behavior; and (9) Optimization, Analysis, and Scheduling addresses how modeling techniques may be used to examine data with the end goal to enlighten human factors researchers on device or system design.

Special thanks to Vincent Duffy for the significant contributions to the conference on Digital Human Modeling and Applied Optimization. All papers in this book were either reviewed or contributed by the members of editorial board. For this, I would like to appreciate the board members listed below:

Human Factors and Simulation

Digital Human Modeling and Applied Optimization

Thomas Alexander, Germany
Jasbir Arora, USA
Sue Bogner, USA
Julie Charland, Canada
Zhiqing Cheng, USA
Thomas Convard, France
Brian Corner, USA
Miguel Corticeiro Neves, Portugal
Nicolas Dechy, France
Jasmin Dell'Anna, Germany
Michael Fray, UK
Lars Fritzsche, Germany
Ravi Goonetilleke, Hong Kong
Richard Goossens, Netherlands
Brian Gore, USA
Rush Green, USA
Lars Hanson, Sweden
Daniel Högberg, Sweden
Masaomi Kimura, Japan
Bruce Byung Cheol Lee, USA
Zhizhong Li, China
Ameersing Luximon, Hong Kong
Tim Marler, USA
Russell Marshall, UK
Marco Mazzola, Italy
Myriam Merad, France
Claus Möbus, Germany
Masaaki Mochimaru, Japan
Anabela Pereira, Portugal
Stefan Pickl, Germany
George Psarros, Norway
Klaus Radermacher, Germany
Hanna Barbara Rasmussen, Denmark
Sudhakar Rajulu, USA
James Yang, USA
Zaili Yang, UK

This book is the first step in covering diverse topics in simulation and modeling. I hope this book is informative and helpful for the researchers and practitioners in developing better products, services, and systems.

July 2017 Daniel N. Cassenti

Contents

Human Factors and Automated Agents

Exploring Trust Barriers to Future Autonomy: A Qualitative Look

Joseph B. Lyons[1(✉)], Nhut T. Ho[2], Anna Lee Van Abel[1], Lauren C. Hoffmann[2], W. Eric Fergueson[1], Garrett G. Sadler[2], Michelle A. Grigsby[1], and Amy C. Burns[1]

[1] Air Force Research Laboratory, Wright-Patterson AFB, OH 45433, USA
{joseph.lyons.6, anna.van_abel, william.fergueson, michelle.grigsby.1, amy.burns.3}@us.af.mil
[2] NVH Human Systems Integration, Canoga Park, CA, USA
nhut.ho.51@gmail.com, lauren.c.hoffmann@gmail.com, garrett.g.sadler@gmail.com

Abstract. Autonomous systems dominate future Department of Defense (DoD) strategic perspectives, yet little is known regarding the trust barriers of these future systems as few exemplars exist from which to appropriately baseline reactions. Most extant DoD systems represent "automated" versus "autonomous" systems, which adds complexity to our understanding of user acceptance of autonomy. The trust literature posits several key trust antecedents to automated systems, with few field applications of these factors into the context of DoD systems. The current paper will: (1) review the trust literature as relevant to acceptance of future autonomy, (2) present the results of a qualitative analysis of trust barriers for two future DoD technologies (Automatic Air Collision Avoidance System [AACAS]; and Autonomous Wingman [AW]), and (3) discuss knowledge gaps for implementing future autonomous systems within the DoD. The study team interviewed over 160 fighter pilots from 4th Generation (e.g., F-16) and 5th Generation (e.g., F-22) fighter platforms to gauge their trust barriers to AACAS and AW. Results show that the trust barriers discussed by the pilots corresponded fairly well to the existing trust challenges identified in the literature, though some nuances were revealed that may be unique to DoD technologies/operations. Some of the key trust barriers included: concern about interference during operational requirements; the need for transparency of intent, function, status, and capabilities/limitations; concern regarding the flexibility and adaptability of the technology; cyber security/hacking potential; concern regarding the added workload associated with the technology; concern for the lack of human oversight/decision making capacity; and doubts regarding the systems' operational effectiveness. Additionally, the pilots noted several positive aspects of the proposed technologies including: added protection during last ditch evasive maneuvers; positive views of existing fielded technologies such as the Automatic Ground Collision Avoidance System; the potential for added operational capabilities; the potential to transfer risk to the robotic asset and reduce risk to pilots; and the potential for AI to participate in the entire mission process (planning-execution-debriefing). This paper will discuss the results for each technology and will discuss suggestions for implementing future autonomy into the DoD.

Keywords: Trust · Automation · Autonomy · Military

D.N. Cassenti (ed.), *Advances in Human Factors in Simulation and Modeling*,
Advances in Intelligent Systems and Computing 591, DOI 10.1007/978-3-319-60591-3_1

1 Introduction

Driverless cars, autonomous drone delivery systems, collaborative robots as teammates, robotic concierges/hosts - these concepts are no longer science fiction as they may be coming to a home or business near you very soon. The notion of autonomy dominates contemporary visions for the future. Veloso and colleagues [1] have outlined a number of potential avenues for robotic systems in supporting the human race. Robotic systems are envisioned to support the elderly in their homes with physical movement, decision making, and even companionship. Robotic systems are hoped to revolutionize transportation and delivery systems. Robotic systems can support health care and connect doctors with patients at a distance. Backbreaking factory and warehouse work could be aided through the use of intelligent exoskeletons, as could individuals who have lost mobility due to medical conditions or injuries. Therapy and rehabilitation could be supported with robots. Customer service and of course entertainment are two other domains where robotic systems will likely make a huge impact on society – and in some instances they already are. While the technology possibilities are only limited by one's imagination, there is one core element of each of the above examples that constrains the potential gains for future robotic systems, and that is the fact that all of these systems will need to, at some point, interface with humans. This has led to a burgeoning of the domain of Human-Robot Interaction (HRI) which studies numerous facets of how to improve human-robot interaction. One key challenge in this domain area is the issue of how to foster appropriate levels of trust of the robotic systems – i.e., will humans accept these technologies or reject them?

Trust represents one's willingness to be vulnerable to another entity in a situation where there is some risk and little ability to monitor the other [2]. The trust construct has been applied to trust of technology to represent the "attitude that an agent will help achieve an individual's goals in a situation characterized by uncertainty and vulnerability" [3, p. 54]. Thus, trust is relevant for both interactions with people as well as with intelligent agents such as robots. Chen and Barnes [4] define an agent as a technology that has autonomy, the ability to observe and act on its environment, and the ability and authority to direct actions toward goals. The current paper will use the term "future autonomy" to collectively represent the notion of robotic systems and agent-based technologies, the latter of which may have no physical embodiment. The key attribute of relevance for future autonomy in this context is that such systems will have both the capability and the authority to act in relevant operational scenarios.

Without a doubt, future autonomy is imminent, yet human trust will determine the effectiveness of said technology as humans decide whether or not to use it, and how to use it. The notion of trust calibration, or appropriate levels of trust, is the critical factor in determining the effectiveness of future autonomy. Meaning, the key challenge is in understanding when to trust and when to distrust technology. Inaccurate trust can result in catastrophic errors when humans rely on technology that is faulty or error-prone. Several accidents have been blamed on human overreliance on automated systems such as the Turkish Airlines flight 1951 in 2009 when a pilot relied on autopilot after an instrumentation failure [5]. The inverse is also problematic in that under trust can be detrimental to performance when humans fail to use a reliable technology as evidenced

by the Costa Concordia cruise ship disaster that killed 32 passengers when the ship captain used manual navigation skills instead of a reliable automated navigation tool [5]. Appropriately calibrated trust is challenging because as technology gains in reliability humans tend to trust it more – appropriately so. However, the performance costs of errors are most severe in situations when a highly reliable system is given the highest level of autonomy and that system makes a mistake [6]. This is driven by the habit of humans to reduce their monitoring of highly reliable systems, which could make compensation, correction, and adaptation to novel demands more difficult when the technology fails. This paradox of automation has motivated the research community to examine the drivers (and detractors) of human trust of technology.

Trust has been a focal topic for researchers in the areas of automation [5] and robotics [7]. While a comprehensive review of this literature is beyond the scope of the current paper, the human-machine trust literature has identified a number of key trust antecedents including: performance [7], transparency [4, 8], perceived benefits of use [9], prior experiences with the system to include error types (i.e., false alarms and misses) and the timing of errors [5, 10], interactive styles (etiquette) [5], anthropomorphism [11], and individual differences such as one's perfect automation schema [12], to name a few. Yet despite the burgeoning literature on human-machine trust, little field work has been done to examine the trust barriers among **real** operators to **real** tools that have **real** consequences in the world (R3) for trust or distrust. One such study found that pilot trust of an automated safety system in fighter aircraft was driven by performance considerations (reliable performance and system behavior that does not interfere with the pilot's ability to fly and fight), transparency, perceived benefits and logical (compelling) rationale for why the technology was needed, and familiarity of system's behavior [13]. It is likely that these same dimensions will be important considerations for future autonomy. Further, as technology increases in both decision capability and authority, it is likely that decision making capability and intent of the system will be important trust considerations [14]. Thus, the antecedents of trust for systems that involve a broader range of decision options should involve more intent-based dimensions relative to mere automated systems that have both decision authority and capability but only under the confines of a narrower set of circumstances.

The Department of Defense (DoD) is very focused on technologies for autonomy. Despite the domain of autonomy being quite broad, the notion of trust in autonomy is a persistent theme throughout much of the DoD Research Doctrine [15, 16]. Yet, it is critical to contextualize the target domain when considering trust so that trust considerations have a focused technology as a trust referent. Thus, the current paper will discuss pilot reactions to two future technologies: the Automatic Air Collision Avoidance System (AACAS) and an Autonomous Wingman (AW). AACAS has already undergone flight testing and is a more mature technology than the AW technology is currently.

The Automatic Air Collision Avoidance systems is part of the Air Force Research Laboratory's Integrated Collision Avoidance Program which seeks to integrate the already-fielded Automation Ground Collision Avoidance System (AGCAS) with AACAS. AACAS was designed to mitigate mid-air collisions among fighters by calculating future aircraft trajectories of cooperative and non-cooperative aircraft and using a collision avoidance algorithm to determine if an automatic maneuver is required to avoid aircraft collision [17, 18]. Like prior systems such as AGCAS,

AACAS must avoid interference with the pilots [18] which by avoiding nuisance the pilots should view the system as more trustworthy and be more likely to trust it [13]. The AW is more of a future concept, but would involve the notion of a robotic aircraft that serves as a subordinate to the flight lead. The AW would handle its own flight maneuvers but would be under the direct control of the flight lead to use as needed. Unlike current Remotely Piloted Aircraft (RPAs) the AW would not be remotely piloted but rather would able to respond to higher-level commands from the flight lead. Relative to AACAS, AW would be expected to be capable of handling a broader range of activities, whereas AACAS has one action – avoiding collision with other aircraft.

2 Method

2.1 Participants

The participants were operational F-16 (N = 131) and F-22 (N = 35) pilots at operational Air Force bases. Nine different F-16 units were visited, 4 of which were outside of the Continental United States. Two F-22 units were visited both of which were in the Continental United States. All of the pilots had, at a minimum, completed basic flight training and were operational pilots within the Air Force. The F-16 pilots had an average of 836 flight hrs. and the F-22 pilots averaged 372 h.

2.2 Procedure

Semi-structured interviews were conducted in person at the F-16/F-22 units. The current data were collected as part of a larger set of interviews centered on trust of ground collision avoidance systems. All pilots were first given an informed consent document which discussed the study objectives. Following consent, the pilots were administered a structured interview focused on attitudes and experiences of ground collision avoidance technologies that are already fielded on the F-16 and F-22. Following this set of questions, the pilots were given written descriptions of the two future technologies (AACAS and AW). After the pilots read the descriptions, a few questions were asked relating to their attitudes toward these systems. The current paper focuses on a subset of those data, and in particular, on responses to two questions: (1) In your opinion, what would be the biggest trust barrier with the AACAS system?, and (2) In your opinion, what would be the biggest trust barrier with an autonomous wingman? Responses were recorded by digital recorders (based on approval of the pilots) for later transcription and analysis. The entire interview lasted on average between 20–30 min. Data were coded with NVivo version 11 qualitative analysis software package. Note that each pilot was asked to provide the "biggest" trust barrier but they could provide multiple trust barriers for each technology.

3 Results

The relevant data clusters are reported in Tables 1 and 2 below. As shown in Table 1, the primary trust barriers reported by F-16 pilots for AACAS involved performance-related issues (e.g., reliability, connectivity issues, and concern about interference). The

Table 1. Clusters and frequencies for F-16 pilots. Note: AACAS = Automatic Air Collision Avoidance System.

AACAS	Cluster	Frequency
	Too conservative	3
	Tactical disadvantage	3
	Concern about close formation flight	41
	Interference concerns	44
	Digital problems	44
	Reliability	45
Autonomous Wingman	Changing training	2
	Replacing pilots	5
	Accountability concerns	8
	Being hacked	9
	Adaptation (concerns about the system's ability to adapt)	16
	Hitting me	18
	Added communications requirement	34
	Lack of a thinking human	42
	Reliability	45
	Workload concerns	47

Table 2. Clusters and frequencies for F-22 pilots. Note: AACAS = Automatic Air Collision Avoidance System.

AACAS	Cluster	Frequency
	Reliability	4
	Digital problems	3
	Close formation flight concerns	5
	Cause tactical disadvantage	8
	Interference	11
Autonomous Wingman	Replace pilots	1
	Reliability	2
	Being hacked	2
	Hitting me	2
	Changing training	3
	Accountability concerns	3
	Added communications requirement	4
	Adaptation (concerns about the system's ability to adapt)	6
	Lack of thinking human	8
	Workload concerns	11

primary trust barriers reported by F-16 pilots for the AW included: workload concerns, reliability, and the lack of a human decision maker. As shown in Table 2, the primary trust barriers reported by F-22 pilots for AACAS involve performance issues: concern about interference and that the system could create a tactical disadvantage in combat. The primary trust barriers reported by F-22 pilots for AW involve concern about increased workload, the lack of a human decision maker, and the AW's ability to adapt to novel constraints.

4 Discussion

The present paper examined trust barriers among operational pilots in relation to two forms of future autonomy within the Air Force, namely the AACAS and the AW technologies. While both 4th and 5th Gen fighter pilots served as the samples, the responses were fairly consistent between both sets of pilots; therefore, the data will be discussed across both samples rather than by a specific platform type (i.e., F-16/F-22). For AACAS, the primary concerns for pilots revolved around performance issues. Like prior fielded automated systems on fighter aircraft [13, 17, 18] pilots were very concerned about interference. Pilots did not want AACAS preventing them from getting close enough to other aircraft for training, battle damage checks, or most importantly, during Basic Flight Maneuvers (BFM). These concerns about interference were largely in preventing the pilot from engaging in a maneuver that was desired, essentially demonstrating concerns about false alarms. There were also concerns about the system causing harm by maneuvering one aircraft into another during the execution of an automated avoidance action in close formation. Pilots also reported concerns about the reliability of the system in general (given the complexity of the data links and algorithms required for the system), as well as concerns about the data linkages between cooperative and non-cooperative aircraft. In this case, cooperative aircraft would be those with a similar AACAS system and sensing capability, and non-cooperative would be those without AACAS. Given the speeds and tactical requirements of operating a fighter aircraft, these concerns are logical as pilots need to maintain a tactical edge on the battlefield. Pilots want a system that is both highly reliable, but not prone to nuisance activations (e.g., false alarms – activating when an activation was not necessary). Consistent with the literature on trust of automation [3, 4, 6, 7], performance and reliability are significant drivers of trust of technologies like AACAS. Additionally, pilots reported that they could see value in AACAS if the reliability of the system was very high and interference could be eliminated/minimized. This value was noted mostly as a "last ditch" maneuver to avoid an otherwise imminent collision.

The reported trust barriers for AW were a bit broader than those for AACAS and this may be reflected for two reasons: (1) AACAS is a more mature technology relative to AW and as such the trust concerns from pilots of AW may be driven by an overall uncertainty associated with AW, and (2) AW is intended to operate within a broader array of situations which thus creates greater complexity for trust evaluations. The pilots' top concern was related to the expectation that the AW would add to an already high-workload environment. Operational fighter pilots operate at a high ops tempo and the flight requirements, communication requirements, and operational requirements

create a high workload situation. Adding the complexity of communicating with and "leading" an AW raises concerns that pilots do not want the added workload. Like AACAS, reliability was also an issue for pilots when considering the AW.

In contrast to AACAS, when pilots considered the AW, they reported concerns about the lack of a human decision maker in the cockpit. Given the time-sensitive and dangerous domains that military personnel are faced with, these concerns are logical. Specifically, there are concerns that the system would make the wrong decision when faced with a difficult situation. Herein, it would be useful to highlight the intent-based transparency of the AW to the pilots, as called for in general by [14]. By using intent-based transparency methods the pilots and AW would have more opportunities to establish shared intent, which is crucial in dynamic, morally contentious situations. Shared intent allows two or more entities to establish predictable behaviors/reactions to novel constraints. Shared intent is important in this context due to the fact that pilots reported concerns about accountability for the AW. This is also important because pilots also noted that they have concerns about the AW's ability to adapt to novel demands. The pilots seemed to want the AW to be able to think and respond "like a human," however that may not be the best approach for this human-machine team. A more fruitful approach may involve leveraging the strengths of the AW and building a flight lead-AW relationship in a way that maximizes the strengths and minimize the weakness of each partner. This heterogeneous, but synergistic approach could maximize the effectiveness of the human-autonomy team. Further, the pilots noted concerns about potential hacking of the AW, and the potential for the AW to physically "hurt" the pilot by running into her/him. Thus, while performance-related concerns were definitely present for AW, similar to AACAS, the pilots seemed to also consider intent-based issues in relation to AW. The identification of these trust barriers are important for researchers and designers to consider in the development and fielding of future autonomy. Like AACAS, the pilots reported a number of potent benefits of a system like an AW to include: risk reduction for pilots (i.e., fewer pilots in harm's way), using the AW to engage particularly risky targets or in very risky situations, using the AW to carry additional assets such as weapons and sensors, using the AW to jam surface-to-air missile batteries (i.e., to protect the pilot).

The next section presents a series of recommendations for military organizations seeking to field future autonomy systems. First, performance-related issues will be a paramount concern among operators. Thus, military organizations are encouraged to use videos as a means to "show" the performance and reliability of the system. There are two potential ways in which videos can be incorporated. Videos of operational performance should be shown to highlight both positive and negative exemplars of the system's performance. The positive videos should boost trust, as demonstrated by a prior field study examining trust of the AGCAS system [19]. Yet, care must be taken to avoid situations of over trust as videos have the potential to generate high trust among individuals with little system experience which could negatively impact trust calibration. The videos serve as operational evidence of the system's performance. While videos of negative system performance may cause a decrease in trust they are important for sharing stories among operators and will help the operators to understand the limits of the system. After all, a decrease in trust can be beneficial if it leads to a more accurate calibration of one's trust. The second type of video might include test videos which show the system in scripted scenarios that test the limits of the system. Such

videos would be impossible (and unethical) to create in actual operations, so testing seems like the right opportunity for such videos. Anecdotally for the present study, following the interviews, most of the pilots had an opportunity to discuss AACAS with a subject matter expert (SME) on the system and when that SME showed the pilots a successful test video of the AACAS in a close proximity high-speed pass, the effects on pilot trust were virtually spontaneous. In this case, "seeing is truly believing."

Understanding the intent of the systems also seems to be an important theme emerging from this research. Using intent-based transparency methods should help to foster shared intent between the human and the system [14]. This shared intent, should in turn support predictability for how the system will behave in novel situations. If one understands the rules that govern the system's behavior (i.e., goals, goal priorities, interactive styles, rules of engagement) then the system's reaction to novel demands should be more predictable, at least more understandable. Intent-based transparency could be established through education and joint human-machine training. The educational aspects could focus on the background and purpose of the system, why it was designed, how the system sets and prioritizes goals in changing contexts, and the rationale for decision making processes. More importantly, the human should engage in joint human-machine training to experience how the system reacts to novel demands. Herein, the design of the scenario should be done in such a way as to stress the boundaries of the situation to maximize the range of potential decision options. Again, the interest is in building an understanding of the behavioral rules used to govern the system's behavior, and in establishing some predictability of how the system executes those rules in various conditions. In this sense, having experience with a system reacting to the same or very similar circumstances is less variable than exposure to a smaller subset of encounters with novel stimuli that stress the system's range of behavioral flexibility.

The current research is not without limitations. One limitation is that the study was limited to military personnel and military technologies. Future autonomy in the commercial sector could be perceived differently than military technologies. Further, non-military personnel may be more or less accepting of future autonomy, relative to military personnel. For instance, autonomous cars are beginning to hit the market and recent accidents have been blamed on overreliance on the technology. Military fighter pilots may be more prone to be skeptical of new technologies. A second related limitation is that only military technologies have been considered in this study. Technologies that are available on the commercial market may be perceived differently than military technologies. However, both AACAS and AW fit the criteria for "R3" in that they are **real** technologies, with **real** operators that have the potential for **real** consequences in the world. Finally, the current study involved qualitative data, future research on this topic might include experimental studies to pinpoint the impact of different trust factors on trust intentions and trust-based behavior.

References

1. Veloso, M., Aisen, M., Howard, A., Jenkins, C., Mutlu, B., Scassellati, B.: WTEC Panel Report on Human-Robot Interaction Japan, South Korea, and China. World Technology Evaluation Center, Inc., Arlington (2012)

2. Mayer, R.C., Davis, J.H., Schoorman, F.D.: An integrated model of organizational trust. Acad. Manag. Rev. **20**, 709–734 (1995)
3. Lee, J.D., See, K.A.: Trust in automation: designing for appropriate reliance. Hum. Factors **46**, 50–80 (2004)
4. Chen, J.Y.C., Barnes, M.J.: Human-agent teaming for multirobot control: a review of the human factors issues. IEEE Trans. Hum.-Mach. Syst. **44**(1), 13–29 (2014)
5. Hoff, K.A., Bashir, M.: Trust in automation: integrating empirical evidence on factors that influence trust. Hum. Factors **57**, 407–434 (2015)
6. Onnasch, L., Wickens, C.D., Li, H., Manzey, D.: Human performance consequences of stages and levels of automation: an integrated meta-analysis. Hum. Factors **56**, 476–488 (2014)
7. Hancock, P.A., Billings, D.R., Schaefer, K.E., Chen, J.Y.C., de Visser, E.J., Parasuraman, R.: A meta-analysis of factors affecting trust in human-robot interaction. Hum. Factors **53**(5), 517–527 (2011)
8. Lyons, J.B., Saddler, G.G., Koltai, K., Battiste, H., Ho, N.T., Hoffmann, L.C., Smith, D., Johnson, W.W., Shively, R.: Shaping trust through transparent design: theoretical and experimental guidelines. In: Savage-Knepshield, P., Chen, J. (eds.) Advances in Human Factors in Robotics and Unmanned Systems, pp. 127–136. Springer, Cham (2017)
9. Li, X., Hess, T.J., Valacich, J.S.: Why do we trust new technology? A study of initial trust formation with organizational information systems. J. Strateg. Inf. Syst. **17**, 39–71 (2008)
10. Guznov, S., Lyons, J.B., Nelson, A., Wooley, M.: The effects of automation error types on operators trust and reliance. In: Proceedings of HCI International, Toronto, CA (2016)
11. Pak, R., Fink, N., Price, M., Bass, B., Sturre, L.: Decision support aids with anthropomorphic characteristics influence trust and performance in younger and older adults. Ergonomics **55**(9), 1–14 (2012)
12. Merritt, S.M., Unnerstall, J.L., Lee, D., Huber, K.: Measuring individual differences in the perfect automation schema. Hum. Factors **57**, 740–753 (2015)
13. Lyons, J.B., Ho, N.T., Koltai, K., Masequesmay, G., Skoog, M., Cacanindin, A., Johnson, W.W.: A trust-based analysis of an air force collision avoidance system: test pilots. Ergon. Des. **24**, 9–12 (2016)
14. Lyons, J.B.: Being transparent about transparency: a model for human-robot interaction. In: Sofge, D., Kruijff, G.J., Lawless, W.F. (eds.) Trust and Autonomous Systems: Papers from the AAAI Spring Symposium (Technical Report SS-13-07). AAAI Press, Menlo Park (2013)
15. Defense Science Board (DSB) Task Force on the Role of Autonomy in Department of Defense (DoD) Systems. Office of the Under Secretary of Defense for Acquisition, Technology, and Logistics. Washington, DC (2012)
16. Defense Science Board (DSB) Summer Study on Autonomy. Office of the Under Secretary of Defense for Acquisition, Technology, and Logistics. Washington, DC (2016)
17. Wadley, J., Jones, S.E., Stoner, D.E., Griffin, E.M., Swihart, D.E., Hobbs, K.L., Burns, A.C., Bier, J.M.: Development of an automatic air collision avoidance system for fighter aircraft. In: AIAA Infotech@Aerospace Conference, Guidance, Navigation, and Control and Co-located Conferences. Boston, MA (2013)
18. Jones, S.E., Petry, A.K., Eger, C.A., Turner, R.M., Griffin, E.M.: Automatic integrated collision system. In: 17th Australian Aerospace Congress. Melbourne, AU (2017)
19. Ho, N.T., Sadler, G.G., Hoffmann, L.C., Lyons, J.B., Fergueson, W.E., Wilkins, M.: A longitudinal field study of auto-GCAS acceptance and trust: first year results and implications. J. Cognit. Eng. Decis. Mak. (in press)

A Design Pattern for Working Agreements in Human-Autonomy Teaming

Robert S. Gutzwiller(✉), Sarah H. Espinosa, Caitlin Kenny, and Douglas S. Lange

Space and Naval Warfare Systems Center Pacific, 53560 Hull Street, San Diego, CA 92152, USA
{gutzwill, shunt, ckenny, dlange}@spawar.navy.mil

Abstract. Humans and machines are increasingly reliant upon each other in complex environments and military operations. The near future suggests human understanding of machine counterparts is a required, paradigmatic element. Knowing how to engineer and design for these environments is challenging. The complexity between levels of automation, human information processing, and function allocation authority issues in an adaptive system make it unlikely to find a "one-size-fits-all" approach. There may still be general strategies for engineering in these cases; for example, collaborating and coordinating are familiar requirements of all human team activities, and extend to human-automation teaming. Here, we outline what we believe is one so-called "design pattern" for working agreements. We use the loose structure of prior software design patterns to organize our thoughts on why working agreements are necessary, where and how they are applicable, what instantiating them requires, and how to measure their effectiveness. By choosing the design pattern structure, we end up carefully describing what might work best and what the limits are toward improving human-machine teaming.

Keywords: Human-machine teaming · Working agreements · Design patterns · Human automation interaction

1 Introduction on Working Agreements

In the modern era of software development, many problems are recurring. Fortunately, these problems have repeatable solutions. The accepted format for conveying these solutions has been termed a "design pattern" [1, 2], and can be applied across the spectrum of software engineering, including implementation and structural design [3]. We believe these can be extended in spirit to describing human-autonomy teaming patterns.

Ostensibly, these patterns are useful for multiple reasons. First, they provide the mid-level conceptual representations for common problems. These allow for a sharing mechanism among programmers and designers that focuses less on specifics and more on generalities. Second, the patterns are not so high-level as to be useless in application: having viewed one pattern, a programmer can begin to work, whereas high-level representations require more effort and investment to flesh out. Patterns may help define key hardware and software requirements as well.

D.N. Cassenti (ed.), *Advances in Human Factors in Simulation and Modeling*,
Advances in Intelligent Systems and Computing 591, DOI 10.1007/978-3-319-60591-3_2

These representations are common in software design, but not yet in the interaction between humans and autonomy. However, recently there have been several efforts to create patterns for methods to solve human-autonomy teaming challenges [4, 5]. Indeed, this method may help bridge disparate research efforts by outlining general solutions to problems plaguing human-autonomy partnerships. The lineage of design patterns suggests that human-autonomy teaming patterns should focus on particular techniques, their intention, motivation, applicability, participants, consequences, implementation, known uses, and related patterns.

In this first attempt at a design pattern, are interested in an emerging method for man-machine teaming, working agreements [6]. We use the format of the chapters from Gamma [3] in the next sections where they apply, borrowing from the software community and using it to develop the conceptual representation of working agreements more fully.

1.1 Background and Intent

Working agreements define how and when human-automation teams split tasks, and in what situations responsibilities over these tasks may change. Most of the power of using agreements is in reducing the mismatch between different agents' expectations about the state of the world, and how agents will interact; and the true state or operating model of the agents, which drive intention, and action. The mismatch between how agents represent other agents expected behavior might affect both the human and any automated participants. Often times this mismatch creates serious safety and performance failings, such as the grounding of the ship Royal Majesty. The inability of the crew to confirm that differential modes of automated navigation and GPS navigation information were active and valid [7] created serious issues. The combination of mode confusion, automation surprise (because of mismatched user-machine models of the environment and how each agent should work), and embedded automated commands operating silently, led a simple GPS receiver loss while leaving a harbor to metastasize into a catastrophic grounding of the ship many days later [7].

Working agreements may improve the transparency of automated decision-making systems by clearly indicating, as well as pre-determining what tasks each human and automated agent in a team performs, and under what conditions. Working agreements can even specify particular methods for solutions that could be used, or could not be used or allowed.

Working agreements seem especially appropriate for teaming, as team situations require communication and collaboration [8–10] in a way that is facilitated by (a) articulating tasks and functions, (b) properly allocating those functions among members, and (c) a display of the allocation of tasks among the team [11, 12]. For example, managing tasks is a source of difficulty for supervisory control of unmanned systems. Automation may reduce load by taking control of some of the operators' tasking (thus reducing demand). The tasks themselves form the backbone of an agreement, which can be configured and determine the behavior of the agents.

Still, certain tasks may be off-limits to certain actors (for example, weapons release). A working agreement could specify tasks that the automation cannot perform. However, a conditional property may modify such an agreement – which can be

specified as well. The key is that these function allocations are brought to the surface of human-automation interactions, where they are visible.

1.2 Motivation

Working agreements help make the rules and constraints of human-machine teams explicit. It is especially important to articulate constraints when the roles and responsibilities of automation "adapt" to changing conditions of the operator and/or the environment. The notion of adapting responsibilities between humans and automation differs from traditionally "static" automation (e.g., [13]). Adaptive automation attempts to deal with the complexity and context-specific dynamics inherent in real-world system operations [13]. These situations are often large, complex, and rapidly overwhelm the limitations of human memory and attention [14]. Such adaptive automation seems to be the future of most systems due to greater success than seen in other automation implementations [15]. As working agreements help track and specify the changes in authority and responsibility that accumulate across adaptive systems, they are naturally beneficial.

Many have written about the intricacies of determining how and when automation changes its behaviors [16–18]. In considering how systems should adapt and interact with operators, working agreements could become a centerpiece in making explicit the capabilities and limitations of the automation (and aiding in developing operator expectancies by making them explicit). As a direct effect, human memory demand is reduced through a better, more available representation of what the automation is doing, and when. Most important is that the negotiation between systems and operators about task and function allocations can happen before workload reaches a high level [19], when most traditional solutions would take effect.

There are several key characteristics to a working agreement in human-machine systems; the use of adaptive or adaptable "mixed initiative" automation with multiple actors; a base model to represent the automation capabilities and limitations; and a triggering model in the case of adaptation for representing how and when to shift responsibilities between the human operator and the system. Adaptation in this sense represents an update of who is responsible for what, in real time, and adjusting the associated information displays, task sequences, and task deadlines as required [20].

Explicit definition of goals and tasks, and how they are shared and split between the agents, are necessary steps toward developing good teamwork and communication (e.g., [21, 22]). These same sets of goals and tasks can populate a working agreement structure [6, 23]. They are, in some respects, necessary before a working agreement can be developed, and are at least one way to abstract the tasks, and the methods to accomplish them, in a manner that a machine may understand and process [24].

In the case of working agreements, automation transparency should also be increased. The task-based nature of working agreements help indicate in clear language what the automation should be doing in any foreseeable condition. Tasks and methods to perform them can also be specified in system language, providing some shared understanding. Working agreements will not solve emergent issues that complex systems may create which are not foreseeable. Different methods may be useful for

creating teamwork between humans and artificial neural network-created behaviors, for example [25].

Limitations of the automation can also be articulated in clear task-based language. The system can no longer hide which tasks it is, and is not, performing or going to perform. Allocations are displayed to the operator prior to performance, aiding in transparency and operator trust.

Working agreements may also be available during or displayed after performance to aid in training and building of user mental models. The agreements themselves may be useful when aggregated across a range of users; for example, did Bob set up a different agreement than Jill? What conditions prompted the difference? Were there any performance effects as a result? While there are a myriad of ways to improve operator trust or acceptance of automation behaviors, working agreements may be one of the easier methods to implement, once a task taxonomy is created and methods of performance are catalogued.

1.3 Applicability – When Should You Use This Design Pattern?

The working agreement pattern should be useful when there is at least one human and one computer "agent," each of which may be asked to perform tasks and occasionally share or trade responsibility for their execution. Such configurations are often referred to as adaptive automation [15] or sometimes adaptable automation [17], or mixed-initiative automation systems. In each, there are definable tasks that either the human or the automation can perform. Additionally, their name hinges on the locus of the allocation authority [26], either human "adaptable," or computer "adaptive," systems.

The allocation agent is that which decides how to allocate task responsibility between the participants. The allocation authority, if a computer, can assign incoming and existing tasks based on any number of inputs of varying complexity, including human workload estimation [18], [27] or state changes in the system given a set of parameters. For example, the flight management system – autopilot – in some airliners takes action at the point in landing where human reaction time is sub-par and unsafe. The function is allocated to the computer and taken out of the hands of the human, based on a condition; [28]. If the allocation authority is a human, then the human directs other humans and automation to have responsibility over certain tasks.

1.4 Participants

The human operator determines and sets the base configurations of the working agreements. These include more than just the function allocation elements. Configuration of the working agreement also involves determining the transition points and conditions that may serve to alter function allocations and authority changes to particular elements, classes of elements or more. The involvement of actual end users in this effort is critical to avoid confusing future operators, or anchoring design around inappropriate elements or triggers. Multiple cognitive task analysis methods are available to help determine these [29–31].

As we will discuss in a later section, human-human working agreements are already a familiar concept in some domains. The extension of the design pattern to human-agent and human-autonomy teams is a natural one, and is being explored.

An intelligent agent must also be able to interpret the human's determination and setting of default working agreement configurations, including function allocation, and transitioning conditions (usually based on if - then logic).

1.5 Structure

While we will usually think of working agreements as dictated by the human to the autonomy, they can also be considered a negotiation between the two in which the human has the upper hand and final say. The autonomy may reject roles through considerations of an inability to perform a particular function, and/or due to current configuration. One could also allow agents to bid for particular tasks. While most often this pattern may have a strictly one-way decision process, one can envision a two-way negotiated agreement fully deserving of that title.

Additionally, once a working agreement is set, its presence allows the human and autonomy to work as teammates rather than necessitating a strict supervisory control abstraction, if the agreement has been so specified.

Figure 1 uses a graphical language defined in [5] to illustrate the team structure being employed. In the figure, we see that the human and autonomy are teammates, both using a common collection of tools to perform work processes. While many implementations may look more supervisory in nature (which could be illustrated by a directional edge between human and autonomy) we diagrammed the more general case.

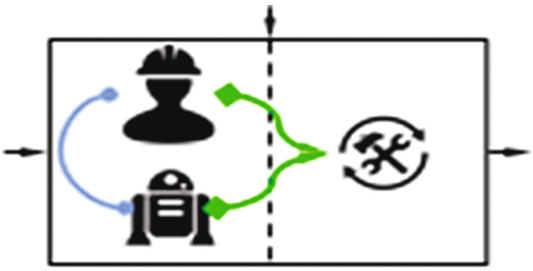

Fig. 1. Working agreements are at their most general a teaming relationship between human and autonomy. [From 4]

The working agreements themselves can be implemented with a variety of structures. However, the recommendation is to use a structure as shown in the following figure. In Fig. 2, we show that an agreement is between two or more agents. Agreements are associated with tasks to be performed. In particular, we are interested in situations where a human is entering into an agreement with an autonomous artificially intelligent agent.

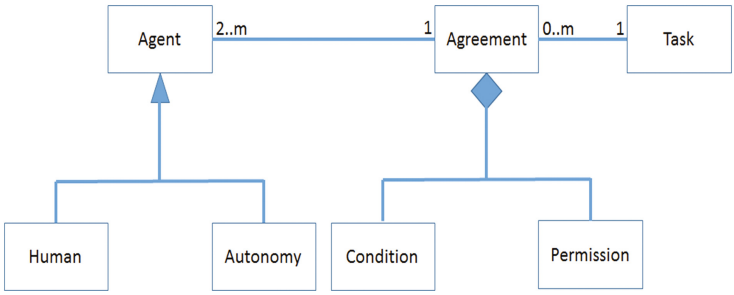

Fig. 2. Working agreement structure using unified modeling language.

We use a task, method breakdown shown in Fig. 3, for an unmanned systems command and control task allocation. Methods can be associated with agents and we can collect data about performance of agents for methods and tasks. Key to working agreements are the conditions under which each set of permissions is valid, and thus, whether the implementation is useful (as discussed next in Sect. 1.6).

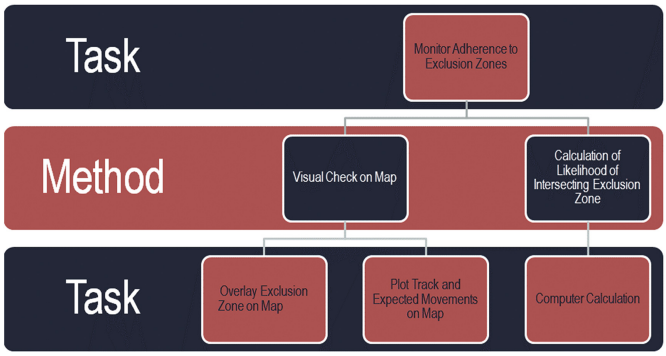

Fig. 3. Example task-method breakdown, as in [21].

1.6 Consequences – What Happens with Pattern Use?

Working agreements are theorized to provide several values to human-autonomy partnerships. A few theories include that agreements should (1) improve teamwork through transparency, and roles clarification; (2) provide a stable representation of the goals and limits of multiple partners in an environment, thereby lessening the burden on memory and training of the human user; and (3) inspire the refinement and definition of tasks and conditions. Better allocation will take advantage of differential skill sets between man and machine, and take into account the information and understanding needed by a human teammate.

Evaluating working agreements is, in essence, about the assessment of the whole system of systems incorporated in the environment. Naturally, performance is a key

parameter. However, additional conditions should be examined, and we consider a few of them here (though this is not an exhaustive list).

First (1) whether there are emergent factors not captured by the task-methods hierarchy should be determined. Emergent factors could easily disrupt performance of the whole system or any of the parts; for example, user fatigue may disrupt whole system performance independent of any helpful effect of a working agreement. Second, (2) is to ensure each party's adherence to the agreement. If an agreement is violated, it might be important to understand the conditions surrounding the violation, but it also means the agreement was not *actually* in place. Third (3), a determination of agent comprehension of the agreement should be made. A user that does not understand the limitations imposed by an agreement will not act properly in the environment, so any performance consequences will not be the result of the agreement. Finally, (4) assessments must ensure there was correct and timely recognition of any triggering elements, events, conditions, and contexts that might comprise the agreement itself. The need for recognition applies to all agents in the agreement.

In order to evaluate the result of a working agreement when it is functioning properly, we turn to the measurement of human-automation function allocation [32]. As agreements define function allocation schemes, once a set of requirements are met, they can be evaluated by a grouping of measures advocated by Pritchett et al., of which we deemed the following as crucial to working agreements:

1. Assessments of user workload, and task loading. This measure may be facilitated by the specific task-based design and task-methods hierarchy breakdown. For example, certain task agreements may generate more or less demand on a human user, or create bandwidth overload on networked systems. There may be optimal agreements, then, that moderate workload and system performance.
2. A measure of authority as compared to a measure of responsibility. In other words, is there an imbalance between the controlling agent and the agent responsible? A working agreement, properly implemented, should directly improve this measure.
3. The stability of the performance and system environment, to the extent it is operationally relevant.
4. The measurement of interruptions, particularly interruption frequency and probability, as well as their effects on operator performance. For example, some function allocation schemes require repeated authorization or input from the human operator, sometimes to the detriment of their performance. Does a particular working agreement improve on, or make this situation worse?
5. The capabilities and limitations of automation and the behaviors that result when they are exceeded by the environment or the user. These may improve, to the extent they are captured in a working agreement, although this is unknown.
6. System cost and performance; is the working agreement improving either, as the result of its effective implementation?
7. How well does the human adapt to any context changes? Some working agreement settings may allow the user to exert more control or allocate more attention to tactics, for example, while others may mean the human is performing more menial labor.

We also suggest that measures of the human's trust in the autonomy may improve through increasing the transparency of function allocation. Of course, one of the gaps identified here is that working agreements and human-autonomy teams in general have not been adjudicated by these measures. Working agreement assessment is a move toward requiring measures of function allocation, and experimental exploration of design.

1.7 Implementation

Working agreement employment will require determination of what tasks are present to be split between human and machine. This is a fundamental function allocation task, and has puzzled engineers of complex systems before. However, here and elsewhere we believe we have a good approach in the application of a task-method hierarchy [24].

We are using this method to determine tasks and methods within a multiple unmanned system command and control environment. Here, supervisory control may be shared between humans and autonomy, creating unique teams [11]. It required the definition of tasks (which were in part derived from subject matter experts), as well as determining the possible conditions surrounding whether automation was capable or should be allowed to perform them.

Working agreements should always be developed in conjunction with user-centered design practices and testing. No amount of a priori assumptions by designers will ever compensate for hands-on, iterative testing with actual users of a system. It is unlikely that all possible effects from all possible combinations of agreements can be understood before users attempt to interact with them. As the autonomy should be viewed as a teammate, the display of the working agreement conditions and status is key in informing the user about the agreement. Efforts should be made to make sure this display is user-friendly and unambiguous through usability assessment and experimentation [33].

It is also critical to ensure that interacting with the agreement occur before operations begin, allowing operators to orient themselves to the situation and conditions. Orientation, as it facilitates communication and coordination, is key to teaming. One could argue that by centering on tasks, a working agreement helps define the work for the team; doing so before work begins may be the most effective approach.

Conditions in which the agreement language itself is unclear may arise. Clarity should be a design goal and should be facilitated by the task-method basis for the agreements and by user-centered design. For example, in air traffic control, there are specific assignments and air space coverage areas that are referenced in agreements, which delineate "who does what" in a verbiage that all parties understand. In the Consequences section above, we discussed some ways to measure the effectiveness of working agreement implementation; these methods may also capture something like language ambiguity problems, whether it is reflected in user trust, particular agreement configuration patterns, workload, and stability.

Implementation may be limited to where there exist definable, separable tasks, roles, and responsibilities. While this will cover most forms of human-automation teaming at a high level, it will not cover others. A good example of something difficult is the automation present in fly-by-wire systems used in high-performance aircraft

which smooth human operator input and maintain flight stability; since the "parts" are not separable it would be very difficult to split tasks out. A similar problem exists when examining basic control of robotic systems that use automation to control robotic arms with high degrees of freedom. In essence, it may be difficult to implement working agreements in automated systems that do not allow for part-task separations.

As noted elsewhere, separating tasks may have important implications for training [34, 35]. Part-task training methods characterize how many automated systems are created, with the automation taking some tasks out of the users' hands. Naturally, the shift of "who does what" between operators and automation affects *what* users learn to perform [36]. Accordingly, the implementation of working agreements may help structure examinations of training with automation. Working agreements could be chosen and enforced experimentally, and measured along with training and skill acquisition of the users, to determine which agreements improve operations, and train the best skills for a given domain [36].

1.8 Known Uses and Related Patterns

The domain of air traffic control (ATC), which depends on proper coordination of aircraft flight paths between multiple human controllers for the duration of a flight, has historically used a working agreement model. The official term is letter of agreement, and they are employed by both the Federal Aviation Administration and by European Organization for the Safety of Air Navigation (EuroControl) [37]. Letters of agreement follow a standard format to supplement procedures that address the needs of particular sectors of airspace. In two ways, these agreements are adhering to our earlier principles for working agreements: (1) that language has to be clearly understood by the parties involved; and (2) that agreements foster the articulation of tasks to enable themselves.

While letters of agreement can cover a variety of scenarios, in general they serve to "(a) define responsibilities and coordination requirements, (b) establish or standardize operating methods, (c) specify special operating conditions or specific ATC procedures, or (d) delegate responsibility for an ATC service" [38]. These letters of agreement are negotiated by the parties involved, which for ATC could mean two airspace sectors, but also between entities [39]. In either case, the agreements define the purpose, scope, responsibilities, and procedure for both parties. Henceforth, parties are equipped with the necessary awareness to coordinate, delegate, and safely proceed with shared ATC procedures. Air traffic controllers are familiar with these agreements between sectors of airspace, and are trained to split tasks within the same sector. A good example of this behavior is within teams assigned to some En Route sectors, who split work between a primary Radar position (R-side) and a secondary Radar Associate operator (D-Side). The Associate supports the R-side operator by taking over housekeeping tasks, such as aircraft handoffs and assisting in separation assurance [40].

Effective teaming and negotiation of the agreement helps define a task allocation schema. In this schema, the D-side acts as a collaborator to help solve difficult conflicts. Much like a working agreement, each team must uniquely determine task allocation and conflict resolution strategies (such as a preference for issuing orders to aircraft to change vector, versus directing them to change altitude, in order to avoid collisions).

Close collaboration and transparency between an R-side and D-side is critical, as not all of these agreements are formal.

As the push toward automation of the national airspace gains momentum, the D-side operation is a natural candidate for supportive automation. With automation systems, the agreements would need to be made formal to enable teamwork. The NASA Ames Airspace Operation Laboratory has been investigating the allocation of tasks between a human air traffic controller and ground based separation assurance automation since 2008 [41]. These experiments specifically target increasing the total number of aircraft in a sector at any given time, while maintaining safety. Several experiments yielded confidence that separation assurance automation is a viable candidate for mediating workload in future, denser airspaces [41]. However, the relationship between the R-side air traffic controller (human) and automation for the D-side is still under investigation.

A 2010 experiment highlighted the human's willingness to delegate housekeeping tasks to the automation [41]. One notable finding was that controllers preferred authority over decision-making tasks, such as approving weather reroutes. However, the majority of controllers indicated post–study that they would still share tasks with the automation, instead of completing them in isolation. This collaboration paradigm mimics the current R-/D-side collaboration between human controllers. It also suggests that whether or not the task-element contains decision-making points, may influence whether an operator will trust that element in the agreement.

Transparency and goal alignment are critical in human-machine teaming. More focused analyses of the data from the 2010 study offered additional insights. Operators have specific preferences in conflict resolution (which the automation in the study did not take into account). Controllers often wanted a different type of conflict resolution than the automation could provide. The automation went about resolving conflicts in a very different manner [42], which violated controller expectancies.

Unlike a human D-Side who could be told a specific way to do a task, or at least could be negotiated with, controllers had to work around the limitations of the automation. Controllers were given no insight or interface for delegating tasks or the methods used to perform them. Implementing working agreements specifically would allow the users to articulate how they want to limit or expand the behavior of the automation, solving some of these problems, and building toward improved human-machine teams.

2 Conclusions

We have written extensively here regarding the use of working agreements between humans and automation. We believe that such agreements are a good way to organize the work of the various agents often in play in complex environments. It is a way to articulate who is doing what work, and the conditions that dictate change. By giving users the power (or denying them the power) to alter explicit expectancies about automation behaviors, better teaming should arise. It is important this power is available a priori, before the performance conditions are put upon the users.

As discussed above, working agreements themselves can be evaluated and assessed. Measurability is not a trivial property, as approaches that can be measured can also be definably improved. What works for some conditions may not work for others; what works for some populations of users may not for others.

The task specification exercise required to formulate agreements provides a valuable reason to articulate tasks that populate a given domain. It is not easy, but benefits the human factors assessment of the user needs and roles, and will help specify the different roles and capabilities of automated teammates.

Acknowledgements. The views expressed in this article are the sole views of the authors and do not reflect official policy or the opinions of the US Government or Department of Defense. This work was funded in part by a NISE ONR project from SPAWAR Pacific, and from the Autonomy Research Pilot Initiative IMPACT project.

References

1. Smith, R.: Panel on design methodology. In: OOPSLA 1987 (1987)
2. Beck, K., Cunningham, W.: Using pattern languages for object-oriented program. In: OOPSLA 1987 (1987)
3. Gamma, E., Helm, R., Johnson, R., Vlissides, J.: Design Patterns: Elements of Reusable Object-Oriented Software. Addison-Wesley, Boston (1995)
4. Lange, D.S., Gutzwiller, R.S.: Human-autonomy teaming patterns in the command and control of teams of autonomous systems. In: HCII 2016 (2016)
5. Schulte, A., Donath, D., Lange, D.S.: Design patterns for human-cognitive agent teaming. In: Harris, D. (ed.) Engineering Psychology and Cognitive Ergonomics, pp. 231–243. Springer, Cham (2016)
6. de Greef, T., Arciszewski, H., Neerincx, M.: Adaptive automation based on an object-oriented task model: implementation and evaluation in a realistic C2 environment. J. Cognit. Eng. Decis. Mak. **4**(2), 152–182 (2010)
7. Lützhöft, M.H., Dekker, S.W.A.: On your watch: automation on the bridge. J. Navig. **55**(1), 83–96 (2002)
8. Cuevas, H.M., Fiore, S.M., Caldwell, B.S., Strater, L.: Augmenting team cognition in human-automation teams performing in complex operational environments. Aviat. Space Environ. Med. **78**(5), B63–B70 (2007)
9. Malin, J.T., Schreckenghost, D.L., Woods, D.D., Potter, S.S., Johannesen, L., Holloway, M., Forbus, K.D.: Making intelligent systems team players: case studies and design issues. Volume 1: human-computer interaction design. NASA Technol. Memo. 104738, 1–276 (1991)
10. Klein, G., Bradshaw, J.M., Feltovich, J.M., Woods, D.D.: Common ground and coordination in joint activity. In: Rouse, W.B., Boff, K.R. (eds.) Organizational Simulation, pp. 139–184. Wiley, Hoboken (2005)
11. Gutzwiller, R.S., Lange, D.S., Reeder, J., Morris, R.L., Rodas, O.: Human-computer collaboration in adaptive supervisory control and function allocation of autonomous system teams. In: Shumaker, R., Lackey, S. (eds.) Virtual, Augmented and Mixed Reality, pp. 447–456. Springer, Cham (2015)

12. Gutzwiller, R.S., Lange, D.S.: Tasking teams: supervisory control and task management of autonomous unmanned systems. In: International Conference on Virtual, Augmented and Mixed Reality, pp. 397–405 (2016)
13. Sheridan, T.B., Verplank, W.L.: Human and computer control of undersea teleoperators, Man-Machine Syst. Lab, Dep. Mech. Eng. MIT. Grant N00014-77-C-0256 (1978)
14. Cummings, M., Mastracchio, C., Thornburg, K., Mkrtchyan, A.: Boredom and distraction in multiple unmanned vehicle supervisory control. Interact. Comput. **25**(1), 34–47 (2013)
15. Kaber, D.B.: Adaptive automation. In: Oxford Handbook of Cognitive Engineering. In: Lee, J., Kirlik, A. (eds.) Oxford University Press, Oxford, March 2013
16. Parasuraman, R., Bahri, T., Deaton, J.E., Morrison, J.G., Barnes, M.: Theory and design of adaptive automation in aviation systems. NAWCADWAR Technical Report-92033-60, pp. 1–44 (1992)
17. Scerbo, M.W.: Theoretical perspectives on adaptive automation. In: Parasuraman, R., Mouloua, M. (eds.) Automation and Human Performance: Theory and Applications, pp. 37–63. Erlbaum, Mahwah (1996)
18. Kaber, D.B., Endsley, M.R.: The effects of level of automation and adaptive automation on human performance, situation awareness and workload in a dynamic control task. Theor. Issues Ergon. Sci. **5**(2), 113–153 (2004)
19. Arciszewski, H., de Greef, T., van Delft, J.: Adaptive automation in a naval combat management system. IEEE Trans. Syst. Man Cybern. Part A Syst. Hum. **39**(6), 1188–1199 (2009)
20. Feigh, K., Dorneich, M.C., Hayes, C.C.: Toward a characterization of adaptive systems: a framework for researchers and system designers. Hum. Factors **54**(6), 1008–1024 (2012)
21. Klein, G., Woods, D.D., Bradshaw, J.M., Hoffman, R.R., Feltovich, P.J.: Ten challenges for making automation a team player in joint human-agent activity. IEEE Intell. Syst. **19**, 91–95 (2004)
22. Hollnagel, E., Woods, D.: Joint Cognitive Systems: Foundations of Cognitive Systems Engineering. Taylor & Francis, Boca Raton (2005)
23. Johnson, A.W., Oman, C.M., Sheridan, T.B., Duda, K.R.: Dynamic task allocation in operational systems: issues, gaps, and recommendations In: IEEE Aerospace Conference, pp. 1–15, March 2014
24. Lange, D.S., Gutzwiller, R.S., Verbancsics, P., Sin, T.: Task models for human-computer collaboration in supervisory control of teams of autonomous systems. In: International Inter-Disciplinary Conference on Cognitive Methods in Situation Awareness and Decision Support, pp. 97–102 (2014)
25. Gutzwiller, R.S., Reeder, J.: Human interactive machine learning for trust in teams of autonomous robots. In: IEEE CogSIMA (2017)
26. Sheridan, T.: Adaptive automation, level of automation, allocation authority, supervisory control, and adaptive control: distinctions and modes of adaptation. IEEE Trans. Syst. Man Cybern. Part A Syst. Hum. **41**(4), 662–667 (2011)
27. Wilson, G., Russell, C.: Performance enhancement in an uninhabited air vehicle task using psychophysiologically determined adaptive aiding. Hum. Factors **49**(6), 1005–1018 (2007)
28. Parasuraman, R., Riley, V.: Humans and automation: use, misuse, disuse, abuse. Hum. Factors **39**(2), 230–253 (1997)
29. Crandall, B.W., Klein, G.A., Hoffman, R.: Working Minds: A Practitioner's Guide to Cognitive Task Analysis. MIT Press, Cambridge (2006)
30. Clark, R., Feldon, D., van Merriënboer, J.J.G., Yates, K., Early, S.: Cognitive Task Analysis, vol. 2006 (2006)
31. Endsley, M.R., Jones, D.: Designing for Situation Awareness: An Approach to Human-Centered Design, 2nd edn. CRC Press, New York (2012)

32. Pritchett, A.R., Kim, S.Y., Feigh, K.M.: Measuring human-automation function allocation. J. Cogn. Eng. Decis. Mak. **8**(1), 52–77 (2013)
33. Kortum, P.: Usability Assessment: How to Measure the Usability of Products, Services, and Systems. Human Factors and Ergonomics Society, Santa Monica (2016)
34. Wightman, D.C., Lintern, G.: Part-task training for tracking and manual control. Hum. Factors **27**(3), 267–283 (1985)
35. Naylor, J.C., Briggs, G.E.: Effects of task complexity and task organization on the relative efficiency of part and whole training techniques. J. Exp. Psychol. **65**(3), 217–224 (1963)
36. Gutzwiller, R.S., Clegg, B.A., Blitch, J.G.: Part-task training in the context of automation: current and future directions. Am. J. Psychol. **126**(4), 417–432 (2013)
37. European Organisation for the Safety of Air Navigation: Common Format Letter of Agreement Between Air Traffic Services Unites (ASM.ET1.ST015 DEL01/02 Ed. 4) (2012)
38. US Department of Transportation Federal Aviation Administration: Air Traffic Organization Policy: Section 3. Letters of Agreement (LOA) (2010)
39. Federal Aviation Administration Los Angeles ARTCC: Los Angeles Air Route Traffic Control Center, CA, U.S.A; Tijuana Terminal Radar Approach Control: Letter Of Agreement (1990)
40. US Department of Transportation Federal Aviation Administration: Air Traffic Organization Policy (2015)
41. Prevot, T., Homola, J., Martin, L., Mercer, J., Cabrall, C.: Toward automated air traffic control—investigating a fundamental paradigm shift in human/systems interaction. Int. J. Hum. Comput. Interact. **28**(2), 77–98 (2012)
42. Mercer, J., Gomez, A., Homola, J., Prevot, T.: A closer look at automation behavior during a human in the loop simulation. In: 33rd IEEE/AIAA Digital Avionics Systems Conference (2014)

Automated Situation Analysis as Next Level of Unmanned Aerial Vehicle Artificial Intelligence

Gunta Strupka[1(✉)], Anatoly Levchenkov[2], and Mikhail Gorobetz[2]

[1] Faculty of Power and Electrical Engineering,
Institute of Industrial Electronics and Electrical Engineering,
Riga Technical University, Azenes street 12/1-504, 1048 Riga, Latvia
Gunta.Strupka@edu.rtu.lv
[2] Faculty of Power and Electrical Engineering,
Institute of Industrial Electronics and Electrical Engineering,
Riga Technical University, Azenes street 12/1-512, 1048 Riga, Latvia
{Anatolijs.Levcenkovs,Mihails.Gorobecs}@rtu.lv

Abstract. In this paper automated situation analysis is discussed together with already accessible advantages of artificial intelligence and control systems of unmanned aerial vehicle. Based on previous researches some new solutions are proposed to fulfill safety tasks in case of traffic, fire and criminal threats. Mostly connected with existing solutions, owing to artificial intelligence and hybrid systems they move to next level and provide better results and guideline for further development.

Keywords: Artificial intelligence · Probabilistic logic · Unmanned aerial vehicles · Programming · Microcontrollers · Automatic control · Path planning · Safety · Security · Traffic · Pattern recognition · Act recognition

1 Introduction and Actual Possibilities of Mechanisms and Autopilot

Automation is the most common term that is used in everyday life, but does its opportunities are fully understood and used? Mostly it is connected with certain actions that automated device is able to do without additional help from user. But possibilities of artificial intelligence (AI) usage are not limited.

Nowadays there are available many technical options on how to improve the ability and durability of unmanned aerial vehicle (UAV). New, lighter and more durable materials are being used, batteries of a new grade and engines with other modifications are being used, as well as improved flight control modules. However, there is a disadvantage to all these technical possibilities – it is impossible to improve the system by improving only one of the fields. As a bad situational example – the time of flight is prolonged by increasing the capacity of batteries, but the weight of the new battery is not taken in count in cases where is used a battery of the same grade with greater capacity but without lighter modules because the factor of effectiveness of the engines

D.N. Cassenti (ed.), *Advances in Human Factors in Simulation and Modeling*,
Advances in Intelligent Systems and Computing 591, DOI 10.1007/978-3-319-60591-3_3

is decreased in this case. The creators of UAV would not allow such a mistake and these improvements are made in accordance with one another.

In parallel to the improvements, the development of autopilot takes place that includes not only the maintenance of height and speed, but also maneuvers (roll, yaw, pitch) and the execution of a plan given in advance. One of the main components of the auto-pilot is the control of the remaining energy to ensure a successful return of the vehicle to its starting point or to ensure at least a successful landing by not being in a free fall. Accordingly created safety systems most often are stagnant and unable to react in non-standard situations as all of the existing solutions are predeveloped and based on the specific logic.

The quadcopter is selected in this research as the most suitable UAV for such task, because of its stability and controllability. However, another type of UAV like helicopters may be used in the tasks, where the speed is more critical.

2 Artificial Intelligence in Control Systems

To improve the mentioned disadvantages, the solutions of artificial intelligence are used. Fuzzy logic has been used in the engine control process to determine and control the maneuvers of the aircraft on the basis of several electro-mechanic aspects.

2.1 AI Types and Hybrid Systems

AI is not a novelty in the field of electrical technology, it is widely used in situations where classical algorithms of regulation and control do not provide the needed result, for example, PID regulator cannot create the needed characteristic curve so the AI is added that would learn or use the existing knowledge of the experts.

To fulfill AI application, usually fuzzy, neural, or genetic algorithms are used. First of mentioned could be used better in situations when normally measurable or technical parameters are discussed, like motor and battery power, speed of wind, geolocation according to its position and in case with other close items mutual position should be taken into account.

Neural and genetic algorithms are able to analyze more sophisticated situations than fuzzy algorithm as for its usage almost all possible variations should be accounted by expert, but for rest - expert is in the role of a trainer. To reach the highest results in AI comprehensive situations, hybrid systems are used, for example, fuzzy and neural generates system with ability to be trained as neural and also predict and analyze as feature of fuzzy.

- Input data set for neural network: $X = \{x_1, x_2, \ldots, x_n\}$
- Set of artificial neural network hidden layers: $L = \{l_1, l_2, \ldots, l_k\}$
- Set of neurons for each j-th hidden layer: $P^j = \{p_1, p_2, \ldots, p_r\}$
- Set of neural network outputs: $Y = \{y_1, y_2, \ldots, y_m\}$
- Weights for each input of i-th neuron of j-th layer: $W_i{}^j = \{w_{i1}, w_{i2}, \ldots, w_{in}, w_{in}\}$
- Bias for each i-th neuron of j-th layer: $b_i{}^j$
- Input analysis function for each i-th neuron of j-th layer: $s_i{}^j = FA(W_i{}^j * X) + b_i{}^j$
- Transfer function for all neurons of j-th layer: $FT^j(s^j)$

Genetic algorithm was regarded as a convenient mean of finding solutions. However, neural networks are more likely to discover the learning errors by matching the input data with the needed output data.

Genetic algorithm for task solution may be described with following steps.

- 1 step: Initialize random set of possible solutions: $S^{(0)} = \left\{ s_1^{(0)}, s_2^{(0)}, \ldots, s_{s_{\max}}^{(0)} \right\}$;
- 2 step: Evaluate each solution with a target function: $V^S = \{F(s_1), F(s_2), \ldots, F(s_p)\}$;
- 3 step: Arrange solutions by evaluation: $\bar{S} = \left\{ \bar{s}_1, \bar{s}_2, \ldots, \bar{s}_p \right\}, \quad F(\bar{s}_1) = opt(V^S)$;
- 4 step: Duplicate best solutions in elite set: $S_E \subset \bar{S}$;
- 5 step: Selection. According to defined selection algorithm select from the set of solutions pairs: $S_C \subset \bar{S}$;
- 6 step: Crossover: According to defined crossover algorithm generate new population from the set of solution pairs:

$$\bar{s}_i \Pi \bar{s}_j \rightarrow s_i' = s_{ij}; s_j' = s_{ji}, \quad i, j = \overline{1, p};$$

- 7 step: Mutation: Random change of one of solution parameter that help to find global optimum of the function:

$$x_j^{s_i'} = x_j^{s_i'} + 1, \quad s_i' \in S', \quad j = rand(\overline{1, k}), \quad i = rand(\overline{1, p});$$

- 8 step: Evaluate new population using target function:

$$V^{S'} = \left\{ F(s_1'), F(s_2'), \ldots, F(s_p') \right\};$$

- 9 step: Arrange new population by the evaluation values:

$$\bar{S}' = \left\{ \bar{s}_1', \bar{s}_2', \ldots, \bar{s}_p' \right\}, \quad F(\bar{s}_1') = opt(V^{S'});$$

- 10 step: Add new population of solution to elite set: $S = (S_E + \bar{S}')$;
- 11 step: Delete last solutions from the population S if its size exceeds predefined population size p: $S = S / \left\{ s_{p+1}, s_{p+2}, \ldots \right\}$;
- 12 step: Algorithm stops by time, generation, convergence or by another predefined criteria. If stop criteria is false then repeat the algorithm from step 4. If true then the result of algorithm is solution s_1.

But fuzzy logic system is method allowing to include infinite amount of levels of truth between full truth and full lies (in binary logic – between the limits of 1 and 0) using also linguistics in the traditional discreet logic that supports the gradation of only truth and lies.

The mathematical model of fuzzy logic is following:

- Each fuzzy variable x consists of a set of n fuzzy values fv: $x = \{fv_1^x, fv_2^x, \ldots, fv_n^x\}$
- Each fv_j is represented by a membership function mf: $fv_j = mf_j(x)$, where $mf \in [0, 1]$

The set of rules are defined for the fuzzy logic, according to Mamdani model or Takagi-Sugeno model. Mamdani model is working with fuzzy variables only: $R_i : IF\ x\ is\ fv_j^x\ then\ y\ is\ fv_k^y$.

For the control of UAV authors propose to use Takagi-Sugeno model, which is using fuzzy conditional part and functional result part. $R_i : IF\ x\ is\ fv_j^x\ then\ y_j = a_j x + b_j$, where a_j – a consequent parameter vector, b_j – scalar offset.

The output y is computed as the weighted average of the individual rules' R_i contributions: $y = \sum_{j=1}^{n} mf_j(x) y_j / \sum_{j=1}^{n} mf_j(x)$.

Within the AI, there are hybrid systems that are the combination of fuzzy logic and other notable systems. They are used to increase the needed result. The most essential hybrid systems are the following [1]:

Fuzzy-neural network hybrid systems. Such system can accurately fulfil the disadvantages of the other as neural networks are able to learn but fuzzy logic – to analyze and foresee in advantage (Fig. 1). This combination can be used easily on a wider scale.

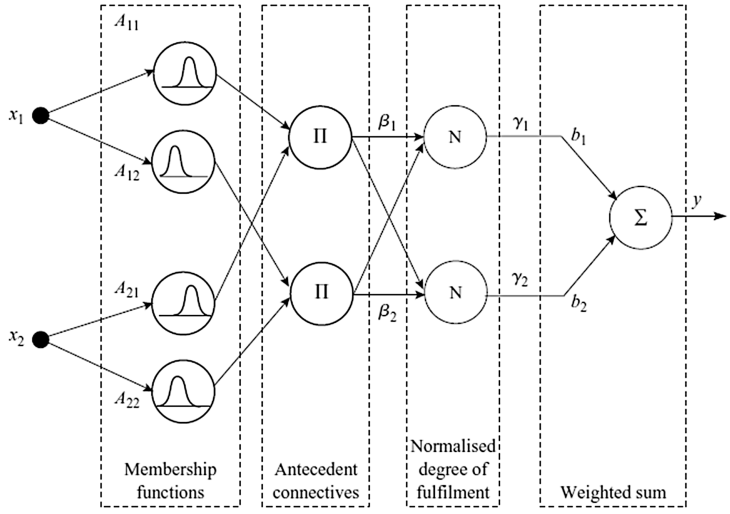

Fig. 1. Example of Takagi-Sugeno model as a neuro-fuzzy network

Fuzzy-genetic algorithm hybrid systems. Such system is able to be useful not only on an academic level due to presence of genetic algorithms, but also on a commercial level as it can regulate and improve the function of affiliation degree, and well regulated

structure of genetic algorithm and FL can search for unknown information and find adequate solutions to the issues.

Fuzzy-PID controller hybrid systems. In several usage ways, such combination works as a hybrid controller where PID controller is used for approximate but fast control while the part of FL systems create or give a task to use other parameters for a better output result [1].

Table 1. Necessity of merging.

Parameter	Fuzzy logic	Neural networks
Output data is needed to create a system	Minimal	Important
Expert knowledge is needed to create a system	Important	Minimal

Unfortunately, the AI group mentioned before in its normal form can be used only in specific situations. In real conditions it is safer to use hybrid systems – systems that are able to learn combined with expert systems.

As depicted in the table, the included logic parameters presented in the Table 1, hybrid systems serve as each others backup and are capable to provide greater control by determining the necessary borders of the inner system values.

2.2 Mathematical Model of the UAV with AI Device

In neural network, analysis and the following trainings are based on pattern recognition. There are plenty of previous researches about pattern recognition that serve as a theoretical basis in this case as well. But it is more important to train neural network to recognize an object or even more – to recognize situation, so UAV could recognize type of object, if this observed object is in the list of addition investigational, it should understand the situation and activity of observed object. At this stage of research network output classification could be divided easily in three results – neutral, warning and dangerous.

In first case there are objects that are standing still like trees or houses. In warning case there are moving objects without markers emblematize any kind of aggression – different transports, people or animals. Also if UAV are working close to any potentially dangerous environment like buildings under construction or power plants it should be taken into account.

In last case, dangerous situations must be recognized, for example, when another object is going to attack AI vehicle, or if UAV performs a guarding function, it should detect dangerous events or accidents and react to them. It is important to remember that the warning category elements should be watched, because they can quickly turn into dangerous.

As seen in Fig. 2 some forms of usage are placed in this diagram. Most important is that analyzing field is linked with traffic and safety. It is necessary to fulfill UAV tasks to improve traffic and safety reasoning. Unmanned aerial vehicles (UAV) plays the most significant role in the improved anti-collision system. It provides the functionality

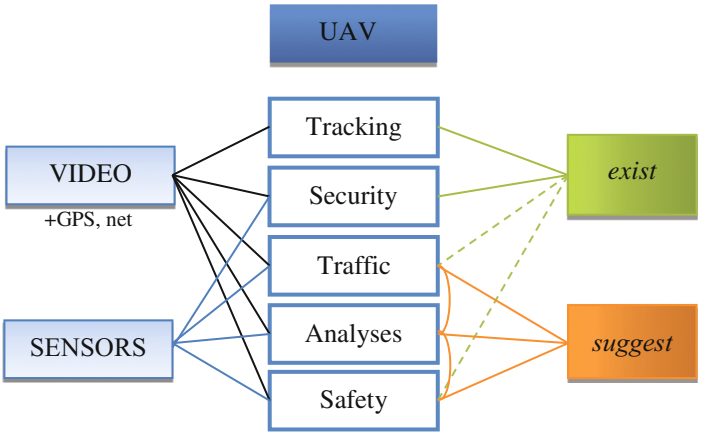

Fig. 2. Structure diagram of UAV usage. From left, the diagram is divided in "classical" usage of quadcopters – for video registration, with GPS and some of network communications included, and sensors that are not used so widely. From right, it is divided in existing usage forms and suggested, with dotted line partly used fields.

of the mobile coordinator for the locations with high probability of collision or in the complicated traffic situations such as congestions.

The quadcopter is the electric vehicle powered by the autonomous power source – accumulator battery.

The structure of the quadcopter equipped with the AI control device is presented in Fig. 3. It contains: four brushless electric motors with high rotation speed, four propellers, flight controller, which controls motion of the quadcopter in horizontal plane – pitch, roll and yaw and vertical movement, electronic speed controller to control speed of motors, accelerometer and gyroscopic sensors to get acceleration and rotation speed in 3 dimensions, GPS receiver for satellite navigation data such as latitude, longitude, altitude, course, speed, bearing, time etc., camera, which provides visual surveillance data, wireless (RF) data transmitter/receiver to communicate with other transport system objects.

The proposed AI algorithms should be used in additional high level controller (highlighted in red), preferably of multi-core based to be able to process all incoming data and ensure the control of the UAV for autonomous flight and goal achievement.

The proposed mathematical model of the quadcopter is based on the study of various models [2–10].

The quadcopter is moving relatively to the stationary inertial reference system associated to the Earth and to the defined orthogonal coordinate axes Ox, Oy, and Oz. Axis Oz directed contrary to the gravity vector.

The coordinate system associated to the quadcopter, has the centre O, which located in the centre of mass of the quadcopter, but the axes OxB, OyB, OzB are parallel and co-directed to the rigid system axes.

The angular position of the apparatus charged with three angles: pitch, roll and yaw, which are respectively determined by rotation around the axes.

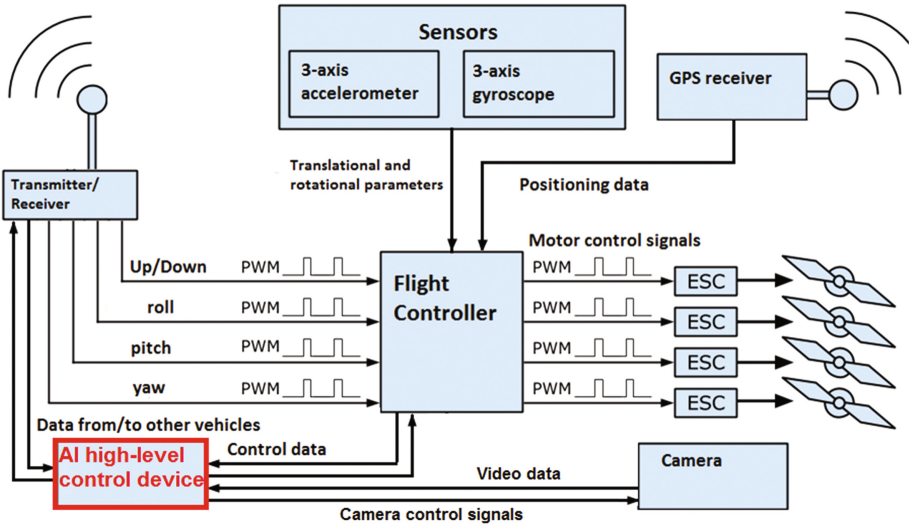

Fig. 3. Main components of quadcopter UAV.

Orientation of the UAV is given as a vector of angles Ω, but the location of the UAV is given as a radius-vector r:

$$\Omega^T = (\varphi, \theta, \psi) \tag{1}$$

$$r^T = (x, y, z) \tag{2}$$

Traction force F_i of each i-th motor is:

$$F_i = b \cdot \omega_i^2 \tag{3}$$

where b – proportional ratio, ω_i – angular velocity of i-th motor.

Vertical acceleration of UAV is:

$$\ddot{r} = g \cdot (0\,0\,1)^T - R \cdot \frac{b}{m} \sum_{i=1}^{4} \omega_i^2 \cdot (0\,0\,1)^T \tag{4}$$

where R – 3 × 3 matrix converting φ, θ, ψ to inertial coordinates using trigonometrical functions, g – gravity constant – 9.81 m/s^2, m – mass of the UAV

Angular acceleration of the UAV is:

$$I\ddot{\Omega} = -\left(\dot{\Omega} \times I\dot{\Omega}\right) - M_G + M \tag{5}$$

where I – inertia matrix, M – rotational torque, M_G – gyroscopic torque

Torques are describes as vectors:

$$M = \begin{pmatrix} Lb\left(\omega_2^2 - \omega_4^2\right) \\ Lb\left(\omega_1^2 - \omega_3^2\right) \\ d\left(\omega_1^2 + \omega_3^2 - \omega_2^2 - \omega_4^2\right) \end{pmatrix} \tag{6}$$

$$M_G = I_R\left(\dot{\Omega} \times (0\,0\,1)^T\right) \cdot (\omega_1 - \omega_2 + \omega_3 - \omega_4) \tag{7}$$

where L – length from the center to the motor, b and d – resistance ratio.

Motion of the UAV is controlled by 4 signals (throttle, roll, pitch and yaw:

$$u^{\tau} = (u_1, u_2, u_3, u_4) \tag{8}$$

where

$$u_1 = d\left(\omega_1^2 + \omega_3^2 + \omega_2^2 + \omega_4^2\right) \tag{9}$$

$$u_2 = d\left(\omega_2^2 - \omega_4^2\right) \tag{10}$$

$$u_3 = d\left(\omega_1^2 - \omega_3^2\right) \tag{11}$$

$$u_1 = d\left(\omega_1^2 + \omega_3^2 - \omega_2^2 - \omega_4^2\right) \tag{12}$$

The equation system of the UAV motion is following

$$\begin{cases} \ddot{x} = -(\cos\varphi\ \sin\theta\ \cos\psi + \sin\varphi\ \sin\psi) \cdot u_1/m \\ \ddot{y} = -(\cos\varphi\ \sin\theta\ \sin\psi + \sin\varphi\ \cos\psi) \cdot u_1/m \\ \ddot{z} = g - (\cos\varphi\ \cos\theta) \cdot u_1/m \\ \ddot{\varphi} = \frac{\dot{\theta}\dot{\psi}\left(I_y - I_z\right) - I_R\dot{\theta}g(u) + L \cdot u_2}{I_x} \\ \ddot{\theta} = \frac{\dot{\varphi}\dot{\psi}(I_z - I_x) - I_R\dot{\varphi}g(u) + L \cdot u_3}{I_y} \\ \ddot{\psi} = \frac{\dot{\varphi}\theta\left(I_x - I_y\right) + u_4}{I_z} \end{cases} \tag{13}$$

Each new or improved function and its mainframe is expressed with multi-objective function (14) that shows what should be taken into account to use quadcopter and swarms as efficiently as possible:

$$F_p^i = \begin{cases} E_i = \int_{n_1}^{n_i} UIdt \rightarrow min \\ T_i = f(E_i, P) \rightarrow max \\ z_i \rightarrow Z_d \end{cases} \tag{14}$$

F_p^i belongs to formation potential of swarm [11]; E_i - consumed electrical energy by UAV, which have to be minimized; T_i - working duration of the UAV; P - set of parameters having influencing on the duration and performance [12]; z_i – distance from current quadcopter to another and Z_d – desired distance between quadcopters in swarm to ensure most optimal communication between team members but cover the broader area without losing communication [11].

3 Future Opportunities

Based on previous researches done in this field, additional options for UAV control system can be stated that could be practically used during the continued research in various, previously covered fields responsible for safety of people, traffic organization and would be able to decide independently or at least to give advices on how to improve the situation, these advices would stay as responsibility and competence for the ground pilot to be accepted or denied.

3.1 Requirements and Usage of the Systems

UAV systems that are able to analyze the surrounding events, know their GPS location, position towards a prospectively horizontal surface, their inner parameters and other widely analyzed information, must use the advantages of AI in a wider usage by analyzing the acquired data from sensors, cameras, and to connect those with information known beforehand.

One of the most important usage of such UAV system could be fire detection and localization. Previously it was organized via certain mission plans [13]. But it would be more progressive to let quadcopter do its routing patrol tasks without obligation to follow its mission plan.

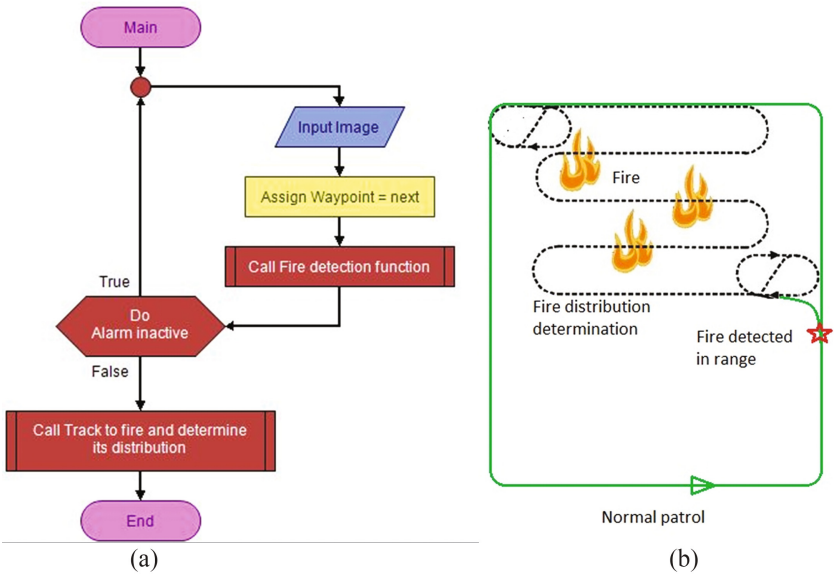

Fig. 4. Algorithm of fire detection by UAV (a) and application of UAV flight plan (b) over its patrolling area

Figure 4a presents process of UAV patrolling. It could be already prepared patrol flight according to flight plan or patrol plan prepared by vehicle placed in new and unknown territory. Input image is combination of visual image and data from sensors. Waypoint is following flight plan as mentioned before, and each time fire detection function is called. If in this case alarm state is still inactive, UAV can start work with next sector. If alarm state is activated by visual, infrared or other data, next function is called out that change flight plan according to location of fire.

In Fig. 4b outer line over perimeter presents optional flight plan, and it would be like parallelogram until something special would be found. In this example, drone could patrol over wood when suddenly noticing fire in its range. So it would decide to change its normal patrol routine and start to patrol in shorter sections to understand the extent of fire damage and give precise information to the supervising institutions.

Many authors have started to work with swarms in case when one or two drones are not enough to do all the tasks at the same time.

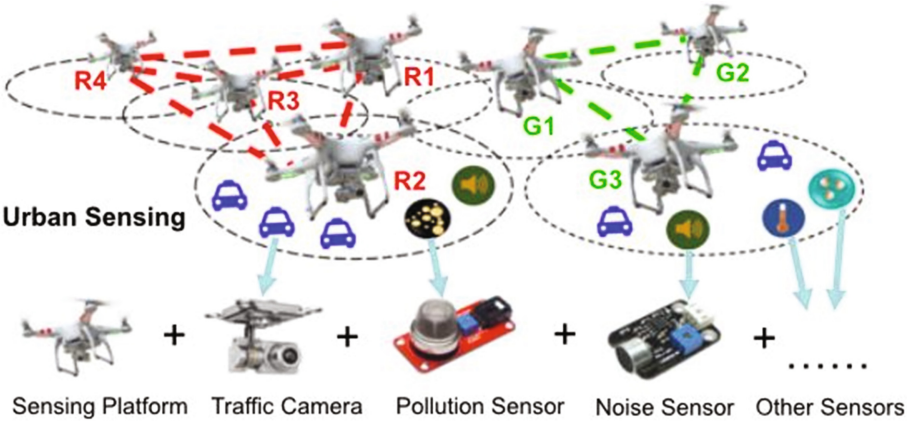

Fig. 5. Urban sensing in transportation using drone swarms [11]

Figure 5 is describing situation when swarm is working on high intension traffic. For one UAV it could take too high power consumption to use all sensors on its platform, but dividing them in groups where each of them is working on its own kind of sensors, would expand their working area together with collected information. Of course, communication should be in very high level to let these swarms to work as a united team.

3.2 Detections According to Input Data and Act Recognition

To work with act recognitions, additional option for image recognitions, AI systems as mentioned in this paper should be used. A significant research has been done in the area of act recognition technology that has given a chance to control a drone or even a whole swarm by using act recognition. [14]. For example, UAV could recognize an attacker with an weapon that is preparing to shoot. Firearms have specific characteristic

technical outlines that can be thought to recognize easier than to recognize gestures or facial expressions. However, this option would be more useful as combined with specific sensors – light and sound sensors to record the shot of a gun, gas sensor, that would catch the trail of gunpowder (this would work only in a close range, of course), as well as the thermo sensor would be the most useful of all mentioned, to recognize the potential threat in the infrared spectrum.

Effectively AI could be used and trained on visual and audial input data like images and video while other sensors mostly serve as binary inputs. Convolutional neural networks may be used for this task. In this contribution lets discuss on recognition according to visual data, and what more – based on RGB (red, green, blue) spectrum. Middle colors like yellow and pink are the easiest to extract. Simplify, each point from image is divided into three main colors and saved as binary image with info only about one color (15).

$$\left(I_b^R, I_b^G, I_b^B\right) \tag{15}$$

That will be combined back into single binary image I_b [14]. In case when certain color is searched initially it is necessary to understand in what proportions it divides. In Fig. 5 it is reasonable to search for green, yellow and orange. If first color will be almost clear, then both other are mix from blue and red and depends from intensity of each. These colors will be searched also to recognize fire.

Problem with fire recognition comes from its unstable color and form. To deal with that it is necessary to prepare Potential fire mask (PFM) [15] that consists from five feature vectors for each pixel (16):

$$PFM = \begin{cases} X^1 \in [R, G, B] \\ X^2 \in [R, G] \\ X^3 \in [R, B] \\ X^4 \in [G, B] \\ X^5 \in [R - G, G - B, R + g + b] \end{cases} \tag{16}$$

Then statistical features of color will be reached and potential of fire presence will be initialized. In order to achieve better results it is recommended to use infrared spectrum with thermal scale and compare it with RGB results [16].

4 Conclusions

The recently most researched UAV possibilities were determined and scenario of further action were offered.

Quadcopter is a good base for further researches as well as its easy construction on modern materials.

Swarm organization is an advancing UAV tendency because in the same way each element communicates with its neighbor or with the team leader device, in the same way they could be used to transfer big amount of information without overloading their signal capacities.

Quadcopter swarms and every single UAV could be used in broad fields, for example delivery, patrolling, safety. They could serve as traffic safety inspectors and even if human actions are taking place. Thanks to artificial intelligence progress, unmanned aerial vehicle accelerate in their applications without human pilot presence and lets them work in places what could be impossible to reach by human because of time consumption or in case of dangerous and aggressive environment.

The described opportunities of unmanned aerial vehicles and their possible tendencies of development will be used as guideline for further research.

Acknowledgements. The research leading to these results has received funding in a frame of Competence Centre of Latvian Electrical and Optical Devices in Industry project No. 1.2.1.1/16/A/00, subproject AERONES.

References

1. Munakata, T.: Fundamentals of the New Artificial Intelligence, vol. 1. Springer, London (2008)
2. Gurianov A.E.: Quadcopter control simulation. Electronic Scientific Journal: Engineering Journal of Don. Bauman Moscow State Technical University (2014). (in Russian)
3. Dikmen I.C., Arisoy A., Temeltas H.: Attitude control of a quadrotor. In: 4th International Conference on Recent Advances in Space Technologies, pp. 722–727 (2009)
4. Luukkonen, T.: Modelling and Control of Quadcopter. School of Science, Espoo, p. 26 (2011)
5. Zhao, W., Go, T.H.: Quadcopter formation flight control combining MPC and robust feedback linearization. J. Franklin Inst. **351**(3), 1335–1355 (2014)
6. Bouadi, H., Tadjine, M.: Nonlinear observer design and sliding mode control of four rotors helicopter. World Acad. Sci. Eng. Technol. **25**, 225–229 (2007)
7. Madani, T., Benallegue, A.: Backstepping control for a quadrotor helicopter. In: IEEE/RSJ International Conference on Intelligent Robots and Systems, pp. 3255–3260 (2006)
8. Murray, R.M., Li, Z., Sastry, S.S.: A Mathematical Introduction to Robotic Manipulation, p. 474. SRC Press (1994)
9. Alderete, T.S.: Simulator Aero Model Implementation, p. 21. NASA Ames Research Center Moffett Field, California (2014)
10. Beard, R.W.: Quadrotor Dynamics and Control, p. 47. Brigham Young University, Provo (2008)
11. Wu, D., et al.: ADDSEN: adaptive data processing and dissemination for drone swarms in urban sensing. IEEE Trans. Comput. **66**(2), 183–198 (2017)
12. Strupka, G., Levchenkov, A., Gorobetz, M.: Algorithm for optimal energy consumption of UAV in maritime anti-collision tasks. In: 56th International Scientific Conference on Power and Electrical Engineering of Riga Technical University (RTUCON) (2015)
13. Santamaria, E., Royo, P., Lopez, L., Barrado, C., Pastor, E., Prats, X.: Increasing UAV capabilities through autopilot and flight plan abstraction. In: 2007 IEEE/AIAA 26th Digital Avionics Systems Conference, Dallas, TX (2007)
14. Nagi, J., Giusti, A., Gambardella, L.M., Di Caro, G.A.: Human-swarm interaction using spatial gestures. In: 2014 IEEE/RSJ International Conference on Intelligent Robots and Systems, Chicago, IL (2014)

15. Duong, H.D., Tinh, D.T.: An efficienty method for vision-based fire detection using SVM classification. In: 2013 International Conference on Soft Computing and Pattern Recognition (SoCPaR), Hanoi (2013)
16. Giitsidis, T., Karakasis, E.G., Gasteratos, A., Sirakoulis, G.C.: Human and fire detection from high altitude UAV images. In: 2015 23rd Euromicro International Conference on Parallel, Distributed, and Network-Based Processing, Turku (2015)

Connected and Automated Vehicle Simulation to Enhance Vehicle Message Delivery

Daniel Barber[1(✉)] and Andrew Best[2]

[1] University of Central Florida Institute for Simulation and Training, Orlando, FL 32826, USA
dbarber@ist.ucf.edu
[2] Univeristy of North Carolina at Chapel Hill, Chapel Hill, NC 27514, USA
best@cs.unc.edu

Abstract. Increased vehicle safety is a driving force in the development of Connected Vehicle (CV) and Automated Vehicle (AV) technologies. Unlike traditional in-vehicle safety features, CV and AV technologies help avoid catastrophes all together with advanced warnings of impending danger and beyond human reaction times. Although extensive efforts are underway in the creation of CV and AV technologies, it is still unclear what the best methods are for alerting drivers to the new information they generate. For example, how should an AV keep passengers informed of where it is going and what corrective actions (e.g. lane changes) it plans to take, and how do we design these systems to engender passenger trust. This paper presents a multi-phased approach to address these issues through simulation for future evaluation and development of multimodal vehicle displays for ease of use and increased safety

Keywords: Human factors · Human-systems integration · Automated vehicles · Driverless cars

1 Introduction

Increased vehicle safety is a driving force in the development of automated vehicle (AV) and connected vehicle (CV) technologies. As U.S Transportation Secretary Anthony Fox stated in a public address at the beginning of 2014, "Vehicle-to-vehicle (V2V) technology represents the next generation of auto safety improvements, building on the life-saving achievements we've already seen with safety belts and air bags," [1]. Unlike safety belts and air bags designed to protect motor vehicle occupants in the event of an accident, CVs avoid catastrophes all together with early warnings about impending danger. While drivers cannot avoid or foresee every possible situation while commuting in a motor vehicle, CVs have the potential to prevent many of the common accidents that occur through improved situation awareness. Accidents that occur from situations such as vehicle following, lane changing or passing, turning through intersections while crossing oncoming traffic, or running red lights and stops signs will no longer jeopardize the safety of fellow motor vehicles on the road. Moreover, AV technologies will take safety further than CV systems, with estimated annual savings of

D.N. Cassenti (ed.), *Advances in Human Factors in Simulation and Modeling*,
Advances in Intelligent Systems and Computing 591, DOI 10.1007/978-3-319-60591-3_4

$1.3 trillion according to Morgan Stanley reports on the economic benefits of driverless cars, with estimated savings of $507 billion due to reductions in accident costs, [2].

The National Highway Traffic Safety Administration released a report in 2014 on the readiness for vehicle to vehicle (V2V) communication that thoroughly describes the need for CVs, the economic impact they will have, and most importantly, the amount of lives they will save [3]. Currently, dedicated short-range communications (DSRC) is a focus for CV success with the latency, accuracy, and reliability needed for V2V communication. At the University of Michigan's Transportation Research Institute (UMTRI), projects such as the Multipath SPAT Broadcast and IntelliDrive are dedicated to improving CV communication [4], but more work is needed regarding the interaction component with the driver. Meaning, although the CVs will provide warnings for potential danger, less is known on how those warnings should be displayed, how often they should be initiated, and if they should change depending on the driving conditions (e.g. night driving, storms).

With V2V and vehicle to infrastructure (V2I) technologies increasing the volume of data available, it is critical that the method in which the vehicle delivers information does not overload drivers. An abundance of research has shown that increased volume and complexity of information results in adverse impacts on decision making performance [5–8] and threatens the benefits of in-vehicle support systems [9–11]. Moreover, older drivers are a growing segment of the population, and it is well known that cognitive and physiological capabilities diminish with age [12]. However, there is a lack of fundamental research on how age may affect acceptance and understanding of AV and CV messages.

It is therefore clear that efforts are needed regarding the interaction component between the automated or connected vehicle and driver. Meaning, although future vehicles will provide warnings for potential danger, less is known on how those warnings should be displayed, how often they should be initiated, if they should change depending on the driving conditions (e.g. night driving, storms), and how age impacts ability of drivers to perceive and acknowledge messages.

The primary objective for this effort was to investigate multimodal AV and CV displays to enable future vehicles to safely and quickly alert drivers of upcoming hazards and automation intent. As part of a multi-phased approach, the research team identified a need for a portable simulation test bed capable of emulating the automated or connected vehicle driving experience. This paper captures the process for identifying requirements for this simulation testbed from literature and project stakeholders and describes the resulting platform and capabilities.

2 Vehicle Messaging Research

Overall, a review of the literature revealed few studies investigating AV passenger interactions. However, a number of CV studies were found that incorporate a variety of different messages, with in-vehicle alerts ranging from email and text to intersection violation warnings (e.g. vehicle running stop sign). The National Highway Traffic Safety Administration (NHTSA) has identified several new messages CVs could make

available including Intersection Movement Assist, Left Turn Assist, Emergency Electronic Brake Light, Forward Collision Warning, Blind Spot Warning/Lane Change Warning, and Do-Not-Pass Warning [13]. Of all identified messages, Forward Collision Warnings (FCW) were the most commonly studied. Within this topic area, researchers studied effects on driver behavior, a driver's engagement in a secondary task, and older and younger drivers' responses to FCW systems.

Koustanai [14] believed that drivers could more effectively use and develop trust in a FCW system with proper training and exposure. To test these hypotheses, their team executed a simulation-based study consisting of 28 participants in which some participants received hands on training with the FCW systems, some participants only read the FCW manual, and the remaining participants had no familiarity with the system. The results showed that drivers with hands on training had no collisions, better reactions in most situations, and reported increased trust [14].

Muhrer et al. [15] conducted a laboratory study regarding driving and gaze behavior while using a FCW and FCW+ (FCW with autonomous braking) system while performing a secondary task. A total of 30 participants ranging in age from 30–40 years old received training on how to use the FCW+ system. The Surrogate Reference Task (SuRT), [16], acted as the secondary task and was used to examine visual attention allocation. Drivers were told to only perform the secondary task when they felt safe to do so. In this experiment, a substantial number of accidents occurred in critical situations without FCW+, but no accidents occurred in critical situations during the use of FCW+. Researchers also discovered that driving with the FCW system did not lead to more engagement in the secondary task. Therefore, a FCW or a FCW + system could help reduce countless vehicle accidents and not cause driver distractions.

A study conducted by Cotte et al. [17] was one of a few studies that researched the impact of automated technologies on elderly drivers. Researchers had 62 participants ranging in age from 30–40 and 65 to 81 years old. Using a driving simulator, participants were instructed to drive 50 MPH with a focus on avoiding collisions. Participants were told that the warning system was not always accurate, and auditory warnings were delivered if they drove too fast, too slow, or were ask risk of a forward collision. If drivers drove too fast or too slow a female's voice reminded them to drive at least 50 MPH. If drivers drove over 57 MPH a police siren went off. The collision warning was a male voice that said, "Brake, brake, brake, brake." The results of the study determined that overall there were no differences between age groups. Researchers did however notice a significant effect when comparing drivers who did and did not receive the warnings. Drivers that received the warning drove much slower than drivers that did not.

In general, a common theme across all studies reviewed was to test different modalities for message delivery. Three modalities are available to alert drivers of safety issues – auditory, visual, and tactile. The review presented determined there is no specific research that shows whether one modality (or combination thereof) is more effective in preventing an accident, nor is the implementation format within a modality consistent. Cotte et al. [17] is an example of this finding, where they employed both voiced auditory messages (e.g. "slow down") and cues (e.g. police siren). Furthermore,

trust is a common concern reported by both researchers and drivers. For example, researchers have tried increasing the level of trust in AV technologies by either giving drivers prior training with the technology [14] or allowing drivers to use technology that shares in their driving goals. An example study testing shared driving goals was Verberne et al. [18], where different Adaptive Cruise Control (ACC) either matched the drivers goals (i.e. energy efficiency, comfort, speed, and safety) or did not, and how that description affected trust. Overall, researchers have conducted numerous studies over the last ten to fifteen years to answer many questions regarding AV technologies; however, with a large focus in recent years on ACC and FCW, there is still a significant amount of research yet to be done to support more recently identified AV messages such as [Intersection Movement Assist, Left Turn Assist, Emergency Electronic Brake Light, Forward Collision Warning, Blind Spot Warning/Lane Change Warning, and Do-Not-Pass Warning].

Within recent studies, a significant lack of research involving older adults was revealed. The majority of the studies conducted with CVs had a maximum participant age range of approximately fifty years old. There is insufficient research to determine how older drivers would perceive or react to AV or CV messages. Therefore, in addition to growing research on different types of messages, much of the research conducted with AV technology should be expanded to elderly drivers. This factor is particularly needed since research shows that research with collision warnings are more likely to benefit older drivers because it helps them compensate for age-related sensory and cognitive changes [17].

Beyond age related research, an area that requires significant focus is modality. Many researchers conducted studies primarily with audio messages (either spoken messages or auditory cues); however, audio messages may be ineffective if there is a lot of noise in the vehicle or if the driver is driving with their windows down [19]. Continued research is needed to determine which of the three modalities would be best suited to alert drivers of a variety of safety messages. For example, do drivers respond better to an audio message versus a tactile message, or both? Perhaps, depending on the urgency of the safety messages, drivers should receive all three modality alerts.

In addition to researching effects of older drivers and modalities, most research focused primarily on FCW, lateral drift, and lane change/merge crash warnings. Basic research is lacking for a number of potentially useful safety applications [20, 21]. Research to date has not focused on alerts for impending/future events including emergency vehicles, wrong way driving, intersection movement assist, and intersection violation warning, especially across different age groups. Moreover, with inclusion of more AV warnings and messages, designers must be cognizant of overloading drivers and passengers, as an abundance of research demonstrates the adverse impacts on decision making performance [5, 6, 22, 23] and loss of benefits from in-vehicle support systems [9–11]. Table 1 below lists automated and connected vehicle messages most likely to benefit from additional research as described, with each safety warning having the potential to significantly impact the number of vehicle accidents and fatalities that occur every year. These messages in addition to those previously investigated must be supported in any AV/CV simulation developed.

Table 1. Automated and connected vehicle messages for future research.

Message	Description
Curve speed warning	Alerts driver to slow down for upcoming turn or changes in road
Intersection movement assist	Alerts driver that it is unsafe to enter the intersection due to conflicting traffic
Intersection violation warning	Alerts driver they are about to commit a violation at an intersection
Pedestrian/bicyclist presence	Alerts driver to a pedestrian or bicyclist presence
Wrong-way driving	Alert driver that someone is driving the wrong-way down a road/coming right at them

3 CV and AV Simulation Development

Upon review of the literature and several meetings with project stakeholders, the team employed an iterative development cycle for development of the simulation software. This cycle including storyboarding of sample scenario events and options for message delivery, to animated 3D video of the storyboard, and eventually software requirements and specifications for implementation. Following this process enabled stakeholders to rapidly review and evaluate testbed capabilities and potential messages quickly.

As an example of this process, the initial storyboard and animated video demonstrated the ability to emulate a driverless car navigating through a commercial downtown district. Within the scenario, the vehicle takes a route through a downtown area, taking several left and right turns at intersections, moving towards a highway onramp, changes lanes, and finally enters the freeway. During execution, the vehicle obeys traffic laws such as maintaining safe distances to traffic, stopping at red lights, and waiting for gaps in traffic when making left and right turns onto connecting roadways. Finally, to highlight how a driverless car would handle an "off-normal" event, the 3D scenario triggered an SUV backing up at the tollbooth for the highway onramp, forcing the driverless car to respond accordingly by stopping before the SUV collided, Fig. 1.

Upon conclusion of multiple scenario revisions, final requirements for the testbed software were determined. It was decided that a custom simulation platform was needed to appropriately capture the types of events and visualizations that existing commercial-off-the-shelf (COTS) driving simulators did not support. Moreover, no existing COTS driving simulation supported switching between manual or driverless modes, as required for the effort. The result simulation platform was developed using the Unreal Game Engine, [24], as it provided a modern development environment for rapid level/scenario creation and flexibility for integrating with 3rd party software applications.

The simulator was designed with the intention of rapid scenario design. Extensible road networks can be constructed from simple building blocks and researchers can construct novel scenarios with ease. The autonomous vehicle was designed for varying levels of communication and with differing safety profiles for investigation of trust in the future.

Fig. 1. SUV reversing at tollbooth, forcing driverless car to react in 3D storyboard simulation.

In addition to simulating autonomous or manually driven vehicles, the testbed required multiple modes of communication with end-users. Therefore, the team identified needs for both a re-configurable dashboard display and an interactive center console, similar to those seen in high-end luxury cars. Furthermore, to support a variety of future experiments, the displays needed to include navigation options, web-browsing/internet, multimedia, multi-touch and voice-controlled interactions. To support this capability, the team modified an existing multimodal interface developed for squad-level human-robot teaming. Described in Barber et al. [25], the multimodal interface includes speech-to-text, simulated radio/voice communications, interactive maps, video, and scripted events. The scripting capabilities include the ability to trigger playing of multimedia (e.g. video), sounds, or modifications to navigation map iconography using time or location-based events. Using these combined features, researchers are able to implement a variety of visual and auditory messages to end-users participating in studies, with information presented on both virtual dashboard and center console displays.

As described in the review of the literature, there is a significant lack of research into how different age populations respond to automated and connected vehicle messages. Usually performed at fixed locations such as a university, many driving simulation studies typically result in a larger percentage of participants in the age range of 18–24. To support low cost and simple transport to locations with populations of interest, the physical platform for the simulation used a commercial-off-the-shelf car gaming cabinet. The gaming cabinet supported disassembly into two smaller pieces and easily fits within a standard door frame. The fully assembled platform, shown Fig. 2,

includes a physical steering wheel supporting manual driving scenarios. Furthermore, when simulating an autonomous vehicle the testbed supports automatic turning of the physical steering wheel, providing additional indicators to passengers of vehicle intent (e.g. turning right).

Fig. 2. Final simulation testbed. Top left: A side view of the complete simulator system. Right: The complete interactive dashboard console display showing the routing and media player panes. Bottom-left: A view from the main screen of the simulator as vehicle navigates environment. The dashboard iconography emulates (with permission) that of the Tesla Model S.

4 Conclusion

In summary, while AV research has advanced significantly over the last ten years, there are still many unanswered questions and gaps in the research. It is apparent that efforts are needed to evaluate best practices for delivery of this information. During the last 15 years, a rapid expansion in the use of robotics for military applications resulted in vendors creating different interfaces for control of each platform. This led to different training requirements for use of each robot, single-use instrumentation and control devices, and increased costs. Addressing this and other interoperability challenges lead to the creation of new standards to ease access, training, and integration of aerial and ground vehicles such as the Joint Architecture for Unmanned Systems (JAUS), [26, 27]. In order to prevent similarly disparate methods of AV signaling across manufacturers and vehicle types, research must be conducted to identify best practices

and guidelines that meet safety requirements for all drivers across age groups. Future efforts should close these research gaps, conducting studies on key questions not yet addressed including the effect AV technology has on older drivers and the importance of communicating safety messages to drivers and the best modality/modalities to be used for that purpose. The simulation testbed described here outlines a capability for rapid development of different driving scenarios and generation of novel messages multimodally to support answering these questions.

References

1. Naylor, N.: National Highway Traffic Safety Administration. 3 Feb 2014. http://www.nhtsa.gov/About+NHTSA/Press+Releases/2014/USDOT+to+Move+Forward+with+Vehicle-to-Vehicle+Communication+Technology+for+Light+Vehicles. Accessed 06 Jan 2016
2. Morgan Stanley. Autonomous Cars: The Future is Now. 23 January 2015 http://www.morganstanley.com/articles/autonomous-cars-the-future-is-now. Accessed 24 Feb 2016
3. National highway traffic safety administration. In: Prelimnary Statement of Policy Concerning Automated Vehicles. United States Department of Transportation, Washington (2014)
4. Robinson, R., Dion, F.: Multipath SPAT Broadcast Project. Michigan Department of Transportation, Lansing (2013)
5. Iselin, E.R.: The effects of information load and information diversity on decision quality in structured decision task. Acounting Organ. Soc. **13**(2), 147–164 (1998)
6. Miller, G.A.: The magic number of seven, plus or minus two: some limits on our capacity for processing information. Psychol. Rev. **63**, 81–97 (1956)
7. Streufert, S.C.: Complexity and complex decision making: convergences between differentiation and integration approaches to the prediction of task performance. J. Exp. Soc. Psychol. **6**(4), 494–509 (1970)
8. Streufert, S.C.: Effects of information relevance on decision making in complex environments. Mem. Cogn. **1**(3), 224–228 (1973)
9. Carsten, O., Nilsson, L.: Safety assessment of driver assistance systems. Eur. J. Transp. Infrastruct. Res. **1**, 225–243 (2001)
10. ECMT. Statement of principles of good practice concerning the ergonomics and safety of in-vehicle information systems. In: New Information Technologies in the Road Transport Sector: Policy Issues. Ergonomics and Safety (1995)
11. Rumar, K.: The basic driver error: late detection. Ergonomics **3**, 1281–1290 (1990)
12. Rakotonirainy, A., Steinhardt, D.: In-vehicle technology functional requirements for older drivers. In: Proceedings of the First International Conference on Automotive User Interfaces and Interactive Vehicular Applications. Essen, Germany (2009)
13. U.S. Department of Transportation. V2V Communications Fact Sheet. http://www.safercar.gov/staticfiles/safercar/v2v/V2V_Fact_Sheet_101414_v2a.pdf. Accessed 14 Oct 2014
14. Koustanai, A., Delhomme, P., Mas, A.: Simulator training with a forward collision warning system: effects on driver-system interactions and driver trust. Hum. Factors **54**(5), 709–721 (2012)
15. Muhrer, E., Reinprecht, K., Vollrath, M.: Driving with a partially autonomous forward collision warning system: how do drivers react? Hum. Factors **54**(5), 698–708 (2012)
16. Mattes, S.: The lane change task as a tool for driver distraction. Qual. Work Prod. Enterp. Future **2003**, 57–60 (2003)

17. Cotte, N., Meyer, J., Coughlin, J.F.: Older and younger drivers' reliance on collision warning systems. In: Proceedings of the Human Factors and Ergonomics Society 45th Annual Meeting. Minneapolis (2001)
18. Verberne, F.M.F., Ham, J., Midden, C.J.H.: Trust in smart systems: sharing driving goals and giving information to increase trustworthiness and acceptability of smart systems in cars. Hum. Factors **54**(5), 799–810 (2012)
19. Singer, J., Lerner, N., Walrath, J., Gill, M.: Warning and message perception under ambient noise conditions: on-road experiment report under crash warning interface metrics 3 program. US Department of Transportation, Washington (2015)
20. Sayer, J., LeBlanc, D., Bogard, S., Funkhouser, S., Bao, D., Buonarosa, M.L., Blankespoor, A.: Integrated vehicle-based safety systems field operational test final program report. U.S. Department of Transportation National Highway Traffic Safety Administration, Washington D.C. (2011)
21. Fitch, G.M., Bowman, D.S., Llaneras, E.: Using wizard of oz technique to evaluate connected vehicles: distracted driver performance to multiple alerts in a multiple-conflict scenario. In: Proceedings of the Transportation Research Board 93rd, Washington D.C. (2014)
22. Streufert, S.: Complexity and complex decision making: convergences between differentiation and integration approaches to the prediction of task performance. J. Exp. Soc. Psychol. **6**(4), 494–509 (1970)
23. Streufert, S.C.: Effects of information relevance on decision making in complex environments. Mem. Cogn. **1**(3), 224–228 (1973)
24. Epic Games. Unreal Engine Epic Games https://www.unrealengine.com/what-is-unreal-engine-4. Accessed 10 Feb 2017
25. Barber, D., Abich IV, J., Phillips, E., Talone, A., Jentsch, F., Hill, S.: Field assessment of multimodal communication for dismounted human-robot teams. In: The Proceedings of the Human Factors and Ergonomics Society Annual Meeting, Las Angeles, CA (2015)
26. Wikipedia. JAUS https://en.wikipedia.org/wiki/JAUS. Accessed 06 Jan 2015
27. Barber, D., Davis, L., Nicholson, D., Chen, J.Y., Finkelstein, N.: The mixed-initiative experimental testbed for collaborative human robot interactions. In: 26th Army Science Conference, Orlando, FL USA (2008)

Measuring Human Trust Behavior in Human-Machine Teams

Jason M. Bindewald(✉), Christina F. Rusnock, and Michael E. Miller

Air Force Institute of Technology, 2950 Hobson Way,
Wright-Patterson AFB, OH 45433, USA
{Jason.Bindewald, Christina.Rusnock,
Michael.Miller}@afit.edu

Abstract. This paper presents a paradigm for distilling trust behaviors in human-machine teams. The paradigm moves beyond diagnostic alarms-based automation definitions of compliance and reliance toward a view of trust behavior that includes automations where the machine has authority to act on behalf of the human-machine team in the environment. The paradigm first determines the purpose of the automation and then relies on three types of authority within the human-machine team to identify what trust behaviors will look like in specific instances. An example using the *Space Navigator* environment demonstrates how trust behaviors can be measured.

Keywords: Trust · Human-machine teaming · Measuring trust

1 Introduction

Influencing trust is not an end goal for automation designers, but a means to another end. Affecting trust is useful to influence human behavior and thereby performance of the combined human-machine team. As trust impacts user adoption of technology [1], measurement of and response to trust is a useful endeavor. However, since trust is a psychological state, we cannot directly measure it. The effect of trust on human behavior may also be complex, as several other factors—including perceived risk, previous experience, system performance, mental capacity, and workload—influence this behavior is influenced by. Therefore, it is desirable to directly describe and understand behavioral changes, which the human's level of trust affect.

This paper describes a paradigm for understanding how trust-based behaviors manifest in human-machine team interaction, and how objective trust-based measures can be designed based upon this interaction. We address the problem by broadening the concepts of compliance and reliance from the automation alarms literature to the broader class of human-machine teams and propose a definition for reliance that encapsulates all trust-based behaviors. Then we provide a paradigm for describing and understanding how trust behaviors are likely to manifest across different automations in response to various agent design factors. These design factors include the automation's intended purpose, the human-machine team's authority to act on the environment, the human-machine team's authority to override actions, and the human-machine team's authority to correct actions.

D.N. Cassenti (ed.), *Advances in Human Factors in Simulation and Modeling*,
Advances in Intelligent Systems and Computing 591, DOI 10.1007/978-3-319-60591-3_5

This paradigm will be illustrated with examples using the Space Navigator [2] simulated agent environment. This environment provides opportunities to vary all of the previously described design factors to create simulated agents that elicit specific human trust behaviors in human-machine teams.

2 Background

2.1 Trust and Trust Behaviors

Trust is *"the attitude that an agent will help achieve an individual's goals in a situation characterized by uncertainty and vulnerability"* [3]. As trust is an attitude—an abstract concept—trust researchers do not want to advocate for better understanding of trust as an end in itself. Rather, research has gravitated toward understanding how trust influences actions and how outside agents and environments influence human trust.

Since trust is an abstract entity, measuring it can be difficult. Measuring trust typically involves the use of subjective surveys, requiring humans to report their level of trust. However, difficulties exist with this measurement as not all humans can accurately characterize or understand their current trust attitudes or may not be willing to report their true attitude. Additionally, a person's trust in another agent can change over time, and subjective measurements only provide snapshots of this attribute at a prescribed time interval. Therefore, subjective trust measures are not necessarily reliable.

To overcome the problems with subjective trust measurement, many researchers have tried to create objective measures of trust. One form of objective trust measures is to associate trust with different psychophysiological human characteristics, such as electroencephalography (EEG) [4] or galvanic skin response (GSR) [4, 5]. Unfortunately, these measures need to be subsequently calibrated against some subjective measure of trust to ensure they provide a meaningful measure of trust.

A second form of objective trust measurement involves indirect assessment by measuring factors that influence trust or behaviors influenced by trust. This second form of trust measurement does not estimate trust. Instead, it accepts the fact that trust is not the end goal, but rather a means toward influencing some other factor.

Factors influencing trust in human-machine teams include the human's automation experience and propensity to trust [6]; the machine teammate's predictability, anthropomorphism, and performance [7]; and the state of the operational environment [8]. Each of these influences on trust provides easier pathways to objective measurement than does trust itself. The primary reason for measuring trust is that trust influences trust-based behaviors or actions taken by a human. Note that the trust definition above states that the trustor has an inherent understanding of the trustee's ability to achieve goals. Further, the presence of vulnerability implies the trustor will be less likely to relinquish goals in the presence of low trust. Goals are achieved through actions and actions can be measured. Several attempts have been made to measure trust behaviors, ranging from rational decision models [9] to behavioral economics trust games [6].

2.2 Compliance and Reliance

The primary manner in which trust behavior has been measured in human-machine interaction is through the concepts of compliance and reliance [10–12]. Human trust in diagnostic automation systems is often expressed through compliance and reliance. In a basic diagnostic automation, the automation monitors the world looking for a predetermined "signal." When the automation detects the signal it alerts the human or suggests an action to the human, otherwise it continues monitoring without alert. In the alarms literature, compliance is a human behavior expressing trust that a diagnostic automation's alert is correct by acting in response to the alert. Reliance is a human behavior expressing trust that a diagnostic automation's non-alert is correct by not devoting human attentional resources to perform the detection task.

Compliance behavior in diagnostic automation systems is inherently active. Inactivity by a human in response to an alert implies non-compliance and a lack of trust in the automation. Therefore, compliance with an alert, whether a recommended action is given or not, implies that an action is taken by the human in response.

The concept of compliance in diagnostic automation is actually a specific form of reliance. This is illustrated using the timelines in Fig. 1. The first timeline illustrates the implicit assumption of the traditional view of compliance and reliance as two separate behaviors. Reliance is a trust behavior that is performed before an action takes place, while compliance is a behavior performed after the automation has acted or made a recommendation. However, the second timeline, takes into account that the automation may reengage at some point. The beginning and ending non-operational times are easy to discern as before and after, and consequently reliance and compliance. However, the interim period between automation operations is difficult to determine, and becomes more difficult as the interim time between automation operations shortens.

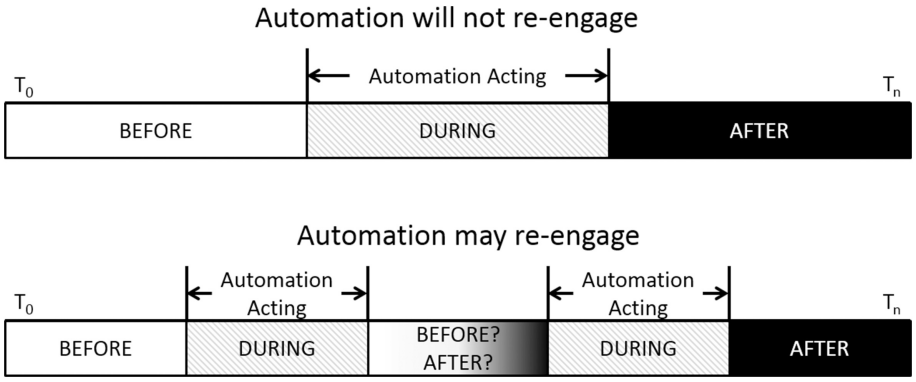

Fig. 1. Two timelines showing recurrence of automation action and its effect on determining whether a non-operational time falls before or after the automation.

As such, we define reliance in human-machine teams as action or inaction demonstrating the human's trust, non-trust, or distrust of the machine. Compliance is a specific form of reliance that only applies for automations that act as recommendation

or diagnose-and-alarm systems: a human deciding to accept the recommendation of an automation and acting in accordance with that recommendation.

It is important to note, as shown in Fig. 2, that trust and reliance cannot be easily decoupled from their antecedents. A host of factors influences the attitude of trust. These factors involve the human, the machine, and the environment in which the h team is acting. Several factors—in addition to trust—influence reliance. Therefore, objective measures of reliance will be difficult to tease out without reducing or eliminating all other influences on the behavior, which is often not possible.

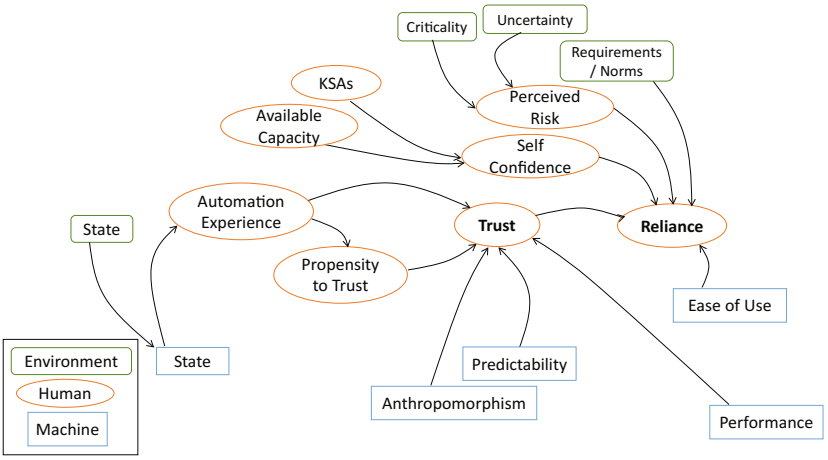

Fig. 2. A causal loop diagram illustrating effects upon trust and reliance [8].

3 Paradigm for Measuring Trust Behaviors

This section presents a paradigm for defining measurable trust behaviors. First, we present assumptions of the paradigm. Then a decision tree illustrates the importance of an automation's purpose and how compliance is actually a specific instance of reliance. The last three sub-sections illustrate that trust behaviors in systems with authority to act upon their environment will include different human actions or non-actions depending upon: (1) the allocation of authority to initiate action, (2) the human's authority to override the automation, and (3) the authority of the human to correct completed actions.

3.1 Assumptions

This paradigm assumes that the human only has one manner in which they can perform actions in the environment. There may be human-machine teaming environments where the human can interact with the automation in several different ways or have choices on how to act. In these cases, reliance and non-reliance may depend on the type of action taken. This paper does not address cases such as these.

Based on the complexities of adding automation into a human-machine team shown in [2], there may be numerous ways that humans will interact with complex sets of automations all within one environment. As such, this paper assumes that only one automation is acting in the human-machine team.

3.2 Automation's Purpose

The first and primary influence on how trust behaviors are measured involves determining the automation's purpose in the human-machine team. Broadly, this category includes systems that alert the human operator to a potential anomaly (perceive), systems that recommend or command the human to take a course of action in response to an anomaly (decide), and systems that are capable of taking action (act). For systems that alert or command the human, reliance on the alert or command is clear and easily monitored. Human action taken that aligns with the alarm or command constitutes reliance on the automation, while action taken contrary to the alert or command constitutes non-reliance.

While the operator's actions illustrate their reliance on the automation, it additionally illustrates the operator's willingness to rely upon the system's ability to have correctly identified the presence of the anomaly or the correct course of action in response to the presence of the anomaly. That is, the human is relying on the system not to produce false alarms or poor commands and illustrating this reliance by taking action consistent with responding to the system. Figure 3 shows actions of a human operator in response to an alert or command-based automation, illustrating trust behavior. This diagram depicts trust-based (reliance) behaviors specifically for alert or command-based automation.

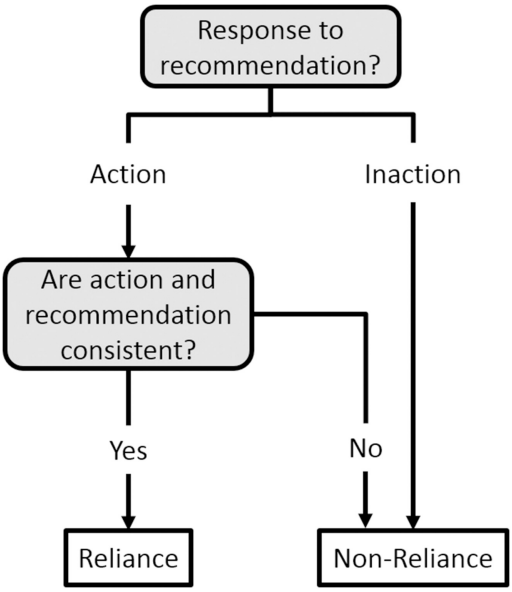

Fig. 3. Decision tree showing how people human-machine teams using alert or command-based automations demonstrate reliance and non-reliance.

In alarm or command-based automation systems, reliance is typically applied to describe a human's action taken when the human trusts the system not to miss an important anomaly. Thus, non-reliance is exhibited by replicating the activity of the automation and monitoring the same data as the automation, an activity that typically does not require interaction with the machine. Therefore, in alarm or command-based automation systems, human activity beyond that enabled through a typical human interface (e.g., eye movement monitoring) must be performed to assess reliance.

However, in human-machine teams where the machine has authority to act, the human is not required to respond to the automation and therefore trust behaviors will differ. The following three sub-sections address automations where the human specifically has authority to act.

3.3 Authority to Initiate Automation

Assuming that an automation is acting in the environment rather than recommending actions, trust behaviors will look different depending on when in the timeline of automation (see Fig. 1) a human action or inaction occurs. In the period before automation activation, trust behaviors are tied to the authority to initiate automation, and the automation's authority to act is tied directly to which entity triggers the automation.

Feigh et al. [13] present a taxonomy of automation triggers, where different factors can trigger automation within a human-machine team. This taxonomy includes, several automation triggers that require the human to activate the automation and others that require the machine to activate the automation. Reliance is manifested differently when the human has authority to activate the automation than when the machine activates automation. The decision tree in Fig. 4 illustrates this dichotomy.

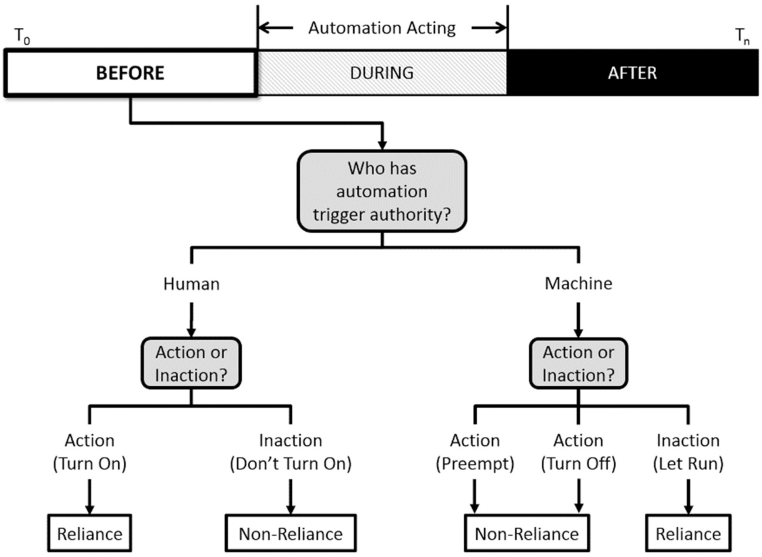

Fig. 4. Assuming the automation is not currently acting, how humans express reliance (via action or inaction) and non-reliance on automation in a human-machine team.

When a human is the one who triggers automation (e.g. cruise control on a car), reliance on the automation is active. He or she must actively engage the automation by turning it on. Whereas, when the human does not rely on the automation he or she can only communicate this through inaction. Inversely, in an automation triggered by the machine (e.g. such as a GPS navigation application automatically re-routing around traffic patterns) the human expresses reliance through inaction by allowing the machine to run. Non-reliance on a machine-triggered automation would then be active, requiring preempting or disengaging it.

3.4 Human Authority to Override

Once an automation has begun to act, the authority to turn an automation off will influence the way trust behaviors are expressed. As Fig. 5 illustrates, when an automation is running, if the human can override the machine, an act of reliance will constitute inaction (i.e. he or she will choose to not turn it off). In this case, an act of non-reliance will look like turning the automation off.

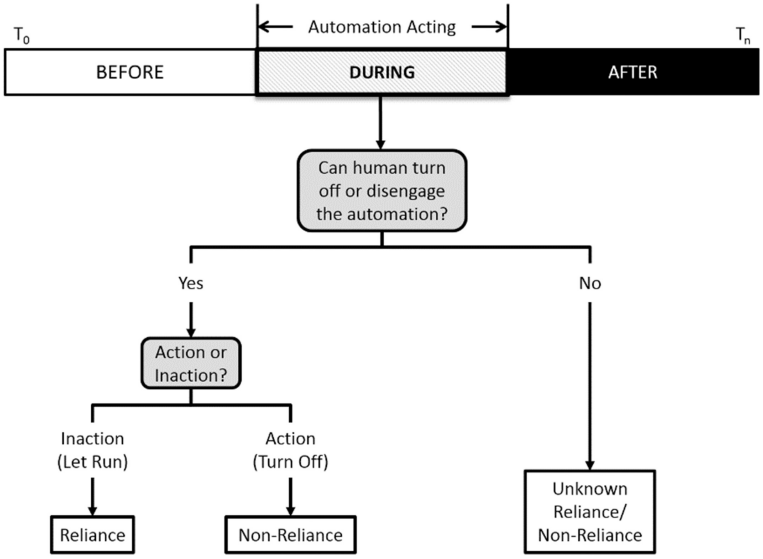

Fig. 5. Assuming the automation is currently acting, how humans express reliance (via action or inaction) and non-reliance on automation in a human-machine team.

However, if the human cannot override the automation once it starts acting (e.g. a ground collision avoidance system [GCAS]), reliance and non-reliance are not distinguishable again until the automation has stopped acting (e.g. not flying again until the GCAS is disabled). Therefore, knowing human override authority is crucial to understanding how measurable trust behaviors will manifest.

3.5 Human Authority to Correct

Once the automation has finished acting, another type of authority that could affect trust behaviors is human authority to correct an action taken by the machine. The ability to correct an action is different from overriding a machine's action in that overriding pertains to turning the automation on or off, while action correction pertains to taking deliberate corrective actions to fix a problem caused by the automation's actions. Authority for the human to correct only pertains once the automation has completed its action. However, authority to override and correct can often be intertwined, where a human overrides and corrects during the same action sequence. As shown in Fig. 6, reliance in a system that allows human correction of the system would be seen as inaction, non-reliance would involve actions.

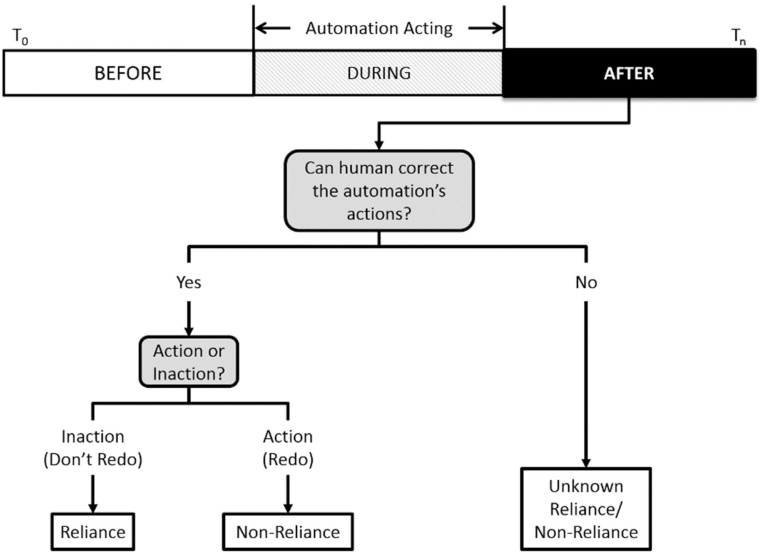

Fig. 6. How humans express reliance and non-reliance on automation in a human-machine team depending on whether they are able to correct the machine's actions.

Because of the manner in which corrective actions work, measuring non-reliance will be an active process. However, since corrective actions are not binary—like the on or off nature of overriding—they may give more insight into degrees of reliance and non-reliance.

4 Example Human-Machine Trust Measures

This section shows an example of measuring human trust behaviors in a human-machine team. Using the *Space Navigator* environment [2], we walk through the four aspects of the automation discussed in the previous section to establish objective measurements of reliance for an automation added to the environment. We then present a brief experimental validation of the measures.

4.1 Experimental Environment

Space Navigator (see Fig. 7) is a tablet-based computer game used in several previous experiments [2, 14, 15] to measure different aspects of human-machine interaction. Within the environment, participants monitor the screen for spaceships to enter from the screen edges and then route the spaceships to their assigned destination planet by drawing with their finger on the touchscreen—including the ability for participants to redraw trajectories. Points accumulate when ships successfully reach their destination planet or pick up bonuses that randomly appear on the screen. Points are lost when spaceships collide with each other or traverse either of two stationary "No-fly Zones." The goal is to amass the most possible points in an allotted time. An automation was designed to help the participant complete a portion of his or her tasks within the environment.

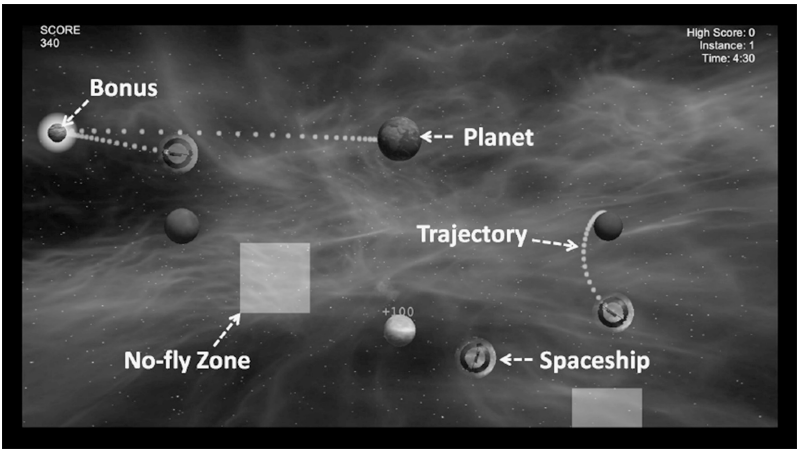

Fig. 7. An example Space Navigator game with several game components highlighted.

Automation: Collision Avoidance. The automation was designed to redraw already drawn trajectories for ships that are about to be involved in a collision. This automation waits until a collision is less than two seconds from occurring to give the human participant time to operate unimpeded. To avoid collisions, the automation redraws the trajectory by stepping the ship backward slightly and starting it back on its previous path.

4.2 Automation Trust Behavior Measures

Automation's Purpose. The collision avoidance automation's purpose is to act on the environment, and is not diagnostic in nature. Therefore, the process for determining reliance measures for diagnostic automations (Sect. 3.2 and Fig. 3) does not apply to this automation. Therefore, the ensuing sections will establish reliance measures.

Authority to Initiate Automation. Having established that the collision avoidance automation is acting on the environment, the next step is to determine what reliance and non-reliance will look like before the automation has triggered. Based on the way the automation triggers (acting upon a detected collision), the machine has the authority to initiate action. Before the automation acts, reliance would constitute inaction by the human when a pending collision is sensed (Let Run). Non-reliance occurs as a human trajectory draw performed on a ship that was nearing a collision (Preempt).

Human Authority to Override. While the collision avoidance automation is acting, the human does not have the authority to override the automation's action. Since the human may not stop the automation, no information can be gained from observing the human allowing the automation to complete its task.

Human Authority to Correct. The human may correct actions taken by the collision avoidance automation: the human can redraw all trajectories drawn by the automation. As such, the human inaction allowing the collision avoidance agent's trajectory to be followed would be reliance (Don't Redo), while redrawing the trajectory would be an example of non-reliance (Redo).

4.3 Notes on Creating Trust Measures

Breaking down the collision avoidance automation according to the preceding paradigm, the researcher can now determine whether trust behaviors (reliance or non-reliance) are measurable and when those behaviors are measurable. Before the automation acts, actions taken (trajectory draws) can be coupled with non-reliance; while the automation is acting, reliance and non-reliance are not measurable; and after the automation has acted, actions taken (trajectory draws) will imply a level of non-reliance on the automation.

The *Space Navigator* example illustrates two key takeaways. First, recurrence of automation action can make it difficult to discern if a trust behavior is preemptive or post-hoc. The collision avoidance automation is a recurrent automation, where it could potentially act on a given ship several times and can act on any number of ships in the environment at any time. As such, it can be difficult to determine if actions represent preemptive or post-hoc non-reliance. However, this distinction may not be important, as both are acts of non-reliance, since there is only one allowable action in the environment (drawing trajectories).

Secondly, just because trust influenced an action, does not mean that it is clearly determinable whether actions taken in the environment are directly related to reliance and trust. As seen in *Space Navigator*, several other factors can be influenced actions. For example, an action perceived as a preemptive collision avoidance action could actually be a rerouting of a ship to pick up a bonus that appeared on the screen. Therefore, researchers must take care to ensure that outside factors are acknowledged and accounted for during evaluation.

5 Conclusion

This paper presented a paradigm for determining measurable trust behaviors in human-machine teams. By understanding trust behaviors for both diagnostic automations and automations with authority to act on their environment, the presented paradigm showed that reliance on automation looks differently depending on how authority is divided within a human-machine team. The *Space Navigator* collision avoidance automation provides a useful example to understand some of the intricacies of the environment. Specifically noting that in environments with recurrent automation, it does not matter whether an act of non-reliance is preemptive or post-hoc and that they both constitute a lack of trust in the automation.

Future work should address cases where multiple users or multiple automations can act within the same environment. Additionally, a study of the types of actions that can be performed within an environment may provide meaningful insight into how humans can demonstrate trust in an automation.

Acknowledgements. The views expressed in this document are those of the author and do not reflect the official policy or position of the United States Air Force, the United States Department of Defense, or the United States Government.

References

1. Lyons, J.B., Ho, N.T., Koltai, K.S., Masequesmay, G., Skoog, M., Cacanindin, A., Johnson, W.W.: Trust-based analysis of an air force collision avoidance system. Ergon. Des.: Q. Hum. Factors Appl. **24**(1), 9–12 (2016)
2. Bindewald, J.M., Miller, M.E., Peterson, G.L.: A function-to-task process model for adaptive automation system design. Int. J. Hum.-Comput. Stud. **72**(12), 822–834 (2014)
3. Lee, J.D., See, K.A.: Trust in automation: designing for appropriate reliance. Hum. Factors: J. Hum. Factors Ergon. Soc. **46**(1), 50–80 (2004)
4. Hu, W.-L., Akash, K., Jain, N., Reid, T.: Real-time sensing of trust in human-machine interactions. Cyber-Phys. Hum.-Syst. **49**(32), 48–53 (2016)
5. Khawaji, A., Chen, F., Zhou, J., Marcus, N.: Using galvanic skin response (GSR) to measure trust and cognitive load in the text-chat environment. In: Proceedings of the 33rd Annual ACM Conference Extended Abstracts on Human Factors in Computing Systems, Seoul (2015)
6. Evans, A.M., Revelle, W.: Survey and behavioral measurements of interpersonal trust. J. Res. Personal. **42**(6), 1585–1593 (2008)
7. Hoff, K.A., Bashir, M.: Trust in automation: integrating empirical evidence on factors that influence trust. Hum. Factors: J. Hum. Factors Ergon. Soc. **57**(3), 407–434 (2015)
8. Rusnock, C.F., Miller, M.E., Bindewald, J.M.: Framework for trust in human-automation teams. In: Proceedings of the 2017 Industrial and Systems Engineering Conference, Pittsburgh (2017, to appear)
9. Freedy, A., DeVisser, E., Weltman, G., Coeyman, N.: Measurement of trust in human-robot collaboration. In: Proceedings of the 2007 International Symposium on Collaborative Technologies and Systems (CTS), Orlando (2007)

10. Dixon, S.R., Wickens, C.D.: Automation reliability in unmanned aerial vehicle control: a reliance-compliance model of automation dependence in high workload. Hum. Factors: J. Hum. Factors Ergon. Soc. **48**(3), 474–486 (2006)
11. Lacson, F.C., Wiegmann, D.A., Madhavan, P.: Effects of attribute and goal framing on automation reliance and compliance. In: Proceedings of the Human Factors and Ergonomics Society 49th Annual Meeting (2005)
12. Chiou, E.K., Lee, J.D.: Beyond reliance and compliance: human-automation coordination and cooperation. In: Proceedings of the Human Factors and Ergonomics Society 59th Annual Meeting (2015)
13. Feigh, K.M., Dorneich, M.C., Hayes, C.C.: Toward a characterization of adaptive systems: a framework for researchers and system designers. Hum. Factors: J. Hum. Factors Ergon. Soc. **54**(6), 1008–1024 (2012)
14. Bindewald, J.M., Peterson, G.L., Miller, M.E.: Trajectory generation with player modeling. In: Canadian Conference on Artificial Intelligence, Halifax (2015)
15. Bindewald, J.M., Peterson, G.L., Miller, M.E.: Clustering-based online player modeling. In: Joint Conference on Artificial Intelligence (IJCAI): Computer Games Workshop, New York (2016)

Occupational Safety Simulators

Analysis of Occupational Security Management Interventions Based on Coupling Human Factors

Yujun Xu[1(✉)], Xuebo Chen[2(✉)], and Qiubai Sun[2]

[1] School of Electronics and Information Engineering, University of Science and Technology Liaoning, Anshan 114051, Liaoning, China
362600074@qq.com
[2] Graduate School, University of Science and Technology Liaoning, Anshan 114051, Liaoning, China
xuebochen@l26.com, lnkdsqb@ustl.edu.cn

Abstract. The objective of this work is to compare the impact of various management factors on safety awareness of staff. Some necessary materials about safety production have been provided by previous works, but internal coupling relationships among factors are often ignored. Lacking of consideration on coupling can make it impossible to give objective and reasonable analyses. Coupling mechanism among workers' and managers' factors in production are analyzed and expressed intuitively by topology. Key nodes in topology were selected and a mathematical model was set up. The variation trends of employee security awareness under different management conditions were simulated through netlogo based on the model we established. Compared with managers' safety awareness, charisma and safety education, supervision can strengthen employees' awareness to a large extent in a short time.

Keywords: Security management system · Human factors · Coupling mechanism · Netlogo simulation

1 Introduction

Unprecedented developed industrialization and machine production have brought about tremendous advantages to human society, at the same time, a large number of production accidents have occurred. In general, production accidents have decreased in recent years, but the overall situation is still grim now [1, 2]. Many scholars at home and abroad now have made a lot of contributions to this field. Human factors have always been thought of as the main accidental factors.

Awareness is the prerequisite of behavior in practice and in part decides real behavior [3]. Principal leaders' safety awareness can largely determine security management level and indirectly affect awareness and behavior of workers [4]. [5] improved theory of Planned Behavior and claimed that attitude can directly affect awareness and behavior, and working pressure can affect group norms and thus influence employees' attitude. Through hypothesis testing, [6] obtained that safety concept and work stress are

D.N. Cassenti (ed.), *Advances in Human Factors in Simulation and Modeling*,
Advances in Intelligent Systems and Computing 591, DOI 10.1007/978-3-319-60591-3_6

significantly associated with unsafe behavior intention and unsafe behavior. [7] showed that self-efficacy, accident experience, job satisfaction and knowledge have close connections with behavior intention, self-efficacy, job satisfaction as well as knowledge were apparently related to actual behavior. [8] concluded that the impact of safety climate on unsafe behavior is not clear, but a statistical association between safety climate and awareness appeared when they had collected sufficient data.

[9] showed that security management poses the most significantly positive impact on security atmosphere. [6] claimed that security management commitment, illegal punishment, safety management practices, stress management and other hazards management can dramatically affect unsafe behavior and intention. [10] proposed: screening and selection of new recruits as well as uninterrupted education and training are needed, so that they can ensure their staff have enough knowledge to avoid unsafe conditions or have ability to properly handle those conditions when they occur. [11] divided managers' behaviors into management practice and design behavior, and verified that management behaviors have a significant positive effect on security motives and knowledge of staff through hypothesis testing. [12] considered that the safety supervision falls under the category of security management, the equating management to supervision is not conducive to the implementation of production safety responsibility.

These documents mainly focused on abstraction of accident factors, available interventions and basic structures. Coupling among factors are often ignored. But from a systemic perspective, actual safety production network, which is composed of mutually associated fundamental elements, is a quite intricate system with numerous coupling relationships [13]. Human error is not the isolated act of a particularly unlucky individual. Rather, it is the result of a chain of events that often culminate in a less than desired outcome [14]. [15, 16] proposed an assumption that there are fundamental elements of all organizations that must work together if safe and efficient operations are to occur. So, analyses of the safety production system will be distorted if coupling relationships are overlooked. Taken together, there is a requirement to insight into the effective integration of human factors in a systematic manner.

The rest of the paper is structured as follows. In Sect. 2, the coupling mechanism among management and employees factors was expressed by topology, and key nodes in topology were selected by measurement indexes of coupling elements. In Sect. 3, we come up with a mathematical model with key factors obtained in Sect. 2. Simulations are performed to assess the efficiency of different management approaches in Sect. 4. Finally, Sect. 5 concludes the paper.

2 Key Nodes in Topology

2.1 An Enterprise Security Topology Network

Topology model is more concise, effective and straightforward than verbal description. It abstracts complex phenomena or systems into structures which consist of nodes and edges. Nodes in topology network can represent anything and links represent interaction among nodes.

For general safety production management system, factors are summarized from previous literatures in Sect. 1. Factors are listed in Table 1 and marked as $V_1 - V_{23}$.

Table 1. Factors of general safety production

Node	Meaning	Node	Meaning
V_1	Working pressure	V_{13}	Risk propensity
V_2	Safety knowledge	V_{14}	Cognitive biases of behavioral risk
V_3	Work experience	V_{15}	Accidents experience
V_4	Security attitude	V_{16}	Past behavior
V_5	Behavior intention	V_{17}	Job satisfaction
V_6	Behavior	V_{18}	Machine, equipment settings
V_7	Safety education and training	V_{19}	Safety climate
V_8	Charisma of managers	V_{20}	Hazard management
V_9	Security awareness of managers	V_{21}	Safety warning
V_{10}	Safety supervision	V_{22}	Safety commitment
V_{11}	Illigal punishment	V_{23}	Performance assessment
V_{12}	Safety management		

As is shown in Fig. 1, the undirected topology model $G = (V, E)$ is established. Wherein, the nodes set$V = \{V_1, V2, \ldots V_{23}\}$ and the edge set E represent the factors listed in Table 1 and the coupling relationships between two factors summarized from previous literatures listed in the last section respectively. Block1 characterizes machines and equipment settings, block2 characterizes the atmosphere, block3 and block4 represent workers' and managers' safety awareness respectively. Human factors are the main objects of our research, so no natural interference has been taken into account. Block1, block2 have been simplified in the topology model and will not be included in the following mathematical model.

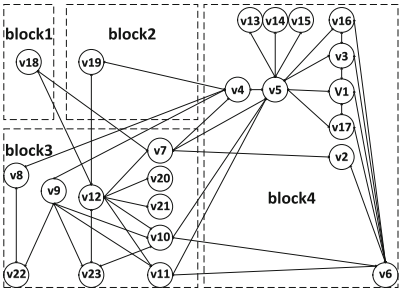

Fig. 1. Topology of enterprise security system

2.2 Selection of Key Nodes

For different nodes, numbers of edges differ, in other word, relationships with others differ. The more edges a node owns, the more impact it can make in the system and the

more important it is. Thus, it can be helpful for improving security status if we know the key nodes in topology, in other words, key factors of security management clearly. In conclusion, there is a need to evaluate the significance of nodes in Fig. 1. Importance evaluation is mainly determined by the following indices:

Importance of Nodes I_i.

$$I_i = L_i + \eta k_i \tag{1}$$

Where L_i represents node load, k_i is node degree, ηk_i is increment. When a node is the end node in a certain long-range connection, $\eta = 0.2$, otherwise, $\eta = 0$ [17]. L_i is decided by node degrees k_i and node betweenness B_i :

$$L_i = \alpha k_i + \beta B_i \tag{2}$$

α is the weight of node degree in the node load, β is the weight of node betweenness in the load node, $\alpha = \beta = 0.5$ [17].

Node Degree K_i.

$$k_i = \sum_{j=1, j\neq i}^{n} e_{ij} \tag{3}$$

$e_{ij} = 1$ when there is an interactive relationship between node i and node j, otherwise, $e_{ij} = 0$.

Node Betweenness B_i.

$$B_i = \sum_{s\neq t} \frac{P_{st}(i)}{P_{st}} \tag{4}$$

Table 2. Indices of key nodes

Node	V_1	V_2	V_3	V_4	V_5	V_6
Node degree	4	3	4	5	12	7
Node betweenness	0.011	0.023	0.011	0.383	0.890	0.191
Node load	2.006	1.512	2.006	2.692	6.845	4.196
Long-range connection	no	yes	no	yes	yes	yes
Connection increments	0	0.2	0	0.6	0.4	0.6
Importance	2.006	1.712	2.006	3.292	4.345	6.696
Node	V_7	V_8	V_9	V_{10}	V_7	V_{12}
Node degree	5	2	5	5	4	8
Node betweenness	0.269	0.036	0.220	0.311	0.215	0.549
Node load	2.635	1.018	2.610	2.656	2.108	4.275
Long-range connection	yes	yes	yes	yes	yes	no
Connection increments	0.8	0.2	0.2	0.4	0.4	0
Importance	3.435	1.218	2.810	3.056	2.508	4.275

Where P_{st} is the total number of shortest paths between nodes s and t, $P_{st}(i)$ is the shortest path that goes through node i.

Indices of 23 nodes are calculated according to the topological structure and the above formulas.12 nodes with high importance are listed out in Table 2.

3 Mathematical Model

The higher the safety consciousness V_5, the less illegal behavior V_6 will be. Safety management V_{12} can be measured by specific elements such as $V_7 - V_{11}$ through the mathematical model. So we basically extract the following factors, $V_1 - V_5$, $V_7 - V_{11}$.

Suppose the total number of employees is n and the i-th employee is denoted by i. According to Sect. 2, their attributes include: work stress x_{i1}, subjective norm x_{i2}, perceived behavioral control x_{i3}, safety knowledge φ_{i1}, familiarity φ_{i2}, attitude x_{i4}, unsafe intention $f(t)$. They take random values in the the continuous interval [0, 5].

Let there be m managers and the j-th manager is denoted by j. According to Sect. 2, individual properties include: safety awareness M_1, charisma M_2, effectiveness of supervision M_3, illegal punishment P, safety training E. We suppose that the above management factors are the same for each employee.

3.1 Managers

Managers' Safety Awareness M_1. Managers' safety awareness has an indirect charisma on front-line staff through its external performance, for instance, legal or illegal inspection, security activities attendance, safety investment share, etc. It takes random value in [1, 10].

Charisma M_2. The greater the managers' external manifestation of security awareness, the more positive their charisma will be and the influence on their staff will also be more positive, and vise versa. It takes random value in [0,1].

Effectiveness of Supervision M_3. Monitor procedures are usually conducted by supervisors who are responsible for overseeing staff. The proportion can represent supervision efficiency. Actually, violators discovered by inspectors just account for a part of the real number. But statistical accident rate obtained in a plant is the baseline for determining whether impose illegal punishment and carry out safety training. It takes random value in [0,1].

$$M_3 = \frac{\psi}{I} \tag{5}$$

Wherein, I is the true number of employees who implement irregularities, ψ is the statistical number of supervised cases.

Illegal Punishment *P*. The level of illegal punishment is proportional to the overall security state, that is the worse the security situation, the severer the illegal punishment. It takes random value in [0,1]. The influence it brings about can see in formulas (7).

Safety Training *E*. Safety training such as training of self-rescue and emergency processing skills will conduct regularly. And training activities will be carried out if the statistical accident rate has exceeded the threshold. It takes random value in [0,1]. The influence it brings about can see in formulas (8).

3.2 Employees

Working Pressure x_{i1}. The traditional incentive theory the pressure efficiency. Appropriate pressure has a positive influence on the working, while higher or lower than the best stress levels will worsen the working performance efficiency [18]. We assume that the highest pressure is $x_m = 5$. When stress exceeds this threshold level, security status will be surely adversely impacted and the worker should be replaced. Workers' pressure will increase with the time and fluctuate with mental and physical situation. The increasing rates z_1 of different workers are not always the same and take random values in [1%, 2%] [19].

$$x_{i1}(t) = \begin{cases} \prod_{1\%}^{2\%} [x_{i1}(t) + z_1]^t + \varepsilon_1, & x_{i1}(t) < 5 \\ x_{j1}(0) \quad , & x_{i1}(t) \geq 5 \end{cases} \tag{6}$$

Subjective Norm x_{i2}. Subjective norm refers to a person's perceived social pressure to engage or not engage in a behavior and it is followed by considering the other people in mind to make oneself acceptable for the people around him. Workers' pressure certainly will paly a part. Subjective norm will also change when manager's factors such as supervision and punishment are in effect. For instance, supervision level, that is, the possibility of being found or punished when they are performing unsafe behavior has a profound influence on subjective norms.

$$x_{i2}(t) = a x_{i1}(t) + b M_3 + c P + \varepsilon_2 \tag{7}$$

Perceived Behavioral Control *xi3*. Perceived behavioral control refers to people's perceptions of their ability to perform a given behavior. And it can be used to predict behavior. Perceived behavioral control is determined by the total set of accessible control beliefs, i.e., beliefs about the presence of factors that may facilitate or impede performance of the behavior. So we assume that safety knowledge φ_1, work experience φ_2 can determine workers' perceived behavioral control to a certain degree.

According to the law of human memory, the probability of memory occurrence is 40%, and then 70% will slip from one's memory [20]. So in the course of education and training E, the level of knowledge φ_1 fluctuates with time. In addition, the outcome

of training can be affected by their managers charisma M_2. With work ongoing, experience will accumulate, work experience φ_2 grow over time with the growth rate z_2. Because of circumstance, accidents and working time each person has experienced are different. The rates take random values in [1%, 2%] [19].

$$x_{i3}(t) = d\varphi_{i1}(0)[1 + (1-\zeta)\Gamma\vartheta M_2 E] + e\varphi_{i2}(0)\prod_{1\%}^{2\%}(1+z_2)^t + \varepsilon_3 \tag{8}$$

$$\xi = \frac{\psi}{n} \tag{9}$$

Wherein, $\vartheta = 0.4$, $\zeta = 0.7$. ξ is the statistical accident rate obtained in plant, if $\xi > 10\%$, $\Gamma = 1.$, that is, training activities will be conducted if the statistical accident rate has exceeded 10%. $\Gamma = 0$, if $\xi \leq 10\%$.

Attitude x_{i4}. Attitude toward a behavior is the degree to which performance of the behavior is positively or negatively valued. According to the improved Theory of Planned Behavior [21], pressure, subjective norms and perceived behavioral control can affect employees' attitude.

In addition, managers'charisma can affect workers' attitude directly [23]. The greater the manager's personality charm, the greater the employee's subjective norms will be influenced by the external performance of managers' safety awareness, otherwise, the smaller.

$$x_{i4}(t) = g[x_{i1}(t) - x_m] + hx_{i2}(t) + kx_{i3}(t) + M_2M_1 + \varepsilon_4 \tag{10}$$

Intention *f(t)*. According to the Theory of Planned Behavior [3], intention is an indication of a person's readiness to perform a given behavior, and it is considered to be the immediate antecedent of behavior. The intention is based on subjective norm, perceived behavioral control and the attitude toward the behavior, with each predictor weighted for its importance in relation to the behavior. In addition, in the improved Theory of Planned Behavior [19], work stress can significantly affect actual behavior through changing behavior intention.

$$f(t) = \alpha_1[x_{i1}(t) - x_m] + \sum_{j=2}^{4}\alpha_j x_{ij}(t) + \varepsilon_5 \tag{11}$$

Wherein, $\alpha_1 = 0.622$, $\alpha_2 = 0.673$, $\alpha_3 = 0.481$, $\alpha_4 = 0.686$ [19].

4 Simulation

4.1 Initialization

314 employees and 16 managers with properties listed in Sect. 3 are set up to complete the simulation. We use arithmetic number with no unit to indicate the situation of safety

awareness. Bigger number equals better safety awareness. The initial average security awareness and the highest safety awareness are set as 3.2 and 5 respectively. The threshold is 3, in other words, the lowest level of qualified safety awareness is 3. Employee whose safety awareness is higher than 3 can be classified as a qualified worker, otherwise, can be classified as the unqualified. People's safety consciousness will fluctuate over time under the management conditions. In the following simulation, consciousness status of the employees changes in steps.

Parameters of functions were derived from published literatures [19–23]. And through repeated testing of simulation, program have been adjusted many times and the final coefficients are shown in Table 3.

Table 3. Coefficients in functions

	$x_{i2}(t)$			$x_{i3}(t)$		$x_{i4}(t)$		
Coefficient	a	b	c	d	e	g	h	k
Value	0.5	0.3	0.2	0.5	0.5	0.518	0.487	0.097
Normalized	0.5	0.3	0.2	0.5	0.5	0.470	0.441	0.088

4.2 Simulation and Discussion

Scenario 1. In scenario 1, Managers' factors such as security awareness M_1, charisma M_2, effectiveness of supervision M_3, safety training E and punishment P are 5, 0.5, 0.4, 0.5 respectively, the level of supervision is 0.4 and managers' factors take the intermediate value. The system under scenario 1 evolves (in steps) as illustrated in Fig. 2. We can see that it requires a long time to reach steady state, step = 1350. The final average level of safety awareness is 3.63. The number of employees whose level of safety awareness is between 4 and 5 is 58. That is, employees with relatively higher level of safety awareness account for 18%. A slight improvement is achieved. In this scenario, promotion of management is imperative.

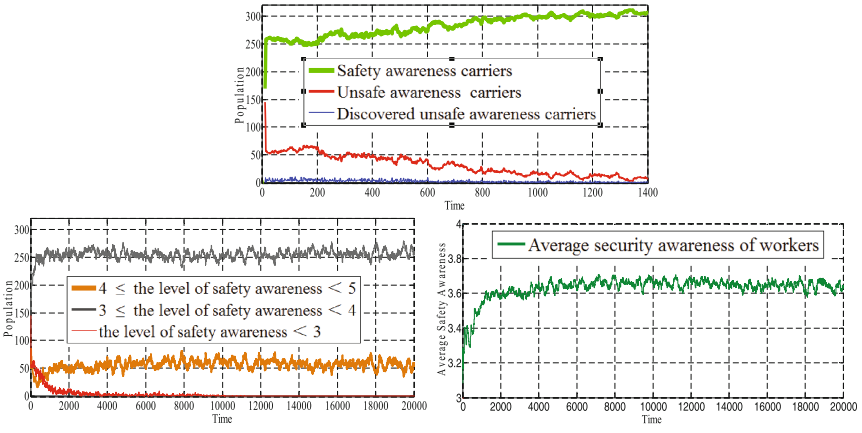

Fig. 2. The changes of employee security awareness in the first scenario

Scenario 2–5. Managers' factors are set as below in Table 4. The system under scenario 2–5 evolves as depicted in Figs. 3, 4 and 5.

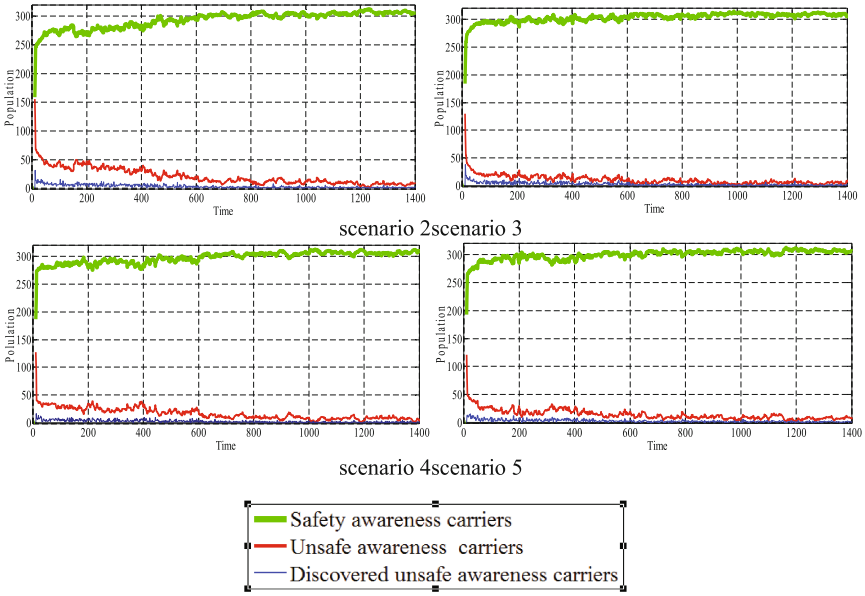

Fig. 3. Overall situation of safety awareness of staff in equilibrium

Table 4. Management conditions in scenario 2–5

Managers' factors	Scenario 2	Scenario 3	Scenario 4	Scenario 5
(M_1, M_2, M_3, E)	(5, 1, 0.4, 0.5)	(5, 0.5, 0.8, 0.5)	(10, 0.5, 0.4, 0.5)	(5, 0.5, 0.4, 1)

(1) It turned out that security awareness of workers can reach equilibrium in different time periods when different management interventions were strengthened.

When administrators' charisma, safety awareness or training efforts is increased, it requires a long time to achieve steady state. Respectively are 1250, 960, and 930 steps. When supervision is emphasized, it requires a much shorter time, 504 steps, to reach equilibrium than in Fig. 2 and other situation in Fig. 3. In addition, feedback is closer and more rapidly follow the actual situation if supervision level is high, so managers can quickly follow up the real situation.

(2) In scenario 2–5, safety awareness status of employees is more better than scenario 1. In scenario 2, the number of workers whose safety awareness is higher than 4 is 62, that is, workers with high safety awareness account for 19%. In contrast, scenario 3 has greatly positive effects, 46% of employees can maintain a high level of safety awareness. In scenario 4 and scenario 5, improvements that training and education achieved can not be disregarded either, employees with a high level of safety awareness can account for 30% and 21% respectively.

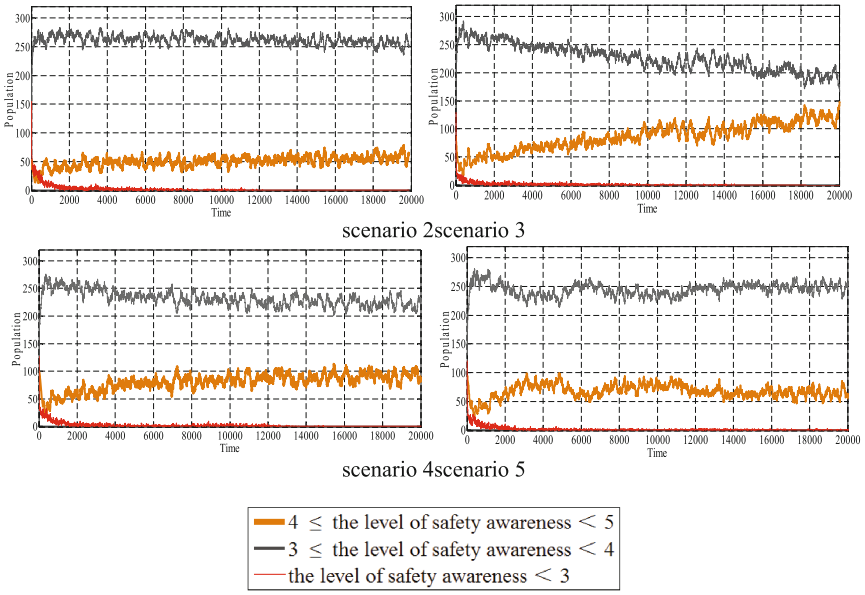

Fig. 4. The distribution of employee safety awareness

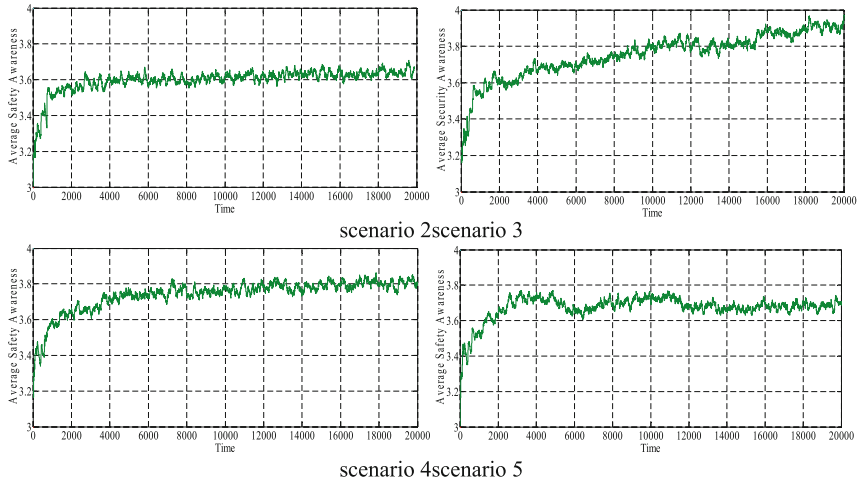

Fig. 5. Average security awareness of workers

(3) From the simulation results show in Fig. 5, compared with other conditions, the improvement is not noticeable in scenario 2, the final average level of safety awareness is 3.66. But if the level of supervision is promoted to 0.8 in scenario 3, the average level of safety awareness can reach 3.92, improvement achieved is considerablely better than other factors. In scenario 4 security awareness of

management layer can bring the final average level of workers' awareness up to 3.83, improvement achieved is relatively better than other factors. In scenario 5, training and education can promote final average level up to 3.72.

5 Conclusion

The trends of security awareness under the different management condition are simulated through netlogo, the conclusions are as following:

Good safety production supervision can bring about the most considerable promotion and improve employees' security awareness most quickly. At the same time, supervision feedback is closer and more rapidly follow the actual situation if supervision level is high and thus managers can quickly follow up the real situation.

In addition, administrators' security awareness can also play a beneficial role in promoting employees' safety consciousness situation. The higher administrators' consciousness is, the higher the safety awareness of employees will be.

Managers' charisma has the smallest effects on employees' safety consciousness. More daringly, we assume that manager's personality charm can not directly affect employee safety consciousness, but will work together with other management factors. We will further study the relationship between Managers' charm and other management factors, in the after work.

To sum up, we can conclude that to achieve the best outcome of safety management, enterprises need to improve their administrators' own knowledge and safety awareness first and try their best to optimize the supervision department structure and staffing. These conclusions can serve as a theoretical basis for improvement of security management and safety awareness.

Acknowledgments. This research reported herein was supported by the NSFC of China under Grant No. 71571091.

References

1. Li, S.C., Xiao, L.: Statistics of industrial accidents in China during the period from November to December in 2015. J. Saf. Environ. **16**(1), 395–396 (2016). (in Chinese)
2. Li, S.C., Xiao, L.: Statistics of industrial accidents in china during the period from January to February in 2016. J. Saf. Environ. **16**(2), 395–396 (2016). (in Chinese)
3. Ajzen, I.: The theory of planned behavior. Res. Nurs. Health **14**(2), 137–144 (2010)
4. Meng, Q.S.: Research on safety awareness of leader based on mine major accidents. Saf. Coal Min. **46**(9), 246–248 (2015). (in Chinese)
5. Fogarty, G.J., Shaw, A.: Safety climate and the theory of planned behavior: towards the prediction of unsafe behavior. Accid. Anal. Prev. **42**(5), 1455–1459 (2010)
6. Liang, Z.D.: Sem-based study on effects of organizational and environmental factors on workers' unsafe behavior. China Saf. Sci. J. **22**(11), 16–22 (2012). (in Chinese)
7. Liang, Z.D.: Sem-based study on effects of individual characteristics factors on unsafe behavior. China Saf. Sci. J. **23**(2), 27–33 (2013). (in Chinese)

8. Cooper, M.D., Phillips, R.A.: Exploratory analysis of the safety climate and safety behavior relationship. J. Saf. Res. **35**(5), 497–512 (2004)
9. Zhang, J.G., Zhang, L.: Study on the influence of enterprise safety climate on enterp rise safety behavior [J]. J. Saf. Sci. Technol. **3**(1), 106–110 (2007). (in Chinese)
10. Makin, A.M., Winder, C.: A new conceptual framework to improve the application of occupational health and safety management systems. Saf. Sci. **46**(6), 935–948 (2008)
11. Cao, Q.R., Li, K., Li, J.L.: Impact of manager's behavior on coalminer's unsafe behavior. J. Manag. Sci. **24**(6), 69–78 (2011). (in Chinese)
12. Guan, S.F.: Safety Management and Supervision of Power Enterprise [J]. Chin. Foreign Entrep. **3X**(9), 92–93 (2014). (in Chinese)
13. Li, W.: The deep-rooted coupling mechanism and emergence of complexity in enterprise integrated innovation system. Sci. Technol. Prog. Policy **26**(5), 73–76 (2009). (in Chinese)
14. Shappell, S.A., Wiegmann, D.A.: Human factors investigation and analysis of accidents and incidents. Encycl. Forensic Sci. **1**(3), 440–449 (2013)
15. Reason, J.: Human Error. Cambridge University Press, New York (1990)
16. Reason, J.: Managing the Risks of Organizational Accidents. Ashgate Publishing Company, Aldershot, Great Britain (1997)
17. Wang, S., WANG, Y., Feng, J.W.: Complex system important node collapse control based on constraint entropy. China Saf. Sci. J. **22**(5), 10–16 (2012) (in Chinese)
18. Li, L., Min, R.: The effects of psychological contract to work stress management. Enterp. Econ. **10**, 5–7 (2007). (in Chinese)
19. Tian, Y.M., Chen, X.B., Sun, Q.B.: Research on inhibition of emergent property of employee unsafe behaviors in bbs management systems. J. Saf. Environ. **16**(2), 174–178 (2016). (in Chinese)
20. Li, N.W., Jin, H.L.: Study on safety attention based on situation cognition theory. China Saf. Sci. J. **23**(9), 58–63 (2013). (in Chinese)
21. Tian, S.C., Liu, F., Yang, L.: Study on miners' unsafe behaviors based on theory of planned behavior. Min. Saf. Environ. Prot. **42**(6), 839–845 (2014). (in Chinese)
22. Li, N.W.: Safety attention attenuation model based on multi-agents modeling. China Saf. Sci. J. **22**(12), 51–57 (2012). (in Chinese)
23. Li, N.W., Huang, J.T., Niu, L.X.: Evolutionary model of miners' violation behavior based on multi-agent simulation. China Saf. Sci. J. **23**(11), 10–15 (2013). (in Chinese)

Group Safety Consciousness Reconstruction Based on the Inclusion Principle

Yangguang Xu[1(✉)], Wei Ye[2], Xuebo Chen[3(✉)], and Qiubai Sun[3]

[1] School of Electronics, Information Engineering,
University of Science and Technology Liaoning, Anshan 114051, China
shine2l683l@sina.com
[2] Faculty of Science and Electronic Information,
Guangdong University of Petrochemical Technology, Maoming 525000, China
yeweill27@l63.com
[3] Graduate School of University of Science and Technology Liaoning,
Anshan 114051, China
xuebochen@l26.com, lnkdsqb@ustl.edu.cn

Abstract. "People" of behavior safety systems composed of people, things and the environment are being regard as object of this research. The interaction relationships of group security awareness are studied with the help of Lotka-Volterra model. According to the organization structure of enterprise, the interaction mode of safety awareness is star type interaction. The interactive relationship between individual security awareness of enterprise employees researched after the overlapping decomposition of Lotka-Volterra model based on the principle of inclusion. The decentralized coordinated control is applied to the reconstruction of the safety consciousness, and the security awareness state feedback controller and the individual relation coordinator are set up to make the security awareness meet the standard. Finally, the simulation results show that the decentralized coordination control can achieve the consistency reconstruction of security awareness. This paper provides reference for the enterprise to make achievements in safety management.

Keywords: Behavioral safety · Safety consciousness reconstruction · Inclusion principle · Lotka-Volterra model · Decentralized coordinated control

1 Introduction

With the rapid development of social economy and science technology, the security problem of human production activities have been more and more attention in recent years, but the accident is still a huge amount, for a long time, the enterprise through the development level of various group organization safety regulations, safety education, safety supervision and inspection. Set up a safety warning signs, safety assessment and safety management methods, but it has little effect, as of August 2, 2014, Jiangsu, Kunshan Rong metal products Co., car wheels polishing workshop dust explosion accidents in paper [1], survey results after the display, the relevant managers and staff safety awareness is weak, ignoring safety rules and regulations do not pay enough

D.N. Cassenti (ed.), *Advances in Human Factors in Simulation and Modeling*,
Advances in Intelligent Systems and Computing 591, DOI 10.1007/978-3-319-60591-3_7

attention to the work of production safety, is the main cause of the accident. In August 12, 2015, Tianjin Binhai New Area in Tanggu Development Zone, Tianjin Dongjiang Bonded Port International Logistics Co. Ltd. is Ruihai dangerous goods warehouse explosion in paper [2]. After the investigation and analysis of the results show that the relevant managers and employees of production safety awareness, ignoring safety rules and regulations, safety production work is not enough attention. The reason is that the human will and the objective reality of the society are in conflict and contradiction, that is, whether the human security management system can be implemented with the improvement of the level of human security awareness? Can the safety consciousness of human being be reconstructed to restrain the emergence of unsafe behavior?

In recent years, domestic and foreign scholars study rarely on the safety awareness. The content of the research is focused on the research of people's safety attitude, safety culture, safety psychology and safety climate. The analysis focuses on the speculation of exploration and qualitative discussion. Jiang proposed a colleague safety knowledge /behavior perception (PCSK/B) model as a means for measuring and predicting the behavior of the individual in paper [3], the study showed that positive safety atmosphere makes the prediction has stronger effect on individual behavior PCSK/B model. Sun Aijun and Liu Mao analyse behavior safety management application in China, put forward exploration of safety education and training mode of our country's workers, strengthen the main responsibility for production safety awareness of enterprises, improve the effectiveness of safety investment in paper [4]. In 2001, TAM and others made a study on the change of the safety attitude of the personnel in the construction, and put forward some constructive and feasible suggestions and measures for the current situation of the weak safety awareness in paper [5]. The safety awareness is divided into 3 dimensions by domestic scholars, using questionnaire investigation and analysis of the civil aviation pilots occupation safety awareness of the status quo, the results show good overall level of civil aviation pilots occupation safety awareness, and strengthen the occupation safety awareness of civil aviation pilots related suggestions are given in paper [6]. Conrad and Bradshaw believe that safety awareness and the occurrence of accidents are inseparable, and do a special study of this, it is found that a good sense of safety can reduce the probability of accidents in paper [7].

Due to interference of anxiety and impulsive, irrational psychological factors in production and technology and other social activities, the group behavior safety management system in the safety awareness of the co evolution is extremely complex, therefore, the study of natural science research methods into the Social Sciences, from the perspective of complex system perspective with the method, the interaction between employee group behavior Lotka-Volterra model of safety management in safety awareness of reconstruction, in order to overcome the influence of anxiety and impulsive irrational psychological factors.

2 Group Security Awareness Dynamic Situation Model

The group is the smallest unit enterprise organization, as a group, each member of the team of different functions, and there is a complex interaction, and the safety consciousness of team interaction is also a relationship between group members.

According to the discrete Lotka-Volterra model modeling method in paper [8], a group of security awareness dynamic situation model composed of different security awareness interaction.

$$x_i(k+1) - x_i(k) = x_i(k)\left(r_i + \sum_{j=1}^{n} A_{ij}x_j(k)\right), i = 1, 2, \ldots, n \tag{1}$$

Where, x_i (k), $(i = 1, 2,\ldots, n,)$ is the security awareness of i-th employee at k-th time, $r_i = [r_1, r_2, \ldots r_n]^T$ is the initial growth rate of employee safety awareness, which is obtained by the statistical analysis of individual behavior safety. A_{ij} is the competition coefficient matrix, which indicates that x_i is the competitive coefficient of x_j.

In order to better fit the actual social network interaction, the following definitions are given.

Definition 1. The interaction matrix $E = (e_{ij})$ is a n-dimensional constant matrix, indicate the interconnection between employee i and employee j, there have

$$0 \leq e_{ij} \leq 1 \tag{2}$$

Which $e_{ij} = 0$ said they did not interact with each other, $e_{ij} = 1$ said employee i direct impact on employee j.

Definition 2. if $E = (e_{ij})$ is the interaction matrix of employee i and employee j, we suppose

$$A_{ij} = \begin{cases} -r_i + e_{ii}a_{ii} & i = j \\ e_{ij}a_{ij} & i \neq j \end{cases} \tag{3}$$

Where A_{ij} is an n-dimensional constant matrix, obtained by individual safety values. And the competitive coefficient matrix is obtained by using this formula.

3 Group Communication Topology

Enterprise security management system is a complex multi index, multi-level system, the organizational structure of the enterprise is refers to between the various departments at all levels of the organization and arrangement of the elements of the relationship between a model.

According to the complex topology structure of the system and the organization structure and job level level, determine the impact of the safety consciousness of the team groups and interaction is the star type structure mode.

Assuming that first employees as the core of the star structure, and its security awareness to play a core role in guiding, n employee safety awareness and security awareness. The interactive model of security awareness:

$$\begin{bmatrix} x_1(k+1) \\ x_2(k+1) \\ x_3(k+1) \\ \vdots \\ x_n(k+1) \end{bmatrix} - \begin{bmatrix} x_1(k) \\ x_2(k) \\ x_3(k) \\ \vdots \\ x_n(k) \end{bmatrix} = \begin{bmatrix} x_1(k) & 0 & 0 & \cdots & 0 \\ 0 & x_2(k) & 0 & \cdots & 0 \\ 0 & 0 & x_3(k) & \cdots & 0 \\ \vdots & \vdots & \vdots & \ddots & \vdots \\ 0 & 0 & 0 & \cdots & x_n(k) \end{bmatrix} \left(\begin{bmatrix} r_1 \\ r_2 \\ r_3 \\ \vdots \\ r_n \end{bmatrix} + \begin{bmatrix} A_{11} & A_{12} & A_{13} & \cdots & A_{1n} \\ A_{21} & A_{22} & 0 & \cdots & 0 \\ A_{31} & 0 & A_{33} & \cdots & 0 \\ \vdots & \vdots & \vdots & \ddots & \vdots \\ A_{n1} & 0 & 0 & \cdots & A_{nn} \end{bmatrix} \begin{bmatrix} x_1(k) \\ x_2(k) \\ x_3(k) \\ \vdots \\ x_n(k) \end{bmatrix} \right) \tag{4}$$

In order to analyze the group interaction and reconstruct the security awareness, the system is decomposed into multiple overlapping and the subsystem is replaced in the extended space.

First, we choose the full rank expansion matrix, the shrinkage matrix and the compensation matrix respectively

$$V = blockdiag\left([I_{11} \quad I_{11} \quad \cdots \quad I_{11}]^T, I_{22}, \quad \cdots, \quad I_{n-1n-1}, \quad I_{nn} \right) \tag{5}$$

$$U = blockdiag\left(\frac{1}{n-1} [I_{11} \quad I_{11} \quad \cdots \quad I_{11}], I_{22}, \cdots, I_{n-1n-1}, I_{nn} \right) \tag{6}$$

$$M_A = \frac{-1}{n-1} \begin{bmatrix} (2-n)A_{11} & A_{11} & \cdots & A_{11} & 0 & \cdots & 0 & 0 \\ A_{11} & (2-n)A_{11} & \cdots & A_{11} & 0 & \cdots & 0 & 0 \\ \vdots & \vdots & & \vdots & \vdots & & \vdots & \vdots \\ A_{11} & A_{11} & \cdots & (2-n)A_{11} & 0 & \cdots & 0 & 0 \\ A_{21} & A_{21} & \cdots & (2-n)A_{21} & 0 & \cdots & 0 & 0 \\ \vdots & \vdots & & \vdots & \vdots & & \vdots & \vdots \\ A_{n-11} & (2-n)A_{n-11} & \cdots & A_{n-11} & 0 & \cdots & 0 & 0 \\ (2-n)A_{n1} & A_{n1} & \cdots & A_{n1} & 0 & \cdots & 0 & 0 \end{bmatrix} \tag{7}$$

where, I_{ii}, (i = 1, 2, … n) is an unit matrix and have same dimensions with competition coefficient matrix.

According to the principle of complex system, the extended system and the original system have the following relations.

$$\tilde{A} = VAU + M_A \tag{8}$$

$$\tilde{r} = Vr \tag{9}$$

$$\tilde{x} = Vx \tag{10}$$

The competitive coefficient matrix of the extended system can be obtained by the inclusion relation:

$$\tilde{A} = \begin{bmatrix} A_{11} & 0 & \cdots & 0 & A_{12} & \cdots & A_{1n-1} & A_{1n} \\ 0 & A_{11} & \cdots & 0 & A_{12} & \cdots & A_{1n-1} & A_{1n} \\ \vdots & \vdots & & \vdots & \vdots & & \vdots & \vdots \\ 0 & 0 & \cdots & A_{11} & A_{12} & \cdots & A_{1n-1} & A_{1n} \\ 0 & 0 & \cdots & A_{21} & A_{22} & \cdots & 0 & 0 \\ \vdots & \vdots & & \vdots & \vdots & & \vdots & \vdots \\ 0 & A_{n-11} & \cdots & 0 & 0 & 0 & A_{n-1n-1} & 0 \\ A_{n1} & 0 & \cdots & 0 & 0 & 0 & 0 & A_{nn} \end{bmatrix} \tag{11}$$

Next, according to the principle of permutation inclusion in monograph [9], Symmetric replacement of subsystem position is conducted for an extended system. Assuming that the extended system has M subsystem, and $M = 2(n-1)$.if extended system $\tilde{x}_p = P_A^{-1}\tilde{x}$, we have

$$P_A = \overleftarrow{\prod}_{k=n-2}^{n-1} p_{Ak(k+1)} \overleftarrow{\prod}_{k=n-3}^{n} p_{Ak(k+1)} \cdots \overleftarrow{\prod}_{k=1}^{2(n-2)} p_{Ak(k+1)} \tag{12}$$

$$p_{Ak(k+1)} = blockdiag\left(I_1, \cdots, I_{k-1}, \begin{bmatrix} 0 & I_k \\ I_{k+1} & 0 \end{bmatrix}, I_{k+2}, \cdots, I_M\right) \tag{13}$$

We can get the competitive coefficient matrix of the extended system

$$\tilde{A}_P = P_A^{-1}\tilde{A}P_A = \begin{bmatrix} A_{11} & A_{12} & 0 & 0 & \cdots & 0 & A_{1n} \\ A_{21} & A_{22} & 0 & 0 & \cdots & 0 & 0 \\ 0 & A_{12} & A_{11} & A_{13} & \cdots & 0 & 0 \\ 0 & 0 & A_{31} & A_{33} & \cdots & 0 & 0 \\ \vdots & \vdots & \vdots & \vdots & & \vdots & \vdots \\ 0 & A_{12} & 0 & A_{13} & \cdots & A_{11} & A_{1n} \\ 0 & 0 & 0 & 0 & \cdots & A_{n1} & A_{nn} \end{bmatrix} \tag{14}$$

After the extension and replacement, the security awareness state vector of the group security awareness competition system is converted into $\tilde{x}_p = \left[x_1^T, x_2^T, x_1^T, x_3^T, \cdots, x_1^T, x_n^T\right]^T$ in the extended system, and the competition coefficient matrix is converted into the $\tilde{A}_P$. Therefore, the diagonal block system of the extended system is composed of the subsystem of the overlapping decomposition of star structure. That is:

$$S_{1j} : \begin{bmatrix} x_1(k+1) \\ x_j(k+1) \end{bmatrix} - \begin{bmatrix} x_1(k) \\ x_j(k) \end{bmatrix} = \begin{bmatrix} x_1(k) & 0 \\ 0 & x_j(k) \end{bmatrix} \left(\begin{bmatrix} r_1 \\ r_j \end{bmatrix} + \begin{bmatrix} A_{11} & A_{1j} \\ A_{j1} & A_{jj} \end{bmatrix} \begin{bmatrix} x_1(k) \\ x_j(k) \end{bmatrix} \right) \quad j = 2, 3, \cdots, n \tag{15}$$

Therefore, the research on the interaction of the security awareness and the reconstruction of the security awareness can be transformed into the study of the interaction between each pair of subsystems and the reconstruction of the security awareness of each group.

4 Pairs of Subsystem Security Awareness Reconstruction

In order to divide the safety consciousness and the consciousness violation of employees, the logic judgment function is introduced:

$$\xi(x,\gamma) = \mathrm{sgn}(\gamma - x) = \begin{cases} 1 & x < \gamma \\ 0 & x \geq \gamma \end{cases} \tag{16}$$

where, γ is safety awareness standard line, If the employee safety awareness is greater than or equal to the standard line, the employee's safety awareness is safe, that is 0, otherwise the violation of consciousness, that is 1.

According to the employee safety awareness questionnaire data and safety behavior data, evaluate the safety awareness of employees, establish a sense of safety and awareness database. We take S_{1j} as an example to reconstruct the security awareness. The goal of refactoring is to realize the security awareness of employees and tend to the ideal security awareness intensity x_{si}.

Assuming that x_1, x_j can be controlled, then the security awareness reconfiguration system is

$$\begin{cases} x_1(k+1) - x_1(k) = x_1(k)(r_1 + a_{11}x_1(k) + a_{ij}x_j(k) + u_1(k)) \\ x_j(k+1) - x_j(k) = x_j(k)(r_j + a_{jj}x_j(k) + a_{j1}x_1(k) + u_j(k)) \end{cases} \quad j = 2, 3, \cdots, n$$

According to the single employee in the upper system, the decentralized feedback controller is designed to make the security awareness stable.

$$u^c(k) = \begin{bmatrix} u_1^c(k) \\ u_j^c(k) \end{bmatrix} = -K_{1j} \begin{bmatrix} x_1(k) \\ x_j(k) \end{bmatrix} \tag{17}$$

Where, $K_{1j} = \begin{bmatrix} k_{11} & 0 \\ 0 & k_{jj} \end{bmatrix}$, and k_{11}, k_{jj} are constants.

In order to make employee safety awareness on stable and consistent, each of the employees need to design a coordination device to coordinate the relationship between them. These basic Coordinator are as follow:

$$u^d(k) = \begin{bmatrix} u_1^d(k) \\ u_j^d(k) \end{bmatrix} = -L_{1j} \begin{bmatrix} x_1(k) \\ x_j(k) \end{bmatrix} \tag{18}$$

Where, $L_{1j} = \begin{bmatrix} 0 & l_{1j} \\ l_{j1} & 0 \end{bmatrix}$, and l_{1j}, l_{j1} are constants.

Integrated formula (17) and (18), a decentralized coordination controller can be obtained for a pair of employees

$$u_{1j}(k) = \begin{bmatrix} u_1(k) \\ u_j(k) \end{bmatrix} = K_{D1j} \begin{bmatrix} x_1(k) \\ x_j(k) \end{bmatrix} \tag{19}$$

Where, $K_{D1j} = \begin{bmatrix} k_{11} & l_{1j} \\ l_{j1} & k_{jj} \end{bmatrix}$.

The decentralized coordination controller for each employee in the system is as follow

$$u_p = -K_D x_p \tag{20}$$

Where, $K_D = blockdiag\left(\cdots, \begin{bmatrix} k_{11} & l_{1j} \\ l_{j1} & k_{jj} \end{bmatrix}, \cdots\right)$

For enterprise management system, decentralized coordination controller can be implemented by managers or virtual robots.

1. Managers through the cognitive, emotional and psychological counseling and other basic methods, advocacy, education, learning and understanding of all countries and enterprises related to safety policies and regulations. Leader will play an emotional advantage in enhancing the safety awareness of local informal groups.
2. An individual with a virtual individual robot is equipped with a radio frequency identification (RFID card) as a fixed or moving object, To assist to complete the demonstration and monitoring of safety awareness and improve the level of employees.
3. Through the interaction between the virtual individual robot and the individual employees to carry out safety education, case study and early warning exercises, the individual's safety consciousness is reconstructed.
4. the level of safety awareness of individual or group put into the performance evaluation indicators of all enterprises.

5 Simulation Analysis

Consider the following system

$$\begin{cases} x_1(k+1) - x_1(k) = x_1(k)(r_1 + a_{11}x_1(k) + a_{ij}x_j(k) + u_1(k)) \\ x_j(k+1) - x_j(k) = x_j(k)(r_j + a_{jj}x_j(k) + a_{j1}x_1(k) + u_j(k)) \end{cases} \quad j = 2, 3, \cdots, n$$

Select a team of 5 employees' security awareness statistical data in an enterprise, using principal component analysis and cluster analysis method, evaluated the safety awareness of employees, can get the comprehensive score of safety awareness of all employees, and the safety awareness score as the safety awareness of reconstruction of the initial state. 1 of employees with a standard safety awareness of the strength of the leading individuals, play a guiding role, and the standard safety awareness intensity of

x_{si} = 500. The initial state is x_i (0) = [500, 350, 420, 450, 380]$^{\mathrm{T}}$. initial growth rate r_i = 0.05.

Set up the standard line of safety awareness $\gamma = 400$, by the formula (2-3-1) can determine the staff 2 and 5 with a sense of violation. So staff 2 and 5 need to reconstruct safety awareness.

Safety awareness competition coefficient matrix

$$A_{ij} = \begin{bmatrix} -1 & -0.06 & -0.05 & -0.04 & -0.03 \\ 0.08 & -1 & 0 & 0 & 0 \\ 0.07 & 0 & -1 & 0 & 0 \\ 0.065 & 0 & 0 & -1 & 0 \\ 0.08 & 0 & 0 & 0 & -1 \end{bmatrix}$$

Adding a state feedback decentralized coordinated control at the initial moment

$$u_{12}(0) = \begin{bmatrix} 0.05 & 0.01 \\ 0.02 & 0.08 \end{bmatrix} \begin{bmatrix} x_1(0) \\ x_2(0) \end{bmatrix}, \; u_{13}(0) = \begin{bmatrix} 0.03 & 0.02 \\ 0.04 & 0.06 \end{bmatrix} \begin{bmatrix} x_1(0) \\ x_3(0) \end{bmatrix},$$

$$u_{14}(0) = \begin{bmatrix} 0.06 & 0.03 \\ 0.05 & 0.04 \end{bmatrix} \begin{bmatrix} x_1(0) \\ x_4(0) \end{bmatrix}, \; u_{15}(0) = \begin{bmatrix} 0.04 & 0.03 \\ 0.02 & 0.07 \end{bmatrix} \begin{bmatrix} x_1(0) \\ x_5(0) \end{bmatrix},$$

The simulation results are shown in Figs. 1 and 2

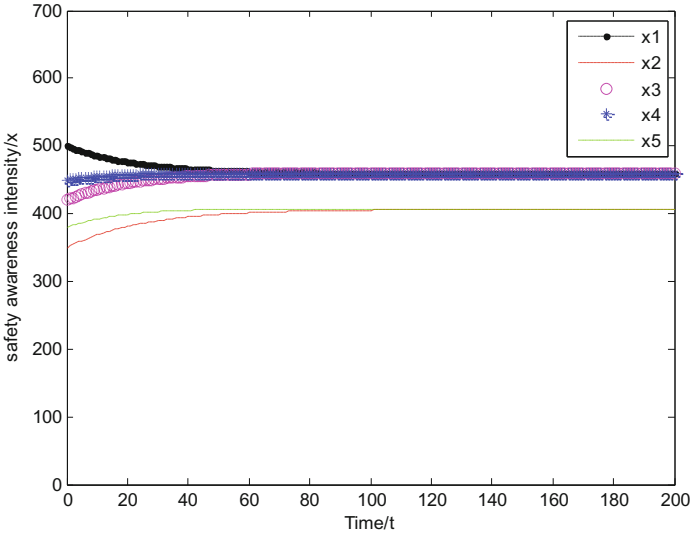

Fig. 1. The change curve of safety awareness intensity without the decentralized coordination control

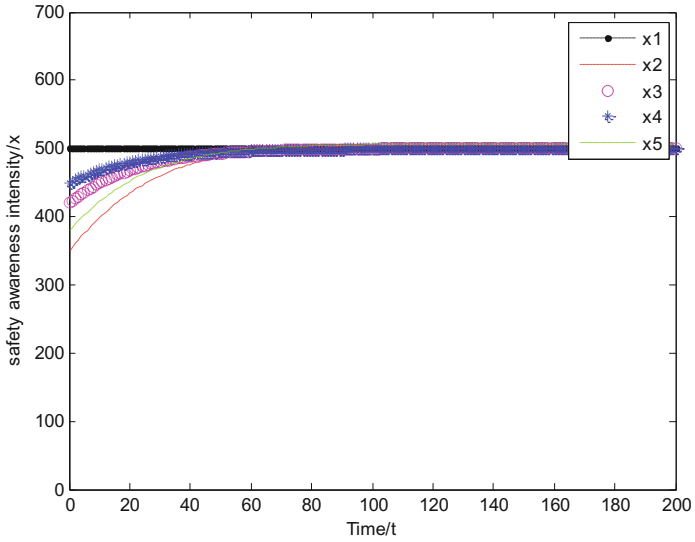

Fig. 2. The change curve of safety consciousness intensity with the added state coordination control

As can be seen from Figs. 1 and 2, in the process of the interaction of safety awareness, if the necessary control measures are not applied, the change curve of the safety consciousness intensity of the original system can not be consistent as shown in Fig. 1. Employees 2 and 5 of the low sense of security awareness, is a violation of consciousness. And the safety awareness of individual leaders is affected by the employees' consciousness of violation of regulations. If the system is decentralized coordinated feedback control, the simulation curve of the system is shown in Fig. 2. The intensity of safety awareness tends to be the ideal safety consciousness, and the goal of safety consciousness reconstruction is achieved.

Acknowledgments. This research reported herein was supported by the NSFC of China under Grant No.71571091

References

1. Kunshan particularly significant explosion accident investigation report. http://news.xinhuanet.com/talking/2014-12/31/c-1113836952.html. (in Chinese)
2. Li, X.Y.: Coping strategies for multi dimensional high risk society: a reflection on the "8.12" special fire and explosion accident in tianjin port. People's Forum **9**, 63–64 (2015). (in Chinese)
3. Jiang, L., Yu, G., Li, Y., Li, F.: Perceived colleagues safety knowledge/behavior and safety performance: "safety climate as a moderator in a multilevel study. Accid. Anal. Prev. **42**, 1468–1476 (2010). (in Chinese)

4. Sun, A.J., Liu, M.: The dilemma of the practice of behavior safety management theory and its solution in China. J. saf. sci. **19**, 58–63 (2009). (in Chinese)
5. Tam, C.M., Fung, I.H.: Study of attitude changes in people after the implementation of a new safety management system: the supervision plan. Constr. Manag. Econ. **19**, 393–403 (2001)
6. Wen, X.Z.: Preliminary study on occupation safety awareness of civil aviation pilots. Chin. Saf. Sci. J. **17**, 26–33 (2007). (in Chinese)
7. Conrad, P., Bradshaw, Y.S.: Helmets, injuries and culture definitions: motorcycle injury in urban indonesia. Accid. Anal. Prev. **28**, 193–200 (1996)
8. Chen, X.B., Sun, Q.B.: Research on the reconstruction of unsafe behavior based on safety consciousness. J. Univ. Sci. Technol. Liaoning, 387–395 (2015) (in Chinese)
9. Chen, X.B.: The principle and application of the system. Sci. Press, 187–189 (2012). (in Chinese)

Safety Awareness Emergence and Behavior-Based Safety Management in Enterprise

Xiaohui Zhang[1(✉)], Xuebo Chen[1(✉)], and Qiubai Sun[2]

[1] School of Electronics and Information Engineering, University of Science and Technology Liaoning, Anshan 114051, Liaoning, China
2275427570@qq.com, xuebochen@126.com
[2] School of Business Administration, University of Science and Technology Liaoning, Anshan 114051, Liaoning, China

Abstract. Some measures of safety management based on cellular automata model are introduced. Firstly, single employee's model could be established. Employees have been divided into three safety states. Each employee has six neighbors which mean hexagon cell is used. Taking employee' s awareness into consideration. Some safety related definitions are given and local transition rules are built. Then three different emergences could be observed in the ideal condition. Overall safety situation shows strong randomness in the different initial conditions and could be divided into three kinds. Key factors of the safety awareness emergence could be found through analysis. Finally, combined with the behavior-based safety management system concept and the key factor above, some specific measures such as education and punishment are put forward. When safety management measure is used, there are only one form of emergence and overall safety situation rises clearly.

Keywords: Safety awareness · Cellular automata (CA) · Model simulation · Behavior-based safety management system (BBS) · Emergence

1 Introduction

Recently, with the rapid development of China, safety production has become an increasingly significant problem. As we still remember that in 2013 the accidents of the explosion of the oil pipeline in Qingdao which caused 62 deaths and 136 disabling injuries, with a combined cost of 750 million Yuan. In 2014, the dust explosion in Kunshan Zhongrong mental products cooperation gave rise to 146 deaths and 114 injuries. Those accidents remind us that we always meet the challenge of work safety. Safety has historically been regarded as an engineering problem. With the study in depth, researchers have become acknowledge that three factors, which can be described as human, equipment and environment, play important roles in enterprise safety. Therefore investigations have been made according to these three factors. Of all the three above, human is in the first place, for human is not only the subject of safety but

D.N. Cassenti (ed.), *Advances in Human Factors in Simulation and Modeling*,
Advances in Intelligent Systems and Computing 591, DOI 10.1007/978-3-319-60591-3_8

also, the object. According to Heinrich, nearly 98% percent accidents were caused by human unsafe factors and only 2% accidents were caused by unresisting factors, based on statistics of 75,000 industrial accidents [1]. That means those 98% accidents could be controlled if appropriate measures are taken. One effective method used to modify unsafe behavior is behavior-based safety (BBS) [2]. BBS is widely applied in Europe and American since 1980s. This method can be induced that human safety awareness and safety habits are not inborn and invariant but could be improved by safety management and training [3]. People could effect and be effected by others. Taking the enterprise as an example. BBS aims to motivate employees to improve their own performance. By effecting and being affected by others, most employees will finally improve their safety awareness. According to BBS, human unsafe awareness and behavior are the root of accidents. Thus, by improving employees' safety awareness, accident rate could decrease.

For over 30 years, BBS has been used in variety of industries such as petroleum industry [4–6], construction [7, 8], the nuclear power industry [9], traffic [10], the transport industry [10, 11], mining [12] and machinery [13, 14].

Among all the researches, one area has received little attention. That is the relation of local interconnection of employees and the emergence of overall safety awareness. This paper, by using cellular automata (CA), model for single employee's safety awareness is established. Different from traditional quadrilateral cell, hexagonal cell is used. After setting local transition rules, overall employee safety awareness emergence in ideal condition could be observed. Thus key factor in the emergence could be found. Finally, combining simulation results and BBS, several measurements are introduced.

2 Model Constructing

Cellular automata (CA) is a discrete model originally discovered in the 1940s by Stanislaw Ulam and John von Neumann [15]. One CA consists of a regular grid of cells, each in one of a finite number of states. For each cell, a set of cells called its neighborhood is defined relative to the specified cell. An initial state is selected by assigning a state for each cell. A new generation is created, according to some fixed rule that determines the new state of each cell in terms of the current state of the cell and the states of the cells in its neighborhood. Typically, the rule for updating the state of cells is the same for each cell and does not change over time, and is applied to the whole grid simultaneously. Although its simple construction, cellular automata is capable of complex behavior [16].

Being different from familiar mathematical models which are based on equations and describe smooth variation of parameters, CA provides a model describing the discrete evolution of many components. Thus CA model is particularly suitable for highly nonlinear regimes [17]. For over 70 years, CA model is well used in mathematics and computer science [18]. It is also used in other areas such as landscape change [19], mapping [20] and virus [21].

CA model is made up of single cell $C_{(i,j)}$, which can be defined as a quaternion:

$$\mathrm{C} = \{L_d, S, N, f\}. \tag{1}$$

(1) In the quaternion, L_d is the 2-dimonsional hexagonal lattice. L_d stands for all employees in this paper and could be described as:

$$L_d = \left\{C_{(i,j)} \middle| i,j \in Z, 0 \le i \le L, 0 \le j \le L\right\}. \tag{2}$$

where (i, j) is the coordinate of one cell in L_d

(2) In the quaternion, S is a set of discrete cell states of one cell. In this paper, S could be defined as safety states of one employee $C_{(i,j)}$. S = {0, 1, 2}, where 0 indicates individual has poor safety awareness, 2 indicates individual has strong safety awareness and 1 indicates individual has general safety awareness which is between poor safety awareness and strong safety awareness. S is used as a qualitative analysis for individual's safety states. Different safety states have different quantization ranges which will be subdivided by safety assessment value introduced below.

(3) In the quaternion, N stands for the neighborhood. Two often-used neighborhoods are the von Neumann neighborhood and the Moore neighborhood (see Fig. 1a, b). Considering that the background of this paper is enterprise safety, those two neighborhoods are not suitable enough for this research. Von Neumann neighborhood's four neighbors seems not enough. Moore neighborhood makes up of four neighbors shared edges and four neighbors shared angles with the central cell. Distances from the center of the central cell to the center of those two kinds of neighbors are different, which means different influence may be exerted to the central cell by those two kinds. Taking those factors into consideration, a hexagon-cell CA model is used in this paper (see Fig. 1c).

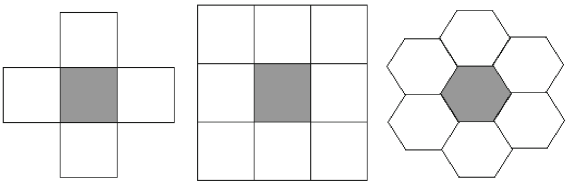

a. von Neumann **b.** Moore **c.** Hexagon

Fig. 1. Two dimensional neighborhood

Because of the special shape of the cell, rectangular coordinate system is not convenient to represent hexagon-cell CA model. Therefore a hexagon-cell coordinate system is introduced in this paper. (see Fig. 2).

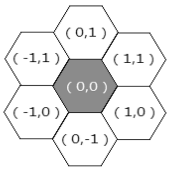

Fig. 2. Hexagon cell coordinate system

For the central cell $C_{(i,j)}$, its neighborhood can be defined as:

$$N_{(i,j)} = \left\{C_{(i,j+1)}, C_{(i,j-1)}, C_{(i-1,j+1)}, C_{(i+1,j+1)}, C_{(i-1,j)}, C_{(i+1,j)}\right\}. \tag{3}$$

(4) In the quaternion, f is transition rule. In CA model, central cell's safety state in t + 1 moment is up to its own state and its neighbors' in t moment. Function f can be defined as:

$$\mathrm{S}_{(i,j)}^{t+1} = f\left(N_{(i,j)}^{t}, S_{(i,j)}^{t}\right). \tag{4}$$

In addition to the above, in order to describe the interaction among employees in the enterprise more accurately several more definitions based on BBS will be introduced below.

2.1 Definition 1: Local Safety Climate S_p

A comprehensive consideration of the neighborhood of the central cell $C_{(i,j)}$:

$$S_p = \sum S_{N_{(i,j)}}^{t}. \tag{5}$$

Where $S_{N(i,j)}^{t}$, represent the safety states of $C_{(i,j)}$'s six neighbors, ranges from 0 to 12.

In this paper, two influence factors are considered. Employees are influenced not only by their own emotions and habits but also by the environment around them. When working in the enterprise, employees' safety awareness would be expressed through their words and behaviors. In local space of one enterprise, employees' safety awareness and their behaviors would continually interact and finally form some kind of safety climate.

2.2 Definition 2: Safety Assessment Value S_v

$$S_v = \mathrm{ranint}[0, 99]. \tag{6}$$

Where ranint [0, 99] means a random integer ranging from 0 to 99. As it mentioned above, S_v gives the specific value of a safety state. The larger the number, stronger safety awareness one employee will have. We all know that changing from one state to another is hardly a transient process, especially human's awareness. Habit formation and awareness changing of employees are a process from quantitative changes to qualitative changes. Under the transition rules established, employee's S_v will change. When S_v is higher or lower than some threshold, employee's safety state will change.

2.3 Definition 3: Overall Safety Situation S_o

The total of the employees' safety assessment value:

$$S_o^t = \sum_{i=0}^{L} \sum_{j=0}^{L} S_{v(i,j)}^t. \tag{7}$$

Which superior limit is $S_{omax}^t = 99L^2$. The superior limit of S_o has only theoretical significance and S_o couldn't reach $99L^2$ in practice.

Using CA model to simulate employee's safety awareness emergence is intuitive. Final emergence can be observed easily. However, there may be a lack of quantitative description for the trend of overall safety awareness. So S_o is introduced in this paper to indicate overall safety awareness in the enterprise. The target of safety management is to promote S_o.

3 Simulations in Ideal Conditions

First of all, transition rules in ideal condition are established. Allocating a random S_v to each employee, which means employees' awareness and behaviors have 100 possibilities. Then these 100 possibilities are divided into three kinds of groups in the ratio of 1:2:1. If S_v is less than 25, the employee has poor safety awareness and his safety state can be represent by 0 in S. If S_v is more than 74, the employee has strong safety awareness and his safety state can be represent by 2 in S. If $S_v \in [25, 74]$, the employee has general safety awareness and his safety state can be represent by 1 in S. Those accord with ideal normal distribution. Those three kinds of groups can be defined as three kinds of heterogeneous individuals that have different character traits. Employees who have strong safety awareness also have strong autonomy. General safety awareness employees are easily influenced by others. Employees who have poor safety awareness also sluggishness. Taking those traits into consideration, specific transition table is shown in Table 1.

According to the transition rule, in the ideal condition, simulations of safety awareness emergence in an enterprise based on Netlogo are carried out. Initial conditions are as follows: sets the number of L_d $26^{2,}$ namely, 676. Allocating each cell with a random S_v successively. Run the program for 50 times. Final emergences could be divided into three cases as below:

Table 1. Transition table

S_v	Safety state	S_p	ΔS_v
[0, 24]	0	[0, 4]	−3
		[5, 9]	0
		[10, 12]	+1
[25, 74]	1	[0, 5]	−2
		6	0
		[7, 12]	+2
[75, 99]	2	[0, 2]	−1
		[3, 7]	0
		[8, 12]	3

Figures 3, 4 and 5(a) shows the final emergence where dark grey cells, light grey cells and white cells represent 0 safety state employees, 1 safety state employees and 2 safety state employees respectively. Figures 3, 4 and 5(b) shows the variation trends of three different safety state employees. Red line, blue line and green line shows 2 safety state employees, 0 safety state employees and 1 safety state employees respectively. Figures 3, 4 and 5(c) shows the variation trend of overall safety situation.

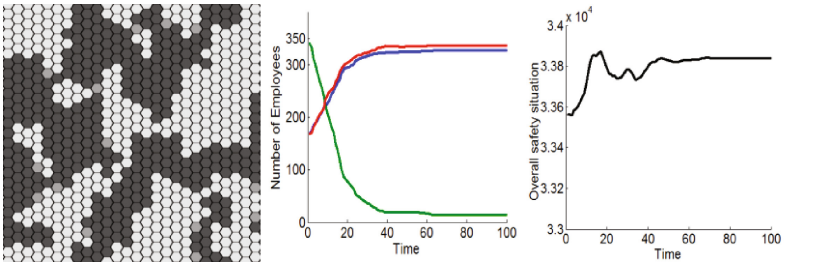

a. finally emergence **b.** trends of three categories situation **c.** trend of overall safety

Fig. 3. Case 1: overall safety situation almost remain unchanged

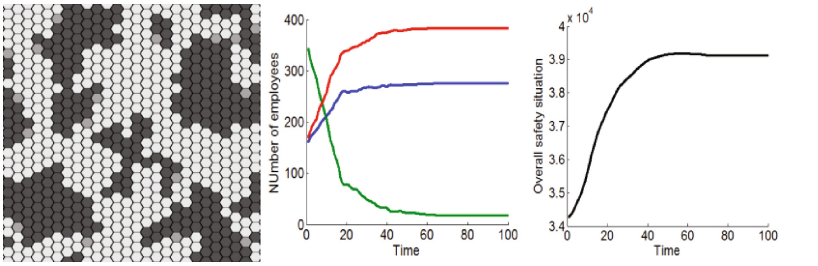

a. finally emergence **b.** trends of three categories situation **c.** trend of overall safety

Fig. 4. Case 2: overall safety situation rise

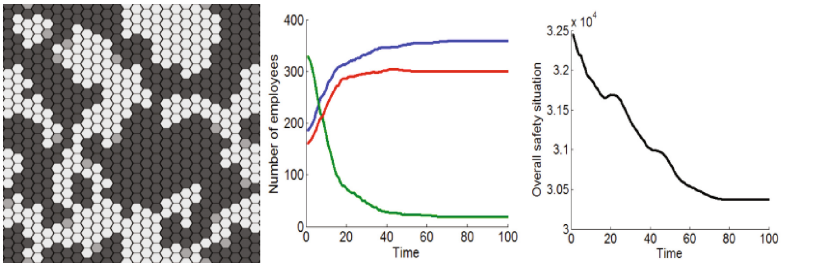

a. finally emergence **b.** trends of three categories situation **c.** trend of overall safety

Fig. 5. Case 3: overall safety situation decline

Based on three cases above, some conclusions could be drawn. Firstly, we could find that final emergences have strong randomness due to employees' initial safety state distribution. Secondly, regardless of final emergences' randomness, general safety employees would be transition to either strong safety state employees or poor safety state employees. So the key factor to increase overall safety situation is the dynamic behavior of general safety state employees.

4 Behavior-Based Safety Management Measures

In order to increase overall safety situation in all initial conditions. Some behavior-based safety managements should be considered. This paper gives two typical management measures: education and punishment.

4.1 Education for General Safety State Employee

Simulations above shows that general safety state employees play an important role in the emergence process. So the first measure is winning over these people. In 1980, Zohar found that safety climate is the overall perception for risky environment in an enterprise [22]. Based on this theory, James and Reichers divided safety climate into psychological climate and organizational climate two parts [23]. Better safety climate could give employees a positive intimation. Therefore production efficiency will rise and accident rate will decrease. Education aiming at general safety state employee could form a good safety culture and climate. After education, employee will reject unsafe behavior in his subconsciousness and learn from their neighbors about safety knowledge. In this way, each employee will improve his own safety awareness. Transition rules for general safety employees should be changed as follows: When local safety climate $S_p \in [0, 3]$, set $\Delta S_v = -2$; When local safety climate $S_p \in [4, 6]$, set $\Delta S_v = 0$; When local safety climate $S_p \in [7, 12]$, set $\Delta S_v = +2$.

Run the program for 50 times and observe results. Being different from the three cases in ideal conditions, this time final emergence has reduced to only one case. After education, the overall safety situation will always rise. Figure 6 is one of the 50 results.

Initial overall safety situation is around 33000. While when measures are taken, S_o rises significantly. In the 50 simulations, $S_o \in [42950, 56400]$ when final permanent state is reached. This result can prove that general safety state employees strengthen their safety awareness gradually after education. However, we also notice that number of poor safety state employees doesn't decrease apparently. Therefore education measures have little effect on poor safety state employees.

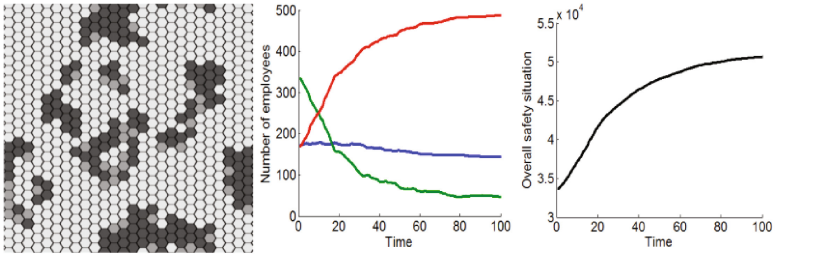

a. finally emergence **b.** trends of three categories situation **c.** trend of overall safety

Fig. 6. Emergence of safety awareness after education

4.2 Punishment for Poor Safety State Employee

Besides education, compulsory measure should also be considered. Thus punishment measures are used when an employee has poor safety awareness and repeated violations. By informed criticism in the whole enterprise and deduction for wages, those employees would realize their faults and pay the consequences. Their safety assessment value would rise rapidly to the general state. We consider that when employee's $S_v \in [0, 10]$, the punishment condition is met. In the next moment, set $\Delta S_v = +50$.

Run the program for 50 times and observe results. Final emergence has been reduced to only one case too. Figure 7 is one of the 50 results. After punishment, the overall safety situation rises more obviously comparing to education measure. In the 50 simulations, $S_o \in [57300, 63000]$ when final dynamic equilibrium state is reached. Besides, the number of poor safety awareness employees reduced obviously. This

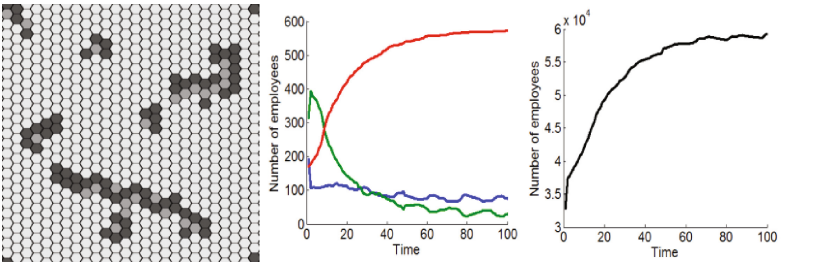

a. finally emergence **b.** trends of three categories situation **c.** trend of overall safety

Fig. 7. Emergence of safety awareness after punishment

results can prove that after punishment measures are used, both general and poor safety awareness employees will gradually raise their safety awareness.

5 Summary

Behavior-based safety management for enterprise employee is a long and arduous work calling for enterprise and employees' corporation. Basing on the CA model, model for single employee's safety awareness and transition rules for group interaction are established. Key factor has been found by analysis three simulation results in ideal conditions. Combining with the key factor and BBS, two management measures are introduced. After the measures are being used, simulations show that general safety state employees have to raise their safety awareness and number of poor safety state employees decreases rapidly. Thus overall safety situation has risen greatly.

Acknowledgments. This work was supported by the National Natural Science Foundation of China under contract number 71571091.

References

1. Heinrich, H.: Industrial Accident Prevention, 2nd edn. McGraw-Hill, New York (1941)
2. Chen, D., Tian, H.: Behavior based safety for accidents prevention and positive study in China construction project. Procedia Eng. **43**, 528–534 (2012)
3. Cooper, M.D.: Goal-setting for safety. Saf. Health Pract. **11**, 32–37 (1993)
4. Zohar, D., Luria, G.: The use of supervisory practices as leverage to improve safety behavior: a cross-level intervention model. J. Saf. Res. **34**(5), 567–577 (2003)
5. Fleming, M., Lardner, R.: Investigating behaviour modification programmes in the offshore oil and gas industry. Ryder-Marsh (Safety) Limited (2000)
6. Ismail, F., Hashim, A.E., Zuriea, W., Ismail, W., Kamarudin, H., Baharom, Z.A.: Behaviour based approach for quality and safety environment improvement: Malaysian experience in the oil and gas industry. Procedia-Soc. Behav. Sci. **35**, 586–594 (2012)
7. Laitinen, H., Marjamaki, M., Paivarinta, K.: The validity of the TR safety observation method on building construction. Accid. Anal. Prev. **31**, 463–472 (1999)
8. Lingard, H., Rowlinson, S.: Behavior-based safety management in Hong Kong's construction industry. J. Saf. Res. **28**(4), 243–256 (1997)
9. Cox, S., Jones, B., Rycraft, H.: Behavioural approaches to safety management within UK reactor plants. J. Saf. Sci. **42**(9), 825–839 (2004)
10. Olson, R., Austin, J.: ABCs for lone workers: a behavior-based study of bus drivers. J. Prof. Saf. **46**(11), 20–25 (2001)
11. Glendon, A.I., Litherland, D.K.: Safety climate factors, group differences and safety behaviour in road construction. J. Saf. Sci. **39**(3), 157–188 (2001)
12. Nai-wen, L., Da-jiang, J.: Application study on behavior-based safety in coal mine behavior management. China Saf. Sci. J. **21**(12), 115–121 (2011)
13. Ray, P.S., Bishop, P.A., Wang, M.Q.: Efficacy of the components of a behavioral safety program. Int. J. Ind. Ergon. **19**, 19–29 (1997)

14. Chandler, B., Huntebrinker, T.A.: Multisite success with systematic BBS a case study. J. Prof. Saf. 35–41 (2003)
15. Sarkar, P.: A brief history of cellular automata. J. Acm Comput. Surv. **32**(1), 80–107 (2000)
16. Wolfram, S.: Statistical mechanics of cellular automata. J. Rev. Mod. Phys. **55**(3), 601–644 (1983)
17. Wolfram, S.: Cellular automata as models of complexity. J. Nat. **311**(5985), 419–424 (1984)
18. Sarkar, P.: A brief history of cellular automata. J. Acm Comput. Surv. **32**(1), 80–107 (2000)
19. Onsted, J.A., Chowdhury, R.R.: Does zoning matter? A comparative analysis of landscape change in Redland, Florida using cellular automata. J. Landsc. Urban Plan. **121**(1), 1–18 (2014)
20. Arsanjani, J.J., Helbich, M., Bakillah, M., Loos, L.: The emergence and evolution of OpenStreetMap: a cellular automata approach. Int. J. Digit. Earth **8**(1), 1–30 (2015)
21. Burkhead, E., Hawkins, J.: A cellular automata model of ebola virus dynamics. Phys. A: Stat. Mech. Appl. **438**, 424–435 (2015)
22. Zohar, D.: Safety climate in industrial organizations: theoretical and applied implications. J. Appl. Psychol. **65**(4), 96–102 (1980)
23. James, L.A., James, L.R.: Integrating work environment perceptions: explorations into the measurement of meaning. J. Appl. Psychol. **74**, 739–751 (1989)

Emergent Research of Employee Safety Awareness Based on Multi-agent Model

Siyuan Fan[1(✉)], Xuebo Chen[1(✉)], and Qiubai Sun[2]

[1] School of Electronics and Information Engineering, University of Science and Technology Liaoning, Anshan, Liaoning 114051, China
1589026384@qq.com, xuebochen@126.com
[2] School of Business Administration, University of Science and Technology Liaoning, Anshan, Liaoning 114051, China

Abstract. In order to strengthen employees' safety awareness and reduce the probability of occurrence of employees' unsafe behaviors, an ABMS-based model was built for emergence of employees' safety awareness. Applying the software of Netlogo and adjusting the values of agents variables such as employee, manager and organization, effect of social environment on employees' safety awareness was simulated dynamically. The research results show that employees' safety awareness is an emergent phenomenon influenced by multiple agents, and that different agents affect employees' safety awareness differently—the agents, ranked in descending order, are as follows: education level, safety training level, emotional intelligence of managerial staff, and the importance the enterprise attaches to work safety; but effect of public opinion on employees' safety awareness has bidirectionality.

Keywords: Safety awareness · Emergence · Complex system · Agent based modeling and simulation (ABMS) · Netlogo simulation

1 Introduction

Recently, with the perfection of safety regulation of government, the number of safety accident showed a tendency of decline. However, the serious accidents still happen from time to time. For example, in July 2015, there was a severe explosion happening in port of Tianjin, which caused nearly 1000 deaths and injuries, with a heavy lost of 6.8 billion. This accident was defined as a extremely severe accident from the investigation team of state council. And the team indicated that this accident mainly is attributed to the weakness of safety awareness [1]. The theory of accident causation chains demonstrate that the essential reasons of accidents stem from unsafety behaviors of human and unsafe state of equipment [2]. A further study on the behavioral safety shows that it has a tight relationship between safety awareness and accident. Good safety awareness can decrease the probability of accident occurrence [3]. From complex system perspective, safety awareness can be regarded as one emergence of complex system in multi-factors' interaction [4]. So, it's very necessary that the research of safety awareness.

D.N. Cassenti (ed.), *Advances in Human Factors in Simulation and Modeling*,
Advances in Intelligent Systems and Computing 591, DOI 10.1007/978-3-319-60591-3_9

Nowaday, in home and abroad, there were few researches of safety awareness from the angel of complex system. The major methods are structural equation model (SEMS) [5] and analytical hierarchy process (AHP) [6]. But these methods still use the single and static thought to analyze the link between safety awareness and the impact factors. It should be use a dynamic analysize to research the emergent level of safety awareness in a period of time. Thereby, there will be some evidence which can help to formulate measures to prevent the happening of accidents. Consequently, here in this paper, by using the emergent property of complex system [7] and agent based modeling and simulation (ABMS) [8], and which apply in the research of safety awareness of employee. Thus, the multi-agents model of emergence of safety awareness will be constructed, which gets some simulation to improve the safety awareness of employee.

2 Model Constructing

The dynamic change of employees' safety awareness is a process that these agents of behavior affect safety awareness. It demonstrates the fact that safety awareness is the emergent phenomenon showed complex system. Then ABMS is the combination of complex system and artificial intelligent technology. According to the model based multi-agent, we can more specific to explain the principle how behavioral agents impact on safety awareness.

2.1 Behavioral Agents

This model is constructed based on complex system and the theory of ABMS. And three kinds of agents are created, employee, manager and organization. Then, every agent is defined different inherent attributes and the range of value by documents [8–10]. And all agents can communicate with social environment. All variables of agents have no units. Meanwhile, the variable "m" is defined as the step length of the simulation (unit day), the variable "n" is defined as the step number, and the range of value is from 0 to 60.

Agent of Employee. Inherent attributes: safety cognition x_1, skilled level x_2, safety attention level x_3, tiredness level x_4, educated level x_5 and the emergent level of safety awareness of employee $F(x_i)$. The range of educated level's value is [1, 10].

(1) In the process of work, tiredness level gradually is increasing. The increasing rate of tiredness level sets as b_m, $b_m \in [1\%, 2\%]$. x_4 can be given as a equation.

$$x_4 = 1.5 \prod_{1\%}^{2\%} (1 + bm)^n + \varepsilon_1 \tag{1}$$

$\varepsilon_{i(i\ =1,2,\ldots,7)}$ is remainders.

(2) $F(x_i)$ is impacted by the variables "$x_{i(i=1,2,\ldots,5)}$:", so

$$F(x_i) = \sum_{i=1}^{5} \alpha_i x_i + \omega_1 \tag{2}$$

The variable "$\alpha_{i(i=1,2,\ldots,5)}$" is defined as the correlation degree between "x_i" and "$F(x_i)$", and $\omega_{i(i=1,2,3,4)}$ is random disturbance term.

Agent of Manager. Inherent attributes: safety training degree y_1, the degree of safety punishment y_2, work emotion y_3, emotional intelligence y_4, the level of safety supervision y_5 and the level of safety management $F(y_i)$. The range of value of variables "y_1" and "y_4" is [1, 10] and [1, 5] respectively.

(1) As time goes by, the safety awareness of employee shows a tendency of decrease, the punishment intensity is introduced for restraining this tendency. The rate of punishment intensity variable is defined "c_m", $c_m \epsilon [3\%, 5\%]$. y_2 can be written as a formula.

$$y_2 = 0.4 \prod_{3\%}^{5\%} (1 + c_m)^n + \varepsilon_2 \tag{3}$$

(2) $F(y_i)$ is impacted by the variables "$y_{i(i=1,2,3,4)}$", so

$$F(y_i) = \sum_{i=1}^{5} \beta_i y_i + \omega_2 \tag{4}$$

The variable "$\beta_{i(i=1,2,\ldots,5)}$" is the correlation degree between "y_i" and "$F(y_i)$".

Agent of Organization. Inherent attributes: the level of safety investment z_1, the degree of safety importance z_2, cohesive force z_3, and the level of safety atmosphere $F(z_i)$. $z_2 \epsilon [0, 10]$.

(1) The level of safety investment is impacted by the enterprise own financial situation and the occurrence frequency of safety accident. So

$$z_1 = 2 \prod_{g=1}^{30} (1 + j_g) \prod_{h=31}^{60} (1 + j_h) + \varepsilon_3 \tag{5}$$

(2) $F(y_i)$ is impacted by the variables "$z_{i(i=1,2,3)}$", so

$$F(z_i) = \sum_{i=1}^{3} \gamma_i z_i + \omega_3 \tag{6}$$

Social Environment. In this model, the social environment has three elements: the equipment aging degree s_1, the comfortable degree of working space s_2, and the pressure of public opinion s_3. Three elements conclude the external affective degree of safety awareness of employee ($F(s_i)$). The variable "s_3" has dual effect on the safety

awareness of employee, $s_3 \epsilon [-10, 10]$. And the level of external safety is impacted by the variables "$s_{i(i=1,2,3)}$", so

$$F(s_i) = \sum_{i=1}^{3} \delta_i s_i + \omega_4 \tag{7}$$

The variable "$\delta_{i(i=1,2,3)}$"is defined as the correlation degree between "δ_i" and "$F(s_i)$".

2.2 The Rules of Interaction

(1) As time goes on, the safety cognition of employee (x_1) shows an improved tendency after accepting safety training. And it has the close connection with educated degree of employee and the degree of safety importance of enterprise.

$$x_1 = d_1 y_1 \prod_{1\%}^{2\%} (1 + \mu_m)^n + d_2 x_5 + d_3 z_2 + \varepsilon_4 \tag{8}$$

The variable "μ_m" is defined as the rate of safety cognition, $\mu_m \in [1\%, 2\%]$. The variable "$d_{i(i=1,2,3)}$" is defined as the correlation degree between "y_1, x_5, z_2" and "x_1".

(2) The degree of work efficiency(x_2) means that employee how to know the degree of job and working space. The variable "a_m" is defined the increasing rate about work efficiency, $a_m \in [3\%, 4\%]$, and the variable "x_2" is impacted by "y_1", "z_2" and "s_1".

$$x_1 = d_1 y_1 \prod_{1\%}^{2\%} (1 + \mu_m)^n + d_2 x_5 + d_3 z_2 + \varepsilon_4 \tag{9}$$

The variable "$a_{i(i=1,2,3)}$" is correlation degree between "y_1, z_2, s_1" and "x_2". In addition, the safety attention level(x_3) is impacted by "x_4, y_1, z_2 and s_3".

$$x_3 = f(x_2) + \phi_1 x_4 + \phi_2 y_1 + \phi_3 z_2 + \phi_4 s_3 \tag{10}$$

The variable "$\phi_{i(i=1,2,3,4)}$" is the correlation degree between "x_4, y_1, z_2, s_3" and "x_3". And the dynamic relation curve between safety attention level(x_3) and the degree of work efficiency(x_2) has different tendency in different times. At the early stage, employee is in the high spirit; in the middle time, the tendency of safety attention of employee shows a rising curve firstly, then, this curve shows a steady situation; finally, with the improvement of tiredness degree, the decreasing speed of safety attention level will be show the gradually rapid tendency. So

$$f(x_2) = q x_2 + \theta n \in [\mathrm{A,B}] \tag{11}$$

The variable "n" is the steps' number, "[A, B]" is defined the value range of step's number.

$$q = (0.6, 0.1, -0.4, -0.2)^{\mathrm{T}}, [\mathrm{A}, \mathrm{B}] = ([\mathrm{A}_i, \mathrm{B}_i])^T = ([0, 10], (10, 25], (25, 45], (45, 60])^T$$

(3) work emotion(y_3) is impacted by the variables "y_4, z_3, s_2, and s_3".

$$y_3 = m_1 y_4 + m_2 z_3 + m_3 s_2 + m_4 s_3 \tag{12}$$

The variables "$m_{\mathrm{i(i=1,2,3,4)}}$" is the correlation degree between "y_4, z_3, s_2, s_3" and "y_3". And the level of safety supervision (y_5) has close relation with the variables "y_3, x_1, x_5, z_1, s_1".

$$y_5 = n_1 y_3 + n_2 x_1 + n_3 x_5 + n_4 z_1 + n_5 s_1 \tag{13}$$

The variable "$n_{\mathrm{i(i=1,2,\ldots,5)}}$" is the correlation degree between "y_3, x_1, x_5, z_1, s_1" and "y_5".

(4) As time goes by, the behavior and psychology of employee gradually become consent. The whole enterprise's cohesive force (z_3) gets a huge improvement under the effect of the variables "x_1, y_1, s_3".

$$z_3 = 1.2\lambda_1 x_1 \prod_{1\%}^{2\%} (1 + \eta_m)^n + \lambda_2 y_1 + \lambda_3 s_3 + \varepsilon_6 \tag{14}$$

The variable "η_{m}" is defined as the rate of group psychology, $\eta_{\mathrm{m}} \in [1\%, 2\%]$. The variable "$\lambda_{\mathrm{i(i=1,2,3)}}$" is the degree of correlation between "x_1, y_1, s_3" and "z_3".

(5) The equipment aging degree (s_1) is increasing with time, but it can reduce the rate of equipment aging degree with the improvement of safety awareness and safety investment. So

$$s_1 = \prod_{i = g, h} [1 + (\kappa_m - e_1 j_i)]^n + e_2 x_1 + e_3 z_2 + \varepsilon_7 \tag{15}$$

The variable "κ_{m}" is defined as the rate of equipment aging degree, $\kappa_{\mathrm{m}} \in [0.5\%, 1\%]$. The variable "$j_{\mathrm{i(i=g,\ h)}}$" is defined as the rate of safety investment, $j_{\mathrm{g}} \in [-2\%, 3\%]$, $\mathrm{n} \in [1, 30]$; $j_{\mathrm{h}} \in [-1\%, 4\%]$, $\mathrm{n} \in [31, 60]$. The variable "e_1" is defined as the correlation parameter between "$j_{\mathrm{i(i=g,\ h)}}$" and "s_1"; the variables "e_2, e_3" is defined as the correlation parameter between "x_1, z_2" and "s_1".

3 Model Initialization

In the experiment of simulation, in order to the result of simulation nearly reaches the reality, according to the references [9–12] and the related questionnaire, finally, it determines the value of all parameters (Tables 1, 2 and 3).

Table 1. Simulation variable coefficients in multi-agent model and their values

Parameters	α_1	α_2	α_3	α_4	α_5	β_1	β_2	β_3	β_4	β_5	γ_1	γ_2	γ_3	δ_1	δ_2	δ_3
Value	0.2	0.35	0.2	−0.2	0.25	0.3	0.2	0.4	0.5	0.3	0.35	0.4	0.25	−0.2	0.3	0.4

Table 2. Simulation weigh coefficients in multi-agent model and their values

Parameters	d_1	d_2	d_3	m_1	m_2	m_3	m_4	n_1	n_2	n_3	n_4	n_5	φ_1	φ_2	φ_3	φ_4
Value	0.3	0.25	0.3	0.5	0.25	0.3	−0.45	0.2	0.1	−0.3	0.2	−0.15	0.2	0.4	−0.3	0.3

Table 3. Correlation coefficients in multi-agent model and their values

Parameters	λ_1	λ_2	λ_3	e_1	e_2	e_3	a_1	a_2	a_3
Value	0.3	0.4	0.2	0.3	0.2	−0.4	0.2	0.1	−0.2

4 The Analysis of Simulation Result of Safety Awareness of Employee

4.1 The No Control Mode

The mode of no control means that the enterprise has no measure with safety awareness of employee. The array [x_5, y_1, y_4, z_2, s_3] is assigned to [1, 0, 1, 0, −10], when the variable "n" equals to 1. The following arrays are all assigned value in the variable "n" equals to 1. As shown in Fig. 1.

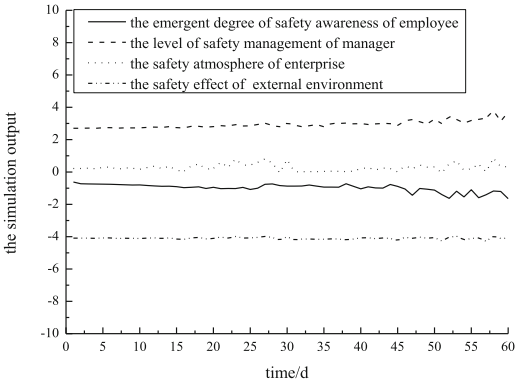

Fig. 1. Simulation output in no control mode

From the simulation output in the Fig. 1: four variables show the steady tendency in the whole curve. It reveals that the output of simulation of four variables has the low value in the initial phase, then four variables all have no improvement. It is possible because of the no control mode that there is no any external or internal element to work safety awareness.

4.2 Benchmark Mode in Controlled Condition

The array[x_5, y_1, y_4, z_2, s_3] is assigned to [5, 5, 1, 5, 5], the output of simulation serve as the criterion of comparison in analytical mode. As shown in Fig. 2.

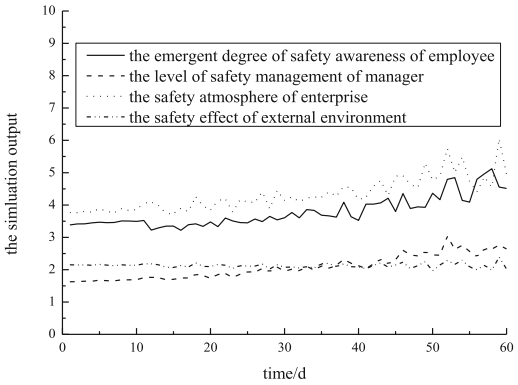

Fig. 2. Simulation output in benchmark mode

4.3 The Analysis of Output of Simulation in the Analytical Mode

To improve the educated degree (x_5), the array [x_5, y_1, y_4, z_2, s_3] is assigned to [10, 5, 1, 5, 5], as shown in Fig. 3.

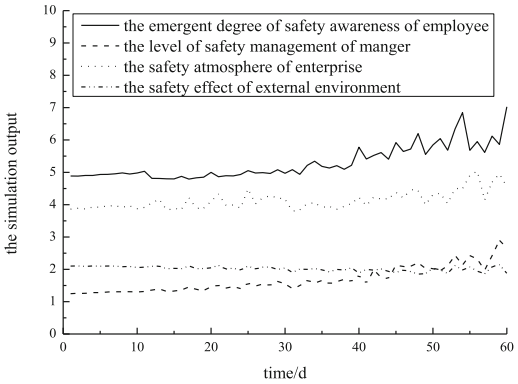

Fig. 3. Simulation output of improved degree of education

In Fig. 3, it demonstrates that the output of safety awareness has a leap in contrasting with the benchmark mode. The improvement of educated degree means that the enterprise hires a group of educated workers. Because these workers have the high level of safety cognition, this makes the safety awareness of employee has a leap. And the cohesive force of enterprise also gets a certain degree of improvement.

To improve the safety training degree (y_1), the array [x_5, y_1, y_4, z_2, s_3] is assigned to [5, 10, 1, 5, 5], as shown Fig. 4.

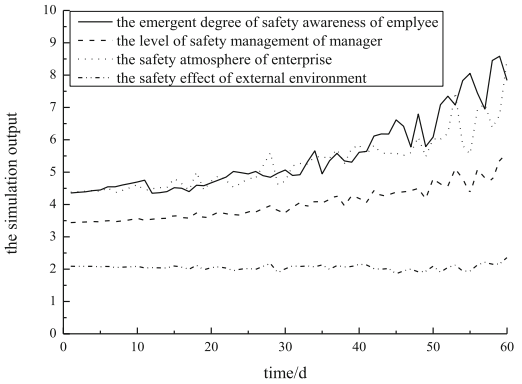

Fig. 4. Simulation output of advanced safety training

In the Fig. 4, to compare with the Fig. 2, the simulation output of the safety awareness of employee has a huge improvement and shows the accelerating tendency. The safety atmosphere also has a certain degree of promotion. It reflects that the level of safety cognition and the work efficiency have been improved, so that the safety awareness of employee creates an enormous improvement. The advance of safety awareness is fed back to the agent of organization, thus the safety awareness of employee and the work efficiency are further enhanced. It constitutes a positive feedback loop.

To improve the emotional intelligence (y_4), the array [x_5., y_1, y_4, z_2, s_3] is assigned to [5, 5, 5, 5, 5], as shown Fig. 5.

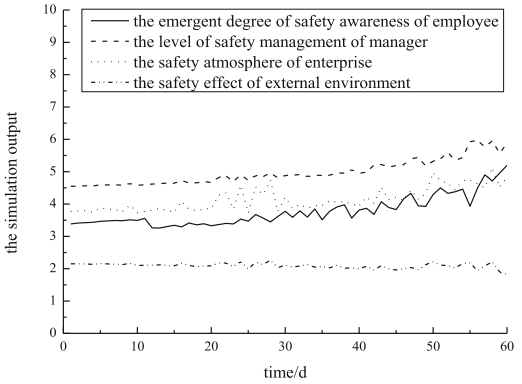

Fig. 5. Simulation output of improved intelligence of managers' emotion

From the Fig. 5, although the level of safety management gets great growth, but the safety awareness of employee almost has no promotion. It shows that the improvement of emotional intelligence has no much effect on the safety awareness.

To improve the degree of safety importance (z_2), the array[x_5, y_1, y_4, z_2, s_3] is assigned to [5, 5, 1, 10, 5], as shown Fig. 6.:

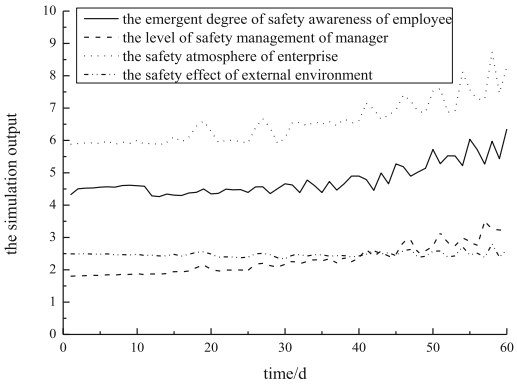

Fig. 6. Simulation output of improved level of safety importance

In the Fig. 6, to compare with Fig. 2, the safety atmosphere has a huge improvement, however, the safety awareness of employee has a small leap in the simulation output. It reveals that safety atmosphere just is the external factor to improve the safety awareness of employee. But employees' own safety cognition has not been substantial improvement. Safety cognition has the conclusive effect on the safety awareness of employee. Only the safety cognition of employee obtains the improvement, the safety awareness of employee can get the fundamental change.

The pressure of public opinion(s_3) has the dual effect on the safety awareness of employee. So the variable "s_3" is assigned to 10 and −10, respectively. So the array is defined as [5, 5, 1, 5, 10] and [5, 5, 1, 5, −10], respectively. As shown Figs. 7 and 8.:

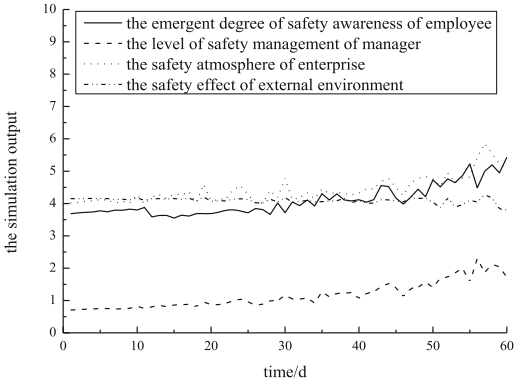

Fig. 7. Simulation output under positive effect of external public opinion

From the Fig. 7, under the positive effect of external public opinion, the safety awareness of employee only has a small growth. Because the enterprise is relatively closed system, the external public opinion only has a little bit influence on the safety awareness of employee.

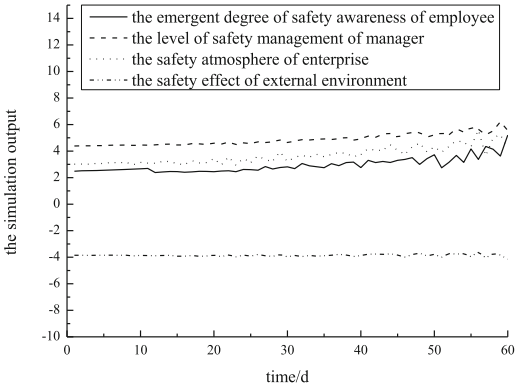

Fig. 8. Simulation output under negative effect of external public opinion

From Fig. 8, under the negative effect of external public opinion, the work emotion of employee has been disturbed, so that safety attention will have a certain degree of decline. However, safety cognition and work efficiency are increasing with time, so the safety awareness of employee has no decline. But managers need to directly face the pressure of social public opinion, the level of safety management must be greatly improved in order to prevent secondary accidents.

From the comparison of Figs. 7 and 8, the safety awareness of employee under the positive effect of external public opinion is higher than the safety awareness of employee under the negative effect of external public opinion. It reveals that enterprises suffer too much the pressure of public opinion, but it may increase the probability of secondary accident.

5 Conclusions

(1) The variation tendency of safety awareness of employee is the dynamic phenomenon of complex system. According to agent based modeling and simulation (ABMS) and the emergent property of complex system, the safety awareness will be simulated and analyzed by the software of Netlogo,

(2) From the analysis of output of simulation in the analytical mode, educated degree has the biggest effect of instant on the safety awareness of employee, the next in importance is safety training and safety train has the chronic effect on safety awareness of employee, the degree of safety degree has a relatively weak effect on the safety awareness of employee. Emotional intelligence and the positive effect of public opinion hardly affect the safety awareness of employee. Therefore, in the

recruitment of enterprise, educated applicants should be retained, and regularly carry out safety training for employees. In order to the safety awareness of employee creates the long-term rapid growth to ensure that the enterprise maintains the long-term zero accident rate.

Acknowledgments. This research reported herein was supported by the NSFC of China (Grant No.71571091, 71371092).

References

1. Huang, P., Zhang, J.: Process Saf. Prog. **34**(4), 313–314 (2015)
2. Henrich, H.W., Petersen, D., Roose, N.: Industrial Accident Prevention. McGraw-Hill, New York (1980). (223 (1998))
3. Conrad, P., Bradshaw, Y.S.: Helmets, injuries and culture definitions: motorcycle injury in urban indonesia. Accid. Anal. Prev. **28**, 193–200 (1996)
4. Holland, J.H.: Emergence: From Chaos to Order, pp. 1–116. Addison Wesley, New York (1998)
5. Kline, R.B.: Principles and practice of structural equation modeling, J. Am. Stat. Assoc. **101**(12) (2006)
6. Beikkhakhian, Y., Javanmard, M., Karbasian, M., Khayambashi, B.: The application of ISM model in evaluating agile suppliers selection criteria and ranking suppliers using fuzzy TOPSIS-AHP methods. Expert Syst. Appl. **42**(15), 6224–6236 (2015)
7. Funtowicz, S., Ravetz, J.R.: Emergent complex systems. Futures **26**(6), 568–582 (1994)
8. Olfati-Saber, R., Fax, A.: RM murray consensus and cooperation in networked multi-agent systems. Proc. IEEE **95**(1), 215–233 (2007)
9. Stroeve, S.H., Blom, H.A.P., Bakker, J.: Contrasting safety assessments of a runway incursion scenario: event sequence analysis versus multi-agent dynamic risk modelling. Reliab. Eng. Syst. Saf. **109**(109), 133–149 (2013)
10. Hofmann, D.A., Stetzer, A.: A cross-level investigation of factors influencing unsafe behaviors and accidents. Pers. Psychol. **49**(2), 307–339 (2006)
11. Li, N., Liu, L.: Coal miners' job burnout structure and questionnaire development. J. Southwest Univ. (Soc. Sci. Ed.) **35**(6), 133–137 (2009). (in Chinese)
12. Yang, C., Chen, X., Sun, Q.: Analysis on impact factors of employees' safety awareness based on structural equation model. China Saf. Sci. J. **25**(1), 34–39 (2015). (in Chinese)

Recognizing Mine Site Hazards: Identifying Differences in Hazard Recognition Ability for Experienced and New Mineworkers

Brianna M. Eiter(✉), Jennica L. Bellanca, William Helfrich, Timothy J. Orr, Jonathan Hrica, Brendan Macdonald, and Jason Navoyski

Pittsburgh Mining Research Division,
Centers for Disease Control and Prevention,
National Institute for Occupational Safety and Health, Pittsburgh, PA, USA
{BEiter, JBellanca, WHelfrich, TOrr, JHrica, BMacdonald, JNavoyski}@cdc.gov

Abstract. To perform a successful workplace examination, miners must be able to find and fix hazards. The goal of the current research project was to identify differences in how workers with varying amounts of work and safety experience search and identify hazards. The NIOSH research team created true-to-life panoramic images that safety professionals, experienced miners, inexperienced miners, and students searched for hazards. The effects of the image context and experience level of the participants on the overall accuracy are explored. The research findings suggest that safety experience and hazard familiarity play a large role in a miner's ability to identify hazards. Findings from this study will be incorporated into training programs focused on improving hazard recognition ability for surface stone, sand, and gravel miners.

Keywords: Eye tracking · Hazard recognition · Virtual reality

1 Introduction

Metal/nonmetal (M/NM) mining saw an increase in the number of fatalities between October 2013 and January 2015 [1]. During this period, 37 miners were fatally injured; that is twice the number of fatalities that occurred in each of the previous two years. Quickly following in July 2015, the Mine Safety and Health Administration (MSHA) issued a program policy letter (P15-IV-01) suggesting that, "miners would benefit from rigorous workplace examinations conducted by experienced and trained examiners." As data collection for this study was completed, in January 2017, MSHA issued a final rule amending the standards for workplace examinations [2]. The amended rule increases regulation of examination recorded content, logistics, and availability. Specifically, the final rule mandates that in addition to a record that an exam has taken place, mine operators must include the location of the exam, hazards found, and mitigation(s) completed. However, this rule does not provide additional guidance for what qualifies a miner to be a "competent person," that is required to complete each exam.

D.N. Cassenti (ed.), *Advances in Human Factors in Simulation and Modeling*,
Advances in Intelligent Systems and Computing 591, DOI 10.1007/978-3-319-60591-3_10

The competent person is defined within the Code of Federal Regulations (30 CFR 56.2) as a person having abilities and experience that fully qualify him or her to perform the duty to which he or she is assigned [3]. In the case of workplace exams, a competent person's primary assignment is to find and fix hazards. Therefore, the skills required for hazard recognition are of key interest. Although the workplace exam regulation is currently under review by the new administration, hazard recognition still poses a safety issue for all M/NM miners. Hazard recognition and mitigation represent a special challenge for the miner because of diverse worker activities that take place in a dynamic environment [4]. Given the complexities and dynamism of the mining environment, it is critical to understand how miners recognize worksite hazards so that NIOSH researchers can identify strategies for how to improve hazard recognition ability and therefore increase the safety and efficacy of workplace examinations.

2 Literature Review

The National Safety Council defines a hazard as "an unsafe condition or activity that, if left uncontrolled, can contribute to an accident" [5]. Hazard recognition is the realization that a condition or behavior can cause harm [6]. Successful hazard recognition requires an individual to possess a complex set of competencies. For instance, knowledge of general and site-specific hazards equips a worker to be better prepared to recognize hazards [7]. An accurate understanding of risk is another critical competency. Inaccurate risk perception can lead workers to ignore or misinterpret cues that signal a hazardous event or activity [8]. Other competencies include the ability to mitigate hazards and communicate risk to others. Mastery of several competencies is therefore critical for miners to be able to successfully recognize worksite hazards. In tasks designed to test hazard recognition abilities, a recognition rate of at least 90% has previously been used as the standard for mastery [9]. Using this criterion, in previous studies testing hazard recognition abilities workers tend to underperform [6, 9, 10].

Prior research suggests that there are factors that may affect hazard recognition ability; one of these factors is experience. Burke et al. [11] show that workers who have experience with a near-miss incident are better able to perceive a similar high risk or hazardous event. Perlman et al. [10] investigated the influence of experience on hazard recognition within the construction industry by comparing the hazard recognition performance of groups with different types [or amounts] of workplace experience. Counter to the authors' prediction that superintendents would successfully identify the most hazards, safety directors outperformed both superintendents and civil engineering students. Perlman et al. attribute this difference to experience and formal safety training, which the superintendents and students did not have [10]. Similarly, results from the mining industry suggest that a lack of *recent* experience working in a particular environment—e.g., because of layoff or filling in for an absent employee—also impacts hazard recognition abilities [9].

Context is another factor that affects the way workers recognize objects in their environment [12]. Objects appearing in a consistent or familiar environment are found more accurately and detected more quickly than objects appearing in an ambiguous or unfamiliar environment [13]. This finding is relevant to hazard recognition because of

the way that miners are typically trained to recognize hazards. During hazard recognition training, miners are oftentimes shown close-up pictures of hazards. While these close-up pictures are helpful at highlighting specific aspects of a hazard (e.g., insufficient berm), the context in which that hazard occurs is absent (e.g., location with respect to the highwall); this information is critical for the miner to learn so that he can successfully search for and find these hazards in his own work environment. Kowalski-Trakofler and Barrett (2003) trained miners with pictures showing only the hazard and with pictures showing the same hazard within the context in which it typically occurs [14]. The results of the study show that miners found fewer hazards following training with pictures that show only the hazard. This suggests that learning about hazards in the context in which they occur (e.g., location or work activity) helps miners recognize them more often later. At a more basic level, larger context pictures have also been linked to increased and easier information extraction, which could better facilitate the understanding of hazards [15].

Context is also important with respect to scene complexity. A number of factors have been identified that reduce visual search performance and make the hazard recognition task more difficult. These factors include area, density, and, most importantly, the number of background items in a scene [16]. Experienced workers may be better able to cope with changes in scene complexity through learned variance in attention. For example, the driving literature shows that experienced drivers increase their visual scanning as the complexity of the roadway increases, suggesting that experienced drivers' improved recognition performance may be due to improved situational awareness that is more necessary and evident in complex scenes [17]. Increased context also leads to improved scene realism, which has been shown to lead to improved training transfer and performance results [18]. Additional items in an image add to the background noise, but also provide realism through reasoning for an action to occur or hazard to be present.

Given that previous research on hazard recognition often used artificial and limited materials, the purpose of the current study was to create a hazard recognition task that more closely parallels—or simulates—the workplace examination. To do this, NIOSH researchers created panoramic images with ample context and asked safety professionals, miners, and students to search the images for hazards as if they were performing a workplace examination at their own worksite. Using this setup, researchers aimed to identify differences in workers' ability to recognize hazards based on context and experience. Findings from this study will be incorporated into training programs focused on improving hazard recognition ability for miners.

3 Methods

3.1 Participants

Fifty-two participants volunteered to take part in the study, but three participants were excluded due to technical difficulties. All participants traveled to the NIOSH research facility in Bruceton, PA. None of the participants received payment for their participation in the study. All participants were screened to verify that they are free of

degenerative vision disorders, have full peripheral vision (−45 to 85°) in both eyes, and have a visual acuity of 20/40 or better [19]. Participants were also screened using Ishihara Plates for color blindness. Participants that were found to have mild or severe colorblindness did not perform significantly worse than the rest of the sample, and were therefore included in the analysis.

For the purposes of this study, participants were divided into four groups: safety professionals, experienced miners, inexperienced miners, and students. Researchers created the groups based on total mining experience (total mining) and experience in current mining position (current position). According to the National Survey of the Mining Population conducted in 2012, the average stone miner has approximately 12.5 years of experience in mining and 7.8 years of experience in their current position; similarly, the average metal and non-metal miner has 10.7 and 12.0 years of total experience and 4.7 and 6.7 years in current position respectively [20]. However, because of sampling constraints, researchers used the following group definitions. Safety professionals had at least 2 years of experience in an environmental, health, or safety position for a mine operator or government agency. Experienced miners had more than 2 years of experience as a laborer, equipment operator, sample taker, foreman, or supervisor. Inexperienced miners had some but less than 2 years of experience as a laborer, equipment operator, sample taker, foreman, or supervisor. Finally, students were defined as a person enrolled in a mining-related program that is not otherwise classified. Any participant pursuing a higher-level degree was grouped as a student regardless of mining experience. All participants, except for students, also reported having completed at least 24 h of MSHA New Miner Training (30 CFR Part 46), and those categorized as experienced miners and safety professionals reported having completed the additional 8 h of MSHA Annual Refresher Training as necessary (30 CFR Part 46) [21]. The demographics of the study participants are shown in Table 1 below.

Table 1. Participant demographic counts and means (standard deviation).

Group	N	Age [yrs.]	Total mining [yrs.]	Current position [yrs.]
Safety professionals	12	47.7 (11.0)	20.3 (13.5)	8.0 (5.7)
Experienced miners	11	39.1 (11.2)	13.8 (11.0)	9.2 (11.1)
Inexperienced miners	12	26.2 (8.2)	0.6 (0.5)	0.3 (0.3)
Students	14	22.9 (2.8)	0.7 (1.1)	N/A

3.2 Materials

The research materials for this study are 32 panoramic images of four locations at a typical surface stone operation: pit, plant, roadway, and shop. There are eight panoramic images taken at each of the four locations. Six images for each location are experimental images, containing hazards, while the other two images are control images, containing zero hazards. The number of hazards per experimental image ranges from two to seven, totaling 101 hazards. The overall breakdown of the hazards is 19 in the pit, 25 at the plant, 26 on the roadways, and 31 in the shop.

The scope of the hazards included in the panoramic images was determined using incident data and subject matter experts. First, NIOSH researchers considered Mine Safety and Health Administration (MSHA) fatal and nonfatal days lost (NFDL) data. Table 2 includes a summary of incidences that occurred at United States M/NM mine sites during the years 2009–2015 compared to classifications of the hazards used in the study. As evident by the numbers, specific hazards were included in the panoramic images in order to represent as many of the accident classifications in as realistic a way as possible as well as mirror the prevalence found in the data. Final decisions on the specific hazards to be included in the images were made with the support of subject matter experts (SME). SME support included feedback from former MSHA inspectors, mine safety professionals, and NIOSH researchers familiar with surface stone mining techniques.

Table 2. Incidence of metal/non-metal mining accidents by classification for years 2009–2015 compared with hazards included in the panoramic images.

MSHA classification	Accident severity			Study hazards
	Fatal	NFDL	Total	
Electrical	5	110	115	8
Entrapment	0	1	1	0
Exploding vessels under pressure	1	65	66	0
Explosives and breaking agents	2	10	12	0
Falling, rolling, or sliding rock	22	65	87	5
Fall of face, rib, pillar, side, or highwall	2	11	13	7
Fire	0	32	32	6
Handling material	0	6473	6473	8
Handtools	0	1851	1851	2
Non-powered haulage	0	55	55	1
Powered haulage	30	1340	1370	32
Hoisting	0	17	17	1
Ignition or explosion of gas or dust	1	23	24	1
Impoundment	0	1	1	0
Inundation	0	2	2	0
Machinery	18	1488	1506	2
Slip or fall of person	14	4641	4655	23
Stepping or kneeling on object	0	378	378	1
Striking or bumping	1	133	134	3
Other	5	475	480	1
Totals	101	17171	17272	101

NIOSH researchers worked with corporate and mine safety professionals from a surface limestone mine site to take the panoramic images. The panoramic images included hazards that were staged onsite at the mine as well as hazards that were enhanced or created using photo editing software. Of the 101 hazards included in the panoramic images, 58 hazards were staged, 22 were enhanced (e.g., rope was brightened to improve visibility), and 21 were created through photo editing (e.g., a stair or part of a berm were

removed from an image). Figure 1 is a panoramic image of the shop; Table 3 includes a description of the seven hazards included in the image, the MSHA classification of the hazards, as well as how the hazards were created. Prior to use in the hazard recognition task, panoramic images were reviewed and evaluated by the aforementioned SME support.

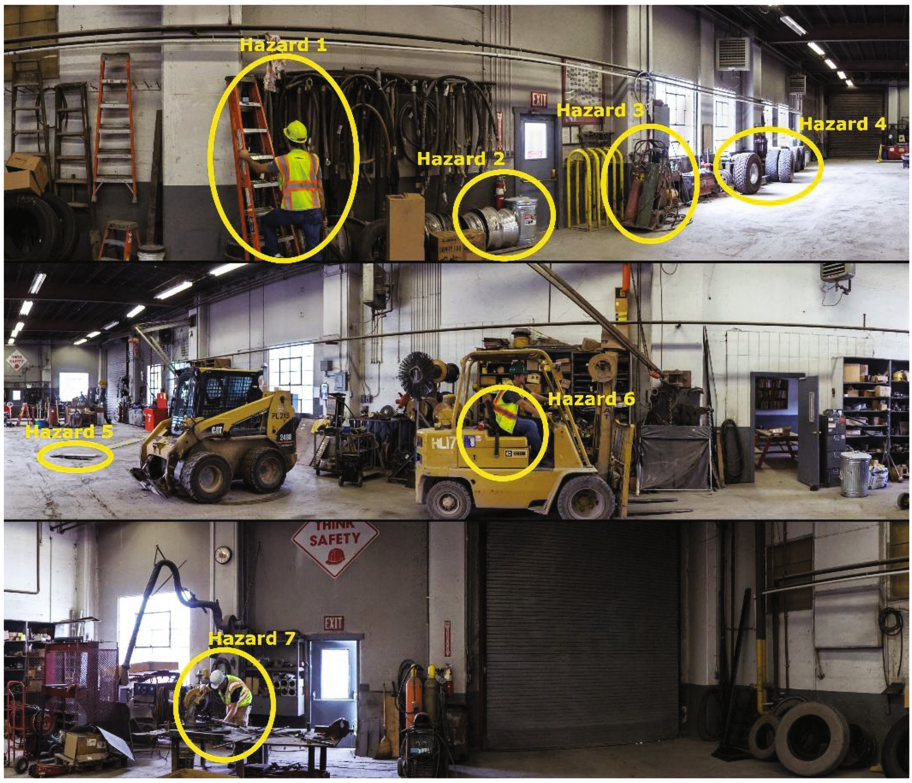

Fig. 1. Panoramic image of the shop (Please visit the following website to view 4 of the NIOSH panoramic images: https://www.cdc.gov/niosh/mining/hazrec.). The NIOSH identified hazards are circled in yellow and labeled Hazard 1–7. Note: the panoramic image is shown in three panels for space purposes.

Table 3. Example hazard descriptions, classifications, and creation method

Hazard	Hazard description	MSHA classification	Creation method
Hazard 1	Incorrect use of ladder	Slip or fall of person	Staged
Hazard 2	Obstructed fire extinguisher	Fire	Staged
Hazard 3	Unsecured gas cylinders	Non-powered haulage	Edited
Hazard 4	Unsecured tires	Handling material	Staged
Hazard 5	Uncovered floor opening	Slip or fall of person	Staged
Hazard 6	Operating without a seatbelt	Powered haulage	Staged
Hazard 7	Working without safety glasses	Machinery	Enhanced

3.3 Virtual Immersion Simulation Laboratory (VISLab)

All testing took place in NIOSH's Virtual Immersion Simulation Laboratory (VISLab) that houses the several display theaters. The system, used to perform the hazard identification task, features a 360-degree panoramic front project display that is roughly 10 m in diameter by 3 m tall. Six high-definition projectors (Titian 1080p 3D, Digital Projection, Kennesaw, GA) create a seamless image that surrounds the user in digital imagery. A motion-tracking camera system (T20, Vicon, Oxford, UK) above the screen provides the capability to track participants and objects within the display space. The 60 Hz data from eye-tracking glasses (ETG 2.0, SensoMotoric Instruments, Teltow, Germany) are used in concert with 120 Hz data from the motion tracking system to calculate the user's gaze point in screen coordinates as the participant moves about the display space. The stimulus images are rendered using an in-house Unity application (Unity technologies, San Francisco, CA). A detailed discussion of the development process for the panoramic images, the calibration of the screen space, the synchronization of the hardware, and the software is described by Bellanca et al. [22].

3.4 Procedure

Upon arriving at the VISLab, researchers obtained informed consent from the study participants to participate in the institutional review board approved protocol. Participants first completed a demographics questionnaire about their training and mining experience and completed the vision screening. Participants were then outfitted with the eye-tracking glasses and a hand-held joystick in their dominant hand. The participants also wore a small backpack to carry the eye-tracking laptop. Lastly, researchers affixed reflective markers to the participants' C7, acromioclavicular joints, sternum, right scapula, and eye tracking glasses frames.

To start the hazard identification portion of the study, participants performed a two-minute simple reaction time test, followed by a static calibration of the motion capture system, and a 3-point calibration using the SMI iView software. Next, an additional 4-point, 10-degree calibration was performed to orient and synchronize the motion capture and eye-tracking systems in order to calculate the point of regard on the 360 screen. After the calibrations, participants reviewed two practice panoramic images to adapt to the setup.

For actual data collection, participants were presented with four blocks of eight panoramic images grouped by location (pit, plant, shop, and roadway). The block orders were distributed across groups, and individual images within the block were randomized per participant. Participants were given up to two minutes to view each image and were instructed to press the joystick button to identify a hazard as quickly and as accurately as possible. Subjects were also instructed to only press the button once per hazard and to assume that all belts and conveyors we in motion. If a participant finished the identification early, they could end the image. Participants were given a break between each block. After all 32 images were completed, the participant was de-instrumented. The hazard identification task typically took about 45 min to 1.5 h to complete.

3.5 Data Post Processing

For each of the 101 identified hazards, regions of interest (ROIs) were defined in the panoramic images using SME support. ROIs were defined as polygons, containing only the hazard. Eye-tracking data was transformed into image data according to the process described by Bellanca et al. [22]. The image scan path data was then processed to identify fixations (e.g., when the eye remains still), using a dispersion algorithm such that the minimum duration is 75 ms and the maximum dispersion is 50 pixels [23]. Given the set ROIs and fixation data, researchers evaluated each button press as a hit or miss based on the central gaze position of the fixation prior. To be a hit, the button press fixation must be (1) within 170 pixels, (2) have at least one fixation prior within 75 pixels of the ROI, and (3) the prior scan path must match the shape of the ROI. Alternatively, a button press could be a late hit, as depicted in Fig. 2. A late hit is defined as a scan path where the last one or two fixations that are no more than one second after the button press meet the hit criteria. The late hit criteria was chosen based on common choice reaction time timing across age and subject variability in order to account for decision making and motor delay [24]. However, no late hits later than 0.5 s were observed. All button presses were visually verified and, if necessary, reviewed by a second person.

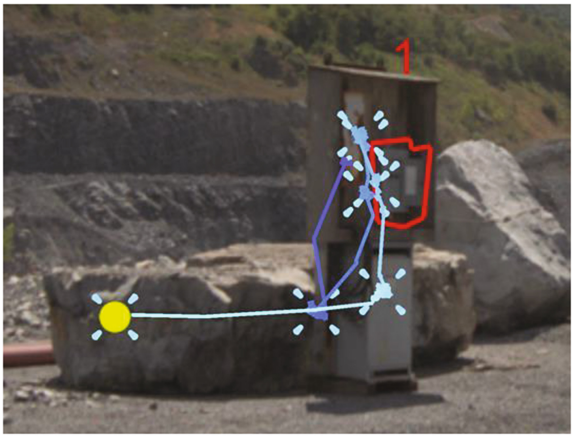

Fig. 2. An example scan path data of a late hit button press identifying the electrical hazard of the open electrical box. The ROI is outlined in red. The scan path before the button press is in blue and gets lighter as time gets closer to the button press. The click icons in blue indicate fixations, and the yellow circle represents the fixation associated with the button press. In this image, the yellow circle is 280 pixels from the edge of the ROI.

From the hit and late hit data, identification accuracy was computed across location and hazard classification for each subject. Because hazards were staged to be as realistic as possible without over saturating an image, it was not possible to achieve equal distributions of hazard classifications across the locations. Therefore, the context variables of location and hazard classification are being analyzed separately. A full

factorial, least squares regression was performed with group and location, and group and classification accounting for participant random effects (JMP, SAS, Cary, NC). For both analysis all statistical assumptions were met.

4 Results

4.1 Location

As was the case in previous studies [6, 9, 10], participants under-performed in the hazard recognition task. With a high score of 78% correct, the average group scores were only 61%, 56%, 50%, and 47% for the safety professionals, experienced miners, inexperienced miners, and students respectively. There were main group ($p = 0.0115$, $F(3, 45) = 4.1$) and location ($p = <0.0001$, $F(3, 135) = 8.2$) effects. As depicted in Fig. 3, accuracy trended downward as safety experience decreased such that the safety professionals performed significantly better than the students did ($p = 0.002$, $F(1, 135) = 10.7$).

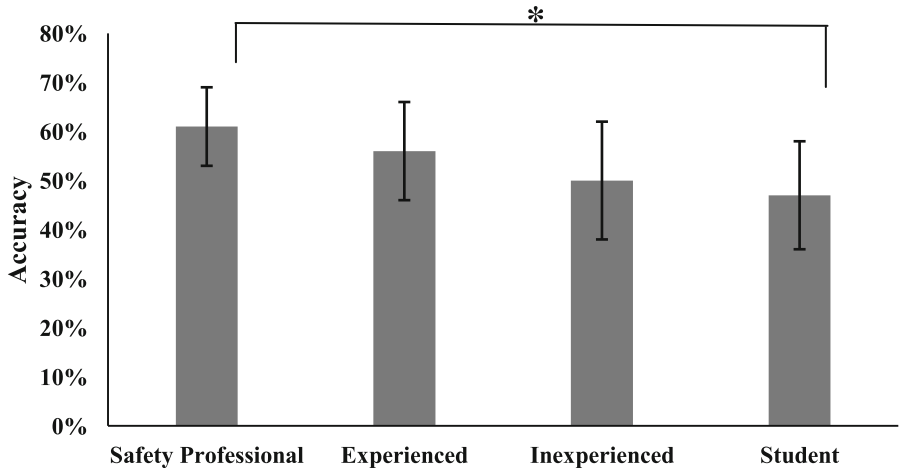

Fig. 3. Bar graph depicting the across subject averages for accuracy, where the error bars represent the standard deviation and the * indicates significance at $\alpha < 0.05$.

The location average accuracy scores were 53%, 55%, 56%, and 48% for the pit, plant, shop, and roadway respectively. Exploring the location effect further, Tukey's range test indicated that the roadway was significantly different from the other three locations with $p < 0.05$.

4.2 Classification

When looking at context versus experience related to hazard classification, only a classification effect was significant ($p = <0.0001$, $F(14, 630) = 31.4$). Figure 4 depicts the average hazard classification accuracy by group, where ignition or explosion had

the lowest success rate, followed by fire, striking or bumping, stepping on object, and electrical all under 50% correct. The top three classification were machinery, handtools, and hoisting, all around 80%.

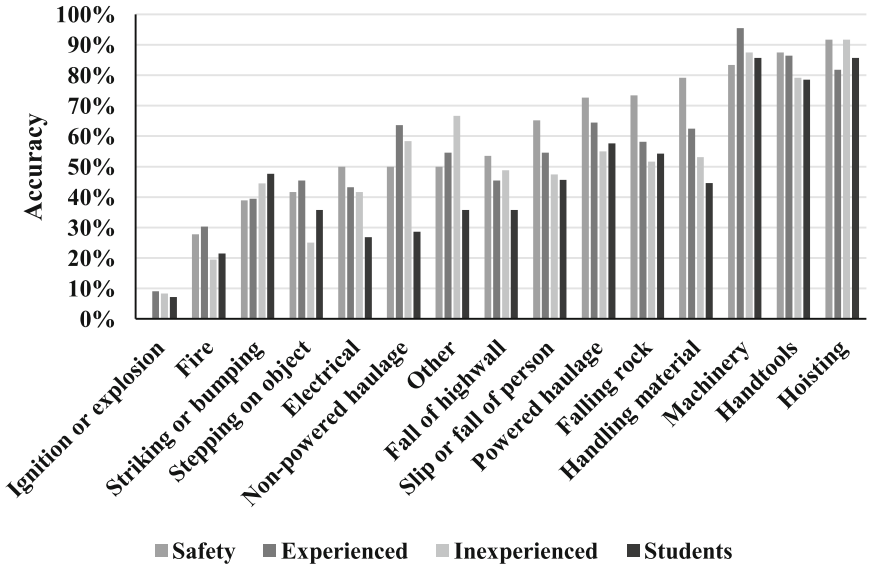

Fig. 4. This bar graph depicts across subject average accuracy by hazard classification.

5 Discussion and Conclusion

A primary goal for this study was to create a hazard recognition task that simulates a workplace examination that a miner would perform. Given the true-to-life images and large projection space, researchers were able to accomplish this goal. Furthermore, because of the realistic content, the panoramic images can be used directly by the industry. However, the applied nature of the images posed analytic challenges. Namely, since the hazard and background content were not evenly distributed, only generalizations of context effects could be examined.

As hypothesized, experience was found to be significant when modeled with location, but interestingly was not significant when analyzed with hazard classification. This weak relationship may suggest that the experience that differentiates location and classification context may be different from that which is being captured by the groups. Dzeng et al. [25] suggested similar reasoning to explain a lack of accuracy differences in their work on visual strategies used by experienced and inexperienced construction workers; where in their case, they suggest that general work experience is not equivalent to safety-specific experience. The current study data aligns with this suggestion, as safety professionals and students have the greatest difference in safety experience and display the only significant result. It may also be possible that the experience difference between the groups in general was not big enough. Specially, the variance of

total mining experience for the experienced miners group was large, as some of the participants were very similar to those classified in the inexperienced miners group. A closer look at the type and quantities of experience may help clarify the lack of significance.

The observed location effect was also not as expected; the results did not align with the hypothesis that scenes that are more complex reduce performance. In the current study, it was predicted that hazard recognition in the shop would be worse than in other locations because the shop images are more enclosed and cluttered. Counter to this prediction, the roadway performance was significantly worse than the other locations. One possible explanation for the reduction in the roadway performance may be due to decreased experience performing exams in this location. As mentioned in the public comments for the workplace exams rule, mine operators are not accustomed to examining roadways as a place of work [2]. The roadway images also tended to include more of the low accuracy hazard classifications such as fire and electrical hazards, possibly leading to an average overall lower score.

The effect of hazard classification may also be due to participants' exposures to hazards. The top three most accurately identified hazards also happened to be the most prevalent in the industry as indicated by MSHA's injury and illness data. Furthermore, trainers typically use the injury and illness data to prioritize their training and safety communications. The data in this study supports the need for training in routine as well as non-routine hazards to eliminate major weaknesses in hazard recognition ability.

As researchers move to translate the work from this study into training, it will be important to incorporate a safety-specific focus that covers common and uncommon hazards. Future work will also include a more in-depth analysis of the scan path, reaction time, and hazard review data to capture a fuller picture of hazard recognition.

Acknowledgments. NIOSH would like to thank Holly Tonini for her help in taking and editing the panoramic images. The findings and conclusions are those of the authors and do not necessarily represent the views of NIOSH.

References

1. Mine Safety and Health Administration. Accident: Illness and Injury and Employment Self-Extracting Files (Part 50 Data). http://www.msha.gov/STATS/PART50/p50y2k/p50y2k.htm
2. Mine Safety and Health Administration: Examinations of working places in metal and nonmetal mines. Final Rule Fed. Reg. **82**, 7680–7695 (2017)
3. Mine Safety and Health Administration: Definitions. In: Code of Federal Regulations. Title30, Part 56.2 (2015)
4. Scharf, T., Vaught, C., Kidd, P., Steiner, L., Kowalski, K., Wiehagen, B., Rethi, L., Cole, H.: Toward a typology of dynamic and hazardous work environments. Hum. Ecol. Risk Assess. **7**(7), 1827–1842 (2001)
5. Mitropoulos, P., Abdelhamid, T., Howell, G.: Systems model of construction accident causation. J. Constr. Eng. Manag. **131**(7), 816–825 (2005)
6. Bahn, S.: Workplace hazard identification and management: the case of an underground mining operation. Saf. Sci. **57**, 129–137 (2013)

7. Albert, A., Hallowell, M.R., Kleiner, B., Chen, A., Golparvar-Fard, M.: Enhancing construction hazard recognition with high-fidelity augmented virtuality. J. Constr. Eng. Manag. **140**(7), 04014024 (2014)
8. Hunter, D.R.: Risk Perception and Risk Tolerance in Aircraft Pilots. Federal Aviation Administration, Washington (2002)
9. Barrett, E., Kowalski, K.: Effective Hazard Recognition Training Using a Latent-Image, Three-Dimensional Slide Simulation Exercise. Report of Investigations, vol. 9527, pp. 1–36. Bureau of Mines, Washington, DC (1994)
10. Perlman, A., Sacks, R., Barak, R.: Hazard recognition and risk perception in construction. Saf. Sci. **64**, 22–31 (2014)
11. Burke, M.J., Scheuer, M.L., Meredith, R.J.: A dialogical approach to skill development: the case of safety skills. HRMR **17**(2), 235–250 (2007)
12. Henderson, J.M., Hollingworth, A.: Eye movements during scene viewing: an overview. In: Underwood, G. (ed.) Eye Guidance in Reading and Scene Perception, pp. 269–293. Elsevier, Oxford (1998)
13. Oliva, A., Torralba, A.: The role of context in object recognition. Trends. Cogn. Sci. **11**(12), 520–527 (2007)
14. Kowalski-Trakofler, K.M., Barrett, E.A.: The concept of degraded images applied to hazard recognition training in mining for reduction of lost-time injuries. J. Saf. Res. **34**(5), 515–525 (2003)
15. Dupont, L., Antrop, M., Van Eetvelde, V.: Eye-tracking analysis in landscape perception research: influence of photograph properties and landscape characteristics. Landsc. Res. **39**(4), 417–432 (2014)
16. Drury, C.G., Clement, M.R.: The effect of area, density, and number of background characters on visual search. Hum. Factors **20**(5), 597–602 (1978)
17. Underwood, G.: Visual attention and the transition from novice to advanced driver. Ergonomics **50**(8), 1235–1249 (2007)
18. Stinson, C., Kopper, R., Scerbo, B., Ragan, E., Bowman, D.: The effects of visual realism on training transfer in immersive virtual environments. In: Proceedings of Human Systems Integration Symposium (2011)
19. FMCSA.: Physical Qualifications for Drivers. Code of Federal Regulations. Title 49, Part 391.41 (2015)
20. McWilliams, L., Lenart, P., Lancaster, J., Zeiner Jr., J.R.: National survey of the mining population, part I: employees. Off. Mine Saf. Health Res. Inf. Circ. **9527**, 252 (2012)
21. Mine Safety and Health Administration: Training and Retraining of Miners Engaged in Shell Dredging or Employed at Sand, Gravel, Surface Stone, Surface Clay, Colloidal Phosphate, or Surface Limestone Mines. Code of Federal Regulations. Title 30 Part 46 (1999)
22. Bellanca, J., Orr, T., Helfrich, W., Macdonald, B., Navoyski, J., Eiter, B.: Assessing hazard identification in surface stone mines in a virtual environment. In: Vincent, G.D. (ed.) Advances in Applied Digital Human Modeling and Simulation, pp. 217–230. Springer, Cham (2016)
23. Salvucci, D.D., Goldberg, J.H.: Identifying fixations and saccades in eye-tracking protocols. In: Proceedings of the 2000 Symposium on Eye Tracking Research and Applications. ACM (2000)
24. Hale, S., Myerson, J., Smith, G.A., Poon, L.W.: Age, variability, and speed: between-subjects diversity. Psyc. Aging **3**(4), 407–410 (1988)
25. Dzeng, R.J., Lin, C.T., Fang, Y.C.: Using eye-tracker to compare search patterns between experienced and novice workers for site hazard identification. Saf. Sci. **82**, 56–67 (2016)

Modeling of Muscle Atrophy and Exercise Induced Hypertrophy

Xianlian Zhou(✉), Paulien E. Roos, and Xinyu Chen

Computational Medicine and Biology Division, CFD Research Corporation, 701 McMillian Way NW, Suite D, Huntsville, AL 35806, USA
{Alex.Zhou,Paulien.Roos,Grace.Chen}@cfdrc.com

Abstract. A better understanding of the time course of changes in muscle performance in response to spaceflight and exercise is required to maintain sufficient muscle function for long duration spaceflight. This paper presents a semi-empirical and dynamic muscle adaptation (atrophy and hypertrophy) model driven by a muscle activation profile that is directly related to muscle exercise intensity and exercise-rest cycles. The effect of muscle adaptation is described by two phenomenological parameters (s, τ), where s is related to the physiological limit of adaption and τ governs rate of adaptation. Both s and τ mathematically depend on the instantaneous muscle activation level (a). The model is calibrated against selected atrophy and hypertrophy experimental data. It was demonstrated that: (1) the model is capable to handle muscle atrophy and hypertrophy in a unified setting; (2) the model can be used for prediction of muscle atrophy during a 6-month spaceflight under two different exercise regimes.

Keywords: Exercise · Muscle activation · Muscle atrophy · Muscle hypertrophy · Spaceflight

1 Introduction

During prolonged spaceflights, such as long duration exploration missions (LDEMs), skeletal muscles undergo gradual changes or adaptations that could cause impaired performance and higher risks of injury during dynamic activities. For muscles, evidence has shown atrophy (reduced mass) and structural and metabolic changes during LDEMs [1], resulting in reduced muscle strength and endurance. Besides muscle atrophy, the loss in muscle strength after mechanical unloading has been attributed to a decrease in neural drive [2]. Numerous studies have been devoted to understanding the physiological mechanisms that affect muscle changes during spaceflight (such as weightlessness, fluid shifts, and muscle unloading). However, the exact mechanisms remain disputed and adaptations may be specific to muscle, fiber, and stimulus type [3]. Postural muscles of the lower limb are particularly susceptible to atrophy during spaceflight, and the extensor muscles more so than the flexor muscles [1]. It has been suggested that muscles have a "set point" for the level of activity required to maintain a constant muscle mass. Cardiovascular exercises with repeated long durations of low intensity contractions result in improved fatigue resistance, while resistance exercises lead to an increased muscle fiber cross sectional area and thereby reduce atrophy.

D.N. Cassenti (ed.), *Advances in Human Factors in Simulation and Modeling*,
Advances in Intelligent Systems and Computing 591, DOI 10.1007/978-3-319-60591-3_11

There is a critical knowledge gap on how the duration of exposure to microgravity and the amount of in-flight exercises affect muscle changes and performance levels. Understanding these relationships is particularly important for LDEMs to destinations such as Mars and asteroids, where the spacecraft may have limited space and hardware for exercises and the astronauts' exploration tasks may be demanding. There are plenty of data on muscle atrophy of astronauts during spaceflights [4] or on ground based models [2, 5]. However, from examining the data in isolation, it is still difficult to predict the timeline of muscle atrophy in space and the effects of exercise countermeasures and to design optimal exercise countermeasure programs for astronauts. Computational models could provide a feasible approach to address this critical knowledge gap by incorporating existing experimental data and deriving quantitative relations regarding disuse induced atrophy and exercise induced hypertrophy.

Previous computational models of muscle adaptation have been developed for underload or disuse [6, 7], overstretch [8] or understretch [7], and overload [7]. Martin et al. [7] presented an agent-based model that generates a tissue-level skeletal muscle response to disuse or immobilization. The model incorporates stochastic tissue-specific muscle fiber architecture parameters and simulates changes in muscle fiber size resulting from disuse-induced atrophy. The models presented in [7, 8] are more phenomenon driven models with simple mathematical expressions and these models can be calibrated to experimental data conveniently. Existing modeling efforts lack detailed representation of physiological processes and consequently might not be able to capture some important physiological changes to muscles under microgravity (e.g. neuromotor control and muscle contraction, morphology, fatigue resistance). In addition, to the best of our knowledge, there exists no model that unifies aspects of atrophy and hypertrophy in the same setting and incorporates the effect of muscle contraction intensity (activation) within the model to study the effects of exercises on muscle adaptation.

The aim of this study was to develop a unified semi-empirical model of muscle adaptation to understand the relation between exercises and muscle hypertrophy and between disuse and muscle atrophy. We first present the theoretical basis of the model and then provide numerical examples to demonstrate model calibration against experimental data. This is followed by an exploratory study on how exercise countermeasures can affect muscle atrophy during long duration spaceflight.

2 Muscle Adaptation Model

Many existing studies have shown that muscle volume can adapt (i.e., increase or decrease) exponentially and then converge toward a homeostatic equilibrium state [9, 10]. In the work by [7], an exponential adaptation equation was introduced to model muscle disuse atrophy due to under-stretch or unload. We introduce a similar equation for normalized muscle anatomical cross-sectional area (CSA) change to account for both muscle fiber atrophy and hypertrophy:

$$\frac{dCSA}{dt} = \frac{s}{\tau} e^{-t/\tau}, \tag{1}$$

where τ is a time constant that controls the adaptation speed. At homeostatic equilibrium of muscle fiber protein breakdown and synthesis, $s = 0$. When protein breakdown is greater than synthesis, $s < 0$ and muscle atrophy is ensued; reversely, when $s > 0$ muscle hypertrophy follows. When s and τ are constant over time, the time integration of the above differential question has an analytical solution:

$$CSA = -se^{-\frac{t}{\tau}} + s + 1, \tag{2}$$

in which we assumed $CSA(t = 0) = 1$. As a result, $CSA(t = \infty) = s + 1$, which indicates the limit of atrophy or hypertrophy. With the analytical expression above, we can rewrite Eq. (1) as:

$$\frac{dCSA}{dt} = \frac{s + 1 - CSA}{\tau}, \tag{3}$$

such that the rate of CSA change depends only on s, τ, and the current value of CSA. Clearly, the sign of $s + 1 - CSA$ determines if muscles experience atrophy or hypertrophy. This equation also eliminates the explicit dependence on the absolute value of time (t) as in (1). Assuming we know $CSA(t = t_n) = CSA_n$ where t_n is the current time point, under the condition of constant s and τ during a time-advancing step, we have CSA at the next time point (t_{n+1}) through analytical integration:

$$CSA(t = t_{n+1}) = CSA_{n+1} = -(s + 1 - CSA_n)e^{-\frac{t}{\tau}} + s + 1 \tag{4}$$

with $t = t_{n+1} - t_n$. This gives us the flexibility to change s and τ from time step to time step and still be able to use the above equation to find the analytical solution to Eq. (3). As long as s and τ are constant, Eqs. (3) and (4) are equivalent and we refer to Eq. (3) as the numerical model and Eq. (4) as the analytical model. Later we will demonstrate the use of this analytical model for calibration of s and τ to experimental data of muscle atrophy and recovery.

To introduce the effect of muscle exercise, we assume s and τ depend on muscle exercise intensity, denoted by muscle activation $(a, 0 < a < 1)$. For the sake of convenience, let's assume the muscle adaptation starts at $CSA(t = 0) = 1$. When muscle activation $a = 0$, the muscle undergoes disuse atrophy, $s < 0$ and $s + 1$ will approach the muscle atrophy limit $(0 < CSA_{atr} = s + 1 < 1)$; and when $a = 1$, the muscle undergoes maximum exercise induced hypertrophy, $s > 0$ and $s + 1$ will approach the theoretical muscle hypertrophy limit $(CSA_{hyp} = s + 1 > 1)$; when $a = a0$ (a balanced or baseline activation level for a muscle) there is no atrophy or hypertrophy and it results in $s = 0$. Therefore, $a0$ indicates a threshold or "set point" at which homeostatic equilibrium of protein synthesis and breakdown is reached. Note that the muscle hypertrophy limit CSA_{hyp} is likely unattainable since no fiber can sustain maximum activation (without rest) for an infinitely long time. Considering these factors, we introduce s as a simple piecewise linear function of a:

$$s = \begin{cases} \frac{a0-a}{a0}\left(CSA_{atr} - 1\right) & a \le a0 \\ \frac{a-a0}{1-a0}\left(CSA_{hyp} - 1\right) & a > a0 \end{cases} \tag{5}$$

Note, other smooth functions can also be considered as long as they pass through the following three points $\{(0, CSA_{atr} - 1), (a0, 0), (1, CSA_{hyp} - 1)\}$.

In light of the above, we can assume that the time constant τ is a function of a as well. Here, we introduce three adaptation time constants, τ_{atr}, τ_{bal}, and τ_{hyp}, corresponding to total disuse atrophy, balance, and maximum hypertrophy, respectively. Similar to the s function, we let τ be the linear interpolation function of a and these three parameters:

$$s\tau = \begin{cases} \frac{a0-a}{a0}\tau_{atr} + \frac{a}{a0}\tau_{bal} & a \le a0 \\ \frac{1-a}{1-a0}\tau_{bal} + \frac{a-a0}{1-a0}\tau_{hyp} & a > a0 \end{cases}. \tag{6}$$

Consequently, we have a dynamic muscle adaptation model, composed of Eqs. (3), (5), and (6), driven by muscle activation level (a). Equation (4) can serve as a numerical integration formula of this dynamic equation and also an analytical solution of this model when s and τ are constant during any time period.

3 Benchmarks and Model Calibration

3.1 Effects of Muscle Activation and Time Constant on Muscle Adaptation

We explored the effects of muscle activation (a) and time constant (τ) on muscle *CSA* adaptation based on the analytical model. In Fig. 1, while τ was kept constant as 10 days and $a0$ (homeostatic equilibrium activation) was set to 0.01, a was changed from 0.0 to 1.0. A larger a resulted in a larger *CSA*. When $a < a0$, *CSA* decreases over time, and when $a > a0$, *CSA* increases. In Fig. 2, a was assigned two values, i.e., 0.0 and 0.5, while τ varied. For each a value, three τ values were tested, i.e., 5, 10, and 20 days. For both a values, the bigger the τ value, the longer the *CSA* took to stabilize.

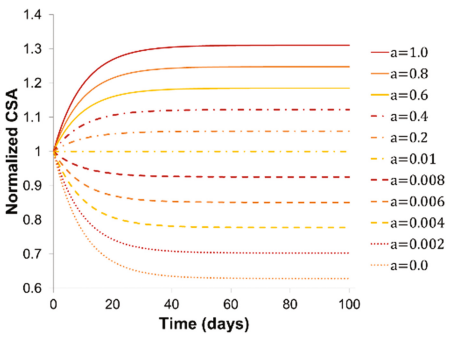

Fig. 1. The effect of muscle activation (a) on muscle physiological *CSA*, given $\tau = 10$ days.

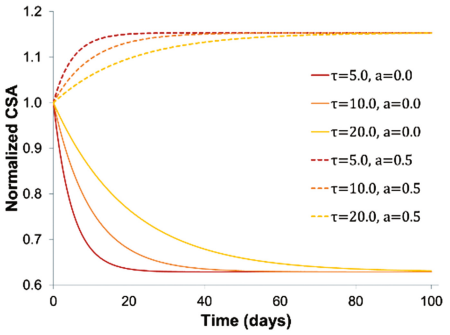

Fig. 2. The combined effect of muscle activation (a) and time constant (τ) on muscle physiological *CSA*.

3.2 Model Calibration with Muscle Atrophy, Hypertrophy, or Recovery Data

Gruther et al. [10] measured muscle layer thickness changes of quadriceps femoris muscles for intensive care unit (ICU) patients who underwent bedrest for up to 100 days. Measurement of muscle layer thickness is often used clinically to document muscle mass [10, 11] and Gruther's data have been interpreted as change in muscle volume [7]. Here we use it to indicate the change in *CSA*. Using a least-square fitting of the analytical model (under zero muscle activation) to all data points, we obtained $s = CSA_{atr} - 1 = -0.603$ and $\tau = \tau_{atr} = 4.0$ days. However, this seemed to under-predict the atrophy limit, which resulted in $CSA_{atr} \cong 39.74\%$ of initial *CSA* (Fig. 3). This is likely because of the relatively small number of data points for post 60-day bedrest and treating all data points equally during fitting. Considering that the muscle volume for subjects who underwent more than 90 days of bedrest reaches around 20% of initial CSA, we fixed $CSA_{atr} = 0.2$, i.e. $s = -0.8$, beforehand. By refitting the equation we obtained $\tau_{atr} = 12.5$ days. Figure 3 illustrates the predicted muscle volume loss with these two sets of coefficients and a comparison with data of [10].

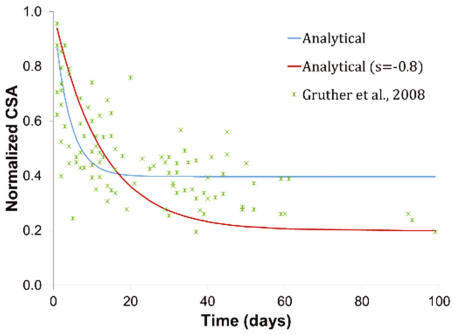

Fig. 3. Muscle volume change versus time with the analytical model (Eq. 4) fitted to data presented in [10].

DeFreitas et al. [9] assessed 25 healthy sedentary men during eight weeks of high-intensity resistance training and presented whole muscle CSAs of their dominant thighs. By our estimates, these men performed high-intensity exercise mostly during days 1, 3, and 5 of each week for about half an hour (excluding resting time between sets). Using a least-square fitting of the analytical model to all data points, we obtained $s = 0.11$ and $\tau = 25.2$ days. The original data collected by [9] and our model predictions are plotted in Fig. 4 to show the agreement.

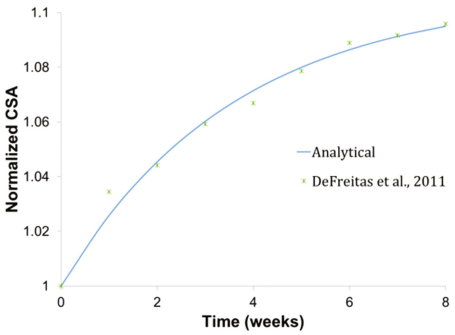

Fig. 4. Muscle volume change versus time with the analytical model fitted to data from [9].

LeBlanc et al. [12] present muscle loss and recovery data on eight healthy subjects after 17 weeks of continuous bedrest and eight weeks of reambulation. MRI muscle volume measurements showed a greater percentage of muscle volume loss in the lower limbs compared to the back muscles during bedrest and rapid recovery after reambulation. The muscle loss was around 16% after five weeks and around 33% after 17 weeks for the ankle plantarflexors (gastrocnemius and soleus); and around 9% after five weeks and around 19% after 17 weeks for the ankle dorsiflexors. For the two subjects who underwent the full eight weeks of reambulation (with a controlled exercise program), the ankle plantarflexors recovered almost fully, while the ankle dorsiflexors recovered to around 94% to their pre-bedrest volume. The level of muscle atrophy was much smaller compared to the data presented by [10], likely because of the conditions of the subjects (subjects in ICU vs. healthy subjects).

To obtain s and τ for the bedrest and reambulation data, we again used a least square fit to obtain their optimal values so that the square of the difference between the experimental data and predicted value using the analytical model was minimized. The optimization was done separately for the bedrest and the reambulation periods. Note that the $CSA(t = 0) = 1$ for bedrest and that the $CSA(t = 17weeks)$ equals its value at the end of bedrest for ambulation, i.e., in the case of the plantarflexors it equals 0.721. The final optimized values for ankle plantar- and dorsiflexors are listed in Table 1. Note for dorsiflexors, s is negative in the reambulation period, meaning they cannot recover to the pre-bedrest volume under the subject's activity level.

To introduce the exercise factors (such as muscle activation a and $a0$), we needed to obtain the values of the following parameters: CSA_{hyp}, τ_{bal}, and τ_{hyp}. From Eqs. (5) and (6), we know when there is no activation $CSA_{atr} = s + 1$ and $\tau_{atr} = \tau$, where the

Table 1. s and τ calculated through optimization for ankle plantar- and dorsiflexors.

	Plantarflexors		Dorsiflexors	
	s	τ (days)	s	τ (days)
Bedrest	−0.371	85.5	−0.232	62.6
Reambulation	0.070	28.6	−0.054	5.1

s and τ values are the ones for the bedrest period. As we are currently unable to determine or obtain data on the baseline activation level, $a0$, for both muscles, we assumed these muscles preserve their volumes if they are under the activation level needed to sustain standing under normal gravity. To calculate muscle activation during standing, we utilized a 3D musculoskeletal model [13, 14] (Fig. 5) with a slightly forward bending posture and obtained $a0 = 0.033$ for the ankle plantarflexors and $a0 = 0.010$ for the dorsiflexors. Since no muscle activations were recorded during the reambulation period, we assume, for simplicity, that average muscle activations during the reambulation period are 0.25 for both ankle plantar- and dorsiflexors. Consequently, we obtained the optimal $CSA_{hyp}, \tau_{bal}, \tau_{hyp}$ values so that the square of the difference between the optimized s and τ values and the predicted values using Eqs. (5) and (6) was minimized (least-square fit). These values are listed in Table 2.

Table 2. Parameter values prescribed and optimized for ankle plantar- and dorsiflexors in τ days.

	a	$a0$	τ_{bal}	τ_{hyp}	τ_{atr}	CSA_{hyp}	CSA_{atr}
Plantarflexors	0.25	0.033	33.6	11.4	85.5	1.311	0.629
Dorsiflexors	0.25	0.010	5.9	2.5	62.6	0.777	0.768

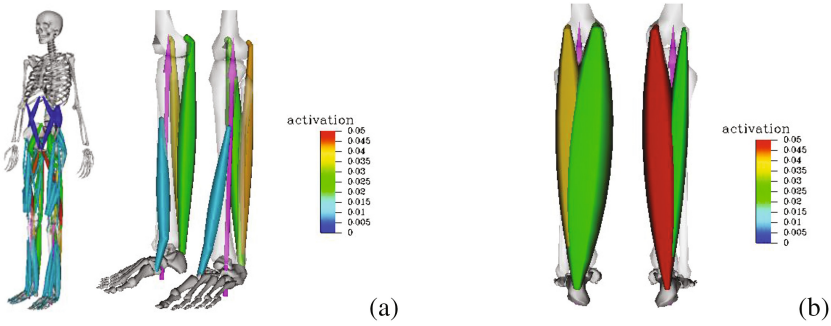

Fig. 5. (a) Muscle activation during standing predicted with a 3D musculoskeletal model [13], treated as baseline activation for maintaining muscle volume. (b) Difference in muscle volume and activation between left (normal) and right plantarflexors (with atrophy) during standing.

Figure 6 shows a comparison of the experimental data by [12] with predictions from the fitted analytical (with s and τ from Table 1) and the numerical model (with parameters from Table 2). The numerical model was solved with a generic implicit

Euler ordinate differential equation (ODE) solver. The model predictions agree well with the experimental data. This demonstrates that the models show the desired behavior and that the model calibration process was accurate.

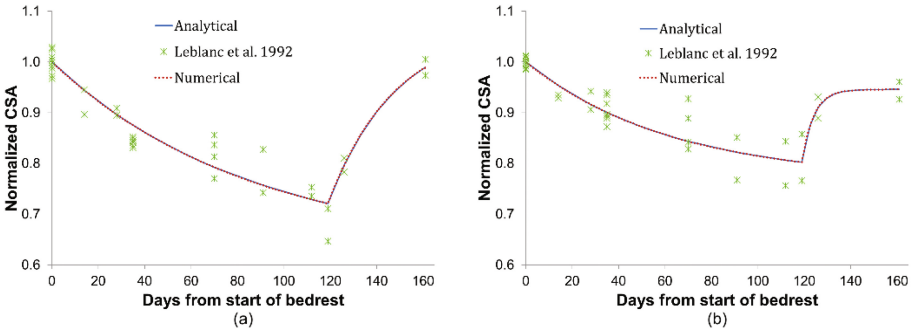

Fig. 6. Normalized muscle CSA change versus time with the analytical model fitted to data presented in [12] and from prediction of the numerical model in (Eq. 3); (a) for plantarflexors and (b) for dorsiflexors.

4 Spaceflight Induced Muscle Atrophy and Effects of Exercise Countermeasures

During long duration spaceflight, crewmembers on the International Space Station (ISS) typically have access to a cycle ergometer, a running treadmill, and a resistance exercise device. US astronauts typically spend less than two hours daily, at least six days per week, using these devices [15]. Exercise regimens varied among crewmembers with on average moderate intensity aerobic exercise performed $\sim$5 h per week and resistance exercise incorporating multiple lower leg exercises 3–7 days per week [16]. We have not found measurements of muscle electromyographical data (EMG) on the ISS during these exercises. Therefore, we refer to similar ground studies to estimate muscle activations. We focus on the gastrocnemius muscle, which is one of the main postural muscles that underwent significant muscle atrophy during a 6-month spaceflight [16]. For the gastrocnemius, the mean maximum and average muscle activation, relative to its maximum voluntary contraction (MVC), during a full crank cycle of ergometer cycling at 90 rpm is 0.5 and 0.17, respectively [17]. The mean maximum and average muscle activation relative to its MVC during one double legged squat lifting a load of 80% the maximum single repetition load is 0.75 and 0.43, respectively [18].

Assuming astronauts work out every day on the ISS for about two hours in the order of cycling, running, and resistance exercise, we created two daily muscle activation profiles for the gastrocnemius (Fig. 7). The first exercise regime, exercise 1, has activation levels (maximum and average) close to the ground activation levels specified above. The second regime, exercise 2, has higher activation levels and slightly longer durations. The intensity and duration of running was intentionally increased more than that of the other exercises to be closer to running intensities on earth. These activation profiles were created in the average sense since in reality the muscle activation

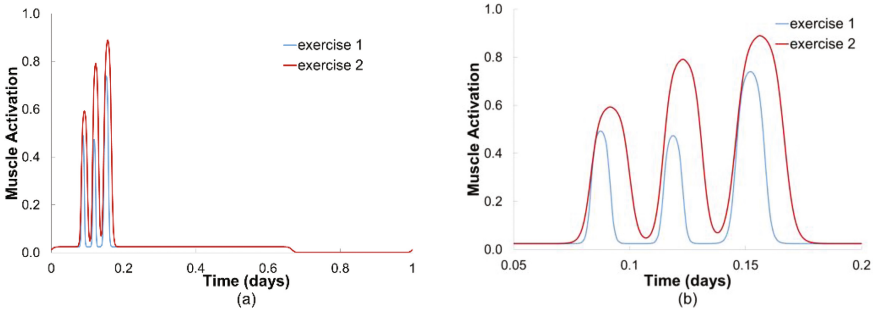

Fig. 7. Muscle activation profiles of gastrocnemius for two daily exercise regimes. (a) Muscle activation profile over the full day with an exercise period, a non-exercise period, and a sleep period, (b) zoomed-in view with the exercise period in detail.

oscillates with much shorter periods (higher frequency). The daily activation profile starts from the astronaut awaking and ends with sleeping for about eight hours. During sleep, we assume the muscle activation level is zero; and during the non-exercise period, we assume the muscle activation level is 0.025 under microgravity (smaller than the baseline value of $a0 = 0.033$ for ankle plantarflexors).

Based on these muscle activation profiles and data fitted earlier for ankle plantarflexors, we simulated dynamic muscle adaption for a 6-month spaceflight (180 days)

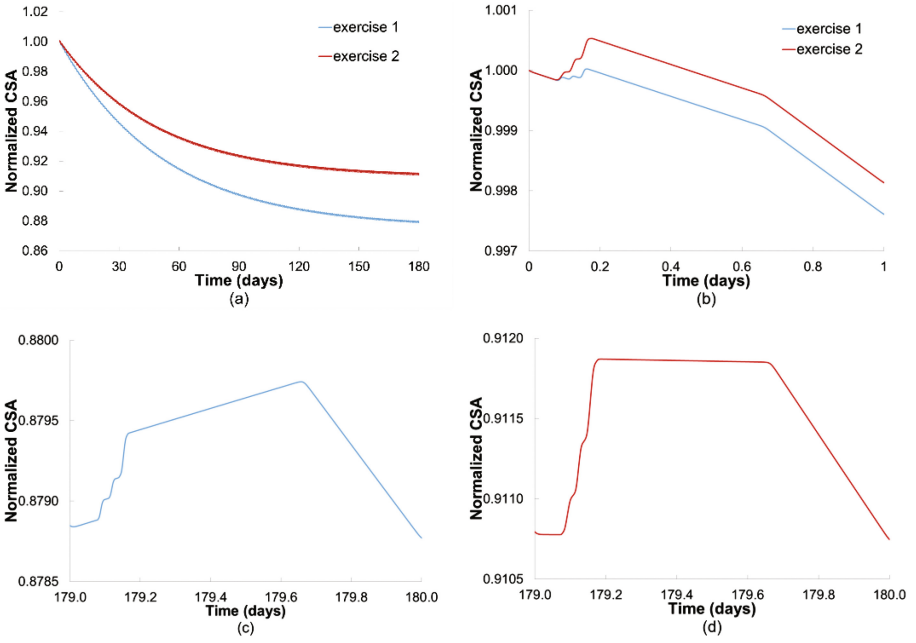

Fig. 8. Muscle adaptation during 6-month spaceflight for exercise 1 (lower intensity) and exercise 2 (higher intensity). Change in muscle *CSA* (a) over the full duration of the spaceflight; (b) on day 1; and (c) and (d) during the last day of the spaceflight.

with the numerical model (Fig. 8). At the end of the spaceflight, muscle atrophy reached around 12% under exercise 1 and around 8.8% under exercise 2. For both exercises muscle atrophy and hypertrophy nearly approached a balance where muscle mass would be maintained.

5 Discussion and Conclusions

Research conducted within NASA's Digital Astronaut Project [19] employed musculoskeletal models to investigate muscle atrophy and metabolic processes [20, 21]. Recently, a musculoskeletal modeling study used a detailed model of the "Advanced Resistance Exercise Device" that is currently used on the ISS for strengthening exercises [22]. It looked at combined muscle moments and did not include actions of individual muscles. However, it does provide important insights into the difference between exercising in microgravity and on earth. Since muscle adaptations during spaceflight depend on muscle activation levels and vary between muscles, individual muscle actions need to be included to better understand these changes.

The present model was calibrated against muscle atrophy data during bedrest and hypertrophy data during resistance training, focusing on overall muscle volume change at tissue or organ level. Within a muscle, different muscle fiber types (e.g. slow-twitch, fast-twitch) respond differently to under- or overloading and muscles undergo a fiber-type transition in response to mechanical stimuli [7]. The present model does not separately treat the adaptation of different muscle types due to lack of data for model calibration. The model can be separately calibrated to arbitrary muscle fiber types as long as specific experimental data are available. We can utilize the same adaptation model with different coefficients calibrated for each fiber type.

The current exploratory study of spaceflight atrophy demonstrated that the model can handle muscle atrophy and hypertrophy in a unified setting. It was demonstrated that the model can predict muscle atrophy during a 6-month spaceflight under different exercise regimes. It predicted overall muscle atrophy was lower with the higher intensity exercise routine (exercise 2; around 12%) than exercise 1 (around 8.8%). These levels are comparable to the $10 \pm 2\%$ of calf muscle atrophy reported in [16]. At the end of the spaceflight, muscle atrophy and hypertrophy nearly approached a balance where muscle mass would be maintained daily. The time course of muscle atrophy in space needs to be further verified when relevant data become available.

Due to its simplicity and relative small number of equations and parameters, the developed muscle adaptation model can be easily integrated with detailed 3D musculoskeletal models and simulations, by altering peak isometric force of individual muscles as a result of the muscle excitation-activation-adaptation mechanism. This was demonstrated using a 3D musculoskeletal model to simulate standing with the peak isometric force of the right plantarflexors decreased (atrophy) while the left ones were kept unchanged (Fig. 5). There was a clear difference in muscle volume and activation between the left and the right side. With this capability, we can further study overall strength change during spaceflight and validate results against existing data.

In conclusion, this study presents a simple semi-empirical muscle adaptation model dynamically driven by disuse or exercise induced muscle activity level (atrophy and

hypertrophy). This model is established on the observation of muscle atrophy or hypertrophy developing in an exponential fashion and reaching a homeostatic state. It introduces a "set point" or threshold of muscle activation at which the muscle maintains homeostatic equilibrium of muscle mass. The model was calibrated against experimental data for specific muscles and was further demonstrated for prediction of the time course of muscle atrophy for astronauts during a 6-month spaceflight mission involving daily exercise routines. This model can serve as a starting point for further studies on muscle physiology in space or other disuse scenarios and help to advise exercise countermeasures to reduce or recover muscle volume loss.

Acknowledgments. The authors would like to thank Dr. Beth Lewandowski of NASA Glenn Research Center and Dr. Lori Ploutz-Snyder of NASA Johnson Space Center for discussion on astronaut exercise routines on ISS and other related issues.

References

1. Ploutz-Snyder, L.L., Jeffrey, R., English, K.L., Haddad, F., Baldwin, K.M.: Risk of impaired performance due to reduced muscle mass, strength, and endurance. Evid. Report, Hum. Res. Program, Hum. Heal. Countermeas. Elem. NASA Johnson Sp. Cent. HRP-47072, pp. 1–80 (2015)
2. Adams, G.R., Caiozzo, V.J., Baldwin, K.M.: Skeletal muscle unweighting: spaceflight and ground-based models. J. Appl. Physiol. **95**, 2185–2201 (2003)
3. Hector, A.J., McGlory, C., Phillips, S.M.: The influence of mechanical loading on skeletal muscle protein turnover. Cell. Mol. Exerc. Physiol. **4**, e8 (2015)
4. Fitts, R.H., Trappe, S.W., Costill, D.L., Gallagher, P.M., Creer, A.C., Colloton, P.A., Peters, J.R., Romatowski, J.G., Bain, J.L., Riley, D.A.: Prolonged space flight-induced alterations in the structure and function of human skeletal muscle fibres. J. Physiol. **588**, 3567–3592 (2010)
5. Du, F., Wang, J., Gao, Y., Wang, H., Wang, Q., Jiang, S., Goswami, N.: A hind limb disuse model inducing extensor digitorum longus atrophy in rats: tail suspension-immobilization. Aviat. Space Environ. Med. **82**, 689–693 (2011)
6. Martin, K.S., Blemker, S.S., Peirce, S.M.: Agent-based computational model investigates muscle-specific responses to disuse-induced atrophy. J. Appl. Physiol. **118**, 1299–1309 (2015)
7. Wisdom, K.M., Delp, S.L., Kuhl, E.: Use it or lose it: multiscale skeletal muscle adaptation to mechanical stimuli. Biomech. Model. Mechanobiol. **14**, 195–215 (2015)
8. Zöllner, A.M., Abilez, O.J., Böl, M., Kuhl, E.: Stretching skeletal muscle: chronic muscle lengthening through sarcomerogenesis. PLoS ONE **7**, e45661 (2012)
9. DeFreitas, J.M., Beck, T.W., Stock, M.S., Dillon, M.A., Kasishke, P.R.: An examination of the time course of training-induced skeletal muscle hypertrophy. Eur. J. Appl. Physiol. **111**, 2785–2790 (2011)
10. Gruther, W., Benesch, T., Zorn, C., Paternostro-Sluga, T., Quittan, M., Fialka-Moser, V., Spiss, C., Kainberger, F., Crevenna, R.: Muscle wasting in intensive care patients: ultrasound observation of the M. Quadriceps femoris muscle layer. J. Rehabil. Med. **40**, 185–189 (2008)

11. Arbeille, P., Kerbeci, P., Capri, A., Dannaud, C., Trappe, S.W., Trappe, T.A.: Quantification of muscle volume by echography: comparison with MRI data on subjects in long-term bed rest. Ultrasound Med. Biol. **35**, 1092–1097 (2009)
12. LeBlanc, D., Schneider, V.S., Evans, H.J., Pientok, C., Rowe, R., Spector, E.: Regional changes in muscle mass following 17 weeks of bed rest. J. Appl. Physiol. **73**, 2172–2178 (1992)
13. Hamner, S.R., Seth, A., Delp, S.L.: Muscle contributions to propulsion and support during running. J. Biomech. **43**, 2709–2716 (2010)
14. Christophy, M., Faruk Senan, N.A., Lotz, J.C., O'Reilly, O.M.: A musculoskeletal model for the lumbar spine. Biomech. Model. Mechanobiol. **11**, 19–34 (2012)
15. Coolahan, J.E., Feldman, A.B., Murphy, S.P.: Simulation of integrated physiology based on an astronaut exercise protocol. Johns Hopkins APL Tech. Dig. **25**, 201–213 (2004)
16. Trappe, S., Costill, D., Gallagher, P., Creer, A., Peters, J.R., Evans, H., Riley, D.A., Fitts, R.H.: Exercise in space: human skeletal muscle after 6 months aboard the International Space Station. J. Appl. Physiol. **106**, 1159–1168 (2009)
17. Neptune, R.R., Kautz, S.A., Hull, M.L.: The effect of pedaling rate on coordination in cycling. J. Biomech. **30**, 1051–1058 (1997)
18. Robertson, D.G.E., Wilson, J.-M.J., St Pierre, T.A.: Lower extremity muscle functions during full squats. J. Appl. Biomech. **24**, 333–339 (2008)
19. White, R.J., McPhee, J.C.: The digital astronaut: an integrated modeling and database system for space biomedical research and operations. Acta Astronaut. **60**, 273–280 (2007)
20. Thompson, W.K., Caldwell, E.E., Newby, N.J., Humphreys, B.T., Lewandowski, B.E., Pennline, J.A., Ploutz-Snyder, L.L., Mulugeta, L.: Integrated biomechanical modeling of lower body exercises on the advanced resistive exercise device (ARED) using LifeMod. In: 44th International Conference on Environmental Systems (2014)
21. Lewandowski, B.E., Pennline, J.A., Thompson, W.K., Humphreys, B.T., Ryder, J.W., Ploutz-Snyder, L.L., Mulugeta, L.: Development of the NASA digital astronaut project muscle model. 2015 Hum. Res. Progr. Investig. Work. Galveston, TX, United States. Poster (2015)
22. Fregly, B.J., Fregly, C.D., Kim, B.T.: Computational prediction of muscle moments during ared squat exercise on the international space station. J. Biomech. Eng. **137**, 121005 (2015)

Medical Simulation: Filling the Training Gap

Human Simulation System for Injury Assessment Due to Repetitive Loading

Sultan Sultan, Karim Abdel-Malek, Jasbir Arora(✉), and Rajan Bhatt(✉)

Center for Computer-Aided Design (CCAD),
Virtual Soldier Research (VSR) Program,
The University of Iowa, Iowa City, USA
{asultan, amalek}@engineering.uiowa.edu,
{jasbir-arora, rajan-bhatt}@uiowa.edu

Abstract. The subject of this research is to investigate human simulation to predict injuries due to the fatigue of a repetitive loading. This work over the past few years has sought to integrate high-fidelity computational methods for stress/strain analysis, namely finite element analysis (FEA), with biomechanics predictions through digital human modeling and simulation (DHMS). Previous work by this group is a simulation environment called SANTOS®, which enables the prediction of human motion, including all aspects of its biomechanics. The SANTOS environment provides a joint- and physics-based predictive dynamics including a muscle model. Repetitiveness of work activity has been shown to be a strong risk factor for cumulative trauma disorders (repetitive strain injuries). Both cumulative load theory and deferential fatigue theory claim that repetitive activities precipitate musculoskeletal injury. The cumulative load theory suggests that repeated load application may result in cumulative fatigue, reducing stress-bearing capacity. Such changes may reduce the threshold stress at which the tissues fail. The deferential fatigue theory proposes that the muscles operating the joints may be differentially loaded and that this may not be proportional to the individual muscles' capabilities. This can create a significant stress concentration in some tissues, causing an injury. This paper presents a local biomechanics model in a virtual environment, whereby the DHMS model calculates the muscle forces and motion profiles (i.e., the kinematics of the motion across time for each degree of freedom for the body). Predictive dynamics, a method developed and implemented by this group, is able to characterize the motion using an optimization algorithm that calculates the motion profiles. These motion profiles and muscle forces are calculated for each task over a repetitive cycle and are used as input for the multi-scale FEA model. The FEA model of the selected joint computes the stresses of the joint components. The system compares the current stresses of the components with the newly yielded strength that has been affected by cyclic loading and indicates the injury status of the components. This paper presents promising results to quantify and predict injury in a particular joint that is undergoing a specific repetitive motion. This integrated system allows one to study the effects of various motions and task parameters on knee joints so as to modify tasks, save analysis time, and reduce the likelihood of injury.

Keywords: Digital human modeling · Multi-scale modeling · FEA modeling · Injury prevention · Fatigue loading

D.N. Cassenti (ed.), *Advances in Human Factors in Simulation and Modeling*,
Advances in Intelligent Systems and Computing 591, DOI 10.1007/978-3-319-60591-3_12

1 Introduction

Musculoskeletal injuries appear as problems in muscles, tendons, ligaments, cartilages, menisci, and bone tissue. These injuries may result from high stress and may potentially advance into chronic conditions [1]. In the US Army, it was reported that about 80% of musculoskeletal injuries for bone stress reactions and stress fractures were located in the lower extremities [2].

In 2006, 82% of the total injuries in the military related to musculoskeletal conditions, and 22% of those were due to knee joint injury [3]. The most commonly injured human body region was the knee joint, followed by the lower back and the ankle joint [4].

The impact of injuries is a loss of manpower, an increase in healthcare costs, and a high probability of disabilities and fatalities. In 2004, over 3 million days of limited duty as a result of lower-extremity injuries took place in the Department of Defense [5]. In addition, there are 27,000 injuries each day in the United States due to sprains of the ankle and knee joints [6].

A fatigue mechanism was suggested as the method of failure of articular cartilage [7]; this is likely either due to a single application of a large load or to cumulative cyclic application of a lower load. Muscle fatigue is simply defined as a decrease in the force-generating capacity of a muscle [8] that can impede task performance and may impair a person's ability to properly execute a task; it may ultimately lead to failure and injury of the joint.

The failure of tissue due to fatigue is explained through two theories: the differential fatigue theory and the cumulative load theory. The first theory states that repetitive loading can alter muscle kinetics and that this changes the joint kinematics pattern and results in stress concentration in the tissue, causing failure [9]. The second theory focuses on the reduction of the stress-bearing capacity of the tissue [10]. It states that, in repetitive loading, there will be a decline in the power capacity of the muscle to a level of threshold stress at which the tissues fail. The work in this study focuses on the cumulative load theory. Sultan and Marler [11] introduced a simple multi-scale model for predicting knee joint injury based on static analysis involving joint torque and external ground reaction forces predicted by the DHM Santos. Sultan and Marler [12] also presented a multi-scale model for predicting a measure for knee and ankle joint injury based on analysis involving motion data and external ground reaction forces predicted by the DHM Santos in conjunction with muscle force computation by the OpenSim software. For different loading capacities, Sultan et al. [13] developed a method to assess the level of injury of knee joint components using finite element modeling in conjunction with neural network analysis.

This study provides a method to measure knee joint component injury for both soft tissues and bones due to a repetitive task cycle. The measuring system is capable of quantitatively assessing the level of injury. The importance of the proposed method is its ability to predict a quantitative scale of the risk of the injury due to a repetitive load duty. This definitely scales the level of injury and indicates proper action for prevention.

2 Method

2.1 Dynamic Prediction System

Predictive dynamics is an approach for simulating human motion with 109 predicted degrees of freedom (DOFs) [14]. These DOFs are represented by joint angles. The relationship between the joint angles and the position of the points on the series of links is defined using the Denavit-Hartenberg (DH) notation [15]. The formulation of the optimization problem includes: (1) determining joint angles as a function of time, (2) optimizing a cost function, and (3) imposing constraints on the motion [16, 17].

In this study, the human motion is predicted using virtual human model named Santos® developed by the Virtual Solider Research program at the University of Iowa. Santos uses physics-based predictive dynamics framework to predict the motion of markers in the form of x-y-z positions and three components of ground reaction forces for walking and stair-ascending tasks in three different loading cases: with no backpack, with a 17 kg backpack, and with a 33 kg backpack, as shown in Fig. 1. Each load case was subjected to seven different repetitive task cycles: 1 cycle, 10 cycles, 100 cycles, 250 cycles, 500 cycles, 750 cycles, and 1000 cycles. The predicted data, which is information about motion data and external forces data (ground reaction forces), is then fed into a muscle force computation model for further analysis.

Fig. 1. Backpack carrying: (a) no backpack, (b) 17 kg backpack, and (c) 33 kg backpack

2.2 Finite Element Analysis

The present study used the same 3D FEA model used by Sultan et al. [13] as shown in Fig. 2. All joint components were meshed using the tetrahedron element (C3D4) with

27109 nodes and 99128 elements. Bone was modeled as an elastic material, and soft tissue was modeled as a hyper-elastic material with the Noe-Hookean method [12]. Contact problems were developed for three pairs of components. In the knee joint model, there were a pair of contact points between the femur cartilage and the patella cartilage, a pair of contact points between the femur cartilage and the tibia cartilage, and a pair of contact points between the femur cartilage and the menisci. The coefficient of friction for the contact problems was 0.01.

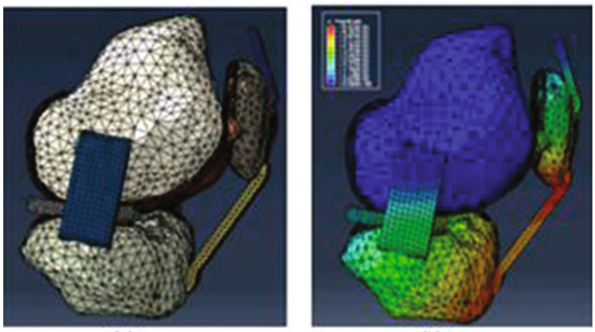

Fig. 2. Knee joint FEA model: (a) tetrahedron mesh element, (b) displacement solution

3 Repetitive Loading and Injury Propensity

Repetition of activities places stress on human physical systems. A repeated load with an inadequate time for recovery from the deformation will increase stress concentration, and this will lower the stress tolerance of the tissue and increase the chance of joint injury.

Differential fatigue theory explains how injury develops from repeated loading through altering muscle kinetics, resulting in joint kinematics and a loading pattern different from the optimum [9]. This places a significant stress concentration on some tissues, causing an injury.

Cumulative load theory explains that repeated load may result in cumulative fatigue, reducing stress-bearing capacity. Muscle fatigue is typically quantified as a decline in the maximal force or power capacity of muscle [10]. This may reduce the threshold stress at which the tissues fail. The work of the present study is based on cumulative load theory and experimental data taken from Kumar [9]. The data was used to construct a mathematical formula to measure the decline of strength of the tissue due to an increase in cycle number. A plot to illustrate the relationship between the strength of the tissue with the number of task cycles is shown in Fig. 3. The curve in Fig. 3 is empirically represented by the following mathematical equation:

$$RS = 75.7395 - 0.0274 * N_r + 1.5446 * 10^{-6} * N_r^2 \quad (1)$$

where **RS** is the percent of reduction of strength, and $\mathbf{N_r}$ is the number of task cycles.

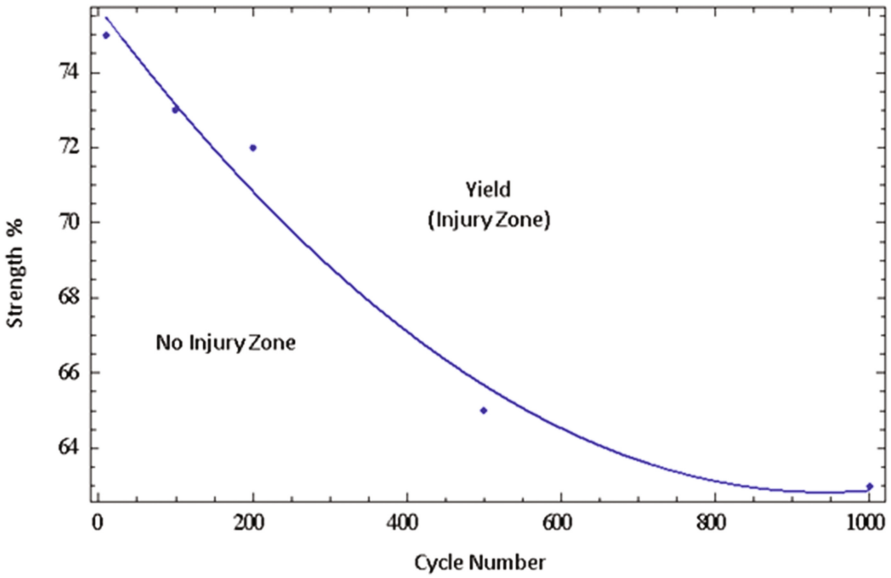

Fig. 3. Declination of strength *vs* number repetitive cycles; data taken from reference [9] and plotted with second-order polynomial regression.

This study used the same algorithm presented by Sultan et al. [13] to assess the level of injury of each component of the joint. The algorithm uses current stress and compares it with the yield stress of a component over the time of the task stride. Due to repetitive loading, the yield stress is no longer a fixed value but changes based on the number of task cycles, as illustrated in Fig. 3. The injury index for the joint components is computed for two tasks: walking and stair ascending. Each task is done with three loading cases: no backpack, 17 kg backpack load, and 33 kg backpack load. All cases were repeated seven times: at one cycle, ten cycles, 100 cycles, 250 cycles, 500 cycles, 750 cycles, and 1000 cycles.

4 Results and Discussion

For a selected task, a dynamic prediction system provides prediction of motion and external forces such as ground reaction forces. Muscle force computation is essentially conducted to determine compression and shear in the joint. A finite element model conducts analysis to compute the field stress at the joint. The present study focuses on the menisci, as this part is in direct contact with the cartilage of the moving joint. The injury

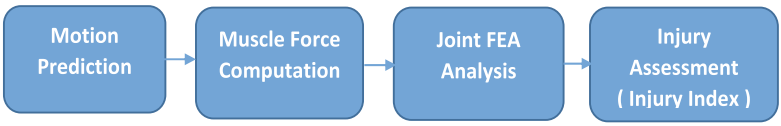

Fig. 4. Injury assessment method

index is simply calculated by evaluating the ratio of current Von Mises stress [18] to the yield stress of a component. A value of less than unity means healthy joint, whereas value of unity or more means risky joint. The complete method of injury assessment is illustrated in Fig. 4. Results of the injury index of the medial meniscus are given in Table 1.

Table 1. Comparison of injury index at different loadings for right knee medial meniscus at 60% of the stride

Number of cycles	Walk			Stair ascending		
	Load-0	Load-1	Load-2	Load-0	Load-1	Load-2
10	0.259	0.298	0.357	0.308	0.349	0.355
100	0.268	0.307	0.368	0.317	0.360	0.367
250	0.281	0.322	0.386	0.333	0.378	0.384
500	0.298	0.342	0.410	0.354	0.401	0.409
750	0.309	0.355	0.425	0.366	0.416	0.423
1000	0.312	0.358	0.428	0.369	0.419	0.427

Load-0 = no backpack, Load-1 = 17 kg backpack,
Load-2 = 33 kg backpack
The injury index at yield point is a unity

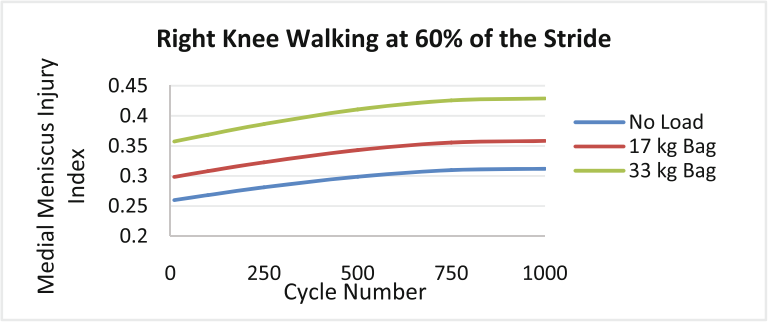

(a)

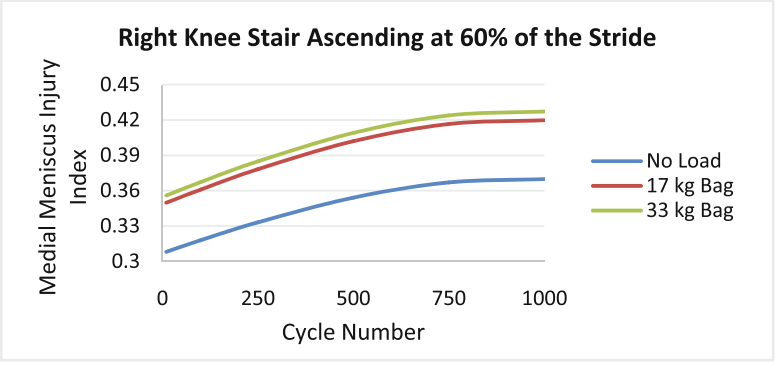

(b)

Fig. 5. Injury index at different cycle numbers: (a) walking (b) stair ascending

The maximum injury index values for the medial meniscus of the right knee joint at 60% of the walking stride for three loading cases as found after 1000 repetitive cycles are 0.312, 0.353, and 0.428, as presented in Table 1. For the same joint under the same walking task, the values of the injury index after 10 repetitive cycles are 0.259, 0.298 and 0.357.

For the stair-ascending task under the same loading cases as the right knee medial meniscus, injury index values of 0.369, 0.419, and 0.427 at 60% of the stair ascending stride were found after 1000 repetitive cycles, as presented in Table 1. After 10 repetitive cycles, the injury index values are 0.308, 0.349, and 0.355. Figures 5(a) and (b) show plots of the injury index for the three load cases under different cycle numbers for the walking and stair-ascending tasks, respectively. A comparison of the injury index values for the medial meniscus and lateral meniscus under the same circumstances for right knee walking is shown in Figs. 6(a) and (b). For the right knee stair-ascending task, the comparison is illustrated in Figs. 7(a) and (b).

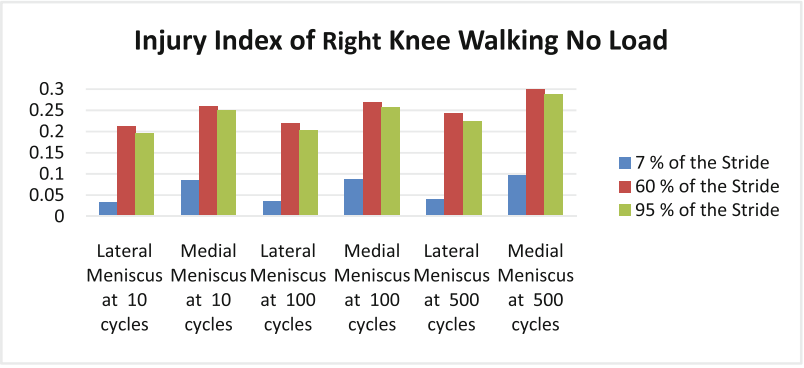

(a)

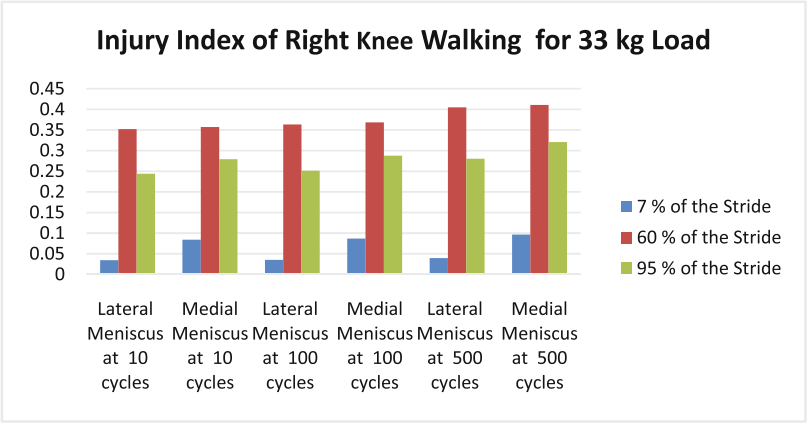

(b)

Fig. 6. Knee components injury index at different cycle numbers: (a) walking with no load, (b) walking with 33 kg backpack

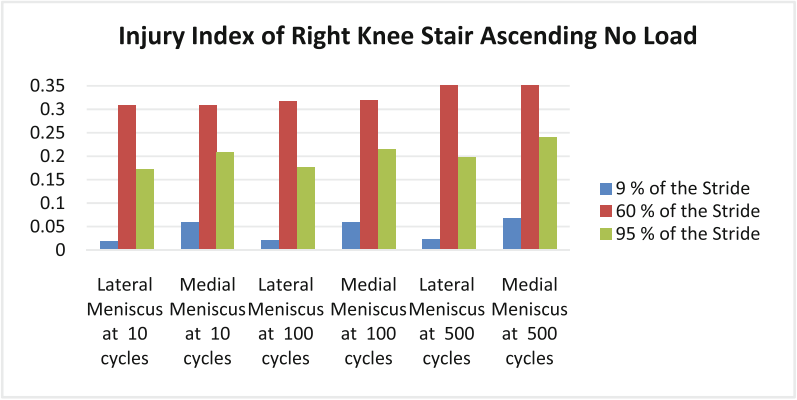

(a)

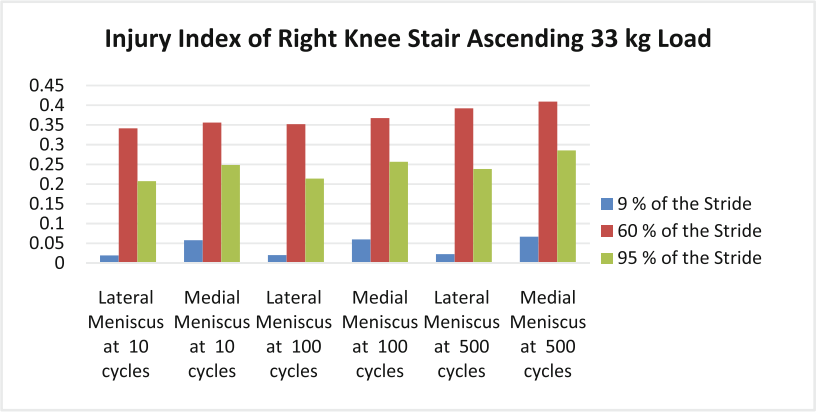

(b)

Fig. 7. Knee components injury index at different cycle numbers: (a) stair ascending with no load, (b) stair ascending with 33 kg backpack

Generally, from the injury index values given in Table 1 and the graphs, it is evident that there is an increase of 15% in the injury index value when the task is repeated for 500 cycles and an increase of 20% when the task is repeated for 1000 cycles. This means that the probability of risk of injury of the menisci of the knee joint is higher by 15% when repeating the task for 500 cycles and by 20% when repeating the task for 1000 cycles.

5 Conclusions

This study has presented a method for injury risk assessment due to a repetitive loading task. A predictive DHM provides dynamic prediction information about motion and external forces. Muscle force in the joint is involved in the analysis of the injury index

of all components, and the stress field of the stride of the task is usually computed by using an FEA model for the joint. The method of measuring injury index due to repetitive loading is a powerful approach as it provides a quantitative measure of the probability of injury when the joint is subjected to a number of loading cycles. The method measures the level of risk of the joint during repetitive loading, and this may direct proper actions for injury prevention.

References

1. Zambraski, E.J., Yancosek, K.E.: Prevention and rehabilitation of musculoskeletal injuries during military operations and training. J. Strength Cond. Res. **26**(7), 101 (2012). National Strength and Conditioning Association
2. Army Report TB MED 592: Prevention and control of musculoskeletal injuries associated with physical training. Technical Bulletin, May 2011
3. Hauret, K.G., Bruce, H., Jones, B.H., Bullock, S.H., Canham-Chervak, M., Canada, S.: Musculoskeletal Injuries Description of an Under-Recognized Injury Problem Among Military Personnel. US Army Report (2006)
4. Danny, L.T., Hollingsworth, J.: The prevalence and impact of musculoskeletal injuries during a pre-deployment workup cycle: survey of a Marine Corps special operations company. J. Spec. Oper. Med. Fall **9**(4), 11–15 (2009)
5. Ruscio, B.A., Jones, B.H., Bullock, S.H., Burnham, B.R., Canham-Chervak, M., Rennix, C.P., Wells, T.S., Smith, J.W.: A process to identify military injury prevention priorities based on injury type and limited duty days. Am. J. Prev. Med. **38**, S19–S33 (2010)
6. Renstrom, P.A.F.H., Konradsen, L.: Ankle ligament injuries. Br. J. Sports Med. **31**(1), 1–20 (1997)
7. Seedhom, B.B.: Conditioning of cartilage during normal activities is an important factor in the development of osteoarthritis. Rheumatology **45**, 146–149 (2006)
8. Gates, D.H., Dingwell, J.B.: The effects of neuromuscular fatigue on task performance during repetitive goal-directed movements. Exp. Brain Res. **187**(4), 573–585 (2008)
9. Kumar, S.: Theories of musculoskeletal injury causation. Ergonomics **44**(1), 17–47 (2001)
10. Enoka, R.M., Duchateau, J.: Muscle fatigue: what, why and how it influences muscle function. J. Physiol. **586**(1), 11–23 (2008)
11. Sultan, S., Marler, R.T.: Multi-scale human modeling for injury prevention. In: 2nd International Conference on Applied Digital Human Modeling, July, San Francisco (2012)
12. Sultan, S., Marler, R.T.: Multi-scale predictive human model for preventing injuries in the ankle and knee. In: 6th International Conference on Applied Digital Human Modeling, July, Los Vegas (2015)
13. Sultan, S., Abdel-Malek, K., Arora, J., Bhatt, R., Marler, T.: An integrated computational simulation system for injury assessment. In: Duffy, V. (ed.) 7th International Conference on Applied Digital Human Modeling. Springer, Cham (2017)
14. Abdel-Malek, K., Yang, J., Kim, J., Marler, R.T., Beck, S., Nebel, K.: Santos: a virtual human environment for human factors assessment. In: 24th Army Science Conference, November, FL, Assistant Secretary of the Army, (Research, Development and Acquisition), Department of the Army, Washington, DC (2004)
15. Denavit, J., Hartenberg, R.S.: A kinematic notation for lower-pair mechanisms based on matrices. J. Appl. Mech. **77**, 215–221 (1995)

16. Marler, T., Knake, L., Johnson, R.: Optimization-based posture prediction for analysis of box lifting tasks. In: Duffy, V.G. (ed.) 3rd International Conference on Digital Human Modeling. Springer, Heidelberg (2011)
17. Marler, R.T.: A study of multi-objective optimization methods for engineering applications. Ph.D. dissertation, University of Iowa, Iowa City, IA (2005)
18. Andriyana, A.: Failure criteria for yielding. CEMEF UMR CNRS 7635, Sophia Antipolis, France (2008)

Image Enhancement Using FUZZY Set

Gunamani Jena[1(✉)], Shubhashish Jena[2], and V. Rajesh Bonam[2]

[1] BVCE JNTUK, Kakinada, AP, India
g_jena@rediffmail.com
[2] CSE BVCE, Amalapuram, India
sjenal998@gmail.com, rajesh.bonam@bvcgroup.in

Abstract. In this paper, FUZZY set is used to deal with image enhancement problems of some uncertain and inaccurate image. The traditional image enhancement method like histogram modification, image smoothing, image sharpening in verse filters and wiener filter for inaccurate and uncertain image is undesirable. As fuzzy system is capable of representing diverse, non-exact, uncertain and inaccurate knowledge of information, it has attracted the attention of for image enhancement. The generalized enhancement algorithm proposed by Dong Liang Peng and Tie-Jun-Wu in 2002 [1] is not suitable for images having very less gray values, lower contrast, more uncertainly and inaccuracy. A novel approach to generalized image enhancement using fuzzy set is proposed in this paper to overcome the problem.

Keywords: FT · Fourier transform · FUZZY set · Membership · FE · Fuzzy enhancement method · GT · Gray transformation

1 Introduction

The improvement of pictorial information for human interpretation and processing of scene data for autonomous machine perception are the root application areas that has shown interest in image processing filed a decade ago. Vision is the foremost trusted source of information compared to other human perception, and image in the basic container of any pictorial information. The two broad categories of image enhancement are,

- Spatial domain methods based on direct manipulation of pixel
- Frequency domain methods [2, 3] are based on modifying the Fourier transform of an image

Fuzzy image processing approach is the collection of how to understand, represent and process the image, their segmentation & features as Fuzzy set. Fuzzy image processing has three main stages: image fuzzification, modification of membership values and image Defuzzification as given in Fig. 1.

The main reason for using fuzzy image processing is

(a) It is a powerful tool for knowledge representation and process.
(b) It can manage the vagueness and ambiguity efficiently.

D.N. Cassenti (ed.), *Advances in Human Factors in Simulation and Modeling*,
Advances in Intelligent Systems and Computing 591, DOI 10.1007/978-3-319-60591-3_13

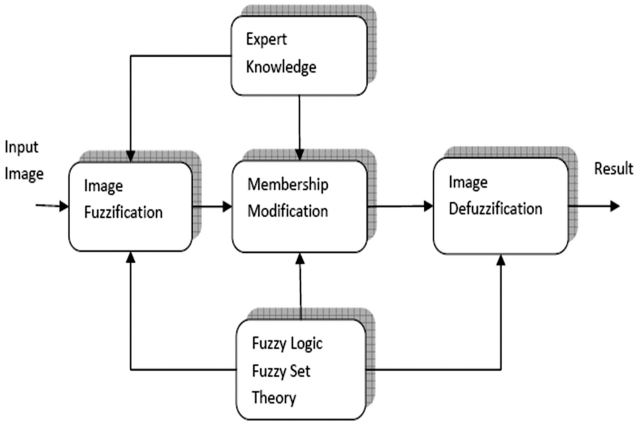

Fig. 1. General structure of fuzzy image processing

2 Existing Method

2.1 Spatial Domain

It is denoted by

$$g(x, y) = T[f(x, y)] \tag{1}$$

Where f(x, y) in the input image, g(x ,y) is the processed image T is the operator on f(x, y). The center of a mark is moved from pixel to pixel from top left corner. The operator T is applied at each location (x, y) to yield g.

2.2 Gray Scale

Here the gray level below the threshold value is mapped to 0 and gray level above threshold value mapped to 255 (Fig. 2).

Original Image Lena

Image with Gaussian noise σ =100

Fig. 2. (a) Original image Lena; (b) Image with Gaussian noise σ = 100

2.3 Histogram Equalization

It involves finding a gray scale transformation function that creates an output image with uniform histogram. But here the problem is how to determine the gray scale transformation function. Histogram equalization image Lena is given below (Fig. 3).

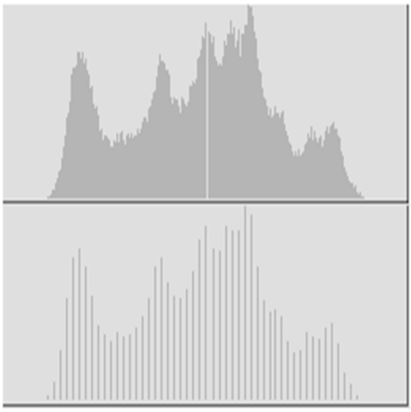

Fig. 3. Histogram equalization of image Lena

2.4 Image Smoothing [4]

Here the technique of neighborhood averaging is employed which results in blurring. We commonly use some weighting function like rectangular weighting function (average) or a triangular weighting function or a Gaussian.

2.5 Averaging

See Fig. 4.

1/9*

1	1	1
1	1	1
1	1	1

Fig. 4. Lena image with Gaussian noise $\sigma = 10$ filtered by average filter

2.6 Gaussian Filter

See Fig. 5.

1/16*

1	2	1
2	4	2
1	2	1

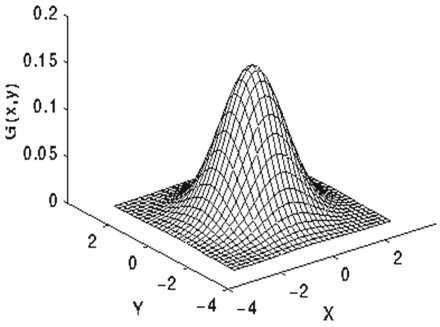

Fig. 5. Gaussian filter

As the above method results in blurring, for edge preserving median filtering is used. Here the pixels with outlaying values are forced to become more like their neighbor. It is a non-liner filter (Fig. 6).

Fig. 6. Lena image with Gaussian noise $\sigma = 10$ filtered by median filter

2.7 Image Sharpening

Here the high frequency components are enhanced as a high positive component is taken at the center. High boost filter can be used when low frequency components are retained along with the high pass image.

2.8 Frequency Domain Methods

Here we enhance the Fourier Transform (FT) of the image. The FT of the image is multiplied by a filter & the inverse transform is taken to enhance the image.

3 Fuzzy Image Enhancement [6–8, 10–12]

It consists of Fuzzification, modification of membership value and Defuzzification. The main power of fuzzy image processing in modification of membership value. First the image data are transformed from gray level plane to the membership plane then appropriate fuzzy technique modify the membership value. This can be a fuzzy clustering a fuzzy rule-based approach and a fuzzy integration approach.

3.1 Generalized Fuzzy Image Enhancement

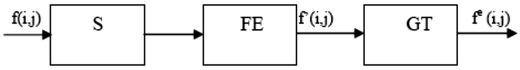

Fig. 7. Block diagram of generalized image enhancement

The smoothing operation S uses median filtering. It is a nonlinear method which suppresses noise and reduces blurring at the same time retains the high frequency components. The fuzzy enhancement method (FE) follows the smoothing operation. The image f*(i, j)* with M *x N* pixels where $f_{ij}\, i = 1, 2...n$, is the gray level of the pixel. The fuzzy set is represented by $\tilde{F}$ which is explained in the proposed method. μ_{ij} is called the fuzzy property plane. The key to the fuzzy enhancement is a contrast intensification operator is T $\left(\mu_{ij}\right)$ (Fig. 7).

Where,

$$\begin{aligned} \mathrm{T}(\mu_{ij}) &= 2(\mu_{ij})^2, \text{where } 0 \leq \mu ij \leq 0.5 \\ &= 1 - 2(1-\mu_{ij})^2, \text{where } 0.5 < \mu_{ij} \leq 1. \end{aligned} \tag{2}$$

The image *f(i, j)* can be enhanced in the property domain by a transformation function $T^{(r)}$

$$\mu'_{ij} = T^{(r)}(\mu'_{ij}) = T(T^{(r-1)}(\mu_{ij})), \mathrm{r} = 1, 2... \tag{3}$$

The enhanced image can be obtained by the following inverse transformation

$$f'_{ij} = G^{-1}\left(\mu'_{ij}\right) \tag{4}$$

Where f'_{ij} is the gray level of the *(i, j)th* pixel in the enhanced image and G^{-1} denotes the inverse transformation of G. The final result is obtained by a gray transformation, GT (t) (Fig. 8).

$$f^{e}_{ij} = t(f'_{ij}) = \frac{f^{e}_{max} - f^{e}_{min}}{f'_{max} - f'_{min}} (f'_{ij} - f'_{min}) + f^{e}_{min} \tag{5}$$

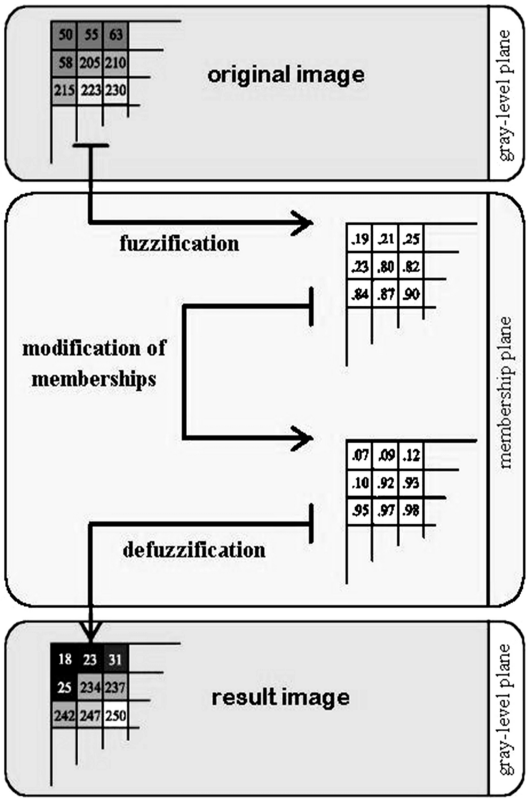

Fig. 8. Fuzzification and defuzzification

4 Proposed Method

As earlier approach proposed method is also divided into three main steps:

(i) Fuzzification
(ii) Iterative computations [9]
(iii) Defuzzification

Given an image f*(i, j)* with M *x N* pixels and f_{ij} levels, and let $f_{ij}\, i = 1,\ 2\ldots n$, be the gray level of the pixel location *(i, j)*. The fuzzy set $\tilde{F}$ corresponding to this image can be written as the following form

$$\tilde{F} = \left(\frac{\mu_{IJ}}{f_{ij}}\right)_{MXN} \tag{6}$$

Where $\left(\frac{\mu_{ij}}{f_{ij}}\right)$, $\left(0 \le \mu_{ij} \le 1\right)$ means the degree of possessing some appointed brightness by the *(i, j)th* pixel with the gray level f_{ij}. This appointed brightness is usually the maximum f_{max} of gray levels in the image. Here $\mu_{ij} = 0$ indicates dark and $\mu_{ij} = 1$ bright. Any intermediate value refers to the grade of maximum gray level of the pixel. A set consisting of all μ_{ij} is called the fuzzy property plane of the image. In [1] μ_{ij} is expressed as

$$\mu_{IJ} = G(f_{ij}) = \left[1 + \frac{f_{\max} - f_{ij}}{F_d}\right]^{-F_c} \tag{7}$$

Where *Fc* and *Fd* denote the exponential and the denominational fuzzifiers, respectively. It is apparent that those two positive constants have the effect of altering ambiguity in the fuzzy property plane. The key to the fuzzy enhancement is a contrast intensification operator (INT). It is calculated using below equation.

$$\begin{aligned} T(\mu_{ij}) &= \sqrt[2]{\frac{\mu_{ij}}{2}} \quad 0 \le \mu ij \le 0.5 \\ &= 1 - \sqrt[2]{\frac{(\mathrm{i} - \mu \mathrm{ij})}{2}} \\ 0.5 &< \mu_{ij} \le 1 \end{aligned} \tag{8}$$

where T is Contrast Intensification Operator (INT). The image *f(i, j)* can be enhanced in the property domain by a transformation function $T^{(r)}$

$$\mu'_{ij} = T^{(r)}(\mu'_{ij}) = T(T^{(r-1)}(\mu_{ij})),\ r = 1, 2\ldots \tag{9}$$

Where $T^{(r)}$ is defined a successive application of T. The enhanced image can be obtained by the following inverse transformation

$$f'_{ij} = G^{-1}\left(\mu'_{ij}\right) \tag{10}$$

Where f'_{ij} is the gray level of the *(i, j)th* pixel in the enhanced image and G^{-1} denotes the inverse transformation of G. The final result is obtained by a gray transformation, GT, of the enhanced image that can be represented as

$$f_{ij}^{e} = t(f'_{ij}) = \frac{f_{max}^{e} - f_{min}^{e}}{f'_{max} - f'_{min}}(f'_{ij} - f'_{min}) + f_{min}^{e} \tag{11}$$

Where the gray level of the *(i, j)th* pixel, the gray maximum and the gray minimum of the final image are denoted by f_{ij}^{e}, f_{min}^{e} and f_{max}^{e} respectively.

Similarly, f'_{min} and f'_{max} indicate the gray maximum and minimum of the image enhanced by FE, respectively. More ever, the following relationships hold:

$$f'_{min} > f_{min}^{e} f'_{max} < f_{max}^{e} \tag{12}$$

5 Proposed Algorithm

The Proposed fuzzy enhancement algorithm is given below.

(i) Input the original image *f(i, j),* let r = 1 and define f_{min}^{e} *and* f_{max}^{e}.
(ii) For each pixel *(i, j)* replace its gray level by the median of the gray levels in its 3 × 3 neighborhood.
(iii) Calculate the fuzzy property plane μ_{ij} corresponding to the filtered image stated above by Eq. (7).
(iv) Transform the fuzzy property plane stated above by (8) and (9) and the result is denoted by μ'_{ij}.
(v) Solve the inverse transformation (10) of G, and the gray level of thefuzzy-enhanced image can be obtained.
(vi) Calculate the gray transform of the image enhanced by the generalized fuzzy enhancement from (11).
(vii) If the enhancement effect is not satisfying, then let r = r + 1 and go to (iv), otherwise the iteration ends.
(viii) Output the final image.

Parameter selection: Here r is taken as 1,
F_c is 2, and F_d is 250.

6 Simulation and Experimental Results

See Fig. 9.

(a) Original Image Lena

(b) Degraded Image

(c)Enhancement using Generalized Fuzzy Image Enhancement

(d) Enhancement using proposed method

Fig. 9. (a) Original image Lena (b) Degraded image (c) A generalized Image Enhancement (d) Enhancement using proposed method

7 Conclusion

Fuzzy system is more suitable for the image enhancement problem where diverse, non-exact, uncertain and inaccurate knowledge of information is available. The generalized image enhancement method using fuzzy set does not work well for images having low gray value and high inaccuracy. The proposed method overcomes the problem and from the simulation analysis it is clear that the result is better than the generalized Fuzzy Image Enhancement.

References

1. Peng, D.-L., Wu, T.-J.: A generalized image enhancement algorithm using fuzzy sets and its application. In: International Conference on Machine Learning and Cybernetics, Beijing, 4–5 November 2002, pp. 820–823 (2002)
2. Gonzalez, R.C., Woods, R.E.: Digital Image Processing. Pearson Education, Upper Saddle River (2003). Chap. 1–5
3. Jain, A.K.: Fundamentals of Digital Image Processing. Prentice Hall, Upper Saddle River (1989). Chap. 1, 7
4. Pal, S.K., King, R.A.: Image enhancement using smoothing with fuzzy sets. IEEE Trans. Syst. Man Cybern. **11**(7), 494–501 (1981)
5. Pal, S.K., King, R.A.: Image enhancement using fuzzy sets. Electron. Lett. **16**, 376–378 (1980)
6. Choi, Y.S., Krishnapuram, R.: A robust approach to image enhancement based on fuzzy logic. IEEE 167–170 (1995)
7. Borgi, A., Akdag, H.: Knowledge based supervised fuzzy-classification: an application to image processing. Anal. Math. Artif. Intell. **32**(1), 67–86 (2001)
8. Farbiz, F., Menhaj, M.B., Motamedi, S.A., Hagan, M.T.: A new fuzzy logic filter for image enhancement. IEEE Trans. Syst. Man Cybern.-Part B: Cybern. **30**(1), 110–119 (2000)
9. Tzafestas, G.S., Raptis, S.N.: Image segmentation via iterative fuzzy clustering based on local space-frequency multi-feature coherence criteria. J. Intell. Robot. Syst. **28**(1), 21–37 (2000)
10. Cheng, H.D., Chen, Y.H., Sun, Y.: A novel fuzzy entropy approach to image enhancement and thresholding. Sig. Process. **75**(3), 277–301 (1999)
11. Kim, T.Y., Han, J.H.: Edge representation with fuzzy sets in blurred images. Fuzzy Sets Syst. **100**(1), 77–87 (1998)
12. Choi, Y.S., Krishnapuram, R.: A robust approach to image enhancement based on fuzzy logic. IEEE Trans. Image Process. **B** (1997)

Medical Simulation Training: Targeting Medical Skills to Emulate Real-Time Field Injuries

Amber Linde(✉), Kevin Kunkler, and Jona Caridha

Medical Simulation and Information Sciences Research Program,
Fort Detrick, Frederick, MD, USA
amber.s.linde.civ@mail.mil

Abstract. Technological advances in modern warfare continue to bring about rapid change in how the military tracks injuries and how the military cares for field injuries. Simulation training experiences should be evaluated on a regular basis, adjusted and adapted to provide crucial training to treat injuries that are happening in the field in real-time. Medical simulation training is only useful to medical professionals if those receiving the training are utilizing medical skills relevant to their patient population. It is important for military medical simulation training curriculums to be flexible and smart. Military medical simulation for the field needs to be updated and tailored to task train medical personnel to care for injuries that are occurring in the field in real-time. Military medical personnel must be able to learn the skill quickly in order to establish a high level of competency before being deployed in the field. This research endeavor was to determine if military medical simulation techniques taught in the current training environment reflect the needed medical skills seen in the Pre-Hospital Trauma Registry (PHTR) data. Tracking injury patterns in the field is crucial not only to determine if current simulation training is accurately mimicking field scenarios, but also to determine if there have been changes in injury patterns since the onset of Operation Iraqi Freedom. This information will facilitate changes/updates in simulation task based training curriculums and research to ensure full competency and complete readiness of medical forces which will result in the best care possible for the injured war-fighter.

Keywords: Medical simulation training · Military · Field injuries · Joint Trauma Registry · En route care · Evacuation

1 Background

A major achievement for any organization (civilian or military) that can offer students access to training on medical simulation technology is the ability to offer their students an immersive, real world training experience with an opportunity to stop, correct, repeat, and master the skill before putting hands on a real patient. The United States military has a long history of using medical simulation to train thousands of medical personnel. It was not until recently, during Operation Iraqi Freedom (OIF),that methods

D.N. Cassenti (ed.), *Advances in Human Factors in Simulation and Modeling*,
Advances in Intelligent Systems and Computing 591, DOI 10.1007/978-3-319-60591-3_14

of medical training in the field were updated to reflect injury patterns reported in the Joint Theater Trauma Registry (JTTR) [1].

Technological advances in modern warfare continue to bring about rapid change in how the military tracks injuries and how the military cares for field injuries. Simulation training experiences should be evaluated on a regular basis and adjusted and adapted to provide crucial training to treat injuries that are happening in the field in real-time. According to the Association of the American Medical Colleges, simulation is defined as "a method used in health care education to replace or amplify real patient experiences with scenarios designed to replicate real health encounters, using lifelike mannequins, physical models, standardized patients, or computers" [2]. The basis of this research paper is to replicate *real health encounters*. Medical simulation training is only useful to medical professionals if those receiving the training are utilizing medical skills relevant to their patient population. It is important for military medical simulation training curriculums to be flexible and smart; in other words, military medical simulation for the field needs to be updated and tailored to train medical personnel to care for injuries that are occurring in the field in real-time and be able to learn the skill quickly in order to establish a high level of competency before being deployed in the field. This will result in providing an injured warrior with the best continuum of care.

As medical simulation training becomes more prominent in US medical schools and in the military, systematic reviews of the literature are revealing stronger evidence of medical simulation training of clinical skills showing translation into improved patient care and improved patient health outcomes [3]. As early as 2009, the literature has captured the usefulness in medical simulation training leading to increased student confidence, allowing for the ability to document improvements in performing medical skills by offering test/retest scenarios, as well as an overall general progression in the attainment of medical knowledge [4].

The basis of this research was not to question the usefulness of medical simulation in training US military medical professionals, but to determine if military medical simulation techniques taught in the current training environment (which can be radically different from place to place) reflect the needed medical skills seen in the field. This will translate to better performance by the medical personnel; which in turn translates into improving patient outcomes.

Tracking injury patterns in the field is crucial to not only determining if current simulation training is accurately mimicking field scenarios, but also to determine if there have been changes in injury patterns since the onset of OIF which can lead to changes/updates in simulation based training curriculums and research topics to ensure full competency and complete readiness of the medical force. This, in turn, will result in providing the injured war-fighter the best care available.

In this regard, the Medical Simulation and Information Sciences Research Program (MSISRP) leveraged the Joint Trauma Registry to track injuries documented in the field, connected tracked injuries to the medical personnel treating the patient, and determined if the simulation training offered to that particular provider in relation to their job category was the appropriate training to care for injuries that were seen in that field environment. Using the results of the data analysis, the MSISRP Medical Simulation and Training (MedSim) portfolio leveraged this data to determine if there is a need to develop a new course of action in selecting simulation training research topics

that are more relevant to the parameters of modern warfare as well as to develop a systematic modeling system that can ensure that simulation training is analogous with medical requirements needed in the field. Two research questions will be addressed:

- Research Question 1: Is the simulation training provided to military medical professionals during training analogous to the medical skills and knowledge needed in the field when compared to injury patterns detected through the Joint Trauma Registry data?
  - H_{0a}: There is no difference between the types of simulation training military medical professionals use to learn medical skills and the types of injuries treated on the battlefield.
  - H_{1a}: There is a significant difference between the types of simulation training military medical professionals use to learn medical skills and the types of injuries treated on the battlefield.
- Research Question 2: Is the medical simulation training research targeted by the MSISRP Medical Simulation Portfolio accurately reflecting research gaps in simulation training when compared to injury patterns detected through the Joint Trauma Registry data?
  - H_{0b}: There is no difference between the injury patterns collected through the Joint Trauma Registry and the MSISRP Medical Simulation Portfolio research topics that aim to improve treatment of these injuries through simulation training research.
  - H_{1b}: There is a significant difference between the injury patterns collected through the Joint Trauma Registry and the MSISRP Medical Simulation Portfolio research topics that aim to improve treatment of these injuries through simulation training research.

2 Aim

The aim of this project was to analyze data collected from the Joint Trauma Registry to determine (1) if military medical simulation training provided during training is relevant to the medical skills and knowledge necessary in real world scenarios, and (2) if relevant medical simulation training research reflects the training needs of injuries documented in the field.

3 Objectives

The following objectives support the hypotheses' that led to the development of the study outcomes:

- Collect injury data from the Department of Defense Trauma Registry (DoDTR) specifically from the Pre-hospital Trauma Registry (PHTR);
- Analyze and determine injury/provider/treatment/evacuation patterns seen in the field;

- Analyze and determine medical simulation training exposure any given medical specialty received prior to deployment;
- Determine if simulation training reflects the injury/provider/treatment/evacuation patterns in the field;
- Determine if research topics released through the MSISRP MedSim Portfolio correlate with the injury patterns captured in the registry.

4 Materials and Methods

The IBM SPSS statistical package was used to run the analysis. Data was used from the PHTR.

5 Data

A sample of convenience was utilized due to the complexities of gathering trauma data from a theatre population. The de-identified data set was provided to MSISRP by the DoDTR which is the data repository of DoD trauma injuries. The data the MSISRP used included trauma data collected from Afghanistan from 2013 to 2014 from the PHTR. This data is specifically collected from prehospital trauma care at the point of injury by all combat forces (Army, Air force, Navy and Marines).

6 Research Design

Using the data collected from the PHTR, data was compiled into SPSS and the frequencies of injuries/treatments/provider/evacuations were generated to address the research questions. For RQ1, battlefield injuries collected and analyzed from the PHTR data provided the background information needed to compare and contrast with the current simulation training education being provided to military healthcare personnel. AMEDD Center and School was contacted to determine the medical simulation training technologies used in medical skills training. The outcomes were cross-referenced with the trauma injuries to determine if medical simulation training accurately coincides with real-time battlefield injuries treated.

To address RQ2, the outcomes of RQ1 were compared the MSISRP MedSim Portfolio to determine if the research topic areas in simulation training accurately research gaps in simulation training when compared to injury patterns captured in the PHTR.

6.1 PHTR Population

The mean age of the trauma injury population in 2013 was 28.63. In 2014 the mean age was slightly younger at 27.36 but did not reflect a significant decrease in age. Out of 394 data points, 94.4% were male, 1.3% were female and 4.3% were unknown (gender not indicated). Out of 394 de-identified trauma patients recorded in the PHTR data

obtained, the United States Army had the highest frequency of trauma patients totaling 261 (66%). The US Marines had 58 (15%) trauma patients, the US Navy had 25 (6%) and local civilians had 22 (6%) trauma patients. Descriptive analysis was conducted on trauma injury patterns based on rank. Rank was analyzed to include the civilian sector; enlisted; officers; and warrant officers.

In order to determine if there were differences in field data types, the PHTR data was categorized into two groups: Battle Injury (BI) and Non-Battle Injury (NBI). The Army, Marines, and Navy had increases in trauma rates when compared to NBI traumas recorded; however, these differences were not significant across the services. Pearson Chi-Square was conducted between the service and injury class (BI vs NBI). From the dataset there was no significance indicated, $\chi^2(7) = 12.866$, $p = .075$.

A description of trauma occurrences comparing rank and branch of service was analyzed using Pearson Chi-Square. From the dataset there was significance indicated, $\chi^2(112) = 458.338$, $p = .000$. Those ranking E4–E6 sustained a majority of the traumas. The US Army had the highest frequency of injuries on and off the field from the data reported on the PHTR.

6.2 Injury Description

The JTTR 2013–2014 provided injury descriptions recording type and treatment methods used for the trauma injury sustained. This section provides the descriptions of injury category, injury, and injury location. The highest occurrence of BI trauma injury was gunshot wounds. NBI trauma accounts were more frequently recorded as pain and "other" related complaints.

Pearson Chi-Square analysis shows a significant difference in the types of trauma injury outcomes between BI and NBI events. BI revealed the top three trauma injuries coming from gunshot wounds, IEDs and RPGs; NBI revealed the top three trauma injuries coming from aircraft crashes, motor vehicle accidents, and "other". From the dataset, a significance was observed between where the trauma occurred (BI vs NBI) and the injury type sustained, $\chi^2(15) = 233.647$, $p = .000$. BI and NBI were evaluated against injury type. Pearson Chi-Square showed significance, $\chi^2(15) = 40.789$, $p = 0.000$.

The locations of the injuries were analyzed and it was determined that 764 injury locations were reported in the data sample. The most frequent injury locations are as follows: 186 head; 97 right leg; 74 left leg; 61 back; 46 right arm; 45 left arm; 42 chest; and 36 in the abdominal region. Using Pearson Chi-Square, a significance was observed between where the trauma location was reported and the service indicated by the trauma report, $\chi^2(210) = 252.61$, $p = .024$.

An examination was conducted on the relationship between the service of the trauma patient and the injury classification. There was not a significance shown in the Pearson Chi-Square analysis $\chi^2(105) = 97.918$, $p = .675$.

BI vs NBI were compared to location of the injury. Location of the injury using Pearson Chi-Square is significant $\chi^2(30) = 45.559$, $p = .034$. Pearson Chi-Square analysis shows a significance between injury location and mechanism of the trauma, $\chi^2(420) = 639.967$, $p = .000$. There was not a significance detected between injury location and injury classification $\chi^2(392) = 433.866$, $p = .071$.

6.3 Provider Description

The JTTR provided generalized data of the provider description to include whether the provider was a medic, a medical officer, a non-medic first responder or unknown. Of the 1,095 medical provider contacts with trauma patients, 69.1% were from medics; 13.3% were from non-medic first responders; 9.8% were from medical officers; and 7.6% were unknown. The majority of points of care providers were medics. Pearson Chi-Square was conducted among the providers and the treatments they provided to trauma patients. A significance was observed, $\chi^2(84) = 364.322$, $p = .000$. Pearson Chi-Square was conducted between the Medics and Medical Officers from the categories of treatments they provided. A significance was observed when comparing treatment category to the medical provider, $\chi^2(28) = 30.589$, $p = .000$.

6.4 Evacuation Description

This section focuses on vehicle type evacuations used at the point of injury in the field according to the data from the JTTR. Of the trauma cases prioritized to include both 2013 and 2014 data, 20% were Urgent, 19% Priority, 15% were Routine (3% were not categorized). Pearson Chi-Square was conducted between the service and evacuation priority. There was no significance indicated, $\chi^2(21) = 25.704$, $p = .218$. Pearson Chi-Square was conducted between the evacuation priority and types of evacuation vehicles used. A significance was indicated in the choice of evacuation vehicles depending on the evacuation priority of a patient, $\chi^2(9) = 88.467$, $p = .000$. Pearson Chi-Square was conducted between the evacuation vehicle and types of evacuation types used. A significance in the use of UH 60 Blackhawk vehicles was noted, $\chi^2(21) = 76.800$, $p = .000$.

7 Discussion

During Operation Enduring Freedom (OEF) in Afghanistan and surrounding areas, approximately 1,800 battle related deaths were recorded and it was estimated that 20,000 people sustained battlefield wounds through November 2014 [5]. The PHTR provided merely a glimpse to the course of action taken to provide trauma care and evacuation strategies for patients. It was noted that the PHTR data call captured a very small number of women service members even though combat positions were opened to women in 2013 [6]. The PHTR recorded five women trauma patients; of those, one patient was labeled as a BI. The percentage of women who were assigned to areas where trauma data was collected is unknown. As such, this study is a comprehensive look at injuries and evacuations for men with the mean age of 28 years old. It includes service members from the Army, Air force, Marines and Navy and included civilian trauma injuries (local and US civilians). This was not an effort to report a detailed study of trauma injuries but to look at recorded field trauma data to compare and contrast existing medical simulation training efforts military medical professional receive prior to deployment to determine if there are medical simulation training research gaps.

7.1 PHTR Population

The PHTR trauma patient data provided valuable insight as to the description of the sample population. As far as frequencies are concerned, it is clear that enlisted personnel serving in the Army had a greater number of traumas reported from both BI and NBI categories. As shown in the results section however, this did not indicate that the Army trauma related injuries were not in proportion with the other services indicated in the PHTR. Across all military services, those ranking E4, E5 and E6 had a significant increase in trauma injuries reported. As the PHTR data did not provide the military operational specialty (MOS) of the trauma patients injured, it is unclear if the risk of injury is specifically correlated to rank or if it is related to the MOS of the patient who happens to be of a certain rank.

The analysis between injuries occurring in the battle field and non-battle field injuries were apparent from the dataset in which trauma injuries were more frequently occurring in BI environments. This was true for all services.

7.2 Injury Descriptions

The PHTR trauma patient data allowed for the analysis of trauma injury descriptions to include BI or NBI, mechanism of injury (i.e. gunshot, blast), anatomical location of injury (i.e. right knee, mouth), and classification of injury (i.e. amputation, burn).

Gunshot wounds were reported as the highest frequency of BI trauma. Laceration injuries were the second highest frequency and pain the third. Pain was reported as the highest frequency of NBI trauma injury. It is unclear what the definition of pain was for the PHTR and how it related to a direct trauma injury. The "Other" category was the next highest entry for NBI and the third was fractures. The pain and other categories for BI represented 20% of the data and 34% for NBI data. It was understood that this could skew the data results for this analysis.

It was surprising that the frequency of gunshot trauma wounds were particularly high considering the literature consistently reported blast trauma injuries were significantly higher than gunshot injuries in the earlier stages of the conflicts during both OEF and OIF [7, 8]. Together, gunshot wounds, IEDs, and RPGs represented 78% of all BI trauma injuries reported on the PHTR. Aircraft crashes, motor vehicle accidents and "Other" represented 61% of all NBI injuries reported in the PHTR. This may explain the differences found in injury classification (BI vs NBI) and the anatomical location of the injury. 764 injury locations were reported in the dataset. The top three injury locations on frequency of occurrence were head, right leg and left leg. The Army and Marines had higher percentages of head trauma; however, the available data for other US services was low and may not be a fair representation of the actual head traumas documented. Head trauma represented the most frequent trauma reported across all services.

Although significance was shown regarding service and injury location; service and injury classification type (i.e. amputation, bleeding) was not significant. This could be due to the violent nature of the trauma itself, however the actions and safety equipment available to the service member being exposed to situations that can result in a severe trauma could possibly be used to predict location of injury patterns in military trauma patients.

As with mechanism of the injury and injury location, there was significance revealed with injury classification (BI and NBI) and injury location. This is not surprising due to the differences in the mechanisms of trauma discussed earlier [9]. This could help in research concerning translating what is learned regarding military traumas (BI and NBI) to civilian traumas based on the environment of the trauma itself.

7.3 Provider Descriptions

The PHTR trauma patient data allowed for the analysis of provider movement during the trauma patient treatment and subsequent movement to an evacuation mechanism. The data captured for the rank/service/background/experience of the provider is unknown. The categories broken down from the data sheet were grouped to include medic, first responder non-medic, medical officer, and unknown. Even though the categories were generalized, the analysis provided insight to provider availability and treatment patterns in a field trauma patient environment in Afghanistan.

As stated in the results section, medics dominated trauma patient point of care by providing 70% of the medical treatment to trauma patients. Analysis of the data revealed treatment categories (i.e. airway management, breathing) and treatments provided (i.e. chest seal, splint) were significantly different between medics and medical officers. Medical officers tend to perform more airway management (15% of the treatments compared to 4% of the Medics) and Medics tend to perform more circulation hemorrhage control management (43% of the treatments compared to 24% of the Medical Officers). Non-Medic First Responders performed circulation hemorrhage control management 74%. This was particularly interesting and shows the importance of understanding the knowledge of medical first aid provider who is at the initial point of care to ensure that those needing medical training are getting adequate instruction to provide crucial point of care delivery of treatment.

7.4 Evacuation Descriptions

Evacuation priorities (urgent, priority) and injury class (BI or NBI) did not show a significant difference which may indicate that triaging patients is standard in trauma patient management. Types of vehicles used for transport were significant and analysis from the dataset revealed the use of aircraft as the preferred mode of evacuation from theatre environments for BI and NBI trauma events. Significance was shown in type of vehicle used in which UH 60 Blackhawk vehicles were the most utilized. In 2012, research acknowledged the high use of UH 60 Blackhawk helicopter as an effective evacuation method for transporting trauma patients which indicates the need for pre-hospital critical care teams assigned to these vehicles [10]. Unfortunately, it is unclear from the PHTR if these teams were aboard these vehicles during the data collection between 2013 and 2014.

7.5 Results: AMEDD Center and School

Regarding Research Question 1: Is the simulation training given to military medical professions during training analogous to the medical skills and knowledge needed in the field when compared to injury patterns detected through Joint Trauma Registry data? There was no difference in the types of training military medical professionals use to learn medical skills with the types of injuries treated on the battlefield when comparing the curriculum with injury, treatments and trauma scenarios reviewed with the AMEDD Center and School; however, the use of simulation training was found to be limited with the majority of simulation training being performed on Rescue Randy mannequins that are modified by the instructors in order to provide the combat injury task training needed to perform the medical task.

In regards to Research Question 2: Is medical simulation training research targeted by the MSISRP Medical Simulation Portfolio accurately reflecting research gaps in simulation training when compared to injury patterns detected through the Joint Trauma Registry data? From the data collected, this was difficult to assess. The reason is the overall ruggedness of manikin technology that can hold up in field exercises simply do not exist on today's commercial market. According to the AMEDD Center and School, the average Rescue Randy manikin averages a lifespan of a little over 12 months. High fidelity systems typically cannot handle the extreme nature of military medical theater training, issues contacting contracting company to repair systems, lack of IT support to connect manikin systems with computer systems, and lack of support available to clean, repair, set up, tear down, store high fidelity simulation systems.

7.6 Treatment and Simulation

Laerdal Difficult Airway Head was used to train all aspects of airway training that were found in the JTTR data (cricothyrotomy, King LT insertion, nasopharyngeal airway, endotracheal tube). Students are provided with lectures on airway maintenance as well as practice their skills on trauma lanes for hands on skills applications. It is not uncommon for a Rescue Randy to be *modified* to allow for the simulation exercise to include making punctures, applying an endotracheal tube etc. Rescue Randy being modified as a simulation method holds true for training on breathing.

For circulation and hemostatic training exercises, limbs taken from a Rescue Randy or the use of 2×4 s for initial training (learning to use a tourniquet) are utilized along with a classroom lecture. Disability and exposure training that involves the use of eye shield, splints, pelvic splints, backboard, C Collars, blizzard blankets, hypothermia kit and ready heat plus covering are typically practiced on another person after a lecture/demonstration is provided by the instructor. These are followed on by scenery driven tasks seen in the trauma lanes.

A gap in simulation training is seen in resuscitation training mainly due to lack of a model that does not require high maintenance to utilize and store. It was also noted that for eye injuries, there is no lateral canthotomy and cantholysis training models available.

7.7 Mechanism Resulting in Injury

The mechanisms collected from the JTTR data included aircraft crash, IED/mine dismount or mounted blast, mortar/artillery, RPG/grenades, collapse/crush from structure, falls, gunshot wounds, fragmentation/shrapnel and motor vehicle accidents utilized Rescue Randy and "modified" Rescue Randy that were simulated with the appropriate scenario for injuries covered in that particular training session. AMEDD Center and School did not have an appropriate model for burn scenarios, in particular a model for escharotomy. The school has created their own model to simulate the training as a model does not exist in the commercial sector.

7.8 Evacuation Simulation Training

Aircrafts and ground vehicles for training purposes take up a lot of space and require maintenance to use for training. TCCC guidelines do not have this capability; however, the Mobile Surgical Team has a Blackhawk and a C130 to use as a simulation tool for advanced student learning.

Litter training simulation is available and the school uses Talon II litters and Skedco litters in conjunction with the Rescue Randy manikin.

8 Limitations

Data from the PHTR was collected from a small population and thus is subject to sampling and non-sampling errors. MEDEVAC and CASEVAC cases were not able to be determined in the data set. Due to the very nature of the data collected it is understood that loss of data would have occurred. The PHTR data call was tasked by USMRMC to provide available trauma data to JPC-1 for the purposes of the research. It is unknown how the data was collected and what data that was provided to the JPC-1. It is unknown at what specific location(s) in Afghanistan the trauma data was collected. All data provided was categorical in nature and was coded for the purpose to conduct Pearson Chi-Square analysis. Civilian, Air force and Navy data had small sample sizes (<5) to be able to successfully run a Pearson Chi-Square analysis.

AMEDD Center and School information concerning simulation systems used was gathered by interview. The instruction is based on availability of equipment and training is not guaranteed to be standardized from one class to the next. There is no repository of simulation systems in current use. There is no repository that can map the use of simulation systems to a particular course curriculum.

9 Conclusion

There is clearly a gap in the manufacturing/development of combat medical simulation training tools that have the ruggedness and fidelity that (1) delivers quality training, (2) has the ability to be used multiple times, (3) is easy to use/store/set-up, and (4) provides enough fidelity to deliver an immersive training experience for the learner.

The AMEDD Center and School is providing the appropriate task curriculum for the injuries seen in the modern battlefield. It needs to be addressed in the military medical simulation and training research community that appropriate actions need to be taken so that suitable simulation training technologies are being leveraged and are readily available to ensure the medical readiness of military medical professionals.

Acknowledgements. We thank the Department of Defense Trauma Registry (DoDTR) for providing valuable data from the Pre-hospital Trauma Registry (PHTR) in order for the research to be conducted. We thank the AMEDD Center and School for providing value insight regarding simulation and training use in their curriculum.

References

1. Brevard, S.B., Champion, H., Katz, D.: Emergency war surgery, chap. 2 (2014)
2. Passiment, M., Sacks, H., Huang, G.: Medical simulation in medical education: results of an AAMC survey, pp. 1–42. Association of American Medical Colleges (2011)
3. McGaghie, W.C., Issenberg, S.B., Cohen, E.R., Barsuk, J.H., Wayne, D.B.: Does simulation-based medical education with deliberate practice yield better results than traditional clinical education? A meta-analytic comparative review of the evidence. Acad. Med.: J. Assoc. Am. Med. Coll. **86**(6), 706–711 (2011). http://doi.org/10.1097/ACM.0b013e318217e119
4. Okuda, Y., Bryson, E.O., DeMaria, S., Jacobson, L., Shen, B., Levine, A.I.: The utility of simulation in medical education: what is the evidence? Mt. Sinai J. Med.: J. Transl. Personalized Med. **76**(4), 330–343 (2009). doi:10.1002/msj.20127. Version of Record online: 29 Jul 2009
5. Goldberg, M.S.: Updated Death and Injury Rates of US Military Personnel During the Conflicts in Iraq and Afghanistan, Working Paper 2014-08, Working Paper Series (2014). https://www.cbo.gov/sites/default/files/113th-congress-2013-2014/workingpaper/49837-Casualties_WorkingPaper-2014-08_1.pdf
6. Raphel, A.: Women in the US military and combat roles: research roundup. Journalist's Resources (2014). http://journalistsresource.org/studies/society/gender-society/women-military-research-roundup
7. Cameron, K.L., Owens, B.D.: Musculoskeletal Injuries in the Military, XIV, Traumatic combat injuries (2015). ISBN: 978-1-4939-2983-2
8. Belmont, P.J., McCriskin, B.J., Sieg, R.N., Schoenfeld, A.J.: Combat wounds in Iraq and Afghanistan from 2005–2009. J. Trauma Acute Care Surg. **73**(1), 3–12 (2012). doi:10.1097/TA.0b013e318250bfb4
9. Schreiber, M.A., Zink, K., Underwood, S., Sullenberger, L., Kelly, M., Holcomb, J.B.: A comparison between patients treated at a combat support hospital in Iraq and a level 1 Trauma center in the United States. J. Trauma Inj. Infect. Crit. Care **64**, S118–S122 (2008)
10. Clark, J.E., Davis, P.R.: Medical evacuation and triage of combat casualties in Helmand province, Afghanistan: October 2010–April 2011. AMSUS **177**(11), 1261–1266 (2012)

Diagnosis of Alzheimer Disease Through an Artificial Neural Network Based System

Ivo Ramalhosa[1], Pedro Mateus[1], Victor Alves[1], Henrique Vicente[1,2], Filipa Ferraz[1], João Neves[3], and José Neves[1(✉)]

[1] Centro Algoritmi, Universidade do Minho, Braga, Portugal
{a68362, a68364}@alunos.uminho.pt,
{valves, jneves}@di.uminho.pt, hvicente@uevora.pt,
filipatferraz@gmail.com
[2] Departamento de Química, Escola de Ciências e Tecnologia, Universidade de Évora, Évora, Portugal
[3] Mediclinic, Arabian Ranches, PO Box 282602, Dubai United Arab Emirates
joaocpneves@gmail.com

Abstract. Alzheimer's Disease (AD) is referred to as one of the most common causes of dementia, which in itself justifies the interest and investment that is made in order to find new biomarkers to identify the disease in its early stages. Indeed, focusing on the hippocampus as a marker for AD, it would be object of analyse different methods of volume measurement and hippocampus segmentation. On the other hand, the computational framework is built on top of a Logic Programming approach to Knowledge Representation and Reasoning, complemented with a computational framework base on Artificial Neural Networks that grip on incomplete, unknown, and even self-contradictory information or knowledge.

Keywords: Alzheimer disease · Biomarker · Hippocampus · Logic programming · Medical imaging · Intelligent systems

1 Introduction

Alzheimer's Disease (AD) is the most common cause of dementia in the world, affecting 20% of the population over 80 years, and being estimated as the cause of 60 to 80% of the death cases. This disease is characterized by initial alterations in the neurofibrillary tangles and the deposit of amyloid- **β** plaque. Later this evolves to variations at the level of the brain structure, causing atrophy [1–3].

In the field of medical imaging, initially images of CT Computed Tomography (CT) and Magnetic Resonance Imaging (MRI) where used to distinguish between AD and other types of dementia. However, medical imaging as assume a more central role in the detection of the disease, with the finding of new biomarkers, not only for detection and follow up of AD, but also to others types of dementia. The uncertainty of the diagnosis of AD, lead to this search of biomarkers that could identify the disease in its early stages, and because a definitive diagnosis requires confirmation, through

D.N. Cassenti (ed.), *Advances in Human Factors in Simulation and Modeling*,
Advances in Intelligent Systems and Computing 591, DOI 10.1007/978-3-319-60591-3_15

cerebral analysis, which associated with the inaccessibility of the brain makes medical imaging fundamental [4, 5].

Initially AD starts to show signs of atrophy in the medial temporal lobe, being entorhinal cortex the first structure to be affected. Rapidly follow by hippocampus, amygdala and para-hippocampus, and structures like the limbic lobe, which correlate with impairments in memory function. These losses spread to other structures, being the more important vascular changes and the cortical atrophy, where the changes in the hippocampus are considered a key biomarker. The moment when AD is detected, normally atrophy is already established in more than one region, showing structures reductions at levels of 20 to 30%. Knowing that the normal AD reduction maintains in levels of 2 to 5% for year, this information suggests that the atrophy in this structures already happens a lot early, making this a parameter for early detection of AD [1, 4, 6].

As mentioned before, hippocampus is a key biomarker in the detection of AD. The early study of hippocampus reported a difference between the dimensions of the right-hand side when compared to the left one, which is smaller. The first studies on the effects of AD in the size of the hippocampus have revealed an area's reduction of 49%, a situation that was already confirmed by other studies [7].

A new variable was introduced in 1991, InterUncal Distance (IUD), obtained from a single slice of a Magnetic Resonance (MR) scan, and used to reflect the incidence of atrophy in the hippocampus. It was proposed that a widening of IUD superior to 30 millimetres would suggest the presence of AD, subsequently supported by a study in which the IUD of healthy people did not exceed such a boundary. Later, in 1993, it were identified correctly all the individuals of a group with early AD and control patients, with analysis of volumes of the hippocampus and temporal horn of the lateral ventricle [7].

MRI biomarkers relating to hippocampus include static and change of hippocampus volumes over time, plus analysis of the shape of the hippocampus. Other studies focus on texture analysis, trying to examine early signs related with the changes in the neurofibrillary tangles and deposition of A**β** plaques, being detectable prior than atrophy in terms of statistics related with image intensities [1]. These studies proved the importance of the hippocampus in an early detection of AD, assuming also as a biomarker of the disease evolution. Indeed, more studies have been made about atrophy in the hippocampus, allowing one to establish boundaries to identify AD, such as other types of dementia and discriminate the changes caused by normal aging. In these studies it was used the measurement of the hippocampus volume, relating this value with established ones. A study carried out from 2010 to 2012, the hippocampus normal size of the control group was 5.202 cubic centimetres and the patients with AD show a decline to 3.853 cubic centimetres [3]. In another study that followed up a group of 518 not at all demented elderly persons through a period of 10 years, with extensive cognitive testing in four stages during that period. The results of the hippocampus volume, from the first measure, showed values of 2.69 cubic centimetres from the left-hand side and 2.76 cubic centimetres from the right one, which lead to a total of 5.45 cubic centimetres, with similar values to the first study [8]. These values were used to establish the standard range of expected values to the hippocampus volume, allowing dataset analyses and the establishment of the patient's health condition.

Solving problems related to AD diagnosis requires a proactive strategy. However, the stated above shows that the AD assessment should be correlated with many variables and

require a multidisciplinary approach. Thus, this paper make a start on the development of an AD diagnosis support system using *Logic Programming* (*LP*) based approach to knowledge representation and reasoning [9, 10] complemented with a computational framework based on *Artificial Neural Networks* (*ANNs*) [11, 12]. ANNs are computational tools which attempt to simulate the architecture and internal operational features of the human brain and nervous system. ANNs can be defined as a connected structure of basic computation units, called artificial neurons or nodes, with learning capabilities. Multilayered feed-forward neural network architecture is one of the most popular ANNs structure often used for prediction as well as for classification. This architecture is molded on three or more layers of artificial neurons, including an input layer, an output layer and a number of hidden layers with a certain number of active neurons connected by modifiable weights. In addition, there is also a bias, which is only connected to neurons in the hidden and output layers. The number of nodes in the input layer sets the number of independent variables, and the number of nodes in output layer denotes the number of dependent variables [12]. Several studies have shown how ANNs could be successfully used to model data and capture complex relationships between inputs and outputs [11, 12].

2 Knowledge Representation and Reasoning

Many approaches to Knowledge Representation and Reasoning have been proposed using the *LP* epitome, namely in the area of *Model Theory* [13, 14] and *Proof Theory* [9, 10]. In the present work, the *Proof Theoretical* approach in terms of an extension to the *LP* language is followed. An *Extended Logic Program* is a finite set of clauses, given in the form:

$$
\begin{aligned}
&\{\\
&\quad \neg p \leftarrow not\ p, not\ exception_p\\
&\quad p \leftarrow p_1, \cdots, p_n, not\ q_1, \cdots, not\ q_m\\
&\quad ?\,(p_1, \cdots, p_n, not\ q_1, \cdots, not\ q_m)\ \ (n, m \geq 0)\\
&\quad exception_{p_1}\\
&\quad \cdots\\
&\quad exception_{p_j}\ \ (0 \leq j \leq k)\ \ \ being\ k\ an\ integer\ number\\
&\}:: scoring_{value}
\end{aligned}
$$

where the first clause stand for predicate's closure, "," denotes "*logical and*", while "*?*" is a domain atom denoting falsity, the p_i, q_j, and p are classical ground literals, i.e., either positive atoms or atoms preceded by the classical negation sign — [10]. Indeed, — stands for a strong declaration that speaks for itself, and *not* denotes *negation-by-failure*, or in other words, a flop in proving a given statement, once it was not declared

explicitly. Under this formalism, every program is associated with a set of abducibles [13, 14], given here in the form of exceptions to the extensions of the predicates that make the program, i.e., clauses of the form:

$$exception_{p_1}, \cdots, exception_{p_j} (0 \leq j \leq k), \ being\ k\ an\ \ integer\ number$$

that stand for data, information or knowledge that cannot be ruled out. On the other hand, clauses of the type:

$$?(p_1, \cdots, p_n, notq_1, \cdots, notq_m) \ (n, m \geq 0)$$

also named *invariants*, allows one to set the context under which the universe of discourse has to be understood. The term $scoring_{value}$ stands for the relative weight of the extension of a specific predicate with respect to the extensions of peers ones that make the inclusive or global program.

In order to evaluate the data, information or knowledge's quality that may be associated to a logic program, an assessment of it, denote as *QoI*, is given by a truth-value ranging between 0 and 1 [15, 16]. Thus, $QoI_i = 1$ when the information is *known* (*positive*) or *false* (*negative*), and $QoI_i = 0$ if the information is *unknown*. Finally, for situations where the extension of a given $predicate_i$ is taken from a set of terms, $QoI_i \in]0, 1[$, i.e.:

$$QoI_i = 1/Card \tag{1}$$

where *Card* denotes the cardinality of the *abducibles* set for *i*, if the *abducibles* set is disjoint. If the *abducibles* set is not disjoint, the clause's set is given by $C_1^{Card} + \cdots + C_{Card}^{Card}$, under which the QoI's evaluation takes the form:

$$QoI_{i_{1 \leq i \leq Card}} = 1/C_1^{Card}, \cdots, 1/C_{Card}^{Card} \tag{2}$$

where C_{Card}^{Card} is a card-combination subset, with *Card* elements. For example, the logic program depicted below, i.e.:

$\{$

$\neg f_1(X, Y, Z) \leftarrow not\ f_1(X, Y, Z), not\ exception_{f_1}(X, Y, Z)$

$f_1(\underbrace{[5,\ 7],\quad \perp,\quad 6.5}_{attribute`s\ values})$

$\underbrace{[0, 8]\ [12, 36][5, 10]}_{attribute`s\ domains}$

$exception_{f_1}(4,\ [30,\ 35],\ \perp) \qquad \ldots \qquad exception_{f_k}(\perp,\ 10,\ [7,\ 8])$

$\}:: 1$ *(once the universe of discourse is set in terms of the extension of one predicate)*

where $\perp$ denotes a null value of the type *unknown*, stands for a logic program that denotes a particular universe of discourse in its initial form. Then, it is now possible to split the *abducible* or *exception* set into the admissible clauses or terms and evaluate their *QoIs*. A pictorial view of this process, in general terms, is given below as a pie chart (Fig. 1).

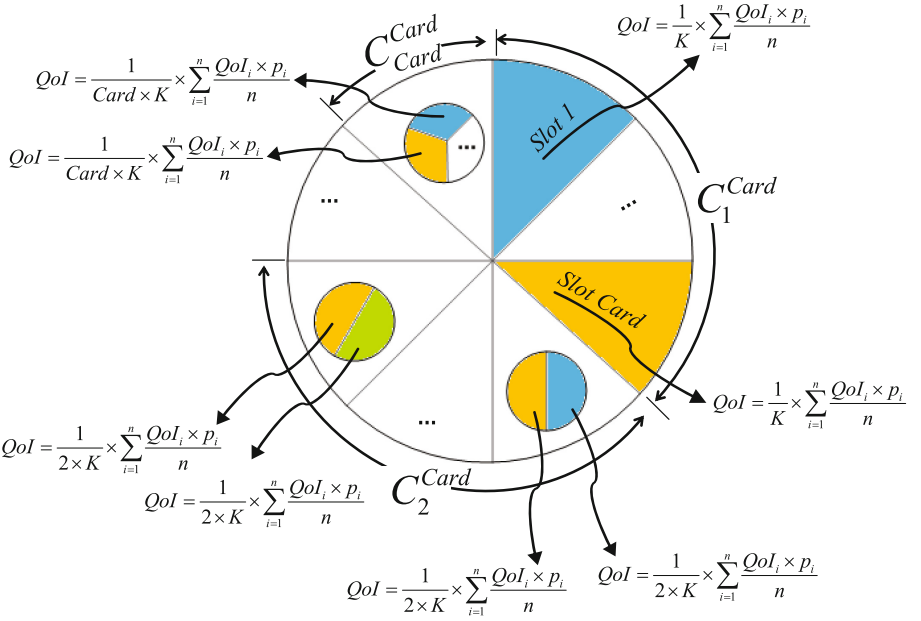

Fig. 1. *QoI's* values for the *abducible* set of clauses referred to above. The clauses cardinality set, K, is given by the expression $C_1^{Card} + C_2^{Card} + \cdots + C_{Card}^{Card}$, where $\sum_{i=1}^{n} (QoI_i \times p_i)/n$ denotes the attributes *QoI's* average of each clause or term. p_i stands for the relative weight of attribute i with respect to its peers, being $\sum_{i=1}^{n} p_i = 1$.

Under this setting, a new evaluation factor has to be considered, which will be denoted as *DoC*, that stands for one's confidence that the argument values or attributes of the terms that make the extension of a given predicate, having into consideration their domains, fit into a given interval [17]. The *DoC* is evaluated as shown in Fig. 2 and computed using $DoC = \sqrt{1 - \Delta l^2}$, where Δl stands for the argument interval length, which was set in the interval [0, 1]. Thus, the universe of discourse is engendered according to the information presented in the extensions of such predicates, according to productions of the type:

$$\begin{aligned} predicate_i - \bigcup_{1 \le j \le m} clause_j(((A_{x_1}, B_{x_1})(QoI_{x_1}, DoC_{x_1})), \cdots \\ \cdots, ((A_{x_n}, B_{x_n})(QoI_{x_m}, DoC_{x_m}))) :: QoI_j :: DoC_j \end{aligned} \tag{3}$$

where $\cup$, m and (A_{xj}, B_{xj}) stand for, respectively, for set union, the cardinality of $predicate_i$ extension and the extremes of the interval where attribute $attribute_i$ may, in principle, be situated.

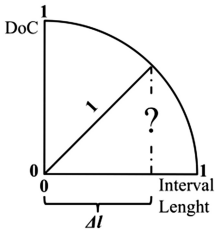

Fig. 2. Evaluation of the attributes' *Degree of Confidence.*

In present study both qualitative and quantitative data are present. Aiming at the quantification of the qualitative part and in order to make easy the understanding of the process, it will be presented in a graphical form. Taking as an example a set of n issues regarding a particular subject, where there are k possible choices (e.g., *absence*, *low*, ..., *high* and *very high*), an unitary area circle, split into n slices, was itemized. The marks in the axis correspond to each of the possible options. Thus, if the answer to issue 1 is *high* the area correspondent is $(k-1)/(k \times n)$ (Fig. 3(a)). Assuming that in the issue 2 are chosen the alternatives *high* and *very high*, the correspondent area ranges between $[(k-1)/(k \times n), 1/n]$ (Fig. 3(b)). Finally, in issue n if no alternative is ticked, all the hypotheses should be considered and the area varies in the interval $[0, 1/n]$ (Fig. 3(c)). The total area is the sum of the partial ones (Fig. 3(d)). In some cases, similar responses to different issues have opposing impact in the subject in consideration. Thus, the contribution of the items with negative impact on the subject in analysis is set as $1/n$ minus the correspondent area, i.e., $(1/n - (k-1)/(k \times n)) = 1/(k \times n)$ for issue 1, $[0, 1/(k \times n)]$ for issue 2 and $[0, 1/n]$ for issue 3.

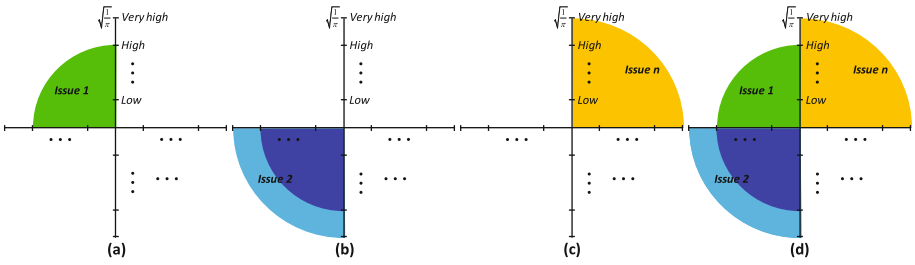

Fig. 3. A view of the qualitative data/information/knowledge processing.

3 Methods

3.1 Data Set

To the purpose of this study, there was a need of a dataset that could provide MRI images of patients with AD. Thus, a dataset from OASIS (Open Access Series of Imaging Studies) was used [18]. OASIS provides MRI data sets of the brain to the scientific community. It was possible to use a dataset of a longitudinal collection of 150 individuals, aged from 60 to 96 years old. Each person was scanned two or more times, having three or four T1-weighted MRI scans for which session. Relating to AD, 72 of the patients were classified as not having dementia, 64 were initially classified with it, which included 51 patients with mild to moderate AD. In 14 of the cases where initial classification reflected not having dementia, later develop to a state of dementia. The dataset also offered information about the patient, such as gender, age, and level of education [18].

In addition to the volumetric feature of hippocampus, there were some non-genetic qualitative factors considered significant. For example, cerebrovascular disease, type 2 diabetes, metabolic syndrome or traumatic brain injury have shown to increase the risk of dementia. On the other hand, the type of diet, physical and intellectual activity may be associated with lower incidences of AD. Characteristics like body weight and blood pressure were also studied involving specific limits with greater risk of having the disease [19]. These factors were included in the dataset for each patient, plus information about the presence of type 2 diabetes, blood pressure, intellectual activity and body weight.

3.2 ImageJ Application to Measure the Hippocampus Volume

ImageJ is an open source java-based image processing program developed at the National Institutes of Health [20]. It provides different processing tools, making possible the use of plugins and macros with different purposes, like the one that we developed to retrieve the hippocampus' volume. With the use of ImageJ the patient MRI stack is opened, the hippocampus position is settled, and corrections to it, if needed, are done. In the dataset used, different stacks were inverted, being used for such a purpose the *Flip Vertically* tool, available from the menu *Image-Transform* to correct them. Searching through the stack series of images, the ones containing the hippocampus are selected. For a better identification of the hippocampus some image processing may be needed, like changes at the contrast levels and brightness.

The data set presents a number of MRI stacks under a sagittal view, making conceivable hippocampus identification. However, other views may be important to check if the hippocampus selection is the correct one. The studies that analyse and compare manual with automate segmentation normally use the sagittal or coronal view. For this purpose, it was used the plugin "*CoronalTP*", which allows to convert the stack to other views. More interesting is that drawing the Region of Interest (ROI) in the selected image allows one to see the selection's points in the other view, which is an aid to make a better identification. In order to assure the correct selection of the

hippocampus, some steps should be made to identify the structures that indicate the beginning and ending of the hippocampus. To this purpose, mechanisms like the one described in [21] must be used to do the manual selection of the hippocampus, and to have a correct measure of its volume. Throughout the *ROI Manager* table, each hippocampus selection is fed to the application's manager, making possible to look at their areas, as well as to other characteristics that were object of selection. Thus, with the ROI that identifies the hippocampus, it is possible to measure such area and evaluate the volume, using the data about the thickness among the MRI slices.

4 Case Study

As a case study consider the knowledge base given in terms of the extensions of the relations depicted in Fig. 4, which stand for a situation where one has to manage information in order to evaluate if a patient is suspected to present AD. The knowledge base includes 150 patients aged between 60 to 96 years old, with an average of 79 ± 17 years old. The gender distribution was 43.6% and 56.4% for male and female, respectively.

The *Type 2 diabetes* column of *Alzheimer Disease Diagnosis* table are filled with 0 (zero) or 1 (one) denoting, respectively, *absence* or *presence*, while in the *Gender* column 0 (zero) and 1 (one) stand, respectively, for *female* and *male*. In order to quantify the information present in the *Risk Factors* table the procedures already described in Sect. 2 were followed. Under this scenario some incomplete and/or unknown data is available. For instance, in case 373 the *Type 2 diabetes* is unknown, which is depicted by the symbol ⊥, while the *Risk Factors* ranges in the interval [0.56, 0.89].

Patient Information

#	Age	Gender	Type 2 diabetes
1	87	Male	0
2	75	Male	1
…	…	…	…
150	65	Female	⊥

Segmentation

#	Hippocampus Volume (cm^3)
1	4.815
2	3.847
…	…
150	5.045

Alzheimer Disease Diagnosis

Attributes of the Feature Vector:	#	Age	Gender	Type 2 diabetes	Hippocampus Volume	Risk Factors
Feature Vector Attributes:	1	87	0	0	4.815	[0.67, 0.78]
	2	75	0	1	3.847	[0.56, 0.78]
	…	…	…	…	…	…
	150	65	0	⊥	5.045	[0.56, 0.89]
Feature Vector Domains:		[60, 96]	[0, 1]	[0, 1]	[3.272, 5.516]	[0, 1]

Risk Factors

#	Education Level	Blood Pressure	Body Height
1	normal/high	normal	normal
2	normal	⊥	normal
…	…	…	…
150	normal	normal/high	⊥

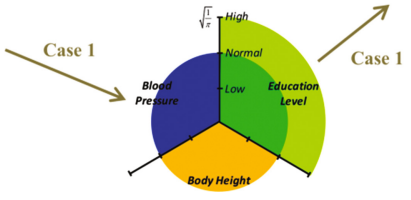

Fig. 4. A fragment of the knowledge base for Alzheimer disease diagnosis.

Applying the algorithm presented in [17] to the table or relation's fields that make the knowledge base for heart failure predisposing risk (Fig. 4), and looking to the *DoCs* values obtained as described before, it is possible to set the arguments of the predicate ***diag****nosis* ***a****lzheimer* ***d****isease* ($diag_{ad}$) referred to below, whose extensions denote the objective function regarding the problem under analyze:

$$diag_{ad} : Age, G_{ender}, T_{ype}2D_{iabetes}, H_{ippocampus}V_{olume}, R_{isk}F_{actors} \rightarrow \{0, 1\}$$

where 0 (zero) and 1 (one) denote, respectively, the truth values *false* and *true*.

The algorithm presented in [17] encompasses different phases. In the former one the clauses or terms that make extension of the predicate under study are established. In the subsequent stage the arguments of each clause are set as continuous intervals. In a third step the boundaries of the attributes intervals are set in the interval [0, 1] according to a normalization process given by the expression $(Y - Y_{min})/(Y_{max} - Y_{min})$, where the Y_s stand for themselves. Finally, the *DoC* is evaluated as described in Sect. 2.

As an example considers a term (patient) that presents the feature vector $Age = 67$, $G_{ender} = 1$, $T_{ype}\ 2\ D_{iabetes} = \bot$, $H_{ippocampus}\ V_{olume} = 4.113$, $R_{isk}F_{actors} = [0.67, 1]$, one may have:

$$\{$$

$$\neg\, diag_{ad}\left(\left((A_{Age}, B_{Age})(QoI_{Age}, DoC_{Age})\right), \cdots, \left((A_{RF}, B_{RF})(QoI_{RF}, DoC_{RF})\right)\right)$$

$$\leftarrow not\ diag_{ad}\left(\left((A_{Age}, B_{Age})(QoI_{Age}, DoC_{Age})\right), \cdots, \left((A_{RF}, B_{RF})(QoI_{RF}, DoC_{RF})\right)\right)$$

$$diag_{ad}\underbrace{\left(\left((0.19, 0.19)(1,\ 1)\right), \cdots, \left((0.67,\ 1)(1,\ 0.94)\right)\right)}_{\substack{attribute`s\ values\ ranges\ once\ normalized\ and \\ respective\ QoI\ and\ DoC\ values}} :: 1 :: 0.79$$

$$\underbrace{[0, 1] \quad \cdots \quad [0, 1]}_{\substack{attribute`s\ domains \\ once\ normalized}}$$

$$\}:: 1$$

5 Artificial Neural Networks

The proposed model for AD diagnosis set above displays how the information comes together to shape a diagnosis. In this section, a data mining approach to deal with this information is considered. It was set a hybrid computing approach to model the

universe of discourse, based on *ANNs*. As an example, let us consider the case given above, where one may have a situation in which an AD diagnosis is paramount. In Fig. 5 it is shown how the normalized values of the interval boundaries and their *DoC* and *QoI* values work as inputs to the *ANN*. The output depicts the AD diagnosis, plus the confidence that one has on such a happening. Has mentioned before, the ANN receives four inputs for each attribute used. Therefore, the input will consist on twenty inputs, regarding the boundaries of the interval, quality of information and degree of confidence.

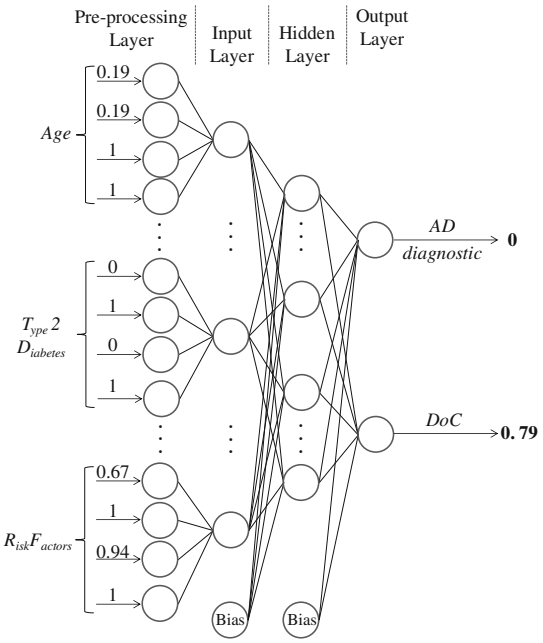

Fig. 5. The Artificial Neural Network topology.

The model was tested on a real data set with 150 examples. Thus, the dataset was divided in exclusive subsets through the ten-folds cross validation [12]. To ensure statistical significance of the attained results, 30 (thirty) experiments were applied in all tests. The back-propagation algorithm was used in the learning process of the ANN. As the output function in the pre-processing layer it was used the identity one. In other layers it was used the sigmoid function.

A common tool to evaluate the results presented by the classification models is the coincidence matrix, a matrix of size $L \times L$, where L denotes the number of possible classes. Matching the predicted and target values create this matrix. L was set to 2 (two) in the present case. Table 1 presents the coincidence matrix (the values denote the average of the 30 experiments). A perusal to Table 1 shows that the model accuracy was 85.3% (i.e., 128 instances correctly classified in 150). Thus, from clinical practice perspective, the predictions made by the *ANN* model are satisfactory, attaining

accuracies higher than to 85%. The sensitivity and specificity of the model were 89.7% and 80.6%, while *Positive* and *Negative Predictive Values* were 83.3% and 87.9%, denoting that the model exhibits a good performance in the diagnosis of AD.

Table 1. The coincidence matrix for ANN model.

Target	Predictive	
	Training set	
	True (1)	False (0)
True (1)	70	8
False (0)	14	58

6 Conclusion

The hippocampus volume reveals himself, one of the most important marker for detecting and following of the AD. However, the diagnostic of AD has shown to be a hard task, as the parameters that cause the disorder are not fully represented by objective data. Furthermore, it is necessary to consider different conditions with intricate relations among them, where the available data may be incomplete, contradictory, and even unknown. In this work the founding of a computational framework was presented. It uses powerful knowledge representation and reasoning techniques to set the structure of the information and the associate inference mechanisms (ANNs based). The ANNs were selected due to their proper dynamics, like adaptability, robustness, and flexibility. This approach not only allows to obtain the diagnosis of AD but it also permits the estimation of the degree of confidence associated with the diagnosis. In fact, this is one of the added values of this approach that arises from the complementarily between Logic Programming (for knowledge representation and reasoning) and the computing process based on ANNs. Future work may recommend that the same problem must be approached using others computational formalisms, namely Case Based Reasoning [22], Genetic Programming [9], or Particle Swarm [23], just to name a few.

Acknowledgments. This work has been supported by COMPETE: POCI-01-0145-FEDER-007043 and FCT – Fundação para a Ciência e Tecnologia within the Project Scope: UID/CEC/00319/2013.

References

1. Sørensen, L., Igel, C., Hansen, N.L., Osler, M., Lauritzen, M., Rostrup, E., Nielsen, M.: Early detection of Alzheimer's disease using MRI hippocampal texture. Hum. Brain Mapp. **37**, 1148–1161 (2016)
2. Alzheimer's Association: 2015 Alzheimer's disease facts and figures. Alzheimer's Dementia **11**, 332–384 (2015)

3. Vijayakumar, A., Vijayakumar, A.: Comparison of hippocampal volume in dementia subtypes. ISRN Radiology 2013, Article ID 174524 (2013)
4. Johnson, K.A., Fox, N.C., Sperling, R.A., Klunk, W.E.: Brain imaging in Alzheimer disease. Cold Spring Harb. Perspect. Med. **2**, a006213 (2012)
5. Bakkour, A., Morris, J.C., Wolk, D.A., Dickerson, B.C.: The effects of aging and Alzheimer's disease on cerebral cortical anatomy: specificity and differential relationships with cognition. Neuroimage **76**, 332–344 (2013)
6. Promteangtrong, C., Kolber, M., Ramchandra, P., Moghbel, M., Houshmand, S., Schöll, M., Bai, H., Werner, T.J., Alavi, A., Buchpiguel, C.: Multimodality imaging approach in Alzheimer disease. Part I: structural MRI, functional MRI, diffusion tensor imaging and magnetization transfer imaging. Dement. Neuropsychol. **9**, 318–329 (2015)
7. Jaba, L.S., Shanthi, V., Singh, D.J.: Estimation of hippocampus volume from MRI using ImageJ for Alzheimer's diagnosis. Atlas J. Med. Biol. Sci. **1**, 15–20 (2011)
8. den Heijer, T., van der Lijn, F., Koudstaal, P.J., Hofman, A., van der Lugt, A., Krestin, G.P., Niessen, W.J., Breteler, M.M.: A 10-year follow-up of hippocampal volume on magnetic resonance imaging in early dementia and cognitive decline. Brain **133**, 1163–1172 (2010)
9. Neves, J., Machado, J., Analide, C., Abelha, A., Brito, L.: The halt condition in genetic programming. In: Neves, J., Santos, M.F., Machado, J. (eds.) Progress in Artificial Intelligence. LNAI, vol. 4874, pp. 160–169. Springer, Berlin (2007)
10. Neves, J.: A logic interpreter to handle time and negation in logic databases. In: Muller, R., Pottmyer, J. (eds.) Proceedings of the 1984 Annual Conference of the ACM on the 5th Generation Challenge, pp. 50–54. Association for Computing Machinery, New York (1984)
11. Vicente, H., Dias, S., Fernandes, A., Abelha, A., Machado, J., Neves, J.: Prediction of the quality of public water supply using artificial neural networks. J. Water Supply: Res. Technol. – AQUA **61**, 446–459 (2012)
12. Haykin, S.: Neural Networks and Learning Machines. Prentice Hall, New York (2008)
13. Kakas, A., Kowalski, R., Toni, F.: The role of abduction in logic programming. In: Gabbay, D., Hogger, C., Robinson, I. (eds.) Handbook of Logic in Artificial Intelligence and Logic Programming, vol. 5, pp. 235–324. Oxford University Press, Oxford (1998)
14. Pereira, L., Anh, H.: Evolution prospection. In: Nakamatsu, K. (ed.) New Advances in Intelligent Decision Technologies – Results of the First KES International Symposium IDT 2009. Studies in Computational Intelligence, vol. 199, pp. 51–64. Springer, Berlin (2009)
15. Machado, J., Abelha, A., Novais, P., Neves, J., Neves, J.: Quality of service in healthcare units. In: Bertelle, C., Ayesh, A. (eds.) Proceedings of the ESM 2008, pp. 291–298. Eurosis – ETI Publication, Ghent (2008)
16. Lucas, P.: Quality checking of medical guidelines through logical abduction. In: Coenen, F., Preece, A., Mackintosh, A. (eds.) Research and Developments in Intelligent Systems XX, pp. 309–321. Springer, London (2004)
17. Fernandes, F., Vicente, H., Abelha, A., Machado, J., Novais, P., Neves J.: Artificial neural networks in diabetes control. In: Proceedings of the 2015 Science and Information Conference (SAI 2015), pp. 362–370. IEEE Edition (2015)
18. Open Access Series of Imaging Studies. http://www.oasis-brains.org/app/template/Index.vm
19. Reitz, C., Mayeux, R.: Alzheimer disease: epidemiology, diagnostic criteria, risk factors and biomarkers. Biochem. Pharmacol. **88**, 640–651 (2014)
20. Rasband, W.S.: ImageJ. U.S. National Institutes of Health, Bethesda, Maryland, USA (1997–2015). http://imagej.nih.gov/ij/
21. Tae, W.S., Kim, S.S., Lee, K.U., Nam, E.C., Kim, K.W.: Validation of hippocampal volumes measured using a manual method and two automated methods (FreeSurfer and IBASPM) in chronic major depressive disorder. Neuroradiology **50**, 569–581 (2008)

22. Carneiro, D., Novais, P., Andrade, F., Zeleznikow, J., Neves, J.: Using case-based reasoning and principled negotiation to provide decision support for dispute resolution. Knowl. Inf. Syst. **36**, 789–826 (2013)
23. Mendes, R., Kennedy, J., Neves, J.: The fully informed particle swarm: simpler, maybe better. IEEE Trans. Evol. Comput. **8**, 204–210 (2004)

Realization of the Principle of Conformal Symmetry in the Structure of the Heart

Galina A. Spirina(✉)

Human Anatomy Department, Ural State Medical University,
Yekaterinburg, Russia
profspirina@gmail.com

Abstract. Knowledge of quantitative rations of intracardiac structures necessary for the implementation of surgical interventions aimed at restoring them. 501 preparation of the fetal heart, people of both sexes and various age morphometric techniques studied the length of the departments of inflow and outflow of ventricles, the heart options. Absolute digital values transferred to the ratio. According to information received the linear dimensions of parts of the inflow, outflow ventricles, the width, the parameters of the heart can be presented in three segments related conformal symmetry. Change one of the parameters in a certain way agreed with the change of the other two. The ratio of length departments inflow, outflow ventricles, their width, calculated according to the formula for determining wurf, is a value close to 1.309. "Golden" wurf (1.309) is the "canon" of the human body, its proportions douse a special aesthetics. Wurf value determines the ratio of the three linear dimensions and not dependent on age. It was found the mean ventricular wurf ranges from 1.24 to 1.30, regardless of age. Similarly interconnected length, width and thickness of the heart. Conformal symmetry principle is reflected in the construction of the ventricles and the heart as a whole, determines the unity in variety of forms heart. Conformity reflects some hard and temporal parameters of macroscopic growth.

Keywords: Heart · Structure · Quantitative analysis · Symmetry

1 Introduction

It is essential to know the quantitative rations of the intracardiac structures in a normal formed heart to perform reconstructive surgeries [1]. Many aspects of heart anatomy are insufficiently covered, one of them is quantitative assessment of intracardiac structures. At the same time, the values of the ventricular input and output sections are used to assess hypertrophia and dilatation of the heart cavities. Morphometry of the heart cavities provides precise anatomical grounds for surgical interference [2]. Solving of problems related to health promotion is inconceivable without thorough study of the basic patterns of personal development and determination of mechanisms regulating organ functioning in pre- and postnatal periods of ontogenesis. Study of morphogenesis of the heart and organ formation at early stages of development is not only theoretical but also a major practical problem. Knowledge of dynamics of organ development and structural peculiarities at different terms of prenatal period allows a doctor to correct developmental pathologies.

D.N. Cassenti (ed.), *Advances in Human Factors in Simulation and Modeling*,
Advances in Intelligent Systems and Computing 591, DOI 10.1007/978-3-319-60591-3_16

2 Aim of Work

Morphometric analysis of ventricular sections, linear dimensions of heart, their interrelation and interdependence.

3 Material and Methods

Using 501 specimens of normally formed hearts of fetuses, children and adults of both sexes and different ages, whose cause of death is other than heart disease, we determined the heart parameters (length, width, thickness). Then these hearts were routinely opened, the length and width of the ventricular input and output were measured. The length of the input ventricular sections was determined as the distance from the fibrous rings of the right and left atrioventricular openings to the center of the heart apex of the respective ventricles, the length of the output sections was determined as the distance from the endocardium of the center of the ventricular apex to the base of the valves of the aorta and pulmonary artery [3]. The obtained absolute numerical values of the ventricular sections and the heart parameters were converted into ratios [1, 4–8]. Falkovsky and Berishvili [1] recommend studying the intracardiac structures using the relationship method. In this case there is no need to recalculate (the data in reference to the body surface and there is a less chance of measurement errors. Taking into account abundant data on influence of the symmetry laws on form-building processes [9, 10], in order to assess the interrelation of the overall heart dimensions, the ventricular input and output, their width, the harmony of heart organogenesis, the wurf value was calculated. Wurf is a value expressing correlation of values of three conformally symmetrical blocks (intervals) connected by one kind of circular symmetry provided that it is equal to 1.31. This value is called the golden wurf. Deviation from this value by more than 5% suggests anharmonic ratio of the values in question. Wurf coefficient is calculated using the following formula:

$$W_n = \frac{(Fn + Fn + 1) \cdot (Fn + 1 + Fn + 2)}{(Fn + Fn + 1 + Fn + 2) \cdot Fn + 1}, \quad (1)$$

where n is a serial number in a numerical sequence [9, 11]. In this case it was assumed that the three dimensions are the members of a harmonic series if their wurfs deviate from the golden wurf by 5% or less, i.e. are within the range 1.24–1.38. For each age group the percentage of samples with the wurf deviating from the golden wurf (1.31) by more than 5% was calculated. The results of the morphometric measurements were processed in Windows 6.0 using standard methods of variation and alternative statistics. For statistical processing we used an in-built analysis suite utilizing descriptive statistics, which included identification of arithmetic mean (M), its tolerance (±m), and root mean square deviation (s). Assessment of certainty of intragroup differences of the studied properties was carried out using Studenťs criterion with a confidence level of 0.95.

4 Results

During our study of age dynamics of the parameters of the ventricular input and output of the heart we used a new approach to its assessment. In this case we proceeded from I.V. Petuhkov's assumptions (1981) that the mysteries of formation of biological bodies lie in conformal or non-Euclidean nature of the space. Linear dimensions of the input and output sections of each ventricle may be presented as three intervals connected by conformal symmetry. A change in one of these parameters is in a certain manner connected with a change in two others. In this regard, the proportions of ratios between the parameters of intracardiac formations within the rage 1.2–1.3 are widely observed in the heart. In every age period elongated of one of the linear dimensions of the ventricles conforms with elongated of the other two dimensions, so that the ratio of the length of the ventricular input and output and their width may be presented as:

Table 1. Average wurf (W) of ventricles of human heart of different ages, relative units

Age	Right ventricle		Left ventricle	
	Wurf value	Wurf deviation from 1.31%	Wurf value	Wurf deviation from 1.31%
Fetuses (weeks):				
16	1.25	4.58	1.26	3.82
20	1.25	4.58	1.26	3.82
24	1.25	4.48	1.24	5.3
28	1.25	4.58	1.24	5.3
32	1.27	3.05	1.24	5.3
Newborn	1.26	3.82	1.24	5.3
Infancy (10 days–1 year)	1.26	2.29	1.27	3.05
1–3 years	1.26	3.82	1.26	3.82
4–7 years	1.26	3.82	1.25	4.58
8–12 years-boys	1.26	3.82	1.25	4.58
8–11 years-girls				
13–16 years-boys	1.26	3.82	1.30	0.76
12–15 years-girls				
17–21 years-youth	1.27	3.05	1.26	3.82
16–20 years-girl				
22–35 years-man	1.24	5.3	1.25	4.58
21–35years-woman				
36–60 years-man	1.25	4.58	1.24	5.3
36-55years-woman				
61–74 years-man	1.25	4.58	1.24	5.3
56–74years-woman				
75–90 years	1.24	5.3	1.24	5.3

$$W = \frac{(C-A)\cdot(D-B)}{(C-B)\cdot(D-A)} \quad A\_\_\_\_\_B\_\_\_\_\_C\_\_\_D, \tag{2}$$

where of the A–B is the length of the input section, B–C is the length of the output section, C–D is their total width approaching 1.31. The ratio of the said three linear dimensions is relatively constant value, similar for the right and left ventricles, irrespective of the age and cardiac index (Table 1). A change is one of these parameters is in a certain manner connected with a change in two others. Correlation of the length of the ventricular input and output and their width calculated using the formula for wurf determination in every age group appears to be close to 1.309. A numerical sequence with such limit is called the wurf sequence, and the value of the limit is called the golden wurf [9]. Study of prenatal period of development serves as the pre-condition for analysis of postnatal states. Linear dimensions of the heart characterize its growth and are most informative [3]. In comparison with the length of the heart, the most variable parameter is its width; the least in absolute value is its thickness. By analogy with a kinematic diagram of human body the heart parameters (length, width, thickness) are presented as trinomial block. As it grows, the proportions of this block change according to the rules of conformal transformation, i.e. a change of one parameter is

Table 2. Wurf value (W) of human heart in ontogenesis, relative units

Age	Wurf value, relative units
Fetuses (weeks):	
16	1.25
20	1.27
24	1.21
28	1.23
32	1.22
Newborn	1.27
Infancy (10 days–1 year)	1.29
1–3 years	1.23
4–7 years	1.22
8–12 years-boys	1.21
8–11 years-girls	
13–16 years-boys	1.23
12–15 years-girls	
17–21–years-youth	1.23
16–20 years-girls	
22–35 years-man	1.23
21–35 years-woman	
36–60 years-man	1.21
36–55 years-woman	
61–74 years-man	1.23
56–74 years-woman	
75–90 years	1.22

correlated with a change of the two others, which in a straighten block is preserved as invariable of circular formations - wurf. In pre- and postnatal periods of ontogenesis, the wurfs of the heart are similar in their value, which proves conformal- geometrical growth transformation of length, width and thickness of the organ. (Table 2).

5 Conclusion

A stable proportional correlation between parameters of the ventricular sections is observed in fetuses and throughout the entire postnatal period of ontogenesis. The identified linear dependence between the length of the ventricular input, output, and their width can be considered as a biomechanical constant, regulating proportional changes of the said parameters. The principle of conformal symmetry reflects in formation of the ventricles and the heart as whole, it is the most common law of morphogenesis, which determines uniformity in a variety of forms of this organ. Conformity reflects some strict and constant space-time parameters of macroscopic growth [10, 12, 13]. Conformal-geometrical growth transformation of the heart ventricles testifies to their development according to the most common laws of morphogenesis.

References

1. Falkovsky, G.E., Berishvili, I.I.: Morphometric research in normal humal newborn. Anat. Arch. **10**, 79–85 (1982)
2. Kuzmina, N.B., Gorodkov, A.Y., Yavorskaya, L.A.: New morphology parameters of left ventricle of human heart. Morphology and morphometry of normal and pathology human heart, Moscow, pp. 56–59 (1990)
3. Avtandilov, G.G.: Morphometry in Pathology, p. 248. Medgiz, Moscow (1973)
4. Feldt, R.H., Du Shane, J.W., Titus, J.L.: The atrioventricular conduction system in persistent common atrioventricular cannal defect. Circulation **42**(3), 437–444 (1970)
5. Kurosawa, H., Becker, A.E.: The conduction bundle at the atrioventricular junction. an anatomical study. Eur. J. Cardiothorac. Surg. **3**(4), 283–287 (1989)
6. Rowlatt, U.F., Rimoldi, H.J.A., Lev, M.: The quantitative anatomy of the normal child's heart. Pediatr. Clin. North Am. **10**, 499–588 (1963)
7. Sweeney, L.J., Rosenquist, G.: The normal anatomy of the atrial septum in the human heart. Am. Heart J. **98**(2), 194–199 (1979)
8. Zuberbuhler, J.R., Anderson, R.H.: Morphological variations in pulmonary atresia with intact ventricular septum. Brit. Heart. J. **41**, 281–288 (1979)
9. Petukhov, S.V.: Biomechanics, Bionics and Symmetry, p. 238. Science, Moscow (1981)
10. Urmancev, Y.A.: Symmetry of Nature and Nature Symmetry, p. 229. Thought, Moscow (1974)
11. Petukhov, S.V.: Highest Symmetries, Transformation and Invariants in Biological Objects, pp. 260–274. Thought, Moscow (1988)
12. Belousov, L.V.: Biology Morphogenesis, p. 239. Moscow University Edition, Moscow (1987)
13. Nalivkin, D.V.: Forms symmetry in inorganic world. Mater. Leningrad Soc. Nat. **75**(1), 27–33 (1965)

Modeling and Simulation for the Extreme Environment

Modeling Operator Workload for the Resource Prospector Lunar Rover Mission

Becky L. Hooey[1(✉)], Jason J.N.T. Toy[2], Robert E. Carvalho[1], Terrence Fong[1], and Brian F. Gore[1]

[1] NASA Ames Research Center, Moffett Field, CA 94035, USA
{Becky.L.Hooey, Robert.E.Carvalho, Terry.Fong, Brian.F.Gore}@nasa.gov
[2] San Jose State University, Moffett Field, CA 94035, USA
Jason.J.Toy@nasa.gov

Abstract. NASA's Resource Prospector mission is an unmanned lunar exploration mission currently in the concept development stage. Early tests have shown that the unique mission characteristics may combine to create the potential for very high workload for operators. This paper applies a taxonomy of workload drivers to identify the contextual variables expected to contribute to operator workload during the mission. Specifically, workload drivers attributed to the environment, task demands, equipment, and operator characteristics are reviewed. This research is intended to support the development of predictive models of operator workload to support the design and evaluation of workload countermeasures for the mission.

Keywords: Lunar rover · Workload · Human-performance modeling

1 Introduction

Resource Prospector (RP) is an in-situ resource utilization (ISRU) lunar rover mission under development by NASA [1]. The primary objective of RP is to prospect for subsurface volatiles on the Moon, particularly in permanently shadowed regions (PSR). The mission will address several of NASA's "Strategic Knowledge Gaps" for lunar exploration and will also address the Global Exploration Roadmap's strategic goal of using local resources for human exploration.

Permanently shadowed lunar craters are high-priority targets for future exploration because of the possibility that they harbor water ice [2]. In the RP mission, the rover will operate on the Moon for 7 to 10 days during a single lunar day at a location where both sun exposure and direct-to-earth (DTE) communication conditions overlap [3, 4]. The solar-powered rover will be capable of entering shadow and operating for up to 6 h before needing to recharge in sunlight [3, 4]. At the end of the lunar day, the sun will set, and the rover is not expected to survive the cold of the lunar night operating solely on battery power [3–5]. The surface mission is short, the environment has many unknowns, and operational constraints (e.g., including high-tempo operations cadence) create unique challenges [3].

These unique mission challenges have the potential to contribute to significant levels of operator workload for the team responsible for maneuvering the rover on the

D.N. Cassenti (ed.), *Advances in Human Factors in Simulation and Modeling*,
Advances in Intelligent Systems and Computing 591, DOI 10.1007/978-3-319-60591-3_17

lunar surface. In an early test [3], several issues relating to operator workload were identified, which prompted this comprehensive investigation of the factors that contribute to operator workload. Because the RP mission is still in the conceptual design phase, there is an opportunity to impact the design to optimize operator workload. The goal of this paper is to identify the contextual factors that may contribute to operator workload with the future objective of mitigating these workload sources through effective countermeasures that may take the form of procedures, appropriate task allocation, automation, and operator interface design.

2 Rover Driver Tasks

Lunar rover operations require a large multi-disciplinary team. It is expected that the RP mission team will be distributed across several NASA centers [3]; Rover drivers are to be located at NASA Ames Research Center along with the flight director, mission manager, science lead, mission system engineers, command and data flow engineers, science planners and prospecting instrument science leads; payload operations leads, systems team and command positions will be located at Kennedy Space Center, and the rover systems team will be located at Johnson Space Center. This paper focuses on the rover driving team, comprised of two operators (a *driver* and *co-driver*) responsible for remotely operating the rover on the lunar surface. The specific task allocation between the two-person driving team has yet to be determined and will be informed, in part, by the results of this workload analysis.

The rover driver task breakdown, shown in Fig. 1 and described next, was derived based on interviews with the RP mission team. In the RP concept, the science team will identify the science station locations (where drilling for surface volatiles will occur). The rover driver team will be responsible for defining a series of waypoints spaced approximately 6 to 10 m apart to maneuver the rover to the science station. Images of the forward view will be captured using mast-mounted stereo cameras and transmitted to the control station. Based on this imagery, the rover driving team will complete a series of tasks including localization (determining where the rover is) and local navigation (determining where the rover will go next) and will then define the location and orientation of the next waypoint. After the waypoint command has been executed, the driver and co-driver will monitor the rover progress, but will not actively control the rover movement. Remote manual control (e.g., rate-controlled driving) has been ruled out because of latency associated with the mission's communication design, and waypoint navigation enables flexibility in path selection and scientific responsiveness [3, 6].

The task of localization is comprised of several subtasks required to verify the location of the rover and its orientation. The rover driver team first assesses the captured image of the forward view and compares the terrain and horizon (when visible) in the captured image with modeled terrain (based on Digital Elevation Models, DEM) and their mental models of the immediate surrounding environment. For example, they may look to see if craters or other terrain features in the camera image match the DEM. If they match, and the rover driver team has confidence in the rover position, they will proceed to the local navigation task. If they lack confidence in the rover position, more images may be captured to help verify the rover location.

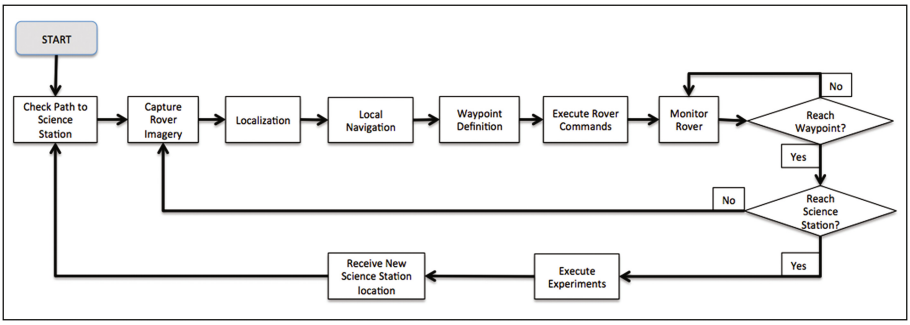

Fig. 1. Resource prospector rover driver tasks

Local navigation includes the task of identifying hazards within the immediate location of the rover and defining a safe hazard-free path that allows the rover to make efficient progress towards the target destination (science station). Hazards including positive obstacles (e.g., rocks) and negative obstacles (craters, holes, etc.) that exceed a specified size, as well as slopes that exceed a specified angle, will be defined in conjunction with the rover's mobility design.

The rover driver team will then identify a hazard free path and set a waypoint and define the rover orientation. Waypoints will be placed 6 to 10 m apart, a value that is determined based on the forward look-ahead distance of the cameras. The rover will continually transmit telemetry (including automatically estimated position and orientation) back to the ground station. However, due to RP's communication design, there will be a transmission delay estimated to be approximately 30 s, with an unknown amount of variability. During remote operations, the rover driver team will monitor a number of parameters including indications that the wheels are slipping. Because odometry will be used as part of pose estimation, wheel slippage could result in the rover traveling less distance than expected.

3 Contextual Factors that Contribute to Rover Driver Workload

Workload represents the task demand of accomplishing mission requirements for the human operator [7]. A taxonomy of *workload drivers* [8] identified four classes of contextual factors that contribute to operator workload for modern human-machine systems, and specifically operators of unmanned vehicle systems. The four classes (see Table 1) include the environment, task, equipment, and operator. *Environment drivers* include degraded visibility, complexity, uncertainty, and environmental elements and stressors. *Task drivers* include task demands, temporal demands, and task structure. *Equipment drivers* refer to the unmanned vehicle, its payload, and the communications link. *Operator drivers* include task proficiency and individual differences.

In the section that follows, we consider the tasks described above and identify workload drivers in each of the four classes within the context of the RP mission. These

workload drivers are derived from interviews with Subject Matter Experts from the RP mission engineering team, as well as literature from other lunar and Mars rover missions (including the Russian Lunokhod 1 and 2 missions [5], lunar analog missions conducted by NASA [3, 4] and the Canadian Space Agency [6], and NASA Mars Exploration Rovers (MER) missions [9]).

Table 1. Taxonomy of workload drivers [8]

Workload driver class	Sub-class
Environment	Degraded visibility Complexity Uncertainty Elements/stressors
Task	Task demands Temporal demands Task structure
Equipment	Vehicle Payload Link
Operator	Task proficiency Individual differences

3.1 Environment Characteristics

Four subclasses of environmental factors were identified, including degraded visibility, complexity, uncertainty, and environmental elements and stressors. When considering environmental factors in lunar rover operations, we must account for both the lunar environment in which the Rover is operating and the operator control room.

Degraded Visibility. RP is expected to operate in lunar polar regions under difficult illumination conditions, including inside PSRs [3]. Operating in these regions is expected to make it difficult to capture good quality imagery that clearly depicts the terrain and potential hazards. Further, when in transit towards the PSRs, low sun elevation (i.e., just a few degrees above the horizon), coupled with uneven terrain, will produce very long, very black shadows [4]. Additionally, the albedo of the lunar surface combined with these shadows will create images with a very challenging contrast. Furthermore, at times the rover may need to be driven directly towards, or directly away from the sun, both of which could produce severe imaging artifacts (overexposure, glare, etc.). All of these may reduce the quality of the captured imagery and increase the cognitive and visual workload required to analyze and interpret the imagery in support of the localization and local navigation tasks.

The challenges of operating in this degraded visibility environment can be informed by past lunar and lunar-analog missions. Previous research [6] using a lunar-analog environment, reported instances of the rover falling into holes or getting stuck when the sun did not illuminate the hole in the ground well, or when holes were hidden by the rover's own shadow. Similar difficulties were expressed by the operators of the Lunokhod 1 mission, who noted that at times fictitious dangers were reported caused by varying illumination conditions [5].

Another difficulty is associated with identifying negative obstacles, such as slopes, cliffs and crater edges, particularly when surface conditions have little textural variation (e.g., uniform soil appearance). In lunar-analog tests [6] it was noted that it "is almost impossible to figure out from cameras where the flat ground stops and the slope starts" (p. 12). Positive obstacles can also be difficult to discern or to assess (e.g., regarding scale or stability). In the same analog environment test, it was noted that at times when the rover drove over rocks that looked benign they ended up being fairly large rocks that were potential hazards for the rover. (p. 15, 17).

Complexity. The complexity of the environment in which the vehicle is operating is defined by the density and nature of hazards that must be avoided. Operators must develop and maintain an understanding of the spatiotemporal relationship of the vehicle relative to the environment, mission objectives, landmarks, and hazards to make decisions about when and how to deviate to avoid these hazards.

Some PSRs are contained inside large lunar craters. In these PSRs, it is expected that the dominant navigation hazards are small craters and their associated ejecta blocks [3]. However, the nature and density of terrain hazards that might be encountered in these areas are not well known. One source of information that can be used to inform expectations about lunar surface complexity is the Russian Lunokhod 1 mission. The vehicle drove 5,224 m in 49 h of driving using 1,695 driving commands including about 500 turns [5]. Sixteen signals were sent for protection against excessive tilt during that time, and approximately 140 craters were traversed at maximum slope angles of 30° [5]. The Lunokhod 1 mission operators reported that they encountered a dangerous situation (e.g., unforeseen entrance into a crater, rolling onto a rock) slightly more often than once per km [5].

The rover drivers may also experience regions that are relatively barren and lack distinguishing features. This can also contribute to workload for the task of localization that requires the rover driver team to compare terrain features captured in the image with those expected based on modeled data.

Uncertainty. The RP mission will travel in regions on the Moon that have never been explored before, and for which only low-resolution maps are available. As such, the density and nature of terrain and hazards are uncertain. One significant source of uncertainty is the composition of lunar regolith in PSRs. Regolith refers to the layer of loose surface material that covers solid rock and comprises dust, soil, broken rocks and other materials. The lunar regolith in PSRs could present driving hazards, including a brittle surface structure that may unexpectedly collapse under the rover, unanticipated depths of loose regolith that could allow the wheels to sink in, unusual electrical charging of the regolith, and poorly understood surface traction [3]. In Lunokhod 1 [5] it was reported that soil properties were found to "differ substantially even in terrain sectors not very distant from one another" [5, p. 1038]. Wheel slippage generally ranged from 0 to 15%, but increased to 20 to 30% on crater slopes [5]. The uncertainty of the surface composition, or even determining what to look for to assess surface stability at the outset, will be a significant workload driver requiring the rover drivers to learn and adapt in real-time during the mission.

Environmental Elements and Stressors. An assessment of the environmental elements and stressors that contribute to workload considers both the rover's environment as well as the rover drivers' environment. With regards to the rover's environment, first we consider the temperature. The temperatures may be expected to be as low as 40 K and as such the surface may contain material lower in density (almost "fluffy") compared to the well-consolidated regolith near the equator [4]. The rover driver will need to be aware of the surface stability to ensure the rover does not become embedded, and to monitor for wheel slippage (which may be an indication of incipient embedding). It is also possible that these temperatures may negatively affect the rover's sensors.

The rover driver team's environment on Earth has not yet been defined for RP, but issues such as temperature, lighting, and noise must be taken into consideration as all of these may increase workload [8]. Also, the distributed nature of RP mission operations necessitates the use of "party-line" voice channels for verbal communication among team members. Both the amount of background chatter and the volume of this chatter may distract rover drivers and contribute to workload.

3.2 Task Characteristics

Task characteristics that contribute to workload may be considered across three categories: Task demands, temporal demands, and task structure [8].

Task Demands. Task demands, including the criticality of the mission, severity of consequences, irreversibility of decisions, and the required level of precision can contribute to an operator's workload [8]. The unique characteristics of the RP mission will place workload demands on the rover drivers: it is an extremely short duration planetary rover mission that requires decisions to be made in real-time and at high cadence. The consequences of failure are high (including possible loss of mission) and will be acutely perceived by the rover driver team.

The rover design is based on a series of decisions that trade-off variables such as cost, weight, power, and robustness. The RP rover that will be built will be relatively lightweight and less robust compared to previous planetary rover missions (although the RP imagery quality will be higher). The nature and density of hazards may require high-precision maneuvering of the rover to avoid hazards while still making efficient progress towards the science station. Waypoint decisions are not reversible once executed given the time delay and there is no way to manually over-ride the rover if a problem or hazard is detected once the rover starts carrying out the command. These factors interact to place demands on the rover driver team to verify and cross-check all decisions before executing. In particular, this will require extended amounts of time localizing the rover to see where it is, where it went, and how to maneuver out of the hazard area. Failure to do this adequately could lead to disabling the rover and prematurely ending the mission without accomplishing critical objectives.

Temporal Demand. The RP mission will be operated 24 h a day for 7 to 10 days using shift-based operations [4]. The mission includes significant temporal pressures given that the rover uses solar power while many of the mission goals require exploring permanently shadowed regions. The science mission must be completed during a single

lunar day, after which the sun will set, and the rover is not expected to survive the cold of the lunar night [4, 5]. Given these time constraints, the rover driver team will be under significant pressure to maximize "speed-made-good" (i.e., the rate of closing distance from a start point to a goal location). The rover drivers will also be pressured to minimize rover idle time – periods when the rover is stationary and waiting for commands. These increases in operational tempo and time pressure have been shown [10] to degrade performance and increase workload.

Task Structure. Task structure variables consider the nature of coordination and collaboration required to accomplish the required tasks within and across a team that may be co-located or distributed [8].

Because the rover will be operated 24 h a day for 7 to 10 days, the driver team will necessarily need to hand off rover control in shifts from one driver to another. Handoffs require tightly coordinated interactions via system interfaces. Factors such as shift changes, interruptions, and distraction, may breakdown coordination, resulting in an unsuccessful handoff and increased workload [11]. As the rover proceeds, the driver develops situation awareness and a mental model of the immediate environment, including locations or rocks, cliffs, craters, and slopes. Transferring this knowledge at shift changes may increase operator workload for both the outgoing and incoming driver.

While it is known that coordination across distributed teams can carry a burden of increased workload, lessons learned from the MER mission suggest that this workload can be exacerbated given the heavy reliance on visual imagery [9]. The MER team, when remotely located, found that discussing images by teleconference required extensive verbal communication. For example, team members referred to familiar shapes, such as, "You can see it's almost like a mini-donut just to the left of the target" [9]. They also referred to structures within the image, such as rocks or shadows, for example, "I find it most convenient to use the shadow as a guide, so starting from the right side of the shadow there's a place where there's kind of two notches in the left of the shadow and then another notch to the left of that" [9]. These exemplify the additional workload required to communicate about visual imagery over voice radio channels when two co-located operators could accomplish the same task by simply pointing at a shared display. On the other hand, while co-locating the science team alongside the drivers may facilitate real-time decision making, it may also add to workload and the possibility of distraction. The co-driver is expected to support the rover driver tasks and has the additional task of relaying communications and requests from the science lead to the driver.

3.3 Equipment Characteristics

Several facets of the rover design itself can also impact operator workload, including the vehicle's physical characteristics, the onboard payload (especially that used to perform tasks associated with vehicle control, navigation, and hazard detection and avoidance), and the features of the command, control and communication link.

Vehicle (Rover) Design. Vehicle characteristics that affect maneuverability and stability such as vehicle size, wheel radius, axle and body clearances, speed and kinematics can directly impact operator workload [2, 8]. The robustness, maneuverability, and stability of the vehicle will determine the size of obstacles that must be avoided as well as the steepness of slopes that the rover can maneuver [2].

Because the RP will explore PSRs with a solar-powered rover, monitoring and managing the rover's power capacity and consumption could be a significant workload driver. While it is anticipated that power management will be the responsibility of other mission controllers, it may still contribute to driver workload, particularly when the driver must maneuver the rover to a location and orientation to allow the solar panels to recharge.

Payload. The rover drivers will use camera imagery to conduct the localization and tactical navigation tasks. These tasks require the rover drivers to use imagery to search for objects and obstacles, and to estimate distance and orientation [12–14] and may require significant effort engaged in camera integration and management. The RP rover may be equipped with multiple cameras (e.g., mast-mounted forward view for navigation and low-mounted hazard cameras) that may be synchronized with model data sources. The task of controlling these camera views and integrating views from multiple sources increases workload [15] associated with the tasks of localization and tactical navigation.

Two variables, look-ahead distance and field of view (FOV), may impact rover driver workload. The look ahead must be at least the minimum stopping or turning distance, and FOV sufficiently wide to encompass the rover width plus a maneuverability and safety margin [2]. Common to many unmanned vehicle domains, the reduced FOV inherent in video imagery (i.e., the "soda-straw effect" or "keyhole effect" [16]) is a source of workload in that it eliminates ambient visual information while imposing a demand for greater camera scanning for successful hazard detection [17].

Image resolution and quality is another potential workload driver. The resolution and quality will be determined based on a number of factors including physical characteristics of the camera and illumination sources (sunlight and rover mounted), as well as a trade-off between quality and transmission speed. Poor image resolution can impair detection of objects that occupy only a small visual angle within an image. Past research [18] showed that extra effort is required to interpret low-quality video feeds, increasing perceptual workload and that decreased resolution and increased scene distortion associated with scene compression may increase cognitive workload in vehicle control, navigation, and object localization tasks.

Communication Link. Rover communication link characteristics including bandwidth, latency, and reliability have been shown to impact operator workload [19]. While the earth-to-moon round trip delay is short and predictable, the communications network and the Deep Space Network (DSN) that is expected to be used for RP introduces an unpredictable and variable latency [3]. Consequently, the round trip latency is expected to range from 10 to 30 s; this inherent variability in latency makes real-time teleoperation (i.e., direct manual control) infeasible [3].

Because of the low data rate and communication delays, combined with the waypoint driving approach, the imagery will be infrequent and physically spaced apart (instead of continuous video feeds). The lack of continuous imagery is expected to increase the workload associated with the task of localization. Rover drivers will not have imagery to show how the current image relates to the image captured at the previous waypoint and it may prove difficult to match the current image with the driver's mental model from the previous image.

Further, with the Earth just above the horizon, line-of-sight radio communications may reflect off of the surface causing multi-path signal interference complicating operations decision making and risk management [4]. When communications are not continuous, or there is severe latency, workload will increase due to additional information processing required to interpret the state of the world based on discontinuous and/or out-of-date information.

3.4 Operator Characteristics

Several aspects of rover driver characteristics can contribute to increased workload including inexperience with rovers in general, with the RP rover specifically, and with operating in the dark, lunar environment [1, 8]. Lack of familiarity with control station tools and lack of experience with specialized driving tasks, such as performing precise parking maneuvers [6] can increase workload, especially when required to be performed under stressful conditions. By definition, the exploratory nature of this mission means that drivers will lack experience with the specific lunar operating environment. Operators of the Lunokhod 1 mission encountered unforeseen environmental hazards slightly more than once per kilometer. This was attributed in part to inadequate driving experience (but also to the modest quality of the images and the poor illumination conditions of the moon) [5].

A wide range of operator individual differences have been identified [8] that may contribute to operator workload including perceptual (e.g., visual acuity, contrast sensitivity, field of view, depth perception), cognitive (e.g., attentional control, spatial ability, perceptual speed, mental rotation, memory, problem solving abilities [20]), and sensorimotor capabilities [21] as well as personality traits, motivational states, and emotional states [22].

Individual characteristics including spatial ability may be a particularly relevant workload driver for RP. Spatial ability refers to the ability to navigate or manipulate objects in a 3-D environment [23] and has been found to be a significant factor in visual display domains, and tasks that involve multitasking, navigation, and visual search [20]. Much research (e.g., [23–26] has shown that operators with a higher spatial ability (i.e., mental rotation, spatial visualization, and spatial memory) perform better on tasks such as navigation, target identification and detection times. The effect of spatial ability on workload is inferred by performance on secondary tasks, a commonly used objective measure of workload.

4 Modeling Workload Drivers and Countermeasures

Maneuvering the rover to meet the science goals of the RP mission is expected to be a high-workload task given the nature of the mission and the unique and challenging operating environment as discussed above. When cumulative workload demands of concurrent tasks exceed acceptable limits, operators are at greater risk for shedding tasks or reduced performance levels, thereby increasing the potential for error and system risk. To guard against these risks, we must carefully examine the workload drivers, and the interactions among them, to predict workload vulnerabilities *before* the mission and rover system design is complete, and thus too expensive to modify.

Many of the workload drivers identified above may be mitigated through effective design of mission procedures, task allocation, rover system design, automation, and interface design. Several such solutions are under consideration by the RP mission design team including driver/co-driver task allocation, hazard detection and avoidance automation, rover preview automation, and graphical overlays to support localization and navigation. However, given the unique operating environment, in-situ human-in-the-loop evaluations of rover driver workload and the effectiveness of these countermeasures are not possible. Therefore an approach that allows for the prediction of workload as a function of proposed countermeasures is required to focus development efforts and support mission and system design. Specifically, our proposed design and evaluation approach uses the validated human performance model, the Man-Machine Integration Design and Analysis System (MIDAS).

MIDAS is a human performance modeling and simulation environment that contains computational cognitive structures that represent the human capabilities and limitations including perception, memory, decision-making, and visual attention [27]. MIDAS inputs include the operators' task and procedures (e.g., localization, local navigation, monitoring) in the form of a task network model, the operational environment (e.g., rover driver console, rover, lunar environment), and operator characteristics (e.g., operator expertise, and fatigue). The MIDAS processes are comprised of a task manager model that schedules tasks, definitions of the state of models within the physical simulation, a library of human primitive models that represent basic behaviors required for all activities, and cognitive models such as operator perception, visual attention, and workload [27].

MIDAS possesses two distinct workload characterizations. The first is an unconstrained representation where MIDAS completes the coded tasks and outputs workload without thresholds to limit task performance. This mode of operation allows model analysts to predict workload spikes and vulnerabilities. The second is an implementation where the MIDAS model completes the coded tasks using thresholds based on the Multiple Resource Theory (MRT). This mode of operation combines a resource conflict matrix and task degradation functions [28] to provide dual-task performance predictions. These model-based workload predictions will enable the identification of workload drivers that are most likely to lead to overload conditions and permit the evaluation of mitigation strategies to balance the workload with the operational demands.

5 Conclusion

In this paper, we applied a taxonomy of workload drivers to identify the contextual variables within the RP mission that are expected to contribute to rover driver workload. We identified workload sources derived from the environment, task demands, equipment, and operator characteristics. With this comprehensive understanding of workload drivers, workload countermeasure will now be developed and evaluated, using predictive models of operator workload to target each workload source. Workload countermeasures may take a variety of forms including procedures, appropriate task allocation, automation and interface design. These analyses are expected to inform the RP concept of operations, operating procedures, and rover design.

Acknowledgments. We would like to thank the members of the Resource Prospector mission team who have shared their insights and experiences including Mark Allan, Matt Deans, Michael Furlong, Mark Shirley, and Vinh To. Also, we would like to thank Mark Micire, Eric Krotkov, and John Paschkewitz for motivating and encouraging this study as part of an effort to model and predict workload in human-machine systems.

References

1. Andrews, D., Colaprete, A., Quinn, J., Bluethmann, B., Trimble, J.: Resource Prospector (RP) - early prototyping and development. In: AIAA Space 2015, Pasadena, CA, pp. 779–793 (2015)
2. Pedersen, L., Han, C.S., Vitus, M.: Dark navigation: sensing and rover navigation in permanently shadowed lunar craters. In: 9th i-SAIRAS, Los Angeles, CA (2008)
3. Trimble, J., Carvalho, R.: Lunar prospecting: searching for volatiles at the south pole. In: SpaceOps 2016 Conference, Daejeon, Korea, pp. 2272–2280 (2016)
4. Trimble, J., Shirley, M.H., Hobart, S.G.: Agile: from software to mission system. In: SpaceOps 2016, Daejeon, Korea, pp. 1012–1019 (2016)
5. Yoshida, K., Wilcox, B.: Space robots and systems. In: Khatib, O., Siciliano, B. (eds.) Springer Handbook of Robotics, pp. 1031–1063. Springer, Heidelberg (2008)
6. Gingras, D.: Deployment of the CSA Teleoperation Robotic Testbed 2 at Rougemont Sand Quarry. Test report, Canadian Space Agency (2014)
7. Hart, S.G.: NASA-Task Load Index (NASA-TLX); 20 years later. In: Proceedings of HFES, Los Angeles, CA, vol. 50, no. 9, pp. 904–908 (2006)
8. Hooey, B.L., Kaber, D.B., Adams, J.A., Fong, T., Gore, B.F.: The Underpinnings of Workload in Unmanned Vehicle Systems. IEEE Trans. Human–Mach. Syst. (2018, in press)
9. Vertesi, J.: Seeing Like a Rover: How Robots, Teams, and Images Craft Knowledge of Mars. University of Chicago Press, Chicago (2015)
10. Liu, D., Peterson, T., Vincenzi, D., Doherty, S.: Effect of time pressure and target uncertainty on human operator performance and workload for autonomous unmanned aerial systems. Int. J. Ind. Ergon. **51**, 52–58 (2016)
11. da Silva, F., Scott, S., Cummings, M.: Design methodology for Unmanned Aerial Vehicles (UAV) team coordination. Technical report HAL2007-04, MIT (2007)

12. McGovern, D.E.: Experience and results in teleoperation of land vehicles. In: Ellis, S. (ed.) Pictorial Communication in Virtual and Real Environments, pp. 182–195. Taylor and Francis, Bristol (1991)
13. McGovern, D.E.: Human interfaces in remote driving. Technical report SAND88-0562, Sandia National Laboratory (1988)
14. Pastore, T.H.: Improved operator awareness of teleoperated land vehicle attitude. Technical report NRAD-TR-1659, Naval Command, Control, and Ocean Surveillance Center, San Diego, CA (1994)
15. Chen, J.Y.C., Durlach, P.J., Sloan, J.A., Bowens, L.D.: Robotic operator performance in simulated reconnaissance missions. Technical report ARL-TR-3628, Hum. Res. Eng. Dir., Army Research Laboratory, Aberdeen Proving Ground, MD (2005)
16. Voshell, M.G., Woods, D.D.: Breaking the keyhole in human–robot coordination: method and evaluation. In: Proceedings of HFES, vol. 49, pp. 442–446, Orlando, FL (2005)
17. McCarley, J.S., Wickens, C.D.: Human factors concerns in UAV flight. Technical report AHFD-05-05/FAA-05-01, University of Illinois at Urbana-Champaign Institute of Aviation, Savoy, IL (2005)
18. Chen, J.Y.C., Haas, E.C., Barnes, M.J.: Human performance issues and user interface design for teleoperated robots. IEEE Trans. Syst. Man Cybern.-C: Appl. **37**(6), 1231–1245 (2007). IEEE Press
19. French, J., Ghirardelli, T.G., Swoboda, J.: The effect of bandwidth on operator control of an unmanned ground vehicle. In: Proceedings of the I/ITSEC, Orlando, FL (2003)
20. Chen, J.Y.C., Barnes, M.J.: Human-agent teaming for multirobot control: a review of human factors issues. IEEE Trans. Hum.-Mach. Syst. **44**(1), 13–29 (2014). IEEE Press
21. Kress, G., Almaula, H.: Sensorimotor requirements for teleoperation. Report R-6279, FMC Corporation, Santa Clara, CA (1988)
22. Szalma, J.L.: Individual differences in human-technology interaction: incorporating variation in human characteristics into human factors and ergonomics research and design. Theoret. Issues Ergon. Sci. **10**(5), 381–397 (2009)
23. Lathan, C.E., Tracey, M.: The effect of operator spatial perception and sensory feedback on human-robot teleoperation performance. Presence: Teleoper. Virtual Environ. **11**(4), 368–377 (2002). MIT Press
24. Rodes, W., Gugerty, L.: Effects of electronic map displays and individual differences in ability on navigation performance. Hum. Factors **54**(4), 589–599 (2012)
25. Baber, C., Morin, C., Parekh, M., Cahillane, M., Houghton, R.J.: Multimodal control of sensors on multiple simulated unmanned vehicles. Ergonomics **54**(9), 792–805 (2011)
26. Chen, J.Y.C.: Concurrent performance of military and robotics tasks and effects of cueing in a simulated multi-tasking environment. Presence: Teleoper. Virtual Environ. **18**(1), 1–15 (2009)
27. Gore, B.F., Hooey, B.L., Haan, N., Bakowski, D.L., Mahlstedt, E.: A methodical approach for developing valid human performance models of flight deck operations. In: Kurosu, M. (ed.) 14th Annual Human Centered Design Conference, pp. 379–388. Springer, Heidelberg (2011)
28. Gore, B.F.: Workload as a performance shaping factor for human performance models. In: 20th BRIMS, Sundance, UT (2011)

Occupant Protection Modeling and Injury Prediction for NASA Human Exploration Spacecraft

Nancy J. Currie-Gregg[1(✉)], Charles Lawrence[2], and Jeffrey Somers[3]

[1] NASA, Langley Research Center, Hampton, VA, USA
n.currie-gregg@nasa.gov
[2] Analytical Mechanics Associates, Inc., Hampton, VA, USA
[3] KBRwyle, Houston, TX, USA

Abstract. Finite element models (FEMs) of both small female and large male anthropomorphic test devices (ATDs) were developed and validated for use in occupant protection analysis for NASA human exploration spacecraft. These models are an important component of the suite of predictive tools which will be used to determine the risk of crew injuries due to spacecraft dynamic loadings. Physical ATD testing and correlation of test results to model predictions was performed to assess uncertainties associated with the FEMs ability to predict ATD responses to spaceflight loading environments. Both quantitative and qualitative metrics were used to assess model correlation quality. Model uncertainty factors were then determined for both small female and large male ATDs for each injury metric specified in NASA requirements.

Keywords: Spacecraft occupant protection · Anthropomorphic test devices · Finite element modeling

1 Introduction

The design of future human spaceflight systems, such as NASA's Multi-Purpose Crew Vehicle (MPCV), introduces new challenges to protect crewmembers from injury due to dynamic loads. Dynamic loads are defined as transient loads less than 500 ms in duration. Many parameters affect the likelihood of crew injury during dynamic spaceflight events. These include extrinsic factors such as g-loading, rate of acceleration onset, and force magnitude and direction; as well as intrinsic factors such as age, gender, and deconditioning incurred by long-duration exposure to microgravity. Injury probability and severity is also greatly influenced by the design of ancillary spacecraft and crew-worn components such as the crew seat, restraint harness, pressure suit and helmet; as well as load attenuating mechanisms that affect the acceleration profiles during loading events, such as landing [1].

Prior studies conducted by NASA's Human Research Program determined an acceptable level of risk tolerance for crew injuries associated with spacecraft landings [2]. Crash and injury statistics from current and previous spaceflight programs, as well as analogous operational environments such as automotive, car racing, and military

D.N. Cassenti (ed.), *Advances in Human Factors in Simulation and Modeling*,
Advances in Intelligent Systems and Computing 591, DOI 10.1007/978-3-319-60591-3_18

aviation, were evaluated. These data provided qualitative risk exposure comparisons from which risk tolerance related to landing impact injuries were established. Crew actions required to be executed immediately upon post-landing, such as emergency egress, were also considered. In addition, a systematic method for defining a set of driving landing scenarios based in part on the probability of occurrence was developed.

A five-point injury severity classification scale was developed to address the unique operational environment of human spaceflight. This classification scheme considers three factors: injury severity, injury effects on the crewmember's capability to self-egress, and influence of the injury on the time for the crewmember to return to flight status. Scores range from "no injury" (class 0) to "life-threatening" (class IV). This injury classification was then combined with a probability of occurrence to define an acceptable level of crew injury risk. Table 1 provides the injury descriptions, classifications and respective acceptable probability of occurrence. NASA requirements for occupant protection were developed based on these acceptable levels of risk.

Table 1. Acceptable risk of crew injury. [2]

Injury description	Injury class	$\geq$95% of dynamic cases	$\leq$5% of remaining cases
Minor	I	<4%	<23%
Moderate	II	<1%	<4%
Severe	III	<0.1%	<0.7%
Life-threatening	IV	<0.1%	<0.7%

NASA requirements for spacecraft occupant protection are based on a combination of Brinkley Dynamic Response (BDR) criteria and injury assessment reference values (IARV) associated with localized anthropomorphic test device (ATD) responses to dynamic accelerations [3]. While the BDR criteria roughly estimates the probability of crew injury or adverse physiological response risk, the criteria have significant limitations and uncertainties exacerbated by seat configuration differences between Orion and the human volunteer data set from which the Brinkley model is based. Further, the limited data used to develop the model and the limitations imposed by the simplifications inherent to the BDR criteria necessitated additional occupant protection requirements for future human-tended spacecraft [4].

The purpose of IARVs is to have occupant protection standards and programmatic requirements based on ATD responses that map to defined critical operationally relevant injury metrics. Among the current IARV metrics are:

- Head injury criteria (HIC_{15})[1]
- Head rotational acceleration limits
- Neck (cervical spine) protection criteria:

[1] A dimensionless measure of head acceleration during a 15-millisecond time interval, measured at the center of gravity of the dummy head.

  - Normalized neck injury criteria (N_{ij})[2]
  - Peak neck axial tension
  - Peak neck axial compression
- Flail
- Peak lumbar axial compression

ATD modeling and physical testing is required to provide predictions of crew injury risk under spacecraft loading conditions in a representative seated environment and to ensure that spacecraft designs meet occupant protection requirements. Current MPCV occupant protection requirements associated with IARVs, shown in Table 2, specify the use of 5th-percentile female Hybrid III (HIII) and the 95th-percentile male HIII ATDs.

Table 2. IARV limits [3]

ATD metric	ATD size	Non-deconditioned		Deconditioned	
		Nominal	Off-nominal	Nominal	Off-nominal
HIC 15	5th Female	375	525	375	525
	95th Male	325	450	325	450
Head rotational acceleration [rad/sec^2]	5th Female	2,500	4,200	2,500	4,200
		2,100	3,600	2,100	3,600
Nij	5th Female	0.5	0.5	0.4	0.4
	95th Male	0.5	0.5	0.4	0.4
Peak neck axial tension force [N]	5th Female	890–1,840		765–1,580	
	95th Male	2,000–3,390		1,720–2,910	
Peak neck axial compression force [N]	5th Female	890–2,310		765–1,990	
	95th Male	2,000–4,360		1,720–3,750	
Flail	5th Female	Pass			
	95th Male	Pass			
Peak lumbar axial compression [N]	5th Female	3,500	4,200	3,000	3,600
	95th Male	6,600	7,800	5,700	6,700

2 Methods

FEMs of both small female and large male HIII ATDs were developed and validated for use in spacecraft occupant protection analysis. These models are an important component of the suite of predictive tools that will be used to determine the risk of crew injuries due to spacecraft dynamic loading given crew seat, pressure suit, restraint harness, and crew impact attenuation system (CIAS) designs. Model performance was characterized by comparing matched ATD responses derived from simulations with the HIII FEMs to results from impact tests with physical HIII ATDs.

[2] Consists of four neck criteria - neck tension-extension, neck tension-flexion, neck compression-extension, and neck compression-flexion.

2.1 ATD Modeling and Simulation

Modeling and simulations were performed using Livermore Software Technology Corporation (LSTC) LS-DYNA® small female and large male HIII ATDs FEMs. The LSTC LS-DYNA® HIII FEMs are commercial off-the-shelf products developed primarily for automotive applications and have not been calibrated nor validated for spacecraft environments. Therefore, physical ATD testing and correlation of test results to occupant FEM predictions was necessary to assess uncertainties associated with the FEM's ability to predict ATD responses to dynamic loading associated with spacecraft applications.

To perform analysis of the loads transmitted to the crew during dynamic events, such as landings, it was necessary to integrate the ATD models with FEMs of the Orion seat/restraint system and key components of the proposed launch and entry pressure suit identified to affect ATD response, such as the helmet.

2.2 ATD Testing

Following initial development of the occupant FEMs, testing was first performed with physical HIII small female ATDs at the Horizontal Impact Accelerator (HIA) facility at the Air Force Research Laboratory (AFRL) at Wright-Patterson Air Force Base (WPAFB). The purpose of the test series was to evaluate localized responses of the physical ATDs in Orion-specific landing orientations, both with and without a representative advanced crew escape suit (ACES) and helmet. The ACES, a pressure suit worn by crewmembers during ascent and entry, can impart forces and moments on the occupant during a dynamic event.

The initial suite of physical ATD tests was not designed to evaluate actual Orion loading conditions but rather to test a range of conditions that envelope or exceed the range of expected dynamics during all Orion landing cases in order to assess occupant FEM capabilities and uncertainties. The test variables included seat orientation and rotation angle, peak G level, and acceleration rise time. From the 160 potential loading combinations, a subset of eight test cases were selected for physical ATD testing. This was the minimum subset determined to be sufficient for model characterization. Impact vectors were varied from single axis, spinal–the primary landing acceleration direction and rear–the primary launch abort acceleration direction, to combined axes–frontal/spinal and rear/lateral. Peak accelerations ranging from 15 to 20 g were selected as they were predicted to yield ATD responses close to the IARV limits defined in the HSIR requirements. Acceleration rise times varied between 70 and 110 ms to determine occupant FEM sensitivity to variations in impact energies. Rise time is defined as the time to peak acceleration.

Dynamic accelerations were achieved using the HIA hydraulic piston, as seen in Fig. 1, that imparts user-specified impact profiles that drive the HIA sled along the sled track. The level of pressure in the piston was used to obtain the desired peak acceleration, while a shaped insert (pin) installed inside the piston was used to tailor the rise time and shape of the impact acceleration. While the majority of the ATD response of interest occurs in approximately a quarter of a second, ATD responses were recorded

throughout the entire test and high-speed video provided critically important ATD kinematics. As seen in previous testing, the HIA facility provided consistent repeatability across all orientations and load conditions tested.

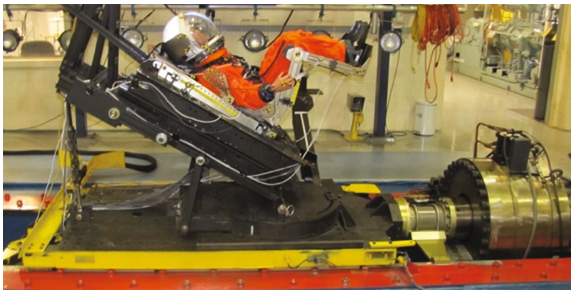

Fig. 1. Suited small female HIII ATD in HIA facility (*hydraulic piston shown on right*).

The first HIA test series, comprised of 35 tests, was conducted with small female HIII ATDs seated in a prototype Orion seat and restrained with a representative five-point harness. The order of the tests was determined to minimize hardware changes such as seat orientation, suited and unsuited ATDs, and pin switches (to change rise time). Each test run was performed at least twice. If the sled driving accelerations or the ATD responses for the first and second test did not match, then a third test was performed. If there were any hardware or instrumentation malfunctions, then the malfunction was resolved and repeat tests were run. Figure 2 shows representative motion of the small female ATD during testing in the HIA facility.

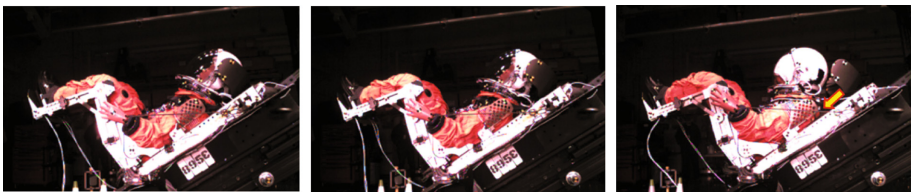

Fig. 2. Motion of the suited small female HIII ATD during HIA testing

The specific ATD configuration used in this study was the automotive HIII ATD with an articulating pelvis and a straight spine. The articulating pelvis, also known as an aerospace pelvis, was required for the ATDs to fit properly into the spacecraft seat, while the straight spine configuration was selected since injury metrics for vertical accelerations are only valid for the straight spine ATD configuration.

Unsuited test runs were performed first in the inclined 60-degree orientation. The 60-degree front/spinal orientation corresponds to an ascent abort landing condition where there are high horizontal winds (50 mph) and a nominal vertical velocity (~20 mph). It was desirable to obtain unsuited data to assess the modeling capabilities before the complexities of the suit and helmet were added to the ATD.

Initial ATD positioning in the seat was found to be a critical factor when comparing physical ATD test results with occupant FEM simulations. Prior to each impact test, the ATD was preloaded into the seat prior to impact by physically pushing the ATD into the seat pan and back while simultaneously tightening the harness straps until the load cells in the restraint harness straps registered 20 lb of preload. Targets on both the ATD and seat, as well as laser scanning measurements, were used to determine the precise position of the ATD with respect to the seat.

Physical ATD sled test results using the small female ATD, both suited and unsuited, were then compared with simulations of the same conditions using the small occupant FEM. To better match test data, modifications to the FEMs were subsequently implemented. The physical and FEM configurations of the small female HIII ATD are shown in Fig. 3.

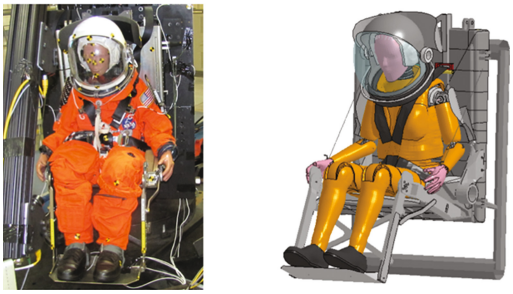

Fig. 3. Suited small female HIII oriented for rearward/lateral impact *(Physical HIII ATD on left and ATD FEM on right)*

An additional series of 17 tests was then performed at the AFRL HIA facility with the large male automotive HIII ATD in both unsuited and suited configurations. Impact directions were identical to those used for the small female ATD testing. However, because of the number of tests conducted with the seat test article and concern with damaging the seat, it was desired to reduce the total number of test conducted with the large male HIII. Since acceleration rise time was shown to have less of an affect than peak G and seat orientation on the correlation between physical ATD test results and FEM simulations, the large male ATD was only tested at an acceleration rise time of 70 ms. Table 3 shows the configurations and masses associated with the physical HIII ATDs that were tested.

Table 3. Physical HIII ATD configurations used in testing.

	AFRL small female	NASA small female	NASA large male
Type	Aerospace	Automotive	Automotive
Weight (unsuited)	110 lb	108 lb	235 lb
ACES helmet/neck ring	11.6 lb	11.6 lb	11.6 lb
Comm Cap	1.3 lb	1.3 lb	1.66 lb
Anchor bar assembly	0.64 lb	0.64 lb	0.64 lb
Suit/boots/cables/misc.	18 lb	18 lb	21 lb
Subtotal	31.5 lb	31.5 lb	34.9 lb
Weight (suited)	142 lb	140 lb	270 lb
Pelvis	Articulating	Articulating	Articulating
Spine	Straight	Straight	Straight
Neck position	Back (−6°)	Neutral (0−0)	Neutral (0−0)

2.3 Model Updates

The ATD FEM was fitted in an Orion seat FEM, which included representations of all of the physical aspects of the seat including the seatback, headrest, shoulder bolsters, seat pan, hip bolsters, foot pan, and restraint harness. Some further modifications to the FEMs were required in order to replicate the physical ATD test conditions. To replicate the preload applied to the physical ATD in the seat prior to testing, a 100-ms preloading phase was added to the simulation prior to applying sled accelerations. During the preload phase a set of static preload forces was applied to various locations within the ATD FEM while a constant preload was simultaneously applied to the cables that attach the harness belts to the seat. Also, since the ATD FEM does not have an articulating pelvis, it is difficult to obtain a close fit between the ATD pelvis and the seat. Thus, a 0.50-inch-thick soft foam padding was added to the occupant FEM between the ATD and the seat to mimic the effect of the pressure suit in this region.

One significant finding from the initial series of tests was the importance of additional crew-worn equipment to the ATD responses. Since the ACES design for MPCV is still under development, no communication cap (ComCap) or anchor bar was placed on the ATD during the initial series of sled tests. However, it was immediately noted that there was insufficient restraint to secure the ACES helmet on the ATD during impacts without the ComCap and anchor bar. Since this configuration would never be acceptable for actual operations, a representative ComCap and an anchor bar that attaches to the helmet ring and fits under the shoulder belts of the harness was used in all subsequent tests to help constrain the helmet from pulling on the head. These features were also implemented in the occupant FEMs. Due to the sensitivities noted in ATD response, it is imperative for additional sled testing to be performed to assess the final Orion seat/suit/restraint configuration.

3 Discussion

It was important to examine the physical ATD test data to ensure repeatability before comparing the data to matched ATD responses derived from simulations. Figures 4, 5 and 6 show a comparison of the repeatability in ATD responses for head rotational velocity and neck upper forces and moment, filtered at CFC 1000 [5], between two representative cases (8932 and 8933). The ATD response repeatability observed in these cases is representative of repeatability observed across the orientations and load conditions run as part of the test program. For the few instances where the repeatability was not as good as that demonstrated for cases 8932 and 8933, additional test cases were run to obtain good repeatability. No more than three tests were ever required in a single configuration.

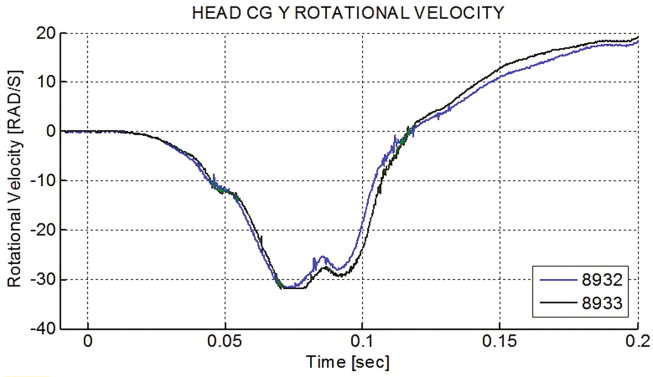

Fig. 4. Head Y-axis rotational velocity (measured at head CG).

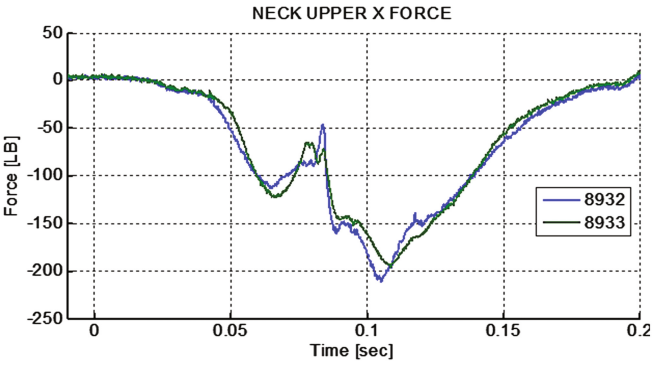

Fig. 5. Neck upper X-axis force.

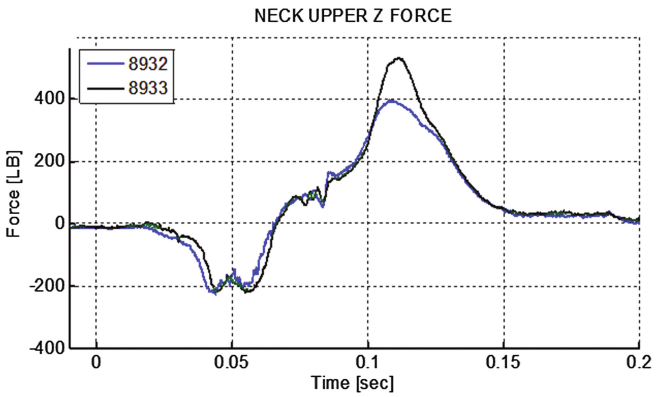

Fig. 6. Neck upper Z-axis force.

To explore potential differences in ATD responses because of the addition of the crew-worn ACES/helmet assembly, data recorded during physical ATD testing with the ACES/helmet assembly were compared with data recorded for the unsuited ATD. Comparing suited ATDs with the ComCap and anchor bar to unsuited ATD sled test results, the injury response is shown to be negatively affected (i.e., the risk of crew injury is increased) by the addition of suit elements. However, head injury criteria (HIC) values were small across the broad spectrum of test cases used in this study. Therefore, it is unlikely that the HIC injury criterion will be exceeded during actual vehicle impact loadings.

The sensitivity of ATD responses to neck position was also briefly explored using two positions: rearward (−6° relative to spinal alignment) versus neutral (0°, aligned with the spine). Magnitudes of neck forces and moments and lumbar forces were found to be sensitive to neck position, depending on the impact direction and seated orientation of the ATD. While current HSIR occupant protection requirements do not specify a required neck position for use during occupant protection requirement validation testing, it is important to use the same neck position when correlating physical ATD test data to occupant FEM results. Further testing to determine sensitivity to the anticipated neck position based on final design of the crew seat, pressure suit and helmet, and restraint system is warranted.

Both the physical ATD and occupant FEM responses exhibit sensitivity to small variations in the initial position of the ATD in the seat. The occupant FEM also showed sensitivity to small variations in the dynamic sled accelerations. The occupant FEM was most reliable for predicting frontal (−X) impacts, which was expected since this orientation is how the ATDs are used for automotive applications. The occupant FEMs do not reliably predict ATD responses to impacts in the +X-axis (rearward) direction. However, since rearward direction impacts are not likely to produce injurious levels of loadings, this is not considered to be a significant issue. The correlation between test and the occupant FEM were mixed in the spinal direction depending on which injury response channel was observed. The occupant FEM predictions were unreliable for the lateral (Y) response which may pose a problem for assessing injury for spacecraft landings without roll control.

In general, the small female occupant FEM results for the head X and Z accelerations, head rotational velocity, neck z-axis force and lumbar z-axis force channels correlated well for both the suited and unsuited physical test data in all orientations except rearward. The occupant FEM tended to under-predict the head X-axis acceleration and over-predict the head Z-axis acceleration, head rotational velocity and lumbar Z-axis force. The head rotational acceleration showed good correlation for the unsuited frontal/spinal cases, as did the neck Y-axis moment.

The large occupant FEM results for the head X and Z accelerations, head rotational velocity and lumbar z force channels correlated well for both the suited and unsuited physical test data in the frontal/spinal orientation. The occupant FEM tended to under-predict the head accelerations and lumbar force and over-predict the head rotational velocity. The lumbar Z force was likely under-predicted due to the fact that the occupant FEM had a curved spine while the physical ATD had a straight spine. Unfortunately, an ATD FEM model with a straight spine is not currently available. The unsuited occupant FEM results for neck Z force and neck Y moment also gave good correlations.

Prior to calculating the modeling uncertainty factors (MUFs), it was necessary to screen the ATD response channels to determine which channels generated usable data. For some response channels, the shape and phasing of the ATD response reasonably matched between ATD FEM simulations and physical ATD test data. In these cases, a MUF can be generated to adjust the magnitude of the ATD FEM simulation response to better reflect the test magnitude. For response channels that did not pass the pre-screening no MUF was calculated.

A multi-step process was used to determine the MUFs. First, a panel of six subject matter experts in injury biomechanics was requested to evaluate the transient responses for all the physical ATD response data. The SMEs were asked to rate each channel as either excellent (4), good (3), fair (2) or poor (1). The ratings were based on how well the ATD FEM simulation prediction matched the physical ATD test data. The SMEs considered the shape of the curves, phasing, and magnitude. The results of the individual ratings were then averaged to derive a composite rating for each channel. Figure 7 depicts an example of a SME rating of "excellent".

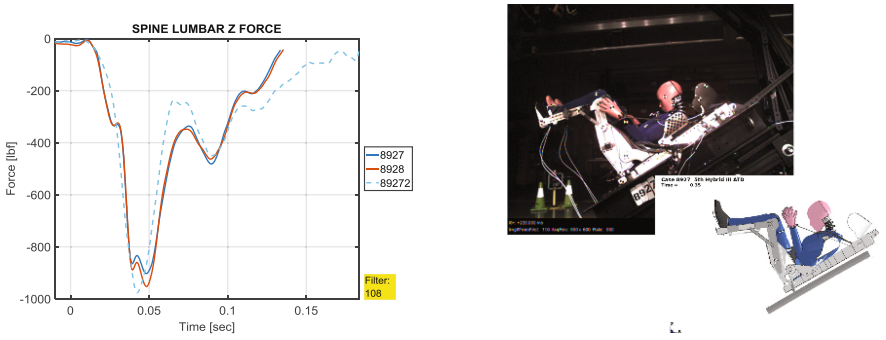

Fig. 7. Comparison of physical ATD test results (*solid lines*) and ATD FEM results (*dotted line*) resulting in a SME rating of "excellent".

The next step for determining acceptable response channels was to develop an objective rating to replace the subjective SME ratings. The International Organization for Standards (ISO) has developed a rating system for dynamic systems that is useful for this application [6–8]. The ISO rating uses a combination of the Correlation and Analysis (CORA) corridor metric with the Enhanced Error Assessment of Response Time Histories (EEARTH) metrics for response history magnitudes, phase, and shape. Each of the individual metrics are weighted and then combined into an overall ISO score. An ISO score of 0.5 was selected as the threshold value and corresponds to a "fair" SME rating (2.0), an ISO score of 0.7 then corresponds to a "good" SME rating (3.0) and an ISO score of 0.9 corresponds to an "excellent" SME rating (4.0).

Instead of deriving a single uncertainty factor that could be applied to the overall occupant FEM, model uncertainty factors (MUFs) were determined for both small female and large male occupant FEMs for each individual injury metric specified in the HSIR. A statistical analysis utilizing the error between the peak occupant FEM and physical ATD results was used to compute predicted errors and error bounds for each response channel. The MUF was defined as a multidimensional variable for each response channel as a function of the following: (1) ATD orientation, (2) whether the ATD is suited or unsuited, (3) the ATD type (i.e., automotive or aerospace), (4) the peak G level, and (5) the impact pulse rise time.

Determining a single MUF for each FEM for all injury metrics would have led to an overly conservative MUF since not all injury metric responses were similarly correlated between the FEM and the test. For some conditions, there was insufficient correlation between the FEM and the test data to compute a MUF for certain injury metric responses; however, as additional data become available it may be added to the available data to either compute MUFs or decrease the value of already existing MUFs.

4 Conclusions

The results derived from physical ATD tests were used to correlate the LSTC small female and large male HIII occupant FEMs, and to derive associated occupant FEM MUFs so the models may be used in future MPCV occupant protection analysis. The occupant FEMs, in conjunction with the MUFs associated with individual ATD IARV metrics, will be useful to provide an initial prediction of the level of occupant protection provided by the integrated Orion seat/suit/restraint/CIAS design under actual spacecraft loadings conditions. Additionally, simulations using the FEMs developed in this study provide a relatively fast and inexpensive method to analyze the potential effects of vehicle or crew equipment design changes on the risk of crew injury.

Verification of spacecraft contractor compliance to NASA occupant protection requirements must be accomplished through physical ATD testing. Thus, one of the most important uses of the occupant FEM developed in this study is to identify the suite of critical dynamic loading conditions to physically test. Improving occupant FEM correlation and MUFs will ultimately reduce the risk of non-compliance with NASA occupant protection requirements.

References

1. Currie, N.J., Lawrence, C.: NASA Engineering and Safety Center Report: Crew Exploration Vehicle (Orion) Occupant Protection, NESC-RP-08-00469. NASA Langley Research Center, Hampton, VA (2012)
2. Somers, J., Newby, N., Wells, J.: Final NASA Panel Recommendations for Definition of Acceptable Risk of Injury due to Spaceflight Dynamic Events, TP-2015-218578. NASA Johnson Space Center. Houston, TX (2015)
3. National Aeronautics and Space Administration, Orion Multi-Purpose Crew Vehicle Program: Human-Systems Integration Requirements, MPCV 70024, Rev. C. NASA Johnson Space Center, Houston, TX (2012)
4. Somers, J., Gohmert, D., Brinkley, J.: Application of the Brinkley Dynamic Response Criterion to Spacecraft Transient Dynamic Events, TM-2013-217380-REV1. NASA Johnson Space Center. Houston, TX (2016)
5. Society of Automotive Engineers (SAE): Instrumentation for Impact Test–Part 1, Electronic Instrumentation, Standard J211/1. SAE International (2014)
6. Barbat, S., et al.: Objective rating metric for dynamic systems. Enhanced Safety of Vehicles, Seoul, Republic of Korea (2013)
7. International Organization for Standardization (ISO): Road vehicles–Objective rating metrics for dynamic systems, ISO/TR 16250:2013(E) (2013)
8. International Organization for Standardization (ISO): Road Vehicles–Objective Rating Metric for Non-Ambiguous Signals, ISO/TS 18571:2014(E) (2014)

Minimizing Human Risk: Human Performance Models in the Human Factors and Behavioral Performance Elements

Brian F. Gore(✉)

NASA Ames Research Center, Moffett Field, CA 94035-0001, USA
Brian.F.Gore@nasa.gov

Abstract. Human space exploration has never been more exciting than it is today. Human presence to outer worlds is becoming a reality as humans are leveraging much of our prior knowledge to the new mission of going to Mars. Exploring the solar system at greater distances from Earth than ever before will possess some unique challenges, which can be overcome thanks to the advances in modeling and simulation technologies. The National Aeronautics and Space Administration (NASA) is at the forefront of exploring our solar system. NASA's Human Research Program (HRP) focuses on discovering the best methods and technologies that support safe and productive human space travel in the extreme and harsh space environment. HRP uses various methods and approaches to answer questions about the impact of long duration missions on the human in space including: gravity's impact on the human body, isolation and confinement on the human, hostile environments impact on the human, space radiation, and how the distance is likely to impact the human. Predictive models are included in the HRP research portfolio as these models provide valuable insights into human-system operations. This paper will provide an overview of NASA's HRP and will present a number of projects that have used modeling and simulation to provide insights into human-system issues (e.g. automation, habitat design, schedules) in anticipation of deep-space exploration.

Keywords: Human Factors and Behavioral Performance · Human performance · Human-systems integration · Systems engineering · Modeling and simulation

1 Introduction

The United States' Department of Defense (US DoD) and the National Aeronautics and Space Administration (NASA) put humans in extreme and hostile environments and require the human to perform optimally in order to successfully accomplish mission goals. Sub-optimal performance in the US DoD and NASA missions has the potential to increase the risks of not completing the mission successfully. A variety of methods to predict human-system vulnerabilities are needed to effectively manage such risks.

D.N. Cassenti (ed.), *Advances in Human Factors in Simulation and Modeling*,
Advances in Intelligent Systems and Computing 591, DOI 10.1007/978-3-319-60591-3_19

Our nation's space program has grown in sophistication and ambition over the recent past. The NASA Human Research Program (HRP) is the result of efforts undertaken by the agency to refocus its efforts on space exploration from the efforts of the Constellation program. The US space program has transitioned from one that focused on completing the International Space Station, to returning to the Moon, to crewed flight to the planet Mars, to one of exploration at greater distances and longer durations from planet Earth with the goal of traveling to Mars and beyond. This focus on exploration has changed the activities that NASA has been undertaking to include activities beyond low Earth orbit (LEO) over a longer duration. The NASA Programs responsible for insuring that success will be attained include the management of Commercial Space Transportation, Exploration Systems Development, Human Space Flight Capabilities, Advanced Exploration Systems, Research and Technology, and Operations.

2 NASA's Human Research Program

The Human Research Program (HRP) resides under NASA's Research and Technology program. The goal of the HRP is to provide human health and performance countermeasures, knowledge, technologies, and tools to enable safe, reliable, and productive human space exploration [1]. The HRP and its researchers are working to develop capabilities, necessary countermeasures, and technologies to support human space exploration, focusing on mitigating the highest risks to crew health and performance and documenting these findings in guidelines and standards. In addition, HRP seeks to develop technologies that serve to reduce medical and environmental risks, to reduce human systems resource requirements (mass, volume, power, data, etc.), and to ensure effective human-system integration across exploration mission systems. HRP ensures maintenance of Agency core competencies necessary to enable risk reduction in the following areas: space medicine; physiological and behavioral effects of long-duration spaceflight on the human body; space environmental effects (including radiation) on human health and performance; and space human factors. The HRP and its researchers are working to improve astronauts' ability to collect data, solve problems, respond to emergencies, and remain healthy during and after extended space travel. Investigators in HRP work to predict, assess, and solve the problems that humans encounter in space through national and international assets and collaborations.

2.1 NASA HRP Structure

As of February 1, 2017, HRP is comprised of five elements: Human Factors and Behavioral Performance, Human Health Countermeasures, Space Radiation, Exploration Medical Capability, and the International Space Station Medical Project. The five Elements are aimed at exploring many facets of human space travel including environmental factors, exercise physiology, habitability, human factors engineering design, medical capabilities, physiology, psychosocial and behavioral health, and space radiation. The HRP's five elements enable scientists and engineers work to predict, assess, and solve the problems that humans encounter in space.

The HRP and its five elements use a risk reduction strategy based on a medical model to guide the research that is to be conducted. The HRP focuses its research investment on investigating and mitigating the highest risks to astronaut health and performance in support of exploration missions. This process describes evidence as the basis for the existence of a risk to the human system, gaps in our knowledge about characterizing or mitigating the risk, and the tasks that need to be carried out in order to produce the deliverables needed to close the gaps and reduce the risk. The evidence for the existence of the risk is documented in the risk evidence reports, the gaps in knowledge represent the questions that need to be answered to mitigate the risk, the tasks characterize the risk or develop mitigation capabilities to reduce the risk to an acceptable level, and deliverables culminate in the final product (standards, guidelines, countermeasures). HRP relies on Design Reference Missions (DRMs), which provide a framework to identify key capabilities and important guiding drivers and assumptions, thus enabling the HRP to focus its research questions on topics highly relevant to NASA's future activities. The exploration missions currently considered include the International Space Station (ISS), lunar, near Earth objects/asteroids, and Mars missions [1].

2.2 Methods Used to Minimize Human Exploration Risks

The multiple lines of critical research that needs to be undertaken by NASA's HRP require that a suite of approaches be used to predict the impact of the complex, long duration mission on the human, and on the human's ability to perform. Ground research occurs in laboratories and analogs that simulate a portion of the spaceflight environment. The International Space Station (ISS) is used to conduct research requiring the unique environment of space, and for validating some of the results from ground-based studies. NASA has also adopted the NASA-STD-3001 to establish a broad set of criteria that ensures that humans are healthy, safe, and productive in space. The approaches used to meet these criteria need to include both the concerns from the human physiology and medical procedures and standards for maintenance and preservation of health, as well as the 'systems' perspective. Specifically, systems that interface with the human: controls, displays, architecture, environment, and habitability support systems. NASA uses a variety of methods to optimize designs for all crew operations both inside and outside the spacecraft in space and on lunar and planetary surfaces. The charter of the Human Factors and Behavioral Performance (HFBP) Element is to perform the research and technology development to support generation of human factors standards and guidelines for human-system hardware, software, procedures, and spacecraft designs as well as to conduct and support research to reduce the risk of behavioral and psychiatric conditions. All of the HFBP research feeds documentation, guidelines, validation of environmental impacts on the human, and HFBP standards within NASA-STD-3001, NASA Space Flight Human Systems Standard, Vol. 2, and the Human Integration Design Handbook [2, 3]. The HFBP Element is subdivided into the Human Factors, the Sleep/BMED, and Team portfolios. Each of these portfolios is guided by a series of risk statements.

2.3 HRP Risk Statements

Six risk statements exist within HRP's HFBP HF Portfolio and serve to guide the research that is completed in order to optimize human performance in space [4]. The risk statements under the HF Portfolio follow.

Risk of Incompatible Vehicle/Habitat Design (HAB). Given that vehicle, habitat, and workspace designs must accommodate variations in human physical characteristics and capabilities, and given that the duration of crew habitation in these space-based environments will be far greater than mission of the past, there is a risk of acute and chronic ergonomics-related disorders, resulting in flight and ground crew errors and inefficiencies, failed mission and program objectives, and an increase in the potential for crew injuries.

Risk of Inadequate Design of Human and Automation/Robotic Integration (HARI). Given that automation and robotics must seamlessly integrate with crew, and given the greater dependence on automation and robotics in the context of long duration spaceflight operations, there is a risk that systems will be inadequately designed, resulting in flight and ground crew errors and inefficiencies, failed mission and an increase in crew injuries.

Risk of Performance Errors due to Training Deficiencies (TRAIN). Given that existing training methods and paradigms may inadequately prepare long-duration, autonomous crews to execute their mission, there is a risk that increased flight and ground crew inefficiencies, failed mission and program objectives, and increased crew injuries will occur.

Risk of Inadequate Mission, Process, and Task Design (MPTASK). Given that tasks, schedules, and procedures must accommodate human capabilities and limitations, and given that ling-duration crews will experience physical and cognitive changes and increased autonomy, there is a risk that tasks, schedules, and procedures will be developed without considering the human condition, resulting in increased workload, flight and ground crew errors and inefficiencies, failed mission and program objectives and an increase in crew injuries.

Risk of Inadequate Human Computer Interaction (HCI). Given that human-computer interaction and information architecture designs must support crew tasks, and given the grater dependence on HCI in the context of long-duration spaceflight operations, there is a risk that critical information systems will not support crew tasks effectively, resulting in flight and ground crew errors and inefficiencies, failed mission and program objectives, and an increase in crew injuries.

Risk of Injury from Dynamic Loads (OP). Given the range of anticipated dynamic loads transferred to the crew via the vehicle, there is a possibility of loss of crew or crew injury during launch, abort, and landing.

Both empirical and computational approaches have been used iteratively to reduce the impact of risks to human exploration.

3 NASA's Human Research Program Use of Modeling and Simulation

Modeling and simulation (M&S) techniques play an integral role when complex human-system notions are being proposed, developed, and tested. NASA Johnston Space Center (JSC) utilizes M&S to represent environments, physical structures and equipment components, crew stations, planets and planetary motions, gravitational effects, illumination, human anthropometric and biomechanics. NASA Ames Research Center utilizes M&S capabilities for airflows, flight paths (e.g., Airspace Concept Evaluation System-ACES), aircrafts, schedules (e.g., Core-XPRT, Science Planning InterFace to engineering – SPIFe, Playbook), human performance prediction (HPMs; e.g. MIDAS, see below), and bioinformatics. NASA's HFBP currently uses a number of these M&S approaches to estimate many aspects critical in the human research roadmap (HRR) in the respective risk's Path to Risk Reduction (PRR) [5].

Seven HRP HFBP (formerly the SHFH and BHP Elements) projects currently underway (or recently completed) serve to reduce gaps in knowledge in the habitability, task design, human automation and robotics integration, and the behavioral performance sleep risks illustrate the manner that M&S approaches have been used to inform the respective risk.

3.1 Computational Model for Spacecraft/Habitat Volume

The Computational Model for Spacecraft/Habitat Volume task set out to create a "bottoms-up" method based on mission attributes and critical task volumes better align with a human-centered design philosophy than the top-down approach that is commonly used [6]. The objective of this ongoing work is to develop a constraint-driven, optimization-based model that can be used to estimate and evaluate spacecraft/habitat volume. The computational model development aims to: Estimate spacecraft/habitat volume based on mission parameters and constraints, provide layout assumptions for a given volume, assess volumes based on a set of performance metrics, and inform risk characteristics associated with a volume. The outcome of this work will provide data to support the HFBP-HAB-09 Gap on technologies, tools, and methods for data collection, modeling, and analysis for design and assessment of vehicles/habitats. This ongoing work is expected to continue through 2017.

3.2 A Tool for Automated Collection of Space Utilization Data

The tool for automated collection of space utilization data task is designed to develop innovative methods to unobtrusively collect detailed and high quality input data without impacting crew time or constraining missions [7]. The objective of this ongoing work is to develop and validate an automated data collection system that delivers data useful in the analysis of space utilization and vehicle habitability

pertaining to crew activities on the ISS as well as potential long duration space missions. The investigation utilizes two independent technologies, 3D RFID-Real Time Location System (RTLS) and Microsoft Kinect 3D volumetric and anatomical scanning tools, and integrates them into a single data collection and integration solution. The project advances the integrated system through a validation exercise that uses the HRP Human Exploration Research Analog (HERA) platform. The significance of this task is that it will provide NASA with a quantitative methodology for collecting data 3D space utilization data that is validated for use in flight analogs and has potential direct applicability for use in in-flight environments. The outcome of this research will provide human performance data to support the needs of the HFBP's Risk of Incompatible Vehicle/Habitat Design and the associated HF portfolio gap HAB-05: We need to identify technologies, tools, and methods for data collection, modeling, and analysis that are appropriate for design and assessment of vehicle/habitats by creating a capability to automatically collect space utilization and other habitation-related questions, questions that need to be answered as the mission lengths increase to months-long durations.

3.3 Human – Automation Interactions and Performance Analysis of Lunar Lander Supervisory Control

This task examined the complex interactions between the astronauts and the vehicle systems and automation required to conduct safe and precise planetary landing tasks. The task produced an integrated human-system model that includes representations of human attention, perception, decision-making, and action for use as an early-stage simulation-based design tool for human-system integration in complex systems [8]. The case study was a piloted lunar landing task. There were four integrated specific aims: (1) Perform a critical analysis of human operator-automation interactions and task allocations, considering information requirements, decision making, and the selection of action; (2) Develop a closed-loop pilot-vehicle model, integrating vehicle dynamics and human performance models, and parametrically analyze and quantify system performance; (3) Conduct experiments in the Draper Laboratory fixed-base simulator to validate critical parameters within the integrated pilot-vehicle model; (4) Extend the model to include the effect of spatial orientation and conduct experiments on the NASA Ames Research Center (ARC) Vertical Motion Simulator (VMS) to investigate the effects of motion cues on pilot performance. The results of the VMS and Draper Laboratory experiments have been used to update the integrated human-system model of the lunar lander. The model represents the cognitive processes and action responses of the human, who can act as both a flying pilot as well as a supervisory pilot. The model blocks have been updated in the Human Performance Model (HPM) library, and the integrated model has been used to run sensitivity analyses to the effect of parameter variation on simulated system performance. The outcome of this research provided research data to support the reduction of the HFBP's

Risk of Inadequate Mission, Process, and Task Design and the associated HF portfolio gap MPTASK-01: we need methods and tools to collect measures of mission, process, and task performance.

3.4 MIDAS-FAST: Development and Validation of a Tool to Support Function Allocation

The MIDAS-FAST[1] project examined the impact that automation has on human manual control performance of a robotic asset, the International Space Station Mobile Servicing System (Canadarm 2) [10]. Robotic manipulations are complex and often involve moving the arm in 7 degrees of freedom, with rotation up to 540 degrees, often possessing optimal camera viewing angles presented on the Advanced Space Vision System screen that need to be set by the crewmember. "Automation" has been proposed as a solution to assist the human guard against errors, which can have disastrous, potentially life threatening, consequences.

The MIDAS-FAST project uses human-performance models with a robotic simulation environment to evaluate the effects of function allocation strategies and task type on operator and system performance in order to evaluate potential human-automation interaction design issues. In this task, the research team (1) developed and validated a model- and simulation-based tool to allow researchers to evaluate various function allocation strategies in space robotics missions and (2) conducted empirical research to investigate human-automation interaction (HAI). The tool used the Man-Machine Integration Design and Analysis System (MIDAS, a NASA Ames HPM tool) [11], the Basic Operational Robotics Instructional System (BORIS, a NASA Johnson Space Center (JSC) training simulation [12], and the Frame of Reference Transformation (FORT) model. FORT was added to the operator model to identify the quality of camera views and control-movement compatibility [13]. FORT contributes to the operator workload, calculated in the human performance software, MIDAS. MIDAS-FAST provides ways for the modeled operator to (1) receive and interpret data from BORIS, (2) assess their own performance as the task is carried out, and (3) adjust their behavior based on FORT and external (BORIS-driven) stimuli.

The MIDAS-FAST task provided a validated model- and simulation-based tool for predicting operator performance when working with a robotic arm in different function allocation situations. The function allocation model, and the empirical research in this effort were used to identify conditions and provide data to develop the tool. The MIDAS-FAST task has integrated the FORT, BORIS and MIDAS models and has developed a combined user interface. The outcome of this research addressed HFBP's Risk of inadequate design of human and automation/robotic integration and the associated HF portfolio gap HARI-01 we need to evaluate, develop, and validate methods and guidelines for identifying human-automation/robot task information needs, function allocation, and team composition for future long duration, long distance space missions [14].

[1] The MIDAS-FAST project arose from the workload monitoring and modeling task of the HRP SHFE portfolio from 2008–2010 [9].

3.5 Modeling and Mitigating Spatial Disorientation in Low G Environments

The goal of this task was to extend a spatial disorientation mitigation software developed for aeronautical use called Spatial Disorientation Analysis Tool (SDAT) to NASA's space applications (e.g. the Shuttle, crew exploration vehicle, Altair, and Mars exploration missions) [15]. This task served three main goals: (1) Enhance the utility of SDAT/SOAS by including appropriate mathematical models for vestibular and visual sensory cues, and CNS (central nervous system) gravito-inertial force resolution into perceived tilt and translation estimates from Massachusetts Institute of Technology's (MIT's) Observer model, and revalidating it using existing aeronautical data sets. (2) Extend the models to describe 0-G, Shuttle, and Altair landing illusions, validating the models using Shuttle and Altair simulator data sets, and current theories (e.g., ROTTR). (3) Extend SDAT/SOAS to consider multiple visual frames of reference, the effects of visual attention and sensory workload, and the cognitive costs of mental rotation and reorientation. The enhanced SDAT/SOAS were validated via simulator experiments. Four key findings from this research were as follows. (1) MIT's Observer model was merged with SDAT; (2) SDAT was enhanced with an attention model termed N-SEEV (noticing-salience, expectancy, effort, and value) and with three new illusion models, verification tests, and comparisons of analytical results produced by SDAT and Observer; (3) SDAT was validated with anonymous data sets of helicopter pilots who experienced spatial disorientation (SD); and (4) an Institutional Review Board (IRB)-approved Space Shuttle spatial orientation survey was completed. The outcome of this research answers a part of HFBP Risk of Inadequate Human-Computer Interaction and the associated HF portfolio gap HCI-03 we need HCI guidelines (e.g., display configuration, screen-navigation) to mitigate the performance decrements and operational conditions of long duration space.

3.6 Space Performance Research Integration Tool (S-PRINT)

The purpose of the Space Performance Research Integration Tool (S-PRINT) task was to build off of earlier validated human performance model work (e.g. MIDAS-FAST) to develop tools and empirically-based guidelines that support human performance researchers, mission planners, automation designers, and astronauts in long-duration missions, specifically human performance in unexpected workload transition situations [16]. These situations, when addressed by fatigued astronauts, constitute worst-case scenarios that require specific, in-depth investigation. S-PRINT helps users anticipate and avoid potential problems related to unexpected workload transitions by identifying the expected effects of operator fatigue, automation system design, and task factors on overload performance, and assure that systems can be designed in such a way as to minimize transient, and long-term impacts of space missions on performance.

The S-PRINT task provided a validated, model-based tool to help researchers evaluate potential long-duration missions, identify vulnerabilities, and test potential mitigation strategies to help ensure effective performance and safe space missions. In addition to the meta-analyses, the project included multiple human-in-the-loop (HITL)

studies to investigate (1) human-automation interaction (exploring, in particular, the effects of automation design factors and failure types on automation bias and complacency), (2) multitasking in overload situations. The results of these studies have been published and contribute to the scientific knowledge in human-automation interaction and human performance in overload. These two topic areas are relevant in numerous Earth-based domains.

The S-PRINT task also developed component models that enable the software to predict; (1) the effects of fatigue (i.e., due to sleep deprivation, sleep restriction, sleep inertia, and circadian cycle effects) on task completion time and task accuracy, (2) the effects of automation design factors (e.g., reliability, degree of automation or function allocation) on operator performance, (3) the effects of failure type on operator performance, and (4) the effects of task factors (i.e., salience, expectancy, effort, and value) on task selection in overload. All of these areas are relevant in Earth-based industries that require around-the-clock operations, involve the use of automation, and offer the potential for situations that put an operator in overload conditions (e.g. medicine, process control, military operations, and transportation). The outcome of this research adds an approach that can be used HFBP's Risk of inadequate mission, process, and task design and the associated HF portfolio gap MPTASK-01: We need methods and tools to collect measures of missions, process, and task performance, and Behavioral Performance (BP) gap Sleep 8 we need to develop individualized scheduling tools that predict the effects of sleep-wake cycles, light and other countermeasures on performance, and can be used to identify optimal (and vulnerable) performance periods during spaceflight [17].

3.7 Occupant Protection Data Mining and Modeling

The risk of injury due to dynamic loads is poorly understood for spaceflight [18]. It is necessary that the risk to crew members associated with dynamic loads be reduced. Many differences exist between the well-documented automotive and military environment (National Highway Transportation Safety Administration, NHTSA and Military Standard, MILSPECS) and those experienced in space flight operations. For instance, the loads experienced in space flight are often a multi-axial, complex impact that is unique to a particular vehicle design, which differences from terrestrial vehicles. Limitations of the current NASA standard require that: (1) a Finite Element (FE) model of test device for Human Occupant Restraint (THOR) Anthropometric Test Device (ATD) be developed, and (2) data mining of existing human injury and response data using the THOR FE model be performed. The purpose of the OP task therefore is to define the scope of dynamic loads reasonably expected in current and future spaceflight systems, identify the appropriate human surrogate(s) for implementing injury assessment reference values (IARVs) appropriate for spaceflight loading conditions, develop IARVs based on Definition of Acceptable Risk (DAR), and validate the IARVs through sub-injurious human testing at nominal landing loads.

In order to develop updated standards, adequate injury assessment tools must be completed. The THOR ATD was chosen as the appropriate human surrogate as it is the most biofidelic ATD available for assessing dynamic loads [18]. The THOR ATD is

limited as the THOR responses are not well correlated to low injury risk. New injury risk functions are therefore needed. The OP risk sets out to develop new functions by comparing the THOR ATD datasets against existing datasets from Wright Patterson Air Force Base and the National Highway Transportation Safety Administration. The data mining portion of the task, requires that each impact case be recreated to determine injury risk. Physical recreation of all impact cases is not feasible. A numerical model of the THOR ATD is being generated since physical recreation of each case is not feasible. An existing THOR FE model is being refined and validated. Additional THOR ATD testing will be conducted at two facilities and ATD response data will be collected to supplement the available THOR ATD validation data. The FE model responses will then be assessed against the physical ATD responses. Once the ATD model is validated, it will be used in the data mining portion of the study. This task contributes to OP-02 and OP-03 by developing an ATD analytical model.

4 Discussion

NASA's HRP needs to study the impact of long duration space flight on human crew members without the luxury of limitless access to the space environment. This fact requires multiple, cooperative approaches to predict when humans will be able to perform optimally and the situations that occur that tax the human capacity for optimal performance. HRP is investing resources into developing valid, predictive capabilities in the modeling and simulation domain. The current article highlights that HRP HFBP has developed models in the HAB, MPTASK, HARI, HCI and OP research areas that seek to reduce the risks to exploration class mission operations.

The computational model development aspect the Habitability risk aims to provide NASA with estimates on the spacecraft/habitat volume based on mission parameters and constraints, provide layout assumptions for a given volume, assess volumes based on a set of performance metrics, and inform risk characteristics associated with a volume. This research will establish the minimum volume required for personal space, exercise, sleep, eat, work and relaxation. Distinct areas for each activity are not going to be possible so NASA is looking to predict the minimum space required to safely conduct the mission. Two ongoing modeling and simulation task in the Habitability risk aim to establish recommendations for future vehicle design layout and minimum net habitable volume (NHV).

The computational model development aspect of the HARI risk aims to develop, and validate methods and guidelines for identifying human-automation/robot task information needs, function allocation, and team composition for future long duration, long distance space missions. One validated model- and simulation-based tool for predicting operator performance when working with a robotic arm in different function allocation situations provided NASA with the capability to augment and perform model manipulations to evaluate different function allocation strategies for future human-robotic systems. This one effort is a necessary step and it is anticipated that future efforts build on the lessons learned by the MIDAS-FAST research team for future function allocation (and HARI) related research tasks.

The computational model development aspect of the HCI risk aims to mitigate the performance decrements and operational conditions of long duration space operations. HCI approaches often require optimization of interface designs so that human performance is maximized. HCI and interface designs rely on the human's ability to receive and encode the information that is presented. In order for this encoding to occur, the human needs to be aware of the information and to attend to the information. As the human's autonomy increases, attention allocation takes on an increasingly important role for critical information intake. The outcome of this research has provided insights into human performance capability in the face of spatial disorientation in microgravity. The attention allocation model that was developed in response to this HCI risk serves as the backbone to many HPMs in use across the field of modeling and simulation.

The computational model development aspect of MPTASK risk aims to reduce the risk to mission performance that are the result of inefficiencies caused by the task, schedule, or procedure design. Two modeling and simulation efforts have been recently completed that address aspects of this very large risk area. The S-PRINT task provided model-based human performance predictions on the effects of automation design factors and failure types on automation bias, and the impact of complacency and multitasking in operator "overload" conditions. This effort produced a general model capability that can be modified with different automation types to examine the impact of context and situation demands on operator performance with the main focus on transitions between overloaded and under-loaded individuals. The interest in this effort was to implement a fatigue model into a human performance model for use by mission schedulers. The scenario that exercised the automation designs was a robotic arm control while dealing with an environmental control and life support system fault. The second MPTASK modeling effort was of a piloted lunar landing task. This effort completed a critical analysis of human operator-automation interactions and task allocations for lunar landing operations (information requirements, decision making, and the selection of action), and developed and validated a closed-loop pilot-vehicle model, integrating vehicle dynamics and HPMs.

The computational model development aspect of the OP risk aims to reduce the risks associated with dynamic loads. One modeling and simulation effort is underway for the OP risk. The OP computation model development is a practical example that illustrates how existing validated datasets can be leveraged to support modeling and simulation approaches to improve algorithms for predicting human performance.

As illustrated in the present article, many distinct modeling and simulation efforts are being completed by NASA's HRP. The investments that have been made in modeling and simulation have already and will continue to provide NASA with a number of validated capabilities. Possessing such capabilities may allow NASA to consider integrating the models together (where feasible) to generate integrated human-system model performance predictions.

5 Conclusions

Extreme and hostile environments require the human to perform optimally in order to successfully accomplish mission goals. Sub-optimal performance in the US DoD and NASA missions has the potential to increase the risks of unsuccessful mission operations. It is only with a comprehensive research program that includes both the empirical research efforts complemented with a modeling and simulation research path that the designs of the habitability, human computer interaction, human automation integration, task and occupant protection will successfully enable the human to perform in extreme environments, such as the one that will be faced in the travel to Mars.

Acknowledgments. This research was funded by the NASA HRP's Space Human Factors and Habitability Element in 2016 and by HFBP in 2017. The author would like to express sincere appreciation to NASA Johnson Space Center, Ames Research Center, and to all reviewers for their input on this document.

References

1. Human Research Program (HRP): Human Research Integrated Research Program Plan. HRP-47052 Revision F, PCN-1. National Aeronautics and Space Administration Johnson Space Center, Houston, Texas (2013)
2. National Aeronautics and Space Administration: Handbook Human Integration Design Handbook (HIDH) NASA/SP-2010-3407, National Aeronautics and Space Administration Washington, DC 20546-0001 (2010)
3. National Aeronautics and Space Administration: Space Flight Human-System Standards, Volume 1 Crew Health and Volume 2 Human Factors, Habitability and Environmental Health. NASA-STD- 3001, vol. 1 and vol. 2, National Aeronautics and Space Administration Washington, DC 20546-0001 (2015)
4. National Aeronautics and Space Administration: Human Research Integrated Research Program Plan. HHPD-HRPCB-15-019. National Aeronautics and Space Administration Johnson Space Center, Houston, Texas (2015)
5. National Aeronautics and Space Administration:: Human Research Roadmap (HRR). National Aeronautics and Space Administration Johnson Space Center, Houston, Texas (2016). https://humanresearchroadmap.nasa.gov/architecture
6. Thaxton, S.: Computational Model for Spacecraft/Habitat Volume. National Aeronautics and Space Administration Johnson Space Center, Houston, Texas (2015). https://taskbook.nasaprs.com/Publication/index.cfm?action=public_query_taskbook_content&TASKID=10193
7. Vos, G.: A tool for the automated collection of space utilization data. National Aeronautics and Space Administration Johnson Space Center, Houston, Texas (2015). https://taskbook.nasaprs.com/Publication/index.cfm?action=public_query_taskbook_content&TASKID=10133
8. Duda, K.R.: Human-automation interactions and performance analysis of lunar lander supervisory control. NASA Taskbook (2013). https://taskbook.nasaprs.com/Publication/index.cfm?action=public_query_taskbook_content&TASKID=9443
9. Gore, B.F.: Man-machine design and analysis system (MIDAS) v5: augmentation, motivations, and directions for aeronautics applications. In: Cacciabu, P.C., Hjalmdahl, M., Luedtke, A., Riccioli, C. (eds.) The Human Modeling in Assisted Transportation 2011, pp. 43–55. Springer, Heidelberg (2011)

10. Wickens, C.D., Sebok, A., Li, H., Sarter, N., Gacy, A.M.: Using modeling and simulation to predict operator performance and automation-induced complacency with robotic automation: a case study and empirical validation. In: Human Factors, vol. 57, no. 6, pp. 959–975 (2015)
11. Gore, B.F., Ahumada, A., Macramalla, S., Oyung, R.: Workload considerations in long duration space operations: a system perspective. HRP Final Report: Workload Tools and Guidelines, Washington, DC: National Aeronautics and Space Administration (2011)
12. Todd, B.K., Fischer, J., Falgout, J., Schweers, J.: Basic Operational Robotics Instructional System (BORIS). NASA Tech Briefs, January 2013; 37; MSC-24850-1 (2013)
13. Gacy, A.M., Wickens, C.D., Sebok, A., Gore, B.F., Hooey, B.L.: Modeling operator performance and cognition in robotic missions. In: Human Factors, vol. 55, no. 1, pp. 861–865 (2011)
14. Marquez, J., Feary, M., Rochlis, J., Bilman, D.: Evidence Report: Risk of Inadequate Design of Human and Automation/Robotic Integration. Human Research Program Space Human Factors and Habitability Element, National Aeronautics and Space Administration Lyndon B. Johnson Space Center, Houston, Texas (2013)
15. Small, R.: Modeling and Mitigating Spatial Disorientation in Low g Environments. NASA Taskbook (2013). https://taskbook.nasaprs.com/Publication/index.cfm?action=public_query_taskbook_content&TASKID=8569
16. Sebok, A.: S-PRINT: Development and Validation of a Tool to Predict, Evaluate, and Mitigate Excessive Workload Effects. NASA Taskbook (2015). https://taskbooknasaprs.com/Publication/index.cfm?action=public_query_taskbook_content&TASKID=10077
17. Whitmire, A.: Evidence Report: Risk of Performance Decrements and Adverse Health Outcomes Resulting from Sleep Loss, Circadian Desynchronization, and Work Overload. Human Research Program, Behavioral Health and Performance Element, National Aeronautics and Space Administration Lyndon B. Johnson Space Center, Houston, Texas (2016)
18. Somers, J., Gernhart, M.: ATD (Anthropomorphic Test Dummy) Injury Metric Development. NASA Taskbook (2016). https://taskbook.nasaprs.com/publication/index.cfm?action=public_query_taskbook_content&TASKID=9877&CFID=231648&CFTOKEN=d3b63ed3a2b28a7d-50A024BA-5056-AA3C-0AA6CD1395A4DACF

When Less is More: Studying the Role of Functional Fidelity in a Low Fidelity Mixed-Reality Tank Simulator

Catherine Neubauer[1(✉)], Peter Khooshabeh[1], and Julia Campbell[2]

[1] US Army Research Lab, Adelphi, USA
catherine.neubauer@gmail.com,
peter.khooshabehadeh2.civ@mail.mil
[2] USC Institute for Creative Technologies, Los Angeles, USA

Abstract. High fidelity military simulators have been a vital part of training and developing warfighters over the last eighty plus years. As military simulator technologies have evolved, continued emphasis tends toward high fidelity as a means to create the most extreme environments that offer novices opportunities to employ a broad spectrum of cognitive and physical skills. However, young and inexperienced trainees may lack the ability to make quick, mature and effective decisions within high fidelity simulators. High fidelity simulators have also proven cumbersome due to a number of factors, which include geographic constraints, limited resource allocation and costly update requirements. This paper explores extreme environment modeling and simulation methods for developing and measuring the effectiveness of low fidelity mixed reality solutions. We also discuss preliminary results from our current project entitled TALK-ON.

Keywords: Tank simulation · Knowledge transfer · Fidelity

1 Introduction

High fidelity military simulators introduce trainees to extreme environments allowing multiple opportunities to practice decision making, effective communication and systems operations that may not otherwise be possible or practical. These simulators can replicate tasks relating to coordinating battle tank maneuvers (e.g., Call for Fire Trainer) [1], calling for fire in an urban environment (e.g., Joint Fires and Effects Trainer System) [1], putting out a fire on a battleship (e.g., Battle Stations 21) [2], conducting dismounted patrols (e.g., Future Immersive Training Environment; FITE) or landing a fighter jet on an aircraft carrier (e.g. Tactical Operational Flight Trainer). High fidelity simulators are able to impose realistic environmental task demands and stressors at the fraction of the cost of live training exercises and are significantly less dangerous [3]. The United States Army is interested in how this technology can elicit human behaviors, emotions and responses within extreme environments in order to accurately assess training effectiveness and transfer of learning [4]. Because high fidelity simulators are designed to replicate real-world tasks as closely as possible, it is a common assumption that using

D.N. Cassenti (ed.), *Advances in Human Factors in Simulation and Modeling*,
Advances in Intelligent Systems and Computing 591, DOI 10.1007/978-3-319-60591-3_20

simulators will expedite transfer of general knowledge and skills required for successful performance in real-world extreme environment settings [5].

The very nature of high fidelity design components, however, may be more detrimental than beneficial to novice trainees. For example, adding 'contextually-relevant stress' (e.g., time pressure, noise and exposure to distressing situations) to training paradigms is desirable so that novices can practice in conditions that are likely to be similar to real-world settings [6, 7]. In performance based research, stress typically drains attentional resources, which are needed for higher order, cognitive tasks and can also impact how we apply effort [8]. These effects are typically found in any performance based environment but are exacerbated when humans are placed in extreme environments and are still novice trainees.

Because of their general lack of previous exposure to other high-fidelity simulators, some would argue that novices require a training environment with high physical fidelity (i.e., high visual, vestibular and kinesthetic realism) [9]. Although potentially useful for skill acquisition if afforded enough repetitions, this is a very costly practice that does not necessarily add to the overall training effectiveness [10]. Consequently, because of the need for optimal performance in such environments, the training environment must foster an easy transition from simulated to real-life performance. For tasks that require higher order cognitive skills related to analytical thinking and decision making, it is paramount to train novices using a scaffolded learning approach, e.g., crawl, walk, run [11], to reach the highest skill level possible when they are exposed to simulators, and eventually, encounter real-life situations.

Therefore, it is our recommendation that simulator fidelity should be measured as a multidimensional construct that consists of physical and functional components, all of which may produce differential effects on trainee behavior and performance. Given the need for newer, more cost effective and mobile training methodologies within extreme environments, the following paper will present work on a current study that has utilized a low fidelity mixed-reality simulator (i.e., an environment which includes both physical and virtual objects) to train individuals on specific domains relating to team cohesion and leadership development. Additionally, we will provide further support to those authors who have argued for the use of low fidelity training environments as long as there is a high replicability between task demands and stressors in both the training and real-life domains.

2 Fidelity Within Simulated Environments

While high fidelity simulators have long been the standard methodology for training novice warfighters, the military is exploring the feasibility of incorporating low fidelity virtual reality or computer-based training simulations (aka "lightweight simulations") [6]. These low fidelity simulations are computer generated, 3D, digital environments, which provide a number of opportunities to model, assess and train specific cognitive aspects of decision making [12]. Additionally, these virtual environments allow the user to interact with them in a seemingly real way with the use of specifically designed

hardware (i.e., head mounted display, sensor capable gloves etc.), typically referred to as 'mixed reality'. Although not as realistic as a physical simulator, these systems are still useful as they are designed to enhance training effectiveness on a specific set of mission skills.

Past research has suggested that a number of factors relate to training and knowledge transfer in simulated environments, which include appropriate levels of fidelity, individual immersion (i.e., how engrossed an individual feels within a particular environment or experience) and trainee presence [6]. These technologies have the ability to mimic visual and auditory stimuli and physical controls of the real environment, which are essential for eliciting behavioral and psychological responses from the human trainee [13]. The degree to which simulators mimic the actual equipment being used is referred to as fidelity [14]. Fidelity in its most basic sense refers to how much the simulation mimics the real world. This construct has been of particular interest to instructional system design specialists and has been subcategorized to include issues relating to *functional*, *physical* and *psychological fidelity* [15]. The term 'functional fidelity' in this case typically refers to the extent to which a simulation successfully reproduces observable human behavior characteristics [15]. For example, a simulation can be said to be high in functional fidelity if it elicits a state of anxiety for users who are anxiety prone in real-life see [11]. Conversely, physical fidelity refers to the physical similarities between a simulated and real environment (i.e., visual, auditory, haptic similarities) [17]; however, the definition of this term has been expanded to include the extent to which a simulated environment can elicit individual differences in cognition and emotional response, (i.e., psychological fidelity) [16], [6]. Although multifaceted, the term fidelity is not mutually exclusive; it is possible that a system can be somewhat low in physical fidelity while still possessing a high level of functional fidelity.

A set of commonalities does exist within many simulated training environments, but these systems vary in their level of fidelity due to a number of factors such as financial, practical and technical feasibility. Sophisticated and expensive simulators can easily recreate the physical environment; however, precise methodology and design is still necessary to implement specific tasks of interest [6]. Generally, it has been assumed that higher levels of physical fidelity relate to better training effectiveness; however, this is not always cost effective [15]. Currently, the acceptable standard for simulation design and implementation is that designers engage in a type of "selective fidelity", which refers to implementing as many of the physical and functional requirements that are deemed necessary and practical [18]. This decision should be dictated by front-end analysis and cognitive task analysis [15]. One of the most prominent examples of the use of selective fidelity is the Advanced Research Projects Agency's (ARPA) simulator network (SIMNET) [19]. SIMNET was designed to implement a network of simulators to train tactical commanders in armored unit deployment; however, only the displays and controls that were deemed necessary and vital to mission effectiveness were implemented, an approach that was referred to as the "60% solution" (i.e., about 60% of the physical fidelity was presented to trainees) [18]. As a result, SIMNET designers were able to develop dozens of SIMNET devices that yielded lower physical and functional fidelity but also allowed for entire battalions to train together. Here, research found that training effectiveness was still relatively high for cognitive tasks (e.g., tactical training) even when the simulation exhibited low

levels of fidelity, such as wallpaper of some of the unused tank knobs and switches [18]. Although the 60% solution was found to be effective for SIMNET, at present the standard for the minimal level of fidelity required in other training simulators is still somewhat variable and not based on any sound principle. It is important to note as well that SIMNET was the precursor to the Close Combat Tactical Trainer (CCTT), a high fidelity battlefield maneuver simulator currently deployed across the Army.

3 Simulation Modeling in Extreme Environments

In order to be effective, teams must be able to adapt to extreme environments, which are dynamic in nature and contain a mixture of known and unknown features that are predominant within military domains. Anticipated task demands can be dealt with via standard operating procedures; however, the ability to anticipate and overcome unknown stressors is more complicated and requires good team cohesion and also high individual and team resilience. Resilience in this context refers to an individual's or team's ability to overcome, learn and eventually grow despite challenging or stressful situations [20]. Due to the lack of simulation modeling standardization, a number of studies have tried to determine the appropriate level of fidelity that is needed in order to maximize training effectiveness when trainees are placed in stressful environments [21].

Generally, previous studies have shown that simulations that are relative low to moderate in their level of fidelity are comparable to high fidelity simulators in that they have the ability to elicit and assess desired learning and performance outcomes. For example, a 1986 study [15] found that individuals who were trained in environments with high functional fidelity but low physical fidelity had more correct solutions and faster response times in a decision making task, compared to persons who trained in high physical but lower functional fidelity conditions. This suggests that task similarity is more important to performance than physical similarity of a system. Similarly, [22] found that a simulator with low physical fidelity was just as good as a simulator with high physical fidelity at accurately assessing changing task demands and team coordination in an aircrew team task [22]. Within the military domain, the Royal Norwegian Naval Academy (RNoNA) has been tasked with comparing the fidelity of two simulated environments, one with a relatively high level of physical fidelity (e.g., the *Aden* simulation) and one with a relatively low level of physical fidelity (e.g., the *Carey* simulation). These two simulations were measured against the training effectiveness of a real life, high demand, live action military task (e.g., the *Dolphin* task) which included the use of small speed boats in a physically demanding environment in order to measure team resilience following a stressful scenario [21]. In the *Carey* simulation trainees had limited technological availability given that the task was based on a scenario set in the 1940's, while the *Aden* simulation was a modern, realistic anti-piracy task and presented trainees with only moderate stressors (e.g., political ambiguity, boredom and mental workload). Results of this study found that the *Carey* training exercise was much better at predicting team resilience in the live training exercise compared to the high fidelity *Aden* simulation. The authors suggest that the task demand was better matched between the *Carey* and live action *Dolphin* exercise, which may have led to better outcomes for the low-fidelity simulator. Here, the *Carey* simulation elicited actual stress and required

a higher level of resilience than the *Aden* simulation (e.g., uncertainty, danger, information ambiguity), which may have increased the functional fidelity of the system.

Previous work in our own lab has also supported the use of a low fidelity simulated training exercise designed to assess team cohesion and resilience to stress [20]. In this context, teammate interaction was an important factor relating to distress and as such we utilized a dyadic team scenario. A manipulation of teammate familiarity (i.e., getting to know a teammate prior to completing the task) was induced to identify whether knowledge and intimacy of a teammate relates to resilience to stress. Teams were responsible for working together to successfully disarm a simulated bomb [23]. This was a PC-based, low fidelity task but it was successful at eliciting high-workload task demands that required successful cooperation and communication among members. In general, we found that team members who were given the opportunity to get to know their team mate prior to the task exhibited more positive facial expressions and engaged in word use related to problem solving and cognitive processing, compared to those who were not given the opportunity to meet prior to the task. Perhaps most importantly, participants also reported an increase in subjective stress from pre to post-task, which confirms our argument that a low fidelity simulation is capable of eliciting desired emotional responses of interest; in this case our goal was to reproduce a stressful environment.

4 Current Trends: Low Fidelity Mixed-Reality Simulations for Training Leadership Development

In the current study, our main goal involved replicating the existing physical tank simulations used in Close Combat Tactical Trainer (CCTT) environments to focus on training platoon leaders within a mixed virtual reality scenario. CCTT utilizes virtual battlefield scenarios in order to train novice tank commanders (TC's) on specific collective training outcomes such as team communication and critical thinking. Furthermore, it has been confirmed that CCTT is effective at simulating tasks that are critical for training entire units. Such tasks include effective communication, maneuverability and navigation capabilities and perhaps most importantly team cohesion and leadership development; however, research has noted that there is room for improvement to support novice training and individual leadership development [24]. Current trends in this domain focus on specifying which stimuli in virtual environments elicit specific types of trainee responses. In order to identify which stimuli are necessary some studies have tasked analysts with talking to experts and journeymen in order to gain subject matter expertise and opinions on what was required to perform specific tasks [18]. Based on past results and several of our own field studies, high physical fidelity of the CCTT might not be cost-effective for training novice tank commanders. Therefore, the reliance on analytical rather than experimental data has provided further support for utilizing the 'selective fidelity' approach and will be reported in the following section.

4.1 Design and Procedure

Traditionally, tank commander training was executed using physical simulators including the Abrams M1A2 tank; however as previously mentioned this is somewhat expensive and is not readily available in other physical locations. Therefore, we have proposed the use of the TALK-ON (Team Assessment and Learner Knowledge Observational Network) system, which is a mixed reality prototype tank simulator (e.g., a virtual reality simulation of an Abrams M1A2 tank) that focuses on assessing and training cognitive and communication skills to a TC in training. Our mixed reality simulator utilizes both virtual reality and physical components of the task including a joystick and radio communication box. Additionally, a head-mounted display (HMD) (i.e., Oculus Rift DK2 HMD) was used which is capable of simulating the visual and auditory scenarios involving specific TC roles as shown in Fig. 1.

Fig. 1. (Left) A Subject Matter Expert (SME) playing the role of the TC in the TALK-ON simulator. (Right) A civilian serves as the controller and executes the commands of the TC through radio communication.

Within our system, the TC is tasked with a number of vital responsibilities including being the tank commander within their own tank and also the director of three other tanks within the platoon. Additionally, users were also provided with some of the physical equipment relating to the task including a radio communication switch and joystick that mimics the commander's actual handle (e.g., a Logitech extreme 3D Pro joystick). These pieces of equipment are designed to replicate the physical CCTT training scenario. This allows the user to interact with some aspects of the physical equipment that are responsible for platoon communication and controlling the turret, gun position and independent scanning of the camera respectively. It is our hope that this implementation will enhance the overall training effectiveness of the physical maneuverability of the system. The following sections will report the results from our initial usability evaluation.

4.2 Results and Discussion

A qualitative usability evaluation of the TALK-ON system was conducted using approximately 15 subject matter experts and others at the Armor Basic Officer Leadership Course (ABOLC). Users included Second Lieutenant trainees, Senior non-commissioned officers (NCO's), contractors and Captains. We had users complete a mission involving tank platoon maneuvering of multiple checkpoints using the TALK-ON system. We will present the three most prominent user experience and fidelity issues that were reported to us.

First, the physical equipment used in the system (i.e., the joystick handle) had incorrect mappings (i.e., the button for screen movement was inverted and didn't support maneuverability on the upwards or downwards plane). The current implementation of the joystick may result in negative transfer of learning and interfere with how the TC's learn to maneuver and control the turret and tactical map. Second, auditory feedback should be provided to users in the form of a mechanical noise as the turret moves back and forth and lastly the loader, who is represented as a virtual human should yell "up" after loading a round of ammunition. The last recommendation is particularly important as this vocal command is what signals that it is ok for the TC to issue a 'fire' command in order to avoid potentially dangerous chamber reverb. Additionally, users also provided a number of feature requests such as increasing the resolution of the HMD, which is typically capable of zooming in at 3, 6, 13, 25 and 50× resolution in the CCTT paradigm. Although the implementation of this zoomability feature will require more time and effort, it has been deemed a 'necessary' task feature that may impact the training effectiveness of tank and platoon checkpoint maneuverability.

Despite recommendations to system improvements, overall, our usability evaluation results suggest that the relatively low fidelity of the TALK-ON system does indeed support basic and fundamental tasks associated with novice TC training and development as well as providing features that are not supported in the CCTT simulation (e.g., being able to pop out of the hatch in order to survey the existing terrain). Additionally, the TALK-ON task requires users to engage in effective communication which is important for relaying important information about the current status of the team. Perhaps more importantly, it is critical that novice users engage in effective communication in order to avoid communicating extraneous, task-irrelevant information (i.e., use of highly emotional words when stressed). As such, the TALK-ON task may lead to further identification of peripheral behaviors relating to leadership development. These include allocating specific task roles to various team members and ensuring that all team members remain aligned with overall team goals. Future iterations of the TALK-ON system will focus on improving the functional fidelity of the system to support fundamental functions such as controlling the tank turret and overriding the gunner's line of sight; these are key tasks that novice Second Lieutenants will practice. Finally, we also hope to improve upon our system to support multiple users in order to simulate the interaction between three independent tank platoon leaders.

5 Conclusions, Recommendations and Implications for Training

Given the high resource constraint, there is a critical need to establish effective and easily applied training regimes for novices who will eventually perform in extreme environments. Traditionally, the military relied on simulators that exhibited high fidelity and physical realism, which is costly and does not ensure high training effectiveness and generalizability [12]. Conversely, PC or virtual reality based simulations are easy to use, operate at a much lower cost and are easily transported to multiple locations. Even though it is not possible to completely recreate an actual combat environment, advances in these training systems have allowed researchers to expose novice trainees to a number of physical and psychological stressors that are typically seen in extreme environments.

Furthermore, scenario-based training simulators are capable of effectively adjusting the level of fidelity presented to trainees in order to identify and assess behaviors of interest within military teams [6]. Although promising, these virtual environments must be able to replicate the task demands and stressors that are placed on the human trainee to be deemed effective. In other words, simulated exercises are relatively good at eliciting, reproducing and training desired behaviors of interest but the design of these exercises must be well thought out in advance. For example, our current work emphasizes the need for effective communication, training and assessment [25], therefore our scenarios and task should utilize high fidelity communication modalities across team members. Additionally, our work and the work of the previously mentioned authors supports the argument that simulation design is best when designers focus on and reproduce only the most necessary and appropriate details of the simulation [21]. Here, designers should conduct a front end analysis and identify specific task components that are necessary for training effectiveness and prioritize simulator capabilities that can increase realism for those factors. One overall goal of instructional design system specialists should be to implement desired learning outcomes in the most cost effective way. The overall findings seem to suggest that simulated environments can be effective training paradigms as long as there is a match between the stressors and task demands within the live and virtual environment [26].

Additionally, several practical suggestions regarding simulator fidelity from Hamstra and colleagues [27] are applicable within this domain. First, it may be useful to conceptualize the term fidelity as a multidimensional construct that goes beyond traditional definitions to include more direct principles relating to effective training and transfer. It has been well established that there is a relationship between fidelity and transfer of learning however, it appears that simply adding more to the system does not necessarily result in better task outcomes. Second, research and design relating to simulated environments should emphasize a shift from physical realism to those functions that coincide with specific learning objectives, due to a number of studies that have found no relationship between decreased physical resemblance and knowledge acquisition [27]. Lastly, the design of simulated systems should emphasize the development and accurate assessment of learning objectives to ensure that transfer of learning to an applied context has occurred.

In our current study, we have suggested the use of a selective fidelity approach in simulation modeling and training that captures a specific, preordained skill set of interest. Additionally, our preliminary usability results have provided further support for the utility of low fidelity simulators as a means for effectively training novices in extreme environments. More specifically we suggest that even if the level of fidelity deviates from the real world it can still be effective if we are careful in designing the system to ensure that the simulation is capable of recreating tasks of interest. As these technologies evolve, instructional system design specialists and military personnel will be interested in implementing newer, more cost effective systems that are capable of eliciting desired human responses and training novices on a specific set of mission skills. Therefore, there seems to be a strong case for 'less is more' when designing and implementing simulated technologies.

Acknowledgements. We would like to acknowledge our multidisciplinary team of researchers. The research reported here is supported by the Mixed-Reality lab at the University of Southern California's Institute for Creative Technologies. Special thanks are made to our system designers Igor Choromanski, David Krum, Ryan Spicer and Edgar Evangelista for their significant contributions.

References

1. Robinson, S.M., Roque, A., Vaswani, A., Traum, D.: Evaluation of a spoken dialogue system for virtual reality call for fire training. In: Proceedings of the 25th Army Science Conference, Orlando, USA (2006)
2. Lawlor, M.: Simulation makes the virtual a reality: immersive environments take sailors to imagination's edge/signal. https://www.afcea.org/content/?q=simulation-makes-virtual-reality
3. GAO. ARMY TRAINING: Efforts to Adjust Training Requirements Should Consider the Use of Virtual Training Devices. Technical report GAO-16-636, GAO, Washington, D.C., August 2016
4. Jenkins, A.P.: Transforming unit training with the science of learning. Mil. Rev. 99–105 (2016)
5. Bossard, C., Kermarrec, G., Buche, C., Tisseau, J.: Transfer of learning in new environments: a new challenge. Virtual Real. **12**, 151–161 (2008)
6. Alexander, A.L., Brunye, T., Sidman, J., Weil, S.A.: From gaming to training: a review of studies on fidelity, immersion, presence, and buy-in and their effects on transfer in PC-based simulations and games. DARWARS Training Impact Group (2005)
7. Morris, C.S., Hancock, P.A., Shirkey, E.C.: Motivational effects of adding context relevant stress in PC based game training. Mil. Psychol. **16**, 135–147 (2004)
8. Matthews, G., Szalma, J.L., Panganiban, A.R., Neubauer, C., Warm, J.S.: Profiling task stress with the Dundee Stress State Questionnaire. In: Cavalcanti, L., Azevedo, S. (eds.) Psychology of Stress: New Research. Nova Science Publishers, Hauppauge (2012)
9. Turner, S., Turner, P., Dawson, L., Munro, A.: DISCOVERing the impact of reality. In: Proceedings of the Third International Conference on Collaborative Virtual Environments, pp. 209–210. ACM Press, New York (2000)
10. Moroney, W.F., Moroney, B.W.: Flight simulation. In: Garlond, D., Wise, J., Hopkin, V.D. (eds.) Handbook of Aviation Human Factors. Lawrence Erlbaum, Mahwah (1999)

11. Finley, D.L.: Simulation-based communications realism and platoon training in the close combat tactical trainer. Technical report, DTIC Document (1997)
12. Elliott, L.R., Dalrymple, M., Regian, W., Shiflett, S.G.: Scaling scenarios for synthetic task environments: issues related to fidelity and validity. In: Proceedings of the 45th Annual Human Factors Meeting, pp. 377–381 (2001)
13. Bonk, C.J., Dennen, V.P.: Massive multiplayer online gaming: a research framework for military training and education (Technical report 2005-1), Advanced Distributive Learning Initiative, Washington, DC (2005)
14. Hays, R.T.: Simulator fidelity: a concept paper. ARI Technical report 490. U.S. Army Research Institute for the Behavioral and Social Sciences, Alexandria, VA (1980)
15. Allen, J.A., Hays, R.T., Buffardi, L.C.: Maintenance training, simulator fidelity, and individual differences in transfer of training. Hum. Factors **28**, 497–509 (1986)
16. Matthews, G., Warm, J.S., Reinerman-Jones, L.E., Langheim, L.K., Guznov, S., Shaw, T.H., Finomore, V.S.: The functional fidelity of individual differences research: the case for context-matching. Theoret. Issues Ergon. Sci. **12**, 435–450 (2011)
17. Becker, A.B., Warm, J.S., Dember, W.N., Hancock, P.A.: Effects of jet engine noise and performance feedback on perceived workload in a monitoring task. Int. J. Aviat. Psychol. **5**, 49–62 (1995)
18. Andrews, D.H., Carroll, L.A., Bell, H.H.: The future of selective fidelity in training devices. Educ. Technol. **35**, 32–36 (1996)
19. Alluisi, E.A.: The development of technology for collective training: SIMNET, a case history. Hum. Factors **3**, 343–362 (1991)
20. Neubauer, C., Woolley, J., Khooshabeh, P., Scherer, S.: Getting to know you: a multimodal investigation of team behavior and resilience to stress. In: Proceedings of the 18th International Conference on Multimodal Interaction, Tokyo, Japan (2016)
21. Mjelde, F.V., Smith, K., Lunde, P., Espevik, R.: Military teams: a demand for resilience. Work **54**, 283–294 (2016)
22. Baker, D., Prince, C., Shrestha, L., Oser, R., Salas, E.: Aviation computer games for crew resource management training. Int. J. Aviat. Psychol. **3**, 143–156 (1993)
23. Kane, B., Fetter, B., Pestaluky, A.: Keep Talking and Nobody Explodes. [Steel Crate Games] Ottawa: Canada (2015)
24. Noble, J.L., Johnson, D.R.: Close Combat Tactical Trainer (CCTT). Cost and Training Effectiveness Analysis (CTEA) (1991)
25. Campbell, J., Lin, R., Khooshabeh, P.: Tank platoon leader training: Army Research Lab Technical report, in review
26. Dieckmann, P., Rall, M., Østergaard, D.: The role of patient simulation and incident reporting in the development and evaluation of medical devices and the training of their users. Work **33**, 135–143 (2009)
27. Hamstra, S.J., Brydges, R., Hatala, R., Zendejas, B., Cook, D.A.: Reconsidering fidelity in simulation-based training. Acad. Med. **89**, 387–392 (2014)

Advancements in Fleet Synthetic Training Systems: A Use Case of Landing Signal Officers

Alexis Neigel(✉) and Heather Priest

Naval Air Warfare Center Training Systems Division, 12211 Science Drive, Orlando, FL 32826, USA
alexis.neigel@gmail.com, heather.priest@navy.mil

Abstract. The advancements of modeling and simulation systems allow individuals to acquire knowledge, demonstrate procedural skills, and practice team tactics, which may be too dangerous or resource-intensive to perform live. In this paper, we describe how advancements in training systems have affected a special population of U.S. Naval aviators, the Landing Signal Officers (LSOs). The primary responsibilities of the LSOs include the safe and expeditious recovery of the Fleet aboard the aircraft carrier. LSOs are required to perform their job in a myriad of extreme environments and aircraft conditions. Considering that a majority of LSO training is obtained on-the-job, it is both impractical and hazardous to continue training in adverse conditions. However, due to modern advancements in Fleet synthetic training, LSOs can gain experience in these adverse conditions by utilizing a training simulator. Currently, LSOs perform approximately six-to-eight hours of training related to performance in extreme environments in the 2H111 dome simulator. Although the 2H111 simulator mirrors many aspects of the aircraft carrier in high fidelity, it is not without its limitations. We describe the current LSO training pipeline and how the Fleet benefits from virtual reality (VR), as well as augmented reality (AR) training systems.

Keywords: Human-Systems integration · Simulated training · Virtual reality

1 Introduction

The training needs of the military have largely facilitated the growth and adoption of modern warfare technology. Historically, one of the primary objectives of the military was to train Warfighters to outperform the adversary while maintaining safety and efficiency to the extent possible. To facilitate these goals, Warfighters utilized the latest advances in modeling and simulation available at the time. For example, in naval aviation, one of the first simulated flight trainers was the "Blue Box," or the Link Flight Trainer that was developed by Edwin Link in 1929. From this point forward, modern training systems have served many purposes. For example, the U.S. Army has successfully trained many infantry operations, including combat missions and advanced mission rehearsals, by capitalizing on simulator-based training [1, 2]. The U.S. Coast Guard has used virtual environments (VE) to successfully train the situational awareness (SA) of crewmembers in battle formation [3]. The U.S. Navy has developed high

D.N. Cassenti (ed.), *Advances in Human Factors in Simulation and Modeling*,
Advances in Intelligent Systems and Computing 591, DOI 10.1007/978-3-319-60591-3_21

fidelity aircraft carrier simulations, which allow submariners, pilots, and other enlisted members to train in adverse sea and weather conditions [4]. Furthermore, many modern training systems are now networked in real-time, thus enabling distributed teams to train on a virtual battlefield synchronously. It is arguable that modern training systems have significantly improved Warfighter performance, as well as the efficiency and cost effectiveness of Fleet training.

1.1 Augmented Reality and Virtual Reality

In many instances, live training is impracticable to perform, resulting in the increased development of virtual reality (VR) and augmented reality (AR) training systems. AR systems "supplement the real, physical world, with virtually-generated objects that appear to coexist in the same space as the real world" [5]. In order to ensure that AR is successful, AR training systems must combine both real and virtual objects seamlessly, run interactively, and allow the user to interact with these objects in real-time [5]. In several studies, AR has been used to successfully train both fine and gross motor skills; however, AR has received limited testing in terms of training conceptual knowledge [6, 7]. This disparity in research is likely due to the level of fidelity required to learn information. For example, general knowledge about a concept can be obtained through low fidelity simulators, such as a desktop training system.

Conversely, VR systems project a computer-generated synthetic environment onto a display, which can include desktop-based trainers, head-mounted displays (HMDs), small-scale simulators (e.g., cockpit simulators or driving simulators), or full-scale simulators (e.g., dome simulators). Thus, VR training systems enable the user to gain conceptual knowledge and practice procedural skills in scenarios that model reality, but are inherently much safer than live training. AR and VR systems help Warfighters to gain exposure to extreme environments or emergency conditions, which they could not experience otherwise. That said, there is currently contention in the literature over how much skill or knowledge can be learned via AR and VR training methods.

It is important to note that not all training systems are created equal, meaning it should not be implicitly assumed that knowledge or skills transfer equivalently across the various types of trainers. One reason for this includes system fidelity (i.e., low, medium, high) [8]. Low fidelity simulation is typically associated with desktop-based training systems because these systems do not necessarily require high quality graphics for learning purposes. Medium fidelity simulation includes large projection screens with realistic controls. High fidelity most closely approaches reality and typically includes a 360-degree view of the environment, realistic controls, and simulated motion within the trainer.

Another type of fidelity worth considering in Warfighter training is cognitive fidelity [9]. Cognitive fidelity is associated with the *perceived* realism of the training, which implies that the training system should maintain a high degree of overlap with what is experienced in reality. To instantiate cognitive fidelity, the technology should facilitate agreement between the action the user performs and the user's intended cognitive action (i.e., the thinking process experienced by the user in reality should be the same as the cognitive process experienced in AR or VR training). Furthermore,

cognitive fidelity can be impacted by many factors including presence, which encompasses factors like immersion, interaction, and engagement [9, 10]. In this same vein, researchers suggest that these factors moderate stress and workload associated with simulated training [11].

Together low, medium, high, and cognitive fidelity can impact the training and transfer of skills in complex tasks [12]. Given this, it is prudent to consider the appropriate level of fidelity when designing training systems and training objectives for the Fleet.

2 Modern Landing Signal Officer Training

One successful example of Warfighter-centric training systems stems from some of the current work at Naval Support Activity (NSA) Orlando. This research has been conducted within a group of Naval aviators, the Landing Signal Officers (LSOs). LSOs have completed at least a Bachelor's degree and obtained certification to serve as a Naval aviator through the fixed-wing training pipeline. LSOs are typically selected based on their previous exemplary performance as a pilot and have demonstrated merit with regard to the ability to understand and land in the carrier environment. Anecdotally, it has been noted that being selected to serve as a LSO is an extremely high honor for Naval aviators and indicates a high degree of skill amongst Naval aviators.

After Naval aviators are designated to serve as LSOs, they attend Initial Formal Ground Training (IFGT) at the LSO School at Naval Air Station (NAS) Oceana in Virginia Beach, Virginia, which is the only school of its kind. The purpose of IFGT is to provide classroom- and simulation-based training to ensure that LSOs receive the necessary training to acquire the skills needed to perform the "safe and expeditious recovery of aircraft" aboard the aircraft carrier [13]. During IFGT, LSOs receive two weeks of classroom-based lectures, which focus on various aspects of waving aircraft and learn more about the recovery of aircraft in adverse sea and weather conditions. Classroom lectures are supplemented by approximately six to eight hours of training with LSO Instructors in the 2H111 dome simulator. LSOs in IFGT also perform several hours of waving at field-based carrier landing practices (FCLPs). Each of these training efforts are designed to prepare the LSOs to perform the procedural and decision-making skills demanded by the position, which will be practiced and developed further aboard the ship.

In addition to obtaining procedural skills and knowledge, IFGT also serves to train the LSOs in several LSO positions under the supervision of a LSO Instructor. These positions include: (1) the Primary LSO, (2) the Backup LSO, (3) the Deck Caller, and, (4) the Air Wing LSO (i.e., CAG Paddles). Students rotate through each of these four positions several times during simulation-based recovery training at the LSO School. Rotating through each LSO position provides exposure to the different roles of the LSO and varies their skillsets for recovery on the aircraft carrier.

Importantly, each of these LSO positions requires very specific skills and responsibilities. According to the LSO NATOPS manual, the Primary LSO position requires visual estimation of the aircraft's glidescope. The Backup LSO position requires the LSO to detect changes to fuel, weights, or winds affecting the aircraft,

clarify any misinformation that may be reported by the Carrier Air Traffic Control Center (CATCC) or the pilot, and declare a waveoff within the appropriate window, if necessary. The Deck Caller is responsible for reporting the appropriate parameters of the waveoff window (i.e., 10 feet or 100 feet) to other LSOs on the platform and visually scan the environment for threats, which impede the safe recovery of the aircraft. These threats include personnel or other materials that may "foul" the landing area. The Deck Caller must immediately declare a foul deck. The CAG Paddles performs all of the above functions while maintaining complete situational awareness (SA) to the status of the deck, aircraft carrier, and pilot. An illustration of these four LSO positions is included in Fig. 1.

Fig. 1. Landing Signal Officer positions (from closest in the foreground to the furthest in the background): CAG Paddles, Backup LSO, Deck Caller, and Primary LSO. These Landing Signal Officers are recovering an F/A-18 Hornet aboard the USS Harry S. Truman (CVN 75) in the Persian Gulf [14].

Following IFGT, a majority of a LSO's training is performed on-the-job using an apprenticeship method. LSOs-in-training, or junior LSOs, must participate in at least six arrested landings every six months or perform twelve arrested landings per year [13]. To obtain day qualifications, LSOs must be involved in twelve landings, ten of which should be arrested landings. To obtain night qualifications, LSOs must be involved in eight landings, six of which should be arrested landings [13].

While on deployment, an apprenticeship model is employed and junior LSOs shadow the Primary LSO, Backup LSO, Deck Caller, and CAG Paddles on the LSO platform. On the platform, the LSOs perform some waving in relatively normal sea conditions. Thus, the training junior LSOs receive beyond this point is relatively individualized and based on the area to which the aircraft carrier deploys. For example, some LSOs may deploy to very cold weather areas, which results in gaining skills related to recovering aircraft on an icy deck. Other LSOs may experience a sandstorm, which changes the skill set and decision-making abilities of the LSO. Typically,

on-the-job training ceases for junior LSOs in extreme sea and weather conditions (i.e., "varsity conditions"). While the junior LSOs must leave the LSO platform at this time, they can continue to observe from the "peanut gallery."

Furthermore, some emergency procedures are far too dangerous or too rare to perform live, such as a barricade. A barricade (akin to a very large, reinforced tennis net) involves arresting an aircraft that has reported some sort of malfunction and it cannot otherwise land without this assistance. Some of the only training the LSOs receive on barricade procedures is performed in the 2H111 simulator during IFGT due to the decreased necessity of barricade use during deployments. This decrease is in part due to modern advancements in the cockpit (i.e., Precision Landing Mode; PLM), but more importantly due to safety concerns associated with the Fleet. Currently, barricade recoveries have generally been phased out by the Fleet due to the cost associated with the design and replacement of barricades, the extreme stress and workload placed on both the pilot and LSO team, and the availability of very senior LSOs to perform the barricade procedure.

3 Future Directions for LSO Training Systems

Although a majority of the simulated training the LSOs receive is performed in the dome simulator, it is not without its limitations. For instance, in one survey, LSOs indicated that the simulator lacks current processing software, which limits effective learning (i.e., errors within the simulator software are distracting during the learning process) [15]. However, on the other hand, anecdotal evidence has indicated that many *junior* LSOs find the simulator to be important for gaining baseline knowledge about waving and recovery prior to deployment to the aircraft carrier [16].

In the case of Landing Signal Officers, it is important that future training systems incorporate important individual differences such as experience in the field (i.e., junior vs. senior LSO) and experience with VR and AR technologies. Training based on experience will better target potential gaps in knowledge or skills that exist between junior and senior LSOs. For example, junior LSOs who have previously deployed to the aircraft carrier have typically performed some initial waving and recovery. Thus, these LSOs come to the LSO School with at least some preliminary knowledge on waving and recovery concepts. However, not all junior LSOs at the LSO School have waved on the aircraft carrier prior to attending the IFGT. This difference in skill changes the effectiveness of training. This disparity in knowledge and skills between junior LSOs is the impetus for the development of desktop-, VR-, and AR-based LSO trainers, designed specifically for the junior LSO group. These training systems ensure that the LSOs have similar skill sets when performing simulator- or field-based landings during IFGT. One method of supplementing simulator-based training for LSOs, as well as across the broader Navy, is to develop desktop- and VR-based training systems, which are more cost effective, portable, and afford individualized training and instruction. These systems could be especially useful to junior LSOs who may require more baseline training related to the waveoff window and aircraft identification in various conditions (e.g., day, night, glare, etc.) prior to completing IFGT at the LSO School. To the best of our knowledge, there are only two efforts focused on the development of AR for training and decision-making in operational

environments for the LSOs. These emergent technologies include a desktop trainer for refresher training (i.e., an overview of potentially perishable LSO skills) and a prototype of a head-mounted VR display [15]. These perishable skills can include appropriately calling a waveoff, crosschecking information at distinct points in the flight path, and performing recoveries in extreme weather conditions. A majority of recoveries are performed in normal sea states, thus LSOs are infrequently exposed to severe sea conditions, which can result in this skill perishing over time. These trainers can simulate these environments and ultimately reduce any gaps in skills or knowledge.

3.1 Current Efforts to Enhance the Training of Landing Signal Officers

One example of a use case for user-centered training technology is the training expansion pack (TEP) that is being developed by scientists and engineers at NSA Orlando [17]. This technology addresses a LSO-specified gap in skill-based training and training effectiveness. Furthermore, the LSO community indicated a desire to have portable VR and AR systems [18]. Thus, the TEP will be designed to be available as both a desktop-based trainer and an AR HMD [17].

Using these different technologies enables targeted training of procedural skills and aircraft-based knowledge. The desktop-based version of the TEP may be more beneficial for training junior LSOs on aircraft type, whereas greater fidelity, which is afforded by the AR version of the TEP, will be required for training LSOs about the waveoff window. Knowledge about aircraft type can be trained using desktop software because this type of training does not require a great deal of immersion. Calling the waveoff window or determining where an aircraft is located in the carrier flight path requires greater simulator fidelity and spatial cues from the environment, which is better enabled by an AR trainer than a desktop trainer.

4 Conclusion

To conclude, the Warfighter has historically benefited from the advancements to training simulators, but there are still many unknowns related to how AR and VR training systems affect Fleet performance over time. More specifically, this chapter discussed how AR and VR trainers are changing to meet the training needs of the LSOs and LSO School. We discussed the importance of studying different levels of training fidelity based on training goals (i.e., the acquisition of conceptual knowledge versus procedural skill). This targeted training technique will be applied in future research involving the Fleet.

Acknowledgements. This work was supported in part by the Navy Innovative Science and Engineering (NISE) program (Section 219) and sponsored by the Office of Naval Research. The views expressed herein are those of the authors and do not necessarily reflect the official position of the Department of Defense, its components, or the organizations with which the individuals are affiliated.

Appendix: Technical Terms

Term	Definition
Aircraft recovery	Procedure of landing the aircraft aboard the aircraft carrier
Arrested landings	When an aircraft engages the deck pendant, purchasing cable, and the arresting wires to absorb energy and stop the aircraft
Backup LSO	Monitor changes to aircraft fuel, weights, or winds that may affect landing; clarify any misinformation reported via CATCC; call a waveoff, if appropriate
Barricade	A large, reinforced net that involves aiding in the recovery and arrest of the aircraft in extreme emergencies
CAG paddles	Maintain complete situational awareness of the deck; perform Primary LSO, Backup LSO, and Deck Caller duties in addition to their own duties
Calling	Calling refers the vocal communication between the LSO and the pilot. For example, one type of call is "WAVEOFF," which indicates to the pilot that the deck is not clear and the pilot cannot proceed to land on the carrier. In this case, the pilot must circle back around to the carrier flight path and proceed to attempt another arrested landing
Clear the deck	Safely recover the aircraft on the landing area and avoiding damage to the deck or deck personnel during recovery
Deck caller	Report the appropriate waveoff window to the LSOs on the platform; scan the environment for events that may foul the deck; call a waveoff, if appropriate
Foul deck	A deck is fouled when an aircraft, weather, personnel, or other objects are present in the landing area
"Peanut gallery"	An area of the aircraft carrier where enlisted members can view aircraft recovery
Primary LSO	Visually estimates aircraft glidescope; confirm pilot information with CATCC; call a waveoff, if appropriate
"Top nugget"	The best performer in a group of first-tour aviators
Varsity conditions	Extreme weather and sea conditions (e.g., pitching deck, sandstorm)
Waveoff window	The point at which an aircraft can safely abort landing on the carrier
Waving	Traditionally, waving used to refer to the action of landing the aircraft on the deck via standardized gestures supplemented with flags or paddles. Today, 'waving' refers to the voice calls communicated between the pilot and LSO

References

1. Hamilton, R.M., Holmquist, J.P.: Training in virtual and augmented realities: an interview with Bruce Knerr. Ergon. Des. **13**, 18–22 (2005)
2. Kaber, D.B., Riley, J.M., Endsley, M.R., Sheik-Nainer, M., Zhang, T., Lampton, D.A.: Measuring situation awareness in virtual environment-based training. Mil. Psychol. **25**, 330–344 (2013)

3. Hammond, M.: Sea fighter analysis. Technical report, United States Coast Guard (2007)
4. Hays, R.T., Vincenzi, D.A.: Fleet assessments of a virtual reality training system. Mil. Psychol. **12**, 161–186 (2000)
5. Azuma, R., Baillot, Y., Behringer, R., Feiner, S., Julier, S., MacIntyre, B.: Recent advances in augmented reality. Technical report. Naval Research Laboratory (2001)
6. Chimienti, V., Iliano, S., Dassisti, M., Dini, G., Failli, F.: Guidelines for implementing augmented reality procedures in assisting assembly operations. In: Ratchev, S. (ed.) Precision Assembly Technologies and Systems, pp. 174–179. Springer, Berlin (2010)
7. Henderson, S., Feiner, S.: Evaluating the benefits of augmented reality for task localization in maintenance of an armored personal carrier turret. In: Proceedings of the 8th IEEE International Symposium on Mixed and Augmented Reality, pp. 135–144. IEEE Press, New York (2009)
8. Trindade, J., Fiolhais, C., Almeida, L.: Science learning in virtual environments: a descriptive study. BJET **33**, 1–18 (2002)
9. Hays, R.T., Singer, M.J.: Simulation Fidelity in Training System Design: Bridging the Gap Between Reality and Training. Springer, New York (1989)
10. Cummings, J.J., Bailenson, J.N.: How immersive is enough? A meta-analysis of the effect of immersive technology on user presence. Media Psychol. **19**, 1–38 (2015)
11. Lackey, S.J., Salcedo, J.N., Szalma, J.L., Hancock, P.A.: The stress and workload of virtual reality training: the effects of presence, immersion and flow. Ergon. **59**, 1060–1072 (2016)
12. Youngblut, C.: What a decade of experiments reveals about factors that influence the sense of presence: latest findings. Technical report. Alexandria Institute for Defense Analyses, Alexandria (2009)
13. Department of the Navy: NATOPS Landing Signal Officer Manual. Training Manual, Office of Naval Research, San Diego (2015)
14. Reyes, R.J.: Landing Signal Officers. Digital image, United States Navy, Persian Gulf. https://commons.wikimedia.org/wiki/File:US_Navy_050209-N-2984R012_Landing_Signal_Officers_(LSO)_watch_as_an_F-A-18C_Hornet_lands_on_the_flight_deck_aboard_the_Nimitz-class_aircraft_carrier_USS_Harry_S._Truman_(CVN_75)_during_aircraft_recovery_operations.jpg
15. Greunke, L., Sadagic, A.: Taking Immersive VR Leap in Training of Landing Signal Officers. In: Proceedings of the IEEE Transactions on Visualization and Computer Graphics, pp. 1482–1491. IEEE Press, New York (2016)
16. Neigel, A.R., Pagan, J., Priest, H.A.: Informal Interviews with Junior Landing Signal Officers. Personal communication, Virginia Beach (2016)
17. McNamara, C.: Flight Deck Crew Training Expansion Pack (TEP) Refresher Course. White paper, Orlando (2016)
18. Neigel, A.R., Priest, H.A.: Waving PLM. Personal communication, Virginia Beach (2016)

Transportation Modeling and Simulation

Comprehensive Assessments of the Effects of Auditory Cognitive Distractions on Driving Safety Across the Lifespan

Nazan Aksan(✉)

University of Iowa, Iowa City, IA 52242, USA
nazan-aksan@uiowa.edu

Abstract. Inexperienced younger (29), middle-aged (29), and older drivers (25) participated in a study evaluating the effects of auditory cognitive distractions on driving safety. Unlike prior research, the secondary tasks were typical of everyday behavior such as listening to a story and participating in a radio quiz. The study also examined driving performance more broadly than prior studies. Outcome measures included speed and lateral control similar to prior studies but in addition included headway maintenance, mean headway time, gap acceptance, mirror use, proper signaling, stopping behavior, intersection scanning. Performance was evaluated in a wider range of driving tasks than prior studies (e.g. included gap tasks such as lane changes, freeway merges, left turns in addition to straightaway car-following). Results showed that older drivers were affected the most by these distractions and that performance was often degraded beyond speed and lateral control to include signaling, mirror use, intersection scanning behaviors.

Keywords: Auditory cognitive distraction · Driving safety · Older driver

1 Introduction

Effect of distraction on driving is of interest to a broad range of specialists and several studies have examined effects of various distractions on driving performance in simulated driving environments [1]. Majority of these studies quantify performance decrements in a few dimensions fundamental to driving safety such as lane keeping and speed control [2–12]. Scenarios tend to be restricted to straightaway road segments with a few intersections and rarely encompass the range of driving tasks any safe driver needs to undertake and are often part of licensing exams (e.g. lane change/freeway merges, intersection with various types of signage controlling rules of right of way, etc.). These trends in study designs provide a limited characterization of the range of decrements in safety relevant behavior that can result from common distractions drivers of all ages engage in behind the wheel, e.g. primarily listening and speaking distractions. The goal of this study was to remedy this shortcoming by examining performance decrements in multiple scenarios with multiple behavioral and electronic sensor indicators that bear on safety beyond lateral and longitudinal control among three age groups: inexperienced younger adults, middle-aged adults, and older adults.

D.N. Cassenti (ed.), *Advances in Human Factors in Simulation and Modeling*,
Advances in Intelligent Systems and Computing 591, DOI 10.1007/978-3-319-60591-3_22

Research to date tends to place an emphasis on being able to inform the most dangerous kinds of distractions that could be reduced with legal statues, enforcement, public information campaigns, and whether knowledge gained from studies can inform infotainment designs. For example, questions such as whether cell phone conversations are more dangerous than in-vehicle passenger conversations to safety [4] or questions such as whether visual tasks affect safety different than cognitive distractions [8–11] are the dominant motivating questions of prior studies. Despite variation in findings across these studies and others, majority report that visual distractions can have more severe consequences on concurrent driving performance relative to tasks that do not require the driver to take their eyes off the road [7, 10]. With a few exceptions however [3], majority of these studies examine speed control as reflected in variability in speed and mean speed, and occasionally lateral control as reflected in standard deviation of lane position. This shortcoming of prior studies was remedied in this study by observing driving performance beyond speed and lateral control measures. To that end, the study included electronic vehicle measures such as headway maintenance, following distance, but also gap acceptance measures. The study also included non-vehicle based measures relevant to driving safety including mirror use, signaling, stopping behavior, smoothness of pedal use and intersection approach. Furthermore, unlike majority of prior studies, driving performance was measured in multiple driving tasks beyond car-following scenarios, such as lane changes, freeway merges, unprotected left-turns, pulling into traffic from park. Finally, performance was examined in distraction conditions that are minimally taxing cognitively: listening to a life story and giving true/false answers to common knowledge questions.

2 Method

2.1 Sample

Younger (29), middle-aged (29), and older drivers (25) passed the initial screening to be recruited into the study. Inclusionary criteria included the following: for younger drivers age between 18 to 25-years and duration of independent driving experience is between 2 to 7 years; for middle-aged drivers age between 28 to 50 years; for older drivers 65 years or older. Exclusionary criteria included the following: neurodegenerative conditions; diagnosis of ADHD, poorly managed major depressive/anxiety disorders, performance in cognitive screening tests consistent with dementia. All drivers had to have a valid driver's license. Average age in the younger driver group was 19.33 years, 37.9 years in the middle-aged, and 74.3 years in the older group.

2.2 Procedure and Design

Following initial screening, participants completed functional assessments including objective and subjective measures pertinent to attention, cognitive function, and questionnaire-based measures of risk-taking preferences/styles, not included in this report. In subsequent visits, participants completed simulated drives in a fixed base, full

cabin, 180° forward field of view, DriveSafety RS600. Each simulated drive lasted 7–8 min and presented several tasks including car-following in a straight road segment and several gap-tasks that included unprotected left turn, lane change, freeway merge, pulling into traffic from parallel park position. The participants were asked to complete this 7–8 min drive under three conditions: listening distraction, true/false answers to common knowledge questions (Q&A), and baseline/no distraction. The order of these distraction conditions was randomized and counterbalanced within each age group.

The listening distraction condition involved a narrative about a life story [x] and answering seven comprehension questions at the end of the drive; the Q&A condition involved evaluating common knowledge statements such as "Chaucer wrote the Canterbury Tales." Performance in these secondary tasks were assessed as percent correctly answered.

2.3 Measures and Data Reduction

Table 1 lists the specific set of measures extracted from each driving task. The drive files were segmented into sections that corresponded to each driving task in each of three distraction conditions prior to computing the performance measures listed in Table 1. The measures obtained from evaluations of the videos were often either ordinal or binary judgments of safety-relevant driver behaviors including mirror use,

Table 1. Driving performance measures from electronic vehicle data and video evaluations in each driving task

	Measures (abbreviation)	Driving tasks/source (E/V)
Performance:		
Speed	Mean speed	All-composite (E)
	Speed control: Std of speed	All-composite (E)
Lateral control	Std of lane position	CF, LT, LC, FW (E)
Longitudinal control	Following distance: Mean headway time	CF, LT, LC, FW (E)
	Headway keeping: Std of headway time	CF, LT, LC, FW (E)
Gap acceptance	Accepted gap size (3, 5, 6, 7, 8, 10 s)	LT, LC, FW, PU (E)
	# of rejected gaps	LT, LC, FW, PU (E)
Attention:		
	Side-view mirror use	All-composite (V)
	Rear-view mirror use	All-composite (V)
	Proper Signaling	All-composite (V)
	Intersection scanning	All-composite (V)
	Intersection approach	All-composite (V)
	Smooth pedal use	All-composite (V)
	Proper stopping point	All-composite (V)

Abbrv. Std = standard deviation; CF = Car following; LT = Left turn; LC = Lane change; FW = Freeway merge; PU = Pulling into traffic from park; E = electronic V = Video; All-Composite = all driving tasks combined

Table 2. P-values associated with the main effects of distraction condition, age, and their two-way interactions on outcome measures.

Outcomes:	Driving task	Distraction	Age	Distraction X age
Mean speed	All	ns	<.001	ns
Speed control	All	ns	.001	.080
SDLP	CF	ns	ns	ns
	LT	ns	ns	ns
	LC	ns	ns	ns
	FW	ns	ns	.056
M_HWT	CF	.094	<.001	ns
	LT	ns	ns	ns
	LC	ns	ns	ns
	FW	ns	ns	ns
SD_HWT	CF	.015	<.001	ns
	LT	.053	ns	ns
	LC	ns	<.001	ns
	FW	ns	ns	ns
Gap size	LT	ns	.085	ns
	LC	ns	ns	ns
	FW	.011	ns	.033
Rejected gaps	LT	ns	.010	ns
	LC	ns	ns	ns
	FW	.089	.100	.024
Side view mirror use	All	ns	ns	ns
Rear view mirror use	All	.001	ns	.016
Proper signaling	All	ns	.055	.037
Intersection scanning	All	<.001	<.001	ns
Intersection approach	All	ns	<.001	ns
Pedal use	All	ns	<.001	ns
Stopping point	All	.039	ns	ns

Abbrv. SDLP = Standard deviation of lane position; M_HWT = following distance mean headway time; SD_HWT = headway keeping, standard deviation of headway time; CF = Car following; LT = Left turn; LC = Lane change; FW = Freeway merge; ns = not significant; All = all driving tasks combined

signaling etc. These judgments captured qualitative aspects of driver performance relative to negotiating the tasks safely. The coders were trained on sample videos and had to achieve a minimum Kappa of .71 prior to being allowed to code the videos independently. The binary/ordinal measures were combined across various tasks to describe performance in the aggregate within a distraction condition, e.g. percent times the driver used proper/correct signaling in the listening distraction condition.

3 Results

Linear mixed models were used to test the effects of distraction, age group, and their interactions. The p-values associated with these effects are shown in Table 2 both for electronic vehicle and video data. Electronic vehicle data was scenario or driving task specific and included lane keeping with SDLP, following distance or mean headway time (M_HWT), headway maintenance (SD_HWT), accepted gap in seconds, and number of rejected gaps. Measures extracted from coding of video clips represent average performance across several scenarios/driving tasks. The direction of effects can be seen from panels of Figs. 1 and 2.

Panels of Fig. 1 show decrements in driving safety across the distraction conditions for each age group for select electronic vehicle data. For headway maintenance, larger scores indicate poorer performance for line graphs in the top panels from car-following (CF) and lane-change (LC) tasks. The overall effect of distraction on headway maintenance was driven largely by the poorer performance of older drivers in both tasks. In contrast, larger scores indicate safer choices for accepted gap and number of rejected gap outcomes for line graphs in the bottom panels from the freeway merge task. Again in both cases, older drivers' gap choices were affected by the distraction conditions to a larger degree than younger and middle-aged drivers consistent with the significant two-way interactions.

Panels of Fig. 2 show decrements in driving safety across the three distraction conditions for each age group using select measures extracted from evaluations of videos. Higher scores represent safer behavior for all four outcome measures. For

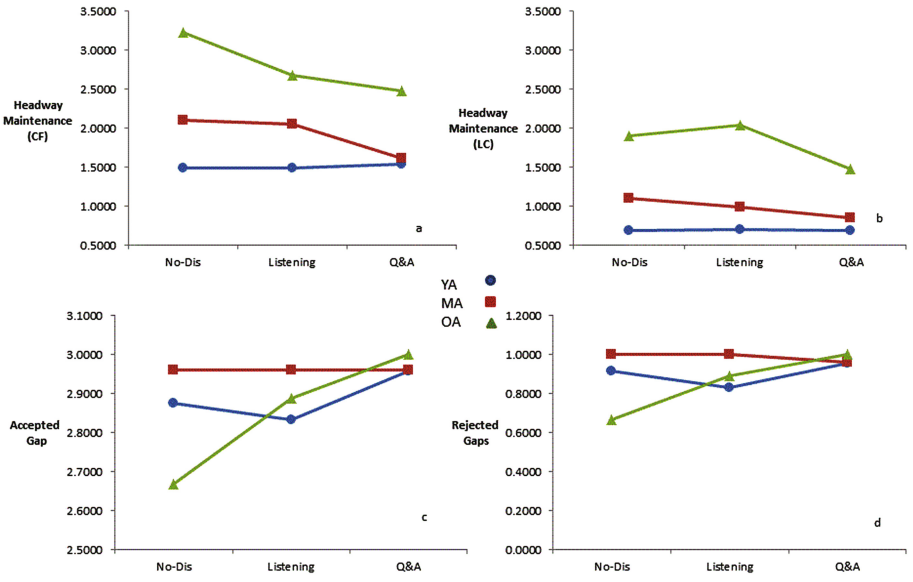

Fig. 1. Effects of distraction and age group on safety relevant behavior extracted from evaluation of videos. Panels (a) and (b) show headway maintenance in car-following (CF) and lane change (LC) respectively, (c) and (d) accepted gap and number of rejected gaps respectively in the freeway merge task. *Abbrv.* YA = Younger adult, MA = Middle-aged OA = Older adult

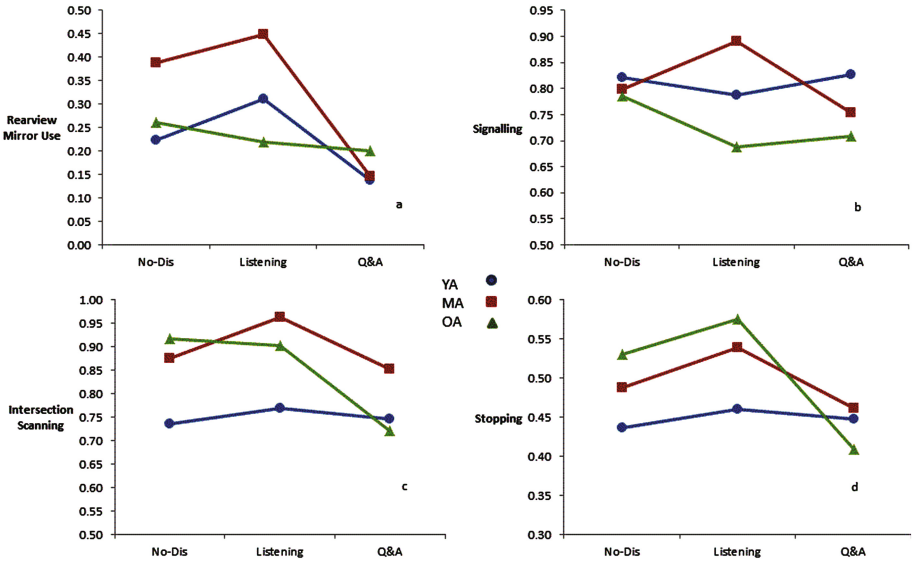

Fig. 2. Effects of distraction and age group on safety relevant behavior extracted from evaluation of videos. Panel (a) rearview mirror use, (b) signaling, (c) intersection scanning, (d) stopping behavior. *Abbrv*. YA = Younger adult, MA = Middle-aged OA = Older adult No-Dis = No Distraction condition

proper stopping point, rearview mirror use, and intersection scanning there was a significant effect of distraction such that on average all drivers performed worse in the Q&A condition. However, some of these effects were qualified by a significant interaction with age group. Effects of distraction were notable for middle-aged drivers in rearview mirror use, signaling and intersection scan. Effects of distraction were notable for older drivers in intersection scan, signaling and stopping. For both middle-aged and older drivers, performance showed an appreciable drop in the Q&A condition relative to listening distraction or both listening and baseline/no distraction conditions. Interestingly, younger driver behavior did not appear to be affected by distraction conditions. However, on all measures other than signaling their average performance was poorer than middle-aged and older drivers.

In terms of secondary task performance, there were significant effects of age, such that older drivers performed more poorly than the middle-aged and younger drivers in both story comprehension in the listening distraction condition and the percentage of correct answers in the Q&A condition, p's < .05.

4 Discussion

The findings showed that several electronic vehicle and video-based evaluations of safety relevant behaviors were affected by auditory cognitive distractions in addition to more common or typical measures of simulator performance such as lane keeping used

in prior studies. These additional measures included adjustments in risk tolerance such as accepted gap size, number of rejected gaps in freeway merge tasks. With greater distraction, all drivers but in particular older drivers waited for larger gaps before choosing to merge. Similarly, following distance and headway maintenance were affected by distractions and in particular for older drivers. Performance decrements were also evident in measures rarely evaluated in prior simulator studies of distraction such as mirror use, signaling, intersection scanning, and stopping behavior. The general pattern in these more qualitative outcomes was that older drivers were adversely affected the most by auditory cognitive distractions. And while the performance of younger drivers did not appear to be affected by distraction conditions, their performance in general was worse than both middle-aged and older drivers on more qualitative aspects of safety relevant behavior.

An important and consistent finding from this study was that auditory cognitive distractions did not lead to severe decrements in performance compared to baseline no-distraction conditions reported in prior studies that involved more demanding cognitive distractions such as working memory tasks [5, 10, 11]. While decrements were significant, those decrements were particularly evident in the Q&A condition rather than the story listening distraction condition. Furthermore, the decrements were most pronounced among older drivers followed by middle-aged drivers but were not evident among younger inexperienced drivers. Collectively those findings reinforce the notion that auditory cognitive distractions typical of everyday conversations and/or listening to quiz/knowledge radio shows are not likely to be associated with severe decrements in vehicle control. Nevertheless, the findings also reinforce the notion that even these relatively mild distractions affect older driver performance significantly. The findings also encourage future research to broaden the scope of outcome measures evaluating the effects of distractions on driving safety relevant behavior beyond lateral and speed control.

Acknowledgments. The study was funded by KPMG: The Toyota Class Action Settlement Safety Research and Education Program to University of Iowa. Sarah Hacker completed the programming of the scenarios; Amanda Farmer and Sayeh Sabbagh completed all of the assessments in the protocol.

References

1. Stutts, J.C., Hunter, W.W.: Driver inattention, driver distraction and traffic crashes. ITE J. **73**, 34–45 (2003)
2. Alm, H., Nilsson, L.: The effects of a mobile telephone task on driver behaviour in a car following situation. Accid. Anal. Prev. **27**, 707–715 (1995)
3. Brookhuis, K.A., De Vries, G., De Waard, D.: The effects of mobile telephoning on driving performance. Accid. Anal. Prev. **23**, 309–316 (1991)
4. Charlton, S.G.: Driving while conversing: cell phones that distract and passengers that react. Accid. Anal. Prev. **41**, 160–173 (2009)
5. Collet, C., Clarion, A., Morel, M., Chapon, A., Petit, C.: Physiological and behavioural changes associated to the management of secondary tasks while driving. Appl. Ergon. **40**, 1041–1046 (2009)

6. Horberry, T., Anderson, J., Regan, M.A., Triggs, T.J., Brown, J.: Driver distraction: the effects of concurrent in-vehicle tasks, road environment complexity and age on driving performance. Accid. Anal. Prev. **38**, 185–191 (2006)
7. Jamson, A.H., Merat, N.: Surrogate in-vehicle information systems and driver behaviour: effects of visual and cognitive load in simulated rural driving. Trans. Res. Part F: Traffic Psychol. Behav. **8**, 79–96 (2005)
8. Victor, T.W., Harbluk, J.L., Engström, J.A.: Sensitivity of eye-movement measures to in-vehicle task difficulty. Trans. Res. Part F: Traffic Psychol. Behav. **8**, 167–190 (2005)
9. Reimer, B., Mehler, B., Coughlin, J.F., Roy, N., Dusek, J.A.: The impact of a naturalistic hands-free cellular phone task on heart rate and simulated driving performance in two age groups. Trans. Res. Part F: Traffic Psychol. Behav. **14**, 13–25 (2011)
10. Reimer, B., Mehler, B., Wang, Y., Coughlin, J.F.: A field study on the impact of variations in short-term memory demands on drivers' visual attention and driving performance across three age groups. J. Hum. Factors Ergon Soc. **54**, 454–468 (2012)
11. Son, J., Reimer, B., Mehler, B., Pohlmeyer, A.E., Godfrey, K.M., Orszulak, J., Long, J., Kim, M.H., Lee, Y.T., Coughlin, J.F.: Age and cross-cultural comparison of drivers' cognitive workload and performance in simulated urban driving. Int. J. Automot. Technol. **11**, 533–539 (2010)
12. Son, J., Park, M.: Comparison of younger and older drivers' glance behavior and performance in a driving simulator. In: 25th ARRB Conference-Shaping the Future: Linking Policy, Research and Outcomes, Perth, Australia (2012)

Exploring the Effects of Perception Errors and Anticipation Strategies on Traffic Accidents - A Simulation Study

Hans van Lint(✉), Simeon Calvert, Wouter Schakel, Meng Wang, and Alexander Verbraeck

Transport and Planning Department,
Faculty of Civil Engineering and Gesciences, Delft University of Technology, Delft, The Netherlands
J.W.C.vanLint@tudelft.nl

Abstract. It is remarkable that drivers (on average) can safely navigate through dense traffic at high speeds—conditions in which the time headways between vehicles are in the same order of magnitude as human reaction times. One explanation for this is the ability of drivers to anticipate on the traffic conditions in their surroundings. In this paper, we study, through simulation, the effects of reaction times, errors in perception and anticipation on the probability of accidents on freeways. To this end we extend an existing model for car following and lane changing with a perception and anticipation model inspired by Ensley's three levels of situational awareness (perception, understanding and projection). By systematically varying driving behavior with different reaction times over a range of perception errors, and anticipation strategies, we compute efficiency effects (capacity and total time spent) and safety effects (the probability density of accidents happening as a function of these different contributing factors and errors). The results provide some evidence that safe driving is robust with respect to perception errors under simple anticipation strategies and small reaction times. When reaction times grow larger, more advanced anticipation strategies are needed to guarantee safe driving.

Keywords: Driving behavior · Awareness · Perception errors · Anticipation strategies · Traffic safety

1 Introduction

On a yearly basis 1.5 Million people get killed and several tens of millions get severely injured in traffic incidents worldwide [1]. Even in countries with the highest road design and regulation standards, such as The Netherlands (570 deaths and 19,000 injured in 2015 [2]), the total economic loss due to traffic unsafety is estimated at € 12.5 billion, or 2.2% of the Gross Domestic Product (GDP), which is more than four times the total delay costs of congestion [3].

In this paper, we focus on the effects of perception errors and anticipation strategies on traffic unsafety. With human reaction times in the same order of magnitude as time headways at capacity flows (between 0.5 and 2 s), *it is remarkable that drivers can*

D.N. Cassenti (ed.), *Advances in Human Factors in Simulation and Modeling*,
Advances in Intelligent Systems and Computing 591, DOI 10.1007/978-3-319-60591-3_23

safely maintain high speeds through dense traffic at all. Even more so when considering the many perception errors humans typically make, e.g. in assessing relative distances and velocities of vehicles close by. One explanation for this phenomenon is the ability of drivers to anticipate on the traffic conditions further downstream and to predict the movement of vehicles in their direct surroundings in the short-term future. This mechanism is well known in control theory and engineering: prediction has a stabilizing effect on control systems with delayed input. However, the intricate balance between reaction time and anticipation is fragile as the sobering statics at the start of this paper confirm. Moreover, whereas perception can be enhanced through technology and perception errors can be automated largely "out of the equation", automation of anticipation and prediction is a much harder problem solve, because it requires the sort of reasoning and intuition that comes natural to humans but is very difficult to capture in mathematical models.

In this paper, we study, through simulation, the effects of reaction times, errors in perception and anticipation strategies on the probability of accidents on free-ways. To this end we extend an existing "collision-free" model for car following and lane changing (the LMRS model) with a perception and anticipation model inspired by Ensley's three levels of situational awareness (perception, understanding and projection). By systematically varying driving behavior with different reaction times over a range of perception errors, anticipation strategies and errors therein, we compute capacity and several safety indicators as a function of these different contributing factors and errors (other contributors such as risk-taking or failing technology beyond the scope of this paper).

2 Overall Simulation Logic

Figure 1 delineates the driving process as modeled in our open-source traffic simulator OpenTrafficSim (OTS) [4]. The overall simulation logic in OTS is that a driver—traveling with a certain strategical plan (a route) on a road stretch—subjectively perceives a portion of the surrounding traffic state. This perception process—potentially affected by the drivers' mental state, preferences, etc—results in a reconstruction of the relevant (instantaneous) state variables and an extrapolation of these into the near future. Using this (anticipated and possibly erroneous) personal state estimate the driver now plans a short-term path (i.e. a trajectory for the next 10–30 s) and executes it in terms of car following or overtaking. Note that OTS does not constrain or impose any specific mathematical model for any of these components.

We will not use the full conceptual OTS model in this paper. First, we will impose errors on perception without an explicit (dynamic) causal model that relates for example workload or other explanatory mental constructs to these errors. Furthermore, we do not consider strategic planning or learning; we do not consider path-planning and execution as separate processes nor do we use a separate vehicle model.

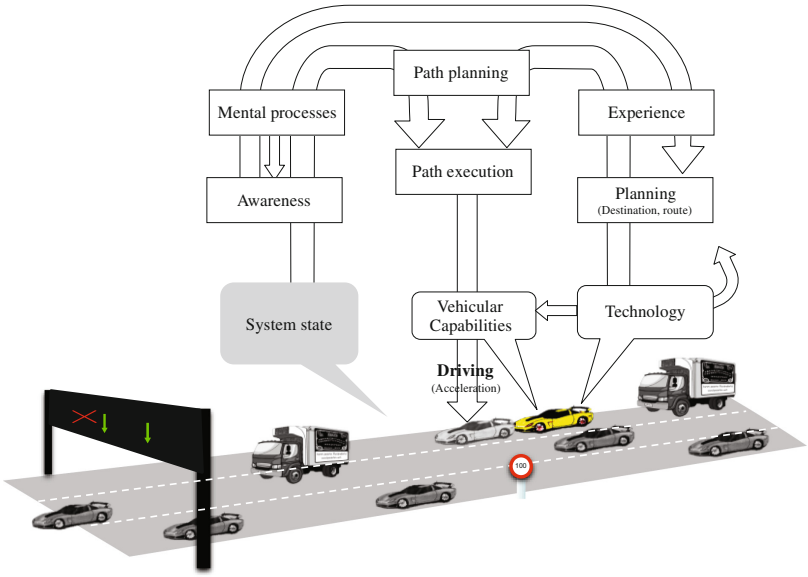

Fig. 1. Schematic delineation of the driving process as modeled in OpenTrafficSim.

3 Mathematical Model for Driving Behavior

Research into traffic flow theory dates back to the 1930s [5, 6] and matured in the 1950s [7, 8] when the first mathematical models for longitudinal driving were developed. Since then many schools of thought have emerged, each characterized by different behavioral assumptions and different ranges of descriptive and (partial) explanatory power for the resulting phenomena. For example, safe-distance models [9–11] assume that drivers maintain a large enough distance headway in case the leader brakes at maximum deceleration; optimal velocity models [12] assume that drivers accelerate to their optimal velocity as a function of the distance headway; whereas approaches in the more general group of stimulus-response models [13–15] make assumptions on how drivers adapt their speed on the basis of speed and headway and a range of additional factors. Incorporating perception and anticipation processes in traffic flow modelling is not new. Most models can straightforwardly be augmented to include reaction times; so-called psycho-spacing (or action point) models [16] incorporate drivers' inertia to observe and respond to small changes in stimuli; whereas multi-anticipatory models [17–19] include terms for anticipation of drivers to traffic conditions further downstream. A recent overview of models for longitudinal driving behavior can be found in [20]. A similar diversity of modelling approaches can be found for lateral driving behavior that governs when drivers change lanes, diverge, and merge [21–25]. What these models have in common is that they are—in principle—collision-free. This is no longer the case, however, if we allow for reaction times (i.e. delayed stimuli) and/or errors in these stimuli or both.

3.1 Lane Change Model

The model we employ is an Integrated Lane change Model with Relaxation and Synchronization (LMRS) [26]. This model offers a parsimonious and integrated approach to lane changing and reproduces several important freeway phenomena such as speed relaxation and synchronization, i.e. following vehicles in adjacent lanes. Although all these effects are captured, the lane change model has only 7 parameters. Below, we highlight the main rationale and refer to [26] for details. Most importantly, LMRS combines multiple lane change incentives into a lane change desire. The desire to change from lane i to lane j that arises from the different incentives is combined into a single desire d^{ij}, expressed as:

$$d^{ij} = d_r^{ij} + \theta_v^{ij}\left(d_s^{ij} + d_b^{ij}\right) \tag{1}$$

In Eq. (1), there is a desire to follow a route (d_r), to gain speed (d_s) and to keep right (d_b), where the subscript b stands for bias to a particular side (left or right). The latter two are included with θ_v which is the level at which voluntary (discretionary) incentives are included. Meaningful desires range between −1 and 1, where negative values indicate that a lane change is not desired (i.e. to stay or to change in the other direction). Values outside of the meaningful range may exist as incentives are added. The weight factor θ_v^{ij} is expressed as:

$$\theta_v^{ij} = \begin{cases} 0, & d_r^{ij} \cdot d_s^{ij} < 0 \; and \; \left|d_r^{ij}\right| \geq d_{coop} \\ \dfrac{d_{coop} - \left|d_r^{ij}\right|}{d_{coop} - d_{sync}}, & d_r^{ij} \cdot d_s^{ij} < 0 \; and \; d_{sync} \leq \left|d_r^{ij}\right| \leq d_{coop} \; d_r^{ij} \cdot d_s^{ij} \\ 1, & d_r^{ij} \cdot d_s^{ij} \geq 0 \; and \; \left|d_r^{ij}\right| \leq d_{sync} \end{cases} \tag{2}$$

The weight factor implies that if both voluntary and mandatory lane-change desires are either negative or positive $(d_r \cdot dv \geq 0)$, voluntary desire is fully included as it coincides with mandatory desire. However, if voluntary desire conflicts with mandatory desire $(d_r \cdot dv < 0)$, the voluntary desire is only partially included. The total desire determines the type of lane change behavior of drivers from three classes: Free Lane Changes (FLC), Synchronized Lane Changes (SLC) and Cooperative Lane Changes (CLC), identified by three thresholds of d_{free}, d_{sync}, d_{coop} as the model parameter:

$$0 < d_{free} < d_{sync} < d_{coop} < 1 \tag{3}$$

Figure 2 gives an overview of the variation of lane change behavior between processes. For little desire, no lane change will be performed. For a somewhat larger desire, FLC is performed requiring no preparation whatsoever. In SLC and CLC, a potential lane changing driver is willing to synchronize their speed with a vehicle on the target lane. This is achieved by following a vehicle in that lane. Concurrently, this will align the vehicle with a gap (if there is a gap); this is thus a simple gap-searching model. In CLC, the potential follower will additionally start to create a gap by following the potential lane changing vehicle.

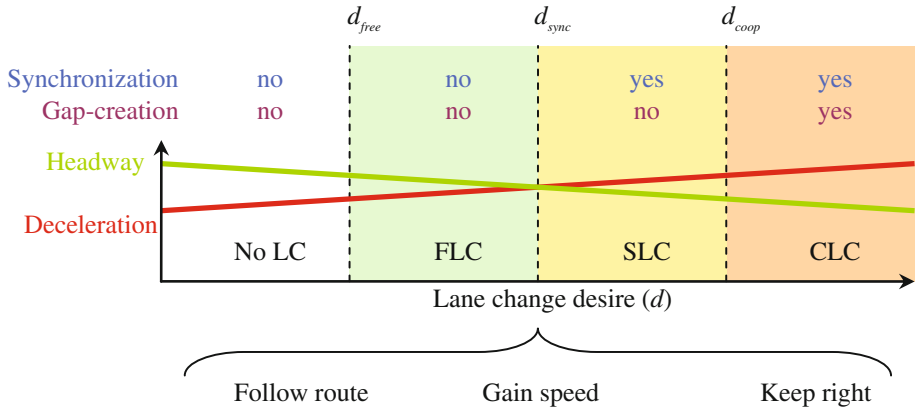

Fig. 2. Overview of LMRS. Lane change desire is based on three incentives. Lane change behavior, including the accepted headway and deceleration for a lane change, varies depending on the level of lane change desire [26].

3.2 Integration of Lane Change Model and Car Following Model

LMRS works with any car following model. Here we use a slightly adapted version of the Intelligent Driver Model (IDM) by Treiber et al. [14]. The acceleration is calculated with

$$\dot{v} = a \cdot \min\left(1 - \left(\frac{v}{v_{des}}\right)^4, 1 - \left(\frac{s^*}{s}\right)^2\right) \tag{4}$$

and

$$s^* = s_0 + v \cdot T + \frac{v \cdot \Delta v}{2\sqrt{a \cdot b}} \tag{5}$$

where s_0 is the stopping distance, Δv is the approaching rate to the leader, s is the gap (net distance headway) and s^* is the dynamic desired gap. The adapted model is referred to as IDM+ because it results in more realistic values for capacity. Integration of lane change and car following model takes place in the gap-acceptance process. In LMRS, a gap is accepted or rejected based on the resulting deceleration that follows from the car-following model. Gaps that result in deceleration that is too large, are rejected as they are unsafe, uncomfortable or impolite. The gap is accepted if both the lane changer (c) and the new follower (f) will have an acceleration that is larger than some safe deceleration threshold $-b^c$. Note that in Fig. 2, we hint that the acceptable headway changes as a function of the lane change desire. For larger lane change desires, larger decelerations and shorter headways are accepted. If the lane change is initiated, both vehicle c and f should update their desired time headway T. When vehicles accept smaller headways than their normal ones, they will gradually relax their headway towards the normal value exponentially with a relaxation time window τ.

When the lane change desire is above the synchronization threshold, drivers will start to synchronize their speed with the leader on the target lane by applying the car-following model. Drivers will apply a maximum deceleration of b, which is considered as a both comfortable and a safe deceleration rate. Finally, if an adjacent leader wishes to change lane with a desire above the cooperation threshold, a gap will be created. Gap creation is similar to synchronization and we again apply the car-following model with a limited deceleration b.

3.3 Modelling Perception Errors and Reaction Time

The original LMRS is a deterministic model without explicit time delay. It does not capture the errors and time delay in situation awareness.

Perception Error Formulation. Important variables (or stimuli) for driving decision-making are the (relative) positions, speeds and accelerations of surrounding vehicles in addition to the ego vehicle speed v. We distinguish the error formulation in these variables. We assume that the error in the ego vehicle speed v is negligeable due to direct feedback from the speedometer. For the errors of position x_s and speed v_s of surrounding vehicles, there is evidence that the error of x_s and v_s is related to distance [27], e.g. the further away the predecessor is, the more difficult to accurately estimate x_s and v_s, and thus the higher the error of s and Δv is. We model the error as a standard Wiener process $w(t)$. The errors in position s and speed v and acceleration $\dot{v}$ of a surrounding vehicle are formulated as:

$$\widehat{x_s} = x_s + \mathrm{w(t)r_s}x_s\alpha \tag{6}$$

$$\widehat{v_s} = v_s + \mathrm{w(t)r_v s}_s \tag{7}$$

$$\widehat{\dot{v}_s} = \dot{v}_s + \mathrm{w(t)r_{\dot{v}}}\,\dot{v}_s \tag{8}$$

where $\alpha = 1$ for leaders, or $\alpha = -1$ for followers. This creates persistence of over- or underestimation. The perceived speed is limited to be non-negative, i.e. $\widehat{v_s} \geq 0$. This Wiener process $w(t)$ has a probability distribution which is the same as the standard normal distribution $N(0, 1)$. However, there is auto-correlation over time. This auto-correlation is described by a value of $\tau = 20$ s. The numerical update scheme is given in equation:

$$w(t) = \begin{cases} e^{-\frac{\Delta t}{\tau}} w(t - \Delta t) + \eta\sqrt{\frac{2\Delta t}{\tau}}, P = 1 \\ \eta, P = 0 \end{cases} \tag{9}$$

where $P = 1$ means the surrounding vehicle was perceived in the previous time step, and $P = 0$ otherwise. Random value η is drawn from the standard normal distribution. Note that, although the acceleration of surrounding vehicles is not directly as the input for car following models, it will be used as the anticipation strategies in the ensuring of this section.

Reaction Time. Including time delay in the model is straightforward in this formulation. We again assume there is no time delay in perceiving the ego vehicle speed, but a fixed time delay t_r for perceiving relative positions, speeds and accelerations of surrounding vehicles:

$$\widehat{x_s}(t - t_r) = x_s(t - t_r) + \mathrm{w(t)r_s}x_s(t - t_r)\alpha \tag{10}$$

$$\widehat{v_s}(t - t_r) = v_s(t - t_r) + \mathrm{w(t)r_v s}_s(t - t_r) \tag{11}$$

$$\widehat{\dot{v}_s}(t - t_r) = \dot{v}_s(t - t_r) + \mathrm{w(t)r_{\dot{v}}}\,\dot{v}_s(t - t_r) \tag{12}$$

One of the powerful features of the OTS simulation environment is that neither reaction times nor scheduling frequency have to be expressed in multiples of the numerical time step with which the simulation is executed. Without going into detail, this results in reaction times that have a stochastic component.

3.4 Modeling Anticipation Strategies

We assume drivers can have the capability to compensate for reaction time t_r by means of one of three anticipation strategies.

- *None*: the simplest case where no anticipation is performed, behavioural stimuli are taken from $t - t_r$; Essentially this comes down to an occlusion of t_r seconds
- *Constant speed*: drivers assume other vehicles move at a constant speed, which is perceived at $t - t_r$, to estimate distance and relative speed at time t;
- *Constant acceleration*: drivers assume other vehicles move with a constant acceleration, which is perceived at $t - t_r$, to estimate distance and speed at time t.

4 Experimental Setup

4.1 Road Network and Scenarios

The experiment is carried out on a motorway corridor with a two plus two lane merge with a lane-drop after the merge (see Fig. 3). This is a very common configuration, that furthermore demands both voluntary and mandatory lane-changes and extensive vehicle interaction, while maintaining a single flow. This means that there are two potential bottlenecks, one at the merge, which heavily depends on vehicle lane changing behaviour, and a second one at the lane-drop, which is obviously more severe. The corridor is 9 km in length in total with the other distances of the various sections indicated in Fig. 3.

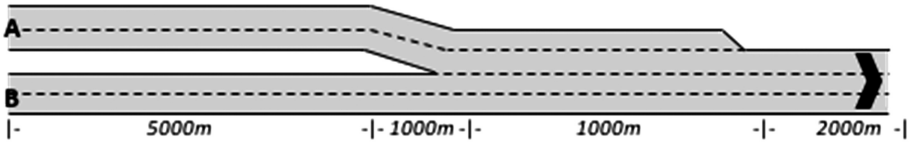

Fig. 3. Experimental network

A basic demand scenario is applied in the experiment that allows the influence of perception errors to be evaluated based on the three main traffic states: *free-flow, (near) capacity flow, and congested flow*. The demand distribution in time is shown in Fig. 4 and is given against the maximum flow on the two inflowing carriageways. The maximum flows on the two carriageways are 3500 veh/hr and 3200 veh/hr for carriageway A and B respectively. Furthermore, the distribution of generated vehicles for both carriageways over the two lanes is 55% for the left lane and 45% for the right lane, while 5% of all traffic are trucks, which are always generated on the right lane. The headways of inflowing traffic are exponentially distributed. There is a model warm-up time of 360 s with a demand set at 0.5 of the maximum flow.

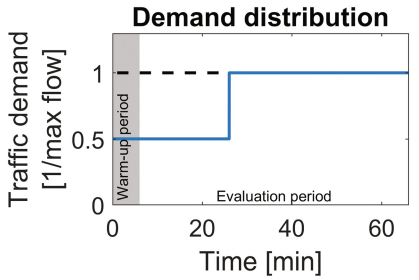

Fig. 4. Demand distributions for the basic demand scenario

For each anticipation strategy there are 36 scenarios by varying the error and reaction time. For the perception error we have r_s = {0.0, 0.02, 0.04, 0.06, 0.08, 0.1}. For the speed error we use $r_{\Delta v} = r_s/5$ = {0.0, 0.004, 0.008, 0.012, 0.016, 0.02}. Finally, for the acceleration error we use $r_{v\cdot} = r_s \cdot 2$ = {0.0, 0.04, 0.08, 0.12, 0.16, 0.2}. While varying the extent of perception errors in our experiment, we scale all error parameter simultaneously, with base parameter r_s where $r_{\Delta v} = r_s/5$ and $r_{v\cdot} = r_s \cdot 2$. For the reaction time we use t_r = {0.0 s, 0.1 s, 0.2 s, 0.3 s, 0.4 s, 0.5 s}.

Due to reaction time stochasticity as mentioned above, these reaction times are lower bounds. Reaction times vary amongst drivers and can be 0–0.5 s larger. Additional to these 36 scenarios, we use 1 'average scenario' with r_s = 0.05 and t_r = 0.25 s for more in-depth comparisons. Note that the deterministic model is given by the scenario with $r_s = t_r = 0$.

4.2 Performance Indicators

In the experiment, we aim to evaluate the effect of driver perception through reaction times and perception errors on traffic flow and safety. We consider *capacity* (max flow sustained for five minutes at the most downstream bottleneck)*; time-to-collision* (TTC) *frequency*, *extreme deceleration frequency* (EDF) and *accident frequency rate*

(AFR). The AFR indicator is defined as the total amount of kilometers driven by all vehicles in a simulation run before a collision occurs.

For each scenario 3 replications are performed. For the safety indicators, this is sufficient, since each run gives many thousands of inter-vehicle observations. We are aware that for estimating capacity, more runs are needed, which due to technical problems was not possible before publication. Note that 3 random arrival patterns of vehicles and their characteristics will result in the 3 replications, but these arrival patterns are equal for all scenarios for a given replication number. The random numbers used for perception do not affect the arrival pattern. This increases comparability of scenarios.

5 Results

5.1 Traffic Flow Performance

Figure 5 visualises capacity values for each anticipation strategy. Note, that results are only given for scenarios in which no collisions have taken place between vehicles. If in all three replications a collision took place, then no result is produced. Otherwise, the figures show the mean value of all available simulation runs. Inclusion of anticipation in driver's behavior can be seen to lead to an improvement in capacity values as well as TTS for increasing reaction times, especially above an initial reaction time value of 0.2 s. There doesn't appear to be any substantial difference between the two anticipation strategies. Given the limited number of replications these results must be taken with reservations.

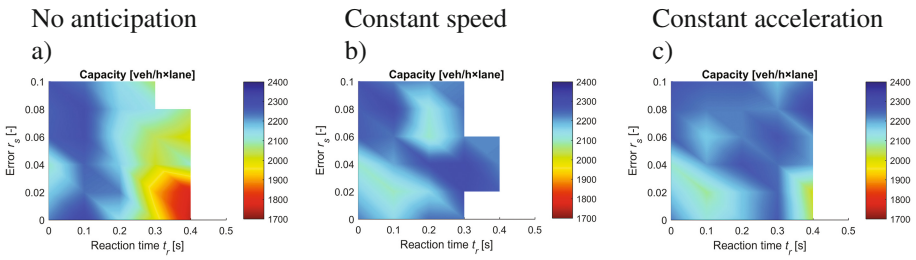

Fig. 5. Traffic flow performance (capacity) for three anticipation scenarios. Note that reaction times are lower bound values; drivers may experience up to 0.5 s additional reaction time

5.2 Traffic Safety Results

The results of the traffic safety indicators: time-to-collision (TTC) and extreme deceleration frequency (EDF) are given in Fig. 7a, b. The accident frequency rate (AFR) results are given in Fig. 8a–c.

The results of the TTC and EDF are shown as probability distributions normalized to lane-kilometers and hours. Figure 7a, shows the constant acceleration strategy performs better than the constant speed strategy, and almost as good as the deterministic model. Without anticipation there are more very small TTC values (1–2 s).

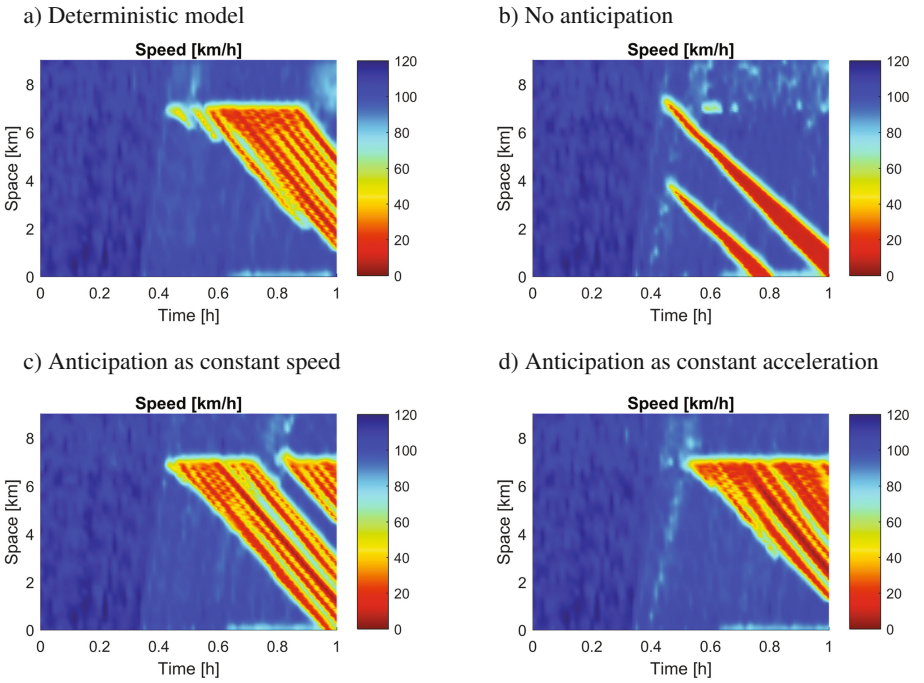

Fig. 6. Congestion patterns for different anticipation scenarios

However, higher but still critical TTC values occur much less frequent. This is not a direct result from the lack of anticipation. Rather, this is a result from the very different congestion pattern in this scenario as shown in Fig. 6b (only two very dense jam waves emerge in this case). With a reduced number of shockwaves, there are simply less fluctuations in speed. A similar performance for safety is found when the EDF is reviewed in Fig. 7b. The EDF performance for no anticipation strategy performs the worst, as may be expected. Anticipation reduces the frequency of extreme decelerations. Again constant acceleration performs close to the deterministic model, and better than the constant speed strategy.

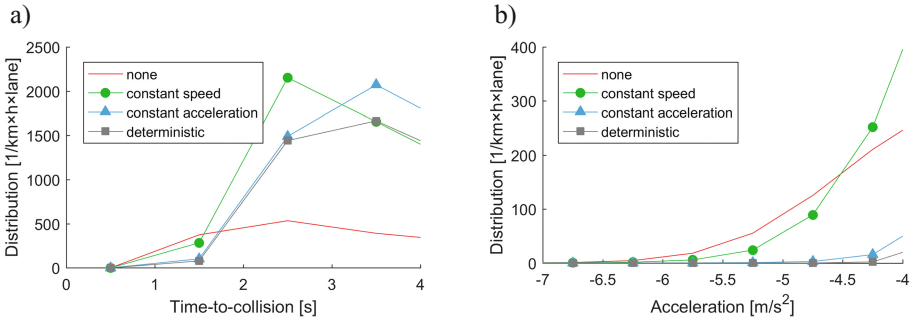

Fig. 7. a–b: Traffic safety performance indicators per anticipation strategy; TTC and EDF

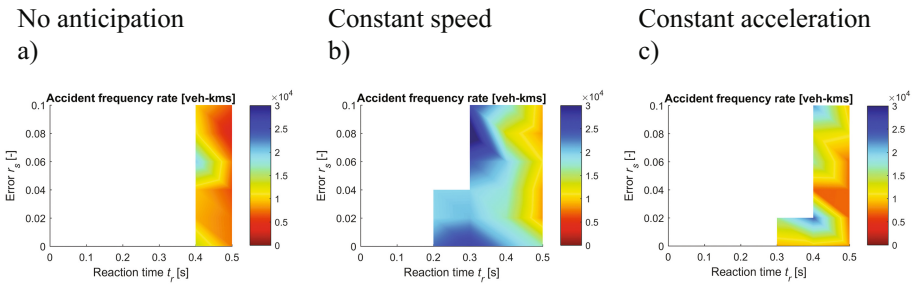

Fig. 8. a–c: Accident frequency rates for three anticipation scenarios. Note that reaction times are lower bound values; drivers may experience up to 0.5 s additional reaction time.

The accident frequency rate (AFR) results show an interesting difference between the three anticipation strategies. The accident rate is the highest (i.e. most kms per accidents) for the anticipation scenario with a constant speed, with the anticipation scenario with constant acceleration anticipation also scoring relatively high compared to no anticipation. Reaction time has a clear influence on the accident rates, with higher reaction times leading to a greater chance of accidents. Again, the perception error does not seem to have any significant influence on the probability of an accident.

6 Discussion and Synthesis

Given our assumptions about collision-free driving (the LMRS model)—the results show that safe driving is fairly robust against the entire range of perception errors we tested under simple anticipation strategies and reaction times of up to a second. Anticipation does *mostly* cancel the effects of reaction time, although more critical situations and more collision occur. The simplest strategy, constant speed anticipation performs slightly worse than constant acceleration anticipation. The latter shows results that are overall close to a deterministic model, that is driving with no perception errors and no reaction time.

There are, however, some limitations. First, we have used a limited number of replications—time restrictions prevented us from doing more. This makes inference on capacity debatable. Second, humans are not good at estimating accelerations. We have incorporated this with a large perception error, but see no significant influence of these large errors. One probable reason for this is that the anticipation time considered in this paper is relatively short—just the time needed to bridge the reaction time delay. When we consider anticipation over longer time periods we hypothesize that more advanced anticipation strategies would pay off.

Future work will focus on testing the same hypotheses in more demanding scenario's in which also scanning frequency (attention span) is taken into consideration.

Acknowledgments. This research is sponsored by the strategic research support programme of the Amsterdam Institute of Advanced Metropolitan Solutions (ams-institute.org).

References

1. Global status report on road safety 2015. World Health Organisation (WHO), Geneva
2. SWOV: Road crash costs. Fact sheet, S.W.O. Verkeersveiligheid (ed.) (2014). www.swov.nl/rapport/Factsheets/UK/FS_Costs.pdf
3. KIM: Mobiliteitsbalans 2013, Kennisinstituut voor Mobiliteitsbeleid (Knowledge Institute for Mobility), Den Haag
4. Van Lint, J.W.C., Schakel, W., Tamminga, G., Knoppers, P., Verbraeck, A.: Getting the human factor into traffic flow models – a new open-source design to simulate next-generation traffic operations. In: Transportation Research Board Annual Meeting, The National Academies, Washington D.C (2016)
5. Greenshields, B.D.: The photographic method of studying traffic behaviour. In: Proceedings of the 13th Annual Meeting of the Highway Research Board, Washington (1934)
6. Greenshields, B.D.: A study of highway capacity. In: Proceedings of the 14th Annual Meeting of the Highway Research Board, Washington, pp. 448–477 (1935)
7. Lighthill, M., Whitham, G.: On kinematic waves II: a theory of traffic flow on long crowded roads. Proc. R. Soc. **A 229**(1178), 317–345 (1955)
8. Richards, P.J.: Shock waves on the highway. Oper. Res. **4**, 42–51 (1956)
9. Pipes, L.: An operational analysis of traffic dynamics. J. Appl. Phys. **24**(3), 274–281 (1953)
10. Newell, G.F.: A simplified car-following theory: a lower order model. Trans. Res. Part B **36**(3), 195–205 (2002)
11. Laval, J., Leclercq, L.: A mechanism to describe the formation and propagation of stop-and-go waves in congested freeway traffic. Philos. Trans. R. Soc. A: Math. Phys. Eng. Sci. **368**(1928), 4519–4541 (2010)
12. Bando, M., Hasebe, K., Nakanishi, K., Nakayama, A.: Analysis of optimal velocity model with explicit delay. Phys. Rev. Lett. E **58**(5), 5429–5435 (1998)
13. Gazis, D.C., Herman, R., Rothery, R.W.: Nonlinear follow-the-leader models of traffic flow. Oper. Res. **9**(4), 545–567 (1961)
14. Treiber, M., Hennecke, A., Helbing, D.: Congested traffic states in empirical observations and microscopic simulations. Phys. Rev. E **62**(2), 1805–1824 (2000)
15. Kerner, B., Klenov, S.: Deterministic microscopic three-phase traffic flow models. J. Phys. A: Math. Gen. **39**(8), 1775 (2006)
16. Wiedemann, R.: Simulation des Strassenverkehrsflusses. Traffic Engineering, University of Karlsruhe, Kalsruhe (1974)
17. Hoogendoorn, S.P., Ossen, S., Schreuder, M.: Empirics of multianticipative car-following behavior. Trans. Res. Rec.: J. Trans. Res. Board **1965**(-1), 112–120 (2006)
18. Treiber, M., Kesting, A., Helbing, D.: Delays, inaccuracies and anticipation in microscopic traffic models. Phys. A: Stat. Mech. Appl. **360**(1), 71–88 (2006)
19. Hoogendoorn, S.P., Ossen, S., Schreuder, M.: Properties of a microscopic heterogeneous multi-anticipative traffic flow model. In: Allsop, R.E., Bell, M.G.H., Heydecker, B.G. (eds.) Transportation and Traffic Theory, pp. 584–606. Elsevier Ltd., London (2007)
20. van Wageningen-Kessels, F., van Lint, H., Vuik, K., Hoogendoorn, S.: Genealogy of traffic flow models. EURO J. Trans. Logist. **4**, 1–29 (2014)
21. Wei, H., Meyer, E., Lee, J., Feng, C.: Characterizing and modeling observed lane-changing behaviour. Trans. Res. Rec.: J. Trans. Res. Board **1710**, 104–113 (2000)
22. Cohen, S.L.: Application of relaxation procedure for lane changing in microscopic simulation models. Trans. Res. Rec.: J. Trans. Res. Board **1883**, 50–58 (2004)
23. Laval, J.A., Daganzo, C.F.: Lane-changing in traffic streams. Trans. Res. Part B **40**, 251–264 (2006)

24. Kesting, A., Treiber, M., Helbing, D.: General lane-changing model MOBIL for car-following models. Trans. Res. Rec.: J. Trans. Res. Board **1999**, 86–94 (2007)
25. Choudhury, C.F.: Modeling driving decisions with latent plans. Massachusetts Institute of Technology (2008)
26. Schakel, W., Knoop, V., van Arem, B.: Integrated lane change model with relaxation and synchronization. Trans. Res. Rec.: J. Trans. Res. Board **2316**(-1), 47–57 (2012)
27. Li, Z., Phillips, J., Durgin, F.H.: The underestimation of egocentric distance: Evidence from frontal matching tasks. Atten. Percept. Psychophys. **73**(7), 2205–2217 (2011)

Human Factors in Modelling Mixed Traffic of Traditional, Connected, and Automated Vehicles

Anshuman Sharma, Yasir Ali, Mohammad Saifuzzaman, Zuduo Zheng(✉), and Md. Mazharul Haque

School of Civil Engineering and Built Environment, Science and Engineering Faculty, Queensland University of Technology, 2 George St, Brisbane, QLD 4001, Australia
{a33.sharma, y2.ali, m.saifuzzaman, zuduo.zheng, ml.haque}@qut.edu.au

Abstract. Connected and automated vehicle technologies are widely expected to revolutionize transport systems, enhancing the mobility and quality of life while reducing the environmental impact. However, in the foreseeable future, connected and automated vehicles will have to co-exist with traditional vehicles, indicating a great research need of modelling mixed traffic flow. In few attempts of modelling mixed traffic flow recently, human factors are largely ignored, despite their critical roles in understanding traffic flow dynamics and effective operation and control of this mixed traffic flow. To properly investigate the role of human factors in mixed traffic, we have designed a series of experiments using a high-fidelity driving simulator. Complementary information is collected using questionnaires. This study can assist in developing accurate, realistic, and robust microscopic traffic flow models.

Keywords: Connected vehicles · Automated vehicles · Human factors · Advanced Driving Simulator · Microscopic traffic flow models

1 Introduction

The connected and automated vehicle technologies have great potential as the solution to massive road transport issues. Experts predict that by the year 2030, connected and/or autonomous vehicles will be mainstream, fundamentally transforming the automobile industry and how humans travel [1]. Such prediction has been supported by numerous studies and research programs [2]. Some key contributions of connected and automated vehicles will be improving traffic safety, reducing emission, enhancing mobility by alleviating traffic congestion and improving overall traffic performance [3].

Connected vehicles are capable to communicate with nearby vehicles as well as external networks. The connectivity can be Vehicle-to-Vehicle (V2V), Vehicle-to-Infrastructure (V2I), and Vehicle-to-Everything (V2X, e.g. pedestrian and electronic devices). Obviously, when driving a connected vehicle a human driver is supposed to

D.N. Cassenti (ed.), *Advances in Human Factors in Simulation and Modeling*,
Advances in Intelligent Systems and Computing 591, DOI 10.1007/978-3-319-60591-3_24

consider the information supplied through the connected system. Therefore, drivers' response to the information assistance becomes critical because it will affect the dynamics of the connected vehicles and thereby the traffic flow, as reflected in the driver assistance system (DAS) studies. Furthermore, it is reasonable to assume that there will be a transition in connected vehicle technology as well as in the penetration of connected vehicles. Also, drivers' adaptation to this new technology requires time [4]. Even a successful adaptation to this technology does not guarantee a full compliance to the system at all time. Thus, it is of utmost importance to: (a) identify the human factors that significantly influence the operation of connected vehicles, both in terms of safety and efficiency; and (b) incorporate these important human factors in developing traffic models. To date, only few researchers have attempted to incorporate these factors [5]. As such, more work is needed due to the emerging nature of the connected vehicle technologies.

Automated vehicles perform the driving tasks without any human intervention. This definition represents the fifth level of automation (level 5) as per vehicle automation classifications by the Society of Automotive Engineers (SAE) [6]. Although drivers do not need to perform the driving tasks, their role of supervisor-cum-operator is crucial [7]. Similar to connected vehicles, there will be a transition in the levels of automation and their penetration in the traffic stream. During this transition phase, depending on the level of automation, drivers need to monitor the driving environment and take over the vehicular control timely for various reasons. Previous studies reported that automation may lead to overreliance, erratic workload, skill degradation, and reduced situation awareness [8].

Meanwhile, traditional vehicles have been modelled extensively since more than 50 years ago. Specifically, microscopic traffic flow models that describe the flow at the individual vehicle level are broadly categorized as car-following models and lane changing models (refer to [9, 10] for a review on each of these models). Human factors are often disregarded in these models which has made them insufficient for explaining the complex interaction between the human driver and the traffic flow. Notably, reaction time is the only human factor that has been extensively used in the modelling.

It is clear from the above discussion that human factors will play an essential role in governing the dynamics of mixed traffic consisting of traditional, connected, and automated vehicles. Unfortunately, human factors are largely ignored both in traffic data collection and in traffic flow modelling. As a part of the on-going effort to model the mixed traffic, this paper presents a comprehensive discussion on the human factors and related issues important for data collection and modelling. In addition, this paper presents one of the first efforts in capturing the human factors for traditional and connected vehicles using driving simulator experiments.

The rest of the paper is organized as follows: Sect. 2 details the important human factors in modelling traditional, connected and automated vehicles; Sect. 3 describes a design of the experiments to incorporate the human factors in modelling mixed traffic; and Sect. 4 summarizes main conclusions and on-going research.

2 Important Human Factors in Modelling Traditional, Connected, and Automated Vehicles

2.1 Traditional Vehicles

Based on the literature, the human factors that govern the traditional vehicles dynamics in the traffic flow are depicted in the Fig. 1. Due to space limitation, the ensuing paragraphs detail only some of the important human factors and their impact on traffic flow.

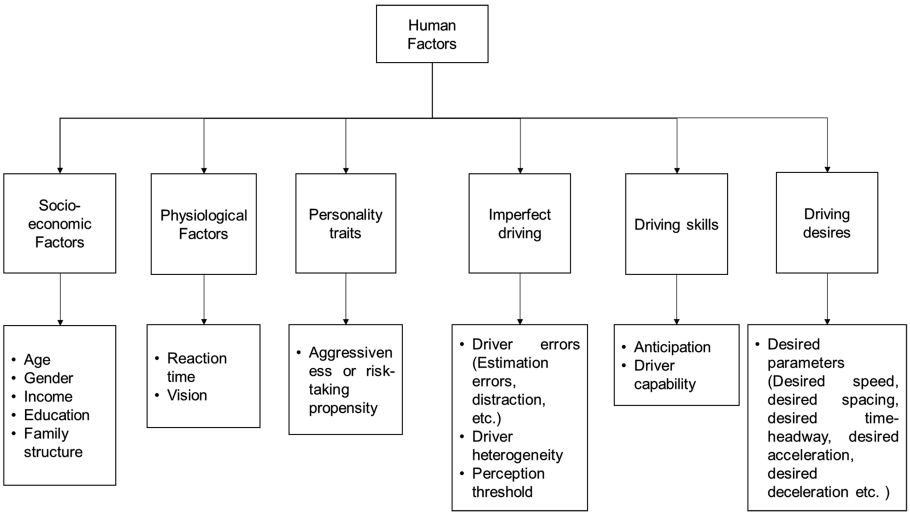

Fig. 1. Human factors critical for modelling traditional vehicles [11, 12]

Socio-Economic Characteristics. These factors refer to a combination of economic and sociological experiences and realities that influence the personality, attitude, and lifestyle of a driver. The main factors are age, income, gender, occupation, education, family background/structure and etc. The effect of socio-economic factors has been widely studied in various fields such as traffic safety [12] and driver compliance [13]. However, limited research studies have considered these factors in traffic flow modelling.

Reaction Time. It is the duration between when a stimulus is observed by the driver and when the driver responses to that stimulus. Some examples of stimulus are sudden acceleration/deceleration of the leading vehicle, a lane changing vehicle ahead, and red traffic light. More specifically, the reaction time has four major psychologic aspects: sensing, perceiving, deciding, and performing an action [14]. Further, the reaction time varies among drivers depending on various factors such as driver's age, gender, driving experience, driving intensity [15], and driver alertness [16].

To describe the stimulus-response relationship such as in the case of car-following, reaction time is an important parameter. Driver reaction time causes traffic instabilities characterized by traffic waves [11], and also reflects inter-driver heterogeneity, i.e. every driver has a different reaction time [17]. Therefore, it is included in many microscopic traffic models (refer [9] for details of these models).

Aggressiveness or Risk-Taking Propensity. Aggressive driving behavior usually neglects other person's right or safety and is intended to hurt/harm another person, either other drivers or pedestrians [18]. Aggressive driving behavior has different forms varying from mild aggressiveness such as flashing lights, honking, tailgating, blocking other drivers, verbal threat, and non-verbal gestures, to extreme aggressiveness such as unsafe lane-changing, speeding, and car ramming [19]. From the modelling perspective, Gasser et al. [20] proposed a car-following model with variable reaction times and aggressiveness of driver and reported that more aggressiveness has a stabilizing effect on the traffic flow characteristics. Moreover, researchers have incorporated risk-taking in some car-following models by considering its psychological and cognitive aspects [21].

Distraction. It pertains to the cognitive and decision-making errors and is caused by the failure of psychological mechanism of attention [22]. Distraction poses serious traffic safety issues [23]. In addition, it impacts braking behavior [24], reaction time [25], and car-following behavior [26]. Recently, Lint et al. [27] have incorporated driver distraction as a parameter to estimate the resultant desired speed and reaction time.

Estimation Errors. These errors also pertain to cognitive and decision-making errors and are caused by the unsuccessful attempt of situation assessment [22]. The most common estimation errors are the inaccurate estimation of the spacing between the driver and the preceding vehicle and the relative velocity. Research related to considering estimation errors in microscopic traffic modelling is also limited. Synthesis of the literature revealed that only one study has attempted to model the estimation errors [11]. This study demonstrates that while small errors have minor impact on traffic waves, large errors may have drastic effects and even lead to crashes.

Driver Heterogeneity. This is defined as the differences in the driving behavior under homogeneous conditions (similar roadway, traffic and weather conditions). It can be classified into two groups: inter-driver heterogeneity and intra-driver heterogeneity. The former illustrates heterogeneity across different drivers, i.e. different drivers have different driving behaviors for the same stimulus and the later describes heterogeneity within the same driver's driving behavior, i.e. the same driver can respond differently for the same stimuli at different times or locations. Both types of heterogeneities have been clearly observed in the real traffic [28]. So far, a few attempts have been made to incorporate driver heterogeneity in traffic models [28]. Driver heterogeneity can lead to a better understanding of traffic flow phenomena such as stop-and-go oscillations, capacity drop, traffic hysteresis flow distribution across lanes, and lane changing maneuvers [29–31]. Moreover, driver heterogeneity also attributes to model calibration errors [11].

Anticipation. Drivers frequently inspect the surrounding traffic situation and anticipate the emerging traffic situation. Driver's such capability is known as anticipation, which can be broadly categorized as temporal anticipation and spatial anticipation (also

known as multi-anticipation) [11]. The former is related to the driver's ability to predict the traffic situation for the next few time intervals and the later describes the driver's ability to take into account several vehicles ahead in decision making. Multi-anticipation has been incorporated in various car-following models and its stabilizing effect on traffic flow has been reported [32].

Perception Threshold. It is defined as the minimum value of the stimulus drivers can perceive and react to [33]. The concept of speed-based and spacing based thresholds was first reported by Michales [34]. Psycho-physiological car-following models (or action point models) consider both local traffic and drivers' perception thresholds in contrast to most traffic flow models where drivers are assumed to respond continuously to an exogenous stimuli, irrespective of how small in the magnitude. Wiedemann [33] is an example of this type of model. Recently, Hoogendoorn et al. [35] presented a data-driven action point model.

Driver Capability. This term was first introduced by Ray Fuller in the Task-Capability Interface (TCI) model, which explains driver behavior through the interaction of driver capability and task demand [36]. Capability of a driver is limited by constitutional characteristics (such as knowledge and skills developed through education and training) and biological capabilities (such as perceptual acuity, reaction time and visual acuity). Furthermore, sensation seeking and distraction are also found to affect driver capability. Previous studies have discovered a correlation between driver capability and time headway selection [37]. Most recently, Saifuzzaman et al. [38] reported that incorporating TCI model into existing car-following models improves the model's performance.

2.2 Connected Vehicles

Human Factors Related to the Deployment of Connected Vehicles. The most critical human factor for the success of connected vehicles is driver behavioral adaptation. It is defined as "*any change of driver, traveler, and travel behaviors that occurs following user interaction with a change to the road-vehicle-user system, in addition to those behaviors specifically and immediately targeted by the initiators of the change*" [39]. Furthermore, the degree of behavioral adaptation according to the 'Qualitative model of behavioral adaption' is the amount of trust a driver has in the system (wherein trust includes 'reliability' and 'competence' of the system), which is determined by the system characteristics such as feedback timing (immediate vs. delayed), amount of usage (amount of exposure) and persistence [40].

Although, drivers' behavioral adaptation to DAS is a widely acknowledged phenomenon, the human centered factors plausible to explain behavioral adaptation are not well established [41]. Behavioral adaptation to connected vehicle technology is possible only if drivers comply with the information provided by the system. Zero compliance will result in zero adaptation. Likewise, degree of compliance will directly influence the degree of behavioral adaptation. In light of this, we propose that drivers' compliance is the sole human factor that governs behavioral adaptation. All the other human factors impact behavioral adaptation through their impact on drivers' compliance.

Driver's Compliance. Drivers' compliance to the information is crucial for the success of the connected vehicles. For example, in relation with variable speed limit system, Hellinga and Mandelzys [42] revealed that safety is positively correlated and travel time is negatively correlated with compliance. Some of the factors that affect driver's compliance are: individual factors such as attitude, subjective norm, habit, distraction, inattention, mindfulness, awareness [43]; situational factors such as traffic conditions, familiarity of road, neighboring vehicle's behavior [44]; and other factors such as the type and presentation of advisory information [44].

For simplicity, we categorize the human factors influencing driver compliance (or the degree of compliance) into four groups, namely, (i) personality traits, (ii) affective, cognitive and psychomotor functions, (iii) acceptance and trust, and (iv) socio-economic characteristics. Some of these factors may be correlated. A field test for examining the freeway merging assistance systems for connected vehicles concluded that the compliance rate is higher for older drivers and is independent of gender [45]. Note that, a full driver compliance (100% compliance) is highly unlikely due to these human factors. Therefore, it is imperative to carry out a comprehensive analysis of human factor impact on the effectiveness of any information assistance system through field or driving simulator experiments prior to its large-scale deployment.

Connected Vehicles' Impact on Human Driving Behavior. Limited research has been conducted using driving simulators or connected vehicle test beds (field tests) to investigate how connected technology influences driver behavior. For instance, using driving simulator experiments, Chang et al. [46] found a significant reduction in driver perception-reaction time while analyzing the rear-end collision warning systems of a connected bus system.

Evidently, connected vehicles will be equipped with devices similar to DAS to receive, process, and then display the kinematic information (position, velocity, acceleration, recommended speed, space-headway, etc.) disseminated by the neighboring vehicles and/or roadside units. During the development stage of connected vehicles, findings from DAS based studies may provide valuable references to understand the potential impact of this new technology on driver's performance. Over the past two decades the impact of different types of DAS (such as vehicle dynamics stabilization systems, information warning, and comfort systems) on driver's performance have been studied in detail. Some intriguing findings are, for example, DAS has the potential of reducing driver errors (e.g. perception, anticipation, and distraction), increasing driving comfort and improving traffic flow [47]. In particular, many studies investigated the impact of DAS on time headway either in field or simulator studies. Almost all the studies reported a decrease in the occurrence of potentially unsafe headways [48, 49]. Furthermore, a shorter reaction time is reported when any anticipatory information was available through DAS [48]. Other positive aspects of DAS are safe speed adaptation [48], collision avoidance [50], and better route selection [51]. Connected vehicle technology is more advanced compared to DAS because it will not only communicate with the surrounding vehicles, but also with the infrastructure and with all other related technologies. Connectivity will help the driver by providing real time and advanced

information related to safe and efficient driving. Therefore, it is reasonable to anticipate that the impact of connectivity on human driving behavior should be more profound than that of DAS in terms of improving safety, comfort and efficiency.

2.3 Automated Vehicles

Major human factors associated with automated vehicles are driver inattention and distraction, situational awareness, overreliance and trust, skill degradation, and motion sickness. Driver inattention and distraction pertain to passive fatigue [52], reduced driver vigilance [53], engagement in secondary activities [54], and etc. Concerns have been raised that automated driving may lead to impoverished situation awareness [54]. In addition, over-reliance on the automation can cause negative behavioral adaptation effects and can be detrimental to safe driving [55]. Skottke et al. [56] reported carry-over effects of highly automated convoy driving such as shorter time headways and increased variability of lateral position in a manual driving task subsequent to brief periods of highly-automated driving. Researchers have argued that re-engaging the driver or shared control has the potential to reduce the detrimental impact of automated driving [8], such as time-dependent takeover of vehicle control by the driver (Level 3 automation). The major issues investigated by the previous studies are the time frame required by the driver to regain the control [57] and after-effects of takeover [58].

3 Driving Simulator Experiment Design

A significant challenge in investigating issues relating to connected and automated vehicles is the lack of field data because these vehicles are not yet operating on a scale suitable for naturalistic research. To overcome this challenge, many researchers choose numerical experiments. While using numerical methods is a reasonable compromise in this circumstance, there is a high risk of oversimplification because an important component, human behavior in the connected environment, is not accounted for. Motivated by the current research needs and limitations of the previous studies, this study seeks to carefully and innovatively design driving simulator experiments to collect vital empirical data. The simulator experiments have been conducted with the CARRS-Q Advanced Driving Simulator at QUT [26]. Two critical factors are considered in order to represent the connected environment realistically in the simulator experiments: design of driving aids and design of connectivity.

Design of Driving Aids. It involves the type of information disseminated and how the disseminated information is presented. Some important factors that have been considered in this research while designing the driving aids are: the content of the aids, the type of the messages, the position of the display, and the duration and frequency of the displayed messages. The content of the driving aids are divided into three categories: (a) continuous information, which is available all the time to the drivers (for example, speed of the preceding vehicle); (b) on-time event-based information, which is available only at the onset of an event (for example, warning about speed violation); and (c) advanced event-based information, which is provided a few seconds earlier of

encountering the actual event (for example, advisory information about congestion ahead). Two types of message presentation are reported in the literature: auditory and imagery messages. Both of these types are incorporated in this study based on needs. For example, the event based information is displayed with a sound to draw driver's attention on those messages. All these messages are carefully presented on the windscreen without obstructing the field of driver view. The design of the driving aids is a crucial part of this study as it has a direct effect on the driving behaviour. All the above-mentioned factors affect the workload of the driver to some extent as the driver needs to understand the presented information, relate it with the driving context and finally act upon it. Hence the information load should be considered judiciously in order to get the optimum benefit from the connected vehicle technology.

Design of Connectivity. In the connected environment, the information is received and transferred by the connected vehicles using V2V and V2I communications. The effectiveness of the information dissemination depends on the penetration and distribution of connected vehicles in the traffic and the distribution of roadside units along the road. Communication impairment is a critical issue that is inevitable in the real-world. Hence, in this experiment, both the perfect communication and communication impairments are included to mimic the connected environment more realistically. In the perfect communication, the flow of information is uninterrupted, whereas no information dissemination (communication loss) or a delay in information dissemination (communication delay) are the characteristics of the communication impairments.

The Experiment. Two scenarios are covered within the scope of this research: baseline (with no connectivity, i.e., traditional vehicles) and connected environment (with both V2V and V2I communications). In the baseline scenario, each participant is asked to drive the vehicle as they normally do with a traditional vehicle (without driving aids). In the connected scenario, information assistance is provided to the participant on the windscreen using the driving aid. Figure 2 is an example, a snapshot

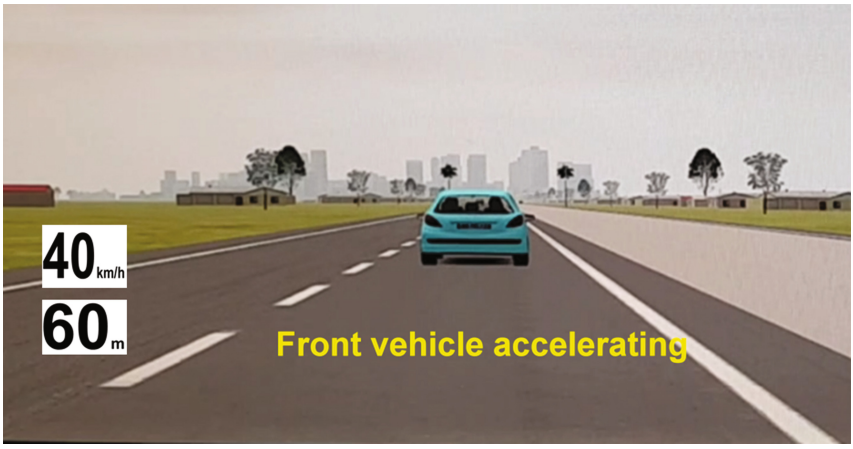

Fig. 2. A visual description of driving aids on the wind screen (Note that 40 km/h and 30 m represent the front vehicle's speed and spacing to the front vehicle, respectively).

of the windscreen when a participant is driving in the connected environment. Each participant needs to complete three driving tasks: car-following (free flow and braking events), lane changing (both mandatory and discretionary), and merging.

A noteworthy feature of connectivity in this research (especially compared with the present DAS) is that the information on some critical events is provided in advance to the driver (about 3–5 s before the occurrence of that event). It is assumed that the connected technology should be smart enough to predict these critical events in advance. For example, when two or more connected vehicles are in front of the driver, the connected vehicle technology should predict and inform the driver in advance about the next braking event of the preceding vehicle. Similarly, it should also be able to inform the drivers about lane closure or traffic state at downstream locations. These advanced information will assist the drivers in tactical decision-making. The experiment design involves all these events. Moreover, to make the experiment more realistic, the connected scenario also incorporates the communication impairments.

Questionnaire Survey Design. To obtain more information related to human factors, pre-drive and post-drive questionnaire surveys have been carried out to understand how human drivers influence, and are influenced by the connected environment. The pre-drive survey involves questions pertaining to socio-demographic information, driving experience, and driving behavior (based on driving anger expression inventory [59]). After each scenario drive participants have to complete NASA Task Load Index (NASA-TLX) [60]. This is to comprehend the required human cost (workload during the experiment) represented by the subscales corresponding to the mental, physical, and temporal demands, frustration, effort, and performance. Finally, the post-drive survey is designed to understand how human factors such as user-acceptance, trust in the technology, and sensation-seeking contribute towards driver's compliance/non-compliance to the information aid.

4 Conclusion

This paper focuses on human factors and their importance for the success of connected and automated vehicles. Furthermore, the paper presents a detail discussion on critical human factors that need to be incorporated in microscopic traffic flow models, especially for traditional and connected vehicles. In addition, this paper also presents the design of a driving simulator experiments for traditional and connected vehicles. Data collected from this driving simulator experiment can assist in developing more accurate, realistic, and robust microscopic traffic flow models, which are important tools for understanding characteristics of mixed traffic flow consisting of traditional, connected, and automated vehicles, and for developing effective operation and control strategies for mixed traffic flow. Such effort is ongoing.

Acknowledgements. This research was partially funded by the Australian Research Council (ARC) through Dr. Zuduo Zheng's Discovery Early Career Researcher Award (DECRA; DE160100449).

References

1. McCarthy, J., Bradburn, J., Williams, D., Piechocki, R., Hermans, K.: Connected & Autonomous Vehicles. ATKINS (2015)
2. Hendrickson, C., Biehler, A., Mashayekh, Y.: Connected and Autonomous Vehicles 2040 Vision (2014)
3. Litman, T.: Autonomous vehicle implementation predictions. Vic. Transp. Policy Inst. 28 (2014)
4. Manser, M., Creaser, J., Boyle, L.: Behavioural adaptation. In: Behavioural Adaptation and Road Safety, pp. 339–358. CRC Press (2013)
5. Talebpour, A.: Modeling driver behavior in a connected environment: Integration of microscopic traffic simulation and telecommunication systems (2015). http://gradworks.umi.com/37/24/3724384.html
6. Smith, B.W.: SAE Levels of Driving Automation. http://cyberlaw.stanford.edu/blog/2013/12/sae-levels-driving-automation
7. Bainbridge, L.: Ironies of automation. Automatica **19**, 775–779 (1983)
8. Saffarian, M., de Winter, J.C.F., Happee, R.: Automated driving: human-factors issues and design solutions. Proc. Hum. Factors Ergon. Soc. Annu. Meet **56**, 2296–2300 (2012)
9. Saifuzzaman, M., Zheng, Z.: Incorporating human-factors in car-following models: a review of recent developments and research needs. Transp. Res. Part C Emerg. Technol. **48**, 379–403 (2014)
10. Zheng, Z.: Recent developments and research needs in modeling lane changing. Transp. Res. Part B Methodol. **60**, 16–32 (2014)
11. Treiber, M., Kesting, A.: Traffic Flow Dynamics. Data Models Simulation. Springer, Heidelberg (2013)
12. Amoros, E., Martin, J.L., Laumon, B.: Comparison of road crashes incidence and severity between some French counties. Accid. Anal. Prev. **35**, 537–547 (2003)
13. Dia, H., Panwai, S.: Modelling drivers' compliance and route choice behaviour in response to travel information. Nonlinear Dyn. **49**, 493–510 (2007)
14. Shiffrin, R.M., Schneider, W.: Controlled and automatic human information processing: II. Perceptual learning, automatic attending and a general theory. Psychol. Rev. **84**, 127 (1977)
15. Mehmood, A., Easa, S.M.: Modeling reaction time in car-following behaviour based on human factors. Int. J. Appl. Sci. Eng. Technol. **5**, 93–101 (2009)
16. Liebermann, D., Ben-David, G., Schweitzer, N., Apter, Y., Parush, A.: A field study on braking responses during driving. I. Triggering Modulation. Ergonomics. **38**, 1894–1902 (1995)
17. Treiber, M., Kesting, A., Helbing, D.: Influence of Reaction Times and Anticipation on Stability of Vehicular Traffic Flow. Transp. Res. Rec. J. Transp. Res. Board. **1999**, 23–29 (2007)
18. Dula, C.S., Geller, E.S.: Risky, aggressive, or emotional driving: Addressing the need for consistent communication in research. J. Saf. Res. **34**, 559–566 (2003)
19. Özkan, T., Lajunen, T., Parker, D., Sümer, N., Summala, H.: Symmetric relationship between self and others in aggressive driving across gender and countries. Traffic Inj. Prev. **11**, 228–239 (2010)
20. Gasser, I., Seidel, T., Sirito, G., Werner, B.: Bifurcation analysis of a class of 'car following' traffic models II: variable reaction times and aggressive drivers. Bull. -Inst. Math. Acad. Sin. **2**, 587 (2007)
21. Hamdar, S., Treiber, M., Mahmassani, H., Kesting, A.: Modeling driver behavior as sequential risk-taking task. Transp. Res. Rec. J. Transp. Res. Board. **2088**, 208–217 (2008)

22. Stanton, N.A., Salmon, P.M.: Human error taxonomies applied to driving: a generic driver error taxonomy and its implications for intelligent transport systems. Saf. Sci. **47**, 227–237 (2009)
23. McEvoy, S., Stevenson, M.: An exploration of the role of driver distraction in serious road crashes. Distracted Driv. Syd. Australas. Coll. Road Saf. 189–211 (2007)
24. Haque, M.M., Washington, S.: The impact of mobile phone distraction on the braking behaviour of young drivers: a hazard-based duration model. Transp. Res. Part C Emerg. Technol. **50**, 13–27 (2015)
25. Haque, M.M., Washington, S.: A parametric duration model of the reaction times of drivers distracted by mobile phone conversations. Accid. Anal. Prev. **62**, 42–53 (2014)
26. Saifuzzaman, M., Haque, M.M., Zheng, Z., Washington, S.: Impact of mobile phone use on car-following behaviour of young drivers. Accid. Anal. Prev. **82**, 10–19 (2015)
27. van Lint, H., Schakel, W., Tamminga, G., Knoppers, P., Verbraeck, A.: Getting the Human Factor into Traffic Flow Models. Transp. Res. Rec. J. Transp. Res. Board. **2561**, 25–33 (2016)
28. Ossen, S., Hoogendoorn, S.P.: Heterogeneity in car-following behavior: theory and empirics. Transp. Res. Part C Emerg. Technol. **19**, 182–195 (2011)
29. Ossen, S., Hoogendoorn, S.: Driver heterogeneity in car following and its impact on modeling traffic dynamics. Transp. Res. Rec. J. Transp. Res. Board. **1999**, 95–103 (2007)
30. Daganzo, C.F.: A behavioral theory of multi-lane traffic flow. Part I: long homogeneous freeway sections. Transp. Res. Part B Methodol. **36**, 131–158 (2002)
31. Kerner, B.S., Klenov, S.L.: Spatial–temporal patterns in heterogeneous traffic flow with a variety of driver behavioural characteristics and vehicle parameters. J. Phys. Math. Gen. **37**, 8753 (2004)
32. Treiber, M., Kesting, A., Helbing, D.: Delays, inaccuracies and anticipation in microscopic traffic models. Phys. Stat. Mech. Appl. **360**, 71–88 (2006)
33. Wiedemann, R.: Simulation des Strassenverkehrsflusses (1974)
34. Michales, R.M.: Perceptual factors in car following. Presented at the Proceedings of the 2nd International Symposium on the Theory of Road Traffic Flow, Paris (1963)
35. Hoogendoorn, S., Hoogendoorn, R., Daamen, W.: Wiedemann revisited: new trajectory filtering technique and its implications for car-following modeling. Transp. Res. Rec. J. Transp. Res. Board. **2260**, 152–162 (2011)
36. Fuller, R.: Towards a general theory of driver behaviour. Accid. Anal. Prev. **37**, 461–472 (2005)
37. Hoogendoorn, R., van Arem, B., Hoogendoorn, S.: Incorporating driver distraction in car-following models: applying the TCI to the IDM. Presented at the 2013 16th International IEEE Conference on Intelligent Transportation Systems-(ITSC) (2013)
38. Saifuzzaman, M., Zheng, Z., Haque, M.M., Washington, S.: Revisiting the Task–Capability interface model for incorporating human factors into car-following models. Transp. Res. Part B Methodol. **82**, 1–19 (2015)
39. Kulmala, R., Rämä, P.: Definition of behavioural adaptation. In: Behavioural Adaptation and Road Safety: Theory, Evidence and Action, pp. 11–22. CRC Press (2013)
40. Rudin-Brown, C., Ian Noy, Y.: Investigation of behavioral adaptation to lane departure warnings. Transp. Res. Rec. J. Transp. Res. Board. **1803**, 30–37 (2002)
41. Saad, F.: Some critical issues when studying behavioural adaptations to new driver support systems. Cogn. Technol. Work **8**, 175–181 (2006)
42. Hellinga, B., Mandelzys, M.: Impact of driver compliance on the safety and operational impacts of freeway variable speed limit systems. J. Transp. Eng. **137**, 260–268 (2011)
43. Hanan, S.A.: An application of an extended theory of planned behaviour to understand drivers' compliance with the school zones speed limit in Australia and Malaysia (2014)

44. Songchitruksa, P., Bibeka, A., Lin, L. (Irene), Zhang, Y.: Incorporating Driver Behaviors into Connected and Automated Vehicle Simulation. Texas A&M Transportation Institute (2016)
45. Hayat, M.T.: Investigating drivers' Responses to Advisory Messages in a Connected Vehicle Environment (2015)
46. Chang, J., Hatcher, G., Hicks, D., Schneeberger, J., Staples, B., Sundarajan, S., Vasudevan, M., Wang, P., Wunderlich, K.: Estimated Benefits of Connected Vehicle Applications: Dynamic Mobility Applications, AERIS, V2I Safety, and Road Weather Management Applications (2015)
47. Brookhuis, K.A., De Waard, D., Janssen, W.H.: Behavioural impacts of advanced driver assistance systems–an overview. Eur. J. Transp. Infrastruct. Res. **1**, 245–253 (2001)
48. Adell, E., Várhelyi, A., Dalla Fontana, M.: The effects of a driver assistance system for safe speed and safe distance–a real-life field study. Transp. Res. Part C Emerg. Technol. **19**, 145–155 (2011)
49. Saffarian, M., De Winter, J.C., Happee, R.: Enhancing driver car-following performance with a distance and acceleration display. IEEE Trans. Hum. -Mach. Syst. **43**, 8–16 (2013)
50. Lee, J.D., McGehee, D.V., Brown, T.L., Reyes, M.L.: Collision warning timing, driver distraction, and driver response to imminent rear-end collisions in a high-fidelity driving simulator. Hum. Factors J. Hum. Factors Ergon. Soc. **44**, 314–334 (2002)
51. Uang, S.-T., Hwang, S.-L.: Effects on driving behavior of congestion information and of scale of in-vehicle navigation systems. Transp. Res. Part C Emerg. Technol. **11**, 423–438 (2003)
52. Desmond, P.A., Hancock, P.A.: Active and passive fatigue states. Stress Workload Fatigue (2001)
53. Neubauer, C., Matthews, G., Langheim, L., Saxby, D.: Fatigue and voluntary utilization of automation in simulated driving. Hum. Factors **54**, 734–746 (2012)
54. Merat, N., Jamson, A.H., Lai, F.C., Carsten, O.: Highly automated driving, secondary task performance, and driver state. Hum. Factors **54**, 762–771 (2012)
55. Regan, M.A.: New technologies in cars: human factors and safety issues. Ergon. Aust. **18**, 6–15 (2004)
56. Skottke, E.-M., Debus, G., Wang, L., Huestegge, L.: Carryover effects of highly automated convoy driving on subsequent manual driving performance. Hum. Factors **56**, 1272–1283 (2014)
57. Zeeb, K., Buchner, A., Schrauf, M.: What determines the take-over time? An integrated model approach of driver take-over after automated driving. Accid. Anal. Prev. **78**, 212–221 (2015)
58. Merat, N., Jamson, A.H., Lai, F.C., Daly, M., Carsten, O.M.: Transition to manual: driver behaviour when resuming control from a highly automated vehicle. Transp. Res. Part F Traffic Psychol. Behav. **27**, 274–282 (2014)
59. Deffenbacher, J.L., Lynch, R.S., Oetting, E.R., Swaim, R.C.: The driving anger expression inventory: a measure of how people express their anger on the road. Behav. Res. Ther. **40**, 717–737 (2002)
60. Hart, S.G., Staveland, L.E.: Development of NASA-TLX (Task Load Index): results of empirical and theoretical research. Adv. Psychol. **52**, 139–183 (1988)

Implementation of a sEMG-Machine Interface for Steering a Virtual Car in a Driving Simulator

Edric John Nacpil[1(✉)], Rencheng Zheng[1], Tsutomu Kaizuka[1], and Kimihiko Nakano[1,2]

[1] Institute of Industrial Science, The University of Tokyo, 4-6-1 Komaba, Meguro-ku, Tokyo 153-8505, Japan
{enacpil, topzrc, tkaizuka, knakano}@iis.u-tokyo.ac.jp
[2] Interfaculty Initiative in Information Studies, The University of Tokyo, 3-8-1 Komaba, Meguro-ku, Tokyo 153-8902, Japan

Abstract. Surface electromyography (sEMG) has often enabled operators to generate electrical muscle signals in order to control robotic arms or prosthetics. Alternatively, sEMG has recently been employed to control other types of equipment such as computer keyboards, which indicates that sEMG-machine interfaces can be a means of controlling actual automobiles or computer-simulated automobiles. Therefore, the current study pertains to a sEMG-controlled virtual car in a PC platform driving simulator. A method is proposed for implementing a sEMG-machine interface that controls the steering of the virtual car.

Keywords: Surface electromyography · Human-machine interface · Driving simulation · Automobile engineering · Control system design

1 Introduction

Surface electromyography (sEMG), a method that records electrical signals generated by muscles, has the potential to control electromechanical devices [1]. For example, researchers have utilized sEMG to control devices such as prosthetics and exoskeletons [2–4]. Other researchers have used sEMG signals to control equipment such as a desktop computer keyboard and a robotic hand [5]. Human subjects performed hand gestures that generated sEMG signals. Multichannel matrix-type surface electrodes measured the forearm muscle signals resulting from these gestures. The control system employed the Monte Carlo Method in order to determine the optimum quantity and positions of electrodes. There was no need to rely on physiological or anatomical knowledge to determine the placement and number of electrodes.

Human subjects have also been able to manipulate a radio-controlled model vehicle with sEMG signals generated by forearm gestures [6]. Multichannel matrix-type electrodes measured muscle signals, and the electrode quantities and positions were determined by the Monte Carlo Method. Various gestures of the right forearm controlled the movement of the model vehicle, including supination and pronation that turned the model vehicle right and left, respectively.

D.N. Cassenti (ed.), *Advances in Human Factors in Simulation and Modeling*,
Advances in Intelligent Systems and Computing 591, DOI 10.1007/978-3-319-60591-3_25

The current study is distinguishable from previous studies because it aims to control the steering of a virtual car in a PC platform driving simulator. Furthermore, unlike other studies that employed matrix-type electrodes, only individual disposable sEMG electrodes are used with electrode quantity and placement being determined by physiological and anatomical knowledge [5, 6, 13]. These electrodes are mounted on human subjects that generate sEMG signals with forearm gestures.

Signal processing circuitry has been designed and constructed for the current study in order to prepare the sEMG signals for analog-to-digital conversion. Computer algorithms have been developed to convert digital sEMG signals to controller signals that are transmitted to a PC. The driving simulator program that runs on the PC responds to the controller signals by steering the virtual car.

What follows is an outline of the steps taken to develop the computer algorithms and to design the signal processing circuitry. Explanations are given with regard to the functions of electronic components and algorithms. A discussion is presented with regard to the experimental application of the steering interface. Recommendations are provided for improvements to the steering interface, and finally consideration is given to alternative hardware and software that could also be used to implement the sEMG-controlled steering.

2 Steering Control System

2.1 Equipment Overview

The control system equipment represented in Fig. 1 includes a commercially available PC laptop that runs the driving simulator software, Virtual Battlespace 2. The laptop is readily powered by a battery so that line noise resulting from an AC power source for the laptop is eliminated.

Avoiding line noise reduces the electrical interference encountered by the sEMG measurement equipment. Commercially available self-adhering Ag/AgCl electrodes are mounted on the skin surface of the test subject in order to measure sEMG signals. In order to improve muscle signal transmission at the skin-electrode interface, conductive wet gel is applied to the adhesive side of the electrodes during the electrode manufacturing process. The data acquisition unit (DAQ) amplifies the sEMG signals so that they are detected by a commercially available, Arduino™ Uno R3 microcontroller. The microcontroller is the component of the DAQ that converts sEMG signals from analog to digital waveforms. After the analog-to-digital conversion, the microcontroller performs a smoothing function on the digital waveforms in order to reduce undesired effects on the sEMG signals such as pull artifacts and electromagnetic interference.

The microcontroller transmits processed sEMG signals to the laptop via a USB connection. Then the driving simulator software on the laptop utilizes these signals to control the steering of a virtual car. Foot pedals control the braking and acceleration of the car.

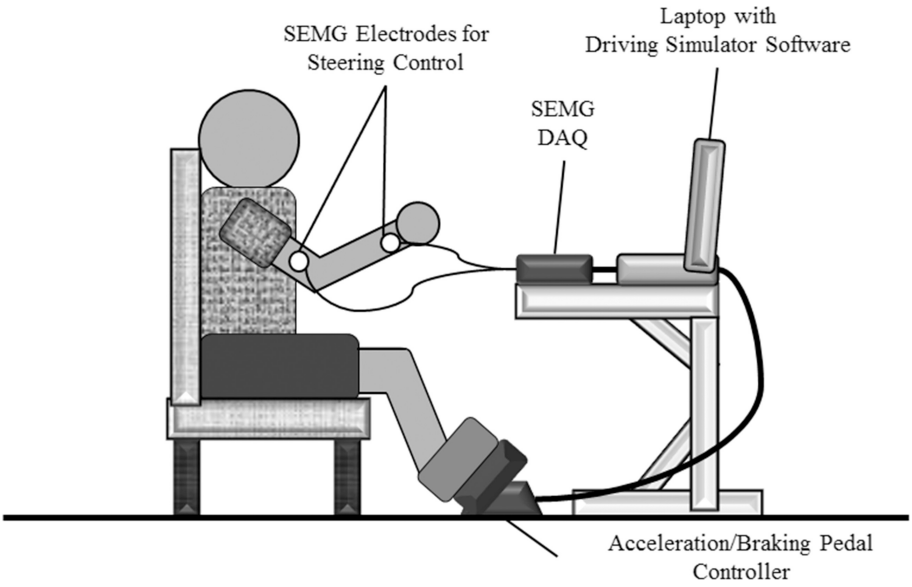

Fig. 1. Schematic of experimental setup for sEMG-machine interface.

2.2 Signal Processing Algorithms

The amplitude of the sEMG signals is considered in the design of the signal processing circuit. The peak-to-peak voltage of sEMG signals ranges from 0 mV to 10 mV [7]. However, the resolution of the microcontroller is 4.9 mV, so sEMG signals with lower amplitudes will not be adequately detected [8]. In order to ensure that the microcontroller can detect the sEMG signals, the investigators have designed and constructed an amplifier circuit that is represented in Fig. 2. In accordance with past sEMG amplifier

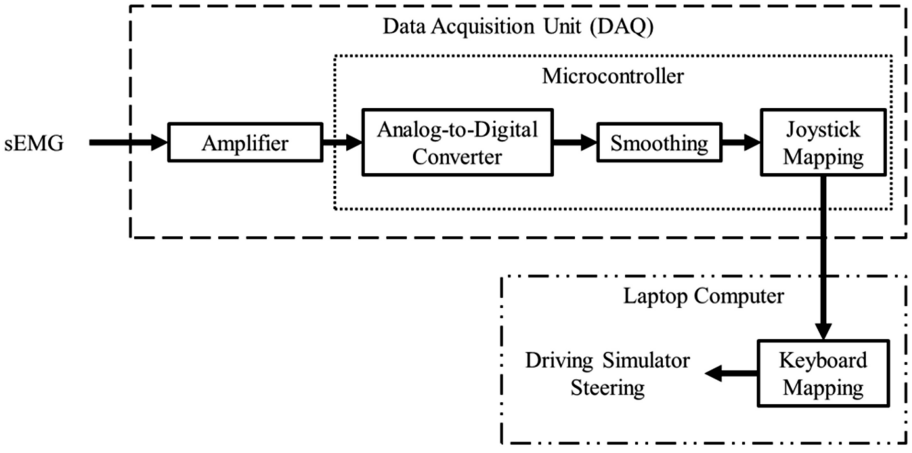

Fig. 2. Block diagram of sEMG signal processing sequence.

designs, the current circuit is comprised of two stages [1]. The first stage, which involves pre-amplification, relies on an operational amplifier to increase the amplitude of the signal in preparation for the second stage of amplification. Performing pre-amplification reduces the energy required by the second-stage operational amplifier. These stages have a combined, calculated voltage gain of approximately 5000 that is within the range of commercially available sEMG measurement equipment [11, 12].

Recording of sEMG signals is partly influenced by the signal-to-noise ratio [7]. Noise can be produced from numerous sources such as: electronic components in the DAQ, external appliances such as light bulbs and computer monitors, and pull artifacts resulting from the movement of sEMG lead wires and sEMG electrodes relative to the skin surface. In order to reduce the influence of noise, the DAQ amplifier contains filters that limit the signal frequency range to between 2 Hz and 530 Hz, approximately. This range is adequate for the recording of sEMG signals, since the usable energy of sEMG signals is between 0 Hz and 500 Hz [7].

The microcontroller uses a 10-bit analog-to-digital converter to digitize the sEMG signal [8]. In order to prevent aliasing, the microcontroller is programmed to acquire the signal at more than twice the maximum frequency of the filtered sEMG signal [9].

Some undesired effects remain in the sEMG signal, even after it undergoes filtering during the amplification stage. Ambient line noise, motion artifacts, and the quasi-random firing rate of motor units in the muscle can influence the signal [7]. In an attempt to reduce this influence, the microcontroller performs a smoothing function, in the form of arithmetic averaging, on the digital sEMG signal. The additional benefit of this process is a more gradual change in amplitude that translates to less erratic steering control in the driving simulator.

2.3 Steering Control Algorithms

Figure 2 shows two steps related to the control of steering. The first step, designated as joystick mapping, is the programming of the microcontroller software and firmware so that the laptop will recognize the microcontroller as a USB joystick. UnoJoy! is a package of firmware and software that implements joystick functionality [10]. The software maps the sEMG signal to a joystick command such as the rightward movement of an analog joystick. On the other hand, the firmware enables the microcontroller to transmit this joystick command to the laptop.

Keyboard mapping, which is the next step towards steering control, involves mapping of joystick commands to the keyboard of the laptop. Since the driving simulator steering is executed through the keyboard, the joystick commands from the microcontroller are mapped to keyboard commands. For example, in order to turn a virtual car to the left, the left arrow key can be pressed on the keyboard. A commercially available software program, JoyToKey, enables a joystick command from the microcontroller to be recognized by the laptop as a press of the left arrow key. Since these joystick commands are the result of sEMG signals, the virtual car can be steered by generating sEMG signals with gestures such as the supination of the forearm.

2.4 sEMG-Machine Interface Design

Designing a sEMG-machine interface involves the assignment of specific gestures to operations of controlled devices. Gestures are associated with sEMG signals that serve as user input for the interface. Past studies have used sEMG resulting from particular gestures to control the operation of different types of devices [5, 6, 13]. Researchers in one study decided to assign 26 different movements of the hand and arm to keyboard functions [13]. With regard to the operation of a model vehicle, pronation and supination of the right forearm corresponded to left turns and right turns, respectively [6]. The control systems for the model vehicle and the keyboard utilized matrix-type electrodes in conjunction with the Monte Carlo Method to select the optimum quantity and position of the electrodes. So knowledge of physiology or anatomy is not required to mount the electrodes onto test subjects. The tradeoffs are: the time and effort involved in the fabrication of the electrode matrix, the acquisition or construction of a multichannel sEMG DAQ, and the development of signal processing algorithms to carry out the Monte Carlo Method calculations. For the current study, such tradeoffs are not necessary, so the more traditional approach involving physiological and anatomical knowledge is used. Two differential electrodes and one ground electrode measure the sEMG signal of an arm muscle. Electrode placement is determined under the guidance of recommendations from SENIAM (Surface Electromyography for the Non-Invasive Assessment of Muscles) [17].

Regardless of the method used in optimizing electrode number and quantity, previous studies involving sEMG-machine interfaces, vary with respect to the selection of gestures, measured muscles, and device operations [5, 6, 13]. The driver of a virtual car in the current study utilizes sEMG signals generated by forearm gestures in order to steer a virtual car in the driving simulator. Multiple combinations of gestures and steering directions are possible. One combination is to have a test subject perform supination with the left forearm to steer the virtual car to the left, whereas supination with the right arm would steer the car to the right. The sEMG of the biceps brachii for each arm would serve as control signals. Table 1 includes this and other configurations. Further configurations are possible, so Table 1 is not an exhaustive list. An optimal set of configurations could be determined through empirical observations gained from driving simulations with varying configurations.

Table 1. Several possible sEMG-machine interface configurations.

Configuration	Steering direction	Gesture	Measured muscle
1	Left	Left forearm supination	Biceps brachii of left arm
	Right	Right forearm supination	Biceps brachii of right arm
2	Left	Left forearm supination	Biceps brachii of left arm
	Right	Left forearm pronation	Pronator teres of left arm
3	Right	Right forearm supination	Biceps brachii of right arm
	Left	Right forearm pronation	Pronator teres of right arm

3 Experimental Applications

Potential experimental applications of the sEMG-machine interface include experiments that aim to determine optimal interface parameters such as gestures performed by the driver and the corresponding muscles to be measured. For example, flexion of the left elbow would generate a biceps brachii sEMG signal that could steer the virtual car to the left. Another possibility is to retain the flexion of the left elbow, but measure the triceps brachii instead. These configurations could be experimentally compared to the configurations in Table 1 that correspond to leftward steering. The control group for these comparisons would represent typical motorists by consisting of licensed automobile drivers who steer the virtual car with a game controller steering wheel. Additionally, drivers could use a gear selection device to simulate an automatic or manual transmission. Comparing this control group with licensed or unlicensed drivers who operate the sEMG-machine interface would allow for an evaluation of sEMG-controlled steering with respect to standard driving interfaces.

Multiple types of criteria may serve as the basis for evaluating the sEMG-machine interface. Driving simulator experiments could focus on the dimension of time such as measuring the amount of time taken for a driver to complete a turn at an intersection or to pass through a series of obstacles such as street cones, pedestrians, or cars. Alternatively, experiments could measure the amount of time or the number of trials for a driver to reach a certain level of driving proficiency such as the completion of a driving course within a target amount of time.

Criteria can also be in the form of surveys that record the subjective experience of test subjects with regard to the operation of the sEMG-machine interface. Test subjects could report the level of difficulty in learning this interface or the preference of this interface over a steering wheel. A more quantitative approach would be obtain a combination of motion capture or video recordings of the gestures performed by subjects during steering in order to evaluate the kinematics of various gesture configurations. It is also possible to record the sEMG signals during a driving simulation to quantify the experience of a test subject.

An emerging criterion for evaluating an interface is intuitive interaction. This research is driven in part by the description of interfaces as being intuitive in everyday speech. Around the beginning of the 21st century, investigations into intuitive interaction have been increasing [14]. Describing an interface as being intuitive can be interpreted in terms of a user being able to interact with the interface through "non-conscious" or "implicit knowledge" [14]. Previous research has focused on measuring intuitive interaction in terms of the "efficiency" and "accuracy" with which an operation is executed [15]. In the context of the current study, "efficiency" is defined as the amount of time to execute a driving maneuver such as the completion of a U-turn. "Accuracy" is defined as the amount of error in the execution of a driving maneuver such as the amount of error in the trajectory of the virtual car relative to a specified U-turn trajectory. The sEMG-machine interface can be compared to a game controller steering wheel in terms of intuitive interaction.

4 Recommendations for Control System Improvement

4.1 Control Feedback

Given that currently planned experiments for the sEMG-machine interface involve a PC platform driving simulator, it is possible to consider further development of the interface for larger scale experiments that involve either a more elaborate driving simulator or an actual car. An improved control system would possess attributes of large-scale or actual driving control systems. Let us then consider the differences between the current interface and the experience of driving an actual car.

Immersive visual feedback is available in the cabin of an actual car. A driver can view the environment in various directions in order to determine the position of the car relative to driving conditions such as the trajectory of the car along a road. The driver also hears sounds and feels vibrations from the car and from other ambient sources such as ambulance sirens or trains. With regard to some setups, such as a rack-and-pinion steering system, the driver can sometimes feel steering resistance and vibration when executing turns.

It is possible to conceive other instances of feedback that are lacking in the current control system. The monitor of the laptop for the current system provides a more limited form of visual feedback that is only in front of the driver. Large projector screens may provide more immersive feedback because the screens occupy a greater portion of the field of view of the driver. A similar result might be achieved with virtual reality glasses.

Furthermore, a speaker or headphone system that is not included in the current setup would provide auditory feedback by replicating sounds from an actual automobile or from other ambient sources. Tactile feedback could also be added by having the driver sit on a moving platform that simulates vibration encountered in an actual automobile. More compact, but perhaps less realistic, feedback might also come from vibrating feedback devices that are directly mounted onto the driver.

4.2 Alternatives for sEMG Measurement Equipment

The sEMG DAQ employed in this study was recently developed and constructed, so it has yet to be tested for long-term accuracy and reliability over the course of multiple experiments. It is possible, perhaps, to overcome this uncertainty by acquiring production sEMG equipment from experienced vendors. One instance of commercially available measurement equipment is the Polymate AP1132. Correspondence with the manufacturer of the Polymate revealed that a software package is available that enables online processing of sEMG signals. Additional software and programming is required, however, in order for the processed signal to be recognized as a control signal by the driving simulator.

Although there is at least one alternative available, pre-experimental equipment testing conducted by the investigators suggests the current DAQ is a promising candidate for driving simulator steering control. However, the DAQ is potentially subject to noise originating from the movement of lead wires attached to the electrodes [7].

Replacing the lead wires with radio transmitters and receivers would eliminate this kind of noise. Alternatively, wireless sEMG sensors may be utilized instead of the current equipment [16].

5 Conclusion

A control system has been developed in order to implement a sEMG-machine interface. The interface is capable of supporting multiple configurations with regard to the muscles that are measured, the gestures that are performed, and the steering operations involved. Multiple experimental applications are possible as a result of this versatility. Although there are options for improvement such as the addition of wireless sEMG measurement capability or devices that convey feedback to the driver, the control system is technologically feasible for driving simulations on a laptop computer.

References

1. Basmajian, J.V., De Luca, C.J.: Muscles Alive: Their Functions Revealed by Electromyography. Williams & Wilkins, Baltimore (1985)
2. Wang, N., Lao, K., Zhang, X.: Design and myoelectric control of an anthropomorphic prosthetic hand. J. Bionic Eng. **14**, 47–59 (2017)
3. Oskoei, M.A., Hu, H.: Myoelectric control systems – a survey. Biomed. Sig. Process. Control **2**, 275–294 (2007)
4. Viteckova, S., Kutilek, P., Jirina, M.: Wearable lower limb robotics: a review. Biocybern. Biomed. Eng. **33**, 96–105 (2013)
5. Nagata, K., Ando, K., Magatani, K., Yamada, M.: Development of the hand motion recognition system based on surface EMG using suitable measurement channels for pattern recognition. In: Proceedings of the 29th Annual International Conference of the IEEE EMBS, pp. 5214–5217 (2007)
6. Takizawa, N., Wakita, Y., Nagata, K., Magatani, K.: A development of the equipment control system using SEMG. In: Lim, C.T., Goh, J.C.H. (eds.) ICBME 2008, Proceedings, vol. 23, pp. 923–926. Springer, Heidelberg (2009)
7. De Luca, C.J.: Surface Electromyography: Detection and Recording. DelSys Incorporated (2002)
8. AnalogRead(). https://www.arduino.cc/en/Reference/analogRead
9. Figliola, R.S., Beasley, D.E.: Theory and Design for Mechanical Measurements. Wiley, Hoboken (2006)
10. Chatham, A., Walmink, W., Mueller, F.: UnoJoy!: a library for rapid video game prototyping using arduino. In: CHI 2013 Extended Abstracts (2013)
11. De Luca, G.: Fundamental Concepts in EMG Signal Acquisition. DelSys Incorporated (2003)
12. EMG100C – Electromyogram Amplifier Module. https://www.biopac.com/wp-content/uploads/EMG100C.pdf
13. Ando, K., Nagata, K., Kitagawa, D., Shibata, N.: Development of the input equipment for a computer using surface EMG. In: Proceedings of the 28th IEEE EMBS Annual International Conference, pp. 1331–1334 (2006)

14. Blackler, A., Popovic, V.: Editorial: towards intuitive interaction theory. Interact. Comput. **27**(3), 203–209 (2015)
15. Chattopadhyay, D., Bolchini, D.: Motor-intuitive interactions based on image schemas: aligning touchless interaction primitives with human sensorimotor abilities. Interact. Comput. **27**(3), 327–343 (2015)
16. BioNomadix 2CH Wireless EMG Amplifire. https://www.biopac.com/product/bionomadix-2ch-wireless-emg-amplifier/
17. SENIAM. http://www.seniam.org/

Advances in Computational Social Sciences

How Triangle Structure in Inter-firm Human Network Affects Bankruptcy Evolution: An Agent-Based Simulation Study with Real and Artificial Data

Shihan Wang(✉), Mohsen Jafari Songhori, Shuang Chang, and Takao Terano

Department of Computer Science, School of Computing, Tokyo Institute of Technology, Yokohama, Japan
ShihanW@trn.dis.titech.ac.jp, mj24l7@gmail.com, {chang, terano}@dis.titech.ac.jp

Abstract. This paper investigates the influence of human factors on the evolution of inter-firm trade network emerging from bankruptcy. In particular, we concentrate on a local interaction mechanism, conceptualized as triangle structure, within the inter-firm human network. An agent-based model is employed to explore the effects of triangle structure-related properties in both real inter-firm human network constructed from empirical data of thousands Japanese firms, and artificially generated ones. The simulation results confirm the influential role of triangle structure-related human factors in bankruptcy: it not only enhances the benefits that firms can obtain from their inter-firm relationships, but also provides firms with few business partners the equal chance to survive in the bankrupt emergency.

Keywords: Human factors · Triangle structure · Bankruptcy evolution · Agent-based simulation · Inter-firm trade network · Social network analysis

1 Introduction

In order to well understand firms' economic activity, the investigation of their business interactions, which is generated as the inter-firm trade network [1], attracts more and more attention in recent years. While inter-firm trade network keeps evolving slowly over time, the evolution can become very dramatic within a short period when facing external influences like bankrupt [2]. As the bankruptcy often transfers as a chain in the inter-firm trade environment [3], it causes serious socioeconomic concerns. Many scholars have made efforts to study the evolution of inter-firm trade network emerged from bankruptcy. They not only analyzed statistical features from empirical data [4], but also modeled the dynamic propagation process using simulation approaches [5]. Despite implications of these studies, some underlying factors of such evolution have often been ignored in the current literature. Among them, social network among senior executives of companies can be crucial, as most of the business operations in companies are decided by senior executives [6]. One of our recent work indicated the

D.N. Cassenti (ed.), *Advances in Human Factors in Simulation and Modeling*,
Advances in Intelligent Systems and Computing 591, DOI 10.1007/978-3-319-60591-3_26

beneficial effect of such inter-firm human network and examined one of its factors (the number of human partners) within this complex phenomenon [7]. In this paper, we aim to extend the previous work and explore other mechanisms relevant to this human factor in the evolution of inter-firm trade network emerging from bankruptcy.

Particularly, we concentrate on a local interaction mechanism, which is conceptualized as triangle structure within the inter-firm human network contributed by senior executives. A closed triangle structure is indicated as the stable cascade with strong ties [8] and has been well studied among inter-firm collaboration networks [9, 10]. We have extracted real data of senior executives who belong to more than one Japanese firms, which links related firms together and build the inter-firm social network consequently.

The empirical data is first analyzed to examine the importance of triangle structure related properties. Then, an agent-based model is developed to further investigate effects of triangle structure-related factors in both real and artificially generated inter-firm human network. By comparing the simulations of various scenarios, we made two main contributions: (1) we evaluate the impact of triangle structure in inter-firm human network on the evolution of inter-firm trade network resulted from bankruptcy; (2) we measure the importance of triangle structure for individual firms in this bankrupt diffusion phenomenon.

The rest of this paper is organized as follows. In Sect. 2, we review triangle structure in inter-firm human network from both practical and theoretical perspectives. Section 3 presents main parts of our agent-based model. In Sect. 4, we describe the overall simulation configuration and detailed setup, whereas several simulations and their results are analyzed in Sect. 5. Finally, we summarize the paper and discuss some potential explorations.

2 Triangle Structure in Inter-firm Human Network

In this section, we firstly review the importance of triangle structure in the inter-firm human network from both practical and theoretical aspects.

2.1 Empirical Data Analysis

We start with analyzing the role of triangle structure in the real inter-firm human network. The dataset is provided by the joint project of TDB (Teikoku Databank LTD) and Tokyo Institute of Technology, which includes more than 10 years' financial information of billions of Japanese companies. In this work, one industry data from 2005 to 2015 are considered as an inter-firm business environment. According to the historical trade records, about 55,000 trade links construct an inter-firm trade network. At the same time, an inter-firm human network with more than 20,000 ties is extracted, by considering two firms sharing the same senior executive members.

A distinguished difference between the inter-firm human and trade network is first observed in data. Although both inter-firm networks follow a power law degree distribution, their topological structure is quite different. Overall, the inter-firm human network holds a stronger community-related feature, where dense connections are held

between firms in each community (with a modularity of 0.64). Moreover, firms in human network have a low and sparse connectivity by separating in more than 200 components, while all firms are connected in two big components by trade linkages.

In addition, empirical analysis results show that triangle closure is a very important property in inter-firm human network. There are in total 320,608 triangles in the real human network, resulting in an average clustering coefficient at 0.467. The overview of triangle structure in the real inter-firm human network is presented in Fig. 1.

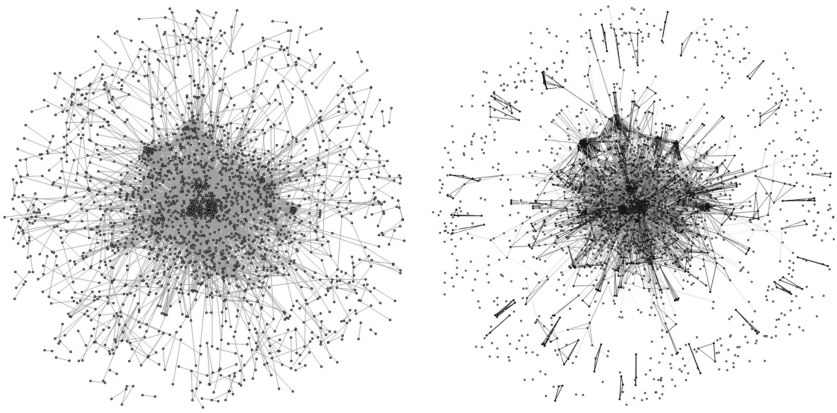

Fig. 1. The observations of the real inter-firm human network. (1) presents an overall snapshot of topology in the network, while (2) represents its triangle closure information, where only close triangle-related edges are shown, and the level of grey scale represents the strength of local clustering coefficient of each firm.

2.2 Theoretical Support

The study of triangle structure (also known as triadic closure or closure) in social phenomenon was pioneered in 1908 by Simmel [11]. He suggested that social 'triad' (a social group with three people) increases the strength and stability between social partners than that in the 'dyad' (two linked people). While 'motifs' with three nodes are emphasized as the cornerstone of building most networks [12], the triangle-related structures are particularly important in social networks [13], where the density of triangles is remarkably high [14]. To simplify the definition, we only consider the closed triangle in the undirected human network as our triangle structure.

Triangle structure in the inter-firm network has also been widely studied in the various organizational phenomenon. In supply network, buyer–supplier–supplier triads offer an interesting managerial decision implications [15]. Phelps's work indicates the beneficial role of 'closure' structure in alliance network on the exploratory innovation of firms [10], while Kreiser suggests that network closure enhances the impact of entrepreneurial orientation on firm's experimental learning [16]. In one recent work, researchers measure the importance of triadic closure within the formation of inter-firm

ties driven by shared directors using exponential random graph models [17]. However, triangle structure in inter-firm human network has not been well studied in the problem of inter-firm trade network evolution rising by bankruptcy.

2.3 Assumption About Importance of Triangle Structure

According to the empirical observation and theoretical base, we propose a hypothesis that: *triangle structure in the inter-firm human network influences the evolution of inter-firm trade network emerging from bankruptcy*. This has been motivating us to further investigate the internal impact of this human factor by agent-based simulation.

3 Agent-Based Model

In order to understand how macro-level phenomenon (i.e. bankrupt evolution) emerge from micro-level factors (i.e. triangle structure-related human factors), an agent-based simulation approach is applied in this work. In total, the agent-based model is proposed to examine two main questions: (1) whether triangle structure in inter-firm human network affects the bankrupt diffusion phenomenon; (2) how human networks with different triangle structure bring a various influence. Investigating these research questions can provide managerial guidelines about proper strategies in defending bankrupt emergencies.

3.1 Entities and State Variables

Three entities and their detailed state variables are given in Table 1. First, the environment entity contains all firms (i.e. agents) and human and trade networks among them. In the environment, simulation time is defined as the timestamp variable, and the average performance of all firms is defined as the social aspiration level [18].

Table 1. Entities and state variables in the model

Entities	Description	State variables
Environment	Overall market environment	agents, timestamp, trade relationship, human relationship, social aspiration level
Agent	Individual firm i	id = i, managers, status, performance, internal fitness, external resource, historical aspiration level
Manager	Senior executive j of firm i	id = j, knowledge vector, fitness

Second, each firm is considered as an agent entity, which holds a status and a performance representing its current economy situation. Among them, the performance is modeled as a weighted summation of the internal fitness and external resource. Moreover, performance history is conceptualized as the historical aspiration level of

agent, it is determined by performance and historical aspiration of the agent at previous simulation time [18].

Third, each firm has a group of senior executives, who are conceptualized as manager entities to measure the inter-firm human relationship. Especially, each manager holds a knowledge set, which is defined as a binary vector. This vector is being updated over simulation period and consequently, that results in updates of fitness.

3.2 Process Overview

An overview of the agent-based model is presented in Fig. 2 [7]. Following the flow, agents take actions to adjust and interact with the environmental over time.

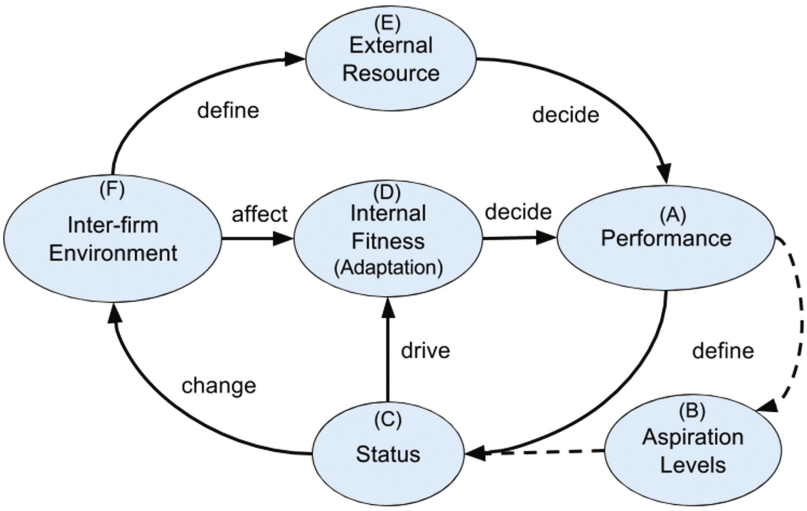

Fig. 2. The overall model flow. According to the circle, each agent holds a performance (A) at every time step. Its economy status (C) is defined by comparing performance with aspiration levels (B), which drives various adaptive behaviors, as well as interactions within the inter-firm environment (F). Then, the agent updates its internal fitness (D) and external resource (E) from self-adaptation and the influence from environment respectively.

3.3 Internal Adaptation

In this model, the design of each agent's internal behaviors follows a common assumption that organizational companies tend to learn from the experience and take actions based on its current performance [19]. In particular, whether its performance attains the goal can determine a variety of economy statuses, which drive this agent to behave differently [20].

By evaluating the performance relative to two well-studied aspiration levels (social and historical aspiration levels [20]), we define three different statuses for agents: healthy, distressed and bankrupt [21], which has been taken in similar risk diffusion

research [22]. The performance of a healthy agent is higher than both aspiration levels, while a distressed agent with a performance in middle starts struggling with the economic emergency. In the worst case, an agent cannot reach the minimum of two aspiration levels and goes bankrupt. In our work, various states transfer from each other. However once an agent is completely failed, it cannot recover from the bankrupt state. The definition formula of performance and details about how agents in different states behave can be referred in our previous paper [7].

3.4 External Interaction

Over time, firms continue interacting with each other in the inter-firm environment. In this regard, trade and human linkages constitute the environmental effects, and they consequently affect the linked firms in various ways.

According to the organizational resource perspectives, inter-firm trade ties are equivalent to the alliance and can provide resource's value to their partners [23, 24]. Thus, the inter-firm trade network affects the external resource of relevant firms in our model.

On the other side, the inter-firm human relationship brings more substantive benefits to social partners [25]. As senior executives communicate with each other during the business actions, they exchange important knowledge [26], which gives social partners access to extra information beyond the local search [27]. Therefore, inter-firm human network affects the internal adaptation of all linked agents. In our model, a firm (i.e. agent) adapts through local search by its managers. With the human relationship, the focal manager can acquire knowledge from both local experience and its social partners. During updates of the fitness, Kauffman NK model [28] is employed to abstractly present the internal situation of each manager. The explanation of external resource and internal adaptation process has been well introduced in our previous paper [7].

4 Simulation Design and Setup

4.1 Simulation Configuration

Both inter-firm trade network and human network are constructed, and they are used as input data for our agent-based simulation. To keep our model consistent with the practical inter-firm environment and validate it implicitly, we apply the extracted real inter-firm human network and artificial inter-firm trade network generated from real properties.

In each simulation run, firstly the inter-firm business environment (i.e. input data) is built, and agents are randomly initialized in three statuses. Following the model flow in Fig. 2, agents keeps adapting, interacting with each other and transiting to different states. Once an agent experienced a completed failure, it goes bankrupt and becomes inactive in the model, which creates new risk to all partners by dissolving its inter-firm links.

Over time, the dissolution of links changes the overall inter-firm environment. Thus, we continuously obverse the features within such evolution to measure the influential factors inside bankrupt propagation process.

4.2 Input Data Generation

This section describes how to generate all inter-firm networks used in our simulations.

As discussed in Sect. 2.1, the inter-firm human network is extracted from real Japanese firms' data and considered as the main input. At the same time, other inter-firm human networks are also generated to examine the effects of different triangle structure-related features. In this paper, average clustering coefficient is considered to measure the density of triangles in a network [29, 30]. In general, higher average clustering coefficient means that the network holds a heightened global triangle structure. In order to obtain resemble networks, we generate artificial networks based on properties of the real inter-firm human network by employing RandNetGen[1] tool. This generator algorithm has been well validated [31] and used to study the effect of a certain topological feature in a network [32]. In this process, we fix the number of nodes (2460 nodes), edges (20041 edges) and degree distribution (power law distribution) of the original network (i.e. real one), but adjust the different average clustering coefficient. The examples of generated networks are shown in Fig. 3 (subfigures (1) – (3)).

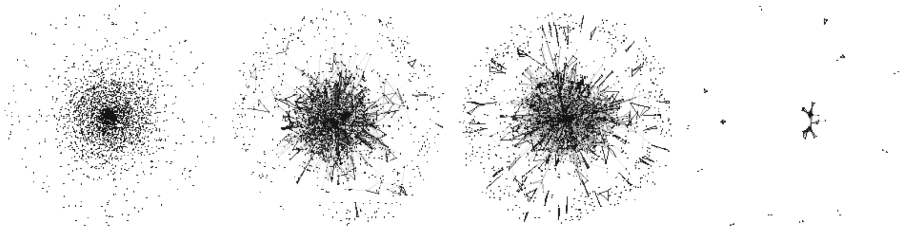

Fig. 3. An observation of triangle closure information in inter-firm human networks. Network (1) and (2) are artificial networks with average clustering coefficient at 0.015 and 0.428 respectively, while network (3) is the extracted inter-firm human network from real data. Panel (4) is a snapshot of the network (3) at time step 10 during the bankrupt simulation.

In addition, the inter-firm trade network with same topological structure is used in all simulations, maintaining the same initial trade environment. The Barabási-Albert model [33] in NetworkX[2] is applied to construct networks with a scale-free property, which matches previous study of the real Japanese inter-firm trade network [34].

[1] Code of RandNetGen can be found in: https://github.com/polcolomer/RandNetGen.

[2] The website of NetworkX library: https://networkx.github.io/.

4.3 Parameter Setting

In our model, there are five senior executives (i.e. managers) in each firm (i.e. agent), which is as same as the real data. Initially, for each simulation run the statuses of all agents are randomly generated once, following a ratio of 1% bankrupt, 9% distressed and 90% healthy. Each simulation is running for 20 timestamps (i.e. 10 years), as each time step represents half a year. Then, this is repeated for 100 experiments. Other parameters corresponding to NK model and variables' definition can be found in our previous paper [7].

5 Simulation Results

In this section, we describe the observation in our simulations and discuss the impact of triangle structure in inter-firm human network in various scenarios. The different scenarios are simulated by importing different input data. We use the same inter-firm trade network with different inter-firm human networks mentioned in Sect. 4.2.

Overall, three sets of results are observed, that are related to (1) whether triangle structure affects; (2) whether triangle structure affects who go bankrupt; (3) whether triangle structure survives.

5.1 Whether Triangle Structure Affects

To study the impact of triangle structure, we first simulate the bankrupt evolution using inter-firm human networks with and without triangle structure (network (3) and network (1) in Fig. 3 respectively). The temporal agent's bankrupt information and social aspiration level are presented in Fig. 4.

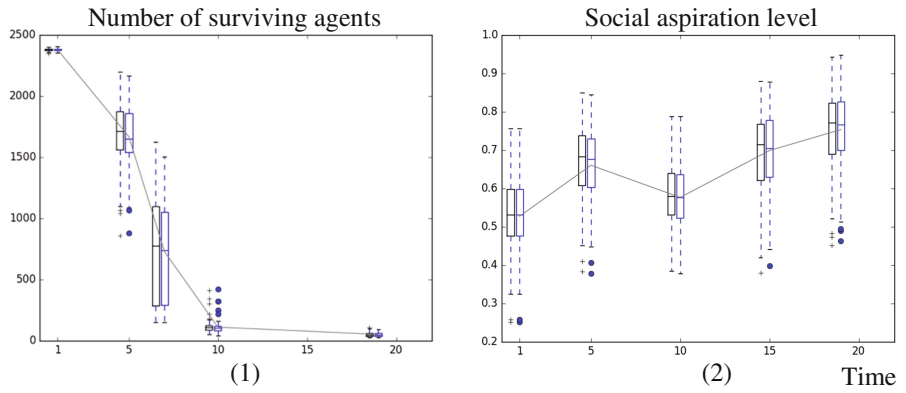

Fig. 4. The number of surviving agents and social aspiration level over time. Blue circle (O) shows information of the real inter-firm human network with average clustering coefficient (abbreviated as CC) at 0.467, while black plus (+) represents the artificial network with 0.015 CC.

Figure 4 shows a similar trend between two scenarios, not only at the median value, but also within the overall scale. This stable phenomenon indicates that presence or lack of triangle structure in inter-firm human network does not significantly affect the global bankrupt distribution and average performance in the inter-firm trade network.

5.2 Whether Triangle Structure Affects Who Bankrupted

In this set of simulations, three inter-firm human networks with different average clustering coefficients are used (network (1) – (3) of Fig. 3). To further study how different triangle structure in inter-firm human network affect the individual firms, some features of evolving human and trade networks are consequently analyzed during the bankruptcy diffusion. Figure 5 shows the comparison among various scenarios, measuring the density of both trade and human network, as well as average clustering coefficient (abbreviated as CC) of the human network.

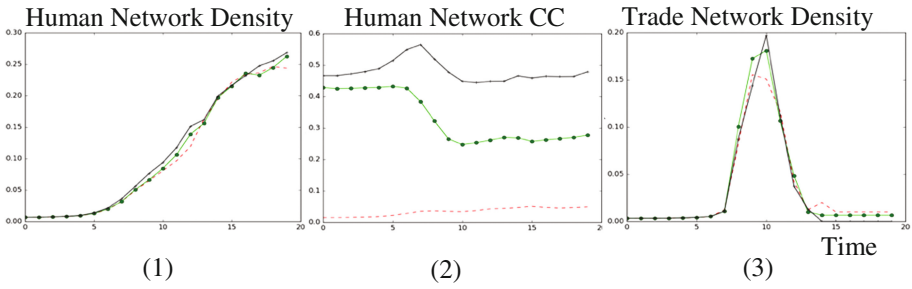

Fig. 5. Three measurements of evolving inter-firm networks over time. The black plus (+) represents the real inter-firm human network with 0.467 CC; green circle (O) contains data of the artificial human network with 0.428 CC; red dotted line (- - -) is the artificial network with 0.015 CC.

In panel (2) of Fig. 5, networks with higher CC keep their advantages on CC during the bankrupt propagation. In the real data case (i.e. black +), the global CC of human network is particularly rising at the early stage of bankruptcy, which implies that firms (i.e. agents) with lower local CC (i.e. within fewer triangles) have higher risk to get bankrupt at the beginning of a bankruptcy emergency.

The different effects of triangle structure in inter-firm human network are also found in subfigures (1) and (3). In general, the higher CC drives a higher density in both human and trade networks. It means, within a human network with higher CC, the firms (i.e. agents) holding high trade and human degree are easier to survive during the bankrupt diffusion. This result shows that triangle structure in inter-firm human network can help firms to obtain more benefits from partners in the inter-firm networks.

Moreover, we observe a correlated influence between the trend of CC in human network and density in trade network. Considering subfigure (2) and (3) together, when triangle structure in human network firstly starts to be widely broken (i.e. CC shows a

quick decrease) at simulation time 7, the density of trade network follows with a dramatic increase, which means most agents with low trade degree are getting bankrupt quickly. Afterwards, the trade density starts to return back, as human network CC becomes stable again around simulation time 10. Such phenomenon suggests that the change of CC in the human network affects which firms go bankrupt in the trade network. For those firms with fewer trade partners, they can still survive in the bankrupt emergency, if their inter-firm human network holds a good triangle structure. It indicates that a stable triangle structure in inter-firm human network can balance the chance of firms with different trade degrees to survive in a bankrupt emergency.

5.3 Whether Triangle Structure Survives

According to clustering coefficient evolution in Sect. 5.2, the CC of inter-firm human networks is getting smooth again in the long term. It drives us to further explore the role of triangle structure in the remaining real human network after dramatic bankruptcy. A snapshot of this real inter-firm human network at simulation time 10 is shown in (4) of Fig. 3.

According to the bankrupt information of Fig. 4, dramatic bankruptcy, as well as CC of inter-firm network, start to reach a smooth state at time 10. Thus, we study this stable network structure (i.e. panel (4) in Fig. 3) held by survived firms at this timestamp. In total, this network has 17 nodes, 21 links and 10 triangles. With average clustering coefficient at 0.43, the survived firms (i.e. agents) holds a strong triangle structure in the human network left. It suggests that triangle structure in inter-firm human network is very significant and helpful for firms to survive after a bankrupt emergency.

6 Conclusion and Discussion

In this paper, we study the impact of triangle structure in inter-firm human network on the evolution of inter-firm trade network emerging from bankruptcy. In particular, an inter-firm human network is extracted from the real Japanese firm data, and used in our agent-based simulation. A series of artificial networks are also generated based on real data, which constructs more scenarios for the simulation experiments. Then, by observing the dynamic evolution of two inter-firm networks, several simulations are analyzed by well-studied measurements. The results present the influential role of triangle structure in inter-firm human network in this phenomenon. Although global triangle-related property does not affect overall bankrupt diffusion distribution obviously, it plays a significant role in determining which individual firms have higher risk of going bankrupt. In general, triangle structure in human network not only enhances the benefits that firms can obtain from their inter-firm relationships. Moreover, the stable triangle structure in inter-firm human network provides individual firms with fewer trade partners the equal chance to survive in the bankrupt emergency.

Similar to any other study, this paper has some limitations that can be potential directions for future research. First, the analysis of simulation results is mostly based on

the macro level in the current work. As firm's strategies related to triangle structure can have implications for the focal firm [15], more micro measurements should be explored to further understand the importance of triangle structure in inter-firm human network. Second, the real inter-firm human network in this work is limited to be extracted from data in one particular industry. Thus, as our model is conceptually designed from general organization theory, we conjecture that the model can be extended to other business environments by feeding extracted features in different data. Finally, more historical data of inter-firm human relationship should be used. We expect to enhance the empirical analysis from various perspectives, exploring not only statistical but also behavioral features within the inter-firm human network.

Acknowledgments. The research is partially supported by the Center for TDB Advanced Data Analysis and Modeling in Tokyo Institute of Technology and JSPS KAKENHI (Grant Number 25240048).

References

1. Ohnishi, T., Takayasu, H., Takayasu, M.: Network motifs in an inter-firm network. J. Econ. Interact. Coord. **5**(2), 171–180 (2010)
2. Aggarwal, C., Subbian, K.: Evolutionary network analysis: a survey. ACM Comput. Surv. (CSUR) **47**(1), 10 (2014)
3. Fujiwara, Y.: Chain of firms' bankruptcy: a macroscopic study of link effect in a production network. Adv. Complex Syst. **11**(05), 703–717 (2008)
4. Hong, B.H., Lee, K.E., Lee, J.W.: Power law in firms bankruptcy. Phys. Lett. A **361**(1), 6–8 (2007)
5. Battiston, S., Gatti, D.D., Gallegati, M., Greenwald, B., Stiglitz, J.E.: Credit chains and bankruptcy propagation in production networks. J. Econ. Dyn. Control **31**(6), 2061–2084 (2007)
6. Robins, G., Alexander, M.: Small worlds among interlocking directors: network structure and distance in bipartite graphs. Comput. Math. Organ. Theory **10**(1), 69–94 (2004)
7. Wang, S., Songhori, M.J., Chang, S., Terano, T.: The impact of human relationship on bankruptcy-related evolution of inter-firm trade network. In: Winter Simulation Conference (WSC), pp. 3405–3416. IEEE Press (2016)
8. Coleman, J.S.: Social capital in the creation of human capital. Am. J. Sociol. **94**, S95–S120 (1988)
9. Schilling, M.A., Phelps, C.C.: Interfirm collaboration networks: the impact of large-scale network structure on firm innovation. Manag. Sci. **53**(7), 1113–1126 (2007)
10. Phelps, C.C.: A longitudinal study of the influence of alliance network structure and composition on firm exploratory innovation. Acad. Manag. J. **53**(4), 890–913 (2010)
11. Simmel, G., Wolff, K.H.: The Sociology of Georg Simmel. Simon and Schuster, New York City (1950)
12. Milo, R., Shen-Orr, S., Itzkovitz, S., Kashtan, N., Chklovskii, D., Alon, U.: Network motifs: simple building blocks of complex networks. Science **298**(5594), 824–827 (2002)
13. Kossinets, G., Watts, D.J.: Empirical analysis of an evolving social network. Science **311**(5757), 88–90 (2006)
14. Newman, M.E., Park, J.: Why social networks are different from other types of networks. Phys. Rev. E **68**(3), 036122 (2003)

15. Choi, T.Y., Wu, Z.: Triads in supply networks: theorizing buyer-supplier-supplier relationships. J. Supply Chain Manag. **45**(1), 8–25 (2009)
16. Kreiser, P.M.: Entrepreneurial orientation and organizational learning: the impact of network range and network closure. Entrepreneurship Theory Pract. **35**(5), 1025–1050 (2011)
17. Howard, M., Cox Pahnke, E., Boeker, W.: Understanding network formation in strategy research: exponential random graph models. Strateg. Manag. J. **37**(1), 22–44 (2016)
18. Greve, H.R.: Performance, aspirations, and risky organizational change. Adm. Sci. Q. **43**(1), 58–86 (1998)
19. Huber, G.P.: Organizational learning: the contributing processes and the literatures. Organ. Sci. **2**(1), 88–115 (1991)
20. Cyert, R.M., March, J.G.: A Behavioral Theory of the Firm, 2nd edn. Prentice Hall, Englewood Cliffs (1963)
21. Cybinski, P.: Description, explanation, prediction–the evolution of bankruptcy studies? Manag. Fin. **27**(4), 29–44 (2001)
22. Basole, R.C., Bellamy, M.A.: Supply network structure, visibility, and risk diffusion: a computational approach. Decis. Sci. **45**(4), 753–789 (2014)
23. Mahoney, J.T., Pandian, J.R.: The resource-based view within the conversation of strategic management. Strateg. Manag. J. **13**(5), 363–380 (1992)
24. Pfeffer, J., Salancik, G.R.: The External Control of Organizations: A Resource Dependence Perspective. Stanford University Press, Palo Alto (2003)
25. Hite, J.M., Hesterly, W.S.: The evolution of firm networks: from emergence to early growth of the firm. Strateg. Manag. J. **22**(3), 275–286 (2001)
26. Bhidé, A.V.: The origin and evolution of new businesses. Oxford University Press, Oxford (2003)
27. Rosenkopf, L., Almeida, P.: Overcoming local search through alliances and mobility. Manag. Sci. **49**(6), 751–766 (2003)
28. Kauffman, S.A., Weinberger, E.D.: The NK model of rugged fitness landscapes and its application to maturation of the immune response. J. Theor. Biol. **141**(2), 211–245 (1989)
29. Newman, M.E.J.: The structure and function of complex networks. SIAM Rev. **45**(2), 167–256 (2003)
30. Schank, T., Wagner, D.: Approximating clustering-coefficient and transitivity. Universität Karlsruhe, Fakultät für Informatik (2004)
31. Orsini, C., Dankulov, M.M., Colomer-de-Simón, P., Jamakovic, A., Mahadevan, P., Vahdat, A., Bassler, K.E., Toroczkai, Z., Boguñá, M., Caldarelli, G., Fortunato, S., Krioukov, D.: Quantifying randomness in real networks. Nat. Commun. **6**(5), 8627 (2015)
32. Colomer-de-Simón, P., Boguñá, M.: Double percolation phase transition in clustered complex networks. Phys. Rev. X **4**(4), 041020 (2014)
33. Albert, R., Barabási, A.-L.: Statistical mechanics of complex networks. Rev. Mod. Phys. **74**, 47–97 (2002)
34. Goto, H., Takayasu, H., Takayasu, M.: Empirical analysis of firm-dynamics on japanese interfirm trade network. In: Takayasu, H., Ito, N., Noda, I., Takayasu, M. (eds.) International Conference on Social Modeling and Simulation, Plus Econophysics Colloquium 2014, pp. 195–204. Springer International Publishing, Cham (2015)

A Preliminary Study of Human Decision-Making, Risk Attitude, and Social Preference on Knowledge Management

Jessica Gu[1(✉)], Ji-Ping Huang[2], and Yu Chen[3]

[1] Graduate School of Frontier Sciences,
The University of Tokyo and Japan Society for the Promotion of Science,
Tokyo, Japan
j.gu@scslab.k.u-tokyo.ac.jp
[2] Department of Physics and State Key Laboratory of Surface Physics,
Fudan University, Shanghai, China
jphuang@fudan.edu.cn
[3] Graduate School of Frontier Sciences, The University of Tokyo, Tokyo, Japan
chen@k.u-tokyo.ac.jp

Abstract. This study aims to introduce a knowledge management (KM) incentive system that induces both monetary and social incentives; probe into the human decision-making nature and attitude towards risks and uncertainty; elucidate the causality between agent's KM motives at microscopic level and organizational outcomes at macroscopic level through strategic individual efforts and social interactions; and unfold the dynamic interplays between intangibles and tangibles. We firstly designed an organizational KM conceptual model with induced monetary incentives that feature: high risk high return for independent effort on innovation (creating new knowledge); low risk low return for dependent effort on imitation (acquiring shared knowledge); and a knowledge bonus which is contributed by collective cooperation and divided based on individual knowledge uniqueness level. Since risks and uncertainty are incorporated, agents have to utilize bounded rationality, psychologically reason upon equal expected utilities, and form strategies when facing two dilemmas: risk seeking vs. loss aversion and competition vs. cooperation. Secondly, we developed a gaming software and implemented the KM model in behavioral experiments to trace the endogenously evolving choices of agents under exogenous policies, capture the dynamic interactions, and observe the emergent properties at macroscopic level through iterations. On top a baseline control setting, three treatments with different interventions were carried out and compared against the baseline. With the empirical evidence obtained, the proposed KM incentive system demonstrated fairness, practicability, and effectiveness. Thirdly, we implemented the KM model into agent-based simulation for systemic prediction and optimization. Through combining the behavioral experiments and agent-based simulation. The microscopic human factors in organizational knowledge management are explored in-depth and the impact on the macroscopic organizational outcomes is revealed and elucidated.

Keywords: Organizational performance · Incentive system · Risk and uncertainty · Competition and cooperation · Agent-based modeling

D.N. Cassenti (ed.), *Advances in Human Factors in Simulation and Modeling*,
Advances in Intelligent Systems and Computing 591, DOI 10.1007/978-3-319-60591-3_27

1 Introduction

In the rapidly growing knowledge economy, knowledge is has been recognized as the key resource of value creation [1] and competitive advantage [2, 3]. Knowledge Management (KM) has been highly valued since its establishment as a formal discipline in 1990s. KM refers to a multi-disciplinary approach to achieve organizational objectives by making the best use of knowledge and improve organizational performance ultimately [4]. Inducing incentives for KM is crucially important, however, the development is still at its infancy. The one that bridges the short-term effort on long-term effect and micro motives on macro outcomes has not yet been available. Besides monetary incentives, bottom-up emergent properties, such as social norms and corresponding impacts on organizational performance are rarely mentioned. Moreover, risks and uncertainty involved in human decision-making are not yet addressed in the KM literature. Hence, this study aims to explore the organizational knowledge management in the context of complex systems under incentive, risks and uncertainty with implementations in both behavioral experiments and agent-based modeling. We propose an organizational KM model with an incentive system that induces both monetary and social incentives; probe into the human decision-making nature and attitude towards risks and uncertainty; elucidate the causality between agent's KM motives at microscopic level and organizational outcomes at macroscopic level; and unfold the dynamic interplays between intangibles and tangibles of value creation.

2 The KM Model

Complex organizational knowledge management is abstracted into a KM model illustrated in Fig. 1. It outlines agent's problem solving KM strategies and its likelihood for success; rules for updating the probabilities, reinforcement learning and knowledge uniqueness; ways of interactions; evaluations of individual successfulness, loss and gains, and collective performance through iterations over time.

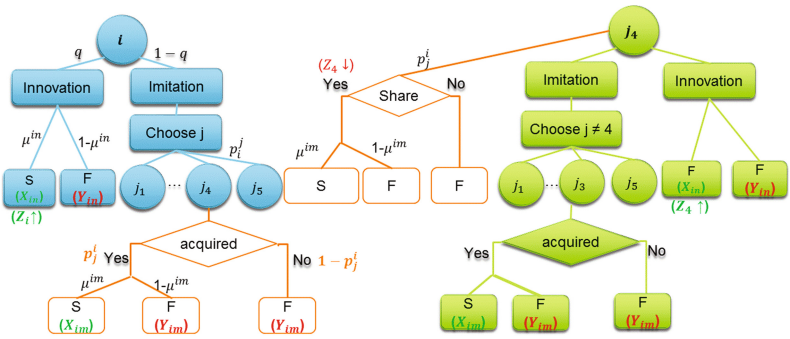

Fig. 1. Framework of the KM model

2.1 The Agent

There are N agents – knowledge workers in an organization. Each agent is striving for better performance and monetary return by choosing either innovation (creating new knowledge independently) or imitation (acquiring shared knowledge dependently). If agent i chooses innovation, under the probability μ^{in} he/she can create a new knowledge and solve the problem successfully, while under the probability $1 - \mu^{in}$ he/she fails. When innovation is successful, agent i's knowledge uniqueness Z_i will increase. If agent i chooses imitation, he/she needs to select whom to learn from and request for the target agent's cooperation. If agent i chooses agent 4, then agent 4 needs to consider whether to cooperate or reject. At this very moment, if agent 4 cooperates and shares his/her knowledge, agent 4 will have to bear a cost of lowering his/her knowledge uniqueness, additionally if agent 4's knowledge uniqueness Z_4 is equal or higher than agent i's, agent i's imitation is successful, otherwise, imitation is unsuccessful. If agent 4 rejects the cooperation request and tries to maintain his/her own competitive advantage, agent i's imitation fails, and agent 4 will not suffer any loss. Agents preserve the freewill to choose either knowledge strategy, choose imitation target and choose to cooperate or not. This freewill is the unique characteristic of human agents. To win, agents have to strategically update the likelihood of choosing innovation q or imitation $1 - q$; the likelihood of choosing other agent p_i^j; and the likelihood of cooperation p_j^i by adaptation and social preferences adjustment.

2.2 The Organization

The organization administrator establishes exogenous policies and managerial interventions to control and optimize the overall outcomes. For instance, managers can adjust the difficulties of the tasks by toning innovation success probability μ^{in}, ranking and promotions intensity Z_i and the size of KM bonus unit B. He/she can also manipulate the information disclosure and accessibility, and adjust the human resources (HR) diversification. It is also the organization's responsibility to evaluate the macroscopic outcomes, such as the organizational performance, the collective knowledge uniqueness, the emergent cooperative culture, and the KM bonus cost effectiveness. The central organizational concern is to identify the best intervention to optimize the macroscopic outcomes.

2.3 The Environment

The environment of the organization is characterized by risk and uncertainty where the successfulness of innovation or imitation is determined by probabilities. Environmental uncertainty can be interpreted as time constrains, incomplete or asymmetric information, cognitive and memory limitations, etc. Meanwhile, innovation is riskier than imitation but yields much higher reward, whereas imitation yields smaller reward but is less risky. Moreover, other agents' choices and performance are unknown. Each agent's choice affects others' payoffs. Incorporating risk and uncertainty is considered more realistic, especially for coping with evolutionary and behavioral aspect of KM.

3 The Incentive System

Incentive is a notion that motivates a human agent to performance a certain action. It is central to all economic activities. Organizations also leverage on incentives to enhance knowledge worker engagement and pursuit collective performance optimization. The role of incentives in organizational behavior has long been studied [5, 6]. Actual strength and value of successful organizations lie in the brainpower of their employees and the connectivity on knowledge sharing, cultural foundation on overall KM effectiveness, and incentives that drive the knowledge processes and forge the organizational norms are crucially important [7]. With previous work laid ahead, this study aims at inducing not only monetary incentives, but also social incentives.

3.1 The Payoff Structure

The monetary incentives for each agent consist of three parts, namely reward for independent innovation, reward for dependent imitation, and knowledge bonus that is determined by the intertemporal cooperation rate $Coop\%$ and bonus unit B. It is then shared based on individual's knowledge uniqueness Z_i. The higher the Z_i, the higher relative ranking position in the organization, thus, the higher bonus one can receive at time t. Vice versa, the lower the Z_i, the lower relative ranking position in the organization, hence lower the bonus one can receive. If the agent has the lowest Z_i, he/she will not receive any bonus from the organization as a penalty. Detailed measurable payoffs and the dynamic update of Z_i is explained in details below.

3.2 The Payoff Function

If agent i chooses innovation, under probability μ^{in} he/she will be successful, hence receives a high return of X_{in}, under probability $(1-\mu^{in})$ he/she will be unsuccessful, hence suffers a big cost Y_{in}. If agent i chooses imitation then he/she selects agent j to learn from, under probability p_j^i agent j will cooperate with agent i, then under probability μ^{im} which is the helpfulness of shared knowledge, agent i. will be successful, hence receive a small return of X_{im}, under probability $(1-\mu^{im})$, agent j's knowledge is not helpful to agent i, hence agent i suffers a small cost of Y_{im}. If agent i chooses imitation then selected agent j, however, agent j rejected the cooperation request under probability $\left(1-p_j^i\right)$, agent i's imitation also is considered as unsuccessful, hence suffers a small cost of Y_{im}. Whether the target can cooperate or not, it is difficult to predict, the initial probability is 0.5 meaning that either accept or reject, and this risk can be manageable through long-term interactions. When trust or altruism emerged, the probability can grow high. At the end of each time, agent's performance π_i and income I_i will be updated, so he/she can adjust the probability of choosing innovation q or imitation $1-q$ in the next time. If agents choose more innovation with high they display a risk seeking behavior while agents choose more imitation with high $1-q$,

they display a loss aversion behavior. Therefore, each individual agent's income I_i at time t, can be calculated by Eq. 1.

$$\begin{aligned} I_i = & q \cdot \left[\mu^{in} \cdot X_{in} - \left(1 - \mu^{in}\right) \cdot Y_{in}\right] \\ & + (1 - q) \cdot \left[p_j^i \cdot \mu^{im} \cdot X_{im} - p_j^i \cdot \left(1 - \mu^{im}\right) \cdot Y_{im} - \left(1 - p_j^i\right) \cdot Y_{im}\right] \\ & + \mathrm{f(B)} \cdot g(Z_i) \end{aligned} \tag{1}$$

where $q \cdot [\mu^{in} \cdot X_{in} - (1 - \mu^{in}) \cdot Y_{in}]$ is the expected utility from independent effort on innovation, $(1 - q) \cdot [p_j^i \cdot \mu^{im} \cdot X_{im} - p_j^i \cdot (1 - \mu^{im}) \cdot Y_{im} - \left(1 - p_j^i\right) \cdot Y_{im}]$ is the expected utility from dependent effort on imitation, and $\mathrm{f(B)} \cdot g(Z_i)$ is the intertemporal knowledge bonus. The expected utilities for both innovation and imitation are kept equal to create the dilemma and ensure that there is no dominant strategy.

3.3 The Bonus Function

In addition to agents' knowledge creation and sharing effort, the organization also rewards them with a knowledge bonus at the end of each round. This knowledge bonus is dynamically changing from time to time. The advantage is of the knowledge bonus is that it bridges the individual self-interests with collective wellbeing. The intertemporal knowledge bonus one can gain is determined by both Eqs. 2 and 3 as shown below:

$$f(B) = \frac{C_{accept}(t)}{C_{request}(t)} \cdot B \tag{2}$$

where $\frac{C_{accept}(t)}{C_{request}(t)}$ is the cooperation rate: number of agents that accepted the cooperation seeking proportion to number of players that requested the cooperation when Imitation is chosen and B is the bonus unit at each period of time.

$$g(Z_i) = \frac{(Z_i - Z_{min})}{\sum_i (Z_i - Z_{min})} \tag{3}$$

which is agent i's ranking position in the organization according to the comparison between his/her knowledge unique with others, where $Z_i(0) \in [0, 1, 2]$. Thus, the higher the cooperation rate, the larger the knowledge bonus size $f(B)$ it is; the higher your relative position in the organization based on the value of Z_i.

μ^{in} is the productivity of a new knowledge is a fixed parameter for each game, e.g. $\mu^{in} = 0.25$; μ^{im} is the helpfulness of the shared knowledge depends on the knowledge uniqueness between agent i and agent j using Heaviside Function:

$$H(Z_j - Z_i) \geq 0 \; \mu^{im} = 1; \; H(Z_j - Z_i) < 0 \; \mu^{im} = 0 \tag{4}$$

Knowledge Uniqueness Z_i Update is guided as follows:
If Innovation is successful, knowledge uniqueness increases by:

$$Z_i' = Z_i + \alpha \cdot (Z_{max} - Z_i) \tag{5}$$

If Cooperation is accepted, knowledge uniqueness decreases by:

$$Z_i' = Z_i - \beta \cdot (Z_{min} - Z_i) \, where \, \alpha > 1 \gg \beta \tag{6}$$

Under such exogenous reward policy, agents need to act strategically when facing a dilemma between the keeping of individual profit and the optimization of collective performance. Hence, the evolving processes of individual behavioral and struggling decision-making is visualized. Furthermore, the most suitable incentive policy, which motivates the agents and unleashes their innovation potentials, can be identified and tested; and the conditions for cooperative and competing behaviors can be identified.

3.4 Two Dilemmas

The agent's iterative decision-makings are cast with two dilemmas, namely risk-seeking vs. loss-aversion, and competition vs. cooperation.

Dilemma 1 on Uncertain Payoffs and Risk Attitude: Loss Aversion vs. Risk Seeking. Many studies have laid a significant foundation for studying human decision-making under risk and uncertainty. Because of incomplete information, time constrains, and cognitive limitations, etc., human agents are not behaving rationally as they think they do. For example, some seminal work, e.g. bounded rationality [8] and prospect theory [9], indicates that people make decisions by bounded rationality and heuristics. These behavioral economics theories reveal that human agents have a hypothetical value function in decision-making that is concave for gains and convex for losses, and much steeper for losses than for gains and overweight small probabilities and underweights moderate and high probabilities event [9]. Hence, when implementing proposed KM incentive model, the key task is to find the critical condition for discovering the human attitude towards KM strategies and tracking the evolving choices on KM strategies to obtain the weighting value that human agents place on each strategy.

Dilemma 2 on Social Preference: Competition and Cooperation. At intra-organizational level, coopetition occurs between individuals or functional units. Based on game theory and social interdependence theories, some studies investigate the presence of simultaneous cooperation and competition among functional units, the antecedents of coopetition, and its impact on knowledge sharing behaviors [10]. For example, the notion of cooperative knowledge sharing is developed to explain mechanisms through which coopetition influences the intensity of knowledge sharing among human agents [11]. The underpinning statement is that while organizational function units need to cooperate, they are likely to face some competition. Under what conditions cooperation can arise is the central concern when designing the incentive system.

A widely studied phenomenon in the social studies of cooperative behavior are the situations known as social dilemmas: namely those where pure rationality leads to collective irrationality [12]. Well-known examples of social dilemmas are the tragedy of the commons, where overuse of shared resource by beneficiaries (such as herders) would result in its ultimate depletion [13], and the phenomenon of free ride, where individuals are tempted to enjoy a common resource without contributing to it [14]. It has been suggested that knowledge sharing can be understood as a special case of a social dilemma [15]. That is, if we consider knowledge as a common resource of an organization, individual workers are often faced with the questions of whether or not, to what extent, and under what circumstances should they contribute to this common property. Thus, this topic is getting attention for investigation in the KM field. Hence, this dilemma aims at utilizing incentive policy to explore the agents KM behaviors when facing competition vs. cooperation. It also aims at elucidating how social norms emerged and organizational outcomes are affected.

4 Behavioral Experiments

The behavioral experiments for the study take place in Department of Physics, Fudan University, Shanghai, China. The purpose for implementing the proposed KM incentive model in the behavioral experiments first is to test the proposed KM model, gain empirical evidence, and demonstrate the applicability of incentive systems for exploring various administrative interventions.

4.1 The Gaming Software Development

The implementation process includes game preparation and gaming software development; participant recruitment, scheduling, briefing, and warm-up trials; four gaming sessions execution; and data analysis. The gaming software is developed in accordance with the proposed KM model illustrated in Fig. 1. It is written in Python and has four modules, namely player interface, control panel, computation engine, and database.

4.2 Baseline and the Interventions

Overall four games exploring different administrative interventions are decided. Game One is the baseline used as a controlled group for comparison, parameter settings are listed in Table 1; Game Two is designed with a big bonus unit for each round. Bonus unit is tuned from $B = 20$ to $B = 30$ for promoting organizational knowledge uniqueness; Game Three is with reputation information disclosing agents' number of cooperation seeking and giving, inducing a social incentive and promoting cooperative culture; and Game Four is with diversified agents, meaning that each agent has different innovation capabilities, e.g. $\mu_1^{in} = 0.1$; $\mu_2^{in} = 0.2$; $\mu_3^{in} = 0.1$; $\mu_4^{in} = 0.4$; $\mu_5^{in} = 0.1$; $\mu_6^{in} = 0.6$. It aims at preserving diversity and optimizing organizational performance. Game Two requires financial delegation from the organization; Game Three uses information control and social incentives; Game Four targets human resource hiring

Table 1. Baseline parameter settings

Notation	Definition	Initial value
μ^{in}	Productivity of the new knowledge	0.25
μ^{im}	Helpfulness of the shared knowledge	0.5
X_{in}	Reward for successful innovation	30
X_{im}	Reward for successful imitation	6
Y_{in}	Cost for unsuccessful innovation	10
Y_{im}	Cost for unsuccessful imitation	2
$Z(0)$	Initial knowledge uniqueness	0 or 1 or 2
B	Bonus unit	20
N	Number of players	6

strategy to create a diversified mix of people with different abilities. The effectiveness of each intervention, agents' adaptive interactions, and collective outcomes are revealed and compared.

4.3 Behavioral Experiments Execution

There are twelve graduate students recruited to participate in the game. There are another two research assistants facilitating the experiments since they are experienced in conducting behavioral experiments. Six participants play each game simultaneously. Hence, participants are divided into two groups playing two games at the same time in separate rooms. Agents are randomly assigned with different User IDs and passwords, so no prior preference or bias is introduced to the experiment. Before formally playing the games, all the participants attend the briefing session as well as the warm-up trials, and hence, they are clear about the rules and familiar with all the functions and features. Each game is played 50 rounds and it lasts for 40 min. At the end of the game, participants are rewarded with cash based on their income score. The player with lowest income cannot receive any financial reward as a penalty; however, he/she receive a small souvenir for devoting time and effort. The budget for each game is RMB600. If shared evenly by five players, each can gain RMB120 for 40-min play, which is roughly two to three times higher than the hourly rate for a part-time job. Thus, during the gaming challenge, participants are highly motivated and engaged.

4.4 Results and Comparisons

To compare with baseline. Table 2 summarizes macroscopic results.

On Organizational Performance. Comparing with Baseline, all other cases with administrative interventions are effective since the problem solving rate has been improved, meaning that the organization successfully solve more problems than the baseline setting.

Table 2. Preliminary result summary

	Organizational Performance (Problem Solving%)	Organizational Innovativeness $\bar{q}$	Cooperation Culture Coop%	Organizational Knowledge Uniqueness	Bonus Cost
Baseline	22.67%	0.48	36%	0.32	348.66
Big Bonus	29.33%	0.52	69.13%	4.16	975.50
Reputation	40.67%	0.46	94.53%	-0.28	928.66
HR Diversification	59.67%	0.64	94%	4.14	925.00

On Cooperative Culture. The organizational cooperation rate (Coop%) has been improved as well, indicating that the interventions are effective on enhancing a cooperative culture. This is particularly noteworthy in the reputation case and the HR diversity case. When reputation information is disclosed, agents have a strong motivation or social pressure to cooperate with others in order to build a good social image. This suggests that reputation or social image is a very effective non-monetary incentive to allow cooperation to arise. In the HR diversity case, when some agents are good at innovation and having very high knowledge uniqueness, he/she has high motivation to capitalize the knowledge, cooperate with others, and transform the knowledge uniqueness to bonus, meanwhile, some agents are poor at innovation and having low knowledge uniqueness, he/she has high motivation to approach the innovative agents for imitation. When knowledge customer finds knowledge supplier, the cooperation rate increases significantly.

On Organizational Knowledge Uniqueness. Not all the three interventions improve organizational knowledge uniqueness, for big bonus and HR diversity cases, the organizational knowledge uniqueness can be very well maintained, while in the reputation case, it is fading away meaning that the collective knowledge is blended among agents under a strong cooperative culture and knowledge sharing engagement. This reveals human irrationality but it makes sense because when reputation information is disclosed, agents are more likely to cooperate and share knowledge to build a good reputation even suffering from individual knowledge uniqueness decrease.

On Organizational Innovation Engagement. The reputation case shows that it is not an effective intervention for maintaining good innovation, since it motivates people to choose more imitation indicated by collective decision-making behavior ($\bar{q} < 0.5$); whereas big bonus and HR diversity cases promote cooperation culture without hurting innovation.

In summary, the developed incentive system is preliminarily proven effective and fair, yet future refinement is needed. Overall, the most cost-effective administrative intervention for enhancing and balancing all aspects of the organizational outcome is the HR diversity policy. The finding suggests that it is the most cost effective way if manager hires employees with diversified innovation ability. It also suggests that diversity is crucially important to the organization in the long-term as a complex adaptive system.

5 The Agent-Based Model, Simulations, and Results

Following the behavioral experiments, the gaming sessions are preliminarily modeled. All the functions and features follow the conceptual framework illustrated in Fig. 1. The agent-based model is modified on top of a previous model developed by the authors (please refer to [16]). The probabilistic decision behaviors are newly modeled. Three variables indicating agent's adaptive decision-making, namely probability of choosing KM strategy q_i, probability of choosing imitation target p_i^j and probability of cooperation r, are crucially important yet difficult to achieve.

5.1 Results and Comparisons

For adjusting the probability of choosing innovation q_i, agents still follows experience-weighted attraction (EWA) learning rule, e.g. updating the strategy attraction factors at each round. However, this KM model has an incentive system that use monetary income to motivate agents for strategic choosing the better options. Hence, a condition is added to the learning rule, that is: if the current round income is less than the recent five rounds' average, the strategy attraction factor B_i^{in} for innovation and B_i^{im} for imitation will not be updated. Five rounds can be adjustable, indicating agents' memory. For probability of choosing imitation target p_i^j, there is no need to add conditions. Based on previous attraction to each target factor A_i^j makes much sense, meaning that if agent j helped agent i successfully improve the performance, agent j's attraction to agent i in the next round will increase by one unit. For the probability of choosing to cooperation r, based on behavioral experiment empirical evidence shown in Fig. 2, agents mostly choose to cooperate when their own knowledge uniqueness Z_i. is higher than the organizational average Z_{avg}, while choose to reject when their own knowledge uniqueness Z_i is lower than the organizational average Z_{avg}. Hence, the probability of choosing to cooperation r, is a rule-based adjustment.

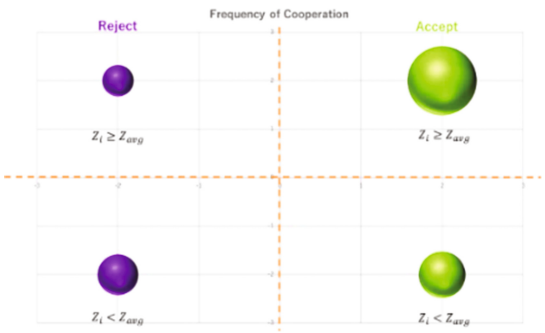

Fig. 2. Frequency of cooperation with reference on knowledge uniqueness

5.2 Results and Comparisons

Preliminary results are generated from the Agent-Based Simulation. Each game is run 1000 rounds. Results are averaged over 10 runs to avoid randomness. Figures 3 and 4. are the baseline results. Organizational vs. Individual Knowledge Uniqueness and Individual Income are steadily improved. Shown in the right chart of Fig. 4, after roughly about 200 rounds, specializatn can be identified, meaning that some agents are specialized in innovation while others are in imitation. More in-depth and detailed investigations on Agent-Based Simulation results are needed in the future work.

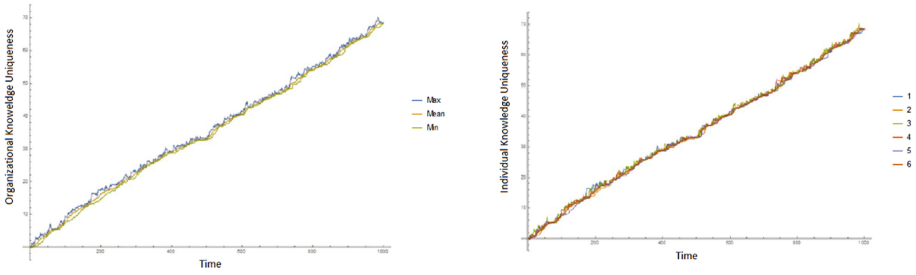

Fig. 3. Organizational vs. individual knowledge uniqueness in baseline case

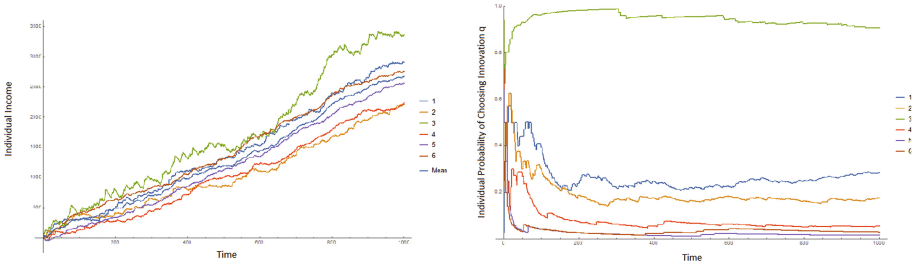

Fig. 4. Individual income and probability of choosing innovation in baseline case

The results of Big Bonus (from $B = 20$ to $B = 30$) and HR Diversity case ($\mu_1^{in} = 0.1$; $\mu_2^{in} = 0.6$; $\mu_3^{in} = 0.1$; $\mu_4^{in} = 0.4$; $\mu_5^{in} = 0.1$; $\mu_6^{in} = 0.2$) are also presented below. However, Reputation case is extremely difficult to model at the moment. Hence, it is expected to be achieved in the future study. From the simulation charts obtained (listed below from Figs. 5, 6, 7 and 8), results are in accordance with the behavioral experiments qualitatively, for instance, the knowledge uniqueness and income in HR diversity case are the highest. However, further investigation is needed, and the model verification needs to be done as well.

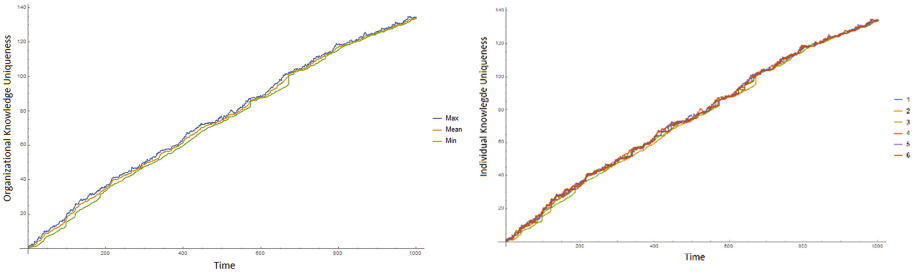

Fig. 5. Organizational vs. individual knowledge uniqueness in big bonus case

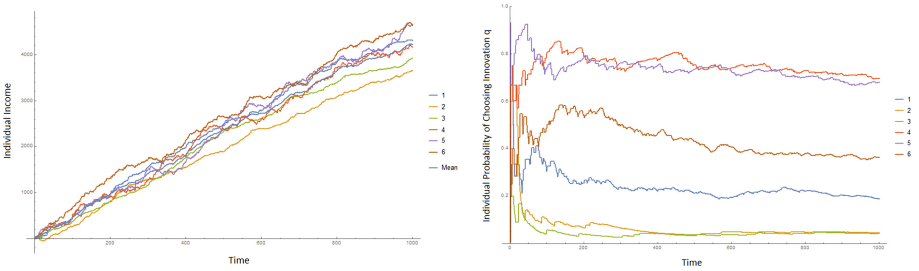

Fig. 6. Individual income and probability of choosing innovation in big bonus case

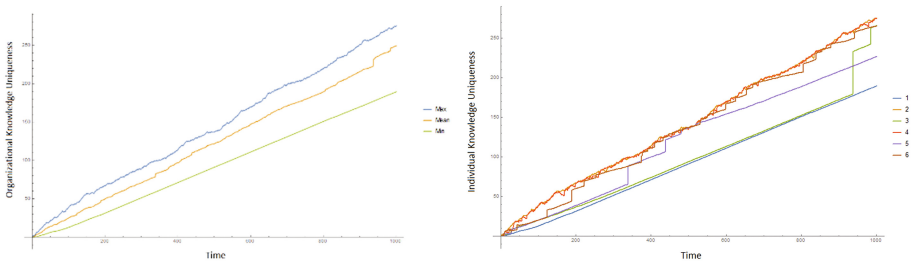

Fig. 7. Organizational vs. individual knowledge uniqueness in HR diversity case

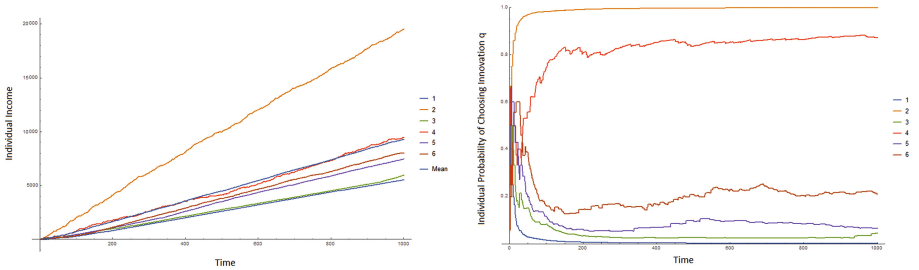

Fig. 8. Individual income and probability of choosing in HR diversity case

6 Discussion

On Reputation, Cooperative Culture and Organizational Performance. Although additional experiments are required to gain statistically significant evidence, it is observed that under the incentive system proposed in this study, human agents exhibit an intrinsic social motivation for building a good reputation on top of the monetary gaining. With interaction among each other throughout time, the cooperative culture as a social norm emerged from the bottom-up. Results indicate, depend on the situation, various intensity of cooperative culture sometimes have positive impact on organizational performance at the macroscopic level, but sometimes negative.

On the Dynamic Interplays Between Tangibles and Intangibles. Through investigation on the dynamic process of the experiments, it is observed that human agents put effort on forming strategies to win. Sometimes they are willing to suffer monetary cost in the short-term to gain social rewards, thus lead to higher profitability in the long-term indirectly. Meanwhile, for organization, it utilizes tangibles e.g. rewards and bonus, to allow intangibles e.g. new knowledge, shared knowledge, and reputation, to emerge. Through time development, in return, the organizational knowledge uniqueness, structure and network reliability, and cooperative culture, etc., foster better problem solving and organizational performance eventually. The KM model of this study demonstrates advantages in observing dynamic interplays between tangibles and intangibles.

On Human Nature in Behavioral KM. Another merit of this study is that the KM incentive model preserves the human free will and social preference on KM decision-makings, and incorporates risk and uncertainty into consideration. These have not yet been receiving enough attention in the field of study. Hence, this preliminary attempt lays empirical foundation and paves the way for establishing a new field of study on behavioral KM in the future.

7 Conclusion

7.1 Achievement

In this preliminary study, an effective incentive system was established successfully to probe into two dilemmas, namely risk-seeking vs. loss-aversion and competition vs. cooperation. Agents' endogenous behaviors against exogenous KM policy-making has been disclosed. Furthermore, administrative interventions on promoting innovation, cooperative culture, and diversity have been identified and evaluated. Through the design of knowledge bonus, it bridges the self-interest agents at the microscopic level to the consideration of organizational benefit at the macroscopic level. Thus, the cooperation arises for gaining indirect benefit. Social interactions and interdependency were incorporated in all four cases, but it was especially highlighted in reputation case, implying that too much cooperation can be good for fostering cooperative culture, but harmful for organizational knowledge. Such integrated approach demonstrated novelty

and versatility in explaining various casual relationships, conditions, and effectiveness of interventions. With the empirical evidence obtained, the proposed KM incentive system demonstrated fairness, practicability, and effectiveness.

7.2 Future Work

The nature of human decision-making, risk attitude, and social preference are broad, complex and deep study. Although the proposed study integrate both behavioral experiment for gaining empirical evidence and agent-based modeling for long-term prediction and optimization, the current progress only achieved preliminary results and the agent-based model needs to be verified rigorously. Hence, in the short-term, more iterative experiments are needed to obtain statistically significant data. In the long-term, future research will keep focusing on the human heuristics at microscopic level, social norms at macroscopic level, and how these influence the organizational behavior and outcomes.

Acknowledgements. The research work was funded by Grants-in-Aid for Scientific Research (#15J07801) of Japan Society for the Promotion of Science, Tokyo, Japan. The authors would like to express their sincere gratitude to the great support.

References

1. Payne, A.F., Storbacka, K., Frow, P.: Managing the co-creation of value. J. Acad. Mark. Sci. **36**(1), 83–96 (2008)
2. Addicott, R., McGivern, G., Ferlie, E.: Networks, organizational learning and knowledge management: NHS cancer networks. Public Money Manag. **26**(2), 87–94 (2006)
3. Drucker, P.F.: Managing in a Time of Great Change. Harvard Business Press, Brighton (2009)
4. King, W.R.: Knowledge management and organizational learning. Springer, US (2009)
5. Herzberg, F., Snyderman, B.B., Mausner, B.: The Motivation to Work. Wiley, Hoboken (1966)
6. Whyte, W.F.: Money and motivation. Harper, New York City (1955)
7. Liebowitz, J., Megbolugbe, I.: A set of frameworks to aid the project manager in conceptualizing and implementing knowledge management initiatives. Int. J. Proj. Manag. **21**(3), 189–198 (2003)
8. Simon, H.A.: Administrative behavior: a study of decision-making processes in administrative organization (1957)
9. Kahneman, D., Tversky, A.: Prospect theory: an analysis of decision under risk. Econometrica: J. Econometric Soc. 263–291 (1979)
10. Armstrong, M.: Employee Reward. CIPD Publishing, Wimbledon (2002)
11. Dalkir, K., Liebowitz, J.: Knowledge Management in Theory and Practice. MIT Press, Cambridge (2011)
12. Kollock, P., et al.: The Possibility of Cooperation, 672–676 (1992)
13. Hardin, G.: The tragedy of the commons. Ekistics, 168–170 (1969)

14. Sweeney, J.W.: An experimental investigation of the free-rider problem. Soc. Sci. Res. **2**(3), 277–292 (1973)
15. Cabrera, A., Cabrera, E.F.: Knowledge-sharing dilemmas. Organ. Stud. **23**(5), 687–710 (2002)
16. Gu, J., et al.: Simulation of an organization as a complex system: agent-based modeling and a gaming experiment for evolutionary knowledge management. In: Kaneda, T., Kanegae, H., Toyoda, Y., Rizzi, P. (eds.) Simulation and Gaming in the Network Society, pp. 443–461. Springer, Singapore (2016)

A Stock Market Model Based on the Interaction of Heterogeneous Traders' Behavior

Ye Yuan[1(✉)], Xuebo Chen[1(✉)], and Qiubai Sun[2]

[1] School of Electronics and Information Engineering, University of Science and Technology Liaoning, Anshan 114051, Liaoning, China
yuanye2882@l26.com, xuebochen@l26.com
[2] School of Business Administration, University of Science and Technology Liaoning, Anshan 114051, Liaoning, China

Abstract. Human factors determine the behavior of people and further influence the interaction of people. In the stock market, traders usually determine their investment strategy not only according to their own viewpoints but also take some advice of others at various degrees. The heterogeneity and irrational behavior of traders in the stock market affect stock price volatility. This paper constructs a model describing the interaction of heterogeneous traders by introducing Lotka-Volterra equation that can properly represent the complex interaction of heterogeneous groups of creatures. We analyze the quantitative variation of heterogeneous traders under various degrees of herding effect, and explore the relationship between stock price and herding effect. Besides, plenty of nonlinear dynamics are shown and we consider that this may available to explain common phenomena in the stock market system.

Keywords: Human factors · Heterogeneous traders · Herding effect · Stock market system

1 Introduction

With the development of system science, it has been found that the research of cross-disciplinary subject is a potential and charming work. The open complex system among system science theory widely exists in the real world. For example, complex interaction and significant heterogeneity exist among a large amount of elements in various systems, such as, ecosystem, human body system and social system. It is obvious that stock prices move up and down and even the global economic situation in the economic system are both related to the character of complex systems. Considering the complex feature, scholars in the economic field are trying to study the causes of stock price volatility in many aspects.

For a review of agent-based financial market models, in [1], Huang and Day discovered that chartists different from fundamentalists are only the active group when the stock price is close to fundamental value. However, new additional fundamentalists

D.N. Cassenti (ed.), *Advances in Human Factors in Simulation and Modeling*,
Advances in Intelligent Systems and Computing 591, DOI 10.1007/978-3-319-60591-3_28

will enter the market and they have no demand at first when the stock price deviates sharply from the fundamental value. As described in [2] by Tramontana et al., there are always some active chartists and fundamentalists in the market. When there was a large deviation between the stock price and fundamental value, new fundamentalists and chartists are both able to entry into the market though their demands are not zero at first.

Heterogeneous traders in agent-based financial market models are classified by the difference of the investment behavior of traders. In our paper, we focus on herding effect that generated by the interaction of plenty of herding behavior of heterogeneous traders. The discussion about the interaction of a group of people appeared in the concept of synergetics in [3]. As described in [3] by Haken, the regularity found in the form of fog and the aggregation of cells is able to explain phenomena in sociology, namely, the behavior of all the people in the group seems to tend to a new idea (or fashion) and people in the whole group behave similarly in a short time. Besides, in [4], Scharfstein and Stein concluded that managers prefer to ignore their own significant informations and follow the investment strategy of other people when they consider their reputation is more important. In [5], Avery and Zemsky showed that speculators in the stock market are able to emerge herding behavior under different dimensions of uncertainty. Herding behavior is related to excess volatility and price bubbles. Herding behavior can also generate snowball effect, since a number of traders prefer to mimic the major investment strategy or the trend in past trends when they are unable to distinguish which information is efficient.

The idea of our model is inspired by following papers, for instance, as described in [6] by Delong, a model was constructed, which contains two kinds of traders (noise traders and sophisticated investors) in the financial market. He also found behavior of traders changed as a response to noise trading and plenty of stylized facts of financial market were successfully explained by the idea of noise trader risk. Besides, the key mechanism in our model is similar to [7, 8]. In our paper, we focus on the interaction between heterogeneous traders and discuss the nonlinear relationship between traders and stock price. We discover that the average rationality and investment attitude in the stock market is greatly influenced by the degree of herding effect.

2 Model Construction

In this section, we seek to explore the interaction between speculators by establishing a model based on [7–9]. We also consider there are two kinds of traders which defined as fundamental traders and noise traders in the stock market model. Each kind of heterogeneous traders is further divided into buyers and sellers. Therefore, we get four kinds of traders (fundamental buyers, fundamental sellers, noise buyers and noise sellers). Generally, the fundamental trader group consists of the rational and experienced individuals (e.g. institutional investors, perspicacious experts and experienced investment analysts). The noise trader represents the people who are irrational and lack of sufficient experiences (e.g. impressionable investors and new traders who just enter into the market etc.). An inspiration comes from complex nonlinear relationship and the famous Lotka-Volterra equations (see [10, 11]) that can be used to demonstrate some

nonlinear dynamics in the stock market. In this paper, we mainly aim at the interaction between heterogeneous traders in the stock market system, and some setup are familiar with [8]. Besides, we use the asset price function mentioned in [9] to represent some dynamics of the stock price. We assume that there is only one asset in the model, and then we draw attention to the interaction relationship between heterogeneous traders under this circumstance. Furthermore, we put forward the discrete Lotka-Volterra equation which contains the information of stock price volatility and the nonlinear interaction relationship between heterogeneous traders as follows:

$$\begin{cases} X_1(t+1) - X_1(t) = k_1 X_1[1 - \sigma_{11} X_1(t)/N + \sigma_{12} X_2(t)/N + \sigma_{13} X_3(t)/N] \\ X_2(t+1) - X_2(t) = k_2 X_2[1 - \sigma_{22} X_2(t)/N + \sigma_{21} X_1(t)/N + \sigma_{24} X_4(t)/N] \\ X_3(t+1) - X_3(t) = k_3 X_3[1 - \sigma_{33} X_3(t)/N + \sigma_{31} X_1(t)/N + \sigma_{34} X_4(t)/N] \\ X_4(t+1) - X_4(t) = k_4 X_4[1 - \sigma_{44} X_4(t)/N + \sigma_{42} X_2(t)/N + \sigma_{43} X_3(t)/N] \\ P(t+1) - P(t) = \lambda \arctan(\theta X_{t+1}) \end{cases} \quad (1)$$

In Eq. (1), the variable X_i (t) represents the total number of individuals in group i (i = 1, 2, 3, 4, representing fundamental buyers, fundamental sellers, noise buyers and noise sellers respectively). The parameter k_i is the nature growth rate of group i, and the parameter N is recognized as growing space in typical Lotka-Volterra equation. However, in this paper, N can be explained as a generalized growing space that is related with the total number of all the traders in stock market. The variable P represents the stock price, and the variable X_{t+1} is the market average investment attitude in t + 1 moment (see Eq. (2)). The parameters λ and θ show the degree of the stock price adjusts to the investment attitude of overall traders. The parameter σ_{ij} shows the degree that group i are influenced by group j, particularly, it represents the degree of the growing limit of group i when $i = j$ (i, j = 1, 2, 3, 4).

3 Model Analysis

The transition between heterogenous traders can be considered as the result of interactions between heterogenous groups of traders. So in our paper, we regard the coefficient of interactions between heterogenous traders as transition rate. In addition, noise traders are willing to understand and follow other people's behavior that is considered as valuable information about the future market trend. They also pay close attention to the passed market trend that is regarded as powerful evidence on probable future market trend. Actually, expectations on the future market trend have a great impact on stimulating plenty of heterogenous groups of traders to pursue maximization of benefits. Besides, fundamental traders use a different strategy to pursue benefits, that is, their expectations on future market trend are based on fundamental value of the stock. They have confidents in the future trend that the stock price will eventually back to its fundamental value no matter how sharply oscillate in the earlier stage. In [8], Lux shown that heterogenous traders can exit and enter into the market in a constant portion. While, in our paper, a relatively free rule that allows heterogenous traders constantly exit and enter into market is proposed.

Different from the total number of heterogenous traders is constant mentioned in [8], in our model, however, heterogenous traders can freely exit and enter into market under various circumstances. Besides, similar with [8], we define that market average investment attitude is related to the difference between the number of total buyers and total sellers. So the market average investment attitude at t + 1 moment in Eq. (1) is:

$$X_{t+1} = \frac{X_1(t+1) + X_3(t+1) - X_2(t+1) - X_4(t+1)}{X_1(t+1) + X_2(t+1) + X_3(t+1) + X_4(t+1)} \tag{2}$$

In Eq. (2), X_t fluctuates in [−1, 1], It means there are more buyers in the market and the overall market emerge a positive state when $X_t > 0$, otherwise, the market under a negative state when $X_t < 0$.

Internal factors in the interaction of heterogenous groups of traders are the transition between them. For instance, fundamental buyers and fundamental sellers will switch between each other when the stock price is higher or lower than the fundamental value. Besides, according to the constantly changing market average investment attitude and the stock price, noise buyers and noise sellers will switch between each other. The transition between fundamental traders and noise traders may occur when other investment strategies can bring much more profits in a relatively short period. In order to focus on the interaction between heterogenous groups of traders, we temporarily consider that there has only one asset in the stock market and a group of traders can not switch to two other groups at the same time at any moment *t*. Following the articles (see [7, 8]), we define the transition rate between heterogenous groups of traders as follows.

3.1 Definition 1

The transition rate from fundamental buyer traders to fundamental seller traders and the opposite transition rate:

$$F_{bs} = v_{bs} exp[-\beta(P_m - P_t)/v_{bs}],\ F_{sb} = v_{sb} exp[\beta(P_m - P_t)/v_{sb}]. \tag{3}$$

The transition rate from noise buyer traders to noise seller traders and the opposite transition rate:

$$N_{bs} = v_{bs} exp[-\gamma X_t - \eta(P_t - P_{t-1})/v_{bs}],\ N_{sb} = v_{sb} exp[\gamma X_t + \eta(P_t - P_{t-1})/v_{sb}]. \tag{4}$$

The transition rate from fundamental buyer traders to noise buyer traders and the opposite transition rate:

$$\begin{aligned} B_{FN} &= v_b exp\{\alpha[[(P_t - P_{t-1})/v_b]/P_t - R - \mathrm{s}|(P_t - P_m)/P_t|]\}, \\ B_{NF} &= v_b exp\{-\alpha[[(P_t - P_{t-1})/v_b]/P_t - R - \mathrm{s}|(P_t - P_m)/P_t|]\}. \end{aligned} \tag{5}$$

The transition rate from fundamental seller traders to noise seller traders and the opposite transition rate:

$$\begin{aligned} S_{FN} &= v_s exp\{\alpha[R - [(P_t - P_{t-1})/v_s]/P_t - \mathrm{s}|(P_t - P_m)/P_t|]\}, \\ S_{NF} &= v_s exp\{-\alpha[R - [(P_t - P_{t-1})/v_s]/P_t - \mathrm{s}|(P_t - P_m)/P_t|]\}. \end{aligned} \tag{6}$$

In Definition 1, the parameter P_m represents the fundamental value to which the stock price tends when market is in equilibrium. v_{bs} and v_{sb} are positive denoting the velocity of transition between buyers and sellers. Similarly, v_b is positive measuring the velocity about transition between fundamental buyers and noise buyers. Relatively, v_s is positive measuring the velocity about transition between fundamental sellers and noise sellers. Traders change their investment strategy when the stock price deviates from the fundamental value, and the time scale of it may be written as $(P_m - P_t)/v_{sb}$. The parameter β and η are positive measuring the strength of stock price influences on fundamental traders and noise traders respectively. Moreover, β and η can also measure the degree of arbitrage behavior of fundamental traders and agitated behavior of noise traders respectively. When facing different values among various investment strategies, traders behave differently, and we use the parameter α to represent the level of the sensitivity of traders. Besides, noise traders prefer to invest a stock when the profit of this investment strategy is higher than the average profit of other investment strategies, and this average profit is represented by R. So the extra revenue they can get may be written as $(P_t - P_{t-1})/v_b/P_t - R$. However, fundamental traders firmly believe the future trend of the stock price will return to its fundamental value sooner or later. We assume the discount rate is s, $0 < s \leq 1$, so the extra revenue they can get may be written as $s|(P_t - P_m)/P_t|$. The parameter γ is positive measuring the strength of the influence that noise traders are affected by market average investment attitude, namely, it can denote the strength of the influence that noise traders are affected by investment behavior of other traders. According to explanations of herd behavior in a lot of papers (e.g. [12–14]), we deem that γ can measure the degree of herding effect in the stock market. From above analyses, we realize that the matrix of the coefficient of interactions between heterogenous traders in Eq. (1) can be described as follows.

$$\begin{bmatrix} \sigma_{11} & \sigma_{12} & \sigma_{13} & \sigma_{14} \\ \sigma_{21} & \sigma_{22} & \sigma_{23} & \sigma_{24} \\ \sigma_{31} & \sigma_{32} & \sigma_{33} & \sigma_{34} \\ \sigma_{41} & \sigma_{42} & \sigma_{43} & \sigma_{44} \end{bmatrix} = \begin{bmatrix} F_{bs} + B_{FN} & F_{sb} & B_{NF} & 0 \\ F_{bs} & F_{sb} + S_{FN} & 0 & S_{NF} \\ B_{FN} & 0 & B_{NF} + N_{bs} & N_{sb} \\ 0 & S_{FN} & N_{bs} & S_{NF} + N_{sb} \end{bmatrix} \tag{7}$$

4 Simulations Analysis

In this section, a mass of simulations are taken on to discover the interactions between heterogenous groups of traders and overall market circumstances under a series of gradually increasing herding effect γ. According to Eqs. 1, 2 and details of parameters mentioned in Definition 1, we start the simulation with a group of representative initialization parameters set up in Table 1.

Table 1. Parameter values in the simulation

Parameter	Value	Parameter	Value	Parameter	Value	Parameter	Value
α	2	v_{bs}	0.5	R	0.08	X_1	30000
β	0.4	v_{sb}	0.5	P	6	X_2	20000
η	0.1	v_b	0.5	P_m	5	X_3	22500
λ	0.2	v_s	0.5	N	100000	X_4	27500
θ	2	s	0.7	k_i	0.0005	γ	1.5–10

4.1 Heterogenous Groups of Traders Affected by Herding Effect

The herding behavior of traders in the stock market propels a large number of traders that actually behave quite different at first miraculously behave in a similar way eventually. Market tends to an unpredictable state that is full of extreme volatility and more likely to generate bubbles and crashes. Obviously, in Fig. 1(a) and (b), all of heterogenous groups of traders keep an exponential growth at first and then tend to an undamped period of oscillation. We consider it is a stable phenomenon because the stock market in our model is an open market and heterogenous traders can freely exit and enter into market. The stable state in this circumstance may not converge to a fixed value. Instead there has a top and bottom limitation in the oscillation, and it is also regarded as relative stable state in Fig. 1(c) and (d). Whereas, in Fig. 1(e) and (f), quite different under the powerful herding effect, it can be found that the tendency of heterogenous groups of traders also keep an exponential growth at first and then turn into an undamped short period of oscillation. Then it tends to a period of sharply oscillation in the end. The reason is that, with the increasing degree of herding effect, blind mimic behavior and irrational speculation behavior of traders gradually emerge in the market. It also leads the overall market circumstance fall into a relatively irrational state. The irrational psychological state of panic and greedy among traders is more easily motivated. Under this circumstance, traders prefer to frequently buy and sell in order to gain more profits, and they consider this investment strategy is highly efficient and speedy to add wealth.

Therefore, the number of heterogenous groups of traders eventually run into a period of sharply oscillation with no apparent limit, and this is a sign of unstable. From microcosmic view, we recognize the herding effect γ surely affect the interaction of heterogenous groups of traders in the stock market.

4.2 The Volatility of the Stock Price Affected by Herding Effect

It is well known that the stock price is affected by the relationship between demand and supply in the market. In Fig. 2, it is shown that the stock price rapidly returns to the fundamental value under a feeblish herding effect and gradually runs into an unstable period of oscillation that centered on the fundamental value under a powerful herding effect. As the value of γ increases, the excess volatility apparently appears, besides, bubbles and crashes can also be found under a powerful herding effect. The explanation may be summarized that a continuous rising during the beginning stage of the bubble will convert a great number of traders to noise buyers who firmly believe that they will gain more profits under the psychology of overconfidence and overoptimistic. For an

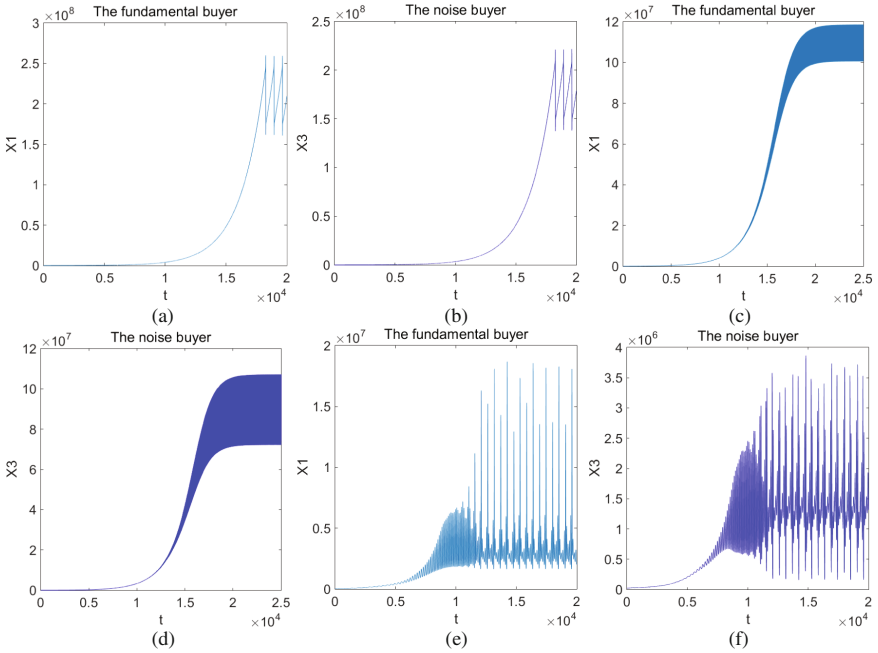

Fig. 1. The quantitative variation of fundamental buyers and noise buyers under different value of γ, 1 (a and b), 2 (c and d), 7 (e and f).

indefinitely extended time span, the rapidly increasing of noise buyers lead to excessive demand that eventually heats up the bubble. With the price excessively deviate from the fundamental value, it seems that the fundamental traders will gain more profits under arbitrage behavior. The prevailing tendency will turn to the investment strategy of fundamental traders. Further, the stock price tends to the fundamental value again with the effect of the increasing fundamental traders. Vice versa, similarly, there is an opposite conclusion in the continuous falling circumstance. The oscillation of the stock price that centered on the fundamental value is generated by the circulative switch between the above circumstances, and it is further intensified by the herding effect. According to Fig. 2(b) and (d), we also find that the high and low price will become higher and lower as the herding effect increases. This phenomenon reveals that bubbles and crashes are more likely to emerge as the herding effect increases.

4.3 *X-P* Phase Diagram, *X-Y-P* Phase Diagram and System Stability Affected by Herding Effect

We introduce the definition of market average rationality as follows.

$$Y_t = \frac{X_1(t) + X_2(t) - X_3(t) - X_4(t)}{X_1(t) + X_2(t) + X_3(t) + X_4(t)} \tag{8}$$

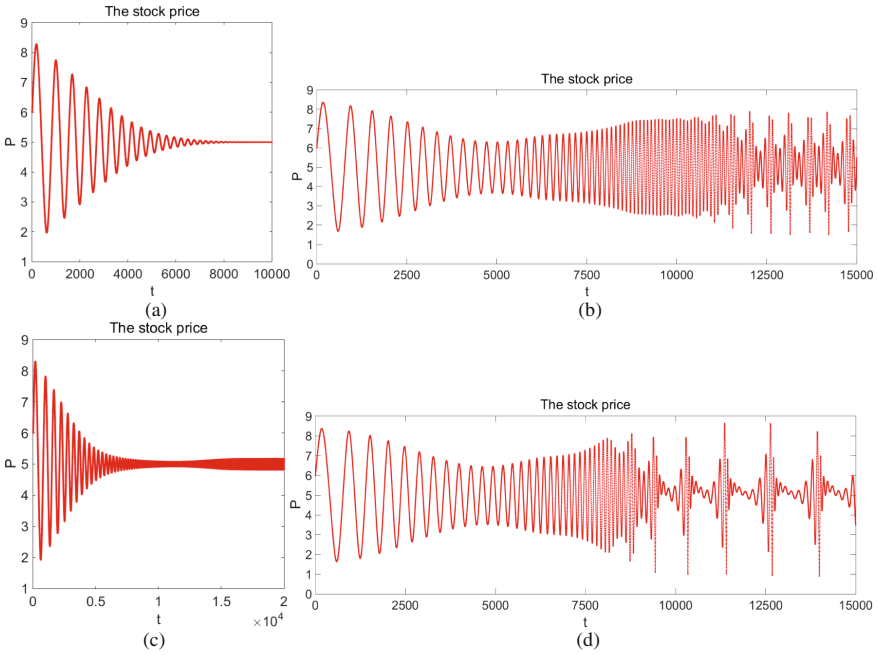

Fig. 2. The fluctuation of the stock price under different value of γ, 1 (a), 7 (b), 2 (c) and 8 (d).

It is assumed that there is a positive relationship between market average rationality and the proportion of fundamental traders. The overall market becomes more rational and stable as the number of fundamental traders increases. Besides, we analyse the character of overall system by following phase diagrams in Fig. 3. We focus on the stability of the overall system. The system gradually tends to the equilibrium point under a feeblish herding effect (e.g. $\gamma = 1$ in Fig. 3(a) and (d)). As the value of γ increases, the trajectory of the system slightly tends to the equilibrium point at first and then changes into a series of limit cycle that centered on the equilibrium point. We found limit cycles in our model is similar to the stable limit cycle in [15]. Moreover, the radius of limit cycle becomes larger as the herding effect increases. We also realize that the system will not stable at the equilibrium point, instead it will stable at a series of limit cycle under moderate intensity of herding effect (e.g. $\gamma = 5$ in Fig. 3(b) and (e)). The unstable state of the system emerges under a powerful herding effect (e.g. $\gamma = 8$ in Fig. 3(c) and (f)), and stable equilibrium points and stable limit cycles are no longer exist. The whole system generates a disorder and chaotic phenomenon. It reveals that the stock market is under a turbulent and rattled circumstance, and various variables are all fluctuated fiercely in the system. Besides, it means that bubbles and crashes will inevitably generate and may result in the outbreak of financial crises in the overall market if there has no external control (e.g. government policies that support the market in time).

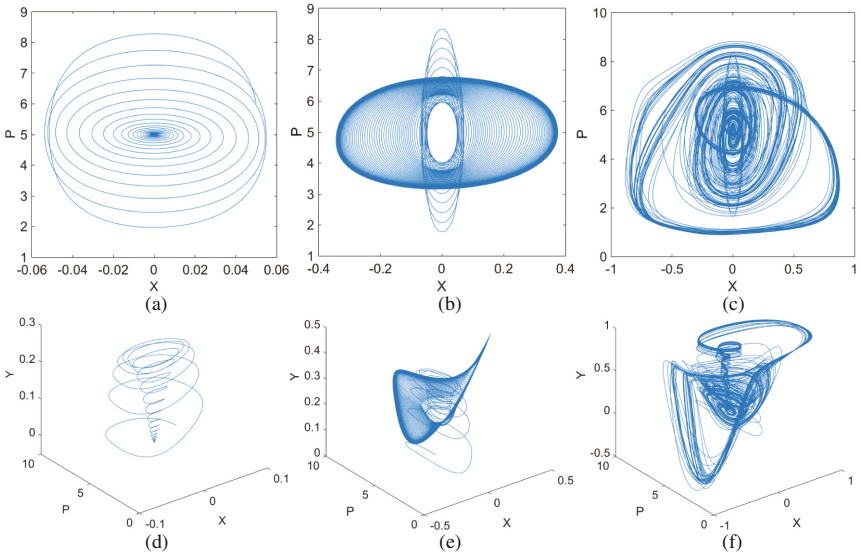

Fig. 3. The relationship among the stock price, market average investment attitude and market average rationality under different value of γ, 1 (a and d), 5 (b and e), 8 (c and f).

5 Conclusions

In our paper, we have proposed a novel agent-based financial market model to explain the dynamics of financial markets. Different from viewpoints in [7, 8], we have focused on the open stock market system by considering a situation in which heterogenous groups of traders may freely exit and enter into the market, which is more close to the realistic market. We introduce Lotka-Volterra equation into our model to highlight the interaction between heterogenous groups of traders. Traders rely on a mix of noise and fundamental trading rules to determine their orders, and these rules indicate a number of investment psychology of traders, which is usually described as herding behavior. In addition, various dynamics and stylized facts of stock markets emerge under different degrees of herding effect. The key outcome delivered by our paper may summarize as follows. With the increase of the degree of herding effect, heterogeneous traders gradually emerge excessive speculation activities, and their decision-making behavior becomes more variable and unfixed. Stock prices gradually deviate from the basic value, which can lead to the tumble of stock prices and even the stock market crash. From the view of a series of phase diagram, dynamics of the stock market system also gradually convert from a steady state to an unstable state. In the future paper, we will refine the model by an in-depth analysis of parameters and introduce a number of new parameters to enlarge the scope of our model. In the end, we hope our work will more or less contributes to the understanding of the real interaction mechanism in the complex economic system and be helpful in formulating and implementing the policy that support the stock market.

Acknowledgements. This research reported herein was supported by the NSFC of China under Grant No. 71371092.

References

1. Huang, W., Day, R.: Chaotically switching bear and bull markets: the derivation of stock price distributions from behavioral rules. Nonlinear Dyn. Evol. Econ. 169–182 (1993)
2. Tramontana, F., Westerhoff, F., Gardini, L.: The bull and bear market model of Huang and Day: some extensions and new results. J. Econ. Dyn. Control **37**(11), 2351–2370 (2013)
3. Haken, H.: Erfolgsgeheimnisse der natur: synergetik, die lehre vom zusammenwirken, Deutsche Verlags-Anstalt (1981)
4. Scharfstein, D.S., Stein, J.C.: Herd behavior and investment. Am. Econ. Rev. 465–479 (1990)
5. Avery, C., Zemsky, P.: Multidimensional uncertainty and herd behavior in financial markets. Am. Econ. Rev. 724–748 (1998)
6. De Long, J.B., Shleifer, A., Summers, L.H., Waldmann, R.J.: Noise trader risk in financial markets. J. Polit. Econ. 703–738 (1990)
7. Lux, T.: Herd behaviour, bubbles and crashes. Econ. J. 881–896 (1995)
8. Lux, T.: The socio-economic dynamics of speculative markets: interacting agents, chaos, and the fat tails of return distributions. J. Econ. Behav. Organ. **33**(2), 143–165 (1998)
9. Foroni, I., Agliari, A.: Complex price dynamics in a financial market with imitation. Comput. Econ. **32**(1–2), 21–36 (2008)
10. Lotka, A.J.: Elements of Physical Biology. William and Wilkins, Baltimore (1925)
11. Volterra, V.: Variazioni e fluttuazioni del numero d'individui in specie d'animali conviventi. Mem. Acad. Lincei **2**, 31–113 (1926)
12. Cont, R., Bouchaud, J.P.: Herd behavior and aggregate fluctuations in financial markets. Macroecon. Dyn. **4**(02), 170–196 (2000)
13. Trueman, B.: Analyst forecasts and herding behavior. Rev. Financ. Stud. **7**(1), 97–124 (1994)
14. Grinblatt, M., Titman, S., Wermers, R.: Momentum investment strategies, portfolio performance, and herding: a study of mutual fund behavior. Am. Econ. Rev. 1088–1105 (1995)
15. Hofbauer, J., Schuster, P., Sigmund, K., Wolff, R.: Dynamical systems under constant organization II: homogeneous growth functions of degree p = 2. SIAM J. Appl. Math. **38**(2), 282–304 (1980)

The Agent-Based Agri-Household Micro-Simulation Platform and Its Application

Xiangyu Wan(✉)

Institute of Quantitative and Technical Economics of CASS, Beijing, China
45440549@qq.com, wanxy@cass.org.cn

Abstract. Based on the agri-household modeling theories and practical needs of agricultural economy research, this paper develop a micro-simulation platform for agri-household modeling, this platform is based on the modern economics theoretical hypothesis of bounded rationality, complex adaptive system and non-equilibrium, it provides a rule-based, independent design, constructive, sharable and reusable software tool for agri-household simulation models. Taking the Chinese food security as an example, we turn to use this platform in modeling and simulating some special agricultural economic environments, the simulation experiments provide quantitative evidence for scientificity and validity of this platform in modeling and analyzing the practical economic issues within the complex adaptive system as well as synthesization and integration system.

Keywords: Agent-based · Agri-household model · Micro-simulation · Food security

1 Introduction

The internal motivation of agricultural economic phenomenon comes from the microscopic state and behavior of farmers. Farmers adjust their status to adapt to the economic environment through behavioral decision making. However, the accumulation of microscopic state constitutes macroeconomic phenomenon. In this way, the essence of study on an agricultural economic problem often is to apprehend the behavior and state of micro farmers. Traditional agricultural economic research is often based on macroscopic empirical data to abstract, analyze and apply farmers' economic status and behavior by the application of typical individual or aggregate analysis model. In fact, the farmer groups in semi-marketization have directly led to the complexity of agricultural research because of the diversity of geographical distribution, the heterogeneity of endowment status and the evolutionary adaptability of behavior decision. Traditional methodology out of micro economic foundation is not enough to seal with such a complexity generally. Therefore, the analysis from the individual perspective of farmers must be included in the scope of agricultural economic research, to form a research pattern cutting from microstate and behavior. This is the so-called "Agricultural Household Model".

As an emerging agricultural economic modeling technology, AHM is an economic model that is used to describe the various relationships within a farmer and is consistent

D.N. Cassenti (ed.), *Advances in Human Factors in Simulation and Modeling*,
Advances in Intelligent Systems and Computing 591, DOI 10.1007/978-3-319-60591-3_29

with the general principle of balanced economic theory. It effectively link farmers' production, consumption and labor supply decision together. It commences with state and behavior of micro farmers, to analyze theories and realities of agricultural economics whose details can be referred to Becker [1], de Brauw et al. [2], Chiappori and Ekeland [3], as well as Blundell and Stoker [4], and so on. The AHM shows a good analytical and predictive ability in a relatively stable economic system [5], which is at the forefront of agricultural economic research, but there are still severe shortcomings.

The first upcoming problem is related to micro-attribution. In AHM modeling process, simply typifying or quantifying their characteristics, obviously can't figure out independent response of different economic agents to economic impact. Accurate research objectives will inevitably require us to involve specific farmers' heterogeneous economic attributes and behavior into our analysis, that is, carry out attribution analysis from the micro level to simulate influence of the external economic conditions and shock on micro-farmers behavior and characteristics. Macroeconomic effects are reflected by the accumulation of attributes and micro-behavior, thereby finally extracting the target information. It's a complex system of adaptation problems in nature. Modern economics argues that the economy is a complex self-adaptive system [6], whose complexity leads to the bounded rationality of economic agent behavior. Agent's adaptability results in the evolution of economic systems, the effects of economic policy are interact under the undescriptive network environment, the "evolution" and "self-organization" are the continuing characteristics of the system. This complex evolutionary mechanism is the biggest problem of economic modeling. Unlike other complex systems, this complexity of the economic system is manifested in four aspects: economic complexity resulting from heterogeneity of attributes, economic complexity resulting from behavioral heterogeneity, economic complexity resulting from interactive networks, and economic complexity resulting from dynamic adaptation. The practical significance of complex system research is critical for the agricultural enterprises with different attributes and behavior, incomplete market participation, expectation of myopia in the economy, and sudden and unexpected agricultural economy. It is urgent to develop a new economic model, to meet dual needs of analyzing and forecasting the real economic problems and updating theoretical economic methodology.

The latest developments in the theory and method of modern economics provide a modeling approach to solve these problems. Based on a completely new methodology, under the interdisciplinary comprehensive knowledge framework of economics, computational mathematics, computer simulation technology, so-called Agent-based Computational Economics (ACE) research system [7] appeared, which builds a research context from a model perspective, treating economic research goals as an evolutionary system consisting of a series of interactions, which allows economists to study economic issues at a deeper and broader level. The microscopic simulation model based on Agent-based computational economics is called the Agent-based economic model. It is an intelligent microscopic simulation model, which regards the economy as an evolutionary system composed of autonomous entities. Through strong computing method (AI) and computing tools (OO) programming, programming is to achieve adaptive capacity, communication skills, learning ability and autonomy of economic intelligence (i.e. Agent), and through the simulation of real economic network to organically

construct the relationship among these agents, and the dynamics of macroeconomics are manifested by the accumulation of micro-individual interactions. In short, Agent-based micro-simulation model is based on real social principle and related economic theory, employing computer modeling methods to build intelligent behavior of micro-individual (Agent), and setting up individual (Agent) interaction, ultimately arriving a stimulation system. The heterogeneity attributes and behaviors of specific agent and their dynamic interaction creates the complexity adaptability of our system. Therefore, our method not only describe intricate adaptability, but also meets demands of Agent-based AHM which stems from the microeconomic behavior and state, bottom-up modeling research as well. Economic model with real existence [8] which is highly valued by the nature, is an effective attempt to consummate AHM.

According to the aforementioned, this paper make a shot to utilize the object-oriented computer programming language—C or C++ language—to establish an agent-based microeconomic simulation model. Through the dynamic simulation of micro-farmers' behavior and the agricultural economy system, this paper observed the agricultural economy phenomenon under micro heterogeneity and dynamic interaction. Then, we apply different environment and impact to the developed simulation model varying from study objectives. Along with our study objectives, particular background and impact were pushed, and this paper compared influence on development path of the agricultural economy, especially on the dynamics of the trend of agricultural prices, with the conventional method in natural science.

2 Modeling Frameworks of Rural Households

As mentioned earlier, the core problem of building a simulation model based on Agent is the effective design of the model, in order to restore the economic reality. Therefore, we must have a relatively fine design and construction of the model. Under the guidance of agricultural experts, according to China's economic reality and related data, and after repeated demonstration and research, we finally established the framework of rural household based the Agent model, which covers the following five aspects: research objectives, data sources, model assumptions, simulation rules and Agent description.

2.1 Research Objective

Whether it can make an effective evaluation of the problems of social focus is the criterion of the applicability of the model, and combined with the reality of China's agricultural economy, the focus of research and the advantages of simulation, we regard China's food security as the evaluation target, design a sudden impact on the agricultural economy, that is the impacts of natural environmental impacts (meteorological or seismic disasters) on food security, in addition, we also focuses on the fluctuation of grain price.

2.2 Data Sources

Due to the need of empirical problems in agricultural economy, we have strict requirements on the reliability of the model. And because the initial data is an important guarantee for the real and reliable model, so the model of heterogeneous individual distribution from micro data on rural development research China Social Sciences Institute of investigation, and the macro data from the statistical yearbook, through abstraction and check to close to the economic reality of our country.

2.3 Model Hypothesis

The effectiveness of economic simulation method based on the Agent depends directly on the degree of users' abstraction of economic reality. Therefore, this study is the primary focus to make reasonable assumptions on the economic system and its operating environment, it is the foundation for the construction of artificial world economy:

1. From the industrial structure, the economic world is consists of the agricultural and industrial sectors; and from the geographical structure, the economic world is divided into urban and rural areas.
2. The economic system is closed, and its internal Agent forms an organic artificial economic network through behavioral interaction.
3. The macro-economic aggregate is formed by the heterogeneous information of the individual, but the macro-economic information and the exogenous shocks directly affect the economic behavior and characteristics of the micro Agent, so as to realize the integration of macro and micro.
4. Through the heterogeneous behavior decision and evolution mechanism of the micro - level economic agent to complete the adaptation of the whole economic system, and this kind of behavior generation and evolution process are based on the rule - based classifier solution, rather than simple mathematical analysis.
5. In the case of economic entities, we assume that the economy consists of rural households, urban households, enterprises (a number of food crop enterprises, a number of cash crop enterprises, a number of industrial enterprises), government and market agents (labor force for labor employment Market and commodity trading products market).
6. There are a kind of food crops, a kind of economic crop, an industrial product and a currency in the economy. The production factors in the production process include labor force, capital, technology or cultivated land, agricultural machinery and fertilizer.
7. The simulated output is a number of macroeconomic indicators in a given environment, including food crop production, purchasing and storage prices and market selling prices, as well as rural labor mobility, which are accumulated from microeconomic realities.

2.4 Simulation Rules

Based on the above assumptions and definitions, microeconomic subjects are organically linked. In this study, the model is the Monte-Carlo simulation, the random pattern of the event causes the behavior and state of the different agents to be heterogeneous, microcosmic individuals in different states adapt to the economic and policy environment by interacting with the dynamic behavior of the surrounding agents and their own behavior, and the associated macroeconomic system evolves with this multi-agent co-evolution. It is also under such a modeling rule that the "emerging" and "self-organized" complex systems can be realized. The macroeconomic indicators in the economy are directly generated by the interaction of the microscopic agents, and the accumulation of microscopic values can be calculated statistically, such as the food crop price index and total output, the overall distribution of cultivated land and the flow of agricultural labor, and so on. Appendix 1 gives the main events that occur in each cycle of each agent in the model.

2.5 Agent Behavior Description

Similar to the actual economic system operating rules, the simulation model established in this study also uses a periodic behavioral evolution model, that is, each type of economic subject has a certain period of its behavior, the same subject in different cycles in the same decision-making mode, but the specific behavior parameters can be completely different, for example, in every economic cycle, farmers need to complete the agricultural cultivation, purchasing and storage, sales and other acts, but the specific species and quantity of cultivation, sale of the price and the object may be different, and the direction of specific behavior changes is the result of the individual's adaptive decision based on the current environment and its own preferences. The key economic behaviors and events of the main agents in the model are as follows:

(1) Artificially issued macroeconomic shocks. This link is a human-computer interaction mechanism, which requires the modeler to design the macro impact in time, including climate, environment, policy, technology and so on.
(2) Rural residents develop planting plans. Farmers determine the ratio of cultivated land to food crops and cash crops; identify other inputs for agricultural production, such as technology, finance, labor, water, etc.; for deterministic factors that affect the planting plan, we use a logical classification to simulate, which mainly includes climate, policy, the purchase price of food crops and cash crops, crop supply and demand, the historical income of farmers, the situation of comparative income between farmers. For the non-deterministic factors affecting the planting plan, we use the GALCS[1] simulation. The other inputs of the farmer are calculated according to the initial situation and experience. Different decision-making responses are different in different regions and different behavior preferences.

[1] GALCS (genetic algorithm learning classifier system). It is proposed by Holland [9] on the basis of genetic algorithm, which is an important mechanism for the evolution of artificial intelligence. Examples of applications in this paper can be found in the famous ASPEN model developed by the American Academy of Urban Studies [10].

(3) Rural residents complete agricultural planting. According to the plan to put into production factors (non-durable inputs to deduct or depreciation), the final calculation of crop yield Y, and accumulated to the corresponding attributes. The C-D function is used in agricultural production, and the specific parameters are estimated based on empirical data.
(4) Urban residents develop labor plans. Urban residents to determine the current labor supply and the supply of labor object. The labor supply equation can use the empirical data to estimate the discrete selection model or the simple behavior classifier; the residents will determine their employment probabilities based on the wages provided by each firm.
(5) Urban residents complete the labor supply (enterprise employment labor force). Residents enter the labor market, and complete the sale of labor, enterprises corresponding to the supply of labor.
(6) Agricultural enterprises make purchasing and storage price, including economic crop and grain crop storage enterprise. Factors to determine the effect of planting plan, we use the logic classification mode to simulate, it mainly includes the policy, crop yield, crop supply and demand situation, the reserve price trend, crop sales price trend, corporate earnings, historical comparison between listed companies' earnings, price comparison between enterprises; as for uncertain factors for the effect of planting plan, we use GALCS simulation.
(7) Agricultural enterprises complete crop storage (farmers sold crops). In accordance with the contract price, enterprises spend the corresponding cost of purchasing and storage, to complete the acquisition. In accordance with the agreed price, farmers sold crop stock and gain earnings. The distribution of market purchasing and storage is depended on the proportion of the share the enterprises offers determined. Farmers and enterprises should timely and accurately record and update transaction, expenditure or income information, as the basis for Agent to make decision making and evolution.
(8) Agricultural enterprises develop sales price. Factors to determine the effect of planting plan, we use the logic classification mode to simulate, which mainly includes the policy, the relationship between supply and demand, crop sales prices, corporate earnings, historical comparison between listed companies earnings, price comparison between enterprises. For the uncertainty factors in the influence of planting plan, we use GALCS simulation.
(9) Industrial enterprises make production plans. Industrial enterprises determine the capital and technology inputs, and use the mode of classifiers, according to the status of enterprises to make decisions.
(10) Industrial enterprises products production. According to the plan to put into production factors (non-durable inputs to deduct or depreciation), the final calculation of crop yield Y, and accumulated to the corresponding attributes. The C-D function is also used in industrial production.
(11) Industrial enterprises make sales price. Factors to determine the effect of planting plan, we use the logic classification mode is simulated, which mainly includes the policy, industrial products supply and demand, the sale price, corporate

earnings, historical comparison between listed companies earnings, enterprise's price comparison (market share). For the uncertain factors in the planting plan, we use GALCS simulation.

(12) Residents pay income tax. Calculate the amount of tax according to the relevant government tax rate.

(13) Residents develop a consumption plan. Using the linear demand function, according to the net income distribution and consumption ratio, to calculate the demand for food crops, calculate the demand for economic crops, calculating the demand for industrial products. The allocation of investment and consumption is given prior.

(14) Residents complete the consumption (enterprise sales products). Residents consume products and pay the cost, enterprises to sell the corresponding goods, access to income.

(15) The enterprise is subject to income tax. Calculate the amount of tax according to the relevant government tax rate.

(16) Enterprises develop the next period production investment (wages). According to the income situation to develop the next period of capital investment and wage levels.

(17) The government sets macro policies and hired labor.

(18) Extracting macroeconomic information at any time. According to research needs timely extraction of macro information, such as food crop production, food crop prices, farmer income, economic aggregate - GDP, and so on.

3 Empirical Results and Evaluation

According to the above design structure, the simulation model is generated. This model is based on the state and behavior of Agent automatically run forward, which is an endogenous economic growth process. In order to ensure the steady state of the simulation, the simulated impacts usually occurs after the 1000th cycle. Each impact is repeated 10 times and the simulation parameters are averaged to reduce the variance.

A series of critical indicators of the model output without any economic impact are presented in Figs. 1, 2 and 3, which is for validity test. Among them, Fig. 1 shows the

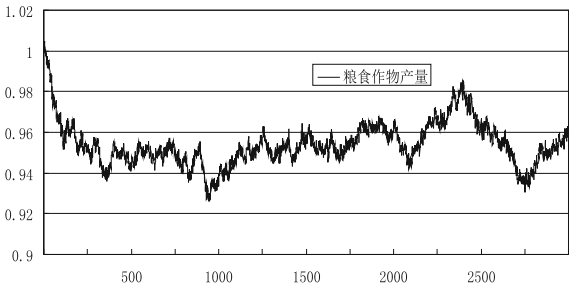

Fig. 1. Grain crop yield under standardized conditions (SC)

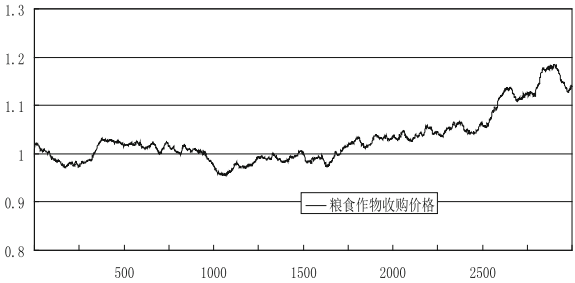

Fig. 2. Grain crop purchasing price under SC

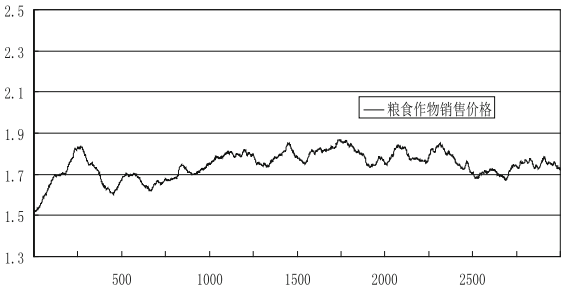

Fig. 3. Average grain crop sale price under SC

dynamic grain crop yield trend, we regard grain output in base year as 1 unit and normalize output, to abate scale deviation arising from simulation. Although the grain yield somehow fluctuates, generally speaking, enthusiasm to planting is not high. On the other side, farmers can hardly convert the land into other purpose due to the limitation of factors such as land, under which grain yield is relatively stable. Figure 2 shows grain purchasing and storage price has been in a gradual uptrend, especially in late stimulation period implying a rising enthusiasm to agriculture. In a downward evolution, however, production increasing induced by price rises will back to normal soon. That is to say, grain crops can never be dominant for a long run in a self-adaptive economy. Although the output and price (adjusted for inflation) have volatility, the overall trend can be smooth. Figure 3 tells the dynamic trend of the average sales price of grain crops. The distinction of purchase-sale price of grain crops enlarged for the existence of middleman. With the continuous development of the economy, the overall profit margin tends to be stable after a dose of games. In other words, positive divergence beyond market can only last in a short term behavior, owing to rationality of grain crops supply market. Given optionality in land allocation, our model allows farmers to decide proportion of two kinds of crops according to their own circumstance.

The experiment of Figs. 4, 5 and 6 is an attempt to solve the new problem. In the 1000th phase of the simulation run, we have imposed a natural disaster on a major grain producing area, which causes a sharp reduction in food production. The economic

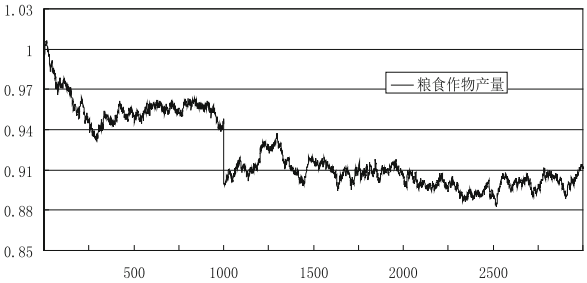

Fig. 4. Grain crop yield under natural environmental impacts (NEI)

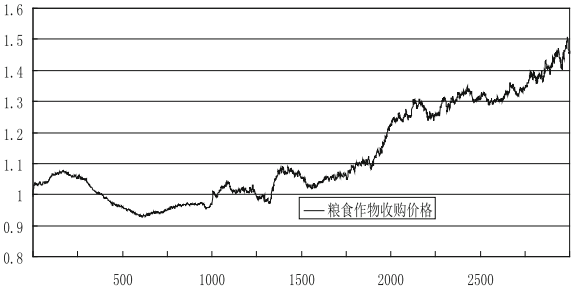

Fig. 5. Grain crop purchasing price under NEI

impact of grain production is firstly market (see Fig. 6), first, in order to make speculative profits, grain brokers significantly increase the food crop market price, while the grain purchasing and storage price growth is relatively slow, with the development of dynamic game, grain enterprises gradually adjust business strategy and improve the purchase price, in order to reply the sale price. Therefore, in the event of food supply disorder, we should first pay attention to the grain market, and be aware of speculation, but for the damaged farmers, we should give appropriate subsidies to encourage their enthusiasm, don't rely too much on the market price of the supply side of the compensation, because the market monopoly has directly led to the acquisition of price rises slow process.

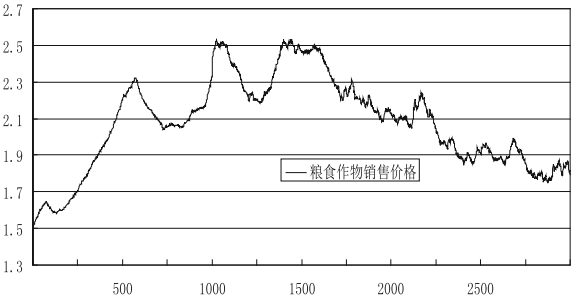

Fig. 6. Average grain crop sale price under NEI

4 Conclusion

In this paper, a micro simulation model based on Agent is proposed to solve the problems existing in the research process. In this model, based on the microscopic simulation technology theory and technology system of the Agent, and using the modern economics of limited rationality, complexity and non-equilibrium and a series of assumptions, and via the modeling method based on rule abstraction of real world economy, we provide a feasible tool for quantificationally figuring the dynamics, emergence and evolution of economic systems. According to China's economic reality and the related data, we do some empirical research on the model, the simulation experiment shows that the evolution of microscopic simulation can reproduce the reality of agricultural economic system, its dynamics is reflected in many traditional research tools cannot describe, especially for describing the evolution process of the price cobweb. The model has the ability to analysis problem of agricultural economy, for our design of the economic shocks, it can give an effective response, and give the development trend. The model also has a strong adaptability, it can respond to economic shocks that lack empirical information, and seek solutions, such as the development trend of agricultural economy under major natural disasters, this is not the ability of the model in general, it provides a tool for studying the emergence of complex systems. The model can meet the requirements of the micro modeling of the integrated system, and realize the integration of micro-macro modeling process; and the modeling theory and method system of the model can be used for reference.

Acknowledgements. This research is supported by Innovation Project of Chinese Academy of Social Sciences.

References

1. Becker, G.S.: A Treatise on the Family. Harvard University Press, Cambridge (1981)
2. de Brauw, A.J., Taylor, E., Rozelle, S.: Migration and Incomes in Source Communities: A New Economic of Migration Perspective from China. University of California, Davis working paper (2002)
3. Chiappori, P.-A., Ekeland, I.: Characterizing Group Behavior. Working Paper. Columbia University, New York (2005)
4. Blundell, R., Stoker, T.M.: Models of aggregate economic relationships that account for heterogeneity. In: Heckman, J., Leamer, E. (eds.) Handbook of Macroeconomics, vol. 6A. Elsevier, Amsterdam (2007)
5. Huffman, E.: Agricultural household models: survey and critique. In: Hallberg, M., et al. (eds.) Multiple Job-Holding Among Farm Families in North America, pp. 79–111. Iowa State University Press, Ames (1991)
6. Arthur, W.B.: Inductive reasoning and bounded rationality. Am. Econ. Rev. **84**, 406–411 (1994)
7. Tesfatsion, L.: Introduction to the special issue on agent-based computational economics. J. Econ. Dyn. Control **25**, 281–293 (2001)

8. Farmer, J.D., Foley, D.: The economy needs agent-based modelling. Nature **460**(7256), 685–686 (2009)
9. Holland, J.H.: Escaping brittleness: the possibilities of general-purpose learning algorithms applied to parallel rule-based systems. In: Michalski, R.S., Carbonell, J.G., Mitchell, T.M. (eds.) Machine Learning, vol. II, pp. 593–623. Morgan Kaufmann, Los Altos (1986)
10. Pryor, B.N.R., Quint, T.: ASPEN: a microsimulation model of the economy. Comput. Econ. **12**(3), 223–241 (1998)

An Agent-Based Approach on Conditional Deterrence

Zining Yang[1(✉)], Kyungkook Kang[2], and Jacek Kugler[1]

[1] Claremont Graduate University, Claremont, CA 91711, USA
{zining.yang, jacek.kugler}@cgu.edu
[2] University of Central Florida, Orlando, FL 32816, USA
kyungkook.kang@ucf.edu

Abstract. This paper provides an integrated structure that defines conditions for the success and failure of deterrence. The conditional deterrence model presented can be applied to global and regional interactions that drive nuclear proliferation. The objective is to further extend the dyadic logic established to anticipate challenges generated by the proliferation of nuclear capabilities and their acquisitions by non-state dissatisfied agents. Key elements included in this assessment are relative capabilities, risk propensity associated with the status quo, and physical exposure to preemptive-attack or retaliation. This work uses ABM to generalize insights to deterrence environments with multiple competing actors. We show that deterrence is stable when the capabilities of a dissatisfied challenger are inferior to that of a dominant and satisfied defender. Deterrence is tenuous when a dissatisfied challenger approaches parity in capability with the dominant and satisfied defender, or when a violent non-state actor obtains nuclear weapon or other WMDs.

Keywords: Agent-based model · Game theory · Deterrence · Relative capabilities · Risk propensity

1 Introduction

In an increasingly globalized and concurrently fractured security environment, the ability of agents to deter others by threats to use weapons of mass destruction (WMD) warrants serious reexamination. The threat of a global nuclear war continues to be the central policy priority, but new security challenges generated by the proliferation of weapons to smaller nations and potential expansion to non-state agents requires assessment.

We develop an integrated simulation model that identifies and addresses security conditions for the success and failure of weapons of mass destruction (WMD) deterrence in the twenty-first century. This study will develop a U.S. defense strategy based on tailored plans to deter the security threats to U.S. vital interests while preserving tractability to assess their unclear trajectories and potential turmoil.

Particularly, our agent-based model responds to the need to reassess the relevance of deterrence as both theory and practice in light of foreign policy challenges facing the U.S. in the twenty-first century. Military leaders have a need to rapidly evaluate, assess,

D.N. Cassenti (ed.), *Advances in Human Factors in Simulation and Modeling*,
Advances in Intelligent Systems and Computing 591, DOI 10.1007/978-3-319-60591-3_30

and reason about deterrence stability when they encounter new political crises in an era of WMD proliferation. However, it is still difficult to find an integrated predictive model for deterrence that takes account of both global and regional interactions in an increasingly globalized and concurrently fractured security environment.

The threat of a global war using nuclear weapons continues to be the central policy priority, but new challenges have concurrently emerged at the regional level. The use of chemical weapons in Iraq, Iran and Syria; the persistent pursuit of nuclear weapon by rogue states such as North Korea; the fastest-growing nuclear program of Pakistan, expected to get 200 nuclear warheads by 2020; the preemptive strikes by Israel against nascent WMD installations in Iraq and Syria (and the threat to do so in Iran); China's rapid nuclear modernization and ballistic missile defense development; Nuclear-backed crisis between Ukraine and Russia; and above all the specter of WMD use by dispersed terrorist groups like ISIS and Al-Qaeda force us to reconsider the effectiveness of traditional deterrence, the leading theoretical and policy framework during the cold war.

The simple and obvious way to avoid war is to eliminate these weapons through disarmament coupled with a robust international verification regime [1–4]. The implications are crystalized in President Obama's nuclear disarmament speech in Prague six years ago and the ongoing debate over the nuclear deal between Iran and the P5 + 1 countries (the U.S., Russia, the U.K., France and Germany) despite attempts by Israel and Saudi Arabia to thwart the deal. According to this "WMD pessimism," only if all of weapons are removed, then war is impossible. In practice, however, the potential for WMD war has not been reduced; rather, it may have increased continually. The estimated arsenal sizes that assure massive destruction among the nuclear powers have monotonically increased since 1945. Apparently, substantial disarmament has not taken place yet despite the persistent political rhetoric of peace.

The second option to prevent WMD war is classical deterrence, sometimes labeled "WMD optimism," based on the logic of balance of terror - the more horrible the prospect of war, the less likely it is to occur [5–8]. This idea of classical deterrence was the backbone of U.S. national security during the Cold War and still continues to be advocated. Recently, Waltz [9], a founder of the neorealist school and prominent advocate of classical deterrence theory, argues that Iran should be allowed to develop and field nuclear weapons in order to balance those deployed by Israel. Waltz contends that a nuclear-armed Iran (and possibly joined by Saudi Arabia and Turkey) would bring stability to the Middle East because war becomes "unthinkable" once nuclear weapons enter the picture. In a similar vein, Mueller [10] also claims that if Iran and North Korea want the bomb so badly, we should let them have it.

In this research as a theoretical response, we raise questions over both the plausibility of disarmament and the validity of classical deterrence at once. Past nuclear stability does not guarantee that all future wars will be waged with conventional weapons. As even Zagare and Kilgour [11] observe, "nuclear war has been avoided not because of nuclear weapons, but in spite of them." Much of previous literature does not address anticipated challenges that may be generated by the acquisition of WMD capabilities by new rising regional competitors, rogue regimes and violent non-state actors. By contrast, this work argues that deterrence remains relevant as a primary strategic goal, but we should not get stuck in the twentieth century. This research will first search for new guidance on what kinds of threats can and cannot be deterred under

which conditions. Then the study will seek to move the framework of deterrence strategy beyond its Cold War roots and construct a more valid policy guidance that would best promote stability and peace in the contemporary world.

In sum, this study has the following major objectives:

(a) To point out how rapidly evolving security challenges make traditional approaches to deterrence unlikely to succeed in an era of WMD proliferation.
(b) To provide a new deterrence concept that can be employed against a wide array of state and non-state actors that challenge U.S. interests.
(c) To anticipate the possibility of crisis before it happens and then analyze the likelihood of escalation into a large-scale war using WMD if a crisis takes place.
(d) To build a predictive simulation model to provide specific insights for foreign policy makers and to offer policy alternatives that are more likely to succeed, given the current state of security environment.

2 Conditional Deterrence Background

In order to understand the stability of deterrence, we assess its conditionality. War by definition is a risk-taking behavior, as no party can be certain of the prospects for victory once war starts. A critical realization is that maintaining the status quo reduces the risk compared to launching a war, but abiding by the status quo produces no additional returns for a dissatisfied party. Modifying the status quo, even when immensely risky, may produce positive returns.[1] Conditional deterrence proposes that war is not an accident, but rather is the outcome of goal-seeking behavior. Following George and Smoke [17], we argue that a challenger may act based on (1) the calculated result from a "risky challenge" over a "certain status quo" and (2) the anticipated opportunity to gain victory or face defeat. The key elements of our assessment include relative capabilities, the risk propensity associated with the relative assessment of the status quo, and an entity's physical exposure to attack or retaliation.

The elements of Conditional Deterrence are generally consistent with prior deterrence modes. A shift in the distribution of capability is critical as it opens the window of opportunity for war. Yet, consistent with previous empirical work we argue that power parity sets the timing conditions for deterrence failure not stability. Once the odds of winning and losing become approximately equal, a dis-satisfied challenger perceives a risky confrontation as an "opportunity" rather than a "danger" [18–21]. We incorporate the novel and measurable concept of exposure, define it as the ability of an

[1] Although risk is defined in various ways by different disciplines, I consider a risky event to be any event where the outcome is not known with certainty in advance. To evaluate an unknown future, I follow the finance approach to the concept of risk where risk represents a quantifiable source of uncertainty, as distinguished by Knight [12]. Specifically, risk is defined in terms of the quantifiable variability of actual outcomes around an expected outcome [13]. Such notions are frequently used in financial risk assessment because it allows risk to be conceptualized in a fashion that can be incorporated into a decision on how much to hedge against or exploit a specific risk (for detailed discussions, see Morgan and Henrion [14], Varian [15], Damodaran [16]). As will be shown later, I will rely on the mean-variance analysis commonly used in financial economics to represent risk.

opponent to inflict massive punishment or retaliation against a previous initiation. Unlike the vague notion of credibility in the context of retaliation, the possession of nuclear weapons and means to deliver them reveals a opportunity to use them. The propensity of actors to assume risk is not assumed to be consistently "averse" rather the full spectrum of a willingness to act is determined by the circumstance in which deterrence is attempted. Risk prone agents can pre-empt assuming no retaliation as can non-exposed agents or parties involved in peripheral conflicts.

This study explores a war and peace mechanism as the strategic risk taking process affected by several conditional factors including (a) relative war-fighting capabilities, (b) WMD holdings, (c) exposure to retaliation, (d) risk preferences associated with political dissatisfaction. Within the analytical framework based on decision theory, such diverse military contingencies under strategic uncertainty will be systemically examined to address the likelihood of choosing war, and then escalating to WMD use. Our results can guide the creation of a computational simulation that incorporates differences in the macro-structural variables (such as the size of arsenal) and in the micro-motivational variables (such as the political dissatisfaction of decision makers). Using an agent-based model method with NetLogo Manipulate programming, the simulation-based deterrence analysis will provide the ability to experiment with different global and regional scenarios and the power of generalization of the insight on strategic stability associated with each policy option. This interactive representation allows practitioners to make more detailed assessment of timing, location, severity, and manipulability of potential crises by reevaluating current political conditions and identifying the thresholds that lead to deterrence failures.

3 The Model

To examine the conditions of deterrence we model deterrence as a strategic risk-taking process. Since decision-makers hope to attain the best *ex post* result, they consider the ex ante position as a trade-off between the anticipated benefit of choosing war, and the risk-adjusted likelihood of the actual outcome. In the context of deterrence, we postulate two interacting parties of a Challenger and Defender, where Challenger has some level of nuclear capabilities that generates risk. Challenger can deliberately threaten the Defender, indicating the foreseeable risks of harm. Accordingly, Defender can decide whether to avoid the risks by making a concession, or choosing to bear the risks through confrontation. Throughout the course of the interaction, withdrawal by either side is permitted. Figure 1 depicts the conditional deterrence framework.

The conditional deterrence rejects the classical deterrence argument introduced by Brodie [5] that a nuclear war is "unacceptable" to all because the costs are "unacceptable." Instead, conditional deterrence postulates that the stability of deterrence depends on whether Challenger would be better or worse off after a nuclear attack. Rational challenges to the status quo are possible and must be managed rather than dismissed. The addition of risk and exposure to the model identifies new and threatening conditions for deterrence failure, as well as raises serious concerns about WMD proliferation.

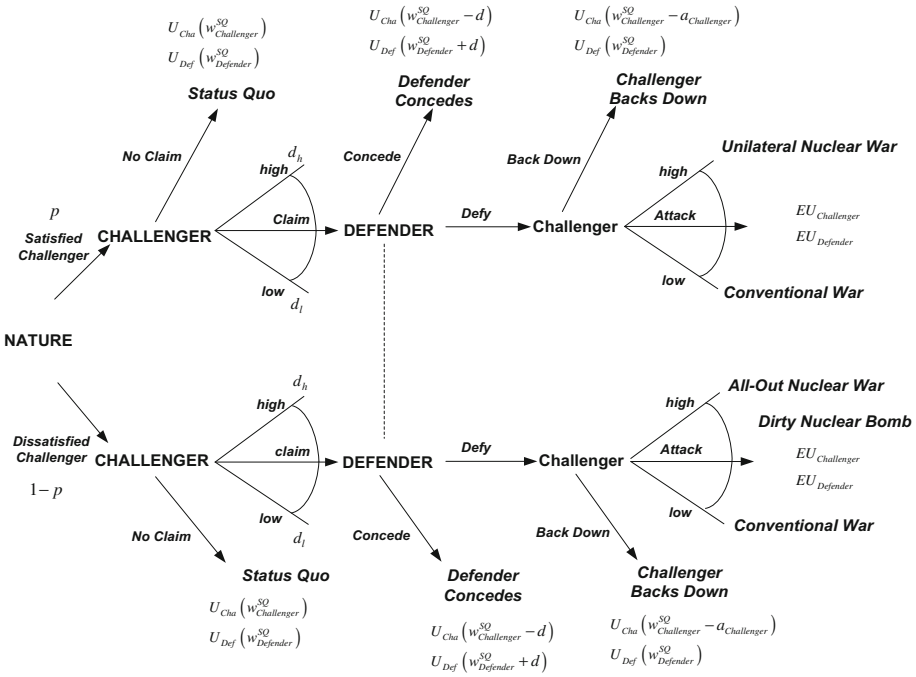

Fig. 1. Conditional bilateral deterrence framework

The question here is whether proliferation threatens stable deterrence further by enabling multiple Challengers to increase nuclear arsenals affecting level of risk, whereas the Defender bears the consequence of providing nuclear "umbrellas" to ponds also rising level of risk. Thus as proliferation proceeds, Defender must choose between concessions that reduce risk, or defiance that increases the risk of war. Such calculations are made by parties fully aware of one another's capabilities, threats, and rising exposure. Stability does not depend on increased costs, but on the decisions of leaders who can choose to initiate or avert conflict. Reducing exposure has even more important consequences. A non-state agent that acquires limited capabilities is tempted to use them understanding that retaliation can produce a follow-up retaliation by third parties. The ABM model extensions suggest exactly this danger.

The starting point in this process relies on the Harsanyi transformation that allows a move by "Nature" to solve an incomplete information game. Defender is assumed to be satisfied, and Nature assigns a positive or negative status quo to Challenger,[2] where satisfaction is determined by the gap between the status quo and Challenger's aspirations. As a result, the challenger may be satisfied or dissatisfied. In the structure, Challenger's status quo evaluation is private information, thus it is unavailable to

[2] This process of adding nature to solve an incomplete information game is suggested by Harsanyi and Selten [22]. It is not equivalent to Powell's [23] "Nature" that imposes the accidental disaster with some positive probability.

Defender at this stage. Defender assesses Challenger's orientation to be either satisfied (with probability p) or dissatisfied (with probability $1 - p$). Formal payoffs are provided in Kang and Kugler [18]. The key equilibrium bilateral results from conditional deterrence are:

> Proposition 1: Under power parity, a dissatisfied Challenger fully exposed to retaliation can initiate a conventional war that may escalate to a WMD level. Stability is tenuous, as the status quo is not the equilibrium outcome.
> Proposition 2: Under extreme asymmetry with conventional and WMD inferiority, a dissatisfied "terrorist" with little or no exposure to nuclear retaliation may initiate limited nuclear or other WMD attack.
> Proposition 3: Under asymmetry, a satisfied or dissatisfied Challenger exposed to Defender's retaliation will not initiate a WMD attack. Deterrence is stable.

Following Yang [24, 25], Yang et al. [26, 27] and Abdollahian et al. [28], We incorporate game theory and system dynamics in an agent-based framework to understand the interactions between different of actors and simulate various scenarios. The agent based formulation could incorporate assessments of policy options that can defuse a conflict or anticipate the long-term effect of decisions made today for the future. To do so detailed information about stakeholder, their positions on critical issues related to WMD, the importance they attach to such outcomes must be added to the assessment of capability, exposure, risk and trust. Before specifying plans for this interactive capability let us review critical outcomes that need to be incorporated in this model.

Our model is implemented in NetLogo with both state actors and non-state actors. Core variables include capability, satisfaction, trust, exposure, and risk. Under this framework, agency matters as individual game interactions, strategy decisions and outcome histories determine an their preferences for proliferation, cooperation, deterrence and conflict. Decisions are constrained or incentivized by the changing global structural environment via conditional deterrence theory, subject to individual actor attributes at any particular time. Emergent behavior on proliferation and deterrence results from individuals' current feasible choice set, conditioned upon past behavior and future expectation. Conversely, regional or global proliferation and deterrence of WMD usage emerge from actors' behavior interactions.

Understanding the interactive political-military effects of structural dynamics and individual agency in multi agent relationships are key elements of a complex adaptive systems approach. Across all, positive feedback mechanisms shift seemingly stable system phenomena towards complexity and catastrophic, far-from-equilibria conditions. Such events force our current scientific understanding to change perhaps radically, considering new possibilities and outcomes that integrate explanations across previously disparate fields. We explore the model's behavioral dynamics via simulation methods to identify paths and pitfalls towards conflict and cooperation, proliferation and disarmamanet, across different actor types.

The model is initialized with the creation of actors, which includes global power, regional power, and non-state actors that have nuclear capability, measured as destruction level. All state actors are exposed while non-state actors are not exposed in terms of their nuclear capability. The third critical agent attribute is level of satisfaction

with the current order of the international system. The lower the level of satisfaction is, the more inclined that actor wants to challenge the dominant powers. Risk attribute contributes as a multiplier when actors evaluate their expected utility of challenging or maintaining the status quo. Different from satisfaction, which reflects the actor's current status, the trust attribute reflects the level of trustworthy measured by previous behavior. Repeated cooperative behavior in the past generates high level of trust, while non-cooperative behavior decreases the level. This attribute will be altered by proliferation of WMD in two ways. Trust can reinforced and cooperation enhanced by the addition of WMD within a cooperative arrangement for example, France nuclear weapons support the British. On the other hand, proliferation can reduce trust and have a negative impact on disarmament agreements or cooperation. Threats of use of WMD during the Cuban crisis 1962 reduced trust and may have prompted the Latin America Nuclear Free Zone agreement of 1967 Cuba's ratification of that treaty in 1992 reestablished trust within region. The most direct manipulator opportunity emerges after a conventional conflict is initiated and challenger chooses to escalate and then defender chooses to retaliate. Such actions have direct effects on relative capabilities that directly connected to the costs inflicted by participants on each other.

Figure 2 shows the high level architecture of our model, which incorporates macro, meso and micro theories, empirics and policy courses of action. In our conditional deterrence framework, agent strategies are adaptive, which affect dyad pairs locally

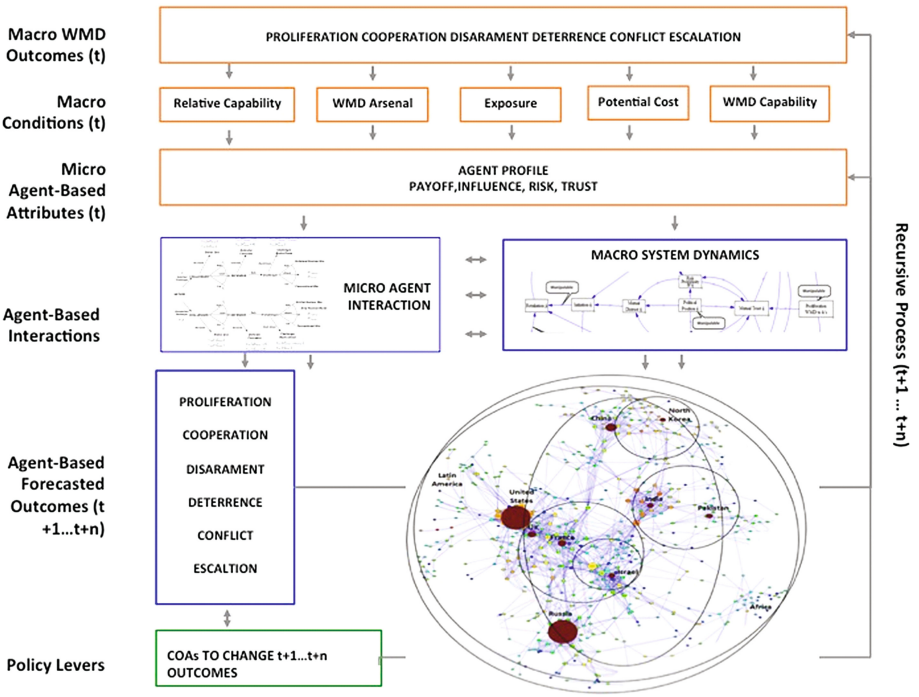

Fig. 2. Model framework

within a proximate radius as first order effects. Other agents, within the system but outside delivery and exposure, are impacted through cascading higher orders. We specifically model individual agent memory or learning from dyadic outcomes as many others do [29–31]. Trust and risk components allows sum of all prior individual behavioral histories and evolutionary through iterations to contribute to each individual and current macro states of proliferation or deterrence. Actors calculate their expected payoff for challenging and not challenging status quo, and the perception of a pair of agents determines the behavior and outcome of their interaction.

The structural approach provides a partial picture of war outcomes that can be further extended with agent based analysis. Japan challenged the US by its attack on Hawaii. The defender shifted risk propensity and then retaliated with full force, eventually terminating the conflict using nuclear weapons. Escalation of conflict differs from initiation of conflict thus far studied. The dynamics of escalation need to be understood to anticipate conflicts with potential to escalate. Such extensions cannot be solved with the current approach.

As an initial effort at a scale integrated framework, this focuses on the coupling of global and regional deterrence and proliferation structures and agency, before enriching subcomponent process detail. Thus agents simultaneously co-evolve as strategy pair outcomes at t to shape outcomes at $t + 1$, thus driving both positive and negative feedback process through $t + n$ iterations. These shape agent attributes which conduct adaptation to a changing environment, summing proliferation, cooperation, disarmament, deterrence, conflict and escalation values. Feedback into subsequent dyadic interaction and strategy choice yields a complex adaptive system representation across multiple scales.

Key will be identifying behavioral symmetry breaks and formally testing for catastrophic or chaotic responses [32] to changes in relative capabilities, exposure, costs and behavior attributes. One approach is to endogenize perturbations and shocks across structural vector values and agent space, to map equilibrium stability and system phase transitions. As domain linkages couple and morph, differential patterns of individual behavioral and system response can be identified through multiple local and global solution trajectories. This can allow us to parameterize the entire conditional deterrence macro-micro model via Monte Carlo simulation methods to explicitly identify and anticipate higher order catastrophic or chaotic, observed system behavior, driven by micro-level agent interactions. More importantly, this provides a portfolio of best response strategies, to help mitigate unwanted outcomes.

To answer the multi actor questions posed by structural conditional deterrence, we strongly believe that integrating macro, meso and micro theories and approach in a complex adaptive modeling framework could give us a handle for the analysis by stakeholders that differ in their assessments of risk, exposure and willingness to accept costs. We are aware that structural models only provide the necessary but not sufficient conditions for evolution of crisis to conflict and the escalation of a war to severe levels that could involve WMD. We use the formal results tested at the national level to develop far more sensitive tools that could provide practitioners with a map that assess the likelihood of initiation and escalation of conflicts and the possible effects of proliferation.

4 Discussion

Conditional deterrence implies that WMD can prevent conflict under narrow conditions, but can lead to WMD imitation, retaliation or exchange under many other structural conditions. Understanding the dynamics of transition between outcome is critical to minimize the likelihood of WMD use in war. Our model shows that WMD free zones - like the Latin American nuclear free zone – can eliminates the possibility of use of WMD even though it does not eliminate or limit conventional conflict. Thus, understanding how to press for a nuclear free zone in the Middle East by persuading Israel and its rivals to remove WMD would not reduce the likelihood of further conventional conflict but would remove the danger of escalation to a WMD confrontation. Likewise a WMD free zone could reduce the likelihood of WMD use by North Korea even though it could encourage South Korea to support reintegration by force. Eliminating WMD diminishes the severity of war and escalation of crisis but does not reduce the frequency or likelihood of such events. A sweet spot can perhaps be detected b a careful assessment of each of these situations.

Conditional deterrence indicates that Global powers cannot abandon WMD because the technology is in place and small rough nation or non sate agents acquiring such capabilities can effectively blackmail the great powers. While a monopoly is no longer feasible, a security oligopoly in which the position of WMD is dominated by the hierarchically great powers holding WMD with global reach can minimize the likelihood of their use. This voluntary or institutionalized collusion of WMD oligopolies would reduce access to WMD and prevents first use by the threat of immediate retaliation would provide safety for participants that lack such weapons. The great power could only maintain within the WMD oligarchy if they develop mutual trust.

References

1. Blair, B., Brown, M., Burt, R.: Can disarmament work? Foreign Aff. **90**(4), 173–178 (2011)
2. Perkovich, G., Acton, J. (eds.): Abolishing Nuclear Weapons: A Debate. Carnegie Endowment for International Peace, Washington (2009)
3. Sagan, S.D.: The case for no first use. Survival **51**(3), 163–182 (2009)
4. Sagan, S.D.: Policy: a call for global nuclear disarmament. Nature **487**(7405), 30–32 (2012)
5. Brodie, B.: The Absolute Weapon: Atomic Power and World Order. Ayer Co Pub, Manchester (1946)
6. Brodie, B.: Strategy in the Missile Age. Princeton University Press, Princeton (1959)
7. Intriligator, M.D., Brito, D.L.: Can arms races lead to the outbreak of war? J. Confl. Resolut. **28**, 63–84 (1984)
8. Mearsheimer, J.: Back to the future: instability in Europe after the cold war. Int. Secur. **15**, 5–56 (1990)
9. Waltz, K.: Why Iran should get the bomb. Foreign Aff. **91**, 2 (2012)
10. Mueller, J.: Atomic Obsession: Nuclear Alarmism from Hiroshima to Al-Qaeda. Oxford University Press, New York (2009)
11. Zagare, F.C., Kilgour, D.C.: Perfect Deterrence. Cambridge University Press, Cambridge (2000)

12. Knight, F.H.: Risk, Uncertainty and Profit. Hart, Schaffner and Marx, New York (1921)
13. Chavas, J.P.: Risk Analysis in Theory and Practice. Academic Press, Cambridge (2004)
14. Morgan, M.G., Henrion, M.: Uncertainty: A Guide to Dealing with Uncertainty in Quantitative Risk and Policy Analysis. Cambridge University Press, New York (1990)
15. Varian, H.R.: Microeconomic Analysis. Norton & Company, New York City (1992)
16. Damodaran, A.: What is the risk-free rate? A search for the basic building block. New York University, Stern School of Business (2008, unpublished papers)
17. George, A.L., Smoke, R.: Deterrence in American Foreign Policy: Theory and Practice. Columbia University Press, New York City (1974)
18. Kang, K., Kugler, J.: Assessment of deterrence and missile defense in East Asia: a power transition perspective. Int. Area Stud. Rev. **18**(3), 280–296 (2015)
19. Kugler, J.: Terror without deterrence: reassessing the role of nuclear weapons. J. Confl. Resolut. **28**(3), 470–506 (1984)
20. Kugler, J., Zagare, F.C.: Exploring the Stability of Deterrence. Lynne Rienner Publishers, Boulder (1987)
21. Organski, A.F.K., Kugler, J.: War Ledger. University of Chicago Press, Chicago (1980)
22. Harsanyi, J.C., Selten, R.: A generalized Nash solution for two-person bargaining games with incomplete information. Manag. Sci. **18**(5-part-2), 80–106 (1972)
23. Powell, R.: Crisis bargaining, escalation, and MAD. Am. Polit. Sci. Rev. **81**(03), 717–735 (1987)
24. Yang, Z.: The freedom of constraint: a multilevel simulation model of politics, fertility and economic development. J. Policy Complex Syst. **2**(2), 3–21 (2015)
25. Yang, Z.: An agent-based dynamic model of politics, fertility and economic development. In: Proceedings of The 20th World Multi-Conference on Systemics, Cybernetics and Informatics (2016)
26. Yang, Z., Abdollahian, M., Neal, Pd: Social spatial heterogeneity and system entrainment in modeling human and nature dynamics. In: Zhang, L., Song, X., Wu, Y. (eds.) Theory, Methodology, Tools and Applications for Modeling and Simulation of Complex Systems, pp. 311–318. Springer, Singapore (2016)
27. Yang, Z., de Neal, P., Abdollahian, M.: When feedback loops collide: a complex adaptive systems approach to modeling human and nature dynamics. In: Duffy, V.G. (ed.) Advances in Applied Digital Human Modeling and Simulation, pp. 317–327. Springer International Publishing, Cham (2017)
28. Abdollahian, M., Yang, Z., Coan, T., Yesilada, B.: Human development dynamics: an agent based simulation of macro social systems and individual heterogeneous evolutionary games. Complex Adapt. Syst. Model. **1**(1), 1–17 (2013)
29. Axelrod, R.: The evolution of strategies in the iterated Prisoner's Dilemma. In: The Dynamics of Norms, pp. 199–220 (1987)
30. Nowak, M., Sigmund, K.: A strategy of win-stay, lose-shift that outperforms tit-for-tat in the Prisoner's Dilemma game. Nature **364**(6432), 56–58 (1993)
31. Nowak, M.A., Sigmund, K.: Evolution of indirect reciprocity by image scoring. Nature **393** (6685), 573–577 (1998)
32. Wolf, A., Swift, J.B., Swinney, H.L., Vastano, J.A.: Determining Lyapunov exponents from a time series. Phys. D: Nonlinear Phenom. **16**(3), 285–317 (1985)

User Experience Modeling

The Virtuality Continuum and Storytelling: Simulation, Interactivity, User Experience and Interaction Design in Virtual and Mixed Environments. A STEAM Based Approach

Jose Luis Rubio-Tamayo[1(✉)], Manuel Gertrudix Barrio[2], and Francisco García García[3]

[1] Ciberimaginario Research Group,
Department of Communication Science and Sociology,
King Juan Carlos University (URJC), Campus de Fuenlabrada, Madrid, Spain
joseluisrubiotamayo@ciberimaginario.es
[2] King Juan Carlos University (URJC), Despacho 234,
Edf. Departamental I, Campus de Fuenlabrada, Madrid, Spain
manuel.gertrudix@urjc.es
[3] Faculty of Information Science (UCM),
Complutense University of Madrid (UCM), Despacho 221,
Avenida de la Complutense s/n, 28040 Madrid, Spain
fghenche@gmail.com

Abstract. Virtual reality and digital environments are phenomena that have several theoretical and experimental approaches different domains research fields. The interactivity, simulation, or immersion in virtual environments help to set new research frameworks for using and implementing digital information and communication technologies. This fact contributes for several researches in order to develop new technological interactive and communicational systems. The relationships between environment, individuals and technology transform when interactive ICT systems are implemented, carrying research to new conceptual frameworks. The current research explores possibilities and potential of digital interactive and immersive environments, in order to contribute to set models to communicate with the technological interfaces, as well as designing new conceptual interaction systems. Thus, design of interactive systems needs to be focuses in practices such as user experience and interaction design, as well as integrate storytelling or specifications such as IMS LD, in order to improve the design of those systems. The research aims also focus in interdisciplinary such as approaches STEAM (Science, Technology, Engineering, Arts and Mathematics). Results describe how virtual reality or emerging ICT have a strong impact in the interaction between individuals and their environments, and open lines of research in aforementioned disciplines (interaction design, user experience, human-computer interaction, video game design or communication systems and processes, or ergonomics and cognitive science), improving interactive process between users, digital information and virtual and physic environments.

Keywords: Communication environments · Computer simulation · Interaction · Simulation · Virtual reality

D.N. Cassenti (ed.), *Advances in Human Factors in Simulation and Modeling*,
Advances in Intelligent Systems and Computing 591, DOI 10.1007/978-3-319-60591-3_31

1 Introduction

Nowadays, the Virtuality Continuum is a key element within the Communication and Information Sciences' context. The Virtuality Continuum can be divided into different levels [1]: virtual reality, augmented reality and augmented virtuality -potentially interesting factors in the abovementioned fields of study. The components of the real world are also relevant in the approach of the virtuality continuum; idea that should be taken into account when designing interactions and approaching them as interfaces. The possibilities for research in this area are relevant when conducting a study based on the different components which can help us to design virtual-physic interactive systems. Among those components: simulation, interaction, user experience, immersion and transformation of the narrative processes, can be found.

The interaction between individuals, environments and/or the information, achieves a multidimensional approach when different layers of the virtuality continuum are interrelated. The interaction surface (or interface) increases when the possibilities of technologies in different levels of virtuality are taken into account. Possibilities to apply and develop new interaction settings and new approaches on the relationship with the information are quickly developing. Thus, this fact allows conceiving and designing new interactive virtual systems based on user experience and needs, and design experiences and interactions with available technologies.

The interrelation between the current interfaces is gathering strength thanks to haptic technologies, virtual environments, augmented reality and the use of open source hardware based on approach to design interactive systems. The experience -that integrates the ergonomic and affective dimension- is a relevant factor in emergent disciplines such as human-computer interaction, interaction design and/or user experience, which allow us to conceive new systems with technological possibilities. These settings show a different level of relationships between humans and computers, since both the real world and different layers of virtual information are being covered. For instance: pervasive games, alternate reality games or high constructivist power environment development, improved by the evolution of the different technological devices. The evolution of those devices and technologies allow us to imagine and develop

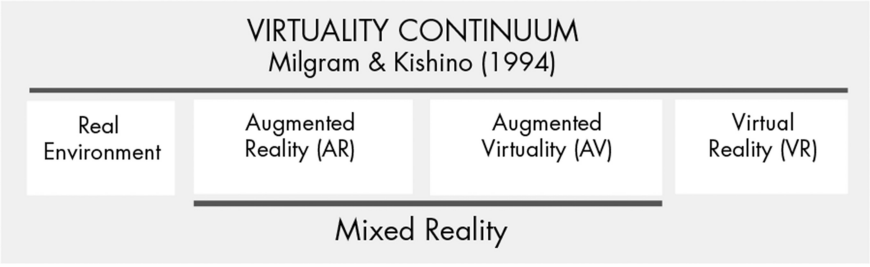

Fig. 1. Representation of the virtuality continuum scale [1]. Those levels are one of the basis in ICT, new media, communication, information and computer sciences research. And enable to position concepts such as interaction, simulation or immersion and to visualize the relationship between users, devices and (virtual or real) environments.

new ways for interacting and communicating, by diversifying the nature of the virtual environments and information, and opening innovative ways to integrate games, scientific research or educational resources in real virtual environments and systems (Fig. 1).

2 Literature Review

Both the research on virtual reality and the range of applications of virtual components are a relevant subject of study, since the first approaches of Lanier [2] and Lanier and Biocca [3] in 1992. Those approaches, mainly theoretical analyse the possibilities of virtual reality and virtual components. In the same year Caudell and Mizell [4] coined the term augmented reality. Two years later Milgram and Kishino [1] put into context both concepts, added the real world dimension, and developed the reality-virtuality continuum approach. The applications in technological contexts and the theoretical dimension are relevant in areas such as video game design and development, game theory, virtual interactive environment designs [5], and user experience in new media [6]. Theories of information and communication [7] are, in this way, relevant to understand the approach of virtual and augmented realities as new ways of creating stories and exploring new ways of interaction, in order to establish standards to conceive and design new systems which keep in mind user experience or user interfaces [8]. On the other hand, simulation or researches in interaction with virtual objects and environments have been relevant and useful in several fields.

The migration of the interaction processes into the virtual dimension is not a recent phenomenon. It has been developed through the study and implementation of virtuality continuum technologies and processes, and applied in several fields of knowledge, such as Engineering, Education, Arts, Psychology and Medicine, to name some. For that reason, and in order to set standards for designing technological systems including virtual environments and interactive approaches, is relevant an interdisciplinary field approach based on STEAM (Science, Technology, Engineering, Art and Mathematics). The evolution of the expressive and creative dimensions through virtual, mixed and augmented reality is an interesting field of research in the mentioned fields, which keeps in mind interaction processes. Part of the scientific literature is observing a transition phenomenon in the artistic and creative disciplines and emergent interacting ways -e.g. from the electronic arts to the virtual arts [9]. The possibilities of interaction are then increased when artistic factors such as interaction design or human-computer interaction are integrated [10, 11]. This fact, on the other hand, increases the possibilities for the user to take an active role in the events or processes, taking part in this process. This would also allow the development of research lines focused on improving interactive components in virtual objects [12]. The mentioned frameworks, strongly influenced by different disciplines and fields of knowledge with dimmed borders, show new and innovative frameworks where Technology, Sciences and the Arts often come together [13]. Science, Technology or Engineering often have an essential role in the interaction processes and the way in which individuals build a relationship with technology and environment, while, on the other hand, information, media and communication sciences are progressively more important in the scientific and technological related areas.

Virtual technologies and environments allow and facilitate the Interactivity and inter-operability between the aforementioned areas. This interoperability and feedback helps integrate the user experience in video games to improve scientific research, augmented reality in cultural heritage, through hybrid disciplines such as cognitive ergonomics. It is also possible to use virtual reality and human-computer interaction to simulate experiences and develop virtual systems [14] to implement processes for training and education in several domains, such Education, Health Sciences or Engineering.

3 Methodology

The methodological framework encompasses different techniques and instruments that address, from different approaches, the relationship between technologies and the creative/innovative processes, in an approach based on virtuality continuum technologies and ways to implement in various domains. This relationship occurs in virtual, mixed, augmented or physic environments, and contributes to design new research frameworks in ICTs. Virtual reality, augmented reality, metaverses, digital manipulatives, video games, alternate reality games (ARGs) and robotics are good examples of components being part of this virtuality continuum approach. Innovative storytelling experiments, creative processes (such as e.g. electronic brainstorming) or interactive artistic innovations occur in virtual environments, medialabs, digital laboratories or fablabs, which are an essential part of research in relationship between individuals, virtual environments, information, and real world.

First of all, a sample of 30 experts and professionals from international laboratories (and medialabs) were interviewed. These professionals develop their activities around virtuality continuum technologies, using augmented reality, game engines, robotics or visual programming, among others. The survey focuses on disciplines such as interaction design, human-computer interaction or cognitive ergonomics. Other theories in ICT research, which approach technology as part of self-perception, were taken into account. The theoretical approaches used in this research are the technology acceptance model or TAM [15], the motivational model (MM) or theory of reasoned action (TRA), which have a strong relationship with aforementioned knowledge areas [16, 17].

Secondly, 60 projects carried out in medialabs that used virtual reality or environments, augmented reality or interactive hardware and devices like robotics, have been analysed. Those 60 projects were developed in twelve laboratories and medialabs that focus in technological, artistic, educational or scientific research (STEAM) with technologies based on the virtuality continuum. To represent this analysis, diagrams and specifications belonging to areas such as engineering were used. This representation uses visual schemes that are distributed by category in the different components of the project.

Among those representative visual schemes, we do an approach, in the first instance, to Unified Modelling Language (UML), which is a modelling language applied to areas such as software engineering, but it's nowadays applied to represent digital systems. We also use the specification called IMS LD to represents dynamics and processes carried in those systems. In order to simplify, mental mappings and

dynamic displays are developed, using also digital data visualization tools. Approaches based on languages and specifications for designing scenarios for innovative interaction have been used as much in pioneering studies [18] as recent research. Part of the aforementioned recent research is focused on creating innovative scenarios and systems for diverse domains such as health science, training, immersive experiences or the application of project-based learning in fields like robotics [19]. The purpose of developing those specifications and visual schematics describing dynamics of such projects is precisely differentiating the components that are part of those interactions, in order to set schemes which help to design systems based on virtual environments, and have as well an approach on interaction design or user experiences.

The structural groups in which the different technological categories, based on reality-virtuality continuum, have been divided for this research are: virtual reality tools, augmented reality tools, game engines, free hardware tools (including robotics), and serious games (including videogames, augmented reality games or ARGs). The study of the interaction between the individuals and the overlapping multilevel layers of information reveals a number of possibilities to be applied in different areas [20]. This phenomenon presents one of its main examples in applying virtual environments and game dynamics to domains such education and training [21], where three components that influence the construction of the interactive environment are observed: the individual, the content (virtual and real information and objects), and the context (environments, interaction dynamics, and processes).

4 Results

The research or conceptual approach to the virtuality continuum has expanded due to technological progress both in digital and interactive technologies, environments and interfaces -which involve an increase on the interaction surface- is wider than ever before. The implication of the immersions, multidirectional interaction, multidimensional and complex haptic surfaces, high quality graphics and sounds lead to a wider range of possibilities to develop complex virtual-physic scenarios and design new systems based on virtual environments and user experiences.

Technologies are also mixed, to the extent that video games are also educational products which can be used also in scientific research, and robotics can be simulated in virtual environments. As it is described in the first part of this paper, the interaction processes are a relevant part of the object of study in this context, and interdisciplinary areas such as interaction design and human-computer interaction are relevant in research in communication and development of virtual environments. In this context, interaction is a relevant phenomenon involving the creative processes, cognitive factors, affective computing and the improvement of interfaces. In an approach based on ergonomics, both the physical dimension of the interfaces and the features of the virtual environment are relevant.

Results, based on the interaction design and the user experience approach, generally show a high rate of acceptance with regards to the structural groups in which technologies have been categorized (virtual environments, augmented reality, game approach).

The perceived usefulness of the results (deeply related to interaction design and human-computer interaction) shows relevant high rates. In fact, the weighted arithmetic shows a value of 4.03 (in a 1–5 Likert scale) related to the perception of the contribution and relevant role of technologies during the development processes. On the same scale, the perception of technologies to support a creative and constructive process shows a value of 3.97. In the other hand, one of the most outstanding factors is that the interaction with peer perception strengthens the creative production, with a value of 4.80 on the same scale.

Video games, game engines, integrated development environments (IDE) or open source hardware have quite a high rate of perception related to the processes and activities related. That is why survey respondents in this research think that the technologies related to the virtuality continuum are the right tools to strengthen creativity in scientific research or artistic work (or STEAM contexts) and for develop virtual environments which help interact with information and peers. Research has an experimental approach that can be strengthen when the subjects interact with technologies based on the virtuality continuum.

This study has also shown trends of moderate-high rate of interest in facts such as human-computer interaction (HCI) and human-environment interaction research, as well as interaction design or other related domains, such as user experience and user-centred design. Thus, the perceived usefulness (PU) of augmented reality tools has a value of 3.86 in a Likert scale (1 to 5). That means that there is an interest to investigate how augmented technologies in scientific research can be integrated. Perceived as easy to use (in an approach based on interaction design, HCI and user experience, among others) for immersive 3D and 2D environments, those also show relative high rates (4.10 and 4.00). Games -mainly serious games, but also video games ARGs-are also perceived as a relevant factor to strengthen creativity and produce innovative ideas (4.34) to be applied in other research scientific and technological fields. That reveals the importance of integrating game theories, approaches and studies in research fields related to interaction, and keep it in mind for develop virtual systems for various goals. Game studies, interaction design, human computer interaction or user experience are interdisciplinary research fields that bring together different branches of knowledge and academic disciplines, focusing on a STEAM approach: fine arts, computing, engineering, ergonomic factors, psychology, anthropology, sociology, communication, design or media studies.

Nowadays, new applications in several research fields have been found and implemented. However, it is necessary to foster research in interdisciplinary fields in order to make the most of technologies framed in the virtuality continuum approach. Simulation – as an approach to representation- will then contribute to deepen the research based on virtuality continuum technologies. Representation needs, therefore, a language, a channel, a message and other elements framed in communication theory. Interactivity needs, on the other hand, to be part the improvement of interfaces for developing new experiences and dynamic systems which allow simulating part of those experiences.

The ability of the objects and (virtual) environments influenced by actions taken by the user shapes the inputs in immersion and interaction. This fact also shows the ability of virtual environments and technological devices to react to the user's behaviour – that

turns into a more complex behaviour as technology progresses. Ergonomics are also related with immersion, simulation and interaction: virtual environments with a lower immersion degree often incorporate the audio visual spectrum of information (sight and sound) and sometimes haptics. More immersive environments, however, include proprioception and/or balance, which open new challenges to design interactive experiences and immersive virtual environments and systems.

User experience also has an important role in the design of applications for dynamic environments based on a virtuality continuum approach. The user experience brings together the aforementioned relationship between the content, the environment and the components; taking into account emotions and creativity as relevant factors.

The approach of the different levels of reality as a continuous line has made a number of important contributions to the field of representation and conception of the space, which holds a strong relationship with the development of systems. The importance of expressive power of virtual and computational media [13], drives us to new interactions between the individuals and the physical and virtual interfaces, objects and environments. The expressive power of the virtual and interactive media establishes new approaches in relationship to the individuals and (physical and virtual) objects, affective implications, actions, environments and objectives, carrying us to develop standards of new systems, keeping in mind languages such as UML or specifications such as IMS LD.

Results also show the need to taxonomically classify and categorise the elements which are studied under the approach based on the virtuality continuum. This taxonomical categorization based on this approach can be done in different ways: technology run processes, interaction levels and dimensions processes, the possibilities of technology for develop projects, specific features of technologies, or gameplay. As abovementioned, pioneer researches [3, 4] focused these issues and developed theoretical approaches. Milgram and Kishino [1] traced a continuous line to study the phenomena described in both approaches, which allow us to understand, visualize and classify the complexity of the relationship between the real and virtual worlds, in order to develop models based on researches in human-computer-environment interaction and user experiences.

This aforementioned context allows us to categorise and demarcate components studied under the approach based on the virtuality continuum -game engines, video games, augmented reality or robotics- and match them with specific actions -simulation, interaction and interface design, immersion-, which will allow a more in-depth analysis of the applications in STEAM contexts. IMS LD is a useful categorization for a design, based on user experience and human-computer-environment interaction, of virtual systems and environments. The interactivity with components of those virtual systems and environments allow to users to experiment things which have been never possible before; and analysing those components requires a mix between quantitative and qualitative methods.

Results show the need to optimise the message and communication processes, as well as the need to develop research focused on interaction systems and interfaces. Communication and information may improve the data transmission, effectiveness and interaction possibilities when integrated in the research on interactivity and technology uses. Research in developing new technological devices and virtual interactive

environments is then an interesting object of study for emerging interdisciplinary STEAM domains. Dynamic flows of information are relevant issues when subjects related to the virtuality continuum are analysed and contextualised: new approaches reveal that information and communication are multidirectional and more complex with virtual, augmented or mixed interactive devices and environments, which allow users to be active subjects in the experience.

5 Conclusions

The study of the components of virtual and interactivity environments provides data about distinctive features of different phenomena, which comprises virtual reality head-mounted displays (HMD), open source hardware, robotics, haptic technologies or motion sensing input devices. That gives us the possibility to explore innovative applications for game engines, video games, integrated development environments, or augmented reality software. Distinctive features of each phenomenon lead us to the design of custom made interactive processes with environments and users, and conceive digital systems with both virtual and real components, and which carry users to new experiential processes. For that, we need to keep in mind not only the current technological features and possibilities, but also the complex features and goals of interactive process and experience desired. This way, simulation applied to the health sciences, involves, for example, a completely different process depending on the sub-domains in which the objectives of the activity are introduced. Virtual simulation for people training in decision-making situations -in case of disasters- is not designed in the same way as the simulation of an operating room for health professionals. The gameplay, environments, game-mechanics, storytelling and interaction processes are completely different. Nevertheless, both situations open lines of research in interaction design, user experience, human-computer interaction, video game design or communication systems and processes, or ergonomics and cognitive sciences, in order to improve the communication flow and interactive process between users, digital information and environments.

Thus, the virtuality continuum approach covers not only environment and object being part of it, but also processes and user's needs and goals, communication processes and information management. Its taxonomical classification (virtuality continuum) is a relevant component to be integrated when designing interactive technological combined with virtual-real systems for different uses, such as: modelling languages, specifications or standards. The development of interactive or immersive environments or experiences will accomplish further research in Science, Engineering, Communication and the Arts.

References

1. Milgram, P., Kishino, F.: A taxonomy of mixed reality visual displays. IEICE Trans. Inf. Syst. **77**(12), 1321–1329 (1994)
2. Lanier, J.: Virtual reality: the promise of the future. Interact. Learn. Int. **8**(4), 275–279 (1992)

3. Lanier, J., Biocca, F.: An insider's view of the future of virtual reality. J. Commun. **42**(4), 150–172 (1992)
4. Caudell, T.P., Mizell, D.W.: Augmented reality: an application of heads-up display technology to manual manufacturing processes. In: System Sciences, vol. 2, pp. 659–669 (1992)
5. Sharp, H.: Interaction Design. Wiley, Hoboken (2003)
6. Albert, W., Tullis, T.: Measuring the user experience: collecting, analyzing, and presenting usability metrics. Newnes, Oxford (2013)
7. Shannon, R., Johannes, J.D.: Systems simulation: the art and science. IEEE Trans. Syst. Man Cybern. **6**(10), 723–724 (1976)
8. Karapanos, E.: User experience over time. In: Karapanos, E. (ed.) Modeling Users' Experiences with Interactive Systems, pp. 57–83. Springer, Heidelberg (2013)
9. Popper, F.: From Technological to Virtual Art. MIT Press, Cambridge (2007)
10. Rogers, Y., Sharp, H., Preece, J.: Interaction Design: Beyond Human-Computer Interaction. Wiley, Hoboken (2011)
11. Baecker, R.M. (ed.): Readings in Human-Computer Interaction: Toward the Year 2000. Morgan Kaufmann, Burlington (2014)
12. Herrera Fernández, E., Fernández Iñurritegui, L.: Diseño de Objetos Gráficos-Interactivos. Icono14 **12**(1), 219–243 (2014)
13. Harrell, F., Harrell, S.V.: Strategies for arts + science + technology research: executive report on a joint meeting of the National Science Foundation and the National Endowment for the Arts (2011)
14. Sedig, K., Parsons, P.: Interaction design for complex cognitive activities with visual representations: a pattern-based approach. AIS Trans. Hum.-Comput. Interact. **5**(2), 84–133 (2013)
15. Davis, F.: Perceived usefulness, perceived ease of use, and user acceptance of information technology. MIS Q. **13**(3), 319–340 (1989)
16. Venkatesh, V., Morris, M.G., Davis, G.B., Davis, F.D.: User acceptance of information technology: toward a unified view. MIS Q. **27**, 425–478 (2003)
17. Dix, A.: Human-Computer Interaction, pp. 1327–1331. Springer, New York (2009)
18. Robinson, P.: Robotics education and training: a strategy for development. Ind. Robot: Int. J. **23**(2), 4–11 (1996)
19. Val, S., Pastor, J.: Robotics in education. Methodology and approach to technical subjects based in projects. ARSA – Adv. Res. Sci. Areas **3**(7), 1917–1921 (2012)
20. Mora-Fernández, J.: Interacciones hipermedia y videojuegos. Icono14 **7**(1), 218–241 (2009)
21. Barab, S., Gresalfi, M., Ingram-Goble, A.: Transformational play? Using games to position person, content, and context. Educ. Res. **39**(7), 525–536 (2010)

Simulating Seat Discomfort: An Experimental Design for Using Digital Human Models

Annika Ulherr(✉), Florian Zeller, and Klaus Bengler

Chair of Ergonomics, Technical University of Munich,
Boltzmannstr. 15, 85748 Garching, Germany
{Annika.Ulherr,Bengler}@tum.de, fzellerl@gmx.de

Abstract. It was the aim of the project UDASim, funded by the German ministry of education and research, to develop a tool for car seat discomfort assessment within the virtual design phase. Seat discomfort depends on a variety of parameters whose correlations are unknown. Therefore, we have chosen an artificial neural network approach using the computational results of three digital human models as input. The training data were computational results based on data from a large-scale seat discomfort study with real test subjects. The digital human models simulated all subjects and experiment conditions, so the experimental design was essential for the project goal. We describe the conducted experiment, its design and the different measurements required by the digital human models. Additionally, we explain the related measurement systems and the choice of test subjects.

Keywords: Digital human model · Discomfort · Seating · Experiment design

1 Introduction

Customers expect that car seats are comfortable and that comfort requirements need to be fulfilled [1]. To reduce time and costs associated with the product development process, computer simulations during the virtual design phase increasingly replace physical evaluations. This shift within the product development process increases the efficiency and competitiveness of the OEMs [1]. Typically, seat comfort assessments require a physical prototype for test persons to be able to evaluate seats during comfort studies. Besides being time consuming and cost-intensive, subject studies are only partially reproducible due to changing physical and psychical conditions of test persons. Since consequential design changes are more expensive in later phases of the product development process [2], seat comfort assessments should be conducted during the virtual design phase. Well-established methods to evaluate human interaction with products within virtual environments are simulations using digital human models [3]. Digital human models should be validated tools that ensure reproducible and objective findings.

Seating discomfort depends on various parameters such as seat pressure distribution [4] and posture [5]. Humans process sensations by combining sensory inputs simultaneously [6]. The same applies for the subjectively perceived seating discomfort, it bases on the different modalities involved. Therefore, a method to predict seat discomfort needs to consider several parameters.

D.N. Cassenti (ed.), *Advances in Human Factors in Simulation and Modeling*,
Advances in Intelligent Systems and Computing 591, DOI 10.1007/978-3-319-60591-3_32

The project UDASim ('Umfassende Diskomfortbewertung für Autoinsassen durch Simulation' [Eng. meaning 'Global discomfort assessment for vehicle passengers by simulation']), funded by the German ministry of education and research (BMBF), aimed to develop a tool to predict the global seat discomfort based on various discomfort parameters using digital human models. The seat discomfort prediction tool was implemented as an artificial neural network since the interrelations of different discomfort factors are not verified yet [7].

The input parameters for the artificial neural network were the computational results of three established digital human models: the multi-body system AnyBody, the FE-model CASIMIR and the 3D-CAD human model RAMSIS. A large-scale seat discomfort study with human subjects provided the training data for the artificial neural network. Therefore, the three digital human models had to be able to simulate all test subjects and experiment configurations. The authors will present and explain the experimental design, the measurement systems and test procedures of the conducted seat discomfort study.

2 Relevant Theories of Seat Comfort and Discomfort

In the middle of the 20th century, comfort and discomfort were seen as two distinct states or the opposite poles of a continuous scale [8, 9]. Yet, the current state of research indicates that comfort and discomfort are not contrasts but rather separate entities, which can occur simultaneously [10]. Physical features effect both comfort and discomfort, but only for comfort is the aesthetic design essential too [11]. Since also psycho-social factors as emotions and expectations influence the comfort feeling, Looze et al. claim that the correlation of objective measurements, e.g. seat pressure, with discomfort must be stronger than with comfort [11]. Vink and Hallbeck proposed a comfort/discomfort model in which comfort is strongly related to the personal expectations [12]. This emphasizes the assumption that discomfort correlates better with objective parameters than comfort.

Previous research focused on relationships between single objective measures and discomfort in seating [11]. Specifically, posture and movement [5, 13], seat pressure distribution [4] and muscle activity [14, 15], were previously investigated; these are all biomechanical factors, which influence seat discomfort sensations [10]. Focusing on single parameters, however, only partially represents reality as humans tend to not separate sensations and merge all sensory inputs into one feeling [6].

Therefore, a comprehensive discomfort analysis must consider multiple parameters in combination. To date, there is no knowledge about the correlations between various factors, e.g. seat pressure and movement, and their effects on seating discomfort. An artificial neural network approach, using pressure measurements, a subjective rating of the aesthetic design, anthropometric and demographic data as input and overall seat discomfort as output, showed that the relationship between the subjective rating, pressure, and anthropometric and demographic data is mainly non-linear [16]. Apparently, artificial neural networks are a more fitting method to predict seat discomfort compared to a statistical model [17].

3 Objectives

The aim of the project UDASim was to shift the evaluation of seat discomfort to an earlier phase in the product development process using three digital human models. OEMs already use well-established digital human models as objective evaluation tools in the seat development process. Each digital human model can simulate single discomfort parameters.

The research approach was based on the assumption that discomfort factors must be considered together instead of by themselves [7]. Hence, the correlations of the established discomfort parameters are unknown, the project partners decided to use an artificial neural network to predict seat discomfort based on computational results of the three involved digital human models.

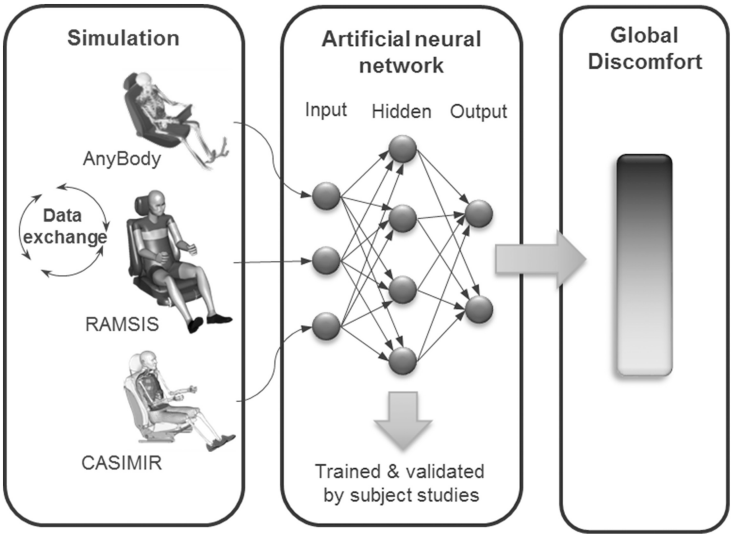

Fig. 1. Discomfort prediction procedure intended by the project UDASim [7].

Figure 1 shows the workflow used to predict global seating discomfort using three digital human models: AnyBody, CASIMIR and RAMSIS. An artificial neural network is able to predict data after a training phase. During this phase, the network recognizes patterns between presented input and corresponding output data. A test phase follows to validate whether the training was sufficient. Therefore, the artificial neural network receives input data and calculates output data based on the training before. The difference between the generated output and the recorded output defines the performance of the artificial neural network. A large-scale subject study conducted at the Chair of Ergonomics of the Technical University of Munich provided the needed training and validation data sets.

The training data set for an artificial neural network needs to have the same data format specified for its usage to fulfill the intended purpose. In our case, the artificial

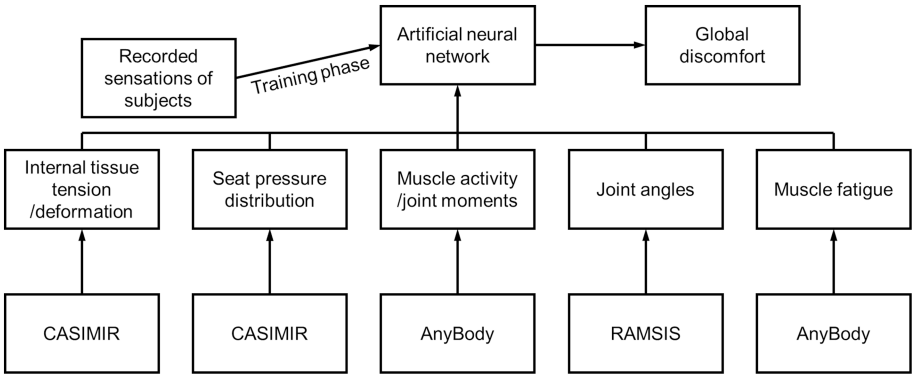

Fig. 2. Flowchart for predicting the global seat discomfort via artificial neural network using parameters calculated by AnyBody, CASIMIR and RAMSIS.

neural network should process computational results from the three digital human models involved (see Fig. 2).

Therefore, the experimental design needed to ensure that all subjects and experimental conditions were suitable for simulations to produce the needed computational results for the training and validation.

4 Methods

4.1 Requirements

Before planning the experiment, the project partners specified the needed measurement categories and the corresponding measurement systems to provide input parameters for the digital human models. Table 1 shows the required measures and their necessity.

Table 1. List of required measurements necessary for the simulation by the three digital human models (AnyBody, CASIMIR, RAMSIS).

Measure	Needed for
Anthropometry	AnyBody, RAMSIS
Body weight	AnyBody, RAMSIS
Sitting posture	AnyBody, CASIMIR, RAMSIS
Contact points with test rig	AnyBody, RAMSIS
Position of subject in the seat	CASIMIR, RAMSIS
Seat pressure distribution	CASIMIR
Contact forces of the feet	AnyBody, CASIMIR
Contact forces with steering wheel	AnyBody (were simulated)
Maximum forces of the legs	AnyBody (were simulated)
Weight on the seat	AnyBody
Adjustment of the seat	RAMSIS, CASIMIR
Subjective discomfort value	Training of the artificial neural network

The digital human model CASIMIR defined the demands on the test subjects. CASIMIR/Automotive is a finite element (FE) simulation tool, which has FE-models of three different persons representing the anthropometries of a female of the 5th percentile body height, of a male of the 50th percentile body height and of a male of the 95th percentile body height. Within the project, modelling new persons was not possible and only minor adjustments for the existing models were feasible. Therefore, the participants had to be as similar to the available models as possible. Body dimensions are normally distributed and independent of each other, so it is almost impossible to find two persons with identical measurements. The project partners therefore decided to use the body height of the three, modelled persons with a range of ±2 cm as a participation requirement. Female participants had to be within the range from 1.52 m to 1.56 m (subject group: F05) and male participants either between 1.76 m and 1.80 m (subject group: M50) or within the range from 1.85 m to 1.89 m (subject group: M95).

The possession of a driver's license was also mandatory since the experiment design resembled a driving task. The realistic driving task was equivalent to driving on a highway, included pressing the gas pedal constantly with the same force.

The existence of detailed FE-models, suitable for CASIMIR, were the requirements for the used car seats of the study.

4.2 Experimental Setup

Each of the three associated partners provided one automobile seat, which fulfilled the requirements. Combined with the intended three different car packages, the construction of the experimental setup had to be adjustable for nine configurations in total.

The experimental setup provided the possibilities to switch between the three different seats and to adjust the position of the seat in the longitudinal direction as well as the heights of the floor and the pedal system. The adaption mechanisms functioned

Table 2. Measurement systems used in the experiment.

Measurement system	Needed for measuring
Two cameras (Sony HDR-SR10)	Subject's anthropometry with PCMAN [18]
Three cameras (Sony HDR-SR10)	Subject's sitting posture with PCMAN [18]
Personal scale	Body weight
Stadiometer	Body height
Two pressure measurement plates (four shear force sensors type 745 B-1kN)	Ratio of body weight on the seat and horizontal Force component of the left foot
Rotary potentiometer (Vishay Spectrol 357-0-0-103)	Force on and position of gas pedal (right food)
Industrial scales (MyWeigh HD-150)	Contact forces of the feet on the floor
Tape measures [cm]	Adjustments of setup and seat
Two pressure mats by XSENSOR (PX100:40.40.02, PX100:40.64.02)	Pressure distribution on seat and backrest
Coordinate measuring system (FaroArm)	Defined points on the seat and backrest surfaces
CP-50 scale and body map	Subjective discomfort

mechanically, so that there were less electrical interferences with the measurement systems. Table 2 lists the measurement systems used in the experiment and their necessities.

An Arduino sound module connected to the potentiometer indicated if the force on the accelerator pedal was above or below the intended range of 17 N–18 N.

Two computers recorded the data during the experiment. The software LabView recorded for ten seconds (100 Hz) and saved the data of the potentiometer and the pressure plates via a data-recording module (NI USB-6211). The software TWedge 3.0 recorded for ten seconds (4 Hz) the measurements of the two industrial scales. The software XSENSOR X3 MEDICAL v.6.0 recorded the pressure on the seat and the backrest for ten seconds.

The experimenters measured the coordinates of the steering wheel center point and six points on the surface of the used seat (three defined on seat base and three on the backrest) with the software FARO CAM2 Measure X1.0 to record the individual adjustments made by the subject for each configuration.

Figure 3 shows the experimental setup.

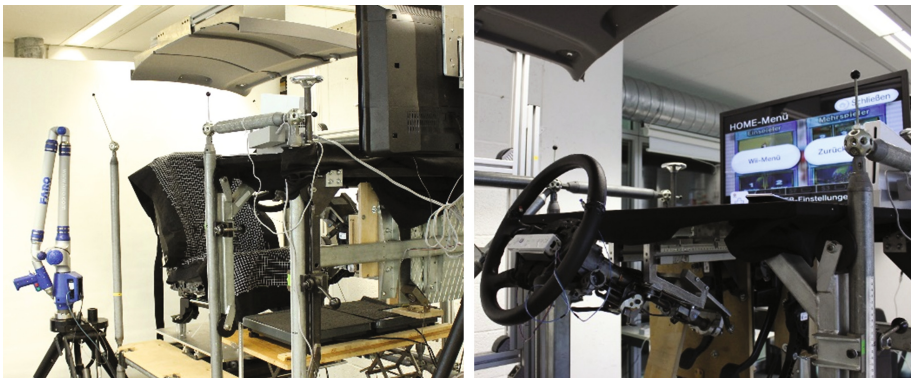

Fig. 3. Left: experimental setup with pressure mats on the seat and coordinate measuring system. Right: steering wheel with integrated Wii remote and video game 'Mario Kart' on the screen in front of the setup. Note: The cameras are out of the photographed area.

The screen placed in front of the test rig was movable upwards and downwards for unobstructed frontal photographing. The monitor was necessary to play a video game as secondary task, to provide an introduction presentation and to present the CP-50 scale and the body map (shown in Fig. 4) during the experiment for the discomfort assessment.

The CP-50 scale is valid and reliable for evaluating seat discomfort [19] and the body map is a combination, of two body maps found in literature [20, 21]. The CP-50 scale consists of a starting point (no discomfort) and five categories with ten scale points each. The subject chooses first a category and then a value to specify the tendency within the category.

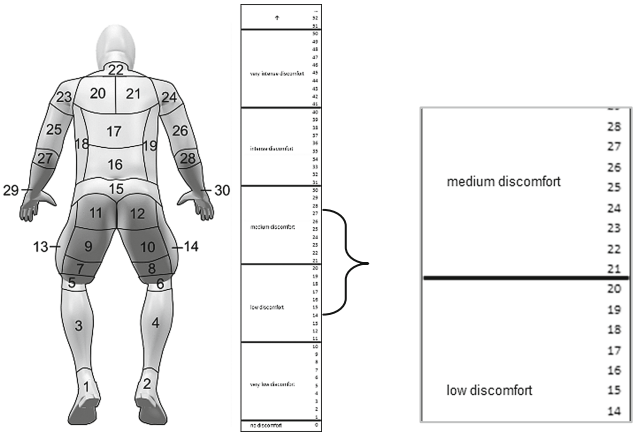

Fig. 4. Left: presented body map and CP-50 scale, consisting of a starting point (no discomfort) and five categories, subdivided in 10 scale points. Right: detail of the scale for better readability.

4.3 Experimental Design

The experiment included in total nine configurations based on the three different seats and three car packages per seat to vary the discomfort parameters.

The three vehicle geometries implemented in the experiment based upon representative chair heights from literature [22] for sports cars, passenger cars and SUVs, shown in Table 3.

Table 3. Representative chair heights from literature [22] and the chair heights implemented in the setup.

	Sports car	Passenger car	SUV
Representative chair height [mm]	135–180	200–250	300–350
Chair height of study [mm]	170	220	320

As in real cars, the positions of seat and steering wheel were identical for every subject in each configuration. The subjects could still conduct needed adjustments of the seat and the steering wheel, including seat height, backrest angle and longitudinal adjustments.

The sitting duration for each configuration was 45 min. A previous study showed no significant differences between discomfort assessments with and without secondary tasks [23]. Therefore, to distract the attention away from sitting and to counteract possible boredom, the subjects had to play Mario Kart (developed and published by Nintendo), a video game in which the player competes in kart races against virtual opponents, on the Nintendo Wii video game console. The Wii remote installed in the steering wheel provided steering control during the kart races. The subjects could accelerate and shoot virtual opponents during the races using two additionally installed buttons on the steering wheel rim. Thereby, the subjects remained in a driving position

with their hands on the steering wheel, the right foot pressing statically the gas pedal and the left foot positioned on the wooden footrest.

Data recording took place four times per configuration: first time directly after the subject sat down and every fifteen minutes afterwards. The subject paused the video game for the measurements. The data collection covered: (i) three simultaneous photos for the posture measurement (ii) the measurements for ten seconds of the pressure plates, the potentiometer, the industrial scales and the pressure mats and (iii) the assessment of discomfort values using the CP-50 scale for 30 body parts and the global discomfort.

After 45 min, the subject rose from their seat and had 15 min free time with the instruction to walk around and not to sit down during the break. While the subject was outside of the laboratory, the experimenters recorded the coordinates of the steering wheel center and the six points on the seat surface. Thereafter, they conducted the necessary changes for the following configuration: switch the seat and/or adjust the test rig for sports car, passenger car or SUV setup.

The experiment duration consisted of 45 min sitting and 15 min break for each of the nine configurations, summing up to a total of 9 h experiment time per subject. To reduce the expenditure of time per day and effects of fatigue, every subject had three appointments of three hours on three different days, at least one week apart. Every subject had a randomized order of the nine conditions.

4.4 Procedure

The recruited test subjects had instructions to wear normal clothes for the experiment. The first appointment started with the measurement of body height and weight. After the measurement, the subject sat down in the test rig. An introductory presentation provided information and instructions inevitable for the experiment. At certain points during the introduction, the subject filled in demographic information (age, gender, and profession), recent aliments in relevant body parts (back, hip, and legs) and provided information about his or her current mood.

To record the anthropometry, the subject stepped out of the test rig and adopted an upright position and a so-called pharaoh-position (left foot elevated, left knee, left hip and left elbow approximately 90°). For each posture, the experimenters took two simultaneous photos from two directions.

Back in the test rig, the subject had to adjust the seat and steering wheel to sit comfortably in a driving position. Thereafter, the subject tested the video game to become acquainted with it. After the experimenters placed the pressure mats on the seat, the subject sat down again and adopted the driving posture including pressing the accelerator pedal, which must both stay the same for the following 45 min. After the experimenters took the pictures for the posture measurement, noted the personal adjustments of the seat and recorded the remaining data, the subject stated the discomfort values. Then the subject started playing Mario Kart until the break for the second round of measurements took place after 15 min. This sequence recurred two more times until the fourth and last data recording occurred after 45 min. During the following break, the subject had the instruction to walk around and not to sit down.

After 15 min, the subject reentered the laboratory where the experimenters had modified the test rig accordingly to the following configuration.

For the sequent two configurations during one appointment, the procedure was the same as in the previous paragraph, starting with the subject adjusting seat and steering wheel and ending with the experimenters modifying the test rig for the next configuration belonging to this or to the following appointment.

The second appointment started with the subject filling out the questionnaire about his or her current mood. After that, the procedures for three different configurations repeated as during the appointment before.

The third appointment was the same as the second appointment. At the end of the third appointment, therefore the end of the experiment for this subject, the subject filled in a final questionnaire with questions about the discomfort evaluation during the experiment.

4.5 Participants

In total, 40 subjects participated in the experiment. Table 4 lists the average age, body height, body weight, and the numbers of participants sorted by the, in paragraph 4.1, defined subject groups.

Table 4. Participants sorted by subject groups.

Group	Gender	Number	Age	Body height	Body weight
F05	Female	13	Ø 23.4 yrs. (SD: 2.5 yrs.)	Ø 154 cm (SD: 1.54 cm)	Ø 57.5 kg (SD: 7.68 kg)
M50	Male	14	Ø 23.6 yrs. (SD: 3.65 yrs.)	Ø 178 cm (SD: 1.28 cm)	Ø 81.2 kg (SD: 7.14 kg)
M95	Male	13	Ø 25.6 yrs. (SD: 4.75 yrs.)	Ø 187 cm (SD: 1.39 cm)	Ø 82.9 kg (SD: 8.13 kg)

Ten participants of each group should provide the data sets for the training of the planned artificial neural network. The validation process of the artificial neural network should use the data of the remaining ten participants.

5 Results

The results of the conducted study are not comparable to other studies in the research field of seating discomfort. Usually studies have the purpose to answer specific research questions. In contrast, the presented study had the assignment to collect data to train and evaluate an artificial neural network to predict seat discomfort. The experiment design's aim was to vary discomfort parameters, among other seat pressure, muscle activity and posture, using different seats, persons and vehicle packages.

After 360 h of experiments, the experimenters recorded 1440 sets of raw data.

$$40\,\text{participants} \times 9\,\frac{\text{configurations}}{\text{participant}} \times 4\,\frac{\text{measurements}}{\text{configuration}} = 1440\,\text{measurements}. \quad (1)$$

The project partners decided to use only the last recorded data set for each configuration, so 360 data sets, as input for the planned artificial neural network to assess seating discomfort. Thereby, the artificial neural network should be able to predict the discomfort after 45 min sitting in a car seat based on the training with 270 data sets, and the validation with the remaining 90 data sets.

The number of discomfort values recorded during the experiments is 44640.

$$1440\,\text{measurements} \times 31\,\frac{\text{discomfort values}}{\text{measurement}} = 44640\,\text{discomfort values}. \quad (2)$$

With every measurement occurring, the subject stated 31 discomfort values. Thirty values for the individual body parts and one global discomfort value. The artificial neural network implementation used only the global discomfort value after 45 min.

The relatively small amount of data, compared to the effort recording the data, used for the implementation of the artificial neural network, leaves the authors with a treasure of data to analyze. The extensive amount of discomfort values combined with a comprehensive set of parameters enables the authors to find further interesting discoveries concerning discomfort evaluations and discomfort studies. The authors plan future publications to present the results of the pending analysis.

For the implementation and outcome of the project's artificial neural network, the authors like to refer to another publication [24].

6 Discussion

The objective of the presented experiment was to gather data for the implementation of an artificial neural network to predict the global discomfort of car seats using computational results of three digital human models. Therefore, the extensive design of the experiments needed to consider several requirements, so the digital human models were able to simulate the subjects and the experiment conditions.

Because of their complexity, the measurement systems in this experiment were very sensitive to disturbances and required the presence of two experimenters to execute each experimental session. Combined with the long duration of the experiment per subject, the study was quite costly in terms of time and resources. Additionally, the recorded data needed post-processing to make it usable for the digital human models.

Lessons-learned from the conducted experiment are that requirements of anthropometric data compared with a long duration of an experiment, makes it harder to recruit participants. Especially the recruitment of female participants fulfilling the requirements of body height was complicated, due to rarity of the height among the population. The cumulative frequency for the German population (18–65 years) of a body height within the range from 1.52 m to 1.56 m is 3.11% according to the last

serial measurement in Germany [25]. To find and motivate women with a driver's license to participate in an experiment with a duration of nine hours, distributed over three days, extended the length of the conducted study. Additionally, the primarily male dominated environment of the mechanical engineering department, where the Chair of Ergonomics is located, reduced the probability to find females meeting the requirements. It took almost a year between the first appointment of the first subject and the last appointment of the last subject.

The participants enjoyed playing Mario Kart on the Wii, controlled by steering wheel movements, as the secondary task. Even though almost all participants imagined that holding the right foot in the same position while driving a kart race would be complicated, it worked out quite well. The relatively low average age might be a reason for that, since young adults are more used to playing games on video game consoles like the Wii than older generations.

7 Conclusion

It is possible to conduct a seat discomfort study in a way that three different digital human models are able to simulate the experiment, the participants and the used configurations afterwards. By presenting the considered requirements, the experimental setup, design and procedure, the authors wanted to share experiences and occurred difficulties with the scientific community. The collected, extensive data most certainly holds very interesting knowledge about effects of, among others, experimental design on seat discomfort.

Acknowledgements. The authors like to thank the German ministry of education and research for funding the project UDASim, and the associate partners (BMW Group, Daimler AG and Ford) for their support.

References

1. Kolich, M.: A conceptual framework proposed to formalize the scientific investigation of automobile seat comfort. Appl. Ergon. **39**, 15–27 (2008)
2. Römer, A., Pache, M., Weißhahn, G., Lindemann, U., Hacker, W.: Effort-saving product representations in design—results of a questionnaire survey. Des. Stud. **22**, 473–491 (2001)
3. Chaffin, D.B., Nelson, C.: Digital Human Modeling for Vehicle and Workplace Design. Society of Automotive Engineers, Warrendale (2001)
4. Zenk, R., Mergl, C., Hartung, J., Sabbah, O., Bubb, H.: Objectifying the comfort of car seats. In: SAE 2006 World Congress and Exhibition. SAE International, Warrendale (2006)
5. Vergara, M., Page, Á.: Relationship between comfort and back posture and mobility in sitting-posture. Appl. Ergon. **33**, 1–8 (2002)
6. Mather, G.: Foundations of Sensation and Perception. Psychology Press, Hove, New York (2009)

7. Ulherr, A., Bengler, K.: Global discomfort assessment for vehicle passengers by simulation (UDASim). In: Proceedings of 3rd International Digital Human Modeling Symposium DHM 2014 (2014)
8. Hertzberg, H.T.E.: Seat comfort. Annotated bibliography of applied physical anthropology in human engineering. WADC Technical report, 30–56 (1958)
9. Shackel, B., Chidsey, K.D., Shipley, P.A.: The assessment of chair comfort. Ergonomics **12**, 269–306 (1969)
10. Zhang, L., Helander, M.G., Drury, C.G.: Identifying factors of comfort and discomfort in sitting. Hum. Factors **38**, 377–389 (1996)
11. de Looze, M.P., Kuijt-Evers, L.F.M., van Dieën, J.: Sitting comfort and discomfort and the relationships with objective measures. Ergonomics **46**, 985–997 (2003)
12. Vink, P., Hallbeck, S.: Editorial: comfort and discomfort studies demonstrate the need for a new model. In: Vink, P., Hallbeck, S. (eds.) Special Section on Product Comfort, vol. 43, pp. 271–276 (2012)
13. Telfer, S., Spence, W.D., Solomonidis, S.E.: The potential for actigraphy to be used as an indicator of sitting discomfort. Hum. Factors: J. Hum. Factors Ergon. Soc. **51**, 694–704 (2009)
14. Hosea, T.M., Simon, S.R., Delatizky, J., Wong, M.A., Hsieh, C.-C.: Myoelectric analysis of the paraspinal musculature in relation to automobile driving. Spine **11**, 928–936 (1986)
15. Durkin, J.L., Harvey, A., Hughson, R.L., Callaghan, J.P.: The effects of lumbar massage on muscle fatigue, muscle oxygenation, low back discomfort, and driver performance during prolonged driving. Ergonomics **49**, 28–44 (2006)
16. Kolich, M.: Predicting automobile seat comfort using a neural network. Int. J. Ind. Ergon. **33**, 285–293 (2004)
17. Kolich, M., Seal, N., Taboun, S.: Automobile seat comfort prediction: statistical model vs. artificial neural network. Appl. Ergon. **35**, 275–284 (2004)
18. Seitz, T., Bubb, H.: Measuring of human anthropometry, posture and motion. In: Digital Human Modeling For Design and Engineering Conference and Exposition. SAE International, Warrendale (1999)
19. Shen, W., Parsons, K.C.: Validity and reliability of rating scales for seated pressure discomfort. Int. J. Ind. Ergon. **20**, 441–461 (1997)
20. Cameron, J.A.: Assessing work-related body-part discomfort: current strategies and a behaviorally oriented assessment tool. Int. J. Ind. Ergon. **18**, 389–398 (1996)
21. Hartung, J.: Objektivierung des statischen Sitzkomforts auf Fahrzeugsitzen durch die Kontaktkräfte zwischen Mensch und Sitz. Garching bei München (2006)
22. Macey, S.: H-POINT. The Fundamentals of Car Design & Packaging (2009)
23. Ulherr, A., Hasselmann, K., Kuhn, K., Bengler, K.: The effect of secondary tasks on the perceived seating discomfort. In: The Proceedings of the 19th Triennial Congress of the International Ergonomics Association (2015)
24. Ulherr, A., Bengler, K.: Simulating seat discomfort: an experimental design for using digital human models. In: 8th International Conference on Applied Human Factors and Ergonomics (2017)
25. SizeGERMANY: Abschlussbericht zur repräsentativen, neuen Deutschen Reihenmessung. Kaiserslautern, Bönnigheim (2010)

A Comparative Study of Virtual Reality and 2D Display Methods in Visual Search in Real Scenes

Juan Carlo M. Figueroa(✉), Raul Alberto B. Arellano, and Janeen Mikee E. Calinisan

College of Engineering, University of the Philippines Diliman, 1101 Quezon City, Philippines
{jmfigueroa, rbalberto, jecalinisan}@up.edu.ph

Abstract. People perform visual search tasks every day: from trivial tasks to emergencies. Classical research on visual search used artificial stimuli to identify factors that affect search times and accuracy. Recent studies have explored visual search in real scenes by simulating them on two-dimensional displays. The scientific community continues to use new technology to formulate better methods and practices. Virtual reality is a new technology that offers its users immersivity and elicits "real" responses. The purpose of this study is to compare search efficiencies in real scenes on 2-D displays and Virtual Reality. A visual search experiment measuring reaction times and accuracy was conducted to evaluate both methods. Results suggest that visual search in real scenes is significantly faster and more accurate in Virtual Reality than in 2-D Displays. These findings could open up new opportunities for visual search research on real scenes and real life scenarios.

Keywords: Ergonomics · Virtual reality · Visual search

1 Introduction

1.1 Background of the Study and Rationale

Visual search is the study of the human ability to distinguish and identify a target among the presence of distractors. Classical and standard methods of visual search studies include the use of artificial objects, such as arbitrary shapes, as search targets on blank artificial backgrounds. Subjects are tasked to search for the target among a number of distractor figures. These studies identified certain features and factors that make targets more visually detectable than others do. Some of the basic factors include shape, size, color, and spatial frequency [1].

These search scenes are typically more complex than the artificial tests used in the classical methods, which is why there have been studies on visual search in real scenes in recent years [2]. Some of these studies include the study of the role of memory for visual search in real scenes [2], the study of the factors that contribute to the seemingly efficient search in real scenes [3] and the parametric modeling of search efficiency in

D.N. Cassenti (ed.), *Advances in Human Factors in Simulation and Modeling*,
Advances in Intelligent Systems and Computing 591, DOI 10.1007/978-3-319-60591-3_33

real scenes [4]. Most of these studies used two-dimensional (2D) displays for their respective experiments.

Recent advances in technology provide opportunities for better research in the scientific community. A new technology that has captured the attention of both the scientific community and the commercial industry is Virtual Reality. Virtual Reality (VR) is a three-dimensional computer generated environment, usually displayed on a flat screen, a room-based system, or a head-mounted display. A unique advantage that VR offers is stereoscopic depth, which makes the viewer see objects in a virtual space and creates the illusion of reality. VR has also been suggested to elicit the sense of presence, which is the ability to make users feel like they are "there" and as a result evokes users to respond the same way in VR as in reality. One of the main determinants of presence is immersivity, which is characterized by factors such as field of view, field of regard, and display size [5].

Virtual Reality has already been used as an alternative tool for scientific research on the human information processing system. Kober and Neuper propose that presence is characterized by increased attention toward stimuli in the virtual environment and decreased attention to irrelevant stimuli [6]. Another study also concluded that immersive environments are better remembered by subjects [7]. VR is also being used in psychology research such as studies on PTSD treatment [8] and natural human behavior.

Visual search in real scenes could possibly be applied in virtual reality. Its application could provide insight on the ecological validity of "point and click" methods currently used in research on complex human processes such as attention and perception [5].

1.2 Problem Statement

There is currently no comparative study on the accuracy and efficiency of visual search in natural scenes between using Virtual Reality tools and 2-D displays, which may provide insight on the ecological validity of current methods.

2 Review of Related Literature

2.1 Classical Visual Search Methods

A study conducted by Wolfe discussed the standard paradigm for visual search [1]. There are two basic methods used in visual search: the reaction time method and the accuracy method. In the reaction time method, reaction time is the dependent measure used. Subjects look for a target along some distractor objects. The subject gives a response to indicate whether the target object is present or absent. Reaction time is analyzed as a function of set size. The set size is the total number of items in a display. The slopes and the intercepts of these reaction time x set size functions are used to infer the mechanics of the search. In the accuracy method, the display is presented briefly. The accuracy is plotted as a function of stimulus onset asynchrony. Classical methods use artificial objects such as letters or shapes as targets on artificial or blank backgrounds which are displayed on two-dimensional displays.

2.2 Visual Search in Real Scenes

A study by Wolfe et al. discussed visual search in real scenes [3]. This study determined if the search for arbitrary objects in real scenes are actually efficient, as believed from an introspective view and determined what guides efficient search in these scenes. The study tested the reliability of using the set size as an index for search efficiency in real scenes. Its reliability was already verified in artificial scenes in previous studies. Set size of a real scene was estimated by labelling objects found in the scene. Six different sets of methods were performed. Each differing whether a word cue or picture cue was presented. Some methods required localization of target objects by using a mouse. Some isolated the target object on a white background while another experiment used a black background. The reaction times for each experiment were compared to determine its efficiency. In analyzing the data, trials were removed if their reaction times fall out of the range depending on the scene presented. Statistical tests were performed to determine if the difference in reaction times for each scene are statistically significant. Results indicated that set size was a poor parameter for measuring search efficiencies in real scenes. It was also concluded that object search is not efficient outside of a scene context and efficient in a scene context. Therefore, it follows that the scene makes an important contribution to the efficiency.

Another study focused on establishing a good measurement of search efficiency in real scenes to replace set size. The researchers studied selected factors: set size, visible size (of target), visual crowding, and eccentricity. Visual crowding was measured using a variable, Ds which described the target-flanker separation in real scenes. Fourteen participants were presented with scene images from two datasets and were tasked to locate a target object. Image attributes (set size, visible size, etc.) were noted. Reaction times were recorded and analyzed against the factors to derive correlations. Results indicated that only visible size and target-flanker separation had significant effect on reaction times. Results indicated that reaction times decreased as visible size increased and as Ds increased [4].

2.3 Virtual Reality and Its Application in Human Factors and Behavior Research

A study conducted by Kozhevnikov and Dhond in 2012 assessed and compared visual-spatial processing of three-dimensional stimuli using non-immersive 2D displays and 3D immersive environments. In this study, experiments that focused on participants performing mental rotation tasks using 2D non-immersive, 3D non-immersive (3D Glasses), and 3D immersive (head mounted display) visual presentations were performed. Results of the experiments indicated that cognitive processing in a 3D immersive environment differs greatly from that in a 2D non-immersive and 3D non-immersive environment. Visual-spatial processing was also different in the immersive environment where participants were encouraged to use a viewer-centered frame of reference during the said tasks [9].

Another study by Lee et al. from 2003 investigated the potential of using virtual reality for cue exposure. The authors conducted the study with 22 male smokers half of

which will be tested with an immersive virtual reality, generated using information from a pilot survey on cues to nicotine craving, while the other half will be tested using pictures, the classical method. Participants were asked before and after the test on the level of their cravings. They have concluded that virtual reality is more effective at eliciting craving symptoms in individuals compared to using pictures, which they attributed to the added spatial stimulus that virtual reality has. This study highlights factors that may contribute to the results of the comparative study of the two methods. By observing how spatial stimulus and its interaction with visual stimulus affect results, this can help further distinguish the effectivity of both methods [11].

A study by Zhang et al. from 2016 compared the performance of participants in 3D/2D visual search tasks using artificial stimuli. The authors conducted an experiment with 16 subjects and used 2 different kinds of television, one with 3D polarization and the other having 3D switch, and recorded their performance and search time. The conditions of the television were found out not to be significant but the two visual methods, 2D and 3D, were significantly different, with the former having significantly longer times. It was concluded that the search environment had an impact on search performance. This information can help the researchers in analyzing results from using real scenes instead of artificial stimuli [10].

Another study by Li et al. also from 2016 investigated the relationship of memory to attention allocation in everyday actions. The authors compared the results of searching in a 3D environment and flat images of that same 3D environment. They had participants roam and search in the 3D environment of an apartment in empty rooms for different objects at each trial. They had another group rested their head and kept still while they comb through images of the 3D environment looking for certain objects. The results they have gathered showed that 2D and 3D search methods are almost the same however body movement allowed better use of memory for participants and help become more efficient in allocating attention by ignoring regions deemed insignificant. According to the authors, this is due to the spatial awareness from roaming the 3D environment compared to the minimal movement of the 2D search [12].

3 Methodology

An integrated methodology of the methods used by Wolfe et al. found in the related literature, which is suitable for both the VR method and 2D method, will be used by the researchers. Among the six methods, the method that exhibited the most efficient result became the basis of the methodology in the current study. The researchers planned their methodology accordingly to take into consideration body movements and memory when comparing methods by holding them constant to reduce contributing factors of variation.

Based on the posit that visual search is efficient in real scenes and the studies on Virtual Reality's ability to elicit real-world responses, the researchers propose that search times and accuracy would be significantly better using a virtual environment rather than two-dimensional displays. To test this hypothesis, the researchers performed a comparative visual search experiment.

3.1 Selection of Test Subjects

Cochran's formula was used to determine the sample size needed for the study.

$$n = \frac{z^2 pq}{e^2}. \tag{1}$$

The confidence level (z) was set to 95% (equal to 1.96), the level of precision (e) was set to 0.1 and the estimated proportion of the attribute (p) was set to 0.5 (q is 0.5 respectively). Given those parameters, the minimum number of randomly selected participants (n) is ninety-six (96).

All subjects were required to have normal or corrected-to-normal, and good color vision.

3.2 Gathering of Quantitative Data

The subjects were divided into two groups depending on the medium used in the visual search. Group A used the VR equipment while Group B used a laptop. The equipment used were the commercially available Samsung Gear VR and a 13-inch MacBook Pro (2011 model).

Each subject was given a short briefing before the task. The subjects were presented with objects as targets. Their task was to locate corresponding targets in five different real scenes and determine whether the target object is present or absent in the scene. The same scenes were shown for both methods to isolate variation due to set size.

For Group A, the subject was asked to adjust the focus of the VR equipment. For Group B, the subject was placed on the apparatus. The apparatus used was an $18 \times 18 \times 24$ inches box with a black background inside to emulate the viewing conditions of a VR. This was to minimize the variation between the two methods.

For each scene, a picture cue was flashed for two seconds before presenting the scene to avoid confusions with the target object. Sceneries are either indoor or urban. The subject responded "present" if they located the target and "absent" if they believe the target is not present in the scene presented. The accuracy and reaction time of the subject were recorded for each scene.

3.3 Gathering of Qualitative Data

Subjects from Group A were exposed to the classical (2D) method while subjects from Group B were exposed to the VR method. The subject was asked to rate how different the two methods were in terms of total visual experience. They were then asked to enumerate the differences or similarities of the two methods.

Each participant was asked in which method they think it would be easier to locate a target and why. This question gave an insight on the factors why the subjects showed a preference on one method over the other.

3.4 Data Analysis of Quantitative Data

The mean accuracy of subjects from both groups were compared. Accuracy was derived as a percentage of total number of correct responses (present or absent) over the number of participants in the method (50). Accuracy was calculated by using the following equation:

$$Accuracy = \frac{\#\,Correct\ Responses}{50} \times 100\%\,. \tag{2}$$

Times where subjects committed an error (i.e. false positive, false negative) were removed. A boxplot was generated with the errorless data for each scene per group to determine the acceptable range of each subgroup. Outliers were removed from the data afterwards.

Two-Sample T-Test was conducted on the response times of Group A and Group B per scene, testing the following hypothesis:

$$H_o : \mu_{2D} - \mu_{VR} = 0. \tag{3}$$

$$H_1 : \mu_{2D} - \mu_{VR} \neq 0. \tag{4}$$

The null hypothesis (H_o) states that the means of the both groups are equal, while the alternative hypothesis (H_1) states that they are not equal.

Test of Two Variances was next conducted on the response times of Group A and Group B per scene, testing the following hypothesis:

$$H_o : \frac{\sigma_{2D}}{\sigma_{VR}} = 1. \tag{5}$$

$$H_1 : \frac{\sigma_{2D}}{\sigma_{VR}} \neq 1. \tag{6}$$

The null hypothesis (H_o) states that the variance of the both groups are equal, while the alternative hypothesis (H_1) states that they are not equal.

3.5 Data Analysis of Qualitative Data

Data visualization was used to help analyze qualitative data. Subjects' ratings of difference in visual experience were graphed according to frequency and the average rating was obtained. Their responses to preferred method were graphed in a pie chart. Subjects' responses to the questions asked were tabulated accordingly to the category they fall under.

4 Results and Discussion

4.1 Study Demographics

One hundred (100) subjects were randomly selected to be a part of the study. Each group consisted of twenty-five (25) males and twenty-five (25) females.

4.2 Quantitative Data: Accuracy

From Table 1, it is seen that VR has a higher accuracy for each scene than 2D. This shows that the VR group is more accurate compared to 2D.

Table 1. Summary of mean accuracy for each scene per group and the difference between them.

Accuracy	2D	VR	Difference
Scene 1	66%	82%	16%
Scene 2	96%	98%	2%
Scene 3	92%	92%	0%
Scene 4	98%	100%	2%
Scene 5	94%	100%	6%

4.3 Quantitative Data: Time

After removing the reaction times of errors, the following boxplot seen in Fig. 1 was generated along with Table 2 showing the acceptable range:

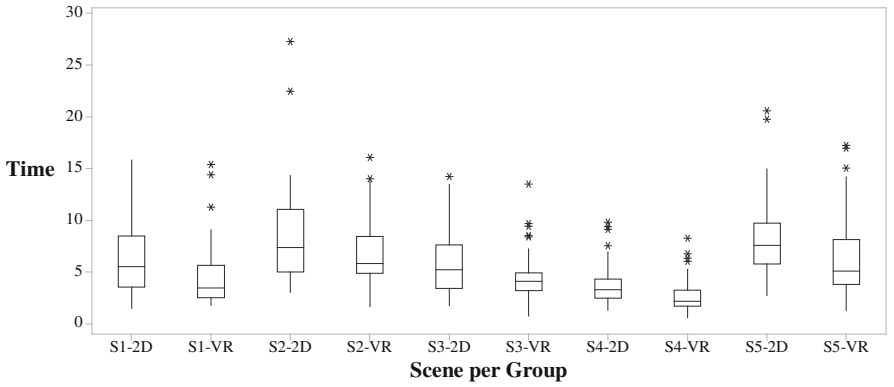

Fig. 1. Boxplot of scene times (in seconds) per group.

Reaction times that exceeded the corresponding limits seen in Table 2 were considered outliers and therefore removed from the analysis.

Table 2. Acceptable range of time (in seconds) for each scene per group.

	2D		VR	
	Lower limit	Upper limit	Lower limit	Upper limit
Scene 1	1.47	15.81	1.77	9.08
Scene 2	3.03	14.30	1.64	13.79
Scene 3	1.75	13.44	0.75	7.24
Scene 4	1.30	6.94	0.60	5.28
Scene 5	2.72	14.98	1.27	14.17

A Two-Sample T-Test for Means was conducted per scene using the adjusted errorless data generating the following results seen in Table 3.

Table 3. Summary of Two-Sample T-Test per scene.

μ	2D	VR	Est. difference	P-Value	Decision
Scene 1	6.38	3.93	2.456	0.002	Reject H_o
Scene 2	7.90	6.29	1.612	0.011	Reject H_o
Scene 3	5.67	3.77	1.895	0.000	Reject H_o
Scene 4	3.39	2.42	0.971	0.000	Reject H_o
Scene 5	7.64	5.95	1.690	0.007	Reject H_o

According to Table 3, the null hypothesis is rejected across all scenes as well indicating that there is significant difference in the mean reaction time of searching an object between 3D and 2D in all of the scenes. It was observed that the mean time of the VR group across all the scenes is smaller compared to the 2D group suggesting they accomplish the task much faster. A one sided Two-Sample T-Test was conducted to test the same null hypothesis and the following alternative hypothesis:

$$H_1 : \mu_{2D} - \mu_{VR} > 0. \tag{7}$$

Results rejected the null hypothesis as well showing the difference of VR and 2D with the performance of the VR group being indeed faster.

A Test of Two Variances was also conducted per scene using the same data generating the following results seen in Table 4.

Table 4. Summary of Test of Two Variances per scene. The lowest P-Value was selected between the Bonett's test and Levene's test results.

σ^2	2D	VR	Ratio	P-Value	Decision
Scene 1	14.235	3.986	3.571	0.012	Reject H_o
Scene 2	10.091	7.819	1.291	0.120	Do not reject H_o
Scene 3	8.093	1.969	4.110	0.000	Reject H_o
Scene 4	1.826	1.227	1.489	0.301	Do not reject H_o
Scene 5	7.644	9.578	0.798	0.520	Do not reject H_o

According to Table 4, the variance of the VR group is smaller in four out of the five scenes (scenes 1, 2, 3, and 4) meaning that the performance of the subjects was nearer to the mean time or more consistent. Two of these scenes concluded to reject the null hypothesis showing a significant difference in their variance.

Scene 5, however, showed that the VR group had a larger variance but was not statistically proven. Only two scenes rejected the null hypothesis suggesting that overall, there may not be sufficient evidence that proves that the VR group yielded more consistent reaction times than the 2-D group.

4.4 Qualitative Data: Visual Experience

The responses from the qualitative data gathering were summarized in Fig. 2 and Table 5.

According to Fig. 2 and Table 5, most subjects rated that the VR method and the 2D method are different from each other (with an average rating of 7.61). Subjects attributed this difference greatly to the immersivity of VR, which includes the realistic feeling, the depth perception, and the clarity of view to name a few of the subjects' comments.

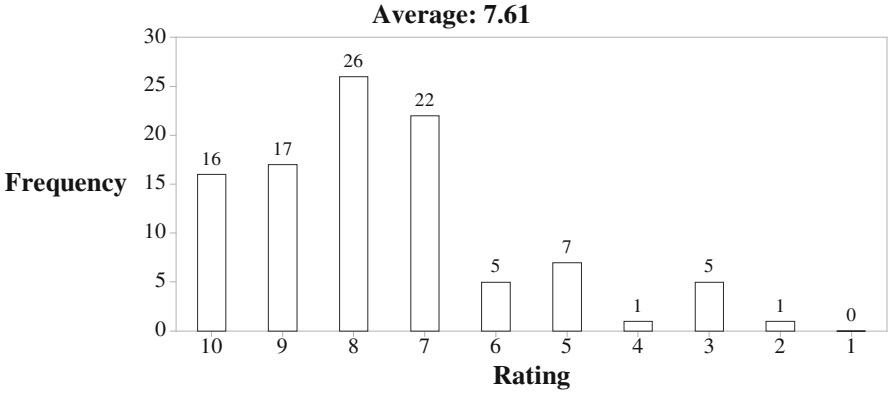

Fig. 2. Frequency of ratings for the difference in visual experience given by the participants.

Table 5. Frequency of most common differences between the VR method and 2D method cited by the participants

Differences	Frequency
Realistic	28
Clarity of view	27
Depth perception	21
Peripheral view	18
Immersivity	12
Spatial awareness	8
Focus	6

4.5 Qualitative Data: Preferred Method

The responses for the preferred method were summarized in Fig. 3, and Tables 6 and 7.

According to Fig. 3, majority of the subjects' preference is the VR method. Similar with the difference in visual experience, immersivity was a major factor in their choice, as seen in Table 6. Subjects who preferred the 2D method chose because of the advantage of seeing everything immediately, as seen in Table 7. Three subjects said that both methods are equally capable and did not have much difference when it comes to visual search tasks. The other two said it would depend on what object they are looking for and in what scene.

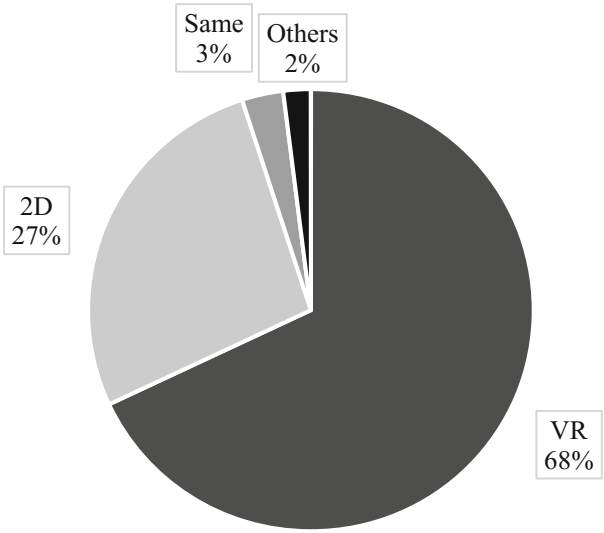

Fig. 3. Pie chart of proportion of preferred method.

Table 6. Frequency of most common differences between the VR method and 2D method cited by the participants

Strength	Frequency
Realistic	18
Depth perception	11
Clarity of view	11
Spatial awareness	9
Immersivity	7
Detail	6
Focus	6
Scaling	6
Peripheral view	5

Table 7. Frequency of most common differences between the VR method and 2D method cited by the participants

Strength	Frequency
Immediate visual	11
Flat	3
Bigger view	2
Stable	2
Clarity	2
Familiarity	2

5 Conclusion

Overall, the test subjects who used the VR method showed a better performance in visual search. The statistical tests indicated that their reaction times are significantly faster (by an average estimate of 28.62%) and more accurate as compared to those who used the 2D method in all scenes. It also indicated that the VR method results are more consistent and stable. Furthermore, majority of the subjects preferred using VR in visual search due to its immersivity, field of depth, and clarity of the visual experience.

6 Areas of Further Study

6.1 Localization of Target Objects

Guessing strategies based on the typicality of the target object in a scene are common for visual search especially for indoor scenes [3]. For instance, a subject will normally search for a remote control either on the couch or on table of a living room. To minimize possible guessing, localization of the target object can be done. This may strengthen the accuracy of results presented in the current study. Further studies can be done using better Virtual Reality equipment (one which allows localization or interaction with objects in virtual space). Although such tools are already available in the market, logistical and financial limitations prevented the researchers from using these tools.

6.2 Wider Range of Scenes and Targets

One of the limitations of the methodology used in this study is the restricted range of scenes. A study conducted by Zhang did not address the natural scenes (e.g. forests) due to the different context of these scenes, such as spatial knowledge [9]. Due to lack of incorporation of more natural scenes in the previous literatures, it would be interesting to include these scenes in future research.

6.3 Incorporation of Movement, Interaction, and Auditory Features

The current study was limited to exploring Virtual Reality only as a visual medium. Incorporating movement and interaction with the environment, also being key features

of VR, into the experiment could provide more insight on visual search efficiencies in real-life settings. Including auditory features that mimic real life scenarios could also maximize the level of presence and immersivity experienced by the users and increase the ecological validity of the method.

References

1. Wolfe, J.M.: Visual search. In: Pashler, H. (ed.) Attention. University College London Press, London (1998)
2. Le-Hoa Võ, M., Wolfe, J.: The role of memory for visual search in scenes. Ann. N. Y. Acad. Sci. **1339**(1), 72–81 (2015)
3. Wolfe, J.M., et al.: Visual search for arbitrary objects in real scenes. Atten. Percept. Psychophys. **73**(6), 1650–1671 (2011). Web. 2 Dec 2016
4. Zhang, X., et al.: Parametric modeling of visual search efficiency in real scenes. PLoS One **10**(6), e0128545 (2015). Web. 2 Dec 2016
5. Wilson, C.J., Soranzo, A.: The use of virtual reality in psychology a case study in visual perception. Comput. Math. Methods Med. **2015**, 1–7 (2015). Web. 2 Dec 2016
6. Kober, S.E., Kurzmann, J., Neuper, C.: Cortical correlate of spatial presence in 2D and 3D interactive virtual reality: an EEG study. Int. J. Psychophys. **83**(3), 365–374 (2012). Web. 2 Dec 2016
7. Sutcliffe, A., Gault, B., Shin, J.-E.: Presence, memory and interaction in virtual environments. Int. J. Hum.-Comput. Stud. **62**(3), 307–327 (2005). Web. 2 Dec 2016
8. Nelson, R.J.: Is virtual reality exposure therapy effective for service members and veterans experiencing combat-related PTSD? Traumatology **19**(3), 171–178 (2013). Web. 2 Dec 2016
9. Kozhevnikov, M., Dhond, R.P.: Understanding immersivity: image generation and transformation processes in 3D immersive environments. Front. Psychol. **3**, n. pag. (2012). Web. 2 Dec 2016
10. Lee, J.H., et al.: Experimental application of virtual reality for nicotine craving through cue exposure. CyberPsychol. Behav. **6**(3), 275–280 (2003). Web. 2 Dec 2016
11. Zhang, Y., et al.: A comparative study on 3D/2D visual search performance on different visual display terminal. In: Hale, K., Stanney, K. (eds.) Advances in Neuroergonomics and Cognitive Engineering, pp. 233–242. Springer, Cham (2016). Web. 2 Dec 2016
12. Li, C.-L., et al.: Memory and visual search in naturalistic 2D and 3D environments. J. Vis. **16**(8), 9 (2016). Web. 2 Dec 2016

Using Cognitive Modeling for Adaptive Automation Triggering

Daniel N. Cassenti(✉) and Vladislav D. Veksler

U.S. Army Research Laboratory, Human Research and Engineering Directorate,
459 Mulberry Point Rd., Aberdeen Proving Ground, MD 21005, USA
{daniel.n.cassenti.civ,
vladislav.d.veksler.ctr}@mail.mil

Abstract. The Multi-Level Cognitive Cybernetics (MLCC) [1] approach provides a methodological approach to studying adaptive automation and advancing its development across multiple levels of analysis. We follow up on the previous paper [1] by focusing on the cognitive modeling level of MLCC. Adaptive aids must only be triggered when the inclusion of the aid will boost performance relative to what it would be without the aid. Computational cognitive modeling provides a means to represent the cognitive sequence that completes a task. Using cognitive modeling and MLCC, we discuss two ways to provide optimal triggering for adaptive automation. First, models will provide a mapping of which cognitive stages caused the most difficulty for individuals and therefore aids may be designed to support those cognitive functions. Second, models may provide information about optimal thresholds for determining when a user is having difficulty, allowing more timely aid interventions than without the model.

Keywords: Cybernetics · Cognitive psychology · Human factors · Computational modeling · Research methods

1 Multi-level Cognitive Cybernetics

The multi-level cognitive cybernetics (MLCC) approach provides a model of human-computer interaction and suggests mutual adaptation between technology and the user occur over time [1]. Assuming human adaptation as a given, the MLCC approach focuses on enabling research that would lead to more effective adaptation in technology. Mutually adaptive systems, however, require both systems to provide information that will allow the other to adapt. Thus, even with human adaptation as a given, the MLCC approach requires a deep understanding of human cognition. In Subsects. 1.1–1.3, we outline the basic principles of MLCC and adaptive automation. In Sects. 2–5, we detail the more direct purpose of this paper, which is to describe the cognitive modeling level of MLCC and its utility to human factors research.

1.1 Cybernetics

Cybernetics [1, 2] is the study of communication and control between agents and their environments in closed-feedback loops. This field mirrors the ideal framework necessary

D.N. Cassenti (ed.), *Advances in Human Factors in Simulation and Modeling*,
Advances in Intelligent Systems and Computing 591, DOI 10.1007/978-3-319-60591-3_34

to study the interactions between technology and users. Technology should enrich a user's interactions with the environment in an attempt to accomplish goals that both the user and the technology share.

1.2 Cognition

Cognitive science is the study of human mental processes and therefore a necessary component of the MLCC approach, which permits understanding the human aspect of the closed-feedback loop system between humans and technology. There are several ways to represent cognition, but according to the MLCC approach, cognition is broken down into stages. The representational format provides a sequential approach to account for how a goal is accomplished from initial state to an end goal state. Figure 1 below outlines the stages of cognition along with corresponding stages in the technology portion in MLCC.

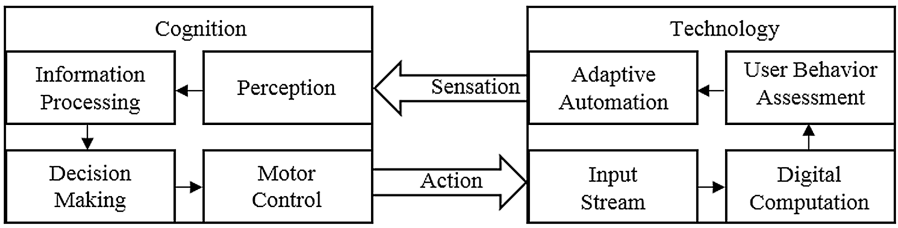

Fig. 1. The stages of cognition and adaptive technology in the MLCC framework [1].

Sensory output from the technology (e.g., the visual interface, warning sounds) enter through the user's sensory organs and initiate cognitive processing, beginning with the conversion of raw sensations to perceptual representations that can be understood by the user. These representations are filtered in the information processing stage to facilitate focus on the important elements from the perception stage. Once these elements are isolated, a decision-making stage works to process a course of action and feed that desired action into motor control processing. Motor behavior produces the action and this is in turn processed by the technology.

Admittedly, this represents a simplified view of cognition to facilitate understanding. One missing element from the model is the learning process. We assume that learning occurs, but do not necessarily divulge how this is done in the current MLCC approach. That said, learning allows the user to adapt to the technology and accomplish goals, which are set by both the user and the technology.

1.3 Triggering Adaptive Automation

Several areas of human factors research focus on building static systems that work with a human user's cognitive needs. However, there are many differences between

individuals, which makes it useful to design technology that adjusts to an individual's capabilities to complete a goal. This technology capability is referred to as adaptive automation [3] and it allows the environment (i.e., interfaced through technology) to adjust to the human as well as vice-versa.

With adaptive aids, the technology must sense the user's state. If the technology senses that the user is having difficulty at any stage of cognition, it will activate an aid to attempt to improve the user's performance. There are several schemas related to the timing of the adaptive aid that may be adopted, discussed in Sects. 1.3.1–1.3.3.

1.3.1 Always On or Always Off

The non-adaptive timing schemas include having the aid always activated or always deactivated. Obviously, the always-off schema would defeat the purpose of having the aid in the first place.

A little less troubling is the always-on schema. After all, if the aid is there to help, then it stands to reason that having it always available would improve performance. However, there are several reasons to avoid having an always-on aid. First, although automated aids are intended to reduce mental workload (i.e., mental demands placed on limited cognitive resources, see [4]), if the workload is reduced too much, distraction can increase and performance may subsequently decline [5]. Also, *automation bias* [6] is a situation in which a user gets a sense of complacency with an aid and accepts all of its choices rather than scrutinizing them for errors. Automation bias is similar to the concept of misuse (i.e., overreliance). Finally, a user's workload may not be reduced by the aid, rather it is possible that an aid that is always on may change the task into a vigilance task, due to the nature of monitoring the reliability of the aid. If the task becomes vigilance, this can increases the amount of mental demand and effort required to perform the task [7]. To avoid these problems, an aid should only be activated in times of need to increase or maintain user performance.

1.3.2 Automation Triggered by the Environment

One way of judging whether the user needs an aid is to gauge the amount of complexity or difficulty that exists within the environment, which increases the processing demands placed upon the user (and task) [8]. Complexity can be judged based on the Four V's of Big Data: (1) Volume–amount of information, (2) Velocity–how fast information is getting to the user, (3) Variety–the diversity of information formats, and (4) Veracity–the need to also judge how accurate the source of information is [9]. If any of these factors are too great, then the aid could be triggered under the assumption of increased difficulty and an anticipated decrease in performance.

There is reason to think that automation triggered by the environment is not always ideal. For example, some individuals have a higher capacity for processing information (i.e., working memory capacity) and are therefore able to handle greater demands from the environment [10]. An aid activated based on environment demands would be disruptive for high-performing users, and still insufficient for low-performing ones.

1.3.3 Automation Triggered by Human Behavior

Of the timing schemas, automated aids would be best triggered by some behavior detected from the user that indicates a current or forthcoming decrease in performance

as it more directly addressed when the user has actual difficulty rather than guessing. This idea provides the foundation for three of the four levels in MLCC. First, the triggering of automation may be left to the user to decide. This first metacognitive level would be an explicit action on the part of the user (e.g., a keypress) to indicate a desire for the aid to be activated based on the user's self-evaluation of task performance. The second level is performance. Instead of waiting for the user to activate the aid, the adaptive automation would monitor performance over time and when person declined below a specified threshold, the aid would be activated. This assumes that the task is continuous in nature and can be constantly monitored. A third level is to rely on several physiological indicators of difficulty. Heart rate variability [11], electrodermal activity [12], and pupil diameter [13] are examples of physiological indictors and stress-related triggers that could activate an aid during times of stress or performance decline. As in the performance level, physiological variables could have thresholds assigned and, once they are exceeded and stabilized above the threshold, trigger adaptive automation.

1.3.4 Conclusions

While adaptive technologies hold promise, it is unclear what type of automated support is necessary and it is unclear when to trigger that automated support. We discuss an approach to these problems below. Specifically, the question of what type of automation is necessary is examined through a cognitive modeling framework in Sect. 3. The question of when to trigger automation support is explored in Sect. 4. The answers to these questions may help improve human factors design of adaptive aids.

2 Cognitive Modeling and MLCC

The level of MLCC that does not fit with the others is cognitive modeling. Instead of supplying information directly to the technology as the user performs the task, cognitive modeling may provide information on what type of aid to trigger and when to trigger the aid in the future. We will discuss these mechanisms in general in Subsects. 2.1 and 2.2, then proceed to more in-depth discussion in Sects. 3 and 4.

Cognitive modeling is the process of building simulations in computer software designed for the purpose of representing human cognition. The models may provide answers about which procedural memories (i.e., cognitive steps that transform representation to advance to a goal state, see [14]), declarative memories (i.e., bits of informational knowledge, see [15]), and modules (i.e., sets of cognitive processes dedicated to particular types of mental computations, see [16]) are needed to perform the task. These models also typically present timing information as the length of time it takes to execute a cognitive step, which are embedded in the sequence of procedural steps needed to move from initial to goal state.

2.1 Sources of Complexity

Figure 1 represents the cognitive stages in the human side of the closed-feedback loop between user and technology and any of these stages can be required for complex

processing. With the possible exception of eye tracking (discussed below), there is very little that can be inferred from self-initiated, performance-based, or physiological-based automated aid triggers that indicate which stage of cognitive processing is difficult for the user. Without this information, the user's software will be uninformed about what type of aid will help. If the user is not having any difficulty with perception, but a perceptual aid is offered at a sign of difficulty, it will not help and could serve to undermine performance, as discussed above.

The cognitive modeling level could provide answers about the cognitive stages that frequently cause difficulty for the user. The task of the modeler is to assemble all the mental components that are necessary to move the task from initial state to goal state. The use of these components can translate into a measure of complexity or difficulty. There are two types of storage that may be used in a cognitive model – short- and long-term memory. Long-term memory is the set of all memories, whereas short-term memory is the set of memories active at any given time. For example, a model of event counting [17] may require individuals to search a large set of long-term memories to cover all possible numbers needed, but the complexity of the task is low because only as much as one declarative memory is needed in short-term memory at once. If the step count were up to 50, you would only need to know the next number is 51 to successfully execute the next step. In contrast, a model of air-traffic control [18] would require that several declarative memories be coordinated at once as the operator must keep track of several planes and their trajectories simultaneously.

Another way of judging complexity may be based on the length of procedural execution—the number of steps completed during task completion. With each new step, there is a chance for error, and that each additional step requires more time. Thus, accuracy and response time measures of performance have a greater chance of worsening.

Finally, the activation of various system modules is an additional way to judge complexity. Cognitive architectures employ different components, or modules, for varying cognitive functionality. For example, in the ACT-R cognitive architecture [19] there are instances where the procedural, goal, visual, declarative, and motor modules may be instantiated simultaneously. In general, modules are considered different cognitive resources that do not interfere with each other (see [20]). Each employed module is an additional source for error, and multiple requests on the same module are a source for cognitive bottlenecks. Therefore, the number of modules active in parallel, and the number of demands on each module are both potential measures of complexity.

Given that a cognitive sequence is mapped out in a cognitive model, the modeler can segment the sequence into the broader cognitive stages from Fig. 1. The stages with the highest complexity would inform the design of adaptive aids.

2.2 Temporal Dimension

Models may also indicate when to trigger adaptive aids. As discussed above, there are possible performance and physiological indicators of the need for assistance in a task. When these aids should be triggered is a separate question. Unlike figuring out which cognitive stage required aided assistance, figuring out the temporal dynamics of aid triggering is not dependent on a cognitive modeling system, such as ACT-R. Instead,

simpler, statistical modeling that describes patterns of accuracy, response time, and physiological measures over time should be enough to determine optimal triggering of adaptive aids for any given continuous task. More description of this method is provided in Sect. 5.

3 Isolating Cognitive Difficulties

As described above, there are explicit factors that could indicate difficulty in performance during specific stages of task completion. In this section, we address the stages themselves and articulate examples of adaptive aids that may help. We will use two example tasks to illustrate aids: piloting an aircraft and intelligence analysis.

Piloting commercial aircraft involves tracking numerous displays, indicators, and meters and also manipulating controllers, flipping switches, and pressing buttons. This situation creates higher perceptual and motor control demands, especially for amateur pilots, which involve the first and fourth stages of cognition in the MLCC approach. However, the information processing and decision-making demands are relatively light and the solutions to problems are usually rote and determined *a priori*, at least in normal air and functional conditions. This is not to say that amateur pilots have not faced difficult decision-making, but these situations are atypical (e.g., a time of emergency), so this example will focus on perception and motor control.

Intelligence analysis is lighter on perceptual and motor control demands than piloting. Perceptual issues have arisen with intelligence analysis systems (see [21]), but generally the software is built to reduce a user's potential perceptual difficulty. The difficulty with intelligence analysis lies with filtering important information from distracting data (i.e., the information processing stage) and making decisions based on that information. Aids that help intelligence analysis should be focused on the stages between perception and motor control.

3.1 Perception

The extent to which perception presents difficulty depends heavily on the task. In the case of piloting an aircraft, the range of visual stimuli is enormous. See Fig. 2 for an example.

Fig. 2. The interior of an airbus cockpit obtained from a public domain image stock.

Each display in Fig. 2 represents a possible target of visual perception. Although any given display may be relatively simple to interpret, the challenge for less experienced pilots is to locate the display of interest amid a myriad of other displays. Current automation includes alarms or indicators that direct the pilot's attention to the gauge that is most important. Piloting an aircraft provides an obvious case for adaptive aids targeting perception, however, providing aids for more difficult cognitive tasks in the cockpit is not as straightforward. The difference between current aids in an aircraft and those argued for here is how adaptive they are to user state. Whereas current aids will trigger when the need arises, adaptive aids could measure response time and only trigger when the pilot is slow to respond. Cognitive models should help with the determination of when perceptual aids are needed.

For example, ACT-R has a *buffer stuffing* mechanism [22] in which any stimulus appearing by itself in ACT-R's environmental window (i.e., ACT-R's visual representation of the environment) is automatically included in a visual buffer. Although, ACT-R's environmental window is not complex enough to perceive a cockpit in an aircraft, if it could, it would have difficulty locating a single display that requires attention. If a different modeled task has high perceptual workload demands, the difficulty of programming that aspect of the task (i.e., supplying the model with declarative and procedural memory) would in turn make it clear to the modeler that cognitive limits will be on perception and aids (i.e., alarms) should be made to support it.

3.2 Information Processing

Although the displays in a cockpit may be initially difficult to locate, once the source of the alarm is determined, the information associated with the alarm may not be difficult to process. For a better example, consider the work of an intelligence (intel) analyst, who must process a lot of data in order to gain situational awareness to potential threats [23] and make recommendations to mitigate these threats. The data flowing to the intel analyst is not always important to the situation, therefore the analyst faces high mental demands in filtering and sorting data to arrive at a list of situation-pertinent information.

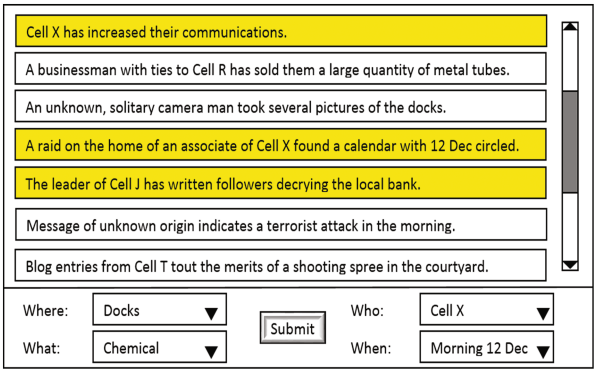

Fig. 3. An example of an information processing aid from a planned experiment.

As in the above example, the modeler can interpret difficulty of a task on information processing based on the amount of declarative and procedural memory involved in cognitive processes relating to isolating options leading to the decision-making stage. A computer aid that may help is one that uses text analytics to process a textual feed and highlight information deemed important when the user has difficulty. Figure 3 represents an example.

3.3 Decision-Making

The intel analyst task is a good example for the decision-making stage as well. Once the data from the feed has been sorted, the intel analyst must turn to making a decision about elevating a potential threat. In the planned experiment represented in Fig. 3, the participants will be asked to determine what the information from the feed might indicate about the where, what, who, and when of a terrorist attack. The experiment represents a definite simplification of the intel analysis process as participants will not judge the source reliability, credibility, or recency of the data (see [24]).

A modeler finding the decision-making stage to be the most complex of the stages can recommend aids assist in the user's decision-making process. Deploying these types of aids should be performed with extreme caution. In the example from Fig. 3, the computer aid could fill in guesses for any of the four decisions that need to be made. However, the software would know ground truth. To make it more realistic, the software in that experiment would be designed to have a certain probability of recommending the incorrect answer. We can assume the probability of error with real-world software would be higher. Just like any adaptive automation, an aid for decision-making should only be deployed when the user is showing signs of current or pending performance decline.

3.4 Motor Control

The motor control involved in the intel analysis task from Fig. 3 is not difficult (i.e., moving and clicking a mouse), thus a motor aid would not be helpful. However, a pilot has a host of motor programs that need to be carefully selected while operating an aircraft. A modeler who must program a large set of motor programs would know that a task will present challenges to the user. Motor aids would activate when the user is in need and execute actions for the user. Again, this should only be done when the operator is showing signs of performance decline.

4 Deriving Performance and Physiological Thresholds

A different type of modeling may be employed for deriving thresholds for the timing or aid triggering compared to understanding the type of aid that should be activated. Determining thresholds involves statistical modeling, in particular time series analysis presents an intriguing option. The setting of a performance threshold could be as simple as selecting a proportion correct threshold as the aid trigger. However, this suggestion

should not be applied blindly; modelers need to consider the type of task (e.g., life-and-death versus benign decision-making), task parameters, or the overall difficulty of the task. Threshold should be based on empirical observation first and modified by other considerations (e.g., subject matter expert input). We will focus on the former in this section.

4.1 Detecting Patterns in Performance Over Time

The modeling system, IMPRINT (i.e., Improved Performance Research Integration Tool; [25]) is one of the few modeling systems that explicitly predicts mental workload values for tasks. When workload reaches a critical value in an IMPRINT model, the interval is considered to be a time of overload and the model will choose one of several mitigation strategies to overcome a state of too much demand on limited mental resources. Examples of mitigation strategies include giving up on a task outright or prioritizing other tasks until the resources are freed to perform them all. A situation like this would appear as a pattern of performance suddenly dropping and maintaining lower performance. Software detecting this pattern should trigger adaptive automation.

Task sets where this happens are not difficult to imagine. However Cassenti et al. [26] found that tasks do not typically follow a sudden-drop-off pattern. Instead, task performance gets more difficult over time in a largely steady manner. Some of these patterns were best characterized as hyperbolic functions, so did approach an asymptote. For these, a threshold could be determined somewhere around the apex of the curve. Other cases were found to be linear and would give no indication of when to set a performance threshold for an aid. In this case, a threshold could be determined based only on parameters such as how critical mistakes are for the task.

An alternative method is to use data from self-initiated aids to set performance thresholds. If the participants in previous studies consistently showed a tight range of performance that they tolerated on a given task before initiating an aid, these patterns can be transferred to the software and used for new users.

4.2 Connecting Physiological Data with Performance

Setting performance thresholds can be completed through observation, but this approach has two drawbacks. First, the task must be one where performance may be judged during task execution. If performance can only be judged by a final response, then a performance threshold for an adaptive aid would not work. Second, a performance threshold only allows intervention once performance is already showing decline. Physiological readings solve both these problems since they are constantly being generated during a task, relate to a stressor that affects performance, and can potentially predict increases in workload and stress during performance, which are generally linked to declines in performance, prior to user awareness of such a decline.

Physiological measures like heart rate variability [11], electrodermal activity [12], and pupil diameter [13] are empirically supported in the literature, but there is little consensus on which cognitive-related variables they are associated with. However, this

is not necessary information, if it is established that they are all tied to some stressor that can affect performance. We propose collecting physiological measures for different tasks and using this data in time series analyses to see how performance varies with any number of the measures. Any plateaus or apexes in performance can be cross referenced to a measure's readings and those ranges used as thresholds for adaptive aids.

4.3 Referencing Cognitive Stage to Eye Tracking

Previously, we made two statements that do not apply to eye tracking and thus place eye tracking into a different category than other physiological measures. First, the cognitive stage that presents difficulty for the user requires cognitive modeling subsequent to the task because there is no indication of what stage caused difficulty during task execution. Second, we stated that physiological variables do not have consensus links to their particular stressor. Researchers can use eye tracking to figure out where the gaze is directed, thus patterns of eye tracking can indicate where the user is attending. If attention is directed away from critical information and toward irrelevant information, software with adaptive automation could assume that the stressor of a visually complex display is interfering with the ability to complete the perceptual stage of processing. If this information could be processed in real time, then the software could deploy an adaptive perceptual aid during times of difficulty.

5 Dynamic Modeling of Individual Differences

Employing a cognitive model to predict when automation may be useful requires that each model is tailored to: (1) each individual's in-task experiences, and (2) each individual's pre-task biases and capabilities. The first of these issues is one of matching human-model experiences and decisions, and the second has to do with dynamic fitting of free model parameters to each individual's behavior.

Model tracing is a cognitive-modeling technique used for matching human-model in-task experiences. Model tracing involves feeding a participant's experiences to the cognitive model. If the user and model choose different strategies, software would overwrite model actions with user actions in the model's memory. This method was employed in computerized instructional aids called "cognitive tutors" for students learning high school math in Pittsburgh [27]. The goal of building these models was to provide individually-tailored instructions to overcome repeated errors and missing concepts. The advantage of model tracing is the ability to query the model for predicted user actions and potential user errors at any decision point, then override model decisions with user decisions, thereby keeping model and human experiences as close as possible.

Pre-task individual differences are just as important as in-task experiences. Different individuals have varying learning rates, explorative tendencies, and pre-task preferences that will affect adaptive aid triggering. For example, if the individual has a strong preference against using pull-down menus when using software applications, this may cause unexpected task-execution paths. Dynamic parameter fitting may be

used to adjust free model parameters based on known data points, so as to make better individual predictions for future behavior. This method was employed to predict performance of individual F-16 pilot teams [27, 28] and is employed in software that predicts optimal training schedules based on individual performance histories [29]. When computational limitations may prevent in-task, best-fitting parameter exploration for each individual, the parameter predictions may be cached for each task [30].

6 Conclusions

In this paper, we discussed how cognitive modeling may provide the guidance we need to trigger the right kind of aid, when it will aid performance. There are several modeling approaches that have implications for cognition. However, we recommend three explicit approaches. First, for modeling the stages of cognition, ACT-R [19] represents the best option. It is not only the most studied of cognitive modeling systems and therefore the most developed, but the goal of ACT-R models is generally to model in a cognitively plausible fashion. So unlike other cognitive modeling systems that take an artificial-intelligence approach (i.e., optimizing solutions), ACT-R models mistakes and problems; in other words, it is more human. Since the point of adaptive aids is to help the user who is showing signs of difficulty, ACT-R represents the best option for modeling. Second, we recommend statistical modeling for performance and physiological threshold information. Though, we should note that physiological measures have a large noise factor, so in this case, stable points of physiological measures should be calculated rather than triggering aids based on momentary fluctuations. Lastly, we recommend dynamic modeling to account for individual user differences.

We wish to conclude by making it clear that the approach outlined here is based on our theorizing on this subject. We hope that this paper may act as a starting point for discussion and refinement of our approach to adaptive automation. Surely, with all of the complexity in this approach, flexibility to feedback must be prioritized.

References

1. Cassenti, D.N., Gamble, K.R., Bakdash, J.Z.: Multi-level cognitive cybernetics in human factors. In: Hale, K.S., Stanney, K.M. (eds.) Advances in Neuroergonomics and Cognitive Computing, pp. 315–326. Springer, New York (2016)
2. Wiener, N.: Cybernetics or Control and Communication in the Animal and the Machine. Wiley, New York (1948)
3. Kaber, D.B., Riley, J.M., Tan, K.W., Endsley, M.R.: On the design of adaptive automation for complex systems. Int. J. Cogn. Ergon. **5**, 37–57 (2001)
4. Wickens, C.D.: Multiple resources and performance prediction. Theor. Issues Ergon. Sci. **3**, 159–177 (2002)
5. Cassenti, D.N., Kelley, T.D.: Towards the shape of mental workload. In: 50th Annual Meeting Human Factors and Ergonomics Society, pp. 1147–1152. HFES, Santa Monica (2006)

6. Skitka, L.J., Mosier, K.L., Burdick, M.: Does automation bias decision-making? Int. J. Hum.-Compt. Stud. **51**, 991–1006 (1999)
7. Byrne, E.A., Parasuraman, R.: Psychophysiology and adaptive automation. Biol. Psychol. **42**, 249–268 (1996)
8. Hart, S.G., Staveland, L.E.: Development of NASA-TLX (task load index): results of empirical and theoretical research. Adv. Psychol. **52**, 139–183 (1988)
9. Siewert, S.B.: Big data in the cloud. Data Veloc. Vol. Var. Veracity, 4–21 (2013)
10. Cowan, N.: Working Memory Capacity. Psychology Press, New York (2012)
11. Segerstrom, S.C., Nes, L.S.: Heart rate variability reflects self-regulatory strength, effort, and fatigue. Psychol. Sci. **18**, 275–281 (2007)
12. Schaefer, F., Haarmann, A., Boucsein, W.: The usability of cardiovascular and electrodermal measures for adaptive automation. In: Westerink, J.H.D.M., Ouwerkerk, M., Overbeek, T.J. M., Frank Pasveer, W., de Ruyter, B. (eds.) Probing Experience, pp. 235–243. Springer, Dordrecht (2008)
13. de Greef, T., Lafeber, H., van Oostendorp, H., Lindenberg, J.: Eye movement as indicators of mental workload to trigger adaptive automation. In: Schmorrow, D.D., Estabrooke, I.V., Grootjen, M. (eds.) International Conference on Foundations of Augmented Cognition, pp. 219–228. Springer, Heidelberg (2009)
14. Gupta, P., Cohen, N.J.: Theoretical and computational analysis of skill learning, repetition priming, and procedural memory. Psychol. Rev. **109**, 401–448 (2002)
15. Knowlton, B.J., Squire, L.R.: Remembering and knowing: two different expressions of declarative memory. J. Exp. Psychol.: Lear. Mem. Cogn. **21**, 699–710 (1995)
16. Duric, Z., Gray, W.D., Heishman, R., Li, F., Rosenfeld, A., Schoelles, M.J., Wechsler, H.: Integrating perceptual and cognitive modeling for adaptive and intelligent human-computer interaction. Proc. IEEE **90**, 1272–1289 (2002)
17. Cassenti, D.N., Reifers, A.L.: Counting on ACT–R to represent time. In: 49th Human Factors and Ergonomics Society Meeting, pp. 1167–1172. HFES, Santa Monica (2005)
18. Loft, S., Sanderson, P., Neal, A., Mooij, M.: Modeling and predicting mental workload in en route air traffic control: critical review and broader implications. Hum. Factors **49**, 376–399 (2007)
19. Anderson, J.R., Lebiere, C.: The Atomic Components of Thought. Erlbaum, Mahwah (1998)
20. Jongman, G.M.G.: How to fatigue ACT–R. In: Second European Conference on Cognitive Modelling, pp. 52–57 (1998)
21. Kase, S.E., Roy, H.E., Cassenti, D.N.: Visualizing approaches for displaying measures of sentiment. In: 20th International Command and Control Research and Technology Symposium, p. 94990H. International Society for Optics and Photonics, Annapolis (2015)
22. Stewart, T.C., West, R.L.: Cognitive redeployment in ACT-R: salience, vision, and memory. In: Eighth International Conference on Cognitive Modeling, pp. 313–318. Taylor & Francis/Psychology Press, Oxford (2007)
23. Endsley, M.R.: Toward a theory of situation awareness in dynamic systems. Hum. Factors **37**, 32–64 (1995)
24. Hanratty, T.P., Newcomb, E.A., Hammell II, R.J., Richardson, J.T., Mittrick, M.R.: A fuzzy-based approach to support decision making in complex military environments. Int. J. Intel. Inf. Tech. **12**, 1–30 (2016)
25. Allender, L.: Modeling human performance: impacting system design, performance, and cost. Simul. Ser. **32**, 139–144 (2000)
26. Cassenti, D.N., Kelley, T.D., Carlson, R.A.: Modeling the workload-performance relationship. In: 54th Annual Human Factors and Ergonomics Society Meeting, pp. 1684–1688. HFES, Santa Monica (2010)

27. Anderson, J.R., Corbett, A.T., Koedinger, K.R., Pelletier, R.: Cognitive tutors: lessons learned. J. Learn. Sci. **4**, 167–207 (1995)
28. Jastrzembski, T.S., Gluck, K.A., Rodgers, S., Krusmark, M.: The predictive performance optimizer: mathematical modeling for performance prediction. In: 18th Conference on Behavior Representation in Modeling and Simulation, pp. 141–142. BRIMS, Sundance (2009)
29. Jastrzembski, T.S., Rodgers, S.M., Gluck, K.A., Krusmark, M.A.: Predictive performance optimizer: U.S. Patent No. 8,777,628. U.S. Patent and Trademark Office Washington, DC (2014)
30. Fisher, C.R., Walsh, M.M., Blaha, L.M., Gunzelmann, G., Veksler, B.: Efficient parameter estimation of cognitive models for real-time performance monitoring and adaptive interfaces. In: 14th International Conference on Cognitive Modeling, pp. 113–118. ICCM, University Park, PA (2016)

Applied Digital Human Modeling and Simulation

Validation of Interruption Management Stage Model: Can We Develop the Human Cognitive Behavior Model in Interruptive Working Environment?

Byung Cheol Lee(✉)

School of Science and Engineering, Texas A&M University-Corpus Christi,
6300 Ocean Drive, Corpus Christi, TX, USA
byungcheol.lee@tamucc.edu

Abstract. Interruptions are prevalent phenomena in modern working environments, and their negative effects are widely admitted; yet, few studies have been conducted on how to successfully manage unnecessary interruption, and there are not many interface design guidelines to minimize the negative effects of interruptions. Using a customized computer software tool, a study was carried out to investigate the effects of interruptions on the different types of interruption management stages. The results showed that the scheduled stage showed the best quantitative performance ($F[2, 331] = 4.71$, $p < 0.01$) and the negotiated stage demonstrated the best qualitative performance ($F[2, 74] = 7.85$, $p < 0.001$). The results provide potential interface design guidelines in interruptive human - system interactions.

Keywords: Interruption · Interruption management · Interface design

1 Introduction

Interruptions are unavoidable and frequent phenomena in modern working environments. As an internet and other information technologies become an indispensable necessity in workplaces, overloaded information may directly devastate human performance. Such diverse and high volume of information relentlessly pours into on us as long as we are connected with information systems. Multi-tasking that concurrently handle multiple information and tasks seems to be one of the essential capabilities required in a modern job description. A majority of workers are exposed to increasing amounts of fragmented, simultaneous task resources, and their attention span cannot be maintained till one task is completed. Due to such highly dynamic, ubiquitous, reactive and multimodal features of work, inopportune and unfavorable interruptions are common in current working spaces.

Generally, task interruptions negatively influence the performance outcomes. Unexpected and unmanageable interruptions cause personal stress that can negatively affect performance [1]. Interruptions can increase mental and physical workload, reduce efficiency and deteriorate psychological consequences such as feelings of "time pressure" and overloaded responsibility [2, 3]. Moreover, they may result in frequent errors,

D.N. Cassenti (ed.), *Advances in Human Factors in Simulation and Modeling*,
Advances in Intelligent Systems and Computing 591, DOI 10.1007/978-3-319-60591-3_35

hesitations and delays in a decision-making process, slow tasks, frustration, and anxiety [4–6]. These are mainly due to that cognitive resources are not properly allocated across tasks [7–10]. A study asserted that interruptions cause to an average of 2.1 working hours loss per day in the US companies [11]. Although interruptions may play a positive role in simple and low cognitive demanding tasks, a broad range of detrimental effects have been more prevailed [12, 13].

Notwithstanding the acknowledging of adverse effects of interruptions, the solutions to minimize the effects are very limited, and most interruptions are not easy to avoid. 59% of email recipients in workplace check emails within 20 min they received because they are anxious if they might miss some important information [14]. During the interruption, suspended goal need to be resumed at the point that enables to remember a previous task state. Ideally, the best way to eliminate the negative effects of interruptions is to recognize an exact spot the task was interrupted and resume properly, without having redundant actions and skipping step [15]. The more specifically recognize how and where task had been suspended, the more efficiently and accurately it can proceed toward achieving the pending goal. However, practically, it seems to impossible to develop such approach for perfectly eliminating all interruptions.

One probable way to minimize the negative effects of interruptions is to develop user interface (UI) design guidelines about how to deal with interruptions in multi-tasking. Trafton et al. [15] investigated to find opportune moments to interrupt users. This coordination approach estimated the cost of interruption by sensory input analyses of interruption task environments and scheduled parallel activities in the period of lower mental workload. However, this approach was limited to the abstract level of interruption interactions and lacked consideration of the different level of efforts to handle interruptions. In addition, it failed to provide specific UI design guidelines.

As another approach, Latorella [16] suggested an interruption management stage model, and this model described human interruption management in the information processing framework and task environment [16, 17]. The model also provided the measures to evaluate the degree of interruption management and deleterious effects of interruptions. The model consists of four different modes. First, the immediate mode immediately delivers interruptions regardless of the status and progress of primary tasks. Interruptions are delivered at the soonest possible moment. Subjects cannot control the occurrence of interruptions. Second is the negotiated mode, which is when the subjects are aware that the interruption will occur and support negotiation of the occurrence of interruptions. A certain type of supports can be given to control when the interruption will be initiated. The third mode is mediated. This mode uses an intermediate agent to handle interruptions and to notify the timing and order of interrupting tasks. For an example, an autonomous broker such as a PDA (personal digital assistant) is actively involved in deciding when is the best to interrupt the user. Fourth is a scheduled mode, in which interruptions occur on a prearranged schedule. The person can expect when interruptions happen.

This study investigated how human task performance can be influenced from interruptions by three different user interface (UI) designs. We devised three different UI design interruption delivering mechanisms by Interruption Management Stage Model and interruption coordination methods [16, 17], and we empirically measured quantitative and qualitative task performance by each UI design. We assumed that the

task performance in each interruption delivering mechanism may show different results, and predicted that the results will highlight the complex relationship between task interrupting modes and their effects on task performance. We tested this prediction in controlled laboratory experiments using a custom-developed application with different types of tasks. In the end, this study can contribute to develop a human cognitive behavior model in interruptive working environments and suggest potential solutions to reduce detrimental effects of unexpected and unnecessary interruptions.

2 Experiment

Controlled laboratory experiments with a within-subject design were conducted to validate interruption management stage model. In this study, the effects of interruption were measured in task completion time and the frequency of errors committed by participants.

2.1 Subjects

Thirty-nine participants were recruited in the study. All participants were college students who were in their junior year (44%) or their senior year (56%) in the engineering program. The average age of participants was 23. Thirteen were females, and 26 were males. All participants were familiar with general computer use and had enough competency in basic mathematic problem-solving. All participants were eligible for incentives if they completed in the experiment. The IRB (Institutional Review Board) protocol was reviewed and approved prior to testing to ensure the protection of human subjects in research.

2.2 Variables and Measures

Types of Tasks. The participants performed a series of tasks, which consists of predetermined order of two task types: cognitive tasks (mental arithmetic problem tasks) and skill tasks (sentence typing tasks). Figure 1 shows the experiment framework for this study.

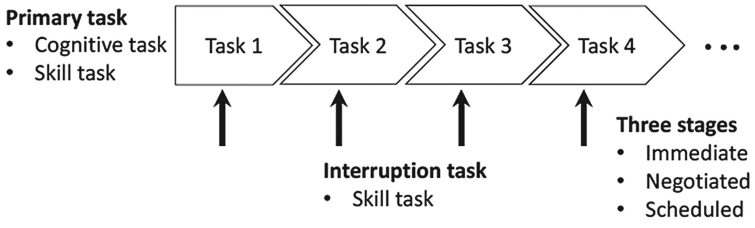

Task Set	Primary Task	Interruption Task
Cog-Skill	Cognitive task	Skill task
Skill-Skill	Skill task	Skill task

*Cognitive task = Mental arithmetic problem task
**Skill task = Sentence typing task

Fig. 1. Experiment framework

Cognitive tasks are vulnerable to individual difference, and maintaining uniform difficulty of tasks is the key for objective measurement of the task performance. To do so, only word problems with similar lengths (average 45 words) were used. The length of word problem added mental workloads and made the interruptions be at a cognitive process. Additionally, simple mathematic operations were required to solve questions, and all questions were selected from a seventh-grade-level math test book. Finally, calculators or computers were not allowed in the experiment to extend cognitive process in question-solving. Table 1 shows some sample questions for cognitive and skill tasks.

Table 1. Sample questions for cognitive and skill task

Cognitive task: math question solving*
Your school cafeteria makes its delicious tuna salad by adding 2 pounds of mayonnaise to every 3 pounds of canned tuna. Canned tuna costs $1.50 per pound and mayonnaise costs $0.75 per pound. How many pounds of tuna salad can the cooks prepare for $100?
a. 88 1/3 b. 33 1/3 c. 55 d. 30
Physical task: sentence copying**
Type the following sentences in given space.
Another approach to definitions of the quality of healthcare is directly connected with patient safety, which can evidently be confirmed by reviewing some definitions of patient safety. One study described healthcare quality as the eligibility of the recommended medical treatments and Berwick expounded.

*: All questions were selected from grade 7th math textbook [20]. Only word problems were selected.
**: Sentences were arbitrary composed but the number of words was limited between 40 and 45. This number is based on average typing words per minute for clerical workers [21].

Interruption Management Stages. This study evaluated three interruption delivering modes that are based on Latollera's Interruption Management Stage Model [18, 19]. The model suggested four different types of coordinating human interruptions as user interfaces. However, only three types were applied in this study. First, the immediate mode immediately delivers interruptions regardless of the status and progress of primary tasks. Subjects cannot control the occurrence of interruptions. Second is the negotiated mode, which is when the subjects are aware that the interruption will occur and support negotiation of the occurrence of interruptions. Subjects can control when and where to deal with interruptions in this mode. The third is a scheduled mode, in which interruptions occur on a prearranged schedule. Subjects can expect when interruptions happen. These three modes were designed and embedded in a custom-developed computer simulated task program.

Task Performance Measure. Task performance measurement was divided into two types: quantitative measure and qualitative measure. As a quantitative measure, task completion time was assessed, and correct answers for cognitive tasks and typographical errors for skill tasks were counted as qualitative measures. Task completion time covers time to complete both a primary task and an interrupting task, and it includes resumption lag, which is "return time" to primary tasks after the completion of

an interrupting task. The resumption lag not only influences a task completion time but also makes difficult to return the resuming spot. Qualitative task measures were developed based on the task types. To minimize the chance of getting right answers accidently, the choice of "I don't know" was also given to participants. Typographical errors in skill tasks included not only spelling errors but also punctuation and capitalization errors.

2.3 Procedure

Each subject was asked to fill out a demographic questionnaire and consent form before the experiment, and a ten-minute training session with several sample tasks was provided. The subjects then performed four different task sets that were assigned in a predetermined order. The order of task sets was fully counterbalanced. Each subject experienced all three different interruption management stages randomly. A none-interruption scenario consisted of pairs of cognitive and skill tasks, and the results were used as a performance reference.

When the experiment started, a primary task was placed on the computer screen. Then, interruption tasks were given by interruption management stages, popping-up on a new screen. Once the subject answered the interruption question, he/she clicked an "OK" button and automatically returned to the interrupted primary task. The experiment included three scenarios per subject, and each scenario continued for 10 min. In an immediate mode, interruption tasks appeared without any indications. In a negotiated mode, when subject clicked the button the screen, interruption tasks were showed up, and, in a scheduled mode, participants had interruption tasks after fifteen seconds with count-down clock and clicking sounds.

3 Results

We performed repeated measures analyses on task completion time as a quantitative task performance. To evaluate the performance of the two different task types on the same basis, Time Performance Ratio (TPR) (Table 2) per subject, which is the standardized task completion time ratio between task completion time with interruptions and without interruptions, was introduced. A two-way ANOVA with repeated measures showed a significant effect of task sets on TPR ($F[1, 331] = 11.24$, $p < 0.001$). It also showed a significant effect of interruption management stages on TPR ($F[2, 331] = 4.71$, $p < 0.01$). No interaction effect was observed.

Paired comparisons showed that the TPR of Cognitive/Skill task sets (mean = 156.43, SD = 12.16) was significantly higher than Skill/Skill task sets (mean = 136.27, SD = 8.78) in the immediate stage. Similar patterns were shown in the scheduled stage, but in the negotiated mode, the results of two task sets were not significantly different. Regarding the effect of interruption management stages, the scheduled stage (mean = 116.28, SD = 12.01) took shortest task completion time, and the negotiated stage took longest time (mean = 168.84, SD = 9.97).

Table 2. Descriptive statistics of Time Performance Ratio (TPR)

Time Performance Ratio (TPR)* (Primary/interrupting task)	Mean	Median	Standard deviation
Cognitive/skill task set			
Immediate	156.43	156	12.16
Negotiated	169.07	168	11.95
Scheduled	123.11	123	15.33
Skill/skill task set			
Immediate	136.27	138	8.78
Negotiated	168.61	167	6.95
Scheduled	109.45	110	7.11

$* \; Completion\ Time\ Ratio\ (TPR) = \frac{Task\ Compltion\ Time\ with\ Interruptions}{Task\ Compltion\ Time\ without\ Interruption}$

As qualitative measurements for task performance, wrong answer rates in mental arithmetic questions and typographical error rates in sentence typing tasks were chosen. To compare two different task types, we have to use the ratio of two measurements: wrong answer rate ratio (WARR) and the typo rate ratio (TRR), which are the standardized values for two measurements. WARR was applied to Cognitive/Skill task sets, and TRR was used for Skill/Skill sets.

Table 3 shows descriptive statistics for each subject's WARR and TRR. A two-way ANOVA with repeated measures showed a significant effect of task sets on WARR and TRR ($F[1, 74] = 12.61$, $p < 0.001$). It also showed a significant effect of interruption management stages on WARR and TRR ($F[2, 74] = 7.85$, $p < 0.001$). No interaction effect was observed.

Paired comparisons showed that the WARR and TRR have the same patterns of the results with TPR. WARR of Cognitive/Skill task sets (mean = 139.42, SD = 17.61: immediate stage, mean = 125.89, SD = 13.41: scheduled stage) was significantly higher than TRR of Skill/Skill task sets (mean = 122.27, SD = 7.51: immediate stage, mean = 109.45, SD = 5.55: scheduled stage) in the immediate stage and the scheduled

Table 3. Descriptive statistics of typo rate ratio and wrong answer rate ratio

Wrong answer rate ratio (WARR)[a] Typo rate ratio (TRR)[b] (Primary/interrupting task)	Mean	Median	Standard deviation
Cognitive/skill task set			
Immediate	139.42	141	17.61
Negotiated	105.21	105	11.89
Scheduled	125.89	123	13.41
Skill/skill task set			
Immediate	122.27	120	7.51
Negotiated	103.67	104	4.33
Scheduled	109.45	111	5.55

[a] $Wrong\ Answer\ Rate\ Ratio\ (WARR) = \frac{Wrong\ Answer\ Rate\ with\ Interruptions}{Wrong\ Answer\ Rate\ without\ Interruption}$

[b] $Typo\ Rate\ Ratio\ (TRR) = \frac{Typo\ Rate\ with\ Interruptions}{Typo\ Rate\ without\ Interruption}$

stage, but in the negotiated stage, the results of two task sets were not significantly different. Regarding the effect of interruption management stages, the negotiated stage (mean = 104.44, SD = 8.57) had the lowest error rate, and the immediate stage had the highest rate (mean = 130.86, SD = 14.06).

4 Discussion

Interruptions more negatively affected task completion time on the negotiated stage. Figure 2 shows that TPR's of the negotiated stage were higher than those of the immediate and the scheduled stages ($F[2, 331] = 7.11$, $p < 0.001$). In negotiated stage, participants had not much experienced the time pressure to complete the task, and interruptions were managed by their control. This stage can be regarded as a sequential process, not a parallel process. It means that the time lags between primary and interrupting tasks in the negotiated stage are longer than those in other stages. Comparing task completion times of different task types, as also shown in Fig. 3, Cognitive tasks were more influenced from interruptions than Skill tasks ($F[1, 331] = 11.88$, $p < 0.001$). Since cognitive tasks require more mental resources for task completion, more switching time to interrupting tasks and returning time to interrupted tasks are required. The long switching time and returning time make it difficult to retrieve cues for the interrupted goal and delayed the transition to the new task [22]. Accordingly, a memory load is the main factor we have to consider the interruption effects on quantitative performance. Cognitive tasks needed more memory loads than sensory

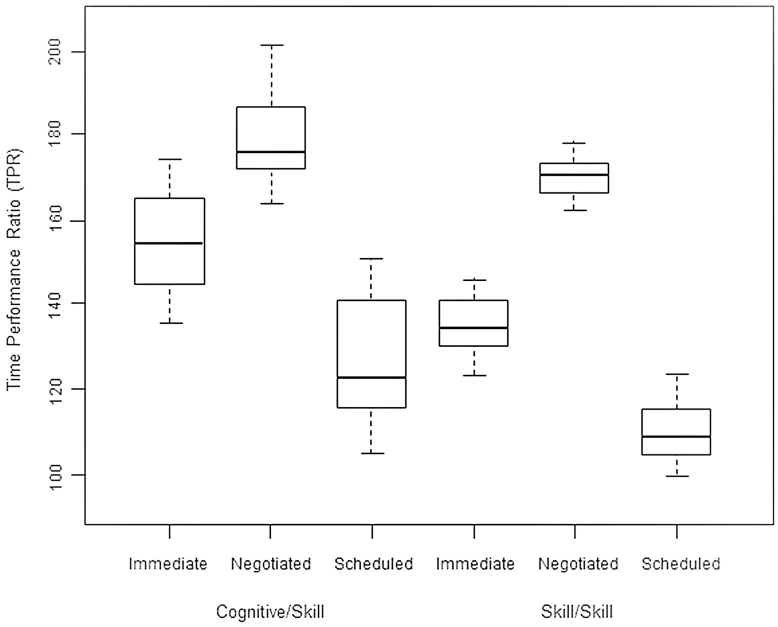

Fig. 2. Quantitative task performances by interruption management stages

information-based skill tasks. High memory loads caused the degradation of task performance in cognitive tasks, and cognitive tasks were more vulnerable to interruptions. However, in the negotiated stage, there was no significant difference.

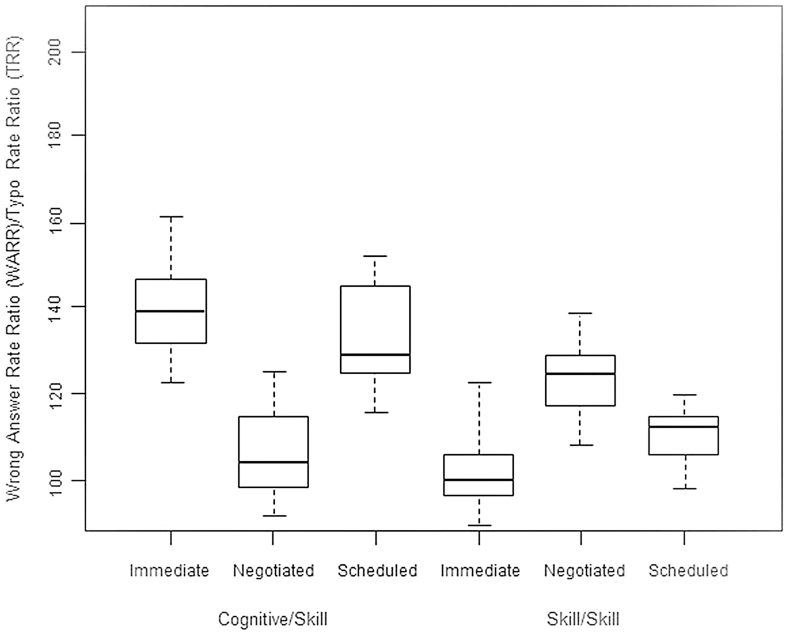

Fig. 3. Qualitative task performances by interruption management stages

Interruption effects on qualitative performance showed different results than on quantitative performance. The negotiated stage generated the fewest errors, and the immediate stage made the most frequent errors in cognitive and skill tasks. Contrary to the results of task completion time, time pressure is the main factor affecting qualitative task performance. In the negotiated stage, participants focused on the task without time pressure, which contributed the low level of error rates. Within the task sets, skill task sets had a higher number of errors than cognitive task set. One probable cause of this high error rates in skill tasks is task similarity. the same type of primary/interruption tasks easily interferes and confuses the cue-goal connection [22, 23]. In addition, well-trained consistent motor behaviors are vulnerable to disruptions from interruptions and are difficult to retrieve and resume interrupted cues [22, 24].

5 Conclusion

The study investigated the effects of interruptions on different information management stages and task types. For the quantitative measure, since the scheduled stage showed the best task completion time performance, it is considered as the most efficient

interruption management approach. For the qualitative measure, the negotiated stage demonstrated the best performance on cognitive and skill tasks, and it could be the most effective approach. However, some tasks in the negotiated stage were conducted in a sequential way. Thus, it may not an appropriate interruption management stage.

This study also has some limitations. Some designs of interruption management stages were not enough to reflect the original concepts suggested by Latorella. Also, the individual difference needs to be more actively considered. The experiments were limited to college students who major in engineering. Other areas and ages may provide more comprehensive and representative results.

In conclusion, different stages of interruption management show different degrees of interruption effects, and the results can apply to design the efficient and effective interface between human behavior and unnecessary interruptions.

References

1. Cohen, S.: Aftereffects of stress on human performance and social behavior: a review of research and theory. Psychol. Bull. **88**, 82 (1980)
2. Carayon, P.: Stressful jobs and non-stressful jobs: a cluster analysis of office jobs. Ergonomics **37**, 311–323 (1994)
3. Yeh, Y.-Y., Wickens, C.D.: An investigation of the dissociation between subjective measures of mental workload and performance. University of Illinois, Urbana-Champaign (1984)
4. Eyrolle, H., Cellier, J.-M.: The effects of interruptions in work activity: field and laboratory results. Appl. Ergon. **31**, 537–543 (2000)
5. Gillie, T., Broadbent, D.: What makes interruptions disruptive? A study of length, similarity, and complexity. Psychol. Res. **50**, 243–250 (1989)
6. Kreifeldt, J., McCarthy, M.: Interruption as a test of the user-computer interface. In: JPL Proceedings of the 17th Annual Conference on Manual Control, pp. 655–667 (1981). (SEE N 82-13665 04-54)
7. Alm, H., Nilsson, L.: The effects of a mobile telephone task on driver behaviour in a car following situation. Accid. Anal. Prev. **27**, 707–715 (1995)
8. Anderson, J.R., Bothell, D., Byrne, M.D., Douglass, S., Lebiere, C., Qin, Y.: An integrated theory of the mind. Psychol. Rev. **111**, 1036 (2004)
9. Bailey, B.P., Iqbal, S.T.: Understanding changes in mental workload during execution of goal-directed tasks and its application for interruption management. ACM Trans. Comput.-Hum. Interact. TOCHI. **14**, 21 (2008)
10. Card, S.K., Moran, T.P., Newell, A.: The Psychology of Human-Computer Interaction. CRC Press, Boca Raton (1983)
11. Freedman, D.: What's Next: The Cost of Competence. Inc.Com, New York (1997)
12. Bainbridge, L.: Diagnostic skill in process operation. In: International Conference on Occupational Ergonomics, pp. 7–9 (1984)
13. van Solingen, R., Berghout, E., van Latum, F.: Interrupts: just a minute never is. Softw. IEEE. **15**, 97–103 (1998)
14. Gonzales, M.M., Dickinson, L.M., DiGuiseppi, C., Lowenstein, S.R.: Student drivers: a study of fatal motor vehicle crashes involving 16-year-old drivers. Ann. Emerg. Med. **45**, 140–146 (2005)

15. Trafton, J.G., Altmann, E.M., Brock, D.P., Mintz, F.E.: Preparing to resume an interrupted task: effects of prospective goal encoding and retrospective rehearsal. Int. J. Hum.-Comput. Stud. **58**, 583–603 (2003)
16. Latorella, K.A.: Investigating interruptions: implications for flightdeck performance. National Aeronautics and Space Administration, Goddard Space Flight Center (1999)
17. McFarlane, D.C., Latorella, K.A.: The scope and importance of human interruption in human-computer interaction design. Hum.-Comput. Interact. **17**, 1–61 (2002)
18. Latorella, K.A.: Investigating interruptions: an example from the flightdeck. In: Proceedings of the Human Factors and Ergonomics Society Annual Meeting, pp. 249–253. SAGE Publications (1996)
19. Latorella, K.A.: Effects of modality on interrupted flight deck performance: implications for data link. In: Proceedings of the Human Factors and Ergonomics Society Annual Meeting, pp. 87–91. SAGE Publications Sage CA, Los Angeles (1998)
20. Linderman, B.: Word Problems Homework Booklet, Grades 7–8. Instructional Fair, Tucson (1999)
21. Ostrach, T.R.: Typing Speed: How Fast is Average: 4,000 Typing Scores Statistically Analyzed and Interpreted. Five Star Staffing, Inc., Orlando (1997)
22. Altmann, E.M., Trafton, J.G.: Memory for goals: an activation-based model. Cogn. Sci. **26**, 39–83 (2002)
23. Lee, B.C., Duffy, V.G.: The effects of task interruption on human performance: a study of the systematic classification of human behavior and interruption frequency. Hum. Factors Ergon. Manuf. Serv. Ind. **25**, 137–152 (2015)
24. Wickens, C.D., McCarley, J.S.: Applied Attention Theory. CRC Press, Boca Raton (2007)

An Evaluation Method for Human Fatigue in Virtual Maintenance Simulation Based on the Cube Model

Yimin Li(✉), Qing Xue, Minxia Liu, and Jingqian Wen

School of Mechanical Engineering, Beijing Institute of Technology, 100081 Beijing, China
3406ll422@qq.com, xueqing@bit.edu.cn

Abstract. This study presents an evaluation method for human fatigue in virtual maintenance simulation based on the cube model which concluded that human fatigue can be decided by posture, force and time during the operations. This paper analyses the feasibility on applying the cube model to the virtual maintain simulation for human fatigue evaluation. According to the analysis, a new posture level determination method in virtual maintenance simulation is put forward based on the advantage that virtual human's data of joints can be acquired in real time. Besides the theory deduction, this paper also provides a practical example of virtual maintenance to show the feasibility of the evaluation method.

Keywords: Human fatigue evaluation · The cube model · Virtual maintenance simulation · Posture level determination method

1 Introduction

With the rapid development of the virtual reality technology, a great reformation named virtual maintenance technology happens on the equipment maintenance field. The application of virtual maintenance technology mainly includes maintainability design, protection plan and maintenance staff training. In the field of maintainability design, using the virtual maintenance technology to carry out the prediction and analysis on the early period of the equipment design can insure the good maintainability of equipment, decrease the cost in future maintenances and increase the efficiency of design [1].

Human factor is a very significant attribute for maintainability design, appropriate human factor design can enhance work efficiency and reduce the operation fatigue for workers. Human fatigue evaluation is an important part of human factor evaluation, it can guide and amend the equipment design, judge the rationality of equipment maintenance process and reduce the occupational injury while workers carry out practical operation. The impact of human fatigue run through all equipment design, operation and maintenance [2]. So, it's considerable to research human fatigue evaluation method in virtual maintenance simulation which is a significant part of the virtual maintenance technology.

Human fatigue is mainly caused by muscle fatigue in maintenance operations. In current situation, there are two kinds of researches in muscle fatigue. One is to predict

D.N. Cassenti (ed.), *Advances in Human Factors in Simulation and Modeling*,
Advances in Intelligent Systems and Computing 591, DOI 10.1007/978-3-319-60591-3_36

muscle fatigue by using fatigue models and another one is to evaluate the risk of musculoskeletal disorders (MSD) which is the expression of accumulated muscle fatigue. Several models which try to objectively predict muscle fatigue have been proposed in public, such as the muscle fatigue model based on force-pH relationship in computer graphics which is applied to visualize the muscle fatigue in a working time [3]. There are many related studies for the risk of MSD evaluation research. Several techniques are available for evaluating the risk of MSD, such as Ovako Working Posture Analyzing System (OWAS), Quick Exposure Check (QEC), Rapid Upper Limb Assessment (RULA) and so on [4]. Although predicting muscle fatigue directly in virtual maintenance simulation can get a specific result, the operation is complex and the result is hard to be used in the maintainability comprehensive assessment. So it seems more reasonable to assess human fatigue by evaluating the risk of MSD with a simple result in virtual maintenance.

The cube model is a classic method to assess the risk of MSD in practical and the result is brief, which is very appropriate for the maintainability comprehensive assessment. So this article analyses the feasibility of applying the cube model in virtual maintenance simulation to evaluate human fatigue and develops the criteria principles based on the advantages of virtual maintenance simulation. Besides the theory deduction, this paper also provides a practical example of virtual maintenance to show the feasibility of the evaluation method.

2 The Cube Model

The methodology of the cube model was mentioned by Putz-Anderson who pointed out that the worker is at risk of developing a CTD (Cumulative Trauma Disorder) when high repetition is combined with forceful and awkward postures on the condition of insufficient recovery time [5]. Kadefors summarized related papers and developed the methodology into the cube model in 1994 [6].

The basis of the cube model is from scientific data which indicates that the risk to acquire work related musculoskeletal disorders during working is to a large extent dependent on three interrelated factors. The factors encompassed by the cube model are postural strain (Posture), external force exertion in pushing/pulling or in manual materials handling (Force) and static or repetitious loads (Time). Each factor can be divided into three levels coding by 1, 2, 3. The numbers 1, 2, 3 indicate the low level, medium level and high level respectively.

From an ergonomic evaluation point of view, these basic factors are heavily interrelated. For example, working under high force level may be accepted while time is in a low level, whereas working under low force level may be unacceptable while time in a high level. So how to determine the relationships of the factors is a huge contribution of the cube model.

The cube model suggests a formula for risk prediction that essentially is these factors multiplied. It can also be applied to human fatigue evaluation. The formula showed in (1).

$$A = Posture * Force * Time \tag{1}$$

Because each factor of the cube model has three kind of levels, there will be 27 cases of A level. Depending on the result of A level, the analysis of work status may be termed acceptable ($A \leq 5$), conditionally acceptable ($5 < A < 10$), or unacceptable ($A \geq 10$).

It's a research challenge to confirm the demand criteria of each factor. The demand criteria outlined in Table 1 [7] from the related paper of Kadefors and Sperling.

Table 1. Criteria principles of basic demand dimensions of the cube model

Dimension	Posture	Force	Time
1	Hand in optimal working zone (waist level, close to the body) Shoulder abduction/flexion <15°	Below 1.0 kg	<1 h per day on and off; continuously <10 min; Repetitively: <0.1 c/min (shoulder), <1 c/min(hand), <20 c/min (fingers)
2	Hand near optimal working zone Shoulder abduction flexion between 15° and 45°	Between 1.0 kg and 2.3 kg	Between 1 and 4 h per day on and off; between 10 and 30 min continuously; Repetitively: 0.1–2.5 c/min (shoulder), 1–10 c/min (hand), 20–200 c/min (fingers)
3	Hand at or above shoulder level or arm extended outside optimal working zone Shoulder abduction/flexion exceeding 45°	Surpass 2.3 kg	More than 4 h per day on and off; more than 30 min continuously; Repetitively: >2.5 c/min (shoulder); >10 c/min (hand), >200 c/min (fingers)

3 Analysis

From the formula (1) and the demand criteria in Table 1, it can clearly find that the cube model is very suitable for computerized assessment. In fact, the cube model has been applied in software like ErogoSAM. ErogoSAM is SAM (Sequence-based activity and method analysis with a module added that also predicts the physical workload on the operator, making it possible to identify points of high load during a working cycle. It offers a tool for the production engineer when it is necessary to take ergonomic considerations in a workplace design.

ErgoSAM assessment has been tested at the Torslanda final assembly plant of Volvo Car Corporation and at the ITT Flygt plant for large submersible pumps at three different balances and compared with two different methods of assessing biomechanical load [8]. So, it's reasonable to think that it's suitable to use the cube model in virtual maintenance simulation if it has similar service environment with ErgoSAM.

As the introduction above, the function of ErgoSAM is to do the risk assessment of a task in a planned but not yet existing workplace which is very similar to carry out maintainability assessment for equipment designed as both the object assessed is not

really existed. No matter in production or maintenance, the assessor has to specify each factor of assessments. The assessor not only needs structures information necessary for the ergonomic assessment but also reaches a more detailed conception of the future for the planning process as a whole. So the assessor and the object assessed are very similar between the environment of ErgoSAM and virtual maintenance simulation. So, it's very appropriate to consider the evaluation method is feasible in virtual maintenance simulation with the verification of ErogoSAM.

The virtual human maintain equipment designed adopt continuous actions following the maintenance operation sequence in virtual maintenance simulation. The external force exerted in virtual human can be seen as a constant and the time is also fixed during a single maintenance operation. So it's credible to use the criteria principles of force and time in Table 1 in a single maintenance operation assessment. A simplified criteria principles is shown in Table 2 based on the continuity of virtual human's operation.

Table 2. Criteria principles of force and time in the cube model

Dimension	Force	Time
1	Below 1.0 kg	Continuously <10 min
2	Between 1.0 kg and 2.3 kg	Between 10 and 30 min continuously
3	Surpass 2.3 kg	More than 30 min continuously

The criteria principles of posture in Table 1 is confined to the shoulder and hand/wrist without heavy back loading and other part of human body. It's acceptable to use this criteria principle for workplace plan because workers generally have only hand operations in a fixed workplace. However, the workers usually have to apply all his body to finish a maintenance operation. The criteria principle of posture in Table 1 may not be suitable applied in maintenance operation assessment. Based on the above analysis, this paper presents a method to determine the posture level in virtual maintenance simulation.

4 Determination Method of Posture Level

There are special advantages of the virtual maintenance simulation. One is that the data of virtual human can be acquired in real time. It's feasible to judge the posture of virtual human based on the data of joints. If the posture level database is build, it can realize computerized assessment for posture level to the posture judged.

The virtual human is drove by joints data. The virtual human showed in Fig. 1 is from Makereal 3D which is a software serving 3D modeling and process simulation. From Fig. 1, the virtual human contains 52 joints and 90 degrees of freedom of freedom (DOF). Like the waist in Fig. 1, it contains 3 DOFs and each DOF has its control scope.

Users control DOF value of joints to drive virtual human to simulate the maintenance process. From the drive mode, the virtual human posture can be defined according to special rule under the joints data. Based on the above analysis, this article proposes a rule for virtual human posture definition.

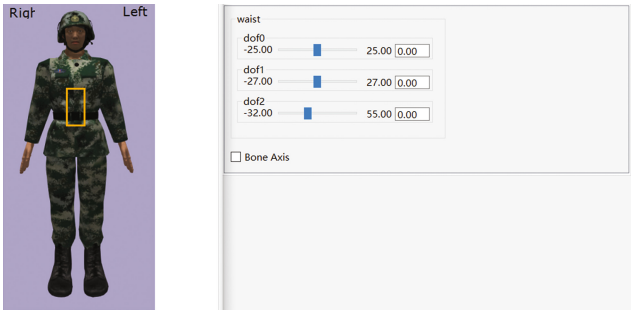

Fig. 1. Virtual human in Makereal 3D

Because of the complexity of human body, it's unwise to build a precise human exercise model. With a view to the maintenance operation, the main parts of human body that participate in exercising are neck, upper limbs, lower limbs and torso. So the human maintenance posture model can be simplified as the combination of the posture of four parts mentioned above. The posture description is showed in Table 3.

Table 3. The posture description of human part

Part	Code	Posture description
Neck	1	Both flexion and lateral bending less than 30°, and axial twist less than 45°
	2	Flexion or lateral bending over 30°, or axial twist over 45°
	3	The backward bending over 20°
Upper limbs	1	Both of elbows are below the shoulders
	2	One of elbow is above the shoulder
	3	Both of elbows are above the shoulders
Lower limbs	1	Knees bend less than 35°
	2	One leg raised; supported by the other foot
	3	At least one knee bend over 35°
	4	Both of knees bend over 90°
	5	Walk
	6	At least one knee touchdown
	7	Both of feet below the hips
	8	Both of feet as high as hips
	9	Move by hands and knees
	A	Supination
	B	Prostrator
	C	Lay on side
Torso	1	All of flexion, lateral rotation and axial rotation less than 20°
	2	Bending between 20° and 45°, lateral rotation or axial rotation less than 20°
	3	Bending over 45°
	4	Flexion less than 20°, one or both of lateral rotation and axial rotation over 20°
	5	Bending between 20° and 45°, lateral rotation and axial rotation over 20°

The posture of four parts can be classified with the description and coded by serial numbers in Table 3. The combination of the codes consist of the neck code, upper limbs code, lower limbs code and torso code successively. It can describe 540 maintenance postures in theory. Using the judgement flow chart to classified the posture of neck, upper limbs, lower limbs and torso based on the real-time joints data of virtual human respectively, a determination of virtual human's posture can be get and stored in a form of posture codes. Take the neck judgment flow chart as an example in Fig. 2.

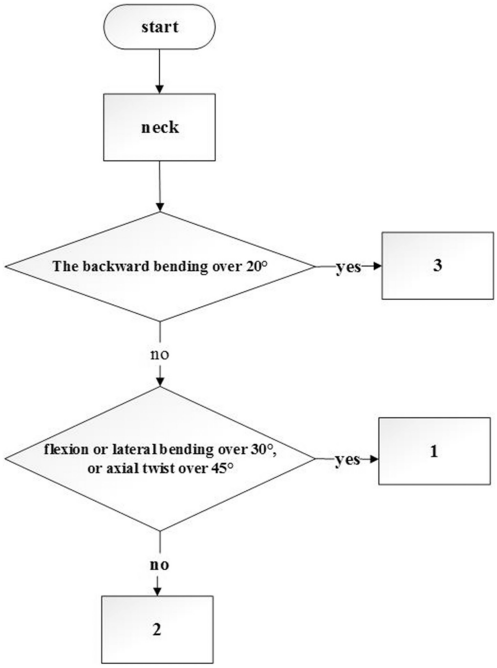

Fig. 2. The neck judgment flow chart

Under the posture type of virtual human that has been determined, it is necessary to determine the posture fatigue level corresponding to each posture. This paper consults the results of posture fatigue level experiment done by Kong [9]. Kong determined the posture fatigue level of 375 posture and presented the experiment result in 1–9 scaling.

Because some postures in the combination we made did not really exit, this paper determines the classification of posture fatigue level shown in Table 4.

According to the data of Table 4, a posture fatigue judgment database is formed to carry out the fatigue determination for virtual human's real-time posture. Like the maintenance posture in the left of Fig. 3, the virtual human kneels down and bends over. The code of this posture is 1361 based on the judgment flow charts. According to the posture fatigue judgment database, the fatigue level of code 1361 is 2. The result is same as the auto judgement of Makereal 3D in the right of Fig. 3. In the right of Fig. 3,

Table 4. The classification of posture fatigue level

Fatigue level	Posture code
1	1111, 1114, 1142, 1151, 1152, 1161, 1171, 1172, 1174, 1181, 1182, 11A1, 1211, 1251, 1271, 1272, 1281, 1282, 12A1, 1311, 1351, 1371, 13A1, 2111, 2151, 2152, 2171, 2172, 2181, 2182, 2211, 2271, 2282, 2371, 3151, 3171, 3181, 3211, 3271, 3281, 3311, 3371
2	1112, 1113, 1115, 1121, 1122, 1123, 1124, 1131, 1132, 1133, 1134, 1141, 1143, 1144, 1145, 1153, 1154, 1155, 1162, 1163, 1164, 1165, 1173, 1175, 1183, 1184, 1185, 1191, 11B1, 11C1, 1212, 1213, 1214, 1215, 1221, 1222, 1224, 1231, 1232, 1233, 1234, 1241, 1242, 1243, 1244, 1245, 1252, 1253, 1254, 1255, 1261, 1262, 1263, 1264, 1273, 1274, 1275, 1283, 1284, 1291, 12B1, 12C1, 1312, 1313, 1314, 1321, 1322, 1324, 1331, 1332, 1334, 1341, 1342, 1344, 1352, 1361, 1362, 1363, 1364, 1372, 1373, 1374, 1375, 1381, 1382, 1384, 13B1, 13C1, 2112, 2113, 2114, 2115, 2121, 2122, 2123, 2124, 2131, 2132, 2133, 2134, 2141, 2142, 2143, 2144, 2145, 2153, 2154, 2155, 2161, 2162, 2163, 2164, 2165, 2173, 2174, 2175, 2183, 2184, 2185, 2191, 2212, 2213, 2214, 2215, 2221, 2224, 2231, 2232, 2233, 2234, 2241, 2242, 2243, 2244, 2245, 2251, 2252, 2253, 2254, 2261, 2263, 2264, 2272, 2273, 2274, 2275, 2281, 2284, 2291, 2311, 2312, 2313, 2314, 2321, 2324, 2331, 2332, 2341, 2342, 2343, 2344, 2351, 2352, 2354, 2361, 2362, 2364, 2372, 2373, 2374, 2381, 2382, 2384, 3111, 3112, 3113, 3114, 3121, 3124, 3131, 3132, 3134, 3141, 3142, 3143, 3144, 3145, 3152, 3154, 3161, 3162, 3164, 3172, 3173, 3174, 3175, 3182, 3184, 3191, 3211, 3212, 3214, 3221, 3241, 3242, 3243, 3244, 3251, 3252, 3254, 3261, 3262, 3272, 3273, 3274, 3275, 3282, 3284, 3314, 3342, 3344, 3351, 3352, 3354, 3355, 3361, 3372, 3373, 3374, 3381, 3382, 3384
3	1125, 1135, 1223, 1225, 1235, 1265, 1285, 1315, 1323, 1325, 1333, 1335, 1343, 1345, 1353, 1355, 1365, 1383, 1385, 2125, 2135, 2222, 2223, 2225, 2235, 2255, 2265, 2283, 2285, 2315, 2322, 2323, 2325, 2333, 2334, 2335, 2345, 2353, 2355, 2363, 2365, 2375, 2383, 2385, 3115, 3122, 3123, 3125, 3133, 3135, 3153, 3155, 3163, 3165, 3183, 3185, 3213, 3215, 3222, 3223, 3224, 3225, 3231, 3232, 3233, 3234, 3235, 3245, 3253, 3255, 3263, 3265, 3283, 3285, 3291, 3312, 3313, 3315, 3321, 3322, 3323, 3324, 3325, 3331, 3332, 3333, 3334, 3335, 3341, 3343, 3345, 3353, 3355, 3362, 3363, 3364, 3365, 3375, 3383, 3385

Fig. 3. A posture of virtual human and the assessment result of the cube model

there is no value filled in to define the time and force attributes in the operation. Both of them applied initial value 1 for computerized calculation, so the level of the cube model method for this virtual human posture is 2 and the assessment is acceptable.

5 Case Analysis

In this paper, a case of replacing a wheel of truck is presented to illustrate the human fatigue evaluation method in virtual simulation based on the cube model. Before the assessment, it is necessary to divide the whole maintenance process into different but consecutive maintenance events. Because the changes may cause the transform of force attribute, the divide principle considers the change of tools and postures. According to the divide principle, whole maintenance process in this case is divided into 8 maintenance events showed in Table 5. The Table 5 also shows the time and force attributes of each maintenance event which is estimated by actual.

Table 5. The maintenance events in replacing a wheel of truck

Event number	Event	Force (kg)	Time (s)
1	Close to the wheel	0	10
2	Jack up the truck	2	180
3	Loosen the bolt with a socket wrench	10	30
4	Loosen the bolt by hands	1	60
5	Remove the wheel	5	45
6	Put on spare wheel	5	45
7	Tighten the bolts by hand	1	60
8	Tighten the bolts with a socket wrench	10	60

Follow event number in Table 5, control the virtual human to do the virtual maintenance simulation in Makereal 3D like Fig. 4.

The maintenance events constitute the maintenance simulation in sequence, so it's necessary to evaluate each maintenance event in the whole simulation. When doing a single evaluation for maintenance event, the assessors need to pick up a key frame of the maintenance event and input the time and force attributes, then click the analysis bottom. The data will transmit to the database for the final analysis. After analyzing each maintenance event, the results of the analysis are given in a histogram. The result of this case is presented in Fig. 5.

From Fig. 5, the events of 1, 2, 4, 7 with green pillars mean that the human fatigue evaluation is acceptable. For the events with yellow pillars which mean that the human fatigue evaluation is conditionally acceptable, we found that the operator is kneeling down with superior force by dating from the maintenance simulation. However, it's all passed for the short work time. There is no red pillar which means that the human fatigue evaluation is unacceptable. From the above, the human fatigue evaluation for this maintenance event is supposed to be acceptable.

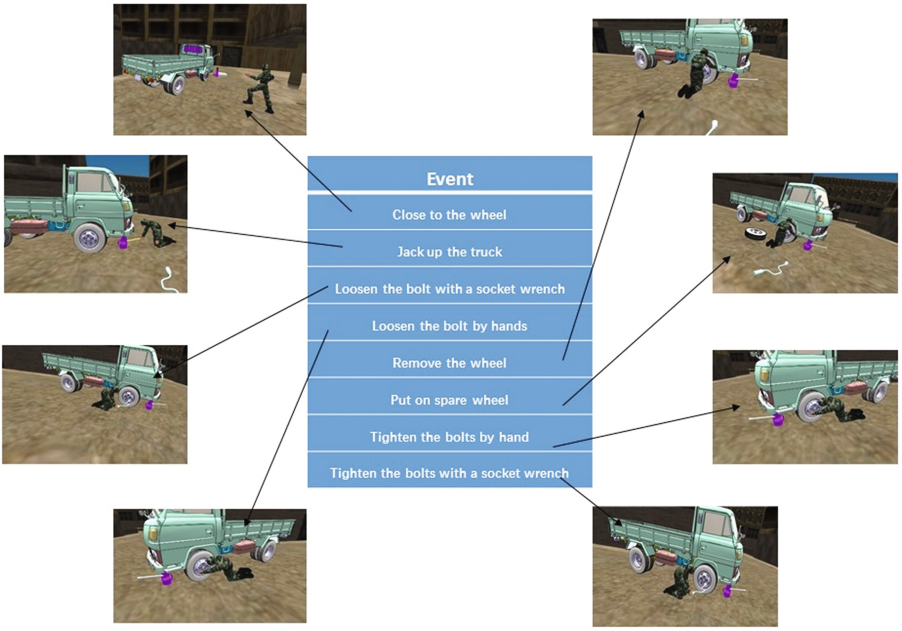

Fig. 4. Virtual maintenance simulation of replacing a wheel of truck

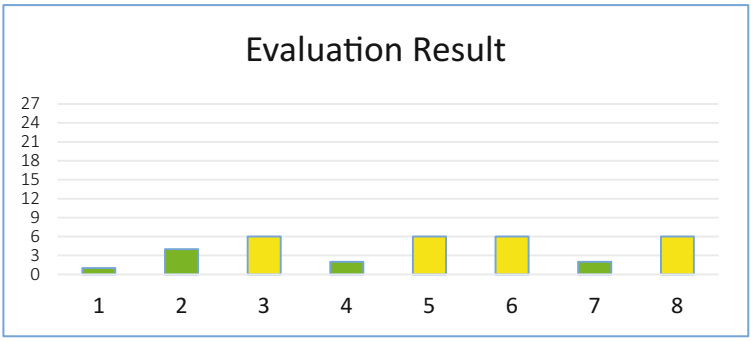

Fig. 5. The evaluation result of replacing a wheel of truck

6 Discussion

This paper analyses the feasibility of applying the cube model in virtual maintenance simulation. According to the analysis, a new posture level determination method in virtual maintenance simulation is put forward based on the advantage that virtual human's data of joints can be acquired in real time. On the basis of theory, a case is presented to illustrate specific assessment process and the results of evaluation can server for the comprehensive evaluation of maintainability design.

However, there is still something insufficient with this research. For example, it is necessary to amend the criteria principles with the application object change in practical situation, but the evaluation method for human fatigue in virtual maintenance simulation applies classic criteria principles for force and time in the cube model. The other one is that it's depend on assessors to input value for the time and force attributes for each maintenance event. But the value is subjective when given, which makes the operation more difficult.

For the current dilemma, this paper considers that it is necessary to carry out research on criteria principles of force and time for maintenance. It will enhance the credibility of the evaluation results of the method mentioned. For the time and force attributes, this article has done some researches. For example, we try to read the length of each maintenance event simulation for its time attribution, but the maintenance event simulation time is greatly different from the actual maintenance time. As for the force, there is no efficient method to get the force information from the virtual maintenance simulation itself. So this paper proposes an opinion that it is necessary to research the maintenance process information expression and connect maintenance process information with evaluation module to realize automated assessment for human fatigue.

Acknowledgments. I would like to thank to my tutors for their suggestions and the engineers for their help of module exploitation.

References

1. Wang, W., Li, G.: Research and development of virtual maintenance simulation technology (in Chinese). J. Syst. Simul. **23**(9), 1751–1757 (2011)
2. Wang, W., Tang, X., Li, Y.: Human fatigue analysis based on maintenance simulation (in Chinese). In: National Conference on Virtual Reality and Visualization (2006)
3. Komura, T., Shinagawa, Y., Kunii, T.L.: Creating and retargetting motion by the musculoskeletal human body model. Vis. Comput. **16**(5), 254–270 (2000)
4. Ma, L., Bennis, F., Chablat, D., et al.: Framework for dynamic evaluation of muscle fatigue in manual handling work. In: IEEE International Conference on Industrial Technology, Chengdu, China (2008)
5. Putz-Anderson, V.: Cumulative trauma disorders: a manual for musculoskeletal diseases of the upper limbs. Appl. Ergon. **19**(4), 332 (1988)
6. Kadefors, R.: An ergonomic model for workplace assessment. In: Proceedings of the IEA 1994, vol. 5. International Ergonomics Association, pp. 210–212 (1994)
7. Laring, J., Forsman, M., Kadefors, R., et al.: MTM-based ergonomic workload analysis. Int. J. Ind. Ergon. **30**(3), 135–148 (2002)
8. Laring, J., Christmansson, M., Kadefors, R., et al.: ErgoSAM: a preproduction risk identification tool. Hum. Factors Ergon. Manuf. Serv. Ind. **15**(3), 309–325 (2005)
9. Kong, L.: Research on comfort evaluation of job posture. Forest. Labor Saf. **22**(1), 22–25 (2009)

Optimization-Based Simulation of the Motion of a Human Performing a Horizontal Drop Jump

Mahdiar Hariri(✉), Toyin Ajisafe, and Jangwoon Park

Texas A&M University–Corpus Christi, 6300 Ocean Dr, Corpus Christi, TX 78412, USA
Mahdiar.Hariri@tamucc.edu

Abstract. The 'Hybrid Predictive Dynamics Method for Digital Human Modeling' is used in this work to analyze the dynamics of a human performing a "Drop Jump" task. The 'Hybrid' prefix mentioned in the literature recently [1] refers to the use of motion capture data for improving human motion simulations. This use of motion capture compensates for the inherent weaknesses of purely theoretical motion prediction due to deficiencies in computational power or available theoretical backgrounds. In this work, using motion capture data, an optimization based 3-D motion tracking of a human model performing a "Horizontal Drop Jump" is presented, as the first step in the simulation/prediction of such a motion. Based on the evaluation of the motion, dynamics properties of the motion are calculated which include ground reaction forces, joint torques and metabolic energy. The human model starts in a standing posture on top of a small box (low elevation from the ground), while jumping down the box, he changes his posture into a ready to jump pose with his two feet on the ground in-line and parallel to each other. After a brief recoil, he accelerates his center of gravity in the upward and forward direction and lifts off from the ground with an initial velocity in the same direction as his past acceleration. In the air, he will have a projectile motion and then he lands in his final position. The human model is a 55 degree of freedom (DOF) robot defined by Denavit-Hartenberg parameters. The base of the model is considered to be the hip point of a human. The orientation and position of this base in the global reference frame is defined by 6 DOF (3 position and 3 orientation). The robot includes 5 open-loop kinematic branches all originating from the base of the robot and ending in left hand, left foot, head, right hand and right foot. The remaining 49 DOF of the robot are revolute joints used in these 5 branches. Based on a motion capture set of data, motion is generated by a multi-objective optimization approach minimizing the difference between the location of markers on an actual human and the location of those same markers on the digital human model. All the forces, inertial, gravitational as well as external, are known, except the ground reaction forces are known. Therefore, it will be possible to calculate the total sum of ground reaction forces and moments. In the next step, joint torques are calculated using Lagrange's equations.

Keywords: Digital human · Robotics · Drop jump · Predictive dynamics · Kinematics · Dynamics · Virtual reality

D.N. Cassenti (ed.), *Advances in Human Factors in Simulation and Modeling*,
Advances in Intelligent Systems and Computing 591, DOI 10.1007/978-3-319-60591-3_37

1 Introduction

Predictive dynamics, developed recently [2–7], is a novel approach for simulating human motion in the digital human modeling field. It is a term that is coined to characterize the prediction of human motion in a physics-based world. Most of the known information for modeling a human motion task such as walking, running, aiming, kneeling, going prone, etc. usually appears as inequality constraints. These constraints represent the limitations of the environment (e.g. non-adhesive contact areas), the limitations of the digital human model (e.g. joint angle or torque limits) and the limitations of the motion task (e.g. those requirements that differentiate crawling from walking).

The non-contact external forces are all assumed to be known during the motion. Design variables are the joint angle profiles. An arbitrary motion (a set of joint angle profiles for all joint angles) of the avatar (humanoid robot) is used as an initial guess. Based on the value of design variables, the kinematic analysis of the model is carried out using the Denavit-Hartenberg method. It is assumed that the digital human has several non-adhesive contact areas with only the horizontal ground. All the forces except the ground reaction forces are known, which are the inertial, gravitational and external forces.

The possibility of generating the arbitrary motion using the given ground contact areas is ensured by using the Zero Moment Point (ZMP) constraint. When ZMP constraint is satisfied, we are sure that it is possible to find unilateral distributed contact forces on those contact areas to satisfy dynamic equilibrium equations [8]. In other words, neglecting the limitations of the digital human and the motion task, when ZMP constraint is satisfied, we are sure that it is possible to generate the arbitrary motion using the given ground contact areas if enough friction exists between these areas and their boundary with the support surface.

Based on this motion, the required external contact forces and moments that should act on each separate contact area are calculated such that dynamic equilibrium equations hold. Using these contact forces and moments, the required torques at all joints are calculated. Physical constraints such as constraints on joint angles and torques are imposed. This renders a feasible (realistic and possible) motion. Best motions are selected (motion is optimized) based on human performance measures, such as speed, energy and comfort which act as objective functions in the optimization formulation. Predicting motion in this way allows one to use avatars to study how and why humans move the way they do, given a specific scenario.

The methods to study human locomotion can be broadly divided into two categories: predictive methods and tracking methods. Predictive methods treat human motion planning as an optimization problem from which the optimal motion and forces are obtained by minimizing a performance measure subjected to physical constraints [9–15]. The advantage of predictive methods lies in their predictive capabilities, which allow novel motions to be obtained by solving an optimization problem under various conditions. However, a limitation of predictive methods is that completely natural motion is hard to obtain because the constraints and objective functions only partially represent the human neural control system [16–20].

Tracking methods are another important approach used in the literature to study human locomotion [21–25]. The benefit of tracking methods is that they use the actual

human motion and therefore are more accurate in a general sense. Tracking methods have become prominent in the literature. In the robotics field, tracking control methods are used to generate online motion synthesis for humanoid robots. In the biomechanics field, tracking methods have been used to analyze human motions and calculate muscle excitations and forces. However, there are two major drawbacks of tracking methods: (1) the approach is limited by the accuracy and amount of available experimental data; and (2) novel motions cannot be predicted.

The 'Hybrid Predictive Dynamics Method for Digital Human Modeling' is used in this work which uses the benefits of 'Tracking' a motion along with the benefits of 'Predicting' a motion. The 'Hybrid' prefix mentioned in the literature recently [1], refers to the use of motion capture data for improving human motion simulations. This use of motion capture compensates for the inherent weaknesses of purely theoretical motion prediction due to deficiencies in computational power or available theoretical backgrounds. Before the introduction of 'Hybrid' method, many tasks had been developed without any use of motion capture. However, instead of using motion capture, additional task-specific constraints had been used in those formulations in order to improve the motion simulation. Such examples can be seen in [2, 3, 4].

Drop jumps help train reactive strength, i.e., the capacity to quickly reverse downward center of mass (CoM) velocity following landing [26]. This is important in order to effectively execute many sport- and physical activity-related movement sequences. Horizontal drop jumps (HDJs) are commonly used to train reactive strength and assess lower extremity explosive power in children and adults [27, 28]. Further, there is a positive association between horizontal jumps and movements like sprinting and agility maneuvers [10, 29]. Single-leg HDJ was found to improve sprint time and ability to change direction [31]. Drop jumps generally involve braking and propulsion phases, which are characterized by the deceleration and subsequent acceleration of the CoM, respectively. The braking phase is associated with considerable lower extremity joint flexion, while the propulsion phase is associated with joint extension.

A previous study involving HDJs from a 40 cm high box reported average vertical GRFs of 2500 N and 5000 N at touchdown and takeoff, respectively [32]. The same study reported angular displacements of 10, 33, and 44 degree of flexion at the hip, knee, ankle respectively, during the flexion (braking) phase following touchdown on the force plate. They reported angular displacements of 44, 55, and 58 degree of extension at the hip, knee, ankle respectively, during the flexion (braking) phase following touchdown on the force plate.

2 Motion Capture Procedure

The participant was a male (age: 21 years; height: 180.3 cm; mass: 93.6 kg) and was one of thirteen young adults who participated in a study that investigated joint loading asymmetry during HDJ. Participants were included, if they were between the ages of 18 to 29 years. They were excluded, if they indicated any neuromuscular condition, including previous or current injuries that may affect their ability to perform drop jumps. Participants provided written informed consent prior to participating. Texas A&M University-Corpus Christi Institutional Review Board approved this study (IRB # 103-15).

Participants were asked to refrain from strenuous physical activity 36 h prior to visiting the lab for data collection. Participants wore tight-fitting exercise clothing and running shorts/exercise tights in order not to occlude the retroreflective markers that were affixed to specified landmarks. Participants' anthropometrics were measured in order to estimate their joint center locations and segmental inertia in consistence with Vicon's (Vicon, Oxford Metrics, Oxford, UK) plug-in gait full body model. Participants' height and weight were measured using a stadiometer and digital scale combination (Tanita, Tokyo, Japan).

Participants performed a general warm up by walking on a Woodway Curve non-motorized treadmill (Woodway World, Waukesha, WI) for five minutes and performed three to five HDJs from a 41 cm high box. Following warm up, participants were fitted bilaterally with 34 Retroreflective markers according to Vicon's Plug-in Gait full body model. Markers were affixed to the participants' head (front and back), shoulder, clavicle, sternum, upper arm, elbow, wrist, second metacarpophalangeal joint, anterior and posterior superior iliac spines, thigh, knee, tibia, ankle, heel, and second metatarsophalangeal joint. Joint angular displacements were captured with a 12-camera VICON motion capture system sampled at 100 Hz. An AMTI force plate (Advanced Mechanical Technology Inc., Watertown, MA) was used to acquire ground reaction forces.

We instructed participants to stand on a box (41 cm high), drop vertically onto the force plate below (without pushing or jumping off), minimize contact time on the force plate, and jump as far forward as they could upon contacting the force plate. The force plate was located 8 cm in front of the box. Participants' plane of jumping progression (forward) coincided with the anterior-posterior axis (Y-axis) of the lab coordinate, while their medial-lateral and vertical axes coincided with the X- and Z-axes of the lab's coordinates, respectively. Movement initiation was delineated as the first non-zero vertical CoM velocity. Touchdown and takeoff from the force plate were defined as the instants when vertical GRF exceeded and fell below 40 N, respectively.

Movement termination was delineated as the last zero vertical CoM velocity. A trial was deemed valid, if participants fully contacted the force plate with both feet and maintained their balance all through takeoff and eventual touchdown off the force platform. Participants were instructed to walk back and mount the drop box after executing a jump.

Raw marker data were automatically digitized and smoothed with a low pass Butterworth filter with a cut-off frequency of 6 Hz. Bilateral hip, knee and ankle joint sagittal angles and moments were calculated using the inverse dynamics method implemented within VICON's Dynamic Plug-in Gait model. Mean and standard deviation (SD) values were calculated for hip, knee and ankle joint sagittal angular displacements and moments across five trials for each condition.

3 The Digital Human Model

The digital human model is a full-body, three dimensional avatar as shown in Fig. 1. It is modeled as a 55 degree of freedom branched mechanism. Six degrees of freedom specify the global position and orientation of the coordinate frame attached to the pelvis of the digital human and 49 degree of freedom represent the revolute joints which model the human joints and determine the kinematics of the digital human.

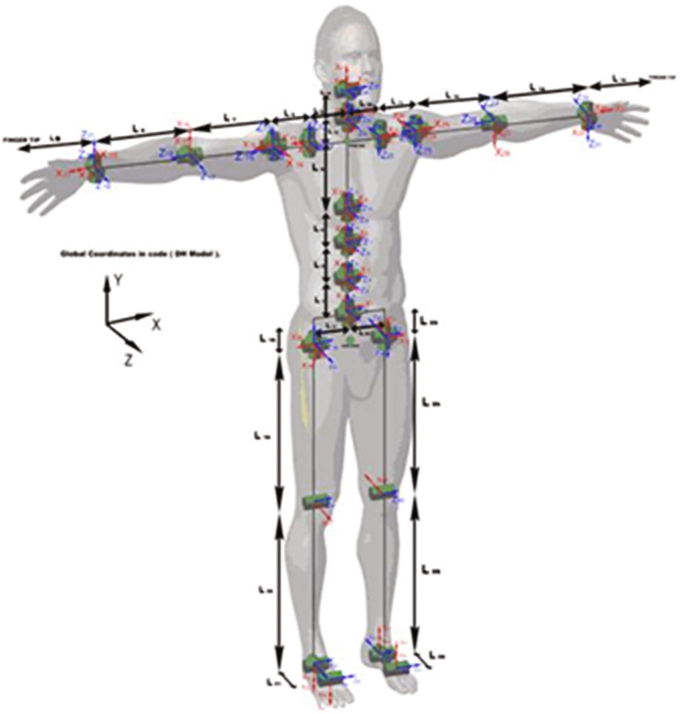

Fig. 1. The structure of the digital human avatar

4 The Kinematics of the Digital Human

Denavit and Hartenberg (1955) suggested a systematic method to formulate the kinematics of a general 3 dimensional open loop robot, now known as the D-H method. Each of the joints in the open loop robot (open loop chain) should possess only one degree of freedom (either purely revolute or purely prismatic) to be modellable by the D-H method.

We use the D-H method in predictive dynamics to address the forward kinematics calculations of our digital human model. The Denavit-Hartenberg (D-H) method was created in the 1950's to systematically represent the relation between two coordinate systems but was only extensively used in the early 1980's with the appearance of computational methods and hardware that enable the necessary calculations. The method is currently used widely in the analysis and control of robotic manipulators. The D-H method is based upon characterizing the configuration of link i with respect to link (i–1) by a (4 × 4) homogeneous transformation matrix representing each link's coordinate system. This method represents each link coordinate system in terms of the previous link coordinate system. The position of a point in any of the local coordinate frames can be expressed in global reference frame by the D-H method.

Assume that the global coordinate frame in the D-H method is numbered as coordinate frame 0. Consider a branched open-loop robot such as a digital human. Assume that point A is attached to a coordinate frame denoted respectively in the D-H table as coordinate frame number m in branch b of that open loop robot. Let the local position vector of point A in that local coordinate frame be given by $\mathbf{L_A} = (x_A \;\; y_A \;\; z_A \;\; 1)^T$. Let the global position vector of the point A be given by $\mathbf{G_A} = (X_A \;\; Y_A \;\; Z_A \;\; 1)^T$. Then, $\mathbf{L_A}$ can be related to $\mathbf{G_A}$ by the following formula:

$$\mathbf{G_A} = [X_A \quad Y_A \quad Z_A \quad 1]^T = \left[{}^{\mathbf{0}}\mathbf{T}_{\mathbf{m,b}}\right][x_A \quad y_A \quad z_A \quad 1]^T = \left[{}^{\mathbf{0}}\mathbf{T}_{\mathbf{m,b}}\right]\mathbf{L_A} \tag{1}$$

In the above formula, $\left[{}^{\mathbf{0}}\mathbf{T}_{\mathbf{m,b}}\right]$ is the 4×4 homogeneous transformation matrix from coordinate frame number m in branch b to the global coordinate frame. $\left[{}^{\mathbf{0}}\mathbf{T}_{\mathbf{m,b}}\right]$ can be calculated from the formula:

$$\left[{}^{\mathbf{0}}\mathbf{T}_{\mathbf{m,b}}\right] = \left[{}^{\mathbf{0}}\mathbf{T}_{\mathbf{1,b}}\right]\left[{}^{\mathbf{1}}\mathbf{T}_{\mathbf{2,b}}\right]\left[{}^{\mathbf{2}}\mathbf{T}_{\mathbf{3,b}}\right]\mathbf{L}\left[{}^{\mathbf{s-1}}\mathbf{T}_{\mathbf{s,b}}\right]\mathbf{L}\left[{}^{\mathbf{m-1}}\mathbf{T}_{\mathbf{m,b}}\right] \tag{2}$$

Each transformation matrix $\left[{}^{\mathbf{s-1}}\mathbf{T}_{\mathbf{s,b}}\right]$ is given by:

$$\left[{}^{\mathbf{s-1}}\mathbf{T}_{\mathbf{s,b}}\right] = \begin{pmatrix} C_{s,b} & -S_{s,b}C\alpha_{s,b} & S_{s,b}S\alpha_{s,b} & a_{s,b}C_{s,b} \\ S_{s,b} & C_{s,b}C\alpha_{s,b} & -C_{s,b}S\alpha_{s,b} & a_{s,b}S_{s,b} \\ 0 & S\alpha_{s,b} & C\alpha_{s,b} & d_{s,b} \\ 0 & 0 & 0 & 1 \end{pmatrix} \tag{3}$$

$$where: \begin{cases} S_{s,b} \equiv sin(\theta_{s,b}), & C_{s,b} \equiv cos(\theta_{s,b}) \\ S\alpha_{s,b} \equiv sin(\alpha_{s,b}), & C\alpha_{s,b} \equiv cos(\alpha_{s,b}) \end{cases}$$

The four values for the D-H parameters $\theta_{s,b}, d_{s,b}, \alpha_{s,b}, a_{s,b}$ are typically entered into a table known as the D-H Table. However, for the simplicity of notation in the rest of this section, let us assume only one branch and denote coordinate frame m in branch b by coordinate frame i. Therefore, the four parameters $\theta_i = \theta_{s,b}$, $d_i = d_{s,b}$, $\alpha_i = \alpha_{s,b}$ and $a_i = a_{s,b}$ (depicted in Fig. 2) are defined as:

(1) θ_i is the joint angle, measured from the x_{i-1} to the x_i axis about the z_{i-1}.
(2) d_i is the distance from the origin of the coordinate frame *(i-1)* to the intersection of the z_{i-1} axis with the x_i axis along z_{i-1} axis.
(3) a_i is the offset distance from the intersection of the z_{i-1} axis with the x_i axis to the origin of the frame i along x_i axis.
(4) α_i is the offset angle from z_{i-1} axis to z_i axis about the x_i axis.

Besides the global position, the global velocity and acceleration of each point attached to each local coordinate frame can be obtained by differentiating Eq. (1) with respect to time.

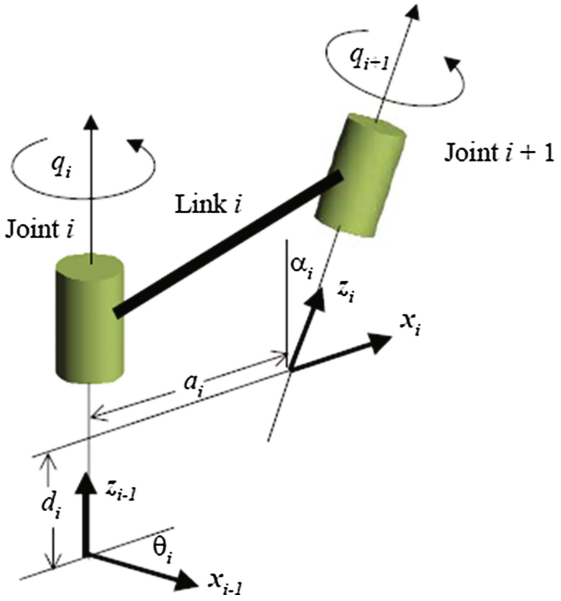

Fig. 2. Depiction of the D-H parameters

5 The Dynamics of the Digital Human

There are several methods in robotics for the calculation of torques in an open loop robot (open loop chain). For these calculations, it is always assumed that all the external forces and the mass of the links are known. In this work, calculation of torques at joints is accomplished by the Recursive Lagrangian method. It is accomplished by defining 4×4 homogeneous transformation matrix $\mathbf{D_i}$ and 4×1 homogeneous vectors $\mathbf{E_i}, \mathbf{F_i}$, and $\mathbf{G_i}$ as follows.

Given the mass and inertia properties of each link, and the external force $\mathbf{f_K^T} = \begin{bmatrix} {}^k f_x & {}^k f_y & {}^k f_z & 0 \end{bmatrix}$ and the moment $\mathbf{h_K^T} = \begin{bmatrix} {}^k h_x & {}^k h_y & {}^k h_z & 0 \end{bmatrix}$ for the link k defined in the global coordinate system, then the joint actuation torques τ_i are computed for i = n to 1 as:

$$\tau_i = tr\left[\frac{\partial \mathbf{A_i}}{\partial q_i}\mathbf{D_i}\right] - \mathbf{g}^{\mathbf{T}}\frac{\partial \mathbf{A_i}}{\partial q_i}\mathbf{E_i} - \mathbf{f_k^T}\frac{\partial \mathbf{A_i}}{\partial q_i}\mathbf{F_i} - \mathbf{G_i^T}\mathbf{A_{i-1}}\mathbf{z_0} \tag{4}$$

Where:

$$\begin{cases} \mathbf{D_i} = \mathbf{I_i}\mathbf{C_i^T} + \mathbf{T_{i-1}}\mathbf{D_{i+1}} \\ \mathbf{E_i} = m_i{}^{\mathbf{i}}\mathbf{r_i} + \mathbf{T_{i+1}}\mathbf{E_{i+1}} \\ \mathbf{F_i} = {}^{\mathbf{k}}\mathbf{r_f}\delta_{ik} + \mathbf{T_{i+1}}\mathbf{E_{i+1}} \\ \mathbf{G_i} = \mathbf{h_k}\delta_{ik} + \mathbf{G_{i+1}} \end{cases} \tag{5}$$

With $\mathbf{D_{n+1}} = \mathbf{0}$ and $\mathbf{E_{n+1}} = \mathbf{F_{n+1}} = \mathbf{G_{n+1}} = \mathbf{0}$; $\mathbf{I_i}$ is the inertia matrix for link i; m_i is the mass of link i; $\mathbf{g}$ is the gravity vector; ${}^{\mathbf{i}}\mathbf{r_i}$ is the location of center of mass of link i in the local frame i; ${}^{k}r_f$ is position of the external force in the local frame k; $\mathbf{z_0} = [0 \quad 0 \quad 1 \quad 0]^T$ for a revolute joint and $\mathbf{z_s} = [0 \quad 0 \quad 0 \quad 0]^T$ for a prismatic joint. δ_{ik} is Kronecker delta.

The first term in torque expression is the inertia and Coriolis torque, the second term denotes the torque of force due to gravity, the third term is the torque due to external force, and the fourth term represents the torque due to external moment.

6 Optimization Formulation

In order to track the motion capture data, b-spline approximating curves are used to represent the motion of each of the 55 human model joints (degrees of freedom). The b-spline control points are chosen to be the design variables of an optimization problem. The optimization problem finds the control points that minimize the error between the marker locations on the human subject in the motion capture data and the location of those points on the digital human model. This is an initial version of the optimization problem that just minimizes the below objective function:

$$f(\mathbf{q}) = \int_{t=0}^{T} \sum_{i=1}^{n_{markers}} \left((X_i(\mathbf{q}) - X_{i_{Seed}})^2 + (Y_i(\mathbf{q}) - Y_{i_{Seed}})^2 + (Z_i(\mathbf{q}) - Z_{i_{Seed}})^2 \right) dt \qquad (6)$$

In the above formula, q_k is the value of the k'th joint angle during the motion at each time t. $\mathbf{q}$ is the vector that contains the q_k values for all values of k from 1 to 55 (55 joints). The $\mathbf{q}$ vector is a function of the $\mathbf{c}$ vector which is the collection of the control points of the b-spline curves mentioned in the previous paragraph. As mentioned there, the members of the $\mathbf{c}$ vector are the actual design variables of the optimization problem. The relation between $\mathbf{q}$ and $\mathbf{c}$ depends on the time discretization strategy that can change based on each problem and is not discussed in this paper. So, for simplicity, in this paper, one can just assume that $\mathbf{q}$ are the design variables of the optimization problem.

Also, in formula (6), X_i, Y_i, Z_i are the coordinates of the marker point i on the digital human in the global reference frame during the motion at each time t. That point needs to be as close as possible to the location of the marker point i in the motion capture data (seed data) with coordinates $X_{i_{Seed}}, Y_{i_{Seed}}, Z_{i_{Seed}}$.

Based on this motion, the required external contact forces and moments that should act on the digital human model are calculated such that dynamic equilibrium equations hold. Using these contact forces and moments, the required torques at all joints are calculated using the recursive Lagrangian formula. Therefore, by simply tracking the motion, we are able to analyze the dynamics of the motion such as ground reaction forces (and therefore joint torques).

7 Initial Results for the "Horizontal Drop Jump" Task

The initial kinematics result for this simulation (tracking) is shown in Fig. 3. The anthropometry of the digital human is scaled to match as closely as possible to the motion capture human subject, so that it can replicate the motion acceptably.

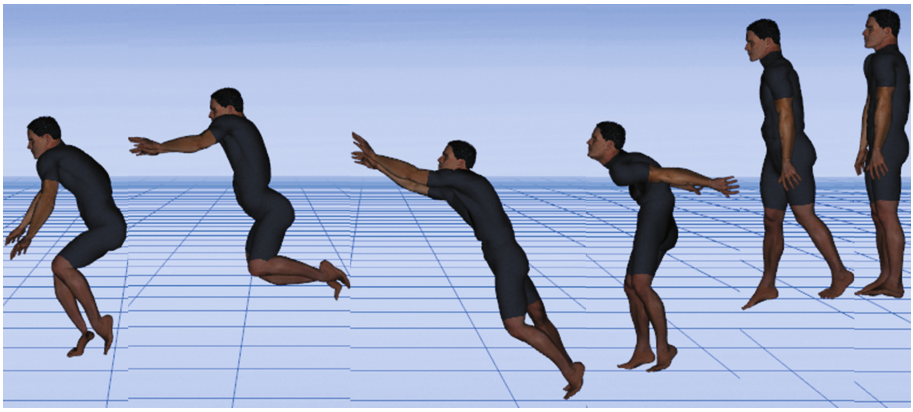

Fig. 3. Slides of drop jump motion tracking for the digital human model.

As seen in Fig. 4, the ground reaction decreases to zero while the avatar is in the air (flight phase) and reaches its maximum value just before take off. This shows a pattern of GRF that matches the measured values for a horizontal drop jump task.

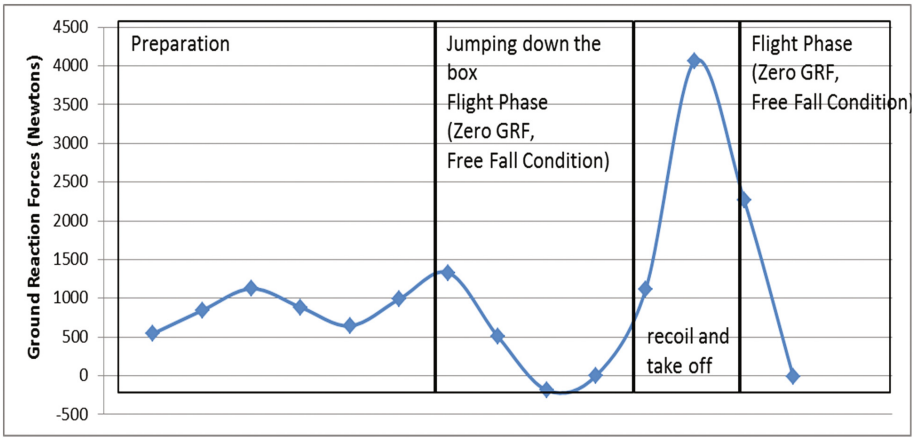

Fig. 4. Calculated history of ground reaction forces for the digital human model.

As seen in Fig. 5, the torque at the knee joint reaches its maximum value just before take off, when maximum value of GRF also occurs.

Fig. 5. Calculated history of knee torques for the digital human model.

References

1. Hariri, M.: The hybrid predictive dynamics method for analysis, simulation and prediction of human motion. In: ASME International Design Engineering Technical Conferences, vol. 6: 12th International Conference on Multibody Systems, Nonlinear Dynamics, and Control, Charlotte, North Carolina, USA, 21–24 August 2016 (2016)
2. Xiang, Y., Chung, H.J., Mathai, A., Rahmatalla, S., Kim, J., Marler, T., Beck, S., Yang, J., Arora, J.S., Abdel-Malek, K.: Optimization-based dynamic human walking prediction. In: SAE Digital Human Modeling Conference, June 2007, Seattle, WA (2007)
3. Hariri, M., Arora, J., Abdel-Malek, K.: Optimization-based prediction of aiming and kneeling military tasks performed by a soldier. In: ASME 2012 IDETC: Human Modeling and Simulation for Engineering, 12–15 August 2012, Chicago, IL, USA (2012)
4. Hariri, M., Arora, J., Abdel-Malek, K.: Optimization-based prediction of a soldier's motion: stand-prone-aim transition task. In: New Trends in Mechanism and Machine Science: Theory and Applications in Engineering, pp. 459–467 (2013)
5. Hariri, M., Xiang, Y., Chung, H.J., Bhatt, R., Arora, J., Abdel-Malek, K.: Simulation and prediction of the motion of a human in a vertical jumping task. In: ASME 2013 Dynamic Systems and Control Conference, 21–23 October 2013, Stanford University, Palo Alto, CA (2013)
6. Marler, R., Rahmatalla, S., Shanahan, M., Abdel-Malek, K.: A new discomfort function for optimization-based posture prediction. SAE Technical Paper 2005-01-2680 (2005). doi:10.4271/2005-01-2680

7. Gill, P.E., Murray, W., Saunders, M.A.: SNOPT: an SQP algorithm for large-scale constrained optimization. SIAM J. Optim. **12**, 979–1006 (2002)
8. Mahdiar, H.: A study of optimization-based predictive dynamics method for digital human modeling. Ph.D. Dissertation, The University of Iowa (2012)
9. Ackermann, M., van den Bogert, A.J.: Optimality principles for model-based prediction of human gait. J. Biomech. **43**(6), 1055–1060 (2010)
10. Bessonnet, G., Chesse, S., Sardain, P.: Optimal gait synthesis of a seven-link planar biped. Int. J. Robot. Res. **23**(10–11), 1059–1073 (2004)
11. Bessonnet, G., Seguin, P., Sardain, P.: A parametric optimization approach to walking pattern synthesis. Int. J. Robot. Res. **24**(7), 523–536 (2005)
12. Bessonnet, G., Marot, J., Seguin, P., Sardain, P.: Parametric-based dynamic synthesis of 3D-gait. Robotica **28**(4), 563–581 (2010)
13. Chevallereau, C., Aoustin, Y.: Optimal reference trajectories for walking and running of a biped robot. Robotica **19**, 557–569 (2001)
14. Davy, D.T., Audu, M.L.: A dynamic optimization technique for predicting muscle forces in the swing phase of gait. J. Biomech. **20**(2), 187–201 (1987)
15. Eriksson, A.: Optimization in target movement simulations. Comput. Methods Appl. Mech. Eng. **197**, 4207–4215 (2008)
16. Bottasso, C.L., Prilutsky, B.I., Croce, A., Imberti, E., Sartirana, S.: A numerical procedure for inferring from experimental data the optimization cost functions using a multibody model of the neuromusculoskeletal system. Multibody Syst. Dyn. **16**(2), 123–154 (2006)
17. Capi, G., Yokota, M., Mitobe, K.: Optimal multi-criteria humanoid robot gait synthesis—an evolutionary approach. Int. J. Innov. Comput. Inf. Control **2**(6), 1249–1258 (2006)
18. Leboeuf, F., Bessonnet, G., Seguin, P., Lacouture, P.: Energetic versus sthenic optimality criteria for gymnastic movement synthesis. Multibody Syst. Dyn. **16**(3), 213–236 (2006)
19. Marshall, R.N., Wood, G.A., Jennings, L.S.: Performance objectives in human movement: a review and application to the stance phase of normal walking. Hum. Mov. Sci. **8**(6), 571–594 (1989)
20. Vaughan, C.L.: Theories of bipedal walking: an odyssey. J. Biomech. **36**(4), 513–523 (2003)
21. Delp, S.L., Loan, J.P.: A computational framework for simulating and analysing human and animal movement. Comput. Sci. Eng. **2**(5), 46–55 (2000)
22. Fregly, B.J., Reinbolt, J.A., Rooney, K.L., Mitchell, K.H., Chmielewski, T.L.: Design of patient-specific gait modifications for knee osteoarthritis rehabilitation. IEEE Trans. Biomed. Eng. **54**(9), 1687–1695 (2007)
23. Lin, Y.C., Walter, J.P., Banks, S.A., Pandy, M.G., Fregly, B.J.: Simultaneous prediction of muscle and contact forces in the knee during gait. J. Biomech. **43**(5), 945–952 (2010)
24. Mahboobin, A., Cham, R., Piazza, S.J.: The impact of a systematic reduction in shoe-floor friction on heel contact walking kinematics-a gait simulation approach. J. Biomech. **43**(8), 1532–1539 (2010)
25. Thelen, D.G., Anderson, F.C.: Using computed muscle control to generate forward dynamic simulations of human walking from experimental data. J. Biomech. **39**(6), 1107–1115 (2006)
26. Bobbert, M.F., Huijing, P.A., van Ingen Schenau, G.J.: Drop jumping. II. The influence of dropping height on the biomechanics of drop jumping. Med. Sci. Sports Exerc. **19**, 339–346 (1987)
27. Lazaridis, S., Bassa, E., Patikas, D., Giakas, G., Gollhofer, A., Kotzamanidis, C.: Neuromuscular differences between prepubescents boys and adult men during drop jump. Eur. J. Appl. Physiol. **110**, 67–74 (2010)

28. Bassa, E.I., Patikas, D.A., Panagiotidou, A.I., Papadopoulou, S.D., Pylianidis, T.C., Kotzamanidis, C.M.: The effect of dropping height on jumping performance in trained and untrained prepubertal boys and girls. J. Strength Cond. Res. **26**, 2258–2264 (2012)
29. Holm, D.J., Stalbom, M., Keogh, J.W., Cronin, J.: Relationship between the kinetics and kinematics of a unilateral horizontal drop jump to sprint performance. J. Strength Cond. Res. **22**, 1589–1596 (2008)
30. Hunter, J.P., Marshall, R.N., McNair, P.J.: Relationships between ground reaction force impulse and kinematics of sprint-running acceleration. J. Appl. Biomech. **21**, 31–43 (2005)
31. Antonio, D.I., Martone, D., Milic, M., Johnny, P.: Vertical- vs. horizontal-oriented drop-jump training: chronic effects on explosive performances of elite handball players. J. Strength Cond. Res. (2016)
32. Kovacs, I., Tihanyi, J., Devita, P., Racz, L., Barrier, J., Hortobagyi, T.: Foot placement modifies kinematics and kinetics during drop jumping. Med. Sci. Sports Exerc. **31**, 708–716 (1999)

Concept of Formalized Test Procedure for Proactive Assessment of Ergonomic Value by Digital Human Modelling Tools in Lean Product Development

Dan Högberg[1(✉)], Erik Brolin[1], and Lars Hanson[1,2]

[1] School of Engineering Science, University of Skövde, 541 28 Skövde, Sweden
{dan.hogberg, erik.brolin, lars.hanson}@his.se
[2] Industrial Development, Scania CV, 151 87 Södertälje, Sweden

Abstract. A concept of a formalized test procedure for proactive assessment of ergonomic value by digital human modelling (DHM) tools in lean product development (LPD) is proposed and described. The objective of the formalized procedure is to integrate the utilization of DHM tools in LPD and to support the delivery of ergonomic value and reduce waste in product and production development processes. A design process model is illustrated and described, and examples are given of how to specify and work with ergonomic value in the process.

Keywords: Digital human modelling (DHM) · Ergonomics · Lean product development (LPD) · Design · Process · Assessment · Formalized · Test procedure

1 Introduction

In contemporary product development processes (PDP), design is typically performed by the assistance of digitalization tools, where products, vehicles, workstations or systems are designed in virtual worlds using computer aided design and engineering (CAD/CAE) tools. In line with this, digital human modelling (DHM) tools have been developed to assist designers to consider ergonomics and human factors in virtual design processes [1–3]. A trend when using digital human modelling (DHM) tools for ergonomic design is to simulate sequences of the human-system interaction rather than a few static instances [2, 4–6]. This is rational since it can enable the simulated interaction to better represent the nature of the real interaction, and hence increases the chance that simulation outcomes provide the DHM tool user with reliable decision support in relation to the quality of the proposed design. Simulating sequences of tasks requires the DHM tool to be able to predict motions of the digital manikin that resemble how a real human is likely to move while performing the tasks [6–8]. The DHM tool also needs to be able to predict motions for how humans of different characteristics are likely to move while performing the tasks, e.g. variety related to body size, strength or range-of-motion [9]. Another important feature of DHM tools when simulating sequences is to enable the DHM tool user to instruct the digital

D.N. Cassenti (ed.), *Advances in Human Factors in Simulation and Modeling*,
Advances in Intelligent Systems and Computing 591, DOI 10.1007/978-3-319-60591-3_38

manikin of what tasks to perform in the virtual environment [6, 10]. A DHM tool to be used in this context also needs to have ergonomics evaluation functionality, able to assess task sequences, to give feedback to the tool user about the quality of the design in relation to set ergonomic constraints and targets. An example of an evaluation method that offers an aggregated assessment of ergonomic load over time, related to working postures and movements, action forces, manual materials handling and repetitive loads of the upper limbs, is the EAWS (ergonomic assessment worksheet) method [2].

Another, but associated, perspective on contemporary product development processes (PDP) is that these processes often follow the philosophies and principles of lean product development (LPD) [11]. Central in modern ways to carry out product development is the focus on '*Do the right thing*' and '*Do the thing right*'. The 'Do the right thing' aspect has the concept of delivering *value* to all stakeholders as the central objective. The 'Do the thing right' aspect focuses on having *efficient processes*, with efficient tools and methods, which assist in creating value while reducing waste, i.e. reduce or remove activities that add no or little value. In addition to this, LPD highlights the importance of '*Continuous improvements'*, where the organization continuously strives to learn and improve the PDP in respect to efficiency and improved understanding of how to deliver value [11].

The concept to focus on *value* in LPD is rational since the expected outcome of a PDP, i.e. the 'product' (physical product or service or a mixture of these), is that the product shall meet or surpass humans' (in their roles as users, customers or stakeholders) expectations. This as a way for the company to please their customers, and a way to render profit, strengthen the brand and increase opportunities for future business. Still, the concept of value is vague and subjective since it lies in the senses of the individual human to perceive and assess, consciously or unconsciously.

A common theme in DHM and LPD is hence the focus on *human*. Another common theme is *product development*, where *product* here may represent anything that physically interacts with humans, e.g. a consumer product, a chair, a vehicle, a workstation etc., together representing a *system*. Based on these commonalities and shared objectives, this paper aims to discuss and suggest an approach for how digital human modelling (DHM) tools can contribute to the overall objective of lean product development (LPD) to deliver value and reduce waste, and do this within an efficient product development process (PDP).

2 Method

By studying the general philosophies and principles of LPD, and reflecting over these in the perspective of DHM tools for ergonomic design, potential contributions from the utilization of DHM tools in LPD are recognized. To supplement the perspective, also the adjacent areas ergonomics and general engineering design methodology are studied and referred to. Based on the findings, a conceptual procedure for how to integrate the utilization of DHM tools in LPD to support the delivery of ergonomic value and reduce waste is proposed and described.

3 Results

Fundamental in LDP is to increase *value* while decreasing *waste* ('muda'), *overburden* ('muri') and *unevenness* ('mura') [11]. In the following section, these targets are discussed in the perspective of DHM tools for ergonomic design.

3.1 LPD in the Perspective of DHM

The aim of using DHM for ergonomic design corresponds with the overall objective of the area of ergonomics, i.e. '*…to optimize human well-being and overall system performance*', which is from the definition of ergonomics by the International Ergonomics Association (IEA) [12]. Interpreting this in the eyes of value, the value that is aimed to be created by the means of DHM (and ergonomics) is optimized human well-being and system performance. *Human* here typically refers to the user or operator that uses (interacts with) a *system,* (which can be represented by a tool, product, vehicle, workstation, robot etc., in a context where *human* is seen as one system component) in order to achieve some sort of task. In LPD, value for a given stakeholder can be expressed as '*the total and balanced perception, resulting from all the various benefits delivered through the product lifecycle*' [11]. The interpretation of value in LPD is considered to be wider than in DHM/ergonomics since it has a wider stakeholder perspective, e.g. also comprising value for stakeholders such as shareholders, dealers and suppliers [11]. However, central in successful PDP is that the product satisfies end-user needs. Hence, it is argued that DHM (and ergonomics) can contribute to create value in LPD since proper consideration of user needs, characteristics and limitations within the PDP is needed to deliver genuine value to end-users. This complies with the findings in [13] where it is argued that the area of human factors engineering (HFE), i.e. the engineering application of the field of ergonomics and human factors, can make substantial contribution in LPD.

The main contribution of DHM is in virtual stages of the PDP where there is no physical product to be tested by real people. Contemporary DHM tools can primarily assist engineers to consider quantifiable and less subjective aspects, e.g. concerns like fit, reach, field of vision, biomechanical load and assumed level of comfort, belonging to the area of physical ergonomics [12]. Naturally there are many more perspectives than those, even within the area of ergonomics, to create value in the PDP but still, failing to thoroughly consider such fundamental user requirements, for a variety of user characteristics, e.g. related to anthropometric diversity, would risk the ambition to deliver excellent value to end-users.

From a waste ('muda') perspective DHM tools can assist in reducing the risk for the greatest waste, i.e. that the result of the PDP is a product that no, or just few users, wants since it is perceived to offer low or no value. Examples would be the design of tools or workstations that leads to discomfort or work-related musculoskeletal disorders (WMSDs), or a vehicle that only accommodates and offers comfort to a fraction of the targeted population. Such scenarios would represent the most wasteful type of iteration in the PDP, i.e. that the PDP is needed to be started all over again. Even though iterations typically are needed in the PDP in order to find best product solutions, and

indeed is a way to enhance knowledge, iteration loops are preferably to be kept 'small' [14]. And, to further reduce waste, iterations are preferably 'front loaded', i.e. performed at early conceptual or embodiment stages of the PDP where changes are less costly and simpler to carry out, especially when the design is done in virtual worlds. Still, decisions and definitions in all phases of the PDP are to be based on a higher degree of knowledge than is often the situation in current PDP [11]. DHM tools enable a more knowledge-based approach towards making design decision related to physical ergonomics issues in the PDP, and can hence act as means to reduce waste by preventing or reducing large time-consuming and expensive iterations and assist in ensuring final product value.

One perspective of DHM in relation to overburden ('muri') is the efficiency of the DHM tools, and the integration of DHM tool usage within the PDP and the compatibility with other engineering tools. DHM tools ought to be acknowledged as one of the common engineering tools to be used when physical ergonomics issues are to be dealt with in the PDP. For that, DHM tools must be easy and efficient to use by any engineer that needs to consider issues of physical ergonomics in the PDP, i.e. to support his or her task to balance ergonomic requirements towards other product requirements in order to identify the design solutions that creates the greatest value. The complexity to model and simulate the physics of humans and the interaction with the surrounding system is a large undertaking for DHM tools developers. This has led to a situation where most efforts in DHM tool development has concentrated on advancing software functionality. However, further development of DHM tool usability and compatibility with the PDP and other engineering tools is also claimed to be required to reach a stage where engineers can get the desired level of efficiency and effectiveness from using DHM tools in the PDP. Examples of steps towards this objective is an approach to integrate DHM tool usage in the general PDP [15], and the development of a module in a DHM tool that assists engineers to efficiently and effectively consider the complexity of anthropometric diversity in the PDP [16]. Another perspective on overburden, and more from the 'Do the right thing' perspective, is the fact that a central feature of ergonomics is to support the design of sustainable human-system interactions. For example, ergonomic knowledge can be applied to ensure that products and associated use tasks are designed and performed without risk for overburden. Hence, DHM tools used for ergonomic design can assist in preventing overburden of the human, and also of the system that the human interacts within.

The third target to reduce in LPD is unevenness ('mura'). In the perspective of DHM this could refer to having stable processes for how to utilize DHM tools as means to assist delivery of value in the PDP. This calls for procedures for how to specify and handle value delivered by ergonomics in the PDP, and procedures for how to utilize DHM tools to evaluate whether set objectives are met or not by generated design proposals. A stable process of using a DHM tool would lead to similar results regardless who is using the tool or when, and also give comparable results when evaluating different design proposals. This put demands on the DHM tool functionality itself, e.g. related to the repeatability of simulation results, but also on the procedures of utilizing the tools in the PDP.

Next section builds on the identified connections between LPD and DHM, and suggests a concept of a formalized test procedure for proactive assessment of ergonomic value by digital human modelling tools in lean product development.

3.2 Concept for a Formalized Test Procedure Using DHM

Based on the identified general philosophies and principles of LPD in the perspective of DHM (Sect. 3.1) and general engineering design methodology [17, 18], Fig. 1 illustrates major steps and process flow of a suggested procedure of how to utilize DHM tools in the PDP. The prominent arguments to suggest a formalized test procedure, which guides the engineer through actions of specification and evaluation, is to have stable processes ('mura') for how to proactively advocate and secure ergonomic value of the final product by the assistance of DHM tools. The procedure is also aimed to reduce waste and overburden by promoting formalized actions of the use of DHM in the PDP, where those actions are associated to the delivery of ergonomic value.

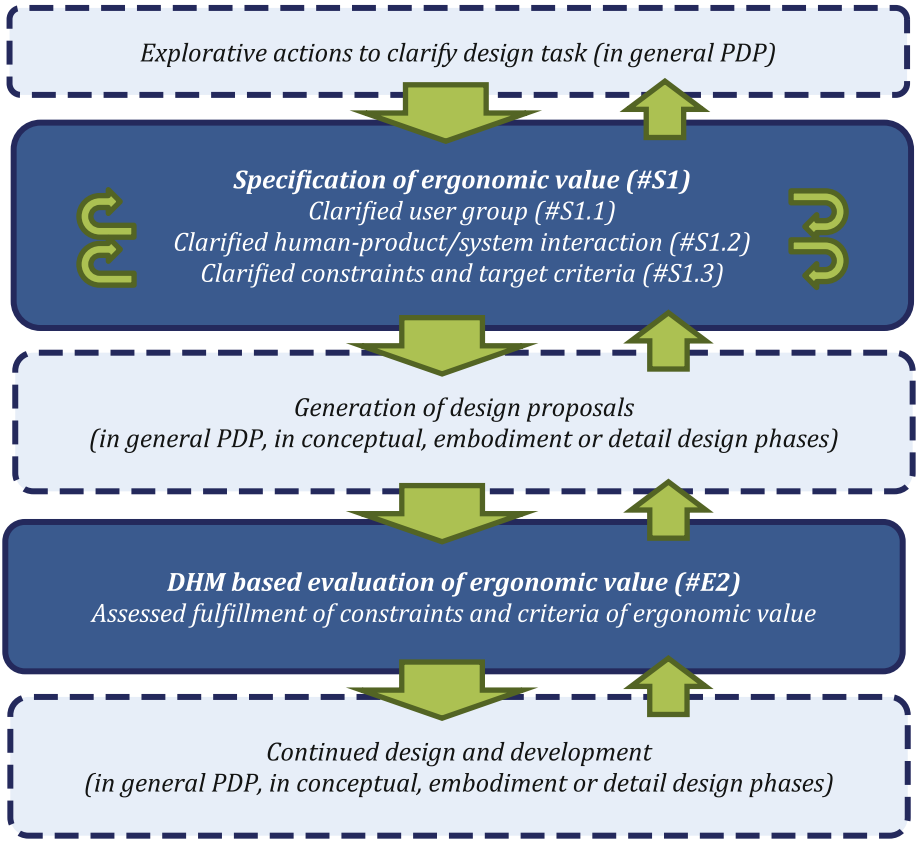

Fig. 1. Major steps and process flow of procedure for utilization of DHM tools in the PDP. Activities in dashed boxes are typically performed within the general PDP in conceptual, embodiment or detail design phases.

Specification. An essential early activity in the PDP is to specify ergonomic value for the product development project at hand (#S1 in Fig. 1), and to do this as clear as possible in relation to the knowledge of the problem space. To state a requirement as 'the product should be ergonomic' would not assist the engineer much, and it would be impossible to know if or when the requirement is fulfilled or not. Hence the requirements need to be specified in a way that is supportive and meaningful to the engineer. This can for example be done by the assistance of 'Objective Trees' to clarify queries like 'what is actually meant by that' [17]. Other engineering design methods that can assist the interpretation of vague statements and express them in a manner that is meaningful for the engineer is QFD (Quality Function Deployment) [17] or VFD (Value Function Deployment) [11].

A first important step for being able to deliver ergonomic value is to understand who the receiver of the value is, i.e. to clarify the stakeholders that are to perceive the product as appropriate or superior when it comes to aspects of ergonomics (#S1.1 in Fig. 1). In the context of ergonomics, these are typically the end-users of the product, but may also include internal and external stakeholders [11]. It is often needed to specify what percentage of the targeted stakeholders (a.k.a. target population) that is to be considered in the design process, where this percentage often is referred to as the 'level of accommodation'. Even though the strive to keep the accommodation level as high as possible is a justifiable ambition in the PDP, following the principles of inclusive design [19], there is often a need to reduce the level of accommodation, e.g. to 95%, due to economic or other constraining aspects in the PDP. Worth noticing however is that the objective to meet set accommodation levels is a complex area due to the multivariability commonly involved. This area, in the context of anthropometric diversity, is elaborated upon in [20–23].

In a DHM context it is often practical to think of the manikins in the DHM tools as virtual test persons. This leads to the question of how to establish the virtual test group in the best way. One approach would be to use standard collections of manikins, e.g. established within a company. Another approach would be to assemble a bespoke test group for the design task at hand. The standardized test group approach, possibly adapted according to on what markets the product are to be sold, would follow the 'mura' approach (stable processes), but may lose in precision compared to the approach to create unique test groups for new design tasks. Regardless of approach chosen, [16] describes a module in a DHM tool developed to ease the definition of virtual test manikins, also known as 'manikin families'.

In addition to know who the users are, it is also imperative to have a good understanding of the expected interaction between the user and the product or system being designed, e.g. the tasks that users will perform on or with the product (#S1.2 in Fig. 1). In [24] it is said that '*every good project starts with a task analysis and ends with a user trial*'. A common method to systematically define tasks is hierarchical task analysis (HTA) [25]. In a DHM context it can be practical to think of tasks as the actions that the virtual test manikins are to perform within the virtual world in the DHM tool in order to assess the suggested design from an ergonomics perspective. Analogous to defining the user group, this leads to the question how to establish the task definitions in the best way. One approach would be to use standard definitions of tasks that are critical for ensuring the ergonomic value. For incremental design, where the

product design gradually is developed, it is believed that such standardized task definitions could work well, especially if described in a functional manner (verb + noun), e.g. 'reach seat adjustment controls'. The standardized task descriptions could also be more encompassing, such as 'drive the predefined virtual test route'. Such formalized test procedures of what the virtual test group are to perform in the virtual world when interacting with the suggested product design could for example be established within a company, e.g. per product type. The test procedures would offer a formalized manner to assess design proposals and products, where assessment results can be compared to each other, and would follow a 'mura' approach (stable processes). However, for new or innovative design, unique task definitions may be needed since the interaction patterns would be less known beforehand.

When users and user tasks are clarified, the desired product characteristics or performances, that are to be offered by a successful design solution from an ergonomics perspective, are preferably expressed as constraints ('demands') and target criteria ('aims') (#S1.3 in Fig. 1) [17]. Constraints clarifies the performance that the product must fulfil, expressed in a way so that they can be assessed for fulfillment or not by different design alternatives, e.g. as quantitative limits. Target criteria clarifies the performance aims, expressed in a manner so that they can be used to qualitatively compare different design alternatives in order to recognize better or worse solutions. Target criteria may be ranked for order of importance. Constraints are however not ranked due to the nature of the requirement, i.e. constraints are used to limit the solution space but not for identifying better or worse solutions within the solution space. It is imperative to thoughtfully carry out this specification step since the constraints and target criteria act as control functions in the remaining steps of the PDP. This is particularly important when following a set-based concurrent engineering (SBCE) approach [11], where design solutions are rejected when they fail to fulfill set constraints only, but otherwise are kept in the collection of potential design solutions. This as an approach to find best solutions, endorse opportunities for innovation while reducing risks, but also as a way to encourage continuous knowledge development and learning in the PDP.

As seen in Fig. 1, iterations of the specification activities #S1.1, #S1.2 and #S1.3 are most likely to be needed since they influence each other. In addition to clarify the constraint or target, each specification is to include a description of the method for controlling fulfilment of the constraint or target. In a DHM context, this could for example be to use the DHM tool to make sure that *each member of the virtual test group can reach the seat adjustment controls without larger postural changes from the preferred seated posture*. Such a control method description would however not be fully objective since it contains the word 'without larger', even though the DHM tool may have a prediction functionality to suggest the preferred seated posture. This highlights the complexity to considerer ergonomic value objectively since it is often subjective and individual, where 'larger' could mean something for one user but something else for another user. Still ergonomics needs to be considered in the PDP, in a way that is compatible with contemporary ways of working in PDP. In this example, the wording 'without larger' is added since some postural changes from preferred seating posture is assumed to be accepted by users and would hence expand the solution space, but these postural changes are only accepted up to a certain degree, and

this degree may vary among users. This would be a case where the continuous learning of LPD comes into play. Tests of opinions with real people of which postural movements that would be acceptable or not would help to build general knowledge of ergonomic value, which then is to be documented, shared and learned from. The gained knowledge is preferably fed back into the DHM tool so that future virtual user tests can be performed with enhanced precision, speed and confidence.

Tables 1 and 2 show imaginary examples of extracts from specifications lists to clarify demanded or desired performance of ergonomic value. Table 1 relates to production development and the context of workstation design. Here the work staff (i.e. user group) is pre-specified, typical tasks to be performed at the workstation are pre-specified (i.e. user-product interaction) and the method of assessment is selected as the ergonomics evaluation method RULA (rapid upper limb assessment) [26].

Table 1. Example extract of specification of ergonomic value in workstation design.

Category	Item #	Description	Constraint	Target	Unit	Test method	Source	Date of change	Comment
User group	U.1	Work population, UD1.4					Study 2.2	2016-10-03	Plant X, final assembly
User tasks	T.1	Work tasks, TD3.1					Study 7.1	2017-01-23	General manual assembly tasks at desk
Biomechanical loads	1.1	Assessment of biomechanical loads on user group UD1.4 while doing tasks TD3.1	Max RULA score 4 for 90% of UD1.4 for tasks TD3.1	Max RULA score 2 for 95% of UD1.4 for tasks TD3.1	RULA scores	RULA with UD1.4 and TD3.1	RULA test specification document X13	2017-03-06	Results stored in SAVESYST as item AD.54

Similarly, Table 2 relates to product development and the context of vehicle interior design. Here the targeted market is known, represented by a pre-defined virtual test group, the tasks to be assessed are pre-defined (in the form of a 'formalized virtual test driving routine') and the method of assessment is according to company specific ergonomic assessment criteria.

Table 2. Example extract of specification of ergonomic value in vehicle interior design.

Category	Item #	Description	Constraint	Target	Unit	Test method	Source	Date of change	Comment
User group	U.1	Occupant population, UD4.2					Study 6.2	2016-11-08	Asian market, Drivers
User tasks	T.1	Driving tasks, TD2.6					Study 1.9	2017-02-11	Driving test routine 2.8
Driver ergonomics	1.1	Assessment of driver ergonomics for user group UD4.2 for tasks TD2.6	Green Ergo score for 90% of UD4.2 for tasks TD2.6	Green Ergo score for 97% of UD4.2 for tasks TD2.6	Ergo scores	Method XX with UD4.2 and TD2.6	Method XX test specification document V5A	2017-03-04	Results stored in XX-PLM as item AKDH.6

Evaluation. After the specifications are established, the next step in the general PDP is to develop design proposals that have the potential to fulfill constraints and meet targets to high degree. As shown in Fig. 1, iterations between the specification and the design generation activity are common, e.g. to add, complement and modify specifications according to gained understanding of the problem and solution space in the PDP. This is due to the nature of design where the problem space ('what the problem really is') and the solution space ('what may an appropriate solution be like') are complementing each other, and often are investigated side-by-side [17]. The modification of the specifications is to benefit the current project, but also to enhance knowledge and continuously improve the way product development is carried out.

Iterations are also common between the design generation and evaluation activities. Also in this case there are double objectives, i.e. both to benefit the current project but also for continuous learning and advancements in product development. DHM based evaluation of ergonomic value (#E2 in Fig. 1) is the activity to use DHM tools to assess fulfillment of constraints and criteria of ergonomic value as specified earlier in the PDP (#S1 in Fig. 1). Hence, for the case described in Table 1, the DHM tool is used to evaluate generated workstation design proposals. This by using functionalities in the DHM tool to create the virtual test group, to instruct the manikins to perform the pre-defined tasks and to use the ergonomics evaluation method RULA to assess whether constraints are fulfilled and to what degree targets are met.

For the case described in Table 2, the DHM tool is used to evaluate design proposals of vehicle interiors (total solutions or sub-solutions). This by using functionalities in the DHM tool to create the virtual test group, to instruct the manikins to perform the pre-defined driving test routine and use the company specific vehicle ergonomics evaluation method 'XX' to assess whether constraints are fulfilled and to what degree targets are met.

The evaluation results are then fed back into the general PDP to possibly lead to the removal, modification or combination of design proposals, as well as to promote continuous improvements and learning in the PDP. Design concepts that fulfill constraints are kept within the 'set of potential solutions', according to the principles of SBCE.

4 Discussion

Key features of the suggested procedure are the establishment and utilization of *predefined virtual test groups* and *predefined test tasks*. Another key feature is the emphasis on specifying ergonomic value in the form of *constraints* and *target criteria*, and a *predetermined test method* to evaluate design proposals. This is to achieve an efficient and consistent ergonomics assessment procedure when using DHM tools in virtual phases of the PDP, in accordance to the principles of LPD and especially the 'mura' target (stable processes). This would support judging and comparing design solutions, and supposedly speed up DHM based ergonomics assessments and make the assessments less subjective.

DHM tools enable the performance of virtual user trails, having digital manikins performing tasks in the virtual world. Such virtual user trails are not the only type of

user trials to be used in the PDP. Having real people interacting with real products, performing real tasks in a real context would in most cases be the preferred method, but with the obvious drawback that such tests are impossible to carry out if the product design only exists in a virtual world. However, DHM tools can contribute to increased ergonomic value by giving early feedback to the engineer about physical ergonomics issues, and reduce the risk that large and late design changes are needed. For some issues like anthropometric fit, reach, biomechanical load and visual field the DHM tools can contribute with high precision in the PDP. For other issues like usability, cognitive ergonomics and user experience, common DHM tools are of less value, even though research and development in such areas are carried out [3, 27]. A more readily achievable approach would be to apply the design method personas [17, 28, 29] to the digital human models, transforming the anonymous manikins into characters that represent particular attributes, typically created with input from market research data. Such an approach, which may be called DHM personas, are discussed and exemplified in [30, 31]. In essence, such DHM personas could be the means to inform, support and inspire designers to consider a wider range of ergonomic aspects when making decisions in the PDP. This applies especially for the kind of aspects that are harder to quantify and simulate, such as those related to cognition and user experience. For such issues the DHM tool would have less precision compared to the ability to simulate issues like fit, reach and biomechanics. The tool would rather act as a checklist and screening tool, but still assist engineers in the PDP to consider and discuss additional issues related to ergonomic value.

Acknowledgments. This work has been made possible with the support from VINNOVA (projects: *3D-SILVER* and *Virtual Verification of Human-Robot Collaboration*), and The Knowledge Foundation and the associated INFINIT research environment at the University of Skövde (projects: *Virtual Driver Ergonomics* and *VEAP*) in Sweden, and by the participating organizations. This support is gratefully acknowledged.

References

1. Duffy, V.G.: Handbook of Digital Human Modeling. Taylor & Francis Group, Boca Raton (2009)
2. Schaub, K.G., Mühlstedt, J., llmann, B., Bauer, S., Fritzsche, L., Wagner, T., Bullinger-Hoffmann, A.C., Ralph Bruder, R.: Ergonomic assessment of automotive assembly tasks with digital human modelling and the 'ergonomics assessment worksheet' (EAWS). Int. J. Hum. Factors Model. Simul. **3**(3-4), 398–426 (2012)
3. Alexander, T., Paul, G.: Ergonomic DHM systems - limitations and trends – a systematic literature review focused on the 'future of ergonomics'. In: 3rd International Digital Human Modeling Symposium, Tokyo (2014)
4. Chaffin, D.B.: Improving digital human modelling for proactive ergonomics in design. Ergonomics **48**(5), 478–491 (2005)
5. Keyvani, A., Lämkull, D., Bolmsjö, G., Örtengren, R.: Using methods-time measurement to connect digital humans and motion databases. In: Lecture Notes in Computer Science, vol. 8026 (Part 2), pp. 343–352 (2013)

6. Högberg, D., Hanson, L., Bohlin, R., Carlson, J.S.: Creating and shaping the DHM tool IMMA for ergonomic product and production design. Int. J. Dig. Hum. **1**(2), 132–152 (2016)
7. Bohlin, R., Delfs, N., Hanson L., Högberg, D., Carlson, J.S.: Automatic creation of virtual manikin motions maximizing comfort in manual assembly processes. In: Hu, S.J. (ed.): Proceedings of the 4th CIRP Conference on Assembly Technologies and Systems, USA, pp. 209–212 (2012)
8. Delfs, N., Bohlin, R., Hanson, L., Högberg, D., Carlson, J.S.: Introducing stability of forces to the automatic creation of digital human postures. In: Proceedings of DHM 2013, Second International Digital Human Modeling Symposium, USA (2013)
9. Brolin, E., Högberg, D., Hanson, L., Örtengren, R.: Generation and evaluation of distributed cases by clustering of diverse anthropometric data. Int. J. Hum. Factors Model. Simul. **5**(3), 210–229 (2016)
10. Mårdberg, P., Carlson, J.S., Bohlin, R., Delfs, N., Gustafsson, S., Högberg, D., Hanson, L.: Using a formal high-level language and automated manikin to automatically generate assembly instructions. Int. J. Hum. Factors Model. Simul. **4**(3/4), 233–249 (2014)
11. Pessôa, M.V.P., Trabasso, L.G.: Lean Product Design and Development Journey: A Practical View. Springer, Berlin (2016)
12. International Ergonomics Association. http://www.iea.cc
13. Institoris, M., Bligård, L-O.: Human factors engineering as a supportive tool for lean product development. In: Proceedings of 10th Biannual NordDesign Conference, NordDesign 2014, Espoo, pp. 346–355 (2014)
14. Högberg, D.: Digital human modelling for user-centred vehicle design and anthropometric analysis. Int. J. Veh. Des. **51**(3/4), 306–323 (2009)
15. Hanson, L., Blomé, M., Dukic, T., Högberg, D.: Guide and documentation system to support digital human modeling applications. Int. J. Ind. Ergon. **36**(1), 17–24 (2006)
16. Brolin, E., Högberg, D., Hanson, L.: Design of a digital human modelling module for consideration of anthropometric diversity. In: Duffy, V.G. (ed.) Advances in Applied Digital Human Modeling, pp. 114–120 (2014). AHFE Conference
17. Cross, N.: Engineering Design Methods: Strategies for Product Design, 4th edn. Wiley, Chichester (2008)
18. Pahl, G., Beitz, W., Feldhusen, J., Grote, K.-H.: Engineering Design: A Systematic Approach, 3rd edn. Springer, London (2006)
19. Waller, S., Bradley, M., Hosking, I., Clarkson, P.J.: Making the case for inclusive design. Appl. Ergon. **46**, 297–303 (2015)
20. HFES 300 Committee: Guidelines for using anthropometric data in product design. Human Factors and Ergonomics Society, Santa Monica (2004)
21. Robinette, K.M.: Anthropometry for product design. In: Salvendy, G. (ed.) Handbook of Human Factors and Ergonomics, 4th edn, pp. 330–346. Wiley, Hoboken (2012)
22. Brolin, E., Högberg, D., Hanson, L.: Description of boundary case methodology for anthropometric diversity consideration. Int. J. Hum. Factors Model. Simul. **3**(2), 204–223 (2012)
23. Högberg, D., Brolin, E., Hanson, L.: Accommodation levels for ellipsoid versus cuboid defined boundary cases. Procedia Manuf. **3**, 3702–3708 (2015)
24. Pheasant, S., Haslegrave, C.M.: Bodyspace: Anthropometry, Ergonomics and the Design of Work, 3rd edn. Taylor & Francis, Boca Raton (2006)
25. Stanton, N.A.: Hierarchical task analysis: developments, applications, and extensions. Appl. Ergon. **37**(1), 55–79 (2006)
26. McAtamney, L., Corlett, E.N.: RULA: a survey method for the investigation of work-related upper limb disorders. Appl. Ergon. **24**(2), 91–99 (1993)

27. Thorvald, P., Högberg, D., Case, K.: Applying cognitive science to digital human modelling for user centred design. Int. J. Hum. Factors Model. Simul. **3**(1), 90–106 (2012)
28. Buur, J., Nielsen, P.: Design for usability – adopting human computer interaction methods for the design of mechanical products. In: Proceedings of 10th International Conference on Engineering Design, Praha, pp. 952–957 (1995)
29. Pruitt, J., Grudin, J.: Personas: practice and theory. In: Conference on Designing for User Experiences, San Francisco, pp. 1–15. ACM Press, New York (2003)
30. Högberg, D., Case, K.: Manikin characters: user characters in human computer modelling. In: Bust, P.D. (ed.) Contemporary Ergonomics, pp. 499–503. Taylor & Francis, Boca Raton (2006)
31. Högberg, D., Lundström, D., Hanson, L., Wårell, M.: Increasing functionality of DHM software by industry specific program features. SAE Technical Paper 2009-01-2288 (2009)

Full Body Statistical Shape Modeling with Posture Normalization

Femke Danckaers[1(✉)], Toon Huysmans[1], Ann Hallemans[2,4], Guido De Bruyne[3], Steven Truijen[2,4], and Jan Sijbers[1]

[1] imec - Vision Lab, Department of Physics, Faculty of Sciences, University of Antwerp, Antwerp, Belgium
{Femke.Danckaers, Toon.Huysmans, Jan.Sijbers}@uantwerpen.be
[2] Multidisciplinary Motor Centre Antwerp, University of Antwerp, Antwerp, Belgium
{Ann.Hallemans, Steven.Truijen}@uantwerpen.be
[3] Department of Product Development, Faculty of Design Sciences, University of Antwerp, Antwerp, Belgium
Guido.DeBruyne@uantwerpen.be
[4] Department of Rehabilitation Sciences and Physiotherapy, Faculty of Medicine and Health Sciences, University of Antwerp, Antwerp, Belgium

Abstract. Realistic virtual mannequins, that represent body shapes that occur in the target population, are valuable tools for product developers who design near-body products. Statistical shape modeling is a promising approach to map out the variability of body shapes. The strength of statistical shape models (SSM) is their ability to capture most of the shape variation with only a few shape modes. Unfortunately, the shape variation captured by SSMs of human bodies is often polluted by variations in posture, which substantially reduces the compactness of those models. In this paper, we propose a fast and data driven framework to build a posture invariant SSM. The normalized SSM is shown to be substantially more compact than the non-normalized SSM. Using five shape modes, the normalized SSM is 23% more compact than the non-normalized SSM.

Keywords: Posture normalization · Human body modeling · 3D anthropometry · Statistical shape model · SSM

1 Introduction

When designing near-body products, product developers often rely on virtual design mannequins. The disadvantage of current mannequins is that they are a simplified representation of the population [1]. Statistical shape modeling is a well-known technique in 3D anthropometric analyses. It allows gaining a better understanding of the variation in shape present in a population. SSMs are highly valuable for product designers since ergonomic products for a specific target population can be designed from these models. By adapting the shape parameters of the SSM, a new, realistic shape can be formed. Product developers may exploit SSMs to serve as input for virtual

D.N. Cassenti (ed.), *Advances in Human Factors in Simulation and Modeling*,
Advances in Intelligent Systems and Computing 591, DOI 10.1007/978-3-319-60591-3_39

design mannequins and explore the body shapes belonging to a specific percentile of a target group, to visualize extreme shapes. On the other hand, an SSM can visualize a specific body shape, which is useful for customization. Reed et al. [2] developed a pose modification technique. Nevertheless, posture has a high influence on their results.

When building an SSM from 3D body scans, body posture has a significant influence on the shape modes. Even when the subjects are instructed to maintain a standard pose, there are slight posture variations noticeable, especially in the region of the arms. This is the case in e.g. the Civilian American and European Surface Anthropometry Resource (CAESAR) database [3]. As a result, some shape variances are incorrectly correlated with posture.

Most posture deformation techniques are based on rotating and translating the body parts. In particular, applying linear blend skinning (LBS) to a surface mesh with a simplified skeleton consisting of joints and bones, is a popular approach [4]. Posture normalization is commonly done by transforming each body part separately. The disadvantage of LBS, is that the result may look unnatural, because LBS cannot compensate for muscle bulging.

Another common approach is separating the shape space from the posture space. Wuhrer et al. [5] did a posture-invariant shape analysis using the Laplace operator. This is very computationally intensive for surface meshes with many vertices, because an optimization problem needs to be solved for every vertex. The SCAPE method [6] is a data-driven method that learns a posture deformation model that derives the non-rigid shape deformation as a function of the posture of the articulated skeleton. The advantage of this technique is that it generates more realistic shapes including the simulation of muscle bulging. However, a drawback of SCAPE is that a skeleton has to be defined for every surface mesh, which is time-consuming and error-prone.

In this paper, we propose a fast, skeleton-less, data-driven method to perform statistical shape modeling in a posture invariant way by minimizing the influence of posture, because we solely want to capture body shape variability. The remainder of this paper is organized as follows. First, the approach for building an SSM is detailed. Second, the approach for feature modification and identity removal is described. Then, the technique for posture normalization is discussed. In the results section, the several components of the framework are tested and evaluated. Finally, a conclusion is formulated.

2 Methods

In this section, the developed framework is described. First, an SSM is built from a population of 3D human body shapes [7]. Next, the identity of these training shapes is removed, by modifying the features of each shape so that they are equal to the average features. From these shapes without identity, a posture model is built. This model captures only the posture of a new input shape. The translation of each vertex from the posture model to the mean posture is calculated and applied to the input shape, which results in a posture-normalized shape.

2.1 Statistical Shape Model (SSM)

An SSM is built from a population of N shapes, with every shape consisting of n vertices. The population is represented by a $3n$-dimensional point cloud, where each point represents a shape. This cloud can be represented by a mean shape and $N-1$ eigenmode vectors, where the first eigenmode describes the largest variance in the population, the second eigenmode the second largest variance perpendicular to the first, etc. In an SSM, the mean shape $\bar{\boldsymbol{x}} \in \mathbb{R}^{3n}$ and the main shape modes, the principal component (PC) modes $\boldsymbol{P} \in \mathbb{R}^{3n\times(N-1)}$, are incorporated. This means that a new shape $\boldsymbol{y} \in \mathbb{R}^{3n}$ can be formed by a linear combination of the PCs:

$$\boldsymbol{y} = \bar{\boldsymbol{x}} + \boldsymbol{P}\boldsymbol{b}, \tag{1}$$

with $\boldsymbol{b} \in \mathbb{R}^{(N-1)}$ the vector containing the SSM parameters.

2.2 Feature Modification

A specific feature of an individual's shape, such as its height, can be adapted by adding a linear combination of PCs to the individual's shape vector. The weights for this linear combination, the so-called feature vector, are computed via multiple linear regression of the PC weights on the body features for the population of individuals. By applying a scaled version of the feature vector to the shape vector of an individual, its shape can be adapted to match a specific feature value [8].

Suppose we know f features $\boldsymbol{f}_i = \begin{bmatrix} f_1 f_2 \ldots f_f & 1 \end{bmatrix}^T \in \mathbb{R}^{f+1}$ and the PC weights $\boldsymbol{b}_i \in \mathbb{R}^{N-1}$ of each shape i from the dataset. Then, a mapping matrix $\boldsymbol{M} \in \mathbb{R}^{(N-1)\times(f+1)}$, describing the relationship between the PC weights matrix $\boldsymbol{B} = [\boldsymbol{b}_1 \boldsymbol{b}_2 \ldots \boldsymbol{b}_N] \in \mathbb{R}^{(N-1)\times N}$ and the feature matrix $\boldsymbol{F} = [\boldsymbol{f}_1 \boldsymbol{f}_2 \ldots \boldsymbol{f}_N] \in \mathbb{R}^{(f+1)\times N}$ is calculated by [9]:

$$\boldsymbol{M} = \boldsymbol{B}\boldsymbol{F}^{+}, \tag{2}$$

where $\boldsymbol{F}^{+}$ is the pseudoinverse of $\boldsymbol{F}$. With this mapping matrix, new PC weights $\boldsymbol{b}$ can be generated from given features $\boldsymbol{f}$ as follows:

$$\boldsymbol{b} = \boldsymbol{M}\boldsymbol{f}. \tag{3}$$

2.3 Identity Removal

Next, the identity of each shape is removed. This means that for each shape, the features are adjusted so that they are equal to the average features. As a result, all shapes look similar.

First, the specific PC weight vector $\boldsymbol{b}_i$ of instance i is extracted from the PC matrix $\boldsymbol{B}$ as the i^{th} column vector of $\boldsymbol{B}$. Second, the delta feature vector $\Delta\boldsymbol{f}$, which is the vector that holds the values that should be added to the current features to become equal to the

average features, is calculated by extracting the specific features $\boldsymbol{f}_i$ (defined as the i^{th} column of $\boldsymbol{F}$) of instance i from the average features $\bar{\boldsymbol{f}}$ of the population:

$$\Delta \boldsymbol{f} = \bar{\boldsymbol{f}} - \boldsymbol{f}_i. \tag{4}$$

Next, the delta PC weights vector $\Delta \boldsymbol{b}$ that should be added to the current PC weights to adjust the body shape, is calculated by multiplying the mapping matrix $\boldsymbol{M}$ with the calculated delta features $\Delta \boldsymbol{f}$:

$$\Delta \boldsymbol{b} = \boldsymbol{M} \cdot \Delta \boldsymbol{f}. \tag{5}$$

These delta weights are added to the original PC weights $\boldsymbol{b}_i$ to obtain the PC weights $\boldsymbol{b}_i'$ of the shape with average features:

$$\boldsymbol{b}_i' = \boldsymbol{b}_i + \Delta \boldsymbol{b}. \tag{6}$$

Finally, the new shape without identity, $\boldsymbol{x}_i'$, is calculated by multiplying the new weights $\boldsymbol{b}_i'$ with the PC vectors $\boldsymbol{P}$ of the SSM and adding them to the mean shape $\bar{\boldsymbol{x}}$:

$$\boldsymbol{x}_i' = \bar{\boldsymbol{x}} + \boldsymbol{P}\boldsymbol{b}_i'. \tag{7}$$

After removing the identity of each shape, a new SSM is built from the shapes without identity. The result is a posture model, where the shape variances are mainly the posture variances.

2.4 Posture Normalization

To normalize the posture of a shape, it is corresponded with the statistical posture model by elastic surface registration and the PC weights of this shape, using the posture model, are calculated. Because this model mostly contains posture variations, only the

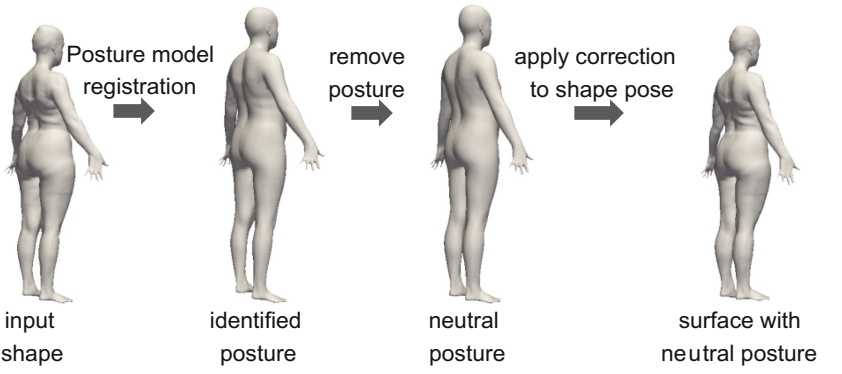

Fig. 1. Example of workflow of posture normalization. Note that the arms are more bent in the original shape than in the posture normalized shape

posture of the target shape is captured. In Fig. 1, the workflow of posture normalization of an example shape is shown.

First, the input shape, $\boldsymbol{x}_j$, is scaled, so it has the same size as the posture model. Then, the posture PC weights $\boldsymbol{b}_j$ of $\boldsymbol{x}_j$ are calculated by multiplying the inverse PC matrix $\boldsymbol{P}$ by the distance vector between each vertex of the input surface mesh and the mean surface mesh $\bar{\boldsymbol{x}}$. These posture PC weights only denote differences in posture compared to the mean posture.

$$\boldsymbol{b}_j = \boldsymbol{P}^T(\boldsymbol{x}_j - \bar{\boldsymbol{x}}). \tag{8}$$

The posture $\boldsymbol{x}'_j$ of the input shape is reconstructed from the calculated posture PC weights $\boldsymbol{b}_j$:

$$\boldsymbol{x}'_j = \bar{\boldsymbol{x}} + \boldsymbol{P}\boldsymbol{b}_j. \tag{9}$$

Finally, the normalized shape $\widehat{\boldsymbol{x}}_j$ is calculated by subtracting the posture influence $\boldsymbol{P}\boldsymbol{b}_j$ on the shape from the original shape $\boldsymbol{x}_j$:

$$\widehat{\boldsymbol{x}}_j = \boldsymbol{x}_j - \boldsymbol{P}\boldsymbol{b}_j. \tag{10}$$

3 Experiments and Results

In this section, the results of the framework are described.

3.1 Statistical Shape Model (SSM)

An SSM was built from 700 subjects (350 men, 350 women) in standing pose from the CAESAR database [3] whose 3D scans were registered using the same template surface mesh, a digitally modeled body consisting of 100k uniformly distributed vertices, shown in Fig. 2. No posture changes were made to these meshes yet.

Fig. 2. Reference mesh, uniformly resampled to 100k vertices.

In Fig. 3, the first three PC modes of the SSM built from the original shapes are shown. There is clearly an influence of posture visible in the third mode.

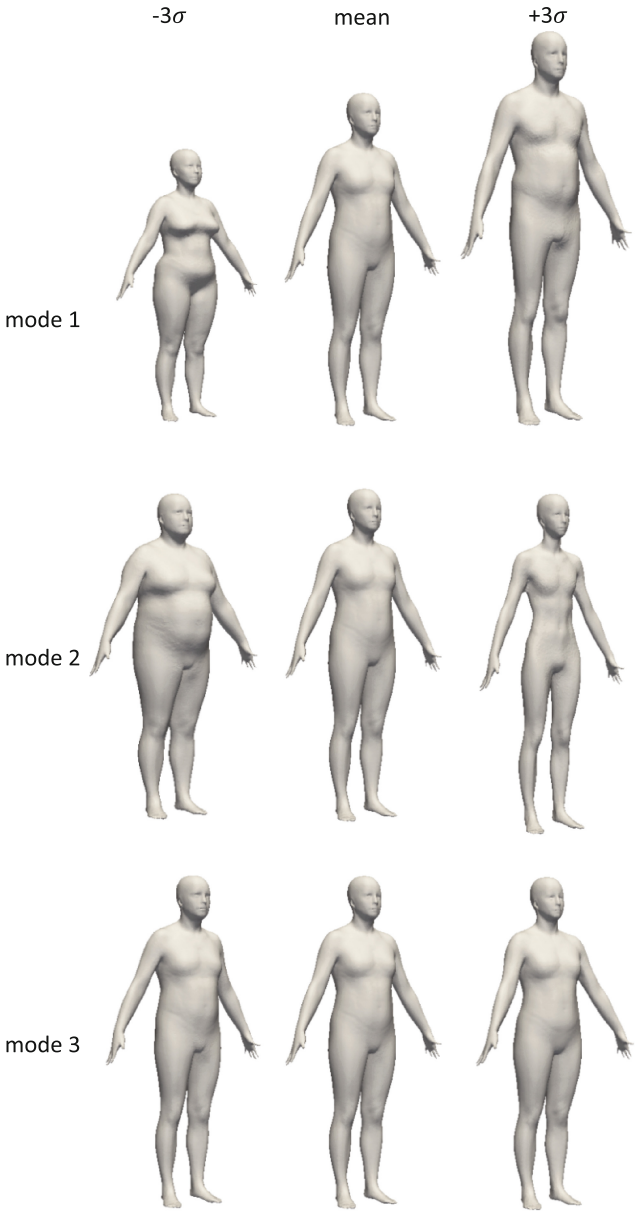

Fig. 3. The first three eigenmodes of the non-normalized SSM, built from the original shapes. A posture variation is clearly noticeable in the third mode, where the position of the arms and shoulders differs.

3.2 Posture Model

In Fig. 4, two examples of identity removal are shown. The resulting shapes look more similar than the original shapes.

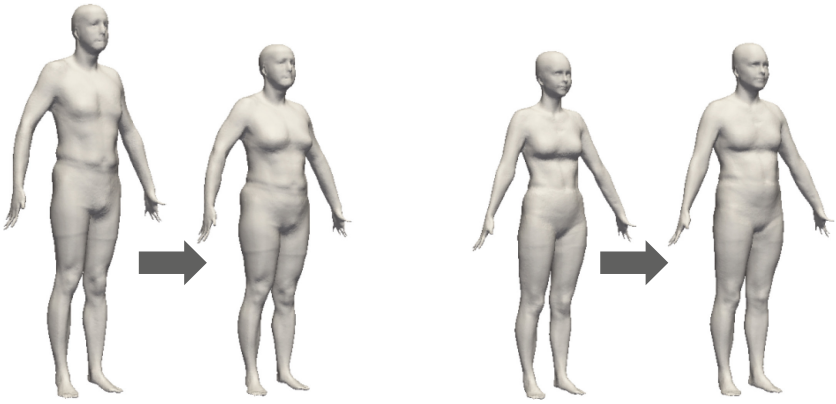

Fig. 4. Two examples of identity removal. The body features are averaged out, so mainly posture differences remain.

The posture model is shown in Fig. 5. The posture model was cut off at 12 shape modes to reduce shape related variations and remove noise from higher modes. This number was empirically determined.

3.3 Poseture Normalization Case

To evaluate the performance of the posture normalization algorithm, the posture of an individual from the CEASAR dataset, which was not included in the dataset of the posture model, was three times slightly modified by applying linear blend skinning (LBS) on the surface mesh [4]. Then, the posture of the modified shapes was normalized. In an ideal case, the normalized shapes are equal to each other. The result of the posture deformation and posture normalization is shown in Fig. 6. The average distance between the posture normalized shape was (1.08 ± 3.60) mm.

Normalizing the posture of a shape took around 10 s on a computer with an Intel® Core™ i7-5960X CP @ 3.00 GHz processor and 23.4 GB memory.

3.4 Normalized Statistical Shape Model

Every input shape of the original SSM was corrected for posture. These shapes served as input to build a new, posture normalized, SSM. The first three shape modes of this posture normalized SSM are shown in Fig. 7.

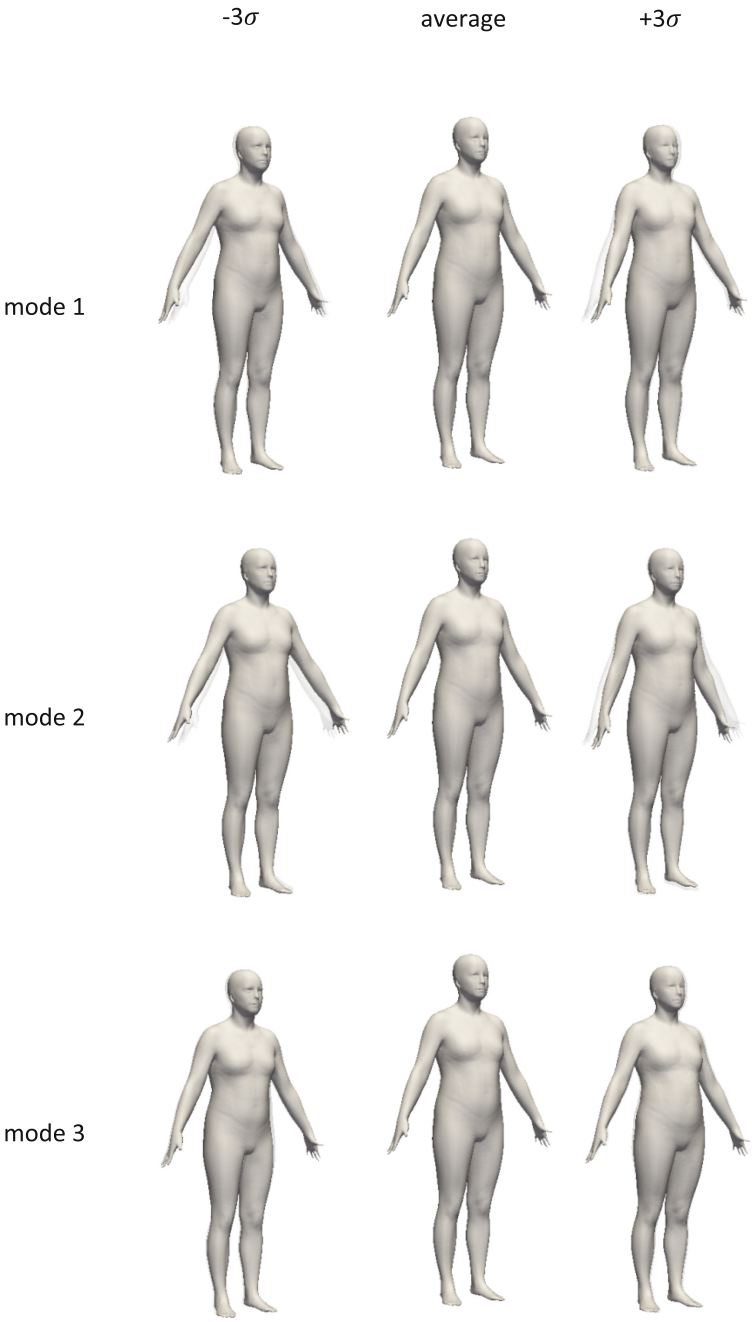

Fig. 5. The first three eigenmodes of the posture model. Posture variation is mainly visible in the region of the arms and torso. For every shape, the average shape is overlaid in light gray to show the difference in posture more clearly.

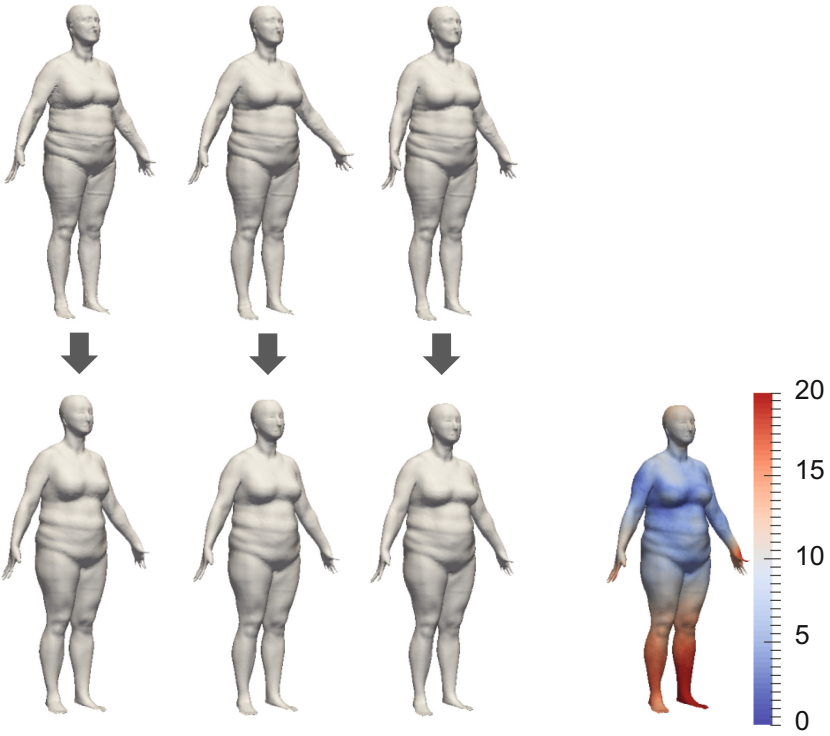

Fig. 6. Posture normalization case. The same input shape was deformed by applying LBS (upper row). The result of the posture normalization algorithm is shown in the lower row. The average distance between the posture normalized shape is shown in the right figure in mm.

3.5 Model Performance – Compactness

Compactness is a widely used measure for quantifying the correspondence quality of an SSM [10, 11]. A compact SSM is a model that can represent body shapes with only a small number of shape modes. The compactness is expressed as the sum of variances of the SSM,

$$C(m) = \sum_{i=1}^{m} \lambda_i, \tag{11}$$

where λ_i is the variance in shape mode i, and $C(m)$ is the compactness using m modes.

The results are shown in Fig. 8. Note that the normalized SSM is more compact than the non-normalized SSM. To describe more than 90% of the shape variation inside the population, the non-normalized SSM requires seven shape modes, while only two shape modes were sufficient for the normalized SSM. Using only one shape mode, the normalized SSM is 16% more compact than the non-normalized SSM. For five shape modes, an improvement of 23% was observed, and an improvement of 25% using ten shape modes. From 14 shape modes, the difference in compactness converged to 27%.

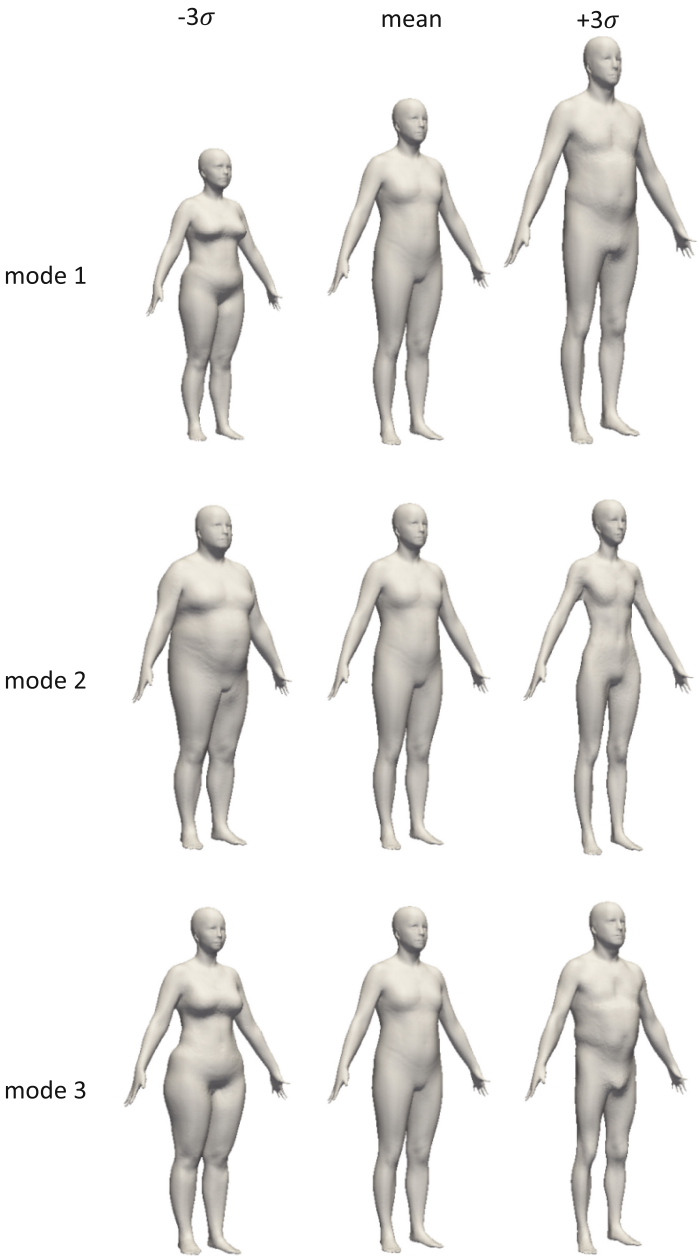

Fig. 7. First three eigenmodes of the posture normalized SSM. The modes describe body shape variances better compared to the shape modes of the non-normalized SSM, shown in Fig. 5. Note that the third mode of the normalized SSM describes mainly gender, while the third mode of the non-normalized SSM describes mainly the position of the arms.

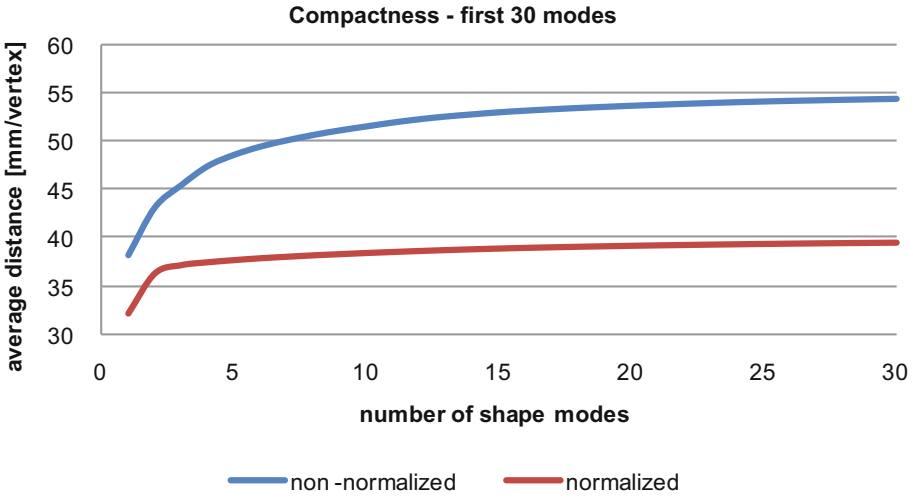

Fig. 8. Compactness graph, first 30 shape modes. The average deviation from the mean shape to describe shapes with a specific number of shape modes is shown. The normalized SSM substantially is more compact than the non-normalized SSM and more of its variance is captured with less modes.

4 Conclusion and Further Work

In this work, we proposed a technique to perform statistical shape analysis in a posture-invariant way. It allows us to study the shape variations in a database of human body shapes in slightly varying postures. The posture model can be used to normalize any shape that is brought into correspondence with this model in a fast and precise way.

The results have shown that statistical shape analysis of a posture normalized population results in more shape related variations than performing the same analysis on a non-normalized population. The normalized SSM is a more compact representation of the population, compared to the non-normalized shape SSM. Hence, less shape modes are needed to describe a certain percentage of the population.

Our SSM is a valuable tool for product designers for creating more realistic, virtual mannequins, that are a better representation of the population, and using this knowledge to improve the ergonomics of their products. It is also a first step towards posture invariant statistical shape analysis of body shapes in varying poses, e.g. for predicting the body shape in seated pose from a body shape in standing pose by mapping the PC weights from one pose to another.

Further fine-tuning of the posture normalization algorithm is necessary. Therefore, we will test our algorithm on multiple body scans of the same person in slightly different postures to validate and optimize the precision of our posture normalization algorithm.

Acknowledgements. This work was supported by the Agency for Innovation by Science and Technology in Flanders (IWT-SB 141520).

References

1. Moes, N.C.: Digital human models: an overview of development and applications in product and workplace design. In: TMCE International Conference (2010)
2. Reed, M.P., Park, B.-K.D., Corner, B.D.: Predicting seated body shape from standing body shape. In: 4th International Digital Human Modeling Conference (2016)
3. Robinette, K.M., Daanen, H., Paquet, E.: The CAESAR project: a 3-D surface anthropometry survey. In: Second International Conference on 3-D Digital Imaging and Modeling (Cat. No. PR00062), pp. 380–386
4. Baran, I., Popović, J.: Automatic rigging and animation of 3D characters. ACM Trans. Graph. **26**(3), 72 (2007)
5. Wuhrer, S., Shu, C., Xi, P.: Posture-invariant statistical shape analysis using Laplace operator. Comput. Graph. **36**(5), 410–416 (2012)
6. Anguelov, D., Srinivasan, P., Koller, D., Thrun, S., Rodgers, J., Davis, J.: SCAPE: shape completion and animation of people. ACM Trans. Graph. **24**(3), 408 (2005)
7. Danckaers, F., Huysmans, T., Lacko, D., Ledda, A., Verwulgen, S., Van Dongen, S., Sijbers, J.: Correspondence preserving elastic surface registration with shape model prior. In: Proceedings - International Conference on Pattern Recognition (2014)
8. Danckaers, F., Huysmans, T., Lacko, D., Sijbers, J.: Evaluation of 3D body shape predictions based on features. In: Proceedings of the 6th International Conference on 3D Body Scanning Technologies, Lugano, Switzerland, 27–28 October 2015, pp. 258–265 (2015)
9. Allen, B., Curless, B., Popović, Z.: The space of human body shapes. ACM Trans. Graph. **22**(3), 587 (2003)
10. Davies, R.H., Twining, C.J., Cootes, T.F., Waterton, J.C., Taylor, C.J.: A minimum description length approach to statistical shape modeling. IEEE Trans. Med. Imaging **21**(5), 525–537 (2002)
11. Zihua, S.: Statistical Shape Modelling: Automatic Shape Model Building. University College London, London (2011)

A Study of Digital Media Art Utilizing 2D Animation: Digital Video Expression Using Projection Mapping and Multi Screen Techniques

Zhipeng Feng(✉) and Kiyoshi Tomimatsu

Graduate School of Design, Kyushu University, Fukuoka, Japan
fengzhipeng_1990@yahoo.co.jp,
k.tomimatsu2008@gmail.com

Abstract. This paper is about the research of the combination of PM technique with traditional animation. It can help designers create a more authentic experience exceeding to traditional animation technique. In PM concrete practicing, designers can shadow movie on an object on regular and irregular surfaces. In recent years, PM technology is applied by more and more film productions, and prevails in many advertisement and art festivals. In the concrete design steps, firstly, makes a cube, two of these cubes' corner has been cut off to create the irregular projection. Two regular projection cubes represent spring and summer, using the bamboo and Lotus character as projected content. The other two irregular cubes represent autumn and winter, using the chrysanthemum and plum character as projected content. And then the second step, the production of projected content, author applied ink painting style to make these four plants animation.

Keywords: Projection mapping (PM) · Multi screen techniques · Animation · Information · Special vision

1 Introduction

In recent years, due to the development of digital technology, traditional hand-painted animation has developed into today's three-dimensional animation, which causes the huge change of animation stylish. But the way of animation display didn't get obvious change. most of them take use of traditional two-dimensional display method (similar to the screen in the theater). so the purpose of this paper is to propose one method of three-dimensional technique display which is based on the combination of three-dimensional projecting technique and projection mapping (PM) technique, quite different from traditional two-dimensional display method.

2 Research Background

In the film display, directors apply Multi- screen (Multi-screen) in some special situation. This method makes several projecting screens together to display and show the total film content in different screens. Also this method can show different contents in

D.N. Cassenti (ed.), *Advances in Human Factors in Simulation and Modeling*,
Advances in Intelligent Systems and Computing 591, DOI 10.1007/978-3-319-60591-3_40

different screens. This kind of display method is applied in many museum and exhibition. Also it is widely used as it can not only provide the full displaying information, but also it can improve the value of the displaying content which has been proved by many studies.

This research is based on the combination of PM technique and Multi-screen technique, to create unique screen display method different from traditional two-dimensional display method. To get full understanding of this field research, firstly, author does some literature study and investigation of the characteristics of animation projector, then studying how to project animation on the irregular objects in various different background environment, and finally do the experiment and test this combination technique to get the experiment result and this paper's conclusion.

3 Projection Animation

3.1 Introduction of Projection Animations

Today, the development of computer technology promotes the digital PM technique. There are three main technical approaches of PM, the first one is known as [MAPPING] technology. The proportion of the general picture of the projector is 16:9 and 4:3 as shown in the shows, generally through the use of projection technique projector projected figure circles, triscreens, in the projecting process, some part of projecting content can be absent. So the PM projection refers to the technique that only the necessary parts are projected out by the digital scale controlling of projector (Fig. 1).

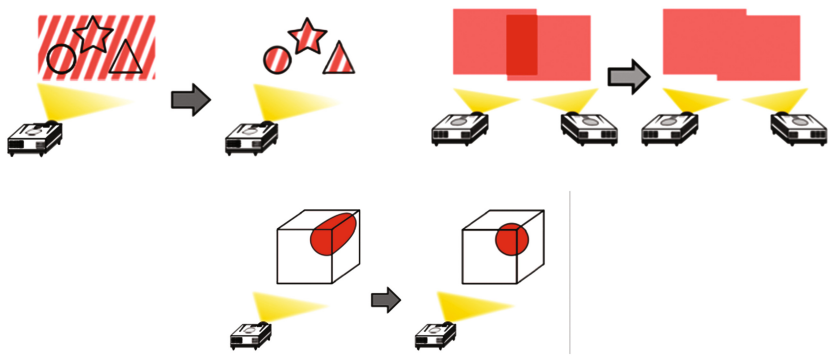

Fig. 1. Mapping, Edge Blending, Projection Mapping

The second one is known as [Edge Blending] technology. Usually the projection area is limited, but by using multiple projectors projection area can be enlarged, which makes it possible to produce large-area films. As shown, when fold the different images together using the general projection technique, but there will be the problem of high brightness. Comparing with PM technique, PM technique can reduce the brightness of overlapping parts. The third one is known as picture adjustment technology. The third

one is known as picture adjustment technique. While the PM technique can correct the deformation and make the projection images more natural.

3.2 Projection Animation Examples

In 2009, a work of art was projected on surface of Hamburger Kunsthalle building in Germany. In this work, the building was operated by two hands moving up and down. Dynamic visual elements, such as moving points, lines, surfaces, bodies, etc., were used to create decomposition and reconstruction, which combines space and time to reconstruct the architecture, presenting the innovatively logic thinking and unique geometric aesthetics. This work showed various levels, was full of diversity, and provided a reference to the consideration of architecture space. This work won the 2009 Cannes Advertising Festival Silver Lion award.

4 Multi-screen

4.1 Introduction of Multi Screen

Multi view screen method has been applied in film as special way. This paper design animation utilizing this method combining with three-dimensional projecting technique to analyze the animation visual characteristics and efficiency, which is main on how this type of animation display to communicate with audiences in the process of information input and information output. Through the experiment, find out the problems of Multi screen animation display, and try to find out the solution (Fig. 2).

Fig. 2. Multi screen examples

4.2 Multi Screen Examples

In 1895, the first Multi-screen works were produced. It was no film clips works produced by French inventor Lumière brothers. After that, the American film maker Edwin Porters produced the world's first Multi-screen editing movie "big train robber" in 1903, Edwin Porters split out ten minutes film into 14 displaying screens. Since then, more and more films have absorbed this kind of display method, the number of

splitimages were more and more rich. For example, In the film of "Lethal (Weapon) (1987)", there was only 1 min and 30 s of fighting scene content, but the screen was divided into 65 small screen to show. Author gets the inspiration of these kinds of displaying technique to carry out this projecting displaying research.

5 Animation Experiment

In the PM projecting and three dimension projecting experiment. Author makes four short small animations as the whole story about traditional Chinese story. They are "spring, summer, autumn and winter" represented by bamboo, lotus, chrysanthemum, plum respectively which are traditional excellent Chinese culture characters. In the four animation contents, the aestheticism expression will represent the gradual change of four seasons (Fig. 3).

Fig. 3. Animation of spring

5.1 Animation of Spring

Spring is the first season of one year, it is also the season symbol world recovery. This spring animation is composed of three elements, including Huizhou architecture, swallow kite and bamboo that are the most local Chinese traditional culture characters. In the beginning of this animation, the Huizhou architecture sweeps. The Huizhou architecture is one of the most important Chinese traditional architecture style, representing Huizhou culture, that is always high application in Chinese and aboard architecture. Huizhou architecture is now popular in Huizhou, Yangzhou, Quzhou Zhejiang area. And its material is mainly brick, wood, which structure is wood frame. Also the rich decoration is high expressing in Huizhou architecture. After the appearance of architecture, there flies into swallow kite from top left corner, appropriately expression of the Chinese old saying in China "Spring comes, the swallow comes back from south." Also, this kite flying is the traditional Chinese custom. Combining the old saying and custom, kite flying is the proper depicting way of "spring comes". The final animation lens of bamboo character is from the bottom of the corner, first appearing a slow growing bamboo with beautiful Chinese traditional music playing, after that bamboo growing into bigger and bigger, full of the whole screen. In this three steps, the expression of "world recovery" comes out apparently (Fig. 4).

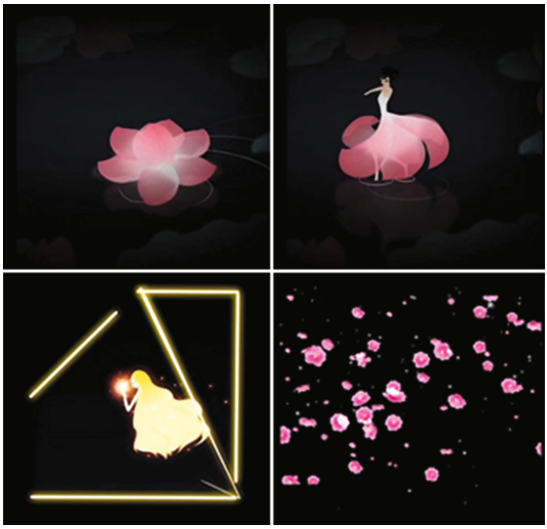

Fig. 4. Animation of summer, autumn and winter

5.2 Animation of Summer

In summer, there are many plants can represent the summer concept in China Jiang Nan area, along by the Yangtze River region. Among these plants lotus is the best representative flower for summer. In ancient China there are many poems praising lotus, the most famous is "Reminiscence", from which this animation get the design inspiration starts from the inspiration of reading this poem. "Reminiscence" is a prose created by Zhou Danni's Neo Confucianism in the North Song dynasty. it is about the high quality of lotus description, praising the lotus faithful character. Because of this reason author utilizes lotus to convert its spirit into this animation to show its nobility characteristic.

5.3 Animation of Autumn

This part animation shows the season transition from autumn to winter through the shape and color changes of chrysanthemum. The front two lens are the color or shape change of traditional Chinese painting, this animation highlights the "new dynamic", much more powerful, combing with the modern design element and traditional element, creating completely different visual experience comparing with the former two animation. In this animation, amount of lines and color changes show the strong impact.

5.4 Animation of Winter

Winter is the last season in the one year, it means it is the conclusion of the whole year. this animation is composed with two elements, plum and snow. In the beginning, there falls amount of snow, along with the snow, there is a small plum blooming quietly,

following by a large plum blooming together. The strong visual comparison between white snow and pink plum gives the viewer fantastic visual feeling.

5.5 The Whole Story of These Four Animations

The four animations present the four season changes, also these four animations constitute the whole season story. The experiment author need to do is displaying them together, String into a whole. So the purpose of this experiment is to display the change of the four seasons in a time. It is also the verification of how to use multi -screen three-dimensional animation technique in reality, and give some suggestion to the future animation display research.

6 Experiment Process

6.1 Prototype

After many years of development, animal technique makes great progress from the original traditional hand-painting to present display with modern elements including language, music, scenes, characters. The content and artistic style of animation have changed a lot.

There are two types of animation from the style classification, one is two-dimensional animation which shows the style of simple and elegant; The other one is now in the paper discussion of three-dimensional technique animation which shows the bizarrerie the space and time display experience. In author‘s four season animations experiment, author tries to prove the feasibility of this multi -screen animation on irregular three-dimensional objects in one space and time, and the high efficient display way of this kind animation (Fig. 5).

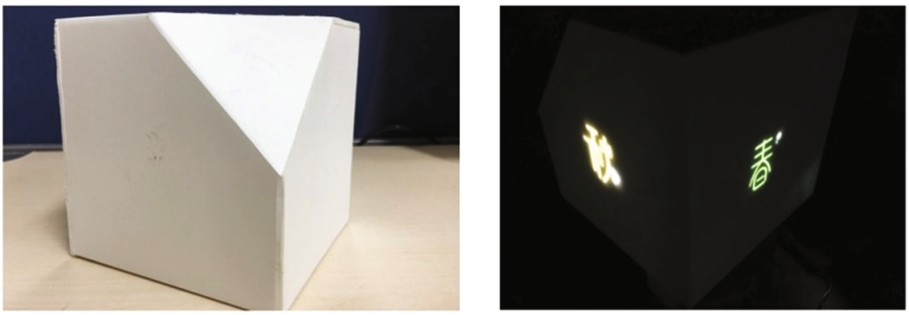

Fig. 5. Prototype

At the beginning of the experiment, making a 15 cm × 15 cm cube as the basic projection. In order to create a special projecting form, author made an equilateral triscreen in each corner of the cube. And in order to get the similar transparent light

display effect, author chooses the foam board to make the model have better transparent feature to build the main experiment structure.

6.2 The Position of Projectors

This experiment is to display four different animations at the same time and same place. In order to display synchronously, author utilizes four linking projectors, adjusting each projector distance, setting the scope of projector to make sure these four animations can be showed in the same scope, and finally make them be the whole coherent season story. These four projection are BENQ No: MP720p, BENQ No. MW512, PLUS No. V-339, SEESE No: M1J11C00489 respectively (Fig. 6).

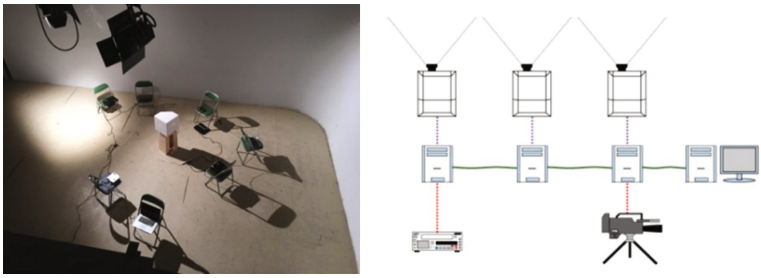

Fig. 6. The position of projectors

6.3 Experiment Questions

Through this experiment, we can find out that there are some problems: (1) As the different type of these four projectors, the projection of resolution and chroma cannot get the same result. Even though, it is not big problem, in the following research and experiment, there is a strong necessary to utilize the same resolution and chroma projectors to solve this problem. (2) The surface is a little bit uneven as the cut of horn between each face transition, such as the extra white line showing in the below figure. If audience views each animation separately, there is no big problem, but if views the four animations together, problem comes out, it seems these four animations are not the total serial story, but unrelated story. (3) The position of each projector and the projecting direction can influence the perception of viewing experience, so in the following research, it should find a better projector placement way. As the above three problems, the future research should be launched to solve them (Fig. 7).

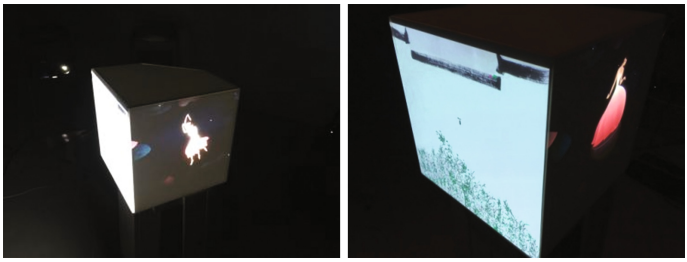

Fig. 7. Projection

7 Conclusion

This research is different with traditional common display design. it is about how to do display taking use of multi-screen and PM technique. The purpose of this research is to provide visual experience in one space and time. By the animation experiment, viewer can get the unusual visual feeling because of the irregular three –dimension projection, the four animations information can be input into viewer's sensory organs synchronously, which brings the viewer's understanding of Chinese culture more clearly and deeply. So though this research, we can get the conclusion that this display method combining with multi-screen and three dimension method can give viewers curiosity experience, at the same time increasing the information input amounts, which will arise efficient information reaction with displaying contents.

In the following future, in order to promote this display technique. Author thinks that the most important one is to do the three –dimension displaying in various environment condition, such as in the water display, in the noising street, how to attract viewers and make sure that they can get efficient information input. So author will continue research in this direction in the future three –dimension technique display research.

References

1. Yun, H.R., Kim, D.W., Ishii, T.: A study of digital media art utilizing the contents of the architecture cultural property. Int. J. Asia Digit. Art Des. (2013)
2. Yamauchi, N., Izuhara, R.: Projection mapping on Tsudumi-mon at Kanazawa Sta. JSSD **63**, 2–60 (2016)
3. Yamamoto, K., Itoh, K., Kikuchi, T.: Proposal of advertising by projection mapping using amid screen. Inst. Image Inf. Telev. Eng. **38**(16), 211–213 (2014)
4. Mori, T.: Automatic generation of cartoon hair animation. ITE Tech. Rep. **40**(11), 45–48 (2016)
5. Ikeda, K.: A study of social impacts of projection mapping. Bull. Fac. Hum. Stud. Seisen Jogakuin Coll. (13), 37–48 (2016)
6. Junichi, S.: Interactive 3D projection mapping with ultra-realistic effects. Inst. Image Inf. Telev. Eng. (2012)

7. Toshiki, N.: Research and development about the direction method of the projection mapping. Inst. Image Inf. Telev. Eng. (2012)
8. Keiko, Y.: Designing physical objects as if they were digital. Inf. Process. Soc. Jpn. (2007)
9. Jung, M.H.: Sensibility classification of flower texture by physical properties (2010)
10. Kana, H.: A study on activity community planning which utilized historic environment as tourist attractions. Architectural Institute of Japan (2007)

Comprehensive Mappings of Postural Angles on a Normalized Plane of Reachability

Raffaele Castellone[1(✉)], Fabrizio Sessa[2], Stefania Spada[3], and Maria Pia Cavatorta[1]

[1] Department of Mechanical and Aerospace Engineering, Politecnico di Torino, Turin, Italy
{Raffaele.Castellone, Maria.Cavatorta}@polito.it
[2] FCA, Manufacturing Engineering Southern Italy, Pomigliano d'Arco, NA, Italy
Sessa.Fabrizio@fcagroup.com
[3] FCA, Manufacturing Planning & Control – Ergonomics, Turin, Italy
Spada.Stefania@fcagroup.com

Abstract. In the industrial context of workstation design, the role of ergonomics in primary prevention of musculoskeletal disorders is increasingly important. Simple tools and guidelines for early postural checks are needed to assist the analyst through the dynamic reality of workstation design. In this work, a method for generating mappings of the operator's reachability is proposed. The reachability plane is normalized with respect to characteristic anthropometric body dimensions so that the postural maps can address any operator, regardless of his/her anthropometry. The mappings of trunk bending and upper arm elevation angles, defined in accordance with the international technical standards, make use of the traffic light scheme to ensure a valid and easy-to-interpret support to the analyst.

Keywords: Human factors · Postural assessment · Reachability comfort · Ergonomic tool

1 Introduction

Reachability assessments represent one of the earliest uses of Digital Human Model (DHM) [1]. Since then, the variables that influence the body posture in reachability tasks (e.g. gender, age, stature) have been widely considered [2], including the discomfort evaluation of arm reaching movements when seated [3].

The motor vehicle is one of the areas where reachability assessments found a specific application. Check on the level of reachability of the different controls and devices on the dashboard is part of the ergonomic analysis of the motor vehicle. Reaching in postural comfort must be possible for different percentiles of users: regardless of the driver's size, the joint angles for the upper limb and for the trunk shall remain within comfortable bounds. Assessment of reaching capabilities using DHM is commonly performed by evaluating each joint of the kinematic chain, terminating in the hand, through the associated ranges of motion [4]. The result is a reach envelope determined entirely by the segment lengths, joint degrees of freedom and joint ranges of motion.

D.N. Cassenti (ed.), *Advances in Human Factors in Simulation and Modeling*,
Advances in Intelligent Systems and Computing 591, DOI 10.1007/978-3-319-60591-3_41

Fewer studies investigate the maximum reach envelope for industrial workstation design. In [5] seated and standing reachability with upright trunk was assessed through experimental tests carried out on male and female subjects with different anthropometries. Later, Parkinson and Reed [6] used a simple virtual manikin for assessing reachability and producing reaching envelopes that are representative of the maximum reachability in space, also considering the mobility of the trunk. In particular, three envelopes related to the maximum reachability in space for the conditions of 0, 30 and 60° of trunk bending were obtained. The postural comfort clearly reduces as the angle of trunk bending increases. In international technical standards ISO 11226 [7] and UNI EN 1005/4 [8], a 60° angle of trunk bending represents the threshold to unacceptable working conditions.

In industrial contexts, it is nowadays binding to run ergonomic assessment in the initial stages of the design and industrialization of new work processes, and DHM programs are increasingly being used to reduce design times and costs [9], and to effectively emphasize primary prevention of musculoskeletal disorders through early recognition and mitigation of the risk factors. However, simpler tools and guidelines that allow early postural checks on potentially critical working points may be of great help to assist the analyst through the dynamic reality of workstation design [10].

The aim of this work is to propose a method for a quick evaluation of the trunk bending and arm elevation angles through the generation of normalized maps of reachability, in which the coordinates of the working point are normalized with respect to characteristic anthropometric body dimensions of the virtual manikin. In the normalized plane, the postural comfort can be estimated for workers of different stature once the coordinates of the working points are scaled to account for the worker's anthropometry.

To ensure a valid and easy-to-interpret support to the analyst, the definition of the trunk bending and arm elevation angles follow the international technical standards [7, 8] and the traffic light scheme is associated with the angle evaluation.

2 Material and Methods

2.1 Obtainment of the Postural Angles

In the initial step of this work, the trunk bending and the upper arm elevation angles were obtained from the virtual simulation of reachability operations. The 3D Static Strength Prediction Program (3DSSPP) software, developed by the University of Michigan [11], was used for this purpose.

The 3DSSPP program is particularly suitable to analyze movements and postures during tasks of manual material handling. More specifically, it has been developed to simulate static postures or slow movements (assuming that the effects due to acceleration are negligible). 3DSSPP allows predicting the posture assumed by the manikin by inputting the coordinates of the point to reach with the hands. In particular, it allows estimating the posture that a person is likely to assume during a reachability task. The posture can be predicted based on a combination of empirical motion tracking data and inverse kinematics [12]. However, the estimated posture may not be the posture that

every person tends to assume due to physical, behavioral and training differences between individuals [13].

National Health and Nutrition Examination Survey (NHANES) is the 3DSSPP's anthropometric database. The 3DSSPP allows the creation of a customized manikin through "scaling" techniques, while a shortcut allows selecting among the percentiles most used in design. In the present work, we selected P5, P50, and P95 male for the reachability simulations.

In this work, we calculated postural angles from simulations of reachability of working points on a plane parallel to the sagittal plane. The X coordinate was set at 200 mm, which represents a point nearly aligned with the elbow joint of a P50 manikin in a rest position. Further investigations confirmed that the same reachability plane for other percentiles (slightly misaligned from the joint elbow) does not produce substantial differences in the posture. The reachability area, in the plane X = 200 mm, was vertically delimited from the hip height to the full stature of the manikin. On the other hand, for the horizontal distance Y, the nearest working points were chosen at 200 mm from the frontal plane without considering the body depth, whereas the farthest points depend on the reachability of the analyzed percentile. Within the reachability area, a grid of working points was then defined.

For each point on the grid, we performed a simulation for predicting the manikin's posture in reaching the working point, and then, for each obtained posture we calculated the two postural angles: trunk bending (α) and upper arm elevation (γ), in accordance with the international technical standards (ISO 11226, UNI EN 1005-4).

The angle of trunk bending (α) is defined in the sagittal plane, as the inclination of the torso with respect to the vertical axis. In particular, the segment that defines the trunk bending is the line connecting two anthropometric points of the manikin, the greater trochanter to the 7th cervical vertebra.

The upper arm elevation angle (γ) is defined as the elevation of the upper arm during task execution with respect to a reference posture. The segment that defines the elevation of the upper arm is the line connecting two anthropometric points of the manikin, the acromio-clavicular joint to the humeral-radial joint. The calculated angle does not depend on the direction of view during the measurement, but it is the real angle in 3D, while the angle of the reference posture of the arm is 13° from the vertical [7, 8].

2.2 Extension of the Mappings

In the second part of the work, we used interpolation methods to extend the postural angle values from the input grid of simulated working points to a much finer grid. In this regard, MATLAB was used to interpolate the values of the postural angles within the reachability plane and, in a further step, to create surfaces of the postural angles with a different number of nodes. The density of the output grid can be set depending on the required degree of detail.

In this work, we used a diverse number of input nodes and different interpolation methods. More specifically, we used three different sizes of the grid: 3×7 (21 work points), 4×7 (28 work points), and 5×7 (35 work points) and applied linear and non-linear spline interpolations.

Figures 1 and 2 show two different surfaces obtained for the upper arm elevation angle. In particular, Fig. 1 represents the initial grid acquired from the reachability simulations; this grid consists of 21 working points, 3 × 7 in size. Figure 2 shows the denser grid of 221 interpolated nodes, 17 × 13 in size. The 3D surfaces allow evaluating what is the behavior of the postural angle in the reachability plane that is chosen for the simulation (X = 200 mm). Each node of the grid corresponds to a value of the analyzed postural angle. A colored scale allows easy quantification of the postural angle.

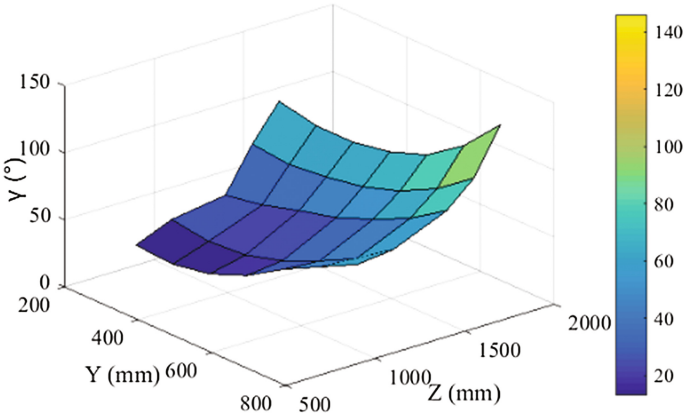

Fig. 1. 3D initial surface. Values of the upper arm elevation (γ) for the initial 3 × 7 grid of work points in the reachability plane.

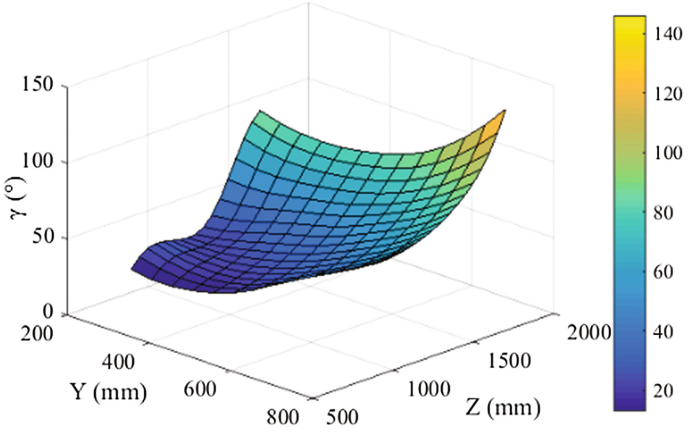

Fig. 2. 3D interpolated surface. Values of the upper arm elevation (γ) for the interpolated 17 × 13 grid of work points in the reachability plane.

2.3 Normalization of the Reachability Plane

In the third and final section of the work, we normalized the mappings of postural angles with respect to characteristic anthropometric body dimensions of the manikin. In particular, the full stature and the arm length of the manikin were used for normalizing the vertical height from the floor and the horizontal distance of the working point, respectively. For this purpose, the anthropometric measures of the three percentiles were taken directly from 3DSSPP, in order to maintain consistency in the anthropometric models. In the normalized plane, the postural angles can be estimated for workers of different body dimensions, once the coordinates of the working points are scaled to account for the worker's anthropometry.

3 Results and Discussions

3.1 Number of Nodes in the Grid and Interpolation Methods

For the validation of the method, we ran a comparison between the angles obtained from the interpolation mappings and the values directly derived from postural simulations. For the comparison, we selected *check points* different from the initially mapped grid of working points. The *check points* were selected among the farthest points from the input grid, in order to highlight the higher differences.

Figure 3 shows the differences between the interpolated and 3DSSPP (reference) values for the trunk bending angle in the case of a 3 × 7 grid. The two graphs refer to the linear and spline interpolation methods.

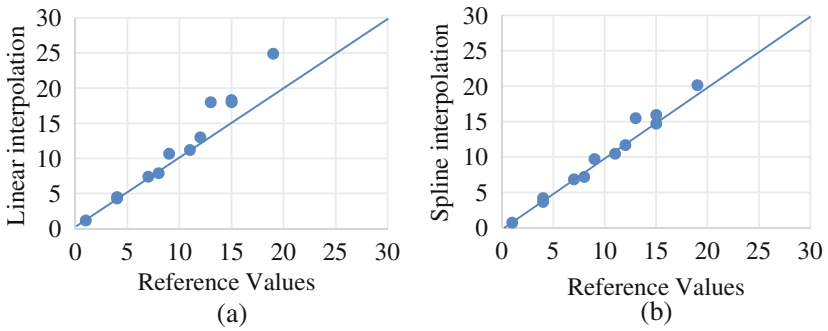

Fig. 3. Correlation of the interpolated values of the trunk bending angle when using a linear interpolation (Fig. 3a) and a spline interpolation (Fig. 3b) for an initial input grid 3 × 7 in size.

In the graphs, the bisector indicates a perfect matching between the interpolated and reference angular values. The coefficient of determination R^2 is given in Table 1. Table 1 shows the R^2 value for each case of interpolation, varying the number of input nodes and the interpolation method. R^2 assumes higher values for the upper arm angle (γ) than for the trunk bending angle (α), for a given number of input nodes and interpolation method. A reason could be that the trunk bending angle (α) assumes lower

values and varies in a narrower range compared to the upper arm elevation angle (γ). Consequently, an error in the trunk bending angle has a greater percentage weight and a greater impact on R^2 (especially for lower R^2 values).

As expected, Table 1 shows a better match for a greater number of input nodes and a non-linear interpolation method. In this work, the angular maps were therefore obtained using a 5 × 7 input grid and the spline interpolation.

Table 1. R^2 values for different interpolation methods and diverse numbers of input nodes.

Postural angle	Interpolation method	Input (3 × 7)	Input (5 × 7)
α	Linear	0.85	0.97
	Spline	0.97	0.98
γ	Linear	0.95	0.97
	Spline	0.99	0.99

3.2 Mappings of the Postural Angles

After choosing the most suitable number of nodes and type of interpolation, the angle of the trunk bending (α) and the angle of upper arm elevation (γ) were mapped for the three selected percentiles. Figures 4 and 5 show the colored map of the two postural angles for the P50 male.

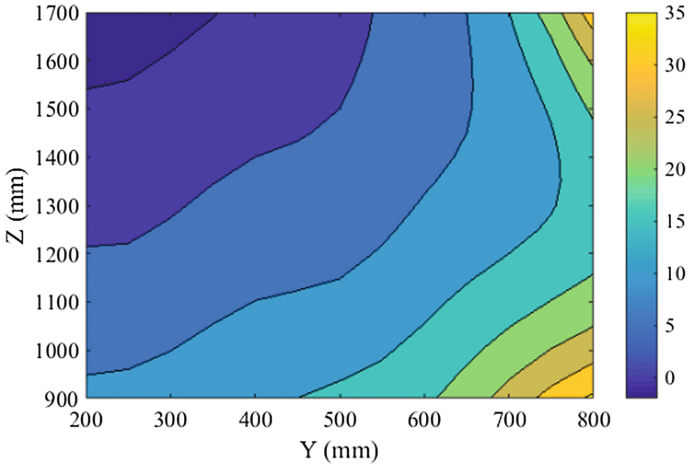

Fig. 4. A colored map of the trunk bending angle (α) in the reachability plane for the P50 male.

Figure 4 shows the values of the trunk bending angle (α). As expected, the bending of the trunk increases with the horizontal distance of the point to reach. Specifically, the maximum values of α are obtained when the horizontal distance is maximum, and the vertical height of the working point is at the limits of the analyzed reachability plane (Z = 900 mm, Z = 1700 mm). On the other hand, for working points closer to the body, α is greater for lower vertical heights from the floor.

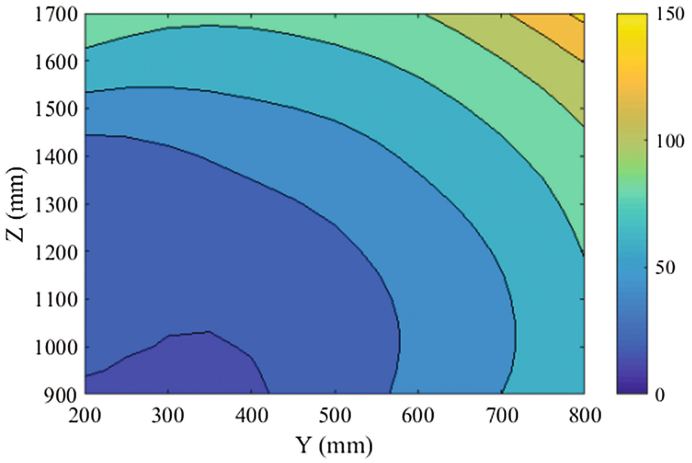

Fig. 5. A colored map of the upper arm elevation angle (γ) in the reachability plane for the P50 male.

Figure 5 shows the upper arm elevation angle (γ). The angular values grow as both the horizontal and vertical distances of the working point increase. The minimum value and the maximum value are in the opposite corners of the mapping.

The comparison of the postural angle mappings among the three percentiles showed significant differences due to the different anthropometry. As expected, the same working point is reached with different postures by the three manikins.

Although the same working point determines different angular values, the postural maps of the different percentiles are similar in shape. Specifically, we observed that manikins of different statures reach in approximately the same manner a working point when the coordinates of the latter are scaled to the manikin's anthropometric size. For this reason, a method to normalize the postural mappings of the different percentiles was studied and is proposed in this work.

3.3 Normalized Maps

In the second part of this work, we normalized the coordinates of the working points with respect to the full stature of the manikin for the vertical height from the floor, and to the arm length of the manikin for the horizontal distance.

Figures 6 and 7 show the two mappings of the postural angles in the normalized reachability plane. These maps were colored in accordance with the technical standards (ISO 11226, UNI EN 1005-4), through the following traffic light scheme:

in particular, for the trunk bending angle (α)

- $0° \leq \alpha < 20°$ acceptable condition (green)
- $20° \leq \alpha < 60°$ condition to be verified (yellow)
- $\alpha \geq 60°$ unacceptable condition (red)

and for the upper arm elevation angle (γ)

- $0° \leq \gamma < 20°$acceptable condition (green)
- $20° \leq \gamma < 60°$ condition to be verified (yellow)
- $\gamma \geq 60°$ unacceptable condition (red)

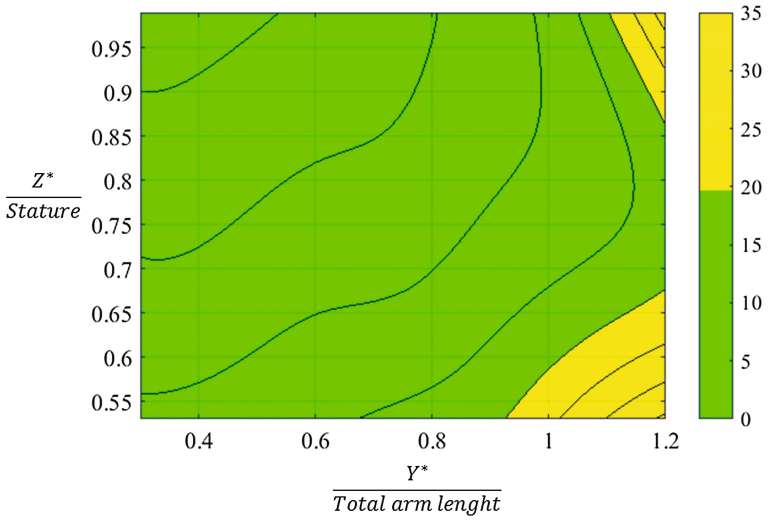

Fig. 6. Traffic light evaluation of the trunk bending angle (α) in the normalized reachability plane for the P50 male.

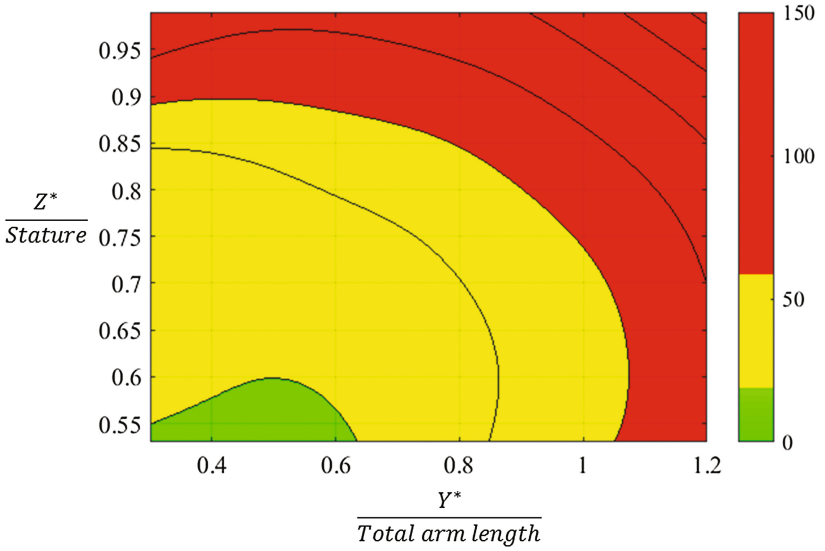

Fig. 7. Traffic light evaluation of the upper arm elevation angle (γ) in the normalized reachability plane for the P50 male.

The traffic light scheme allows for a quick postural evaluation. In the design stage, the analyst may use these mappings to perform reachability checks and estimate the postural comfort of a work task even before it exists and prior to more complex virtual simulations.

At last, we compared the mappings of the postural angles for the three percentiles in the normalized plane of reachability. Figure 8 shows a comparison for a few working points defined in the normalized plane. For illustrative purpose, in Fig. 8 the height of the working points is fixed to 82% of the manikin's stature (approximately the shoulder height), while the horizontal distance is shown on the x-axis as a ratio with the manikin's arm length. The three curves represent the values of the trunk bending angle for the P5, P50, P95 male manikins. Angular values are very similar among the percentiles, and the difference is always limited within 3°.

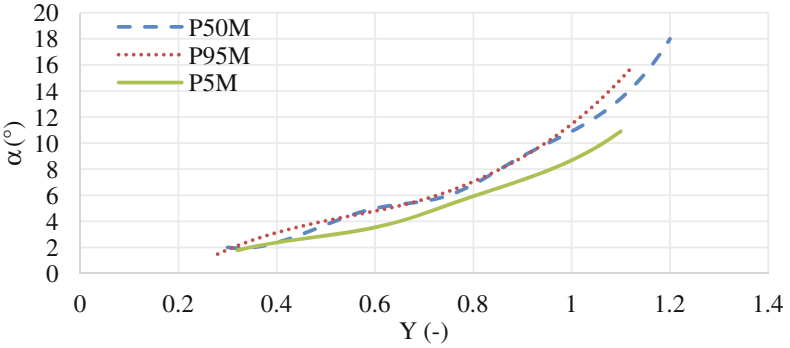

Fig. 8. Comparison of trunk bending angles for the three manikin percentiles. Working points are at shoulder height, while the Y coordinate is scaled to arm length.

Similarly, Fig. 9 shows the comparison between the values of the upper arm elevation angle for the P5, P50, P95 male manikins. In this case, the working points are at a distance from the ground that is approximately equal to the full stature of the manikin.

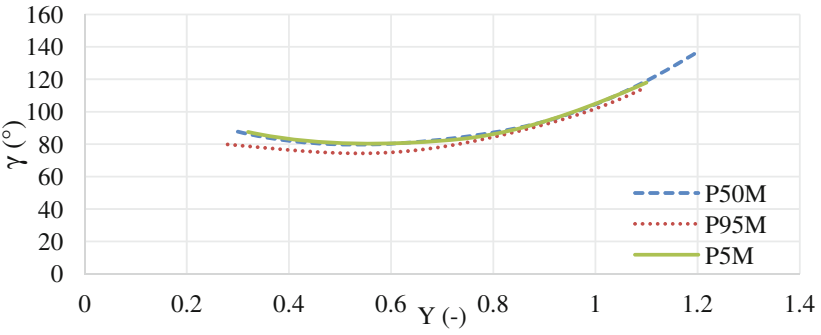

Fig. 9. Comparison of upper arm elevation angle for the three manikin percentiles. Working points are at full stature height, while the Y coordinate is scaled to arm length.

For sake of simplicity, Figs. 8 and 9 plot working points at fixed heights. Additional comparisons were made for the other working points in the reachability plane. These results confirm that the mappings of the postural angles can be used for any given percentile with an acceptable approximation, provided that the working points are normalized with respect to the manikin's anthropometry.

4 Conclusions

In this paper, we conducted a preliminary study of the postural comfort during reachability tests and proposed a method to obtain comprehensive mappings for a normalized reachability plane.

In the normalized plane, the trunk bending and arm elevation angles can be estimated for workers of different stature once the coordinates of the working points are scaled to account for the worker's anthropometry. The traffic light scheme was used to define different comfort zones in accordance with the international technical standards to ensure a valid and easy-to-interpret support to the analyst.

In this paper, the input data were obtained from reachability simulations using a DHM program. However, the proposed method can be applied to postural data obtained from experimental reachability tests. In this case, the mappings could be created from a reduced initial grid of working points, saving time and costs.

References

1. Ryan, P.W., Springer, W., Hlastala, M.: Cockpit geometry evaluation. Joint Army-Navy Aircraft Instrumentation Research Report, 700201 (1970)
2. Chaffin, D.B., Faraway, J.J., Zhang, X., Woolley, C.: Stature, age, and gender effects on reach motion postures. Hum. Factors **42**(3), 408–420 (2000)
3. Chevalot, N., Wang, X.: An experimental investigation of the discomfort of arm reaching movements in a seated position (No. 2004-01-2141). SAE Technical Paper (2004)
4. Reed, M.P., Parkinson, M.B., Klinkenberger, A.L.: Assessing the validity of kinematically generated reach envelopes for simulations of vehicle operators. SAE Trans.: J. Passeng. Cars-Electron. Electr. Syst. **112**(7), 693–697 (2003)
5. Sengupta, A.K., Das, B.: Maximum reach envelope for the seated and standing male and female for industrial workstation design. Ergonomics **43**(9), 1390–1404 (2000)
6. Parkinson, M.B., Reed, M.P.: Standing reach envelopes incorporating anthropometric variance and postural cost (No. 2007-01-2482). SAE Technical Paper (2007)
7. International Standard ISO 11226:2000: Ergonomics – Evaluation of static working postures (2000)
8. EN 1005-4:2005 + A1, 2008: Safety of machinery – Human physical performance – Part 4: Evaluation of working postures and movements in relation to machinery (2008)
9. Chaffin, D.B.: Improving digital human modelling for proactive ergonomics in design. Ergonomics **48**(5), 478–491 (2005)
10. Castellone, R., Sessa, F., Spada, S., Cavatorta, M.P.: Reach posture prediction through a simple multibody model for early design checks. Int. J. Ind. Ergon. (under revision)

11. Chaffin, D.B., Andersson, G., Martin, B.J.: Occupational Biomechanics. Wiley, New York (1999)
12. Zhang, X., Chaffin, D.: A three-dimensional dynamic posture prediction model for in-vehicle seated reaching movements: development and validation. Ergonomics **43**(9), 1314–1330 (2000)
13. The University of Michigan: 3D Static Strength Predication Program, ver. 6.0.5, User's Manual, The University of Michigan, Center for Ergonomics, Ann Arbor, Michigan (2011)

Comparison of Gender Specific and Anthropometrically Scaled Musculoskeletal Model Predictions Using the Sorensen Test

Phillip E. Whitley(✉), Paulien E. Roos, and Xianlian Zhou

Computational Medicine and Biology Division, CFD Research Corporation, 701 McMillian Way NW, Suite D, Huntsville, AL 35806, USA
{Phil.Whitley,Paulien.Roos,Alex.Zhou}@cfdrc.com

Abstract. Modeling gender and anthropometric influence on human response is essential for understanding biomechanical stressors, population task capability, and injury risk. Arbitrary anthropometric musculoskeletal (MSK) models were generated based on gender and anthropometric variables with MSK muscle strength optimized using lower spinal moment generation capacity. Two female (F1, F2) and two male (M1, M2) MSK models were compared using a 300 s Sorensen test simulation for muscle activation, forces, capacity, pain score, and lumbar joint reaction forces and moments. Predicted muscle activation, force, capacity, pain score, reaction shear and compressive force, and reaction pitch moment followed a body size relationship where M2 > M1 > F2 > F1. The anthropometric MSK model generation process created variants that were not simply proportionally scaled versions of the reference model in dimension and strength. The smallest MSK model (F1) exhibited comparatively higher capacity than the other models in agreement with literature.

Keywords: Musculoskeletal models · Anthropometric scaling · Sorensen test · Lumbar model · Anthropometry

1 Introduction

Modeling gender and anthropometric influence on human response is essential for understanding biomechanical stressors, population task capability, and injury risk. We have developed the capability to generate specific, strength-scaled anthropometric musculoskeletal (MSK) models based on gender and anthropometric variables. These scaled MSK models were compared using the Sorensen test.

2 Methods

The anthropometric basis for this effort was a principal component analysis of the ANSUR II survey [1]. New MSK models were created through scaling of a reference 50th percentile gender version of the Christophy et al. [2] lumbar spine model. Starting

D.N. Cassenti (ed.), *Advances in Human Factors in Simulation and Modeling*,
Advances in Intelligent Systems and Computing 591, DOI 10.1007/978-3-319-60591-3_42

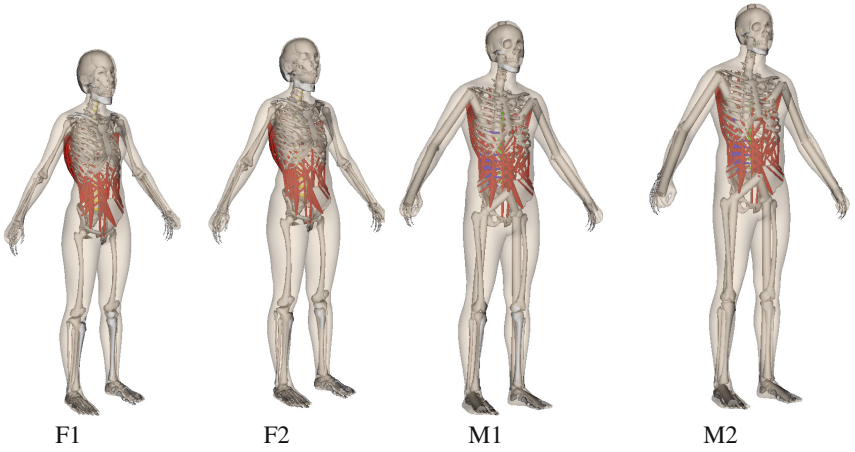

Fig. 1. The four generated models with the musculoskeletal lumbar model shown together with the 3D mesh model.

with specific desired body measurements, the automated process described by Zhou et al. [3] scaled the body habitus, skeletal linkage system and the lumbar vertebral characteristics to those associated dimensions. Male model muscle strength was optimized based on reported lower spinal moment generation capacity of the specified gender associated anthropometry [4–6]. Female model muscle strength was scaled relative to the male model based on Marras et al. [7]. Two female (stature/body mass: F1:1.60 m/49.9 kg and F2:1.68 m/63.3 kg) and two male (stature/body mass: M1:1.78 m/81.5 kg and M2:1.89 m/97.7 kg) MSK models, Fig. 1, were generated for comparison simulation. In the development of this method, the original Christophy model was the basis for scaling but the muscle strength factors were also optimized.

Figure 2 compares the maximum isometric strength about the L3–L4 intervertebral joint for the four generated models.

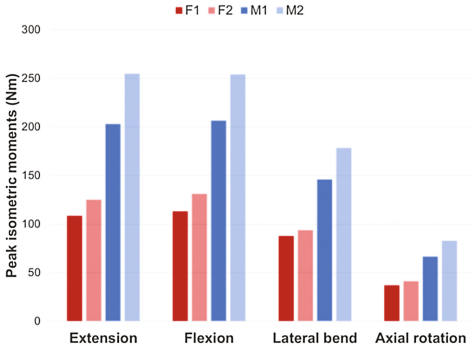

Fig. 2. Comparison of the maximum isometric moment about L3–L4 intervertebral joint for the four generated models.

Capacity – Muscle exertional capacity was predicted using a method reported by Zhou et al. [8]. This semi-empirical muscle force capacity model is an extension of a Hill-type muscle model and is capable of handling the full range of neural excitations (maximal or submaximal) and varying contractile conditions. This model builds on reported muscle fatigue model concepts [9–11] which classify muscle fibers into three mutual exclusive states: resting, activated, and fatigued states. The capacity value range was 0 to 1.

Pain score – A pain score was developed based on the metabolic requirements for muscle exertion and muscle nociceptor response to interstitial metabolites that estimated the potential for the onset of exertional muscle pain. The muscle metabolic model was linked to the musculoskeletal model to predict interstitial concentrations of ATP, Lactate and hydrogen ion (pH) based on muscle demand. The Bhargava et al. phenomenological metabolic model [12] was utilized and represented by linear combinations of different heat/work components further modeled as functions of time, physiological parameters (such as mass fractions of fibers), physical parameters (such as length, mass, etc.), and empirical constants (such as basal heat rates). The skeletal muscle energy consumption was supported by continuous supplies of ATP. The metabolic model predicted the extracellular pH and lactate concentration, but intracellular ATP does not diffuse across the cell membrane due to its molecular size. Rather, ATP is released into the interstitial space when the muscle contracts. Li et al. [13] demonstrated that during contraction tension, muscle releases ATP into the muscle interstitial space in an almost linear fashion related to tension force. A linear curve fit was performed relating the interstitial ATP concentration to the muscle force from this work, which produced a statistically significant ($p < 0.05$), fit with an $r^2 = 0.8$. The regression equation as determined was:

$$[\text{ATP}]\text{nM} = 111 + 36.6 * (\text{Force}) \tag{1}$$

The tension limit range was 0 to 53 N, which yielded an [ATP] from 78 to 1670 nM. The interstitial space concentrations of hydrogen ions, lactate and ATP accumulate and diminish over time, which gives a time course of pain development. Hydrogen ions are rapidly buffered back to a physiological pH and lactate leaves the interstitial space through diffusion into capillaries. However, there are many ways that ATP is utilized in the muscle interstitial space. The accumulation and utilization of ATP in the model was estimated through a general first-order response with a time constant of 200 s to approximate the combined effects of extracellular ATP half-life [14, 15], subjective pain response [16] and subjective pain duration [17].

A synergistic relationship has been demonstrated for subjective muscle pain response between hydrogen ions, ATP and Lactate, which was used to calculate a pain score [17, 18]. A response surface regression equation was fit to these subjective data as a function of their study pH, ATP and Lactate levels and is given below:

$$\begin{aligned}\text{Pain Score} = {} & -65.451 + 18.943(\text{pH}) + 0.001(\text{ATP}) + 0.007(\text{LAC}) - 1.365(\text{pH})^2 - 6.95\text{E}-08(\text{ATP})^2 \\ & + 4.256\text{E}-05(\text{LAC})^2 - 0.0001(\text{pH})(\text{ATP}) - 0.0008(\text{pH})(\text{LAC}) \\ & + 1.126\text{E}-06(\text{ATP})(\text{LAC})\end{aligned} \tag{2}$$

Where the final model $r^2 = 0.873$, ($p < 0.001$) and muscle interstitial values are: (pH) in pH units, (ATP) is the concentration of ATP in nM and (LAC) is the concentration of mM. The Pain Score range is limited to 0 to 1. The estimated pH, ATP and Lactate metabolite levels with respect to exercise level [17] were compared to the calculated pain score shown in Table 1.

Table 1. Major metabolite levels, exercise level and predicted pain score.

pH	ATP (nM)	Lactate (mM)	Exercise level	Pain score
7.4	300	1	Resting	0.06
7.3	400	4	Mild	0.22
7.2	500	10	Moderate	0.36
7.0	1000	15	High	0.64
6.8	2000	20	Very high	0.92
6.6	5000	50	Ischemic	1.0

2.1 Comparison of Anthropometric Model Performance

The four anthropometric models were compared using the Sorensen Test. Figure 3 shows the Sorensen test configuration [19] and an oblique view during simulation of the test.

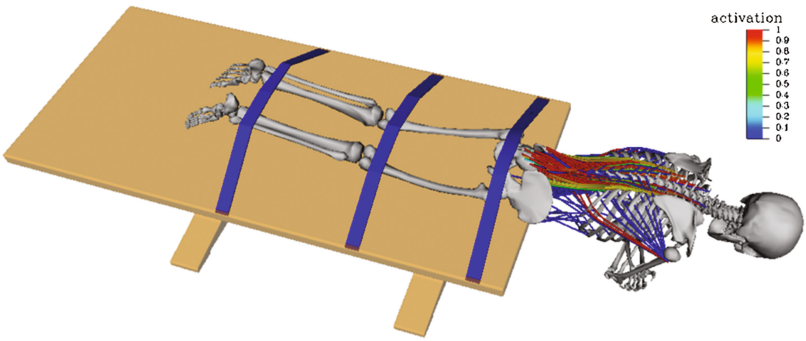

Fig. 3. Sorensen test simulation with muscle activation.

In the Sorensen test, the subject holds their unsupported torso in a horizontal position while the lower body is strapped to a table. The simulation duration was 300 s, approximately twice the normative test value. The simulation predicted muscle activation, forces, capacity, and a pain score along with joint reaction forces and moments at the lumbar functional spinal unit level.

3 Results

The muscle data results were compared across the anthropometric models for the left side. The left and right side muscle results were equivalent across all anthropometric models. Group results were average values across all fascicles within the longissimus thoracis pars lumborum (LTpL) and iliocostalis lumborum pars thoracis (ILpT). The comparisons of the LTpL and ILpT group average activation, force, capacity and pain score are shown in Figs. 4, 5, 6, and 7, respectively.

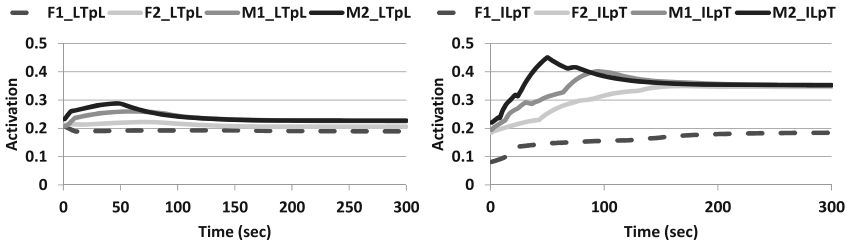

Fig. 4. Group average muscle activation comparisons.

The group average activation results in Fig. 4 show that the ILpT exhibits greater activation than the LTpL. The muscle activation is the fraction of available muscle force contraction employed. Initial activation followed model size variation with the largest model showing the highest activations. While the LTpL reaches asymptotic activation by approximately 100 s, the ILpT required approximately 150 s to reach an asymptote.

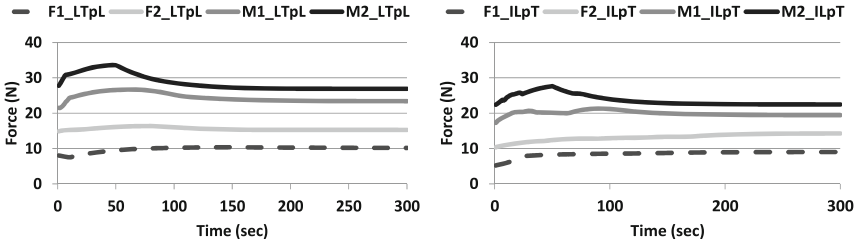

Fig. 5. Group average muscle force comparisons.

LTpL and ILpT group muscle average force comparisons are shown in Fig. 5. As the activation values show the fraction of full muscle contraction force, the actual force predictions show the LTpL generated higher forces compared to the ILpT. Again the force magnitudes are related to the anthropometric model size where the large male (M2) shows the higher forces followed by M1, F2, and F1.

Figure 6 shows the LIpT and LTpL average group capacities. The muscle capacity is an indicator of the muscle fatigue over time. The ILpT capacity approaches 0.75 for

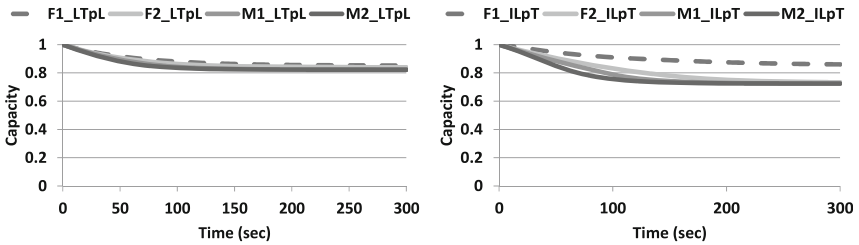

Fig. 6. Group average muscle capacity comparisons.

M2, M1 and F2, but the LTpL capacity is above 0.8 in all cases (lower activation). The ILpT capacity loss follows a body size relationship over the first 100–150 s, except for the F1 model, which shows a minimal capacity decrease.

The LTpL and ILpT average group pain scores are shown in Fig. 7. The ILpT and LTpL exhibit an increase in pain score over time. The pain score time histories show a body size relationship where M2 shows the highest score followed by M1, F2 and then F1. Pain scores of approximately 0.3 would be consistent with just below moderate exercise exertion.

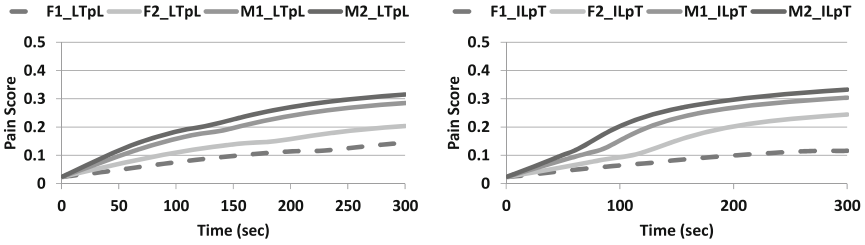

Fig. 7. Group pain score comparisons for erector spinae muscles.

3.1 Intervertebral Disc Joint Reaction Data

The maximum reaction forces and moments for the intervertebral disc (IVD) joints of the lumbar spine are shown in Figs. 8, 9, and 10. The forces in the x direction (back to front, shear), Fx, are shown by vertebral level and anthropometric model in Fig. 8. The highest shear forces are seen at the L2_L3 level followed by L3_L4.

The reaction shear forces at L4_L5, L3_L4, L2_L3, and L1_L2 follow a body size relationship where M2 exhibits the highest force followed by M1, F2 and then F1. The reaction shear forces at L5_S1 follow the same size relationship except for F1 and F2, which are approximately the same shear force. While the Fx time history (not shown) peaks at approximately 60 s for M2 and M1 at all vertebral levels, this peaking response is not seen for either female model.

The forces in the y direction (vertical, compression), Fy, are shown by vertebral level and anthropometric model in Fig. 9. The highest compressive forces were seen at L5_S1 followed by L4_L5 with the other levels close behind showing a similar response.

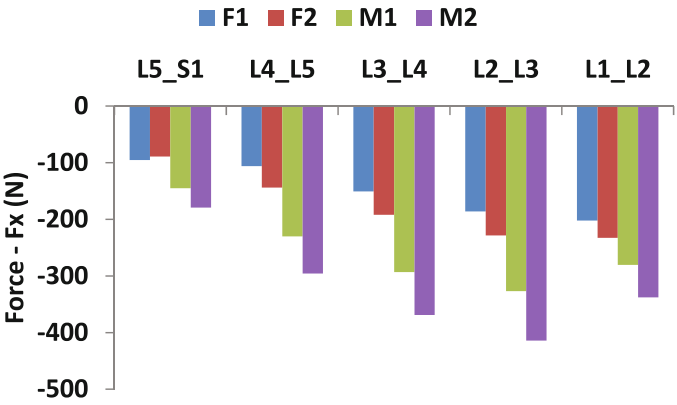

Fig. 8. IVD reaction force Fx by vertebral level and anthropometric model.

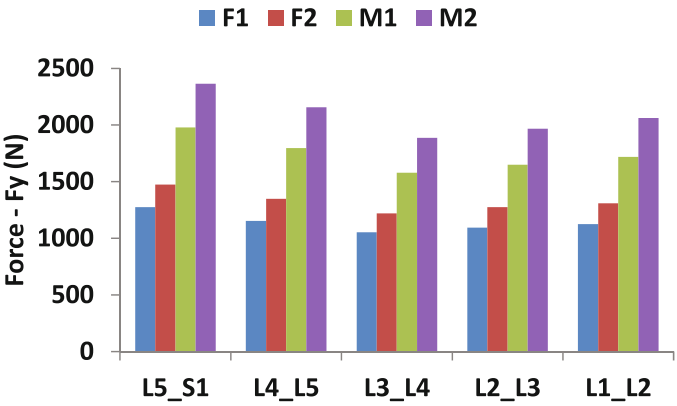

Fig. 9. IVD reaction force Fy by vertebral level and anthropometric model.

A body size relationship was observed with respect to compressive forces. The same force time history peaking response was observed in compression (not shown) in the male models but not in the female models.

The forces in the z direction (lateral shear), Fz, as well as the lateral and axial moments, Mx and My, were extremely small owning to the symmetry of the simulated task and the optimized model performance and were not reported.

The reaction moment about the z direction (pitch), Mz, are shown by vertebral level and anthropometric model in Fig. 10. The highest moments are seen at L5_S1, which are almost double of that at the next highest vertebral level L4_L5. The moments by model show a decrease from L3_L4 to L2_l3 but then and increase from L2_L3 to L1_l2, likely due to the maintenance of the lumbar lordosis by the spinal model constraint.

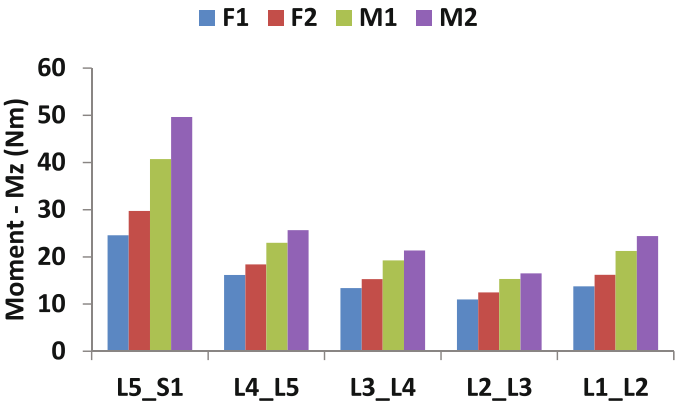

Fig. 10. IVD reaction moment Mz by vertebral level and anthropometric model.

4 Discussion and Conclusions

The anthropometric MSK model generation process created specific variants that were not simply proportionally scaled versions of the reference MSK model in dimension. The predicted results indicate the importance of strength scaling when generating a scaled anthropomorphic model. The differences between the anthropometric models results are related to the variation in back muscle strength as well as the torso mass and moment arm variation by anthropometry. The smallest MSK model (F1) results were notably lower than the other models but studies indicate that females exhibit significantly longer holding times than males [19]. The IVD reaction forces and moments for the Sorensen test follow a body size relationship. Given the nature of the simulated task, sagittal plane moments were significant while minimal transverse or coronal plane moments were observed. While lateral forces were minimal, significant shear and compressive forces by level and significant sagittal plane (extension) moments were observed. Variations by vertebral level for reaction compression and shear as well as sagittal plane moment follow a pattern with change noted in the L3_L4 to L2_L3 region where a parameter reaches a peak or a valley in this region. This pattern is likely due to lumbar lordosis and the model's maintenance of lordosis by the spinal model constraint. The MSK generation approach and predicted results will be further validated through graded Sorensen tests with human volunteers.

References

1. Gordon, C.C., Blackwell, C., Bradtmiller, B., Parham, J., Barrientos, P., Paquette, S., Corner, B., Carson, J., Venezia, J., Rockwell, B., Mucher, M., Kristensen, S.: 2012 Anthropometric Survey of U.S. Army Personnel: Methods and Summary Statistics. NATICK TR-15/007 (2014)

2. Christophy, M., Faruk Senan, N., Lotz, J., O'Reilly, O.: A Musculoskeletal model for the lumbar spine. Biomech. Model. Mechanobiol. **11**, 19–34 (2012)
3. Zhou, X., Sun, K., Roos, P., Li, P., Corner, B.: Anthropometry model generation based on ANSUR II database. Int. J. Digit. Hum. **1**(4), 321–343 (2016)
4. Kumar, S.: Isolated planar trunk strengths measurement in normals: part III — results and database. Int. J. Ind. Ergon. **17**, 103–111 (1996)
5. Kumar, S., Dufresne, R.M., Garand, D.: Effect of body posture on isometric torque-producing capability of the back. Int. J. Ind. Ergon. **7**, 53–62 (1991)
6. Larivière, C., Gravel, D., Gagnon, D., Bertrand Arsenault, A., Loisel, P., Lepage, Y.: Back strength cannot be predicted accurately from anthropometric measures in subjects with and without chronic low back pain. Clin. Biomech. **18**, 473–479 (2003)
7. Marras, W.S., Jorgensen, M.J., Granata, K.P., Wiand, B.: Female and male trunk geometry: Size and prediction of the spine loading trunk muscles derived from MRI. Clin. Biomech. **16**, 38–46 (2001)
8. Zhou, X., Whitley, P., Przekwas, A.: A musculoskeletal fatigue model for prediction of aviator neck manoeuvring loadings. Int. J. Hum. Factors Model. Simul. **4**, 191–219 (2014)
9. Liu, J.Z., Brown, R.W., Yue, G.H.: A dynamical model of muscle activation, fatigue, and recovery. Biophys. J. **82**, 2344–2359 (2002)
10. Xia, T., Frey Law, L.A.: A theoretical approach for modeling peripheral muscle fatigue and recovery. J. Biomech. **41**, 3046–3052 (2008)
11. Frey-Law, L.A., Looft, J., Heitsman, J.: A three-compartment muscle fatigue model accurately predicts joint-specific maximum endurance times for sustained isometric tasks. J. Biomech. **45**, 1803–1808 (2013)
12. Bhargava, L.J., Pandy, M.G., Anderson, F.C.: A phenomenological model for estimating metabolic energy consumption in muscle contraction. J. Biomech. **37**, 81–88 (2004)
13. Li, J., King, N.C., Sinoway, L.I.: ATP concentrations and muscle tension increase linearly with muscle contraction. J. Appl. Physiol. **95**, 577–583 (2003)
14. Gündüz, D., Kasseckert, S.A., Härtel, F.V., Aslam, M., Abdallah, Y., Schäfer, M., Piper, H.M., Noll, T., Schäfer, C.: Accumulation of extracellular ATP protects against acute reperfusion injury in rat heart endothelial cells. Cardiovasc. Res. **71**, 764–773 (2006)
15. Clemens, M.G., Forrester, T.: Appearance of adenosine triphosphate in the coronary sinus effluent from isolated working rat heart in response to hypoxia. J. Physiol. **312**, 143–158 (1981)
16. Arendt-nielsen, L., Graven-nielsen, T.: Muscle pain: sensory implications and interaction. Clin. J. Pain **24**, 291–298 (2008)
17. Pollak, K.A., Swenson, J.D., Vanhaitsma, T.A., Hughen, R.W., Jo, D., White, A.T., Light, K.C., Schweinhardt, P., Amann, M., Light, A.R.: Exogenously applied muscle metabolites synergistically evoke sensations of muscle fatigue and pain in human subjects. Exp. Physiol. **99**, 368–380 (2014)
18. Light, A.R., Hughen, R.W., Zhang, J., Rainier, J., Liu, Z., Lee, J.: Dorsal root ganglion neurons innervating skeletal muscle respond to physiological combinations of protons, ATP, and lactate mediated by ASIC, P2X, and TRPV1. J. Neurophysiol. **100**, 1184–1201 (2008)
19. Demoulin, C., Vanderthommen, M., Duysens, C., Crielaard, J.-M.: Spinal muscle evaluation using the Sorensen test: a critical appraisal of the literature. Joint Bone Spine **73**, 43–50 (2006)

Enhancing User Identification During Reading by Applying Content-Based Text Analysis to Eye-Movement Patterns

Akram Bayat[1(✉)], Amir Hossein Bayat[2], and Marc Pomplun[1]

[1] University of Massachusetts Boston, Boston, MA, USA
{akram, marc}@cs.umb.edu
[2] Iran University of Science and Technology, Tehran, Iran
a_bayat@comp.iust.ac.ir

Abstract. In this study, we introduce a brand new idea for a user identification task that benefits from an effective fusion scheme that combines eye movement with syntactic and semantic word relationships in a text. We perform eye-movement recordings during reading because reading process is an instance of high usability as a very common activity. Currently there are very few studies based on eye-movement based identification during reading because of the complex effects of text content on eye-movement behavior. Our proposed method overcomes this drawback by creating a dynamic model for which we register text input and the model's answer to that input. For this purpose, a vector space representation of text content is interpolated based on fixation duration patterns during reading, leading to high accuracy of identification (an overall accuracy of 98.43%) along with robustness by eliminating the use of common eye-movement characteristics that are sensitive to various factors unrelated to reader identification.

Keywords: Eye movement · Semantic analysis · Word2vec · Word vector representation

1 Introduction

The concept of using eye movements for biometric identification is very new. Unlike other identification methods, eye-movement based identification uses information, which is produced mostly by an individual's brain and is virtually impossible to imitate. This property makes it ideal for the purpose of biometric identification with various applications such as personal security, access restriction, and personalized interfaces.

The human eye exhibit basic types of eye movements in response to internal and external stimuli [1]. Extracting statistical features of those eye-movements can be used in biometric techniques that are actively developing these days.

In the current paper, we propose a new identification technique that combines eye-movement data obtained during the reading and semantic content of the text. This technique could enhance the stability and accuracy of a model that is capable of identifying a user by implementing various learning techniques. Capturing eye-movement during reading is desirable because of presenting an instance of high usability, as it is a

D.N. Cassenti (ed.), *Advances in Human Factors in Simulation and Modeling*,
Advances in Intelligent Systems and Computing 591, DOI 10.1007/978-3-319-60591-3_43

common activity which is familiar to everyone. In addition, reading activity provides the possibility of performing a covert identification. On the other hand, text content influences reading process that makes it very challenging to obtain invariant features from eye-movement data. In a study by Bayat and Pomplun [2], it has been shown that how various eye movement indices are affected by text characteristics. We address this issue by fusing text information into eye movement data. The reason is that we need to account for the different text content and characteristics. Therefore, we not only perform our identification algorithm in a variety of text contents and characteristics, but also fuse semantic content of text with eye movement data.

Section 2 describes the experiment design and data collection. An overview of eye-movement behavior in reading, word vector representations, information fusion and classification results are given in Sect. 3. We conclude the paper in Sect. 4.

2 Experimental Setup

In this section, the experiment that was used to capture users' eye-movement data while reading a set of six passages is described. We use the raw data set that has previously been collected for the work by Attar and colleagues [3, 4]. Forty native English speakers with an average age of 20.4 (SD = 5.35) years participated in the experiment. Each subject read the six passages which were identical for all subjects. Every passage was presented to subjects on three screens in which the background colors were gray and the font was black.

The passages that were used for data collection contained various general topics (food, science, and health) and were taken from the Washington Post News. Each passage had between 230–240 words. Furthermore, these passages exhibit a various range of difficulty levels (plain English, Fairly difficult, difficult) that were previously computed by the Flesch readability ease score algorithm [2]. Figure 1 illustrates the topics and difficulty levels of passages were used in this experiment.

3 Methodology

In this section, we describe the feature extraction method from eye-movement data and text data that we use for building a model for identification. We present our technique for information fusion from eye movement data and semantic text content that leads to obtaining invariant features of eye movement data.

3.1 Eye Movement in Reading

Visual fixation is defined as the act of maintaining of the gaze on a single location. A quick, simultaneous movement of both eyes between two phases of fixations is referred to a saccade [5]. A regular eye movement alternates between saccades and fixations. During reading, the eye-movement guidance system directs the gaze to a location near a word in order to identify that word. Figure 2 shows a sample visual fixation trajectory during reading a text by a sample subject.

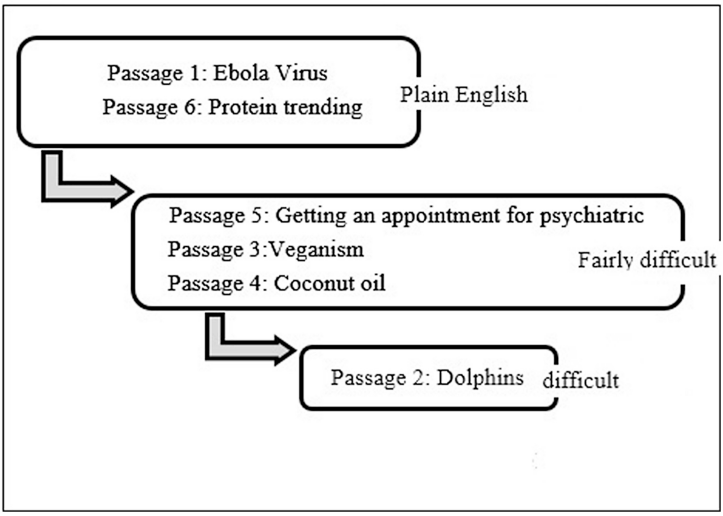

Fig. 1. Topics and difficulty levels of Passages that were used for data collection. For example, the passage 2, "Dolphins", is interpreted as a difficult passage to read by using the Flesch readability ease score algorithm.

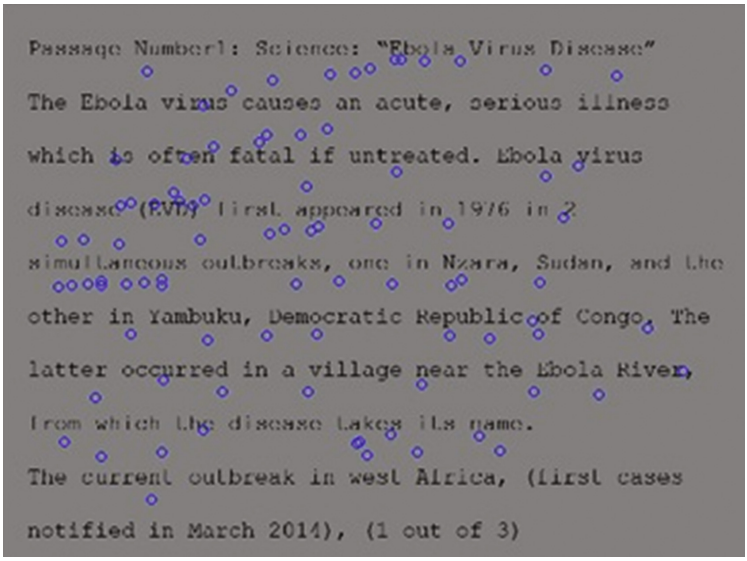

Fig. 2. Fixation positions for a sample subject during reading a sample text. Circles correspond to the fixations.

The previous studies on eye movements during reading have reported the tendency for readers to direct their gaze to the centers of words or slightly left of them for quick identification [6]. However, the distribution of initial fixation locations in a word

depends on many factors related to the visual system and characteristics of text (e.g., length of the word and the duration of prior fixation). In many instances, fixations are located at different distances to a word, which we refer to as a landing site [7]. The landing site could range from the very beginning of the word to its end. Several studies have shown the influence of the eye fixation duration and location on the identification of words during reading [8, 9]. In this work, we consider a bounding box around each word as a proper landing site of fixations for that word. In this study, the number of fixations and the mean duration of fixations in each bounding box (landing site) account for eye movement data for that word.

Figure 3 shows the mean fixation durations (per 20 words) during reading a sample screen for two different subjects. Instead of representing the mean fixation duration in each bounding box, we smooth it by computing the mean fixation duration for 20 words in order to leave out noise and discover the important differences. A significant difference in the mean fixation durations in each bounding box between two different subjects confirms the importance of using the mean fixation duration to distinguish two different subjects.

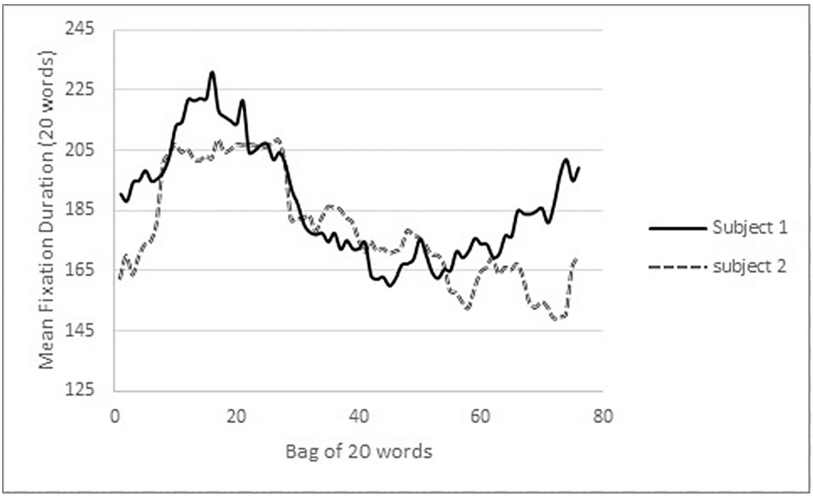

Fig. 3. The mean fixation durations in each bounding box around a word in a sample screen for two different subjects. In order to smooth the data, we take an average of the mean fixation duration over a bag of 20 words on the screen.

3.2 Word Vector Representations

Representing words as unique discrete encoded symbols for training statistical models has been traditionally used in Natural language processing systems. An example is the popular N-gram model used for statistical language modeling. These encodings are arbitrary, and provide no useful information to the system regarding any possible relationships between the individual symbols [10]. In this technique of representing the words, the model share very little of what it has learned about contextually similar

words. For example ‘cattle’ and ‘sheep’ are both domestic animals, four legged, etc., which are represented with no notion of similarity between them. In addition, representing words as unique, discrete symbols leads to data sparsity, needs more data in order to successfully train statistical models. Using distributed representations of words (vector representations) can overcome some of these drawbacks.

Vector space models represent words in a continuous vector space where semantically similar words are assigned to nearby points (words that appear in the same contexts share semantic meaning). By performing simple algebraic operations on the words vectors, for example, vector (“King”) - vector(“Man”) + vector(“Woman”) results in a vector that is closest to the vector representation of the word Queen [11].

Recently, neural-network based word embedding models such as Word2vec models have received an increasing attention. The word2vec software has created by Mikolov and colleagues [12] that provides state-of-the-art vector space word representations. In this work, the vector representations of words in three screens of all six passages are computed using the skip-gram model [12]. This pre-trained Google News corpus word vector model consists of 3 million 300-dimensional English word vectors. Using this vector space model, each word is mapped into a 300-dimensional vector. In this way, we obtain the eighteen, 300-dimesional vectors corresponding to the eighteen screens of six passages. We visualize all 300-dimensional vectors corresponding to all words in all six passages using t-Distributed Stochastic Neighbor Embedding (t-SNE) [13]. The t-SNE is a technique for dimensionality reduction that we use to visualize high-dimensional word vectors (Fig. 4).

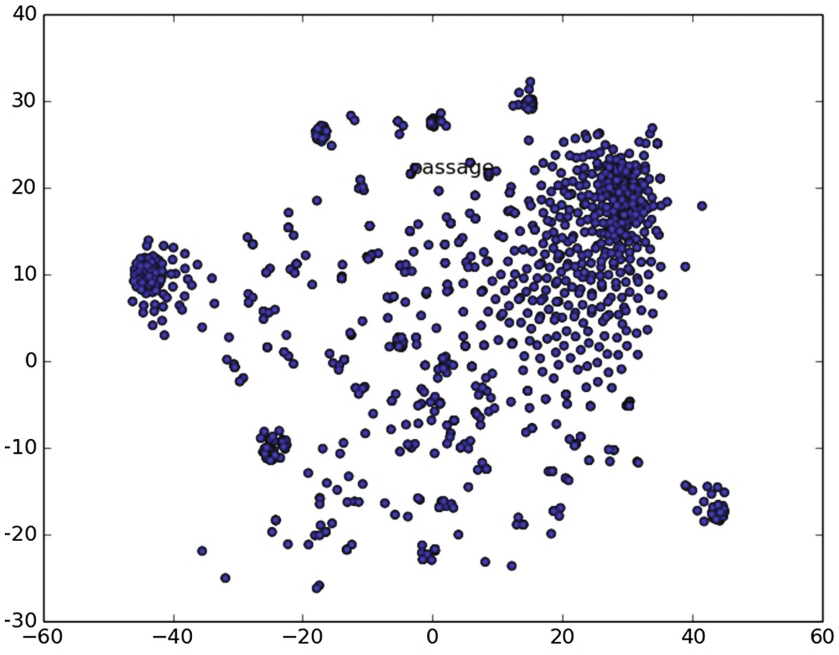

Fig. 4. This view depicts the embedding of all words in six passages (passage 1 through 6 in Fig. 1) where there is a word associated with a data point.

3.3 Information Fusion

In this Section, we introduce our novel and effective fusion scheme that combines fixation patterns with syntactic and semantic word relationships in a text. For this, a weight vector representing eye-movement variables is interpolated in a vector representation of words in each screen of a passage.

We define a weight vector, W_w, as the normalized fixation duration for each word as follows:

$$W_w = \frac{\sum_{i=1}^{i=k} \text{Fixation\_Duration}_i}{\max_{i<N} \text{Fixation\_Duration}_i}. \quad (1)$$

Where $\text{Fixation\_Duration}_i$ is the total duration of k fixations that occur in the landing site of a given word w in each screen with N words. This leads to a fixation weight vector, $\{W_1, \ldots, W_N\}$, for each screen. This vector can be efficiently multiplied by word vector representations in each screen. Our final feature vector, F_S, is the average of all weighted word representations (v) in each screen:

$$F_S = \frac{1}{N} \sum_{i=1}^{i=N} W_i v_i. \quad (2)$$

This feature vector similarly is measured in all six passages and for each subject. In this way, for each subject and for a set of six passages we have a set of eighteen, 300-dimensional feature vector.

Each subject's data is separated to train and test data (3–1 train/test splits) in three different ways. Various classifiers are trained and tested on the set of extracted features. We evaluate the performance of these classifiers using their accuracies. We combine two best individual classifiers to obtain a better result using the average of the probabilities [14]. By combining Logistic and Multilayer Perceptron as our classification algorithms, we reach an overall accuracy of 98.43%.

4 Conclusion

This work presents a novel technique to identify unique individual readers based on an effective fusion scheme that combines eye movement patterns with semantic contents in a text. Previous eye-movement identification methods for reading used intricate eye-movement variables that are sensitive to various factors unrelated to reader identification. In this study, we use only fixation duration patterns for each individual word and combine it with syntactic and semantic representation of that word. The identification result suggests that the extracted features using this technique differ systematically across individuals, which leads to high and consistent identification accuracy.

References

1. Holland, C.D., Komogortsev, O.V.: Biometric verification via complex eye movements: the effects of environment and stimulus. In: 2012 IEEE Fifth International Conference on Biometrics: Theory, Applications and Systems (BTAS), pp. 39–46. IEEE (2012)
2. Bayat, A., Pomplun, M.: The influence of text difficulty level and topic on eye-movement behavior and pupil size during reading. In: 2016 2nd International Conference of Signal Processing and Intelligent Systems (ICSPIS), Tehran, Iran, 2016, pp. 1–5. IEEE (2016)
3. Attar, N., Wu, C., Sia, D., Pomplun, M.: A deeper understanding of optimal viewing position using eye fixations and character recognition on text - viewing and reading tasks. In: ACM ETRA: 2016 Symposium on Eye Tracking Research & Applications, pp. 209–212. ACM ETRA (2016)
4. Attar, N., Fomenky, P., Ding W., Pomplun, M.: Improving cognitive load level measurement through preprocessing psychological data by random subspace method. In: IEEE 2nd International Conference on Human Computer Interactions (ICHCI 2016), pp. 1–6 (2014)
5. Saccade: Wikipedia. https://en.wikipedia.org/wiki/Saccade
6. Just, M.A., Carpenter, P.A.: A theory of reading: from eye fixations to comprehension. Psychol. Rev. **87**(4), 329 (1980)
7. Vitu, F., McConkie, G.W., Kerr, P., O'Regan, J.K.: Fixation location effects on fixation durations during reading: an inverted optimal viewing position effect. Vis. Res. **41**(25), 3513–3533 (2001)
8. Folk, J.R., Eskenazi, M.A.: Eye movement behavior and individual differences in word identification during reading. Eye-Track. Technol. Appl. Educ. Res. 66 (2016)
9. McConkie, G.W., Rayner, K.: The span of the effective stimulus during a fixation in reading. Atten. Percept. Psychophys. **17**(6), 578–586 (1975)
10. Vector representations of words. https://github.com/Russell91/tensorflow-1/blob/master/tensorflow/g3doc/tutorials/word2vec/index.md
11. Le, Q.V., Mikolov, T.: Distributed representations of sentences and documents. ICML **14**, 1188–1196 (2014)
12. Mikolov, T., Sutskever, I., Chen, K., Corrado, G.S., Dean, J.: Distributed representations of words and phrases and their compositionality. In: Advances in Neural Information Processing Systems, pp. 3111–3119 (2013)
13. Maaten, L.V.D., Hinton, G.: Visualizing data using t-SNE. J. Mach. Learn. Res. **9**(Nov), 2579–2605 (2008)
14. Bayat, A., Pomplun, M., Tran, D.A.: A study on human activity recognition using accelerometer data from smartphones. Procedia Comput. Sci. **34**, 450–457 (2014)

Effects of Socks and Shoes on Normal Foot Skin Temperature

Ameersing Luximon[1(✉)], Balasankar Ganesan[1,2], and Abida Younus[1]

[1] Institute of Textiles and Clothing, The Hong Kong Polytechnic University, Hong Kong, China
ameersing.luximon@polyu.edu.hk
[2] Department of FEIT, University of Technology Sydney, Ultimo, NSW, Australia

Abstract. The skin is the major organ of integumentary system of human body and helps to maintain the body temperature, excretes the waste through sweating, protects deepest structures of the human body, and prevent from various problems such as water loss, infection. However, excessive sweating leads to infection in human body especially in the foot such as dermatophyte infection. This study aimed to investigate the foot skin temperature and humidity after wearing socks with shoes. It is a pre-post experimental design study. Ten subjects were selected for this study by convenience sampling methods. In this experiments, humidity and temperature, infrared images were recorded at baseline and post experiment. For this experiment, Infrared camera, HC 520 IN/OUT Temperature/humidity, and the thermometer were used as outcome measurement and the total duration of pre and post-session consists of 3 h. The results revealed that the foot skin temperature was slightly increased in the left foot: 97.02 (mn), 2.51 (SD). Thus, there was no difference observed in temperature changes. However, humidity level increased in socks with shoes experiment in the post-experiment results. At the same time, we observed in the infrared thermal image analysis that there were physiological changes and post-test temperature changes on the skin of foot. In conclusion, this study revealed that socks with shoes are altered the humidity and foot skin temperature.

Keywords: Socks · Foot · Foot skin temperature · Thermal foot · Infrared thermal images

1 Introduction

The skin is one of the largest systems of the human body and it is accounted for 15% of total human body weight. It consists of three layers. The outermost layer is called as epidermis, middle layer as dermis, and the innermost layers are subcutaneous tissue as shown in Fig. 1. The human body temperature is regulated by the autonomic nervous system through sweating, and passively (behavioral) by adjusting room temperature, adding or removing clothes [1]. Skin thickness will be varied from one part of the body place to another body parts. It is also based on the location of body parts of the skin. Generally, the plantar side of foot and hand has a higher thickness of skin is about three to four millimeters [2].

D.N. Cassenti (ed.), *Advances in Human Factors in Simulation and Modeling*,
Advances in Intelligent Systems and Computing 591, DOI 10.1007/978-3-319-60591-3_44

In the human body, the sweating glands can be divided into two types: Apocrine and Eccrine gland. The heat dissipation occurs mainly through evaporation of sweating, and it is mostly regulated by eccrine sweating gland [3, 4]. There is approximately 1.6 to 4 million sweating gland present in the human body [4]. Eccrine glands are mostly present in the forehead, the palm of the hand and sole of the foot. Eccrine gland maintains the thermoregulation of the body through evaporation of sweating. Excessive heat loss will be critical to human survival in the hot environment. It increases the skin temperature and sweat rate leads to excessive blood flow. There are the following physiological body heat mechanisms proposed to maintain or adapt the body temperature in various environmental thermal regulations: vasomotor regulation and sweating [5]. Sometimes, excessive sweating on the foot leads to severe health problems such as tinea pedis. Wearing tight footwear and socks is also one the reason for developing tinea pedis among the age group between 20–50 years. Some of the clothing materials are inducing high temperature in our body, even though, the outside of the temperature and humidity is low [6]. It will alter the core temperature of the human body when the presence of high temperature in the extremities [7]. Therefore, fabrics and clothing are also having the important role in maintaining the thermal regulation of the human body. Some of the previous studies focused on health-related socks such as diabetic socks [8]; compressive socks [9]; non-slip socks for elderly population to prevent the falls [10]. Generally, cotton socks have been used to prevent the excessive sweating and to avoid foot disease such as fungal infections [17]. In clothing research, most of the studies have been focused on other body parts of cloths except socks and foot. However, a sock can be altering the core body temperature due to changes in skin blood perfusion at the foot [11]. However, few kinds of literature reported that sock is the one of cause for developing tinea pedis [12]. Therefore, this study tried to investigate the effects socks with shoes on skin temperature, humidity and blood flow changes in the foot.

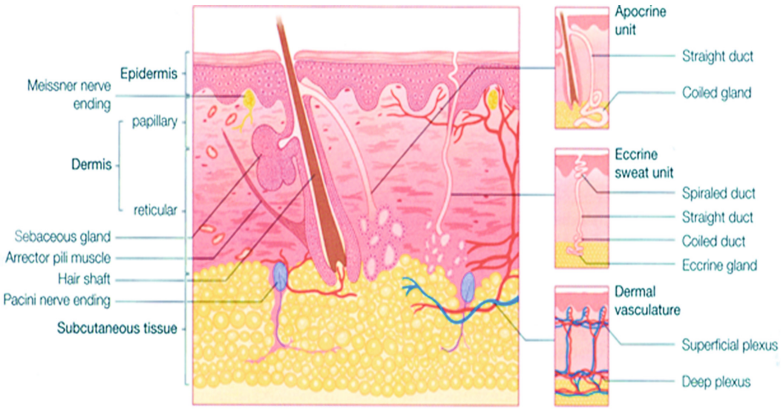

Fig. 1. Skin structure (James et al. [18], adapted and modified)

2 Methods

2.1 Participants

There are ten subjects with an age range between 20–45 years old were selected for this study. All participants were in good health condition. Demographic data of all subjects such as age, gender, health condition, occupation, and educational history were collected and recorded. There were no foot abnormalities or foot infections observed in any of the participants. Informed consent form was obtained from each subject before start the experiment procedures.

2.2 Equipment

Nowadays, Infrared camera thermography system (FLIR Systems) has been used in the medical and allied health field to detect or to diagnose the various health problems such as skin problems, orthopedic or musculoskeletal disorders, neurological related disorders, vascular problems, kidney related disorders, fever, and breast cancer [13–16]. It is considered as non-invasive and non- radiation methods, which is used to measure the skin temperature of the human body. In this study, we used this equipment to measure the baseline score of foot skin temperature and post experiments (after the subject worn the socks for 3 h). The HC 520 IN/OUT Temperature/humidity meter used to measure the humidity inside the foot after wearing the socks. Also, the thermometer was used to measure the foot skin temperature at the baseline and after 3 h of the experiment session.

2.3 Procedures

The first step of this experiment study was conducted with an infrared camera (IR) to find the physiological changes of the foot (Fig. 2c). The IR camera was in fixed into stable position in 45° angle. After that, the subjects were asked to keep their feet in the different position: Anterior, posterior, medial and lateral position. The investigator captured infrared images of the medial, anterior, posterior and lateral position of right and left foot with IR camera system. The second steps of this experiment, all participants were instructed to wear the socks. Temperature and humidity were recorded at the foot with socks. The HC 520 IN/OUT- temperature/humidity meter devices were used to measure the humidity and the temperature (Fig. 2a and b). In addition, all experiments were recorded by taking photos. Then, all subjects were instructed to wear the shoes and wait for 3 h. After 3 h of the first session, temperature and humidity were recorded on both sides of the foot after removing the shoes. The baseline and post-experiment foot skin temperature and humidity of the subjects were recorded. After completing the pre and post experiment of the second session, IR images of were recorded again and stored into the computer for further analysis.

a)

b)

c)

Fig. 2. (a) Humidity/Temperature meter. (b) Thermometer. (c) Infrared camera

3 Statistical Analysis

Demographic characteristics of all subjects such as age, gender, and pre and post temperature mean, the standard deviation was calculated. Infrared data exported into the computer software and InfraTec's state-of-the-art IRBIS ® 3 thermography software package was used for further analysis of skin temperature changes.

4 Results

The details demographic characteristics of subjects such age, mean value, and standard deviation are shown in Table 1. The Table 2 shows the result of pre and post-temperature of this study. The results of pre and post humidity experiments are shown in Table 3. All participants mean age was 39.1 (mn), and the standard deviation

Table 1. Descriptive statistics results

Types/Exp.	Pre experiment			Post experiment	
	Age (m/sd)	Right foot (m/sd)	Left foot (m/sd)	Right foot (m/sd)	Left foot (m/sd)
	39.1 (9.79)				
Temperature		97.6 (1.47)	97.83 (1.65)	96.86 (2.06)	97.02 (2.51)
Humidity		60.2 (9.36)	59.5 (9.3)	75.00 (2.82)	75.00 (2.49)

Table 2. Results of temperature pre and post experiment

Subject	Age	Pre experiment-right foot (F)	Pre experiment-left foot	Post experiment-right foot	Post experiment-left foot
1	37	99.0	99.0	96.0	96.0
2	32	97.0	97.0	94.0	94.0
3	35	100	100	99.0	99.0
4	55	94.6	94.6	94.0	94.1
5	56	96.4	96.4	96.0	96.0
6	27	98.0	98.4	98.0	98.0
7	37	97.0	97.0	95.3	94.2
8	32	98.0	98.0	97.8	98.7
9	35	98.0	99.9	99.4	101.2
10	45	98.0	98.0	99.1	99.0

Table 3. Results of pre and post humidity on the foot

Subject	Pre experiment-right foot	Pre experiment-left foot	Post experiment-right foot	Post experiment-left foot
1	81.0	80.0	81.0	79.0
2	59.0	52.0	78.0	79.0
3	60.0	60.0	73.0	79.0
4	58.0	58.0	75.0	75.0
5	57.0	56.0	77.0	77.0
6	72.0	72.0	73.0	73.0
7	51.0	52.0	74.0	74.0
8	55.0	57.0	73.0	73.0
9	51.0	52.0	74.0	74.0
10	58.0	56.0	72.0	72.0

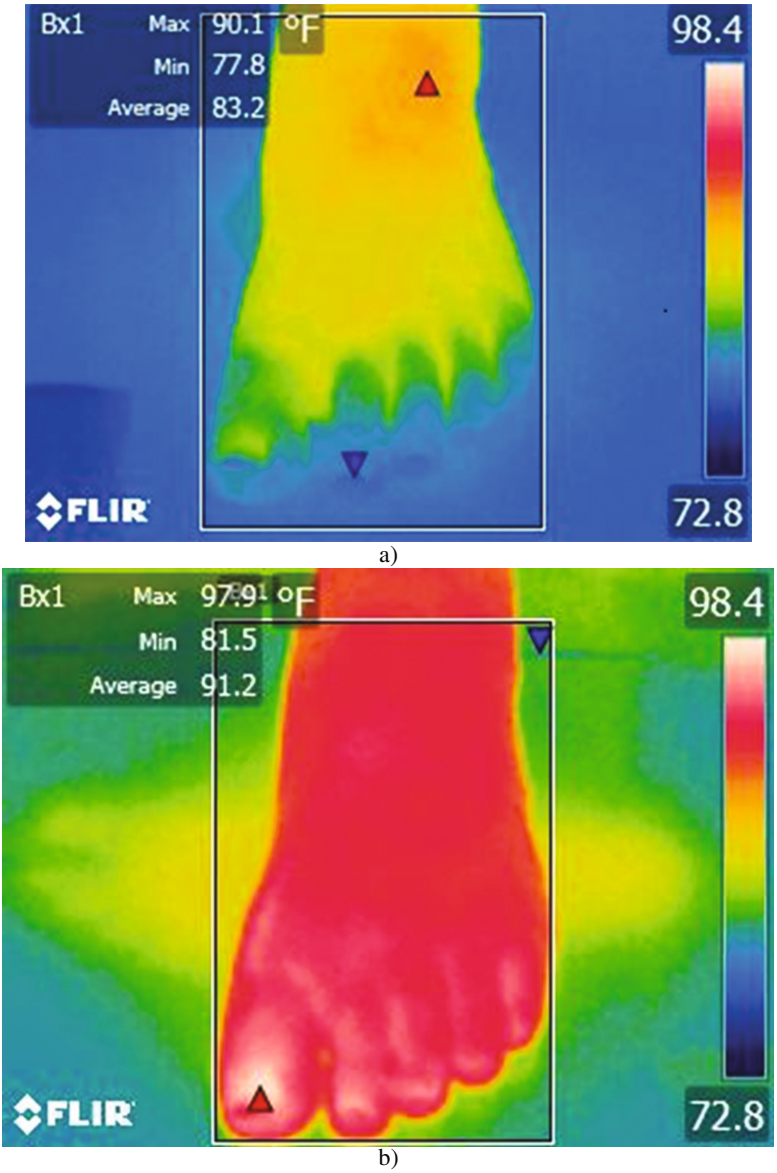

Fig. 3. Thermal pattern on skin before and after the socks experiment: (a) Thermal pattern before the socks experiment; (b) Thermal changes on the skin in the post-experiment evaluation

was 9.79 (SD). The results found that left foot had high temperature and humidity than right (97.02 ± 2.51). Most of the subjects had lower temperature level in the post assessment results than baseline score assessment. This study revealed that subject number 7 had lower foot skin temperature on the post-test result (right foot - 95.3 °F, left foot 94.5 °F) than baseline test (right foot - 97 °F, left foot - 97 °F), and subject

number one had lower (96 °F) in the post experiments than pre-experiment assessment of foot skin temperature (right foot - 99 °F, left foot - 99 °F). Only subject 9 and subject 10 had higher temperature than bassline scores: On subject 9, the temperature level increased from 98 °F to 99.4 F on the right foot and 99.9 to 101.2 increased at left foot. On subject number 10, the baseline score of right foot and left foot was same level (99 °F), and the foot skin temperature increased up to 99.1° at the right foot and 99 °F at the left foot. Although, we observed that not much differences of temperature level in the pre and post socks and shoes experiment results, we noticed that changes in the skin color and foot temperature in the infrared analysis. The results of infrared images showed that more redness represents the blood circulation or physiological changes of the foot after wearing socks and shoes continuously (Fig. 3a and b). It might alter the core temperature of the human body. For instance, the Fig. 3 shows the infrared images of the foot and temperature changes of foot, which shows the ankle and foot skin temperature on the anterior side and it was increased from 90.1 °F to 97.9 °F. Moreover, the infrared images shows the physiological changes (skin color) on the foot after post socks experiment. Also, the temperature changes on the varied from the different areas of the foot. For example, the subject number results showed that the maximum of temperature level was high in the ankle area of the foot and then post study experiment revealed that the temperature was increased on the great toe of the right side foot.

5 Discussion and Conclusion

The purpose of this study was to evaluate the temperature and humidity changes inside the foot, and to compare these parameters with socks with shoes. In this study, we found that mild differences between pre-post skin temperature and humidity changes. However, humidity increased more in the socks with shoe wearing population. Infrared images showed that more physiological changes on skin color and temperatures changes on the foot after post experiment. High temperature changes in the foot might be altering the core temperature of the body and mental stress level impact on feet health as well as productivity of the work. In addition, we observed based on the analysis of infrared thermal images that maximum of foot skin temperature increased in the area of toes on the post experiment and maximum of foot skin temperature on the ankle area. Therefore, selection of materials for socks and shoes are essential to provide appropriate comfort to the feet and reduce the risk of infection and sweating. Future study with using large sample size, with different types of socks materials and thermal infrared imaging study on the foot would be useful to find out the changes of the foot skin temperature and suggesting comfortable and healthy socks.

Acknowledgments. This study was supported by "The Hong Kong Polytechnic University", PolyU research project number: G-YBRJ, and RGC project number: PolyU 156603/16H.

References

1. Kanitakis, J.: Anatomy, histology and immunohistochemistry of normal human skin. Eur. J. Dermatol. **12**, 390–399 (2002)
2. McLafferty, E., Hendry, C.: The integumentary system: anatomy, physiology and function of skin. Nurs. Stand. **27**, 35–42 (2012)
3. Sato, K., Kang, W.H., Saga, K., Sato, K.T.: Biology of sweat glands and their disorders. I. Normal sweat gland function. J. Am. Acad. Dermatol. **20**, 537–563 (1989)
4. Shibasaki, M., Wilson, T.E., Crandall, C.G.: Neural control and mechanisms of eccrine sweating during heat stress and exercise. J. Appl. Physiol. (1985) **100**, 1692–1701 (2006)
5. Kolarsick, P.A.J., Kolarsick, M.A., Goodwin, C.: Anatomy and physiology of the skin. J. Dermatol. Nurses Assoc. **3**, 203–213 (2011)
6. Sullivan, P.J., Mekjavic, I.B.: Temperature and humidity within the clothing microenvironment. Aviat. Space Environ. Med. **63**, 186–192 (1992)
7. Jeong, W.S., Tokura, H.: Different thermal conditions of the extremities affect thermoregulation in clothed man. Eur. J. Appl. Physiol. Occup. Physiol. **67**, 481–485 (1993)
8. Feldman, C.B., Davis, E.D.: Sockwear recommendations for people with diabetes. Diabetes Spectr. **14**, 59–61 (2001)
9. Fletcher, L., Raab, S., Sanderson, S., Vargo, L.: Efficacy of compression socks to enhance recovery in distance athletes. Sport Art **2**, 15–18 (2014)
10. Hatton, A.L., Sturnieks, D.L., Lord, S.R., Lo, J.C., Menz, H.B., Menant, J.C.: Effects of nonslip socks on the gait patterns of older people when walking on a slippery surface. J. Am. Podiatr. Med. Assoc. **103**, 471–479 (2013)
11. Purvis, A.J., Tunstall, H.: Effects of sock type on foot skin temperature and thermal demand during exercise. Ergonomics **47**, 1657–1668 (2004)
12. Cohen, A.D., Wolak, A., Alkan, M., Shalev, R., Vardy, D.A.: Prevalence and risk factors for tinea pedis in Israeli soldiers. Int. J. Dermatol. **44**, 1002–1005 (2005)
13. Hildebrandt, C., Raschner, C., Ammer, K.: An overview of recent application of medical infrared thermography in sports medicine in Austria. Sensors **10**, 4700–4715 (2010)
14. Ishigaki, T., Ikeda, M., Asai, H., Sakuma, S.: Forehead back thermal ratio for the interpretation of infrared imaging of spinal cord lesions and other neurological disorders. Int. J. Therm. Sci. **3**, 101–107 (1989)
15. Gulevich, S.J., Conwell, T.D., Lane, J.M.D., Lockwood, B.M.D., Schwettmann, R.S., Rosenberg, N., Goldman, L.B.: Stress infrared telethermography is useful in the diagnosis of complex regional pain syndrome. Clin. J. Pain **13**, 50–59 (1997)
16. Ng, E.Y.K., Acharya, R.: Remote-sensing infrared thermography. IEEE Eng. Med. Biol. Mag. **28**, 76–83 (2009)
17. Richardson, M.D., Warnock, D.W.: Function Infection: Diagnosis and Management, 3rd edn. Blockwell publishing, Massachusetts (2008)
18. James, W.D., Berger, T.G., Elston, D.M.: Andrew's Diseases of the Skin: Clinical Dermatology, 10th edn. Elsevier Saunders, Philadelphia (2006)

Research on the Competency Model for the Professional Ship Crew

Zhen Liao(✉), Xin Wang(✉), Tuoyang Zhou, Shuang Liu, Gui Cai, and Lei Liu

CIMTEC, 70, Xueyuan South Road, Haidian District, Beijing 100081, China
lzhen24@sina.com, xinwang_thu@l26.com

Abstract. Ocean-going ship plays an important role for the transportation around the world, and the capability of ship crew is crucial for the safety of life and property because of the extremely unpredictable and dangerous circumstance in the ocean. However, the competency characteristics has not been well established, especially in our country. To address this issue, the competency of the ship crew was investigated under current situation in this research. Firstly, the job analysis and literature investigation were utilized to study the potential competency. Secondly, the ship crew were interviewed through the BEI method. At last, a competency questionnaire was designed and conducted for the selected ship crew. The results of questionnaire survey were analyzed trough statistical analysis, which tested the reliability of the competency model for the ship crew. Overall, the proposed model in this research provided a theoretical and technical basis for competency modeling for the ocean-going ship crew.

Keywords: Competency model · Ship crew · Behavioral event interview

1 Introduction

Ocean-going ship crew are usually faced with a series of challenges, such as unpredictable and complex sea condition, fatigue or even capability decline induced by long-time navigation. Although the automation technology was developed greatly for the last decades, it has to be the ship crew to make the final decision under lots of emergences scenarios, which could cause heavy loss of human life and property if the measures were improper or even completely wrong. While dealing with these emergences, the ship crew need to receive visual and auditory information continuously from all kinds of detection and display device equipped in the ship. All of the information were then analyzed and judged by the ship crew based on their knowledge, skills, abilities and experiences, after that the ship crew would make the decisions and give the instructions to the ship through the control device. During these processing procedures described above, the ship crew had to reply on their perceptual ability, cognitive ability and operational ability. In addition, their final performance would also be influenced by the emotion and pressure they experienced at that time. However, the efficient methods are not well investigated and established for the selection, assessment and training of ship crew right now. There are still lots of issues need to be addressed as follows:

D.N. Cassenti (ed.), *Advances in Human Factors in Simulation and Modeling*,
Advances in Intelligent Systems and Computing 591, DOI 10.1007/978-3-319-60591-3_45

- The key characteristics of professional ship crew, which can discriminate the excellent and the common crew, have not been identified by objective and quantitative methodology. At present, the physical examination and academic test occupy the most important part of the ship crew selection for many years. In contrast, the psychological quality and cognitive capability, which may be the more efficient predictors of the performance after a fixed-time training, did not get the attentions they deserve. The cause of this phenomenon is rooted in lack of systematic scientific methodology and model to guide the selection, such that the proper person can be chosen under the acceptable cost of time and economic.
- The comprehensive, systematic and quantitative methods has not be established for the professional ship crew evaluation. A person's quality cannot be assessed precisely if only relying on the academic test score and subjective experience of the administrators during a very short time. Nevertheless, the proper evaluation methods of lots of important characteristics, such as perceptual, cognitive and operational ability, have not been well designed and established for the ship crew in our country. It resulted in lack of effective technique support for selection, assessment and training of ship crew.

Therefore, it is essential to establish a competency model for the professional ship crew to address the issues mentioned above. In 1973, McClelland proposed the concept of "Competency" in the famous paper entitled with "Testing for Competency Rather than Intelligence" [1]. After that, the competency drew lots of attentions from both academic circle and company related to the human resource management around the world. The competency expresses the quality characteristics, such as knowledge, skills, ability, emotion and so on, which can distinguish people with different performance. As a result, the people should possess these characteristics to qualify them for the position. In addition, these characteristics are inherent, stable, and most importantly, can be measured by reliable methods.

Bennis took 90 most successful leaders in USA as research subjects and found out they all possessed four kinds of common characteristics [2]. Based on their 20-year research result, Spencer and Spencer identified four types of ability, which can distinguish the excellent entrepreneurs, and the ordinary based on a research of cross-culture comparison for 216 entrepreneurs. Then they utilized behavior event interview (BEI) to construct five general competency models, including professional, marketing personnel, community service personnel, administrative staff and entrepreneurs [3]. Losey proposed the competency equation, including intelligence, education, experience, quality and interests [4]. Rodriguez et al. compared the Multipurpose occupational system analysis inventory-close-ended (MOSAIC) with the traditional competency assessment tools, and showed that the MOSAIC have the higher economy and stronger generality [5]. Armstrong believed that organized learning played an important role in determining the outcome of the information technology based on the research related to relationship between information technology competency and the enterprise performance [6]. Reisdorff et al. came up with a quantitative method for the comprehensive competency evaluation [7]. Martone thought that the target performance management system based on the competency provided a general framework for improvement of consistency between employee's performance and the organizational

goal [8]. Weissmann also proposed a competency model for the successful leader that consisted of 16 competency characteristics, such as professional skill, honest, trustful, courage to bear and so on [9].

After 2000, lots of research in China focused on the competency gradually. Shi et al. tried to build competency model for the manager in communicating industry through BEI technique [10]. Wang and Chen designed a questionnaire titled with "the key behavior evaluation questionnaire for the management quality" to investigate competency elements of the manager (220 managers with different rank has been studied by the questionnaire), they found that the competency of managers with different rank need to be characterized by the models with different elements [11]. However, none of the methods or results introduced above can be applied to construct the competency model for the professional ship crew in China because of the particularity of the mission and environment (Most of the related research have focused on the competency of managers instead of professional personnel). Therefore it is necessary to study the competency of ship crew in order to support the selection, assessment and training of the ship crew.

2 General Idea and Framework

The basic idea of this research was as following. A complete set of competency characteristics were constructed based on literature investigation firstly. Then the competency set was utilized to design a questionnaire, which would be sent to the ship crew with different ranks. At last, the competency model for ship crew was built through the statistical analysis of the questionnaire survey. In addition, there were three fundamental hypotheses in this research as follows:

- The competency model for ship crew was considered as an integrated structure with different hierarchy and different dimensions;
- The proposed competency model in this research need to have the ability to distinguish the ship crews with different performance;
- The significance of each competency characteristics are different from each other, they could be described quantitatively by the weights.

It took eight steps to accomplish this research (see Fig. 1), which were:

Step 1. Literature investigation, this study investigated plenty of relevant literatures to collect the potential competency characteristics and to establish the general framework of this research.

Step 2. Behavior events interview, BET or in-depth interview, one of the most important method in competency research, is an open investigation technique of behavior retrospect. The ship crews were required to list the key incidents during work, including successful incidents, unsuccessful incidents and negative events. And then, the ship crews needed to describe the whole events in details, such as the cause, the related persons, the process, the result, the duration as well as the involved range. In addition, the ship crews were courage to narrate their thoughts at that time and to summary the successful experience and lessons of failure.

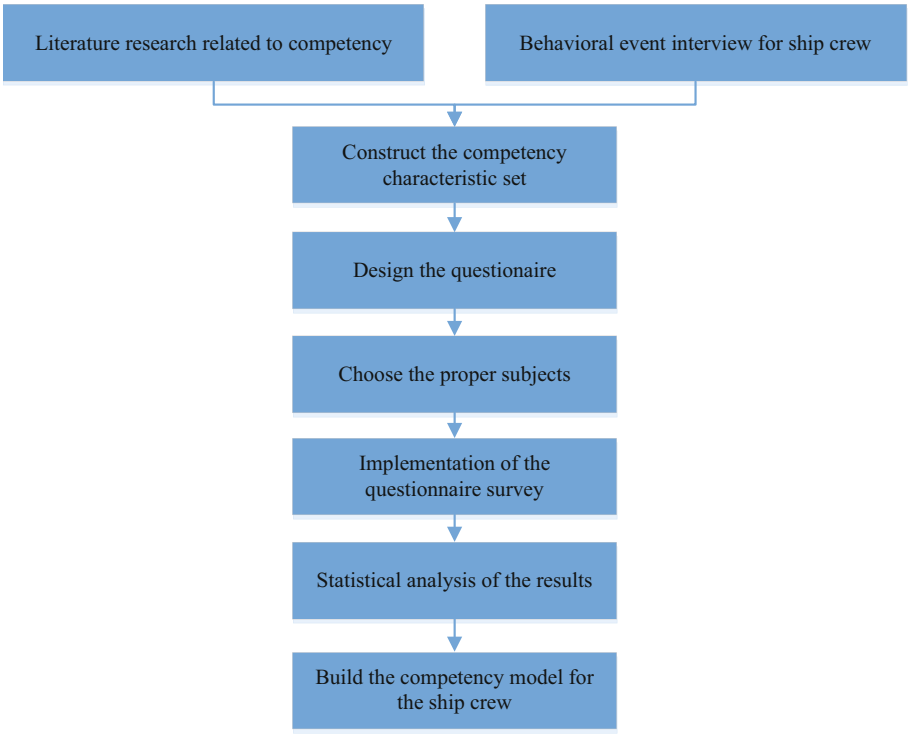

Fig. 1. Research route for the competency model of ship crew

Step 3 and 4. Based on the results of literature investigation and behavior events interview, the competency set has been constructed for ship crew, and then it was utilized to design the ship crew competency questionnaire.
Step 5 and 6. The subjects of the questionnaire investigation were selected according to five factors, which were age, length of service, length of working in ship, professional title, duty & post and educational level. The questionnaires were sent to the selected subjects and taken back for the statistical analysis.
Step 7 and 8. The result of questionnaire survey were analyzed through descriptive statistical analysis. After that, the competency model for ship was therefore established.

3 Result and Analysis

3.1 Potential Competency Characteristics Set

From the relevant research and the behavior events interview, a potential competency characteristic set has been constructed, and it consisted of 55 abilities, which could be distributed into four dimensions. The first dimension was cognitive ability, including

spatial orientation, mathematical reasoning, speed of closure, visualization, flexibility of closure, number facility, originality, fluency of ideas, selective attention, fine manipulative abilities, information ordering, category flexibility, working memory, time sharing, perceptual speed, deductive reasoning, inductive reasoning, written expression, problem sensitivity, long memory (see Fig. 2a). The second dimension was perceptual ability, including peripheral vision, night vision, glare sensitivity, depth perception, visual color discrimination, far vision, sound localization, hearing sensitivity, near vision, speech clarity, auditory attention, oral comprehension (see Fig. 2b). The third dimension was psychomotor ability, including manual dexterity, finger dexterity, response orientation, control precision, arm-hand steadiness, speed of limb movement, multi-limb coordination, wrist-finger speed, reaction time, reaction time and speed abilities (see Fig. 2c). The last dimension was physical ability, including explosive strength, static strength, dynamic strength, trunk strength, dynamic flexibility, gross body equilibrium, endurance, gross body coordination, dynamic flexibility (see Fig. 2d).

The competency questionnaire for ship crew was designed based on the potential competency characteristics set. The questionnaires were sent to the subjects selected according to the factors of age, length of service, length of working in ship, professional title, duty & post and educational level. Finally, the results of this survey were analyzed through the following methods.

3.2 Reliability Analysis

Reliability is referred to as an indicator to evaluate the consistency of measurements. In this research, the Cronbach' α coefficient was utilized to analyze the reliability of the questionnaire. The coefficient represents the internal consistency of each items in the questionnaire, which would lie in between 0 and 1. The questionnaire would be considered to pass the reliability test the Cronbach' α coefficient is greater than 0.6. In this research, the Cronbach' α is 0.932, and the Cronbach' α based on the standardized items is 0.927, which proved the reliability of the questionnaire was sufficiently high. The Cronbach' α coefficients for each dimension were shown in Table 1, which presented that it was reliable to measure the competency of ship crew for all of the dimensions in the designed questionnaire.

Table 1. The Cronbach' α coefficient for each dimension

Dimension	Cronbach' α	Cronbach' α based on the standardized items	Number of items
Cognitive	0.762	0.782	23
Perceptual	0.837	0.835	12
Psychomotor	0.936	0.935	10
Physical	0.905	0.906	9

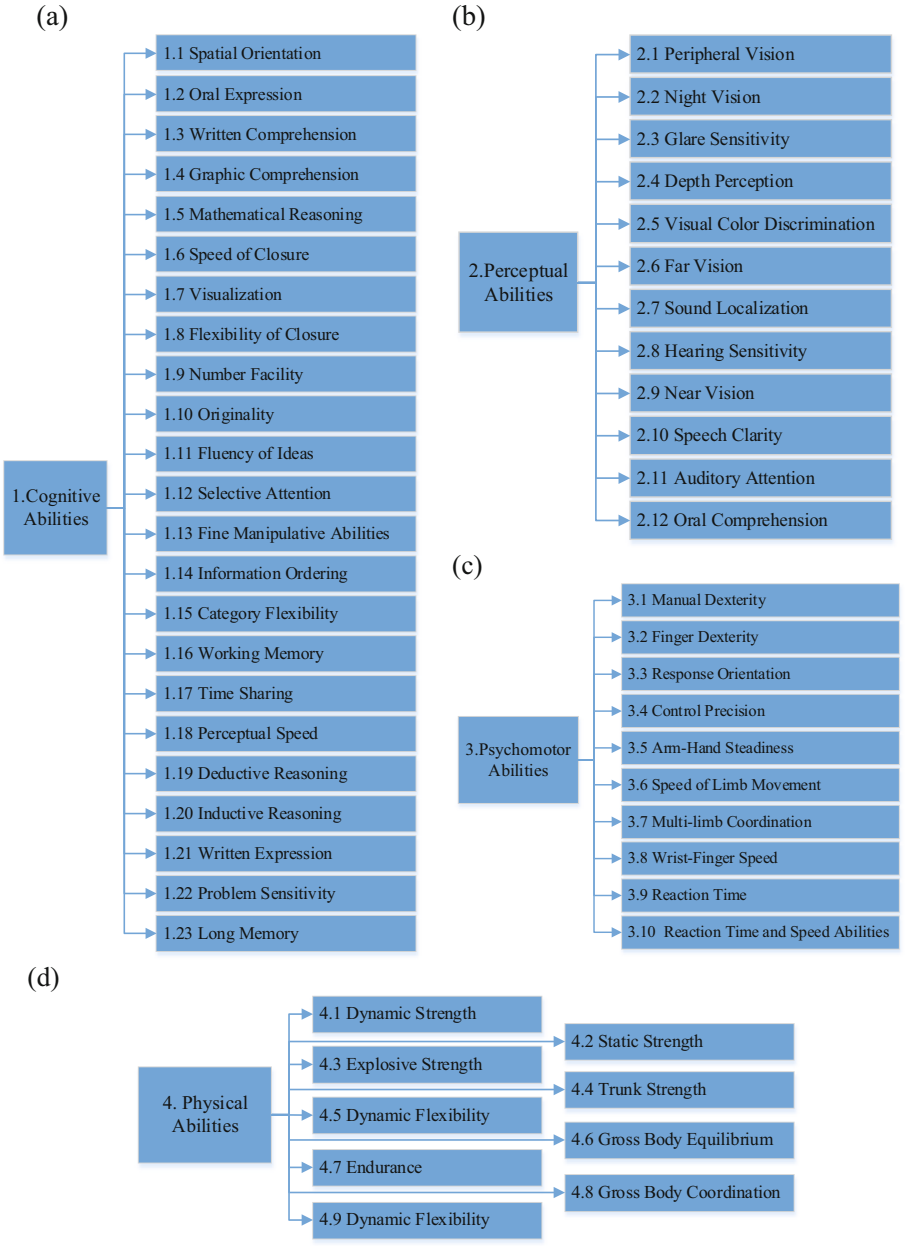

Fig. 2. Competency characteristics (a) for cognitive dimension, (b) for perceptual dimension, (c) for psychomotor dimension (d) for physical dimension

3.3 Competency Model

The raw data of this survey was then analyzed through the decretive statistical analysis, including mean, standardized deviation and order by the mean of items. The calculated results were presented in Table 2, and the 15 most important abilities for the ship crew were shown in Fig. 3. The analysis result were evaluated by several experts from domains of human factors and ship crew training. After that, all the abilities were categorized into three levels: the first level included the abilities with the scores larger than 0.8 (Oral Comprehension, Oral Expression, Written Comprehension, Graphic Comprehension, Speech Clarity, Written Expression, Problem Sensitivity, Inductive Reasoning, Working Memory, Selective Attention, Speed of Closure, Flexibility of Closure, Deductive Reasoning, Time Sharing); the second level included the abilities with the scores between 0.6 and 0.8 (Fine Manipulative Abilities, Information Ordering, Finger Dexterity, Fluency of Ideas, Category Flexibility, Spatial Orientation, Response Orientation, Auditory Attention, Reaction Time, Originality, Long Memory, Hearing Sensitivity, Perceptual Speed, Control Precision, Wrist-Finger Speed, Mathematical Reasoning, Number Facility, Visualization, Reaction Time and Speed Abilities); the third level included the abilities with the scores less than 0.6 (the rest of abilities). The scores of each abilities could be considered as the weight of each items in the competency model after standardized treatment. The competency model with different dimensions and levels was constructed for the professional ship crew as shown in Fig. 4.

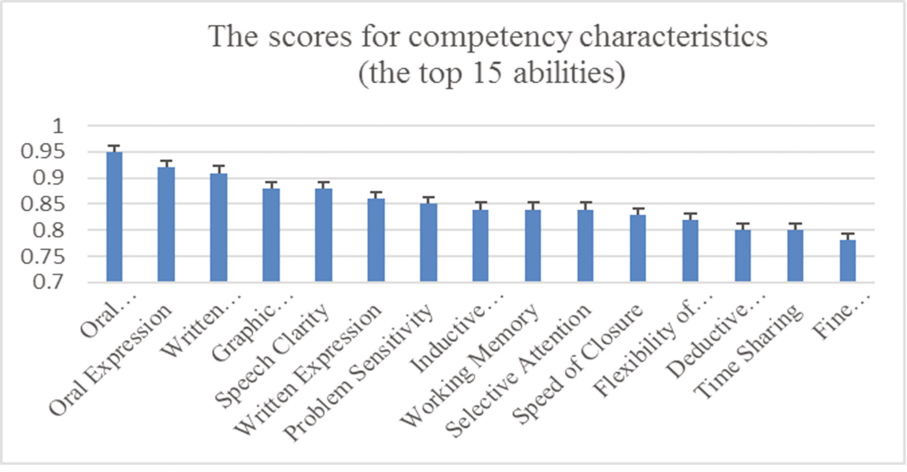

Fig. 3. The scores for competency characteristics (the top 15 abilities)

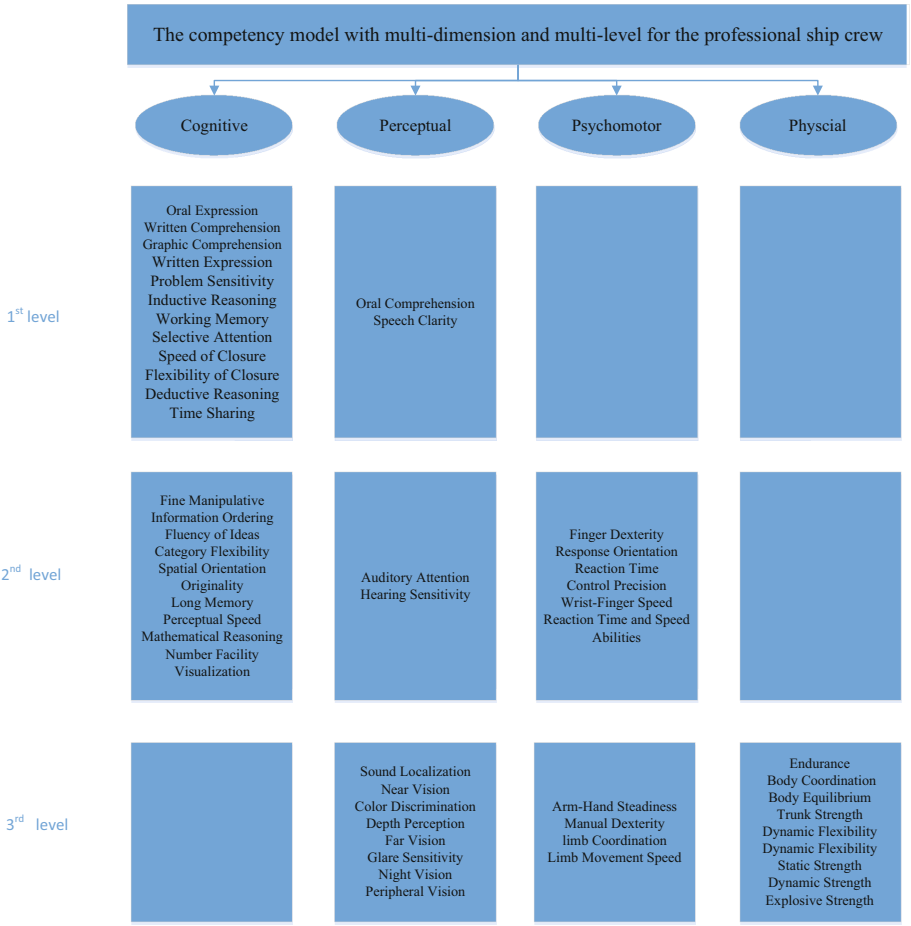

Fig. 4. The competency model with multi-dimension and multi-level for professional ship crew

4 Conclusion

This research proposed a competency model with multi-dimension according to the type of ability and multi-level according to the importance of ability for the professional ship crew via literature investigation, behavior events interview and questionnaire analysis. As indicated in Fig. 4, the cognitive ability is relatively more important compared with the abilities of the other three dimension, and the physical dimension is the least important for the ship crew studied in this research. The reason for this phenomenon lied in a great change of the work nature from labor-intense work to the mental-intense work experience by the ship crew in recent years; this change was contributed by the tremendous improvement of the automation technology. In the future, this research will put more efforts on assessment technology of the abilities and the accurate criterion of the ship crew performance, such that the validity of the

proposed model can be verified in further which would be beneficial to the accurate selection and efficient training of the professional ship crew.

Appendix: Descriptive Statistical Analysis

Table 2. Descriptive statistical analysis for each item

Order	Identifier	Abilities	Mean (score)	Std
1	2.12	Oral comprehension	0.95	0.15
2	1.2	Oral expression	0.92	0.16
3	1.3	Written comprehension	0.91	0.17
4	1.4	Graphic comprehension	0.88	0.19
5	2.10	Speech clarity	0.88	0.17
6	1.21	Written expression	0.86	0.19
7	1.22	Problem sensitivity	0.85	0.21
8	1.20	Inductive reasoning	0.84	0.23
9	1.16	Working memory	0.84	0.19
10	1.12	Selective attention	0.84	0.21
11	1.6	Speed of closure	0.83	0.21
12	1.8	Flexibility of closure	0.82	0.21
13	1.19	Deductive reasoning	0.8	0.24
14	1.17	Time sharing	0.8	0.24
15	1.13	Fine manipulative abilities	0.78	0.19
16	1.14	Information ordering	0.75	0.21
17	3.2	Finger dexterity	0.75	0.31
18	1.11	Fluency of ideas	0.74	0.26
19	1.15	Category flexibility	0.74	0.23
20	1.1	Spatial orientation	0.72	0.27
21	3.3	Response orientation	0.71	0.31
22	2.11	Auditory attention	0.7	0.23
23	3.9	Reaction time	0.7	0.26
24	1.10	Originality	0.68	0.26
25	1.23	Long memory	0.68	0.27
26	2.8	Hearing sensitivity	0.68	0.27
27	1.18	Perceptual speed	0.67	0.34
28	3.4	Control precision	0.67	0.34
29	3.8	Wrist-finger speed	0.67	0.25
30	1.5	Mathematical reasoning	0.64	0.26
31	1.9	Number facility	0.63	0.28
32	1.7	Visualization	0.6	0.35
33	3.10	Reaction time and speed abilities	0.6	0.3
34	3.5	Arm-hand steadiness	0.58	0.34
35	3.1	Manual dexterity	0.58	0.34

(*continued*)

Table 2. (*continued*)

Order	Identifier	Abilities	Mean (score)	Std
36	4.7	Endurance	0.54	0.3
37	2.7	Sound localization	0.52	0.24
38	2.9	Near vision	0.46	0.29
39	2.5	Visual color discrimination	0.46	0.29
40	3.7	Multi-limb coordination	0.46	0.31
41	4.8	Gross body coordination	0.46	0.29
42	3.6	Speed of limb movement	0.45	0.28
43	2.4	Depth perception	0.43	0.27
44	4.6	Gross body equilibrium	0.42	0.27
45	2.6	Far vision	0.41	0.25
46	2.3	Glare sensitivity	0.41	0.26
47	2.2	Night vision	0.4	0.32
48	4.4	Trunk strength	0.4	0.23
49	2.1	Peripheral vision	0.39	0.26
50	4.9	Dynamic flexibility	0.39	0.29
51	4.5	Dynamic flexibility	0.37	0.27
52	4.2	Static strength	0.31	0.27
53	4.1	Dynamic Strength	0.3	0.29
54	4.3	Explosive Strength	0.27	0.27

References

1. McClelland, D.C.: Testing for competence rather than for "intelligence". Am. Psychol. **28**(1), 1–14 (1973)
2. Bennis, W.: The four competencies of leadership. Train. Dev. J. **38**(8), 14–19 (1984)
3. Spencer, L.M., Spencer, S.M.: Competence at Work: Models for superior Performance, pp. 222–226. Wiley, Hoboken (1993)
4. Losey, M.R.: Mastering the competencies of HR management. Hum. Resour. Manag. **38**(2), 99–102 (1999)
5. Rodriguez, D., Patel, R., Bright, A., Gregory, D., Gowing, M.K.: Developing competency models to promote integrated human resource practices. Hum. Resour. Manag. **41**(3), 309–324 (2002)
6. Armstrong, M.: Performance Management. The Cromwell Press, London (1995)
7. Reisdorff, E.J., Stewart, L.T.: Assessing the new general competencies for resident education: a model from an emergency medicine program. Acad. Emerg. Med. **76**(7), 753–757 (2001)
8. Martone, D.: A guide to developing a competency based performance. Employ. Relat. Today **30**(3), 76–82 (2003)
9. Weissman, H.N.: Ethical Principles and Professional Competencies (Handbook of Psychology). Wiley, Hoboken (2003)
10. Shi, K., Wang, J., Li, C.: Assessment on competency model of senior managers. Acta Psychol. Sin. **34**(3), 306–311 (2002)
11. Wang, C., Chen, M.: Management competency model analysis: structural equation modeling assessment. Psychol. Sci. **5**, 513–516 (2002)

Ergonomic Study to Compare Digital Human Modeling Simulation Versus Real Life and Momentum

Caroline Massolino[1(✉)], Salvador Ávila Filho[1], Ivone Cerqueira[1], Renê Pimentel[1], Napoleão Neto[1], and Cristiane Fragoso[2]

[1] UFBA, Federal University of Bahia, Industrial Engineering Program, Salvador, Bahia, Brazil
massolinoccm@yahoo.com.br, {avilasalv,pimentel}@ufba.br, ivonecscerqueira@hotmail.com, napoleao87@gmail.com
[2] IFBA, Instituto Federal da Bahia, Salvador, Brazil
cristianemfl3@gmail.com

Abstract. As part of Vehicle Company ongoing efforts to provide employees a safe and healthy workplace. This study investigated how well ergonomics risk assessments on simulations with digital human models match (DHM) the real-life assessments obtaining on a car assembly line. The purpose is validated physical results comparing to virtual analysis of open hood operation. First off all the method used was measure the computer-aided design at virtual analysis to determine the open hood angle, hinge type, distance between hinge and point of force application, hood center of mass and part weight were collected with a Design Engineer. It was established three different angles to calculate three momentums to compare with a real-life and strength capabilities at DHM. This document concluded the validate results at virtual analysis to real life which means an anticipated force value to open hood operation and the force calculated at virtual analysis.

Keywords: Digital human modeling · Momentum · Dynamometer · Ergonomics · Human factors

1 Introduction

Throughout the vehicle development process, people in different departments use a variety of tools to represent users such as drivers, passengers and operators from assembly process. It appears that recently many different companies have established internal organizations to utilize this new digital human modeling technology. Seven case studies reported [1] describe the successful use of various digital human models to analyze and improve the physical ergonomics of different designs. This view is consistent with the concept of reducing total design and engineering costs by using computer-aided engineering (CAE) and digital mock-up (DMU) methods to achieve rapid, virtual prototype development and testing, as diagrammed in Fig. 1 [2].

We have been using to vehicles assemblers considering different aspects of human–vehicle interaction and when focusing on different physical environmental parameters,

D.N. Cassenti (ed.), *Advances in Human Factors in Simulation and Modeling*,
Advances in Intelligent Systems and Computing 591, DOI 10.1007/978-3-319-60591-3_46

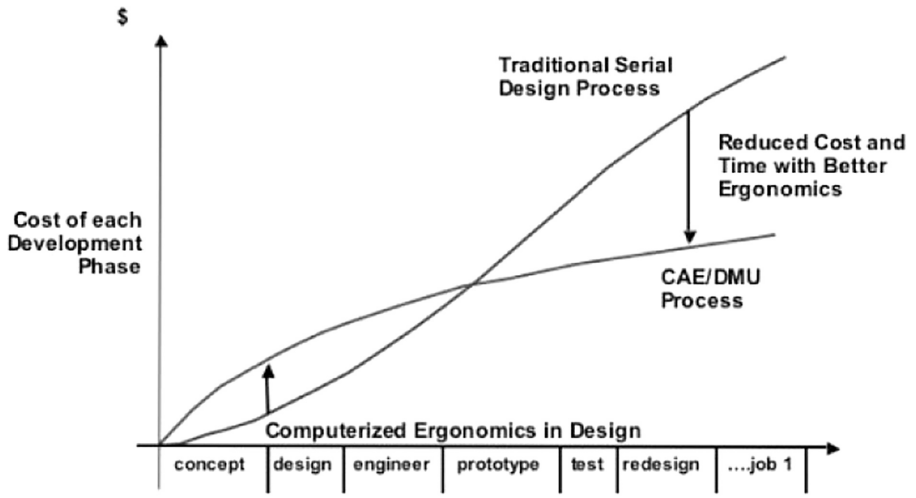

Fig. 1. Typical development phases and hypothetical cost profiles believed to exist when using a DMU (with human simulation) early in the design process compared to not using DMUs, which results in increased prototype building and ergonomics evaluation costs late in the development process.

such as geometry and forces. Traditionally, human–vehicle interactions have been evaluated relatively late in the development process by using physical mock-ups [3]. The integration of human factors is then carried out in laboratory and field experiments, which often are considered very expensive and time consuming [4]. Over the last 31 years, the utilization of human modeling tools has supported ergonomic evaluations in virtual environments, hence reducing the need for physical tests. A human modeling tool is a computer program that utilizes a human model in the creation, modification, presentation and analysis of, for example, human–vehicle interaction [5]. The tools are meant to assist designers and engineers when as part of vehicle company ongoing efforts to provide employees a safe and healthy workplace, the Vehicle Operations Division has launched a proactive ergonomics program. This system has incorporated the use of virtual tools and digital human models (DHM) to assess ergonomic assembly feasibility. Digital human figure models (DHM) are now widely used for ergonomic analysis of products and workplaces. In many organizations, DHM software is a tool of first resort for answering questions relating to physical interaction between people and objects [6]. Digital human modeling (DHM) and virtual human simulation (e.g., 3DSSPP™, EAI Jack®, RAMSIS) have been created to facilitate ergonomic evaluations [7]. Using these tools, the visual scope and reach envelope of users representing specific populations can be analyzed (e.g., EAI Jack®) [8]. Some DHM tools can calculate the biomechanical attributes of manual handling operations (e.g., Anybody® Modeling System, 3DSSPP™) and predict physical fatigue and potential disorder risk. These analytical tools can be used to identify and mitigate ergonomic problems of a designed product, workstation, or job in order to promote human considerations and protect the users, during an early stage of design [7].

Virtual human simulation provides a quick, virtual representation of human beings in a simulated working environment. Physical mock-up is no longer necessary, and multiple aspects can be assessed with rapid computational efficiency. One of the main issues with using virtual human simulation in some applications is that the movement or motion is obtained through inverse kinematics, which gives the virtual human robot-like, unnatural behavior [9].

The aim of integrating ergonomic evaluation methods into virtual reality (VR) is to facilitate the work design process, enhance design efficiency, and lower the design cost. Hypothetically, if a virtual environment (VE) could provide 100% fidelity then the workload and performance in VE should be the same as in a real-life and the strength capabilities to open the hood with a dynamometer. Practically, however, the main concern is whether the indices in VE, which have a limited level of fidelity due to economic and technical constraints, are consistent with the indices in real-life.

The presentation will highlight the advantages of using DHM in identifying ergonomic concerns in advice in the design process. This study investigated how well ergonomics risk assessments on simulations with DHM match the real-life assessments obtaining on a car assembly line. The purpose is validated physical results (dynamometer) and comparing to virtual analysis of open hood operation.

2 Method

The study included three ergonomics simulations cases, four computer-aided design (CAD) analysis and six cars at three different position of open hood angle.

First off all the method used was measure the CAD at virtual analysis to determine the open hood angle, hinge type, distance between hinge, point of force application, hood center of mass and part weight. It was established three different angles to calculate three momentums as posture 1 (Pos 1), posture 2 (Pos 2) and posture 3 (Pos 3) to compare with a real-life (dynamometer) and strength capabilities at DHM.

Force can be measured using multiple set-ups such as a dynamometer (Force Gauge). It is necessary to identify the movement path of the operator (whole body or segment) and the direction of forces (combination likely) that represent that movement path. Establish good coupling between the force gauge and the object (resistance). The goal is to ensure constant contact between the gauge and the object, and avoid any slipping. Record the peak (effectively, the highest force obtained) AND the average force.

Reading during sustained movement (constant velocity). Record values for ALL efforts observed in the movement path. Take these force measurements through the most heavily loaded condition (worst-case scenario).

In the real-life scenario it was measured the force to open the hood using dynamometer at the same three angles at virtual analysis. There were established two positions on CAD, one position at hood to keep the dynamometer during the process to open hood for all three posture: Pos 1, Pos 2 and Pos 3; the second position is a fix point on car chassis in Fig. 2.

After that three different random heights were chosen, but they should be the same during the actual measurement in Fig. 3.

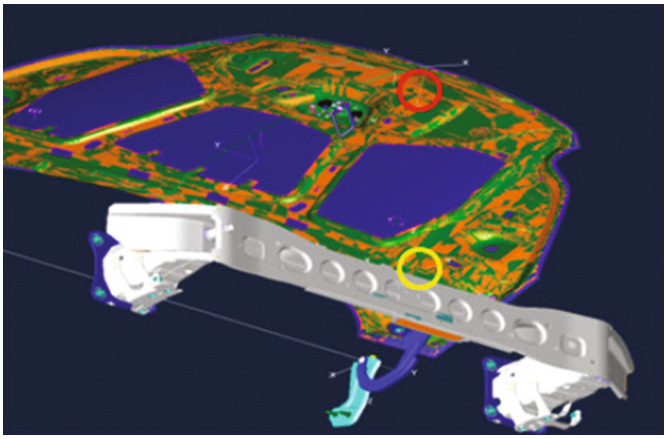

Fig. 2. Computer-aided design (CAD) at virtual analysis to determine the open hood angle and distance between hinge.

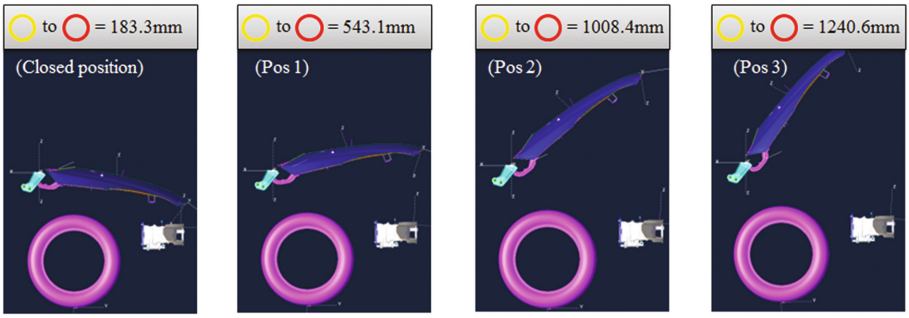

Fig. 3. Computer-aided design (CAD) at virtual analysis to determine the open hood angle and distance between hinge.

Fig. 4. A marking was made on the hood in blue, in order to be able to place the dynamometer during the movement to open hood.

The dynamometer was positioned at real-environment as CAD reference for position 1 (Pos 1), position 2 (Pos 2) and position 3 (Pos 3) in Fig. 4.

According to posture 1 (Pos 1) 543.1 mm of height in Fig. 5, posture 2 (Pos 2) 1008.1 mm Fig. 6 and posture 3 (Pos 3) 1240.6 mm in Fig. 7.

Fig. 5. Position 1 (Pos 1)

In each environment, the momentum calculation in each environment was based on static force as open hood angle, hinge type, distance between hinge, point of force application, hood center of mass and part weight as formula (1).

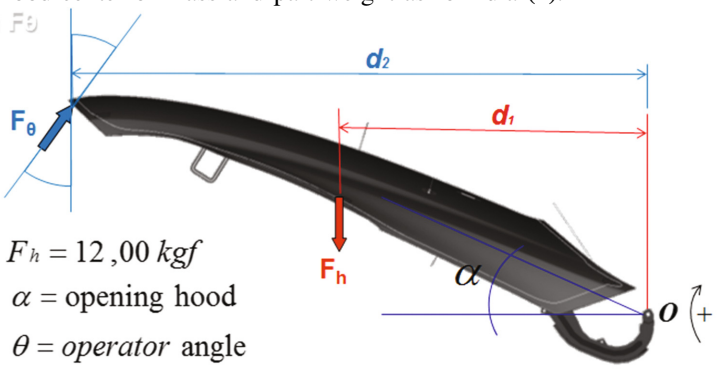

(1)

$$\circlearrowleft + \quad \sum M_o = 0 \therefore \sum M_o = \left(F_o \times d_2\right) + \left(-F_h \times d_1\right) = 0$$

$$F_h = 12{,}00 \times 9{,}8 = 117{,}6N$$

$$F_o = F_h \times \frac{d1}{d2} \therefore \left[F_o = (117{,}6 \times \frac{d1}{d2}) \times \cos\theta \right]$$

Fig. 6. Position 2 (Pos 2)

Fig. 7. Position 3 (Pos 3)

There is DHM (Jack – Siemens) to validate this strength capabilities according to our anthropometric data collected. The version of the Jack Static Strength Prediction (JSSP) tool used by Vehicle Company is the Ergonomics Static Strength Prediction Solver (FSSPS). There are two modes in which an assessment can be performed. The first mode determines the implications of set hand loads that are manually entered into the interface. This mode outputs torques, strengths and percent capable (%Cap) for each joint,

and the %Caps were used to determine if the Task was considered as "acceptable" for that trial. In this mode, the user selects the hand(s) in which the force is applied, if there are any supporting hands or external support, and the frequency at which the force is exerted. For the second mode, the user selects the Solve SSP button once the correct posture of the digital human is attained according to each posture in Fig. 8.

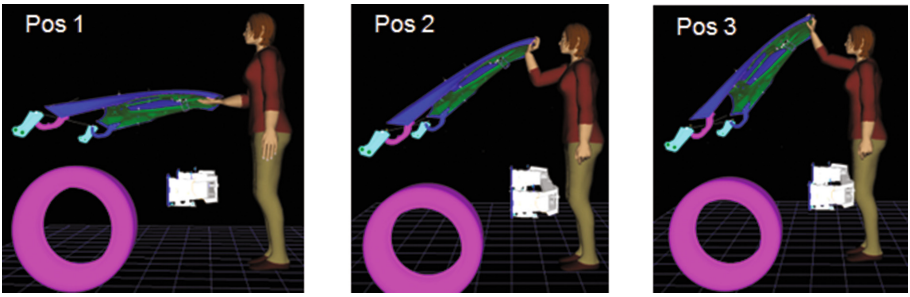

Fig. 8. The DHM (Jack – Siemens) in posture 1, posture 2 and posture 3 at same position as CAD and real-life.

This will show the maximum force that would still make the Task "acceptable". When support hands are used, it was not possible to output values for joints affected by this support (as its force was not measured). For example, if the right hand was used for an insertion, and the left hand was used to support the body, then only right arm values would be output from the FSSPS and the left arm, trunk and leg values would be blacked out in the Solver in Fig. 9.

Fig. 9. The Force Solver or strength capabilities for posture 1, posture 2 and posture 3 at same position as CAD and real-life.

3 Result and Discussion

3.1 Results

This study we have a hood weight as 11 kg we are going to change for next steps the hood hinge angle, operator angle to open the hood, distance 1, distance 2, dynamometer force measurement to each position as soon as.

Posture 1. According to results for posture 1 there are distance 1º 549.29 mm, distance 2º 959.77 mm, weight 107.8 N, hood hinge angle 5.06º, operator to open hood 35.14º total force momentum is 61.1 N. The real-force (dynamometer measure) is 75.18 N. The maximum accepted force according to DHM is 81 N with a frequency to repeat this movement eight hours per day of once each three minutes.

Posture 2. According to results for posture 2 there are distance 1º 446.86 mm, distance 2º 775.94 mm, weight 107.8 N, hood hinge angle 11.41º, operator to open hood 33.61º total force momentum is 58.8 N. The real-force (dynamometer measure) is 63.4 N. The maximum accepted force according to DHM is 74 N with a frequency to repeat this movement eight hours per day of once each three minutes of once each three minutes.

Posture 3. According to results for posture 3 there are distance 1º 347.58 mm, distance 2º 600.2 mm, weight 107.8 N, hood hinge angle 19.58º, operator to open hood 29.61º total force momentum is 52.1 N. The real-force (dynamometer measure) is 52.75 N. The maximum accepted force according to DHM is 104 N with a frequency to repeat this movement eight hours per day of once each three minutes of once each three minutes.

Results showed position (1) 22.9%, position (2) 7.82% and position (3) 1.25% comparing virtual analysis with real life. At DHM environments, results position (1) 32.73%, position (2) 25.85% and position (3) 100% greater than virtual analysis in Table 1.

Table 1. Result comparative

	D1	D2	Weight	θ'	θ''	TOTAL	Real Fθ Car 1	Real Fθ Car 2	Real Fθ Car 3	Real Fθ Car 4	Real Fθ Car 5	Real Fθ Car 6
POS1	549.29	959.77	107.8	5.06	35.14	**61.1**	76.1	76.6	76.1	74.3	75.4	72.6
POS2	446.86	775.94	107.8	11.41	33.61	**58.8**	62.7	65.8	64.7	62	63.1	62.1
POS3	347.58	600.2	107.8	19.58	29.61	**52.1**	52.2	52.9	54.8	52.7	51.6	52.3

According to real force measured with dynamometer at the six cars models to posture 1 in Fig. 10.

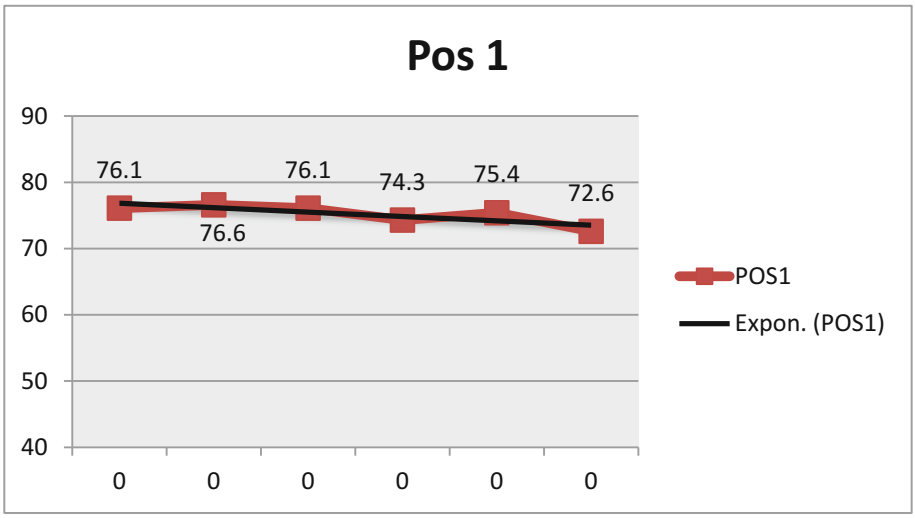

Fig. 10. Results force measurement for all six cars models for posture 1.

According to real force measured with dynamometer at the six cars models to posture 2 in Fig. 11.

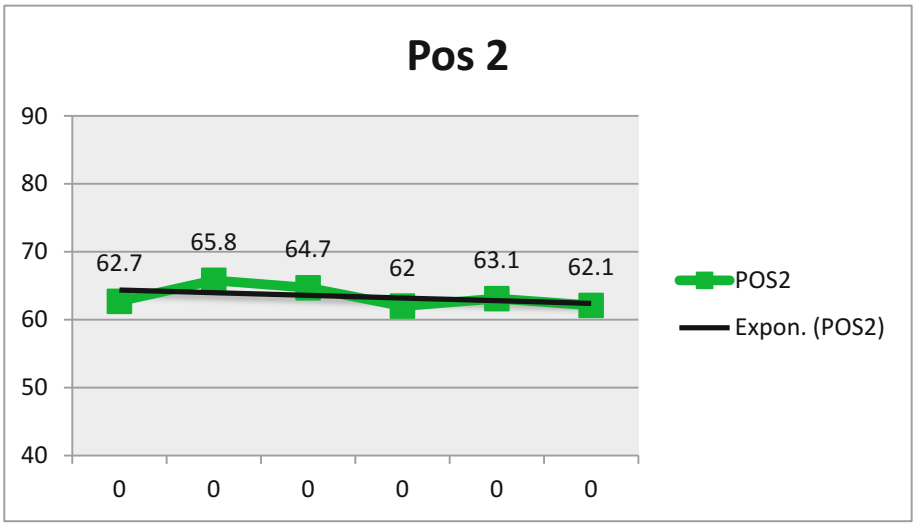

Fig. 11. Results force measurement for all six cars models for posture 2.

According to real force measured with dynamometer at the six cars models to posture 3 in Fig. 12.

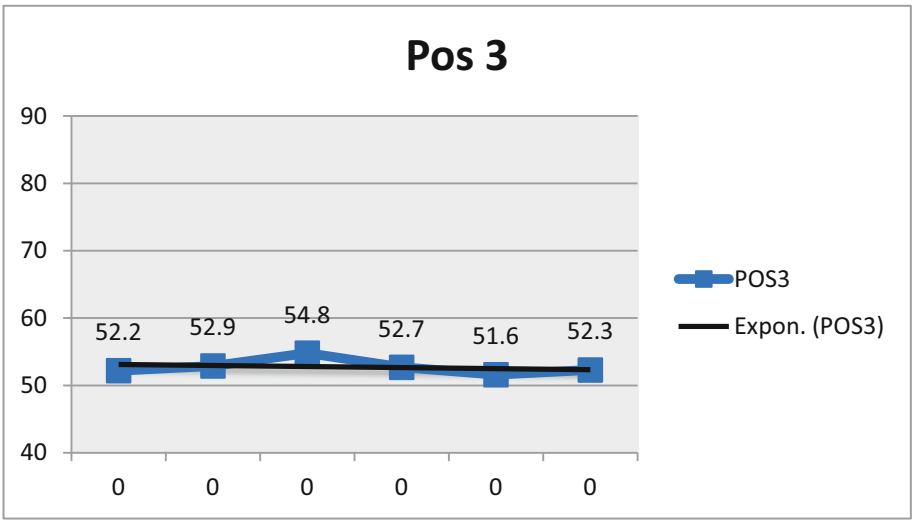

Fig. 12. Results force measurement for all six cars models for posture 2.

4 Conclusion

This document concluded the validate results at virtual analysis to real life (dynamometer) which means an anticipated force value to open hood operation, and the force calculated at virtual analysis is closer than we found at real life results. At DHM showed the operator has a strength capability to open the hood safe and healthy. In summary, the Human in Process Simulate, along with the UGS Jack 8.3 DHM software allowed an assembly process to be evaluated virtually, years and months prior to having physical parts. The effort results between real and virtual studies are different. The virtual effort results are lower compared with real results, but at virtual analysis we can not include some points according to friction, dynamometer calibration, same person are measuring, velocity of measurement, hood clean, center of mass correct, hood weight correct. When we found results of measured closer from virtual and real is when are closer to hinge. The mathematic account is validated. This is the cost associated with fixing a job after it has been released from engineering. The result was an early design change with minimal cost to the company.

References

1. Chaffin, D.B.: Digital Human Modeling for Vehicle and Workplace Design. SAE International, Warrendale (2001)
2. Chaffin, D.B.: Experimental evaluation of a computational shoulder musculoskeletal model. Department of Biomedical Engineering, University of Michigan, Ann Arbor, MI 48109, USA and Center for Ergonomics, University of Michigan, Ann Arbor, MI 48109, USA (2007)

3. Porter, J.M., Case, K., Freer, M.T., Bonney, M.C.: Computer-aided ergonomics design of automobiles. In: Peacock, B., Karwowski, W. (eds.) Automotive Ergonomics. Taylor and Francis, London (1993)
4. Helander, M.G.: Seven common reasons to not implement ergonomics. Int. J. Industr. Ergon. **25**(1), 97–101 (1999)
5. Hanson, L.: Guide and documentation system to support digital human modeling applications. Division of Ergonomics, Department of Design Sciences, Lund University, P.O. Box 118, SE-221 00 Lund, Sweden and Saab Automobile AB, SE-461 80, Trollhättan, Sweden (2006)
6. Parkinson, M.B., Chaffin, D.B., Reed, M.P.: Center of pressure excursion capability in performance of seated lateral-reaching tasks. Clin. Biomech. **21**, 26–32 (2006)
7. Hu, B., Ma, L., Zhang, W., Salvendy, G., Chablat, D., Bennis, F.: Predicting real-world ergonomic measurements by simulation in a virtual environment. Department of Industrial Engineering, Tsinghua University, Beijing, 100084, PR China. And Institut de Recherche en Communications et en Cybernétique de Nantes, CNRS UMR 6597, Ecole Centrale de Nantes, IRCCyN-1, rue de la Noë, BP 92 101, 44321, France (2010)
8. Chaffin, D.B., Nelson, C., Ianni, J.D.: Digital Human Modeling for Vehicle and Workplace Design, pp. 82–87. SAE International, Warrendale (2001)
9. Chaffin, D.B., Erig, M.: Three-dimensional biomechanical static strength prediction model sensitivity to postural and anthropometric inaccuracies. IIE Trans. **23**(3), 215–227 (1991)

Optimization, Analysis and Scheduling

A Comparison Between Physical and Virtual Experiments of Convective Heat Transfer Between Head and Bicycle Helmet

Shriram Mukunthan[1(✉)], Kalev Kuklane[2], Toon Huysmans[3], and Guido De Bruyne[1,4]

[1] Product Development, Faculty of Design Sciences, University of Antwerpen, Ambtmanstraat 1, 2018 Antwerp, Belgium
Shriram.Mukunthan@uantwerpen.be
[2] Ergonomics and Aerosol Technology, Department of Design Sciences, Lund University, Box 118, 221 00 Lund, Sweden
[3] Vision Lab, Department of Physics, University of Antwerp (CDE), Universiteitsplein 1, 2610 Antwerp, Belgium
[4] Lazer Sport NV, Lamorinierestraat 33-37 bus D, 2018 Antwerp, Belgium

Abstract. Thermal performance of five bicycle helmets was evaluated with a thermal manikin head with six zones. Evaluation was made with physical and virtual experimental methods. Ambient temperature maintained at 24 °C and surface temperature of the thermal manikin head was set to 34 °C. Experiments were performed for air velocities of 1.6 m/s and 6 m/s. Heat transfer (W) of four thermal zones was recorded for five helmets and compared with a nude thermal manikin head to assess thermal performance. Virtual experiments were performed using commercial CFD codes with a realizable k-ε turbulence model. Correlation coefficients of 0.78 (1.6 m/s) and 0.79 (6 m/s) were found between physical and virtual experiments. A combined physical and virtual evaluation methodology allows creating a design iteration process with virtual prototypes, physical prototypes and commercially available helmets.

Keywords: Thermal manikin · Wind Tunnel Experiments · Convective heat transfer · Cooling efficiency · Turbulence models · CFD

1 Introduction

Head injury is a major cause of fatal and serious injuries during cycling [1, 2]. Bicycle helmets can reduce the risk of serious brain injuries [3, 4]. The use of helmets during cycling should therefore be encouraged. Thermal discomfort is a major factor influencing the usage of bicycle helmets. Although commercially available helmets are designed with a large numbers of vents, they are not always effective in removing the heat produced by cyclists in the scalp area.

Cyclists tend to avoid helmets especially during the summer time when the temperatures are high [5, 6] resulting in high heat production between head and helmet. Two types of studies are usually performed to understand the cooling effectiveness of headgear: subject studies and object studies. Subject studies, with test persons cycling

D.N. Cassenti (ed.), *Advances in Human Factors in Simulation and Modeling*, Advances in Intelligent Systems and Computing 591, DOI 10.1007/978-3-319-60591-3_47

in a windtunnel in a climatic chamber, are accurate but time consuming. These experiments often result in high variability between different tests for the observed variables such as sweat production [7]. Objects studies, with for example thermal manikins, are a simplification of the real heat loss on a human head, but provide results with less statistical variation. Object studies using thermal manikin are therefore preferred to compare the thermal performance of helmets. Thermal manikin head studies focus on convective heat loss between head and helmet [8], but can also be used to study radiative heat loss [9] and evaporative heat loss [10, 11].

To date, only a limited number of studies have focused on the development of a virtual thermal manikin head that may allow predicting the thermal performance of a helmet design in the early stage of a design process. This study aimed at developing a virtual test method to evaluate the convective heat transfer on a thermal manikin head using commercial numerical methods (CFD). The evaluation was carried out for five complex bicycle helmets and virtual results were compared with physical test results (Fig. 1).

2 Calculation of Convective Heat Transfer and Cooling Efficiency

The basic heat balance of the human body is given by [12]

$$S = M - W - (E_{res} + C_{res} + E_{sk} + C_{sk} + K + R) \quad (1)$$

where M is metabolic rate and W is work rate, quantifying heat production. Heat loss is defined by evaporation (E), convection (C), conduction (K) and radiation (R). Evaporation and convection occurs through respiration (res) and skin (sk) and S is heat storage in the human body.

For bicycle helmets, having a layer of insulating expanded polystyrene, heat loss is predominantly defined by convective heat loss. Convective heat transfer through skin is defined by:

$$C_{sk} = \dot{Q} = hA(T_h - T_a) \quad (2)$$

where, $\dot{Q}$ is heat transfer per unit time, A is area of the object, h is heat transfer coefficient, T_h is Temperature of head, T_a is Temperature of air/fluid.

Cooling efficiency (%) is used in this research to compare the heat loss of helmets as compared to a reference thermal manikin head with no helmet. Cooling efficiency of a helmet is thus defined as the ability of a helmet to dissipate the heat from the head to the environment, relative to a nude head.

$$Cooling\ performance = \frac{Heat\ transfer\ with\ helmet}{Heat\ transfer\ (nude\ head)} X100 \quad (3)$$

3 Methods

3.1 Experimental Setup

Experiments were performed in an open circuit suction type wind tunnel with fans located at the outlet and tubes to streamline the flow into the test section at the inlet (Fig. 2). The test section was 0.5 m high, 0.5 m wide and 1.5 m long. The ambient temperature was set to 24 °C.

The headform that was used for testing resembles the headform used by Liu et al. 1997 for evaluating the heat transfer characteristics of Helmets. The heating system inside the head consists of heating foils wound on the inner side of the zones. The heat transfer between different zones of the head was eliminated through an insulating barrier. The headform was classified into six measurement zones: face, forehead, neck, scalp, left and right ear (Fig. 3). During the test, the surface temperature of the each measurement zone was maintained at a constant temperature of 34 °C.

Fig. 1. Nude headform and helmets used for testing in wind tunnel

Table 1 shows the surface area of the each measurement zone. The testing was done at two air speeds: 1.6 m/s and 6 m/s. The headform was vertically positioned and the test was carried out for 60 min such that the test reaches a steady state in 40 min and the last 20 min of the test were considered for the calculations. The power required at the each measurement zone to maintain the surface temperature of the headform at 34 °C was recorded with a sampling rate of 1 Hz. The power needed to maintain a constant surface temperature were converted into heat flux values, which in turn were used to calculate the heat transfer from the different measurement zones. The convective heat transfer from the head without any helmet was used as the reference for determining the efficiency of helmets.

3.2 Numerical Simulations

A digital model of the headform and the five helmets used for testing were obtained from 3D scanning. The assembly of headform and helmets was done to control the positioning and gap between headform and helmet. The digital version of the helmets and headform were cleaned and simplified to facilitate meshing. The computational

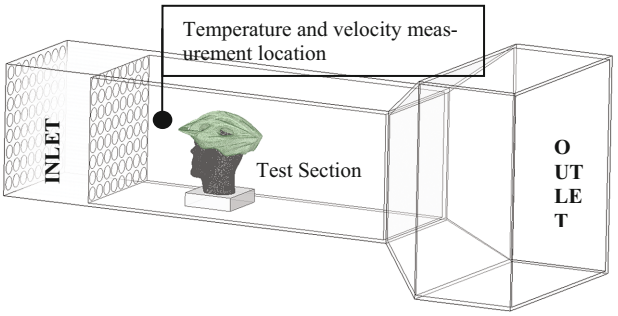

Fig. 2. Nude headform and helmets used for testing in wind tunnel

domain as shown in the Fig. 4 was modelled. This type of domain geometry was chosen to study the air flow patterns in the wake of the headform.

The computational domain that was used for the simulation is different from the domain used in actual testing to understand the air flow patterns in the wake of the headform. The size of the domain also prevents back flow warnings during the simulation.

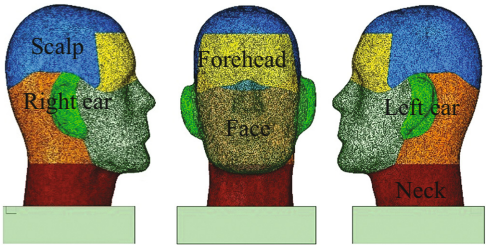

Fig. 3. Measurement zones on the thermal manikin used in physical tests

Meshing of both solid and fluid domain was done using tetrahedral mesh and hexahedral mesh to understand the mesh sensitivity. Tetrahedral meshing was preferred over hexahedral mesh since the desired orthogonal skewness was achieved only with tetrahedral mesh. Fluent meshing was carried out in two steps: Firstly, a surface mesh was generated for all the geometries viz., headform, helmet and the domain. The surface mesh was then refined to desired skewness and the identified critical zones were remodeled to avoid slivers and skewed cells. The surface mesh also allows the user to reposition and adjust the gap between the head and helmet if required. In addition, the surfaces in the headform that come into contact with the helmet were identified and stitched to the helmet surface. This prevents the cells from headform penetrating the helmet and in turn serves as an interface.

Prism layers were modelled on the boundary surfaces that interact with the fluid layer (solid-fluid interface). Prism layers (Fig. 5) are effective to understand the interactions that happen in the solid-fluid interface viz., Forces, fluxes and heat transfer rate etc. The number of prism layers modelled depends on the y+ values desired for

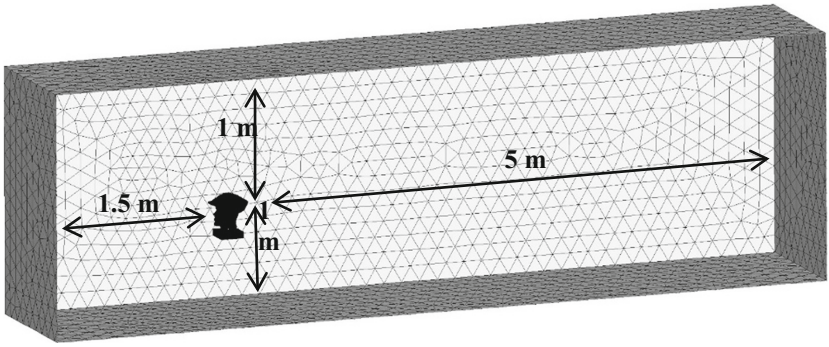

Fig. 4. Head form – Helmet assembly inside the virtual domain

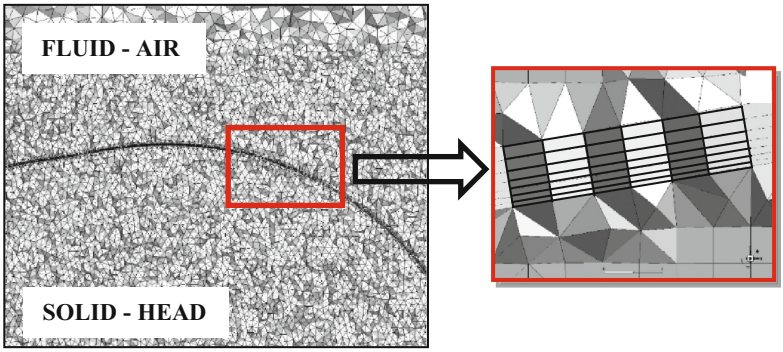

Fig. 5. Solid- fluid interface modelled using prism layers

that particular interface. External parameters like fluid velocity, density, Reynolds number determine the y+ value (Figs. 4 and 5).

A steady state simulation was preferred to a transient one because of the following reasons: The heat transfer between the head and environment is not time dependent and time dependent effects in this test protocol were negligible. In the tests, it was observed that the system reached a steady state after 40 min and hence a steady state simulation was performed.

Pressure based coupled algorithm was used to solve the governing equations. Reynolds-averaged Navier-Stokes equations (RANS) are used by most of the commercial codes to solve the turbulence models. RANS coupled with realizable k-ε turbulence model were used to solve the governing equations. Realizable k-ε model was used for resolving the boundary layer since it has proven to be consistent with the physics of turbulent flows. Second order discretization schemes were used to solve pressure, momentum and energy equations. SIMPLE algorithm was used for pressure-velocity coupling. Enhanced wall treatment was used to model the boundary layer.

The boundary conditions imposed to the model was similar to that of the test. Velocity boundary condition was assigned to the domain inlet. The velocity of fluid

Table 1. Surface area of measurement zones used in physical and virtual tests

	Surface area (m^2)	
Zone	Physical	Virtual
Scalp	0.0616	0.0676
Forehead	0.0146	0.0141
Face	0.0314	0.0324
Ear - right	0.0044	0.0052
Ear - left	0.0043	0.0051
Neck	0.0322	0.0208

was defined in the direction parallel to the length of the domain (X direction). The outlet of the domain was assigned with pressure outlet where the pressure is maintained at atmospheric pressure. No slip condition was assigned to the walls of the domain, headform zones and helmet. This implies that the velocity of the fluid at the wall is set to zero and the roughness of the domain surfaces, head form and helmet cannot be defined by the user.

The temperature of the head form surface was set to 34 °C and the temperature of the domain was set to 24 °C such that a temperature difference of 10° was maintained. No radiation or evaporative heat transfer was modelled since the tests determine the heat transfer through forced convection only. Convergence was assessed by monitoring the default residuals like continuity, energy and velocity. Besides these default quantities heat flux values for each measurement zone on the headform was recorded for every iteration and plotted.

4 Results and Discussion

4.1 Wind Tunnel Experiments

The temperature of the headform zones and the variation was recorded after the test and from the values it is evident that the temperature variation that is observed on the head surfaces is limited to ± 0.2. The total and zonal convective heat transfer values of nude head and 5 different helmet designs are shown in Tables 2 and 3 for wind speeds 6 m/s and 1.6 m/s respectively.

Table 2. Total and zonal heat transfer values from headform tested at 6 m/s

V = 6 m/s	Nude head	Helmets				
		1	2	3	5	17
Scalp	25.15	21.88	21.08	25.50	22.56	21.99
Forehead	6.13	5.50	5.61	5.64	5.86	6.03
Face	14.27	13.95	14.28	14.16	14.30	13.96
Ear- right	1.90	1.68	1.85	1.74	1.89	1.63
Ear-left	1.90	1.94	1.80	1.94	2.06	1.70
Total (W)	49.35	44.95	44.62	48.98	46.67	45.32

Table 3. Total and zonal heat transfer values from headform tested at 1.6

V = 1.6 m/s	Nude head	Helmets				
		1	2	3	5	17
Scalp	12.66	8.72	9.60	11.45	10.75	10.51
Forehead	3.44	3.18	3.33	3.25	3.21	3.05
Face	7.35	7.28	7.11	7.24	7.23	6.95
Ear-right	1.07	0.76	0.95	0.86	1.06	0.91
Ear-left	1.12	0.77	0.98	0.98	1.12	0.93
Total (W)	25.64	20.71	21.97	23.78	23.36	22.34

The heat transfer from head to environment is directly proportional to the airspeed i.e., the speed of the cyclist in real scenario. The scalp region of the head displays higher variation in heat transfer values with and without helmet. This variation in the values of heat transfer from, scalp can be attributed to the design of helmets that were used for testing. From the total heat transfer values, it can be inferred that the helmets with vents on top seem to exhibit similar heat transfer characteristics with Helmet 3 being an exception.

The heat transfer values from individual zones are similar for helmets 5 and helmet 17. Helmet 1 and helmet 2 comparatively exhibit poor heat transfer and ventilation characteristics. Absence of vents could be the reason for helmet 1 to perform poorly. On the contrary, heat transfer to the environment with helmet 2 which has multiple vents is also lesser than helmet 5 and 17. This could be due to a tight fit between headform and helmet 2, which would have resulted in low heat transfer values. Helmet 3 exhibits higher heat transfer values and this can be attributed to the geometry of the helmet. Helmet 3 is provided with channels under the top shell instead of vents and this air channels serve as passage for air, which in turn results in better convection.

4.2 Numerical Simulations

Steady state simulations were carried out using the commercial solver FLUENT. RANS coupled with k-ε model were used to solve the governing energy and momentum equations. The heat flux values recorded after each iteration is recorded and plotted to understand the convergence behavior. Figure 6 shows heat flux plots of measurement zones scalp and face.

The heat transfer rate for the individual measurement zones and the headform is shown in the Tables 4 and 5 for wind speeds 6 m/s and 1.6 m/s respectively. It should be noted that the heat transfer values for the actual test and the simulation do not match. This is due to the following reasons: the domain used in the simulation is different than that of the one used in the actual test. The difference in domain size is to prevent the backflow errors and warnings that arise in the simulation due to insufficient domain length for the flow behind the head to develop and reach a steady state. Increase in length of the domain also allows to understand the air flow pattern behind the head to identify separation, vortices etc.

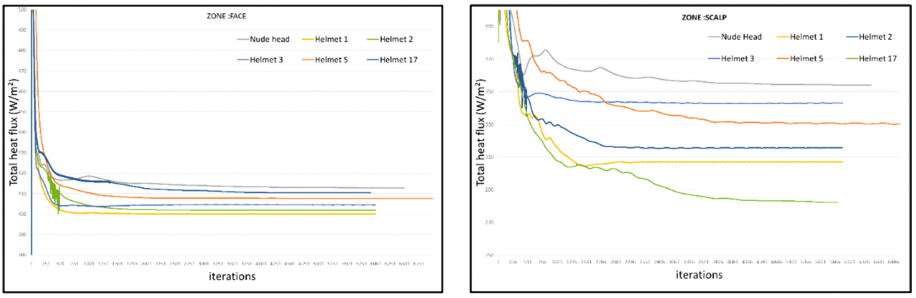

Fig. 6. Heat flux plots of scalp and face

Table 4. Total and zonal heat transfer values from headform tested at 6 m/s in simulated environment

	Nude head	Helmets				
		1	2	3	5	17
Scalp	21.02	18.38	17.59	19.23	17.82	16.68
Forehead	6.46	6.40	6.31	6.04	6.34	6.20
Face	13.38	12.80	13.01	13.09	13.23	13.31
Ear - right	1.75	1.65	1.60	1.79	1.67	1.82
Ear - left	1.90	1.88	1.76	2.03	1.82	1.71
Total (W)	44.51	41.11	40.28	42.18	40.88	39.72

Table 5. Total and zonal heat transfer values from headform tested at 1.6 m/s in simulated environment

	Nude head	Helmets				
		1	2	3	5	17
Scalp	8.38	5.52	7.32	7.05	7.53	7.00
Forehead	3.01	2.74	2.93	2.75	2.84	2.73
Face	5.63	5.44	5.40	5.43	5.53	5.52
Ear - right	0.74	0.66	0.63	0.65	0.68	0.69
Ear - left	0.88	0.76	0.69	0.83	0.80	0.69
Total (W)	18.64	15.11	16.97	16.71	17.38	16.62

The wind speed used in the test cannot be maintained at a constant value and a variation of ±0.2 m/s was observed and this could contribute to the difference in heat transfer values. Also the assembly of helmet and head was made with visual references and so it cannot be considered as identical to test and hence establishing a grid based assembling method should resolve this issue. Other factors that could have contributed to the difference in heat transfer values are for example., the mesh orthogonal skewness, turbulence model parameters. Since all the simulations were ran with identical settings, the cooling efficiency values of the helmets were used to compare the test and simulation results instead of comparing the heat transfer values one-on-one.

4.3 Cooling Efficiency

Cooling efficiency can be used to determine the effectiveness of the vents and thereby the helmet design itself. The efficiency of different helmets when compared to the nude head is shown in Tables 6 and 7.

Table 6. Cooling efficiency of helmets at V = 1.6 m/s

	Cooling efficiency V = 1.6 m/s	
	Physical	Virtual
Helmet 1	80.8	81.1
Helmet 2	85.6	91.1
Helmet 3	92.7	89.6
Helmet 5	91.1	93.2
Helmet 17	87.1	89.2

Table 7. Cooling efficiency of helmets at V = 6 m/s

	Cooling efficiency V = 6 m/s	
	Physical	Virtual
Helmet 1	91.1	92.4
Helmet 2	90.4	90.5
Helmet 3	99.2	94.8
Helmet 5	94.6	91.9
Helmet 17	91.8	89.3

From the cooling efficiency results, it is evident that the results from the test and simulation are comparable. At wind speed 6 m/s, the cooling efficiency of helmet 3 shows a considerable difference and this is due to assembly between the head and helmet. Several simulations carried out after adjusting the positon of the helmet exhibited different efficiency values and as discussed earlier, a grid based helmet positioning method will help in reducing this difference. The difference in cooling efficiency values for helmet 2 at wind speed 1.6 m/s is due to the geometry and fit of the helmet. A solution to this problem could be to test the helmet with a headform that is smaller than the current one which provides a better fit such that interference between head and helmet can be avoided in the virtual model.

4.4 Correlation Coefficient

A correlation coefficient was used to determine the nature of relationship between two set of results. In this case the correlation between the results from wind tunnel tests and simulations were determined. The correlation between two sets of data points is found using Pearson Product-Moment Correlation Coefficient

$$Correl(X, Y) = \frac{\sum(x - \bar{x})(y - \bar{y})}{\sqrt{\sum(x - \bar{x})^2 (y - \bar{y})^2}} \tag{4}$$

where $\bar{x}$,$\bar{y}$ are sample means of two sets.

Using the formula, the correlation coefficient for the physical and coefficient results for wind speed 6 m/s is determined to be 0.79 and the correlation coefficient for wind speed 1.6 m/s is found to be 0.78. The coefficient values clearly indicate that there exist a positive relationship between physical and virtual tests.

5 Conclusion

In this study, a physical and virtual experiment of a thermal manikin with five bicycle helmets was performed to compare both evaluation methods. The study allows validating virtual experiments.

Cooling efficiency ranged from 90.4% to 99.2% at an air velocity of 6 m/s in physical tests and from 90.5% to 94.8% in virtual tests. Cooling efficiency ranged from 80.7% to 92.7% at 1.6 m/s in physical tests and from 81.1% and 93.2% in virtual tests.

A correlation coefficient of 0.79 and 0.78 at wind speeds 6 m/s and 1.6 m/s was found.

This research showed that virtual experiments may serve as an acceptable method to evaluate the thermal performance of helmet design in the early stage of a design process. Additionally, an iterative verification methodology was initiated that allows evaluating virtual prototypes, physical prototypes and commercially available helmets.

Acknowledgements. The wind tunnel tests were performed at the facility of Ergonomics and Aerosol Technology, Department of Design Sciences, Lund University.

References

1. Patel, R., Mohan, D.: An improved motorcycle helmet design for tropical climates. Appl. Ergon. **24**, 427–431 (1993)
2. Fife, D., Davis, J., Tate, L., Wells, J.K., Mohan, D., Williams, A.: Fatal injuries to bicyclists - the experience of Dade County, Florida. J. Trauma-Inj. Infect. Crit. Care **23**, 745–755 (1983)
3. Wood, T., Milne, P.: Head-injuries to pedal cyclists and the promotion of helmet use in Victoria Australia. Accid. Anal. Prev. **20**, 177–185 (1988)
4. Thompson, D.C., Rivara, F.P., Thompson, R.S.: Effectiveness of bicycle safety helmets in preventing head injuries - a case-control study. JAMA – J. Am. Med. Assoc. **276**, 1968–1973 (1996)
5. Servadei, F., Begliomini, C., Gardini, E., Giustini, M., Taggi, F., Kraus, J.: Effect of Italy's motorcycle helmet law on traumatic brain injuries. Inj. Prev. **9**, 257–260 (2003)
6. Orsi, C., Stendardo, A., Marinoni, A., Gilchrist, M.D., Otte, D., Chliaoutakis, J., Lajunen, T., Ozkan, T., Pereira, J.D., Tzamalouka, G., Morandi, A.: Motorcycle riders' perception of helmet use: complaints and dissatisfaction. Accid. Anal. Prev. **44**, 111–117 (2012)
7. Bogerd, C.P., Aerts, J.P., Annaheim, S., Bröde, P., De Bruyne, G., Flouris, A.D., Kuklane, K., Mayor, T.S., Rossi, R.M.: A review on ergonomics of headgear: thermal effects. Int. J. Industr. Ergon. **45,** 1–12 (2015)
8. Brühwiler, P.A.: Heated, perspiring manikin headform for the measurement of headgear ventilation characteristics. Meas. Sci. Technol. **14**, 217–227 (2003)
9. Brühwiler, P.A.: Radiant heat transfer of bicycle helmets and visors. J. Sports Sci. **26**, 1025–1031 (2008)
10. De Bruyne, G., Aerts, J.-M.M., Sloten Vander, J., Goffin, J., Verpoest, I., Berckmans, D.: Transient sweat response of the human head during cycling. Int. J. Industr. Ergon. **40**, 406–413 (2010)

11. De Bruyne, G., Aerts, J.-M.M., Vander Sloten, J., Goffin, J., Verpoest, I., Berckmans, D.: Quantification of local ventilation efficiency under bicycle helmets. Int. J. Industr. Ergon. **42**, 278–286 (2012)
12. Blatteis, C., Boulant, J., Cabanac, M., Cannon, B., Freedman, R., Gordon, C.J., Hales, J.R.S., Horowitz, M., Iriki, M., Janský, L., Jessen, C., Kaciuba-Uscilko, H., Kanosue, K., Kluger, M.J., Laburn, H.P., Nielsen-Johannsen, B., Mercer, J.B., Mitchell, D., Simon, E., Shibata, M., Sz_ekely, M., Szel_enyi, Z., Werner, J., Kozyreva, T.: Glossary of terms for thermal physiology. Jpn. J. Physiol. **51**, 245–280 (2001)

Modeling Transition and Mobility Patterns

Adele Hedrick[1], Ying Zhu[2], and Ken Pu[2(✉)]

[1] Faculty of Science, University of Ontario Institute of Technology, 2000 Simcoe Street North, Oshawa, ON, Canada
adele.hedrick@uoit.ca
[2] Faculty of Business and IT, University of Ontario Institute of Technology, 2000 Simcoe Street North, Oshawa, ON, Canada
{ying.zhu, ken.pu}@uoit.ca

Abstract. We present a solution to model user transitions and mobility patterns without the need of accessing any cloud services, and thus completely preserving user privacy. Our algorithm relies solely on the sensor inputs of the mobile device to gather environmental fingerprints. A real-time hierarchical clustering algorithm efficiently organizes the individual signatures into a hierarchy of meaningful significant locations at various time scale. By applying (normalized) information measure and neural network based learning, we are able to identify the most salient transition patterns that best characterize the mobility data of the user. Our algorithms are completely online, and do not rely on any networked resources. Thus, user can gain insight to their own mobility activities, and has total control of how this information is to be shared with other applications. We will demonstrate using real-life data the effectiveness and efficiency of our approach. Several appealing visualizations will be showcased. The resulting transition models can be utilized towards better user experience for a variety of mobile applications such as activity scheduling and travel route planning.

Keywords: Human mobility · Modeling · Privacy

1 Introduction

Smart devices and mobile computing have become an integral part of the modern everyday life. Most of us carry a relatively powerful computing device that is constantly collecting information using an array of different sensors including the wireless network connectivity. While the smartphones are capable of providing us geolocation and mobility history, much of the algorithms and methods to achieve this require additional cloud services. For instance, Google Maps require access to the cloud Web services and other cellular network based approaches [1] to generate the geolocations and the mobility history of the device. Depending on the situation, user may be concerned with the leakage of privacy while still wish to retain the ability to access and analyze one's own mobility history and patterns. We argue that this can be achieved by leveraging off of the device sensor inputs. Most of the collected sensor information is thrown away and never used in any meaningful way. However, there is a great deal of value that we can derive from the on-device data by applying intelligent data process [2, 3].

D.N. Cassenti (ed.), *Advances in Human Factors in Simulation and Modeling*,
Advances in Intelligent Systems and Computing 591, DOI 10.1007/978-3-319-60591-3_48

Our motivation is to design efficient data analytic processing pipelines that are suitable for the mobile platform in order to achieve the following goals:

1. Summarize the real-time wireless data observations collected by the mobile device in a space-efficient manner.
2. The summarization allows us to construct transition models of the mobile user, and the models can be used to gain insight of the user mobility patterns.
3. The analysis should solely rely on the data collected by the mobile device at the user's discretion. No external cloud services and network exchange are needed to ensure that all the mobility analysis does not lead to any privacy leakages.

2 Background and Problem Definition

Mobile devices have a number of continuous sensors which are sources of data. The most notable one is the on-device wireless network adapter. It naturally gathers the ambient wireless hotspots. Each wireless hotspot has a unique identifier known as BSSID. Modern mobile devices can very efficiently scan the available BSSID's at fixed time intervals. Each scan reports a set of BSSIDs and their relative strengths. We assume that the device continuously gathers a stream of BSSID, and we call this the *raw readings* of the mobile device.

2.1 Definition: Raw Reading

The raw readings are a sequence of BSSID sets and their signal strength, denoted as:

$$\boldsymbol{R} = \{(t_i, B_i) : i = 0, 1, \ldots\} \tag{1}$$

where t_i are the timestamps and B_i is a collection of BSSIDs and their strength.

2.2 Definition: Transition Model

A transition model consists of two parts.

1. *A set of significant locations $X = \{L_1, L_2, \ldots\}$. Each location $\boldsymbol{L}$ is a set of BSSIDs.*
2. *An family of prediction functions: $P_L(t) \in [0, 1]$ that predicts the likelihood that we will be at location L at some time in the future t.*
3. *A transition model: $P(L_1, L_2) \in [0, 1]$ that predicts the likelihood that we will go to location L_2 if the current location is L_1.*

2.3 Problem Definition

This paper describes an end-to-end pipeline that process the data in the raw reading to a transition model.

Given the density of Wi-Fi hotspots, each distinct physical location (e.g. home or office) may yield dozens if not more BSSIDs in the reading. To further complicate the

situation, Wi-Fi signals can fluctuate and intermittently be disrupted due to hardware glitches. Moreover, the distribution of BSSIDs is highly non-uniform. In an urban environment, each physical location may correspond to several dozens of distinct BSSIDs while on the road or in rural areas, each physical location may only have one or two BSSIDs.

The first problem toward our objective of transition modeling is to learn a mapping of BSSID readings to physically significant locations. Our previous work [4] address this specific problem using an unsupervised algorithm. The algorithm constructs a hierarchy of locations with increasing geographical scale. The hierarchy consist of nodes which are physical locations. At successively higher levels, the locations correspond to larger physical scales. The root corresponds to the entire physical range that the mobile phone has covered, while the leaf nodes corresponds to specific locations. For completeness, we will briefly outline our solution for location identification. The physical location hierarchy is used as the basis of the contribution of this paper.

The second sub-problem of transition modeling is to distinguish the significance of the locations on in the hierarchy. Each location corresponds to some node in the hierarchy (to be described later). Since the locations of different granularity and geographical scale, they have unequal degree of *interestingness* for the purpose of constructing the transition model as defined above. In this paper, we will present a scoring function that assigns the degree of *interestingness* of a location. The novelty of the ranking function is that it uses a combination information theory and unsupervised machine learning to *learn* the score of the locations.

3 Hierarchical Localization

In this section, we will describe the method for constructing a multi-scale locations from the raw readings. Reads can refer to our previous publication [4] for any details omitted. For completeness, we will outline the key elements of the hierarchical localization algorithm which are essential for the contribution of this paper as described in Sect. 4.

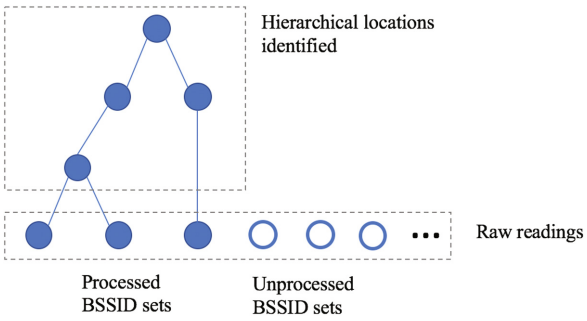

Fig. 1. A partially constructed hierarchy of locations. The leaf nodes are the BSSID sets from the raw readings. Each reading is successively processed and added to a partially constructed hierarchy.

We successively process each reading, and merge it incrementally into a hierarchy of location nodes as shown in Fig. 1. The location nodes near the root cover larger sets of BSSIDs, and thus spanning greater geographical scale. The algorithm is online, and performs well independent of the length of the raw readings.

Let H be the hierarchy constructed by online segmentation. Each node $L \in H$ is a location that has a set of BSSIDs. Due to the online nature of the algorithm, it is possible that a single physical location (e.g. home) can appear multiple times in the location hierarchy. For this reason, we utilize a hash function that can map a set of BSSID to a hash value using *min-wise* [5] hashing. The reason we choose min-wise hashing is that the hash value can be used to perform approximate Jaccard similarity [5] between two sets of BSSIDs.

We are able to construct the following from the raw readings:

1. A hierarchy of locations, with each level having successively broader geographic coverage.
2. A min-wise hash based dictionary of locations where the key is the min-wise hash value of the BSSID set of the location, and the value is the BSSID set.

4 An Information Theoretic and Learning Based Ranking and Modeling

This section presents the main contribution of this paper, namely a scoring function that uses the normalized information measure and a machine learning based score to assess the interestingness of a given location.

At an intuitive level, a location is *uninteresting* if it appears so rarely that it does not contribute to any mobility *pattern*. At the other extreme, a location is equally uninteresting if it spans such large geographical scale that it's nearly always being detected by the device. So, we need to design a scoring function that captures the following two aspects of interestingness:

1. Location should be part of a pattern.
2. The presence at a location should be informative.

Fortunately, there are well established mathematical models that corresponds to the concepts of *pattern* and *information.* The former can be captured by machine learning algorithms, while the later can be described by statistical measure of entropy and mutual information. In this section, we describe a data analytics pipeline that computes a two-dimensional score for locations that reflect the presence of pattern and information.

4.1 From Activity Graph to a Feature Space

Recall that the raw readings R consists of a sequence of timestamped BSSID sets, written (t_i, B_i), where B_i is a set of BSSIDs detected at timestamp t_i.

Definition: Activity Sequence. *Given a location node $L \in H$ with BSSIDs B_L, the activity sequence of L, written A_L, is given as* $\{(t_i, \text{sim}(B_L, B_i) : i = 0, 1, \ldots)\}$.

The activity sequence of L provides the presence of location L over time. The timestamps are absolute values, i.e. UNIX system timestamps. Thus, every t_i is unique. We transform the timestamp into *feature vectors*.

$$f(t) = (\text{month}, \text{day of week}, \text{hour of day}) \tag{3}$$

So, the activity sequence in the feature space becomes a feature activity sequence:

$$F_L = \{(f(t_i), \text{sim}(B_L, B_i)) : i = 0, 1, ..\} \tag{4}$$

4.2 A Neural Network Based Pattern Score

A location is *interesting* if it exhibits a pattern. Neural networks [6] are excellent at capturing *patterns*. By controlling the number of neurons and layers in the network architecture, we can control the degree of complexity of the pattern we seek. For our application, we utilize a shallow multi-layer perceptron (MLP) architecture to fit a best model for the observation derived from F_L. The input to the MLP is the feature vectors $\{f(t_i) : i = 0, 1, \ldots\}$, and the training is done on the output of the activity level $\{\text{sim}(B_L, B_i) : i = 0, 1, ..\}$.

If there exists a distinct pattern, the trained MLP will exhibit high degree of accuracy from the training. Namely the model fits the data well. We stress that the MLP needs to be appropriately designed so that there is no overfitting to the data.

Definition: Predictability. *The predictability of a location $L \in H$, written* $\text{pred}(L)$*, is given as the training accuracy of MLP with the feature vectors as inputs, and activity level as the output.*

Predictability of a location is a measure of the degree of a pattern in the activity sequence of that location. While this will filter out uninteresting locations that have very rare appearances, unfortunately, predictability by itself is not enough to guarantee interesting locations. Consider locations in the hierarchy that span large geographic scale, such as the root location. It's always present, so the activity sequence is nearly: $\{(t_i, 100\%)\}$. This is exceedingly predictable by any MLP, so it will have a very high predictability score. We will address this issue by introducing a second score that measures the amount of information in the distribution in the feature space.

4.3 An Information Theoretic Score

Consider the feature sequence $F_L = \{(f(t_i), sim(B_L, B_i)) : i = 0, 1, \ldots\}$. We can compute a histogram which describes the activity distribution over all possible features.

Definition: Activity Distribution in Feature Space. *Let f be a feature (namely a tuple of month, day of week, hour of day), and $L \in H$ a location in the hierarchy. The activity distribution is defined as:*

$$h_L(f) = \sum_{i:f(t_i)=f} \mathrm{sim}(B_L, B_i) \tag{5}$$

*Namely, $h_L(f)$ is the sum of all the aivities of L during timestamps that match the feature f. We **normalize** the distribution h(f) such that it is a valid probability mass function over the features.*

Definition: Support. *The support of a location $L \in H$, written $support(L)$, is the percentage of features that has activity for the location.*

$$support(L) = \frac{|\{f : h_L f(L) > 0\}|}{n} \tag{6}$$

We use normalized entropy to measure the amount of redundancy exhibited by the activity distribution. Let n be the number of distinct features seen in the feature sequence. The normalized entropy of h_L is given by

$$\hat{E}(L) = -\frac{\sum_f h_L(f)\log(h_L(f))}{\log(n)} \tag{7}$$

The information gained when detecting the presence of a location L is the reduction in the normalized entropy from that of the root location (one with the largest geographical scale). So, the relative information of a location is given by

$$\inf(L) = \left(\hat{E}(\mathrm{root}(H)) - \hat{E}(L)\right) \cdot support(L) \tag{8}$$

Definition: Interestingness Score. *The interestingness of a location L is given by the vector:*

$$\mathrm{score}(L) = \begin{bmatrix} \mathrm{pred}(L) \\ \inf(L) \end{bmatrix}. \tag{9}$$

The score provides a definitive and mathematical ordering of all the locations detected in the hierarchy H. Namely, we c say that L_1 is more interesting than L_2, written $L_1 > L_2$, if we have $\mathrm{pred}(L_1) > \mathrm{pred}(L_2)$ and $\inf(L_1) > \inf(L_2)$. Given that the scoring function is two dimensional, we do not guarantee that all pairs of locations are comparable.

4.4 Transition Modeling

We know present the main thesis of the paper, namely transition modeling of the mobile user.

To identify the interesting locations, we filter all locations in the hierarchy by two thresholds: minimal predictability α and minimal information β. The interesting locations are defined as

$$L^* = \{L \in H : \text{score}(L) > \begin{bmatrix} \alpha \\ \beta \end{bmatrix}\} \tag{10}$$

The appropriate choice for α and β depends on the application. If patterns are of greater importance, α should be increased, and if local precision is required, than β is to be increased. Furthermore, the choices of the thresholds will also determine the number of interesting locations.

As given in Sect. 2, we are to construct a predictable model for individual interesting locations in L^*, and also the transition probabilities. Both are quite straightforward.

The location predication is immediately given by

$$p(L, t) = \text{MLP}_L(f(t)) \tag{11}$$

which is to be computed by the MLP neural network. The transition probability can be constructed from the *interesting sequence*. For each reading (t_i, B_i), we can estimate the location of B_i by the following

$$\text{L}_i = \text{argmax}\{\text{sim}(B_i, L) : L \in L^*\} \tag{12}$$

That is, L_i is the interesting location that has the greatest similarity to B_i. This induces a sequence of *interesting* locations given by

$$R^* = \{L_i : i = 0, 1, \ldots\} \tag{13}$$

The transition probability is given by

$$p(L_1, L_2) = \frac{|\{i \in R^* : L_i = L_1 \text{ and } L_{i+1} = L_2\}|}{|\{i \in R^* : L_i = L_1\}|} \tag{14}$$

5 Experiments

We have gathered approximately one month of data, and ran the transition modeling in an online fashion. In this section, we include the observations from the model and the intermediate steps of the pipeline (Fig. 2).

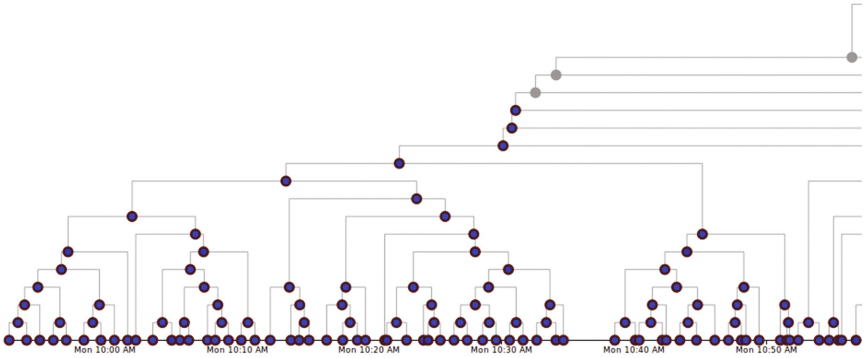

Fig. 2. Part of the online location hierarchy as it is being generated.

Below are samples of various locations and their characterizations based on the interestingness score (Figs. 3, 4 and 5).

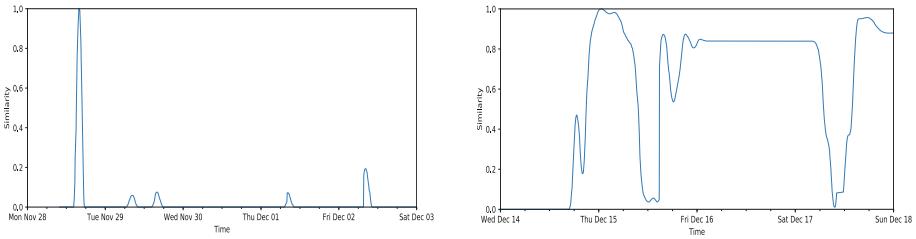

(a) (b)

Fig. 3. Two location activity sequence with LOW predictability and LOW information due to the low degree of support (L) in (a), and lack of pattern in (b).

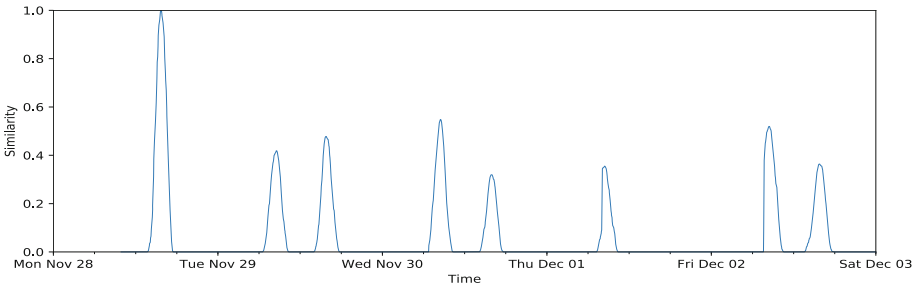

Fig. 4. A location activity sequence with HIGH predictability and HIGH information.

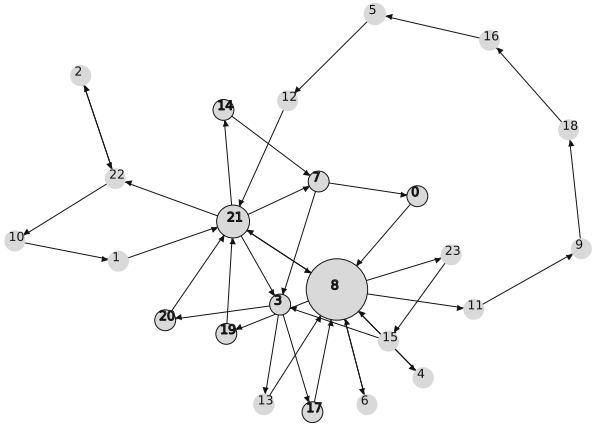

Fig. 5. The transition diagram with illustrating the most significant transitions of the top interesting locations.

6 Conclusion and Future Work

We have presented a complete pipeline that maps raw Wi-Fi scans collected by the mobile device to a transition model of the user without resorting to any additional cloud services, thus preserving the user privacy completely.

The contribution of this paper is the design of a two-dimensional score that assesses the interestingness of a location. The score uses a simple machine learning model (MLP) to capture any patterns if present, and an information theoretic measure to capture the amount of information of a location. Together, we are able to automatically sift out the most interesting locations encountered by the mobile device. This allows us to construct a compact transition model that are capable of:

1. Predict future occurrence of locations in the future.
2. Predict the sequence of locations most likely to occur in the future.

As future work, we would like to investigate ways that the transition model can create a more integrated and engaging user experience without any leakage of the user privacy by means of predicative decision making.

References

1. Mayorga, C.L.F., et al.: Cooperative positioning techniques for mobile localization in 4G cellular networks. In: IEEE International Conference on Pervasive Services. IEEE (2007)
2. Song, C., Qu, Z., Blumm, N., Barabási, A.L.: Limits of predictability in human mobility. Science **327**(5968), 1018–1021 (2010)
3. Jensen, B.S., et al.: Estimating human predictability from mobile sensor data. In: 2010 IEEE International Workshop on Machine Learning for Signal Processing (MLSP). IEEE (2010)

4. Hedrick, A., Pu, K.Q., Zhu, Y.: Hierarchical temporal mobility analysis with semantic labeling. In: Proceedings of 2016 International Conference on Computational Science and Computational Intelligence (CSCI 2016), Las Vegas, NV, 8 p., 15–17 December 2016
5. Cohen, E., Datar, M., Fujiwara, S., Gionis, A., Indyk, P., Motwani, R., Yang, C.: Finding interesting associations without support pruning. IEEE Trans. Knowl. Data Eng. **13**(1), 64–78 (2001)
6. Haykin, Simon, Network, Neural: A comprehensive foundation. Neural Netw. **2**(2004), 41 (2004)

A Combined Statistical Shape Model of the Scalp and Skull of the Human Head

Femke Danckaers[1], Daniël Lacko[2], Stijn Verwulgen[2], Guido De Bruyne[2(✉)], Toon Huysmans[1], and Jan Sijbers[1]

[1] imec - Vision Lab, Department of Physics, Faculty of Sciences, University of Antwerp, Antwerp, Belgium
{Femke.Danckaers, Toon.Huysmans, Jan.Sijbers}@uantwerpen.be

[2] Department of Product Development, Faculty of Design Sciences, University of Antwerp, Antwerp, Belgium
{Daniel.Lacko, Stijn.Verwulgen, Guido.DeBruyne}@uantwerpen.be

Abstract. In this paper, we describe a framework to build a combined statistical shape model (SSM) of the outer surface of the scalp and the inner and outer surface of the skull of the human head. Such an SSM is a valuable tool when designing headgear, as it captures the variability of head geometry of a given population, enabling detailed analysis of the relation between the shape of the scalp and the skull. A combined SSM of the head may allow to work towards population based Finite Element (FE) models e.g. for safety and comfort predictions when wearing headgear. Therefore, a correspondence between the skull and scalp surfaces, originating from MRI scans, is determined using elastic surface registration. The combined SSM shown to be compact, to be able to generalize to unseen instances by adjusting the shape parameters and to be shape specific. Therefore, we can assure that, by adjusting the shape parameters, a broad range of realistic head shapes can be formed.

Keywords: Statistical shape model · Human head · Scalp · Skull · Headgear · SSM

1 Introduction

A statistical shape model (SSM) of the human head is a valuable tool to design headgear, because it captures the variability of head geometry of a population. SSMs are built from 3D scans of a population of shapes. Therefore, they contain much more information than traditional anthropometrical measurements. When designing headgear, SSMs can be employed for ergonomic optimization warranting an optimal fit of the product to the geometry of the head, for a target population [1].

Insight in 3D skin and bone thickness of the human head for specific populations may help to avoid local peak pressure on the head while wearing a helmet in future helmets. Additionally, it may enhance the accuracy of Finite Element (FE) models of the human head that aim at predicting brain damage. The soft tissue layer is expected to

D.N. Cassenti (ed.), *Advances in Human Factors in Simulation and Modeling*,
Advances in Intelligent Systems and Computing 591, DOI 10.1007/978-3-319-60591-3_49

be a contributing parameter in the kinematics of head movement during head impact to affect rotational acceleration and velocity of the human brain. The bone tissue layer is a contributing parameter in the prediction of linear acceleration of the human brain during head impact.

A combined SSM of the head may allow to work towards population based FE models for safety and comfort predictions when wearing headgear. Such an FE head model can be used in simulations, to predict the impact on the head in accidents that cause trauma injuries to determine regional responses [2–5]. Typical FE head models are based on one head shape or the average head, calculated from a population [6–8]. A typical example is the Strasbourg University Finite Element Head Model [9, 10]. This is a very detailed FE model of the human head, with many internal structures included, and based on a single skull. By building an FE model from an SSM, it is adjustable in shape [2, 11], what can lead to more accurate, customizable FE models. Such a statistical FE model is especially useful when designing helmets [5, 12], because the impact on the head in an accident can be studied on different shapes and sizes of human heads, and thus improve the biofidelic characteristics of current FE head models for impact.

Most SSMs of the head only describe the outer skin layer of the head and do not contain information about the thickness of the scalp and the skull [1, 13, 14], while this information is important for e.g. predicting local skin pressure on the head. Claes et al. [15] constructed a combined SSM of the face shape and soft tissue depths for forensic facial reconstruction on an unidentified person's skull. Their technique is labor-intensive, as the researchers had to place manually indicated anatomical landmarks on the surface and measure soft tissue depths at 52 locations.

In this paper, we describe a technique for building a combined SSM of the human head, more specifically, the outer surface of the scalp and the inner and outer surface of the skull. The paper is organized as follows. First, the segmentation of the 3D surfaces from the MRI scans is detailed. Second, the construction of a combined SSM is explained. Next, in the results section, the SSM is subject to quality tests to evaluate the model's compactness, generalizability and shape specificity. Finally, the results are discussed and a conclusion is formulated.

2 Methods

Scalp and skull surfaces are separately segmented from MRI datasets. A reference mesh (a uniformly resampled surface from the dataset) is constructed for the scalp and for the skull, and is registered to all input meshes of each layer, to obtain a homologous point-to-point correspondence. Next, an average mesh is calculated for both the scalp and skull and used as template to register the input scalp and skull meshes for the second time to prevent a biased result. Then, the registered scalp and skull of each subject are merged again.

A combined SSM is built using Principal Components Analysis (PCA) on the corresponded heads. In this SSM, the average surface and skull thickness, and the main variances are incorporated. The process is shown in Fig. 1.

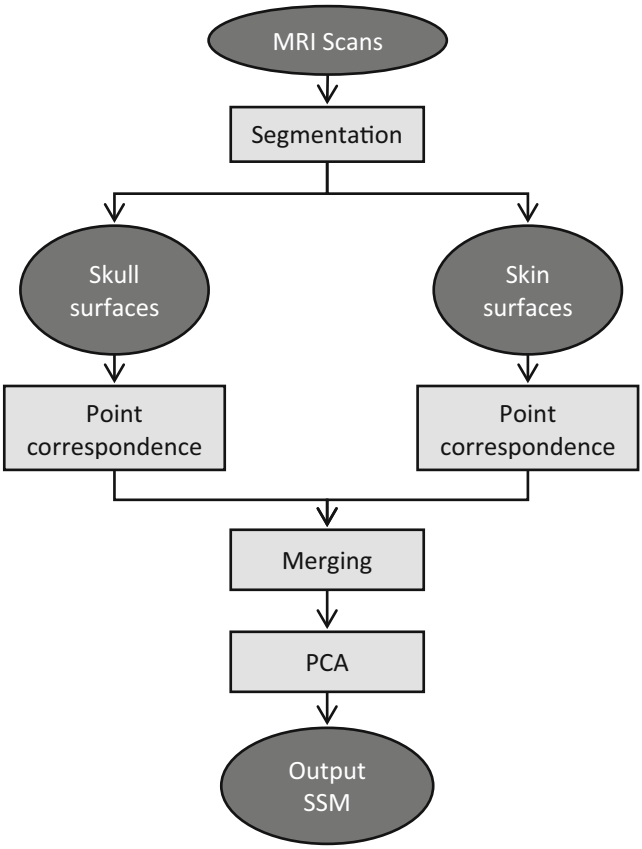

Fig. 1. Framework for building a combined SSM of the skull and scalp.

The training population consisted of 85 MRI T1-FFE-weighted scans (male and female, aged between 20 and 40 years, Western Population) originating from the International Consortium for Brain Mapping (ICBM) database [16]. The scans were acquired using a Philips ACS III 1.5 T scanner in the sagittal acquisition plane, with a slice thickness of 1 mm, an echo time of 10 ms, a repetition time of 18 ms and a flip angle of 30°.

2.1 Segmentation

From magnetic resonance imaging (MRI) scans, the scalp and the skull are separately segmented using the Statistical Parametric Mapping (SPM12) [17] package from MATLAB and converting the outcome to 3D meshes. The skin corresponds with layer 3 and the skull corresponds with layer 4 in SPM12. Scalp and skull were constructed separately by segmentation as different surfaces, because finding correspondences between nearby components is error-prone.

2.2 Statistical Shape Model (SSM)

In this section, the methodology to build a combined skull/scalp SSM is described. The algorithm is based on a previously developed elastic surface registration algorithm [18]. The first part of the framework is surface registration. The registered surfaces are used in the second part of the framework, where an SSM is built. The method is applicable to other layered surfaces as well.

Surface Registration. The first step of surface registration is a rigid alignment. Therefore, in both surfaces corresponding points are identified. This is done by casting a normal ray from each vertex of the reference surface to the target surface. When the normal of an intersection point is in the same direction (within a tolerance) as the normal of the point on the reference surface, that point can be considered corresponding. Another restriction for corresponding points is that the normal may not intersect the surface multiple times before reaching the corresponding point. The corresponding points serve as landmarks for a least-squares rigid alignment step.

In the elastic part of the registration the vertices are allowed to translate separately, while motion is restricted by a stiffness parameter that regulates the strength of the connection with the neighboring vertices and which decreases throughout the iterations. In this way, the movement of neighboring vertices is constrained, resulting in similar movements for nearby vertices. By applying weights to each vertex, the importance of this vertex can be set. If a corresponding point is found, its weight is set to 1.0. If no corresponding point for a vertex of the target mesh can be found, its weight is set to zero. In that case, this vertex simply translates along with its neighboring vertices.

Building a Statistical Shape Model. In the second part of our framework, an SSM is built based on the correspondences of N shapes, with every shape consisting of n vertices, that resulted from the surface registration [19]. To build an SSM, it is important that the surfaces are superimposed by optimally translating and rotating the surfaces to minimize the distance between corresponding points. In this way, shape information is maximally compressed. The optimal poses are determined by Procrustes analysis. The SSM is built by performing principal components analysis (PCA) on the corresponding points of the population.

In this SSM, the mean surface $\bar{\boldsymbol{x}} \in \mathbb{R}^{3n}$ and the main variances or PC modes, represented by $\boldsymbol{P} \in \mathbb{R}^{3n\times(N-1)}$, are incorporated. The population of N shapes is represented by an $3n$-dimensional point cloud, where each point represents a shape as a $3n$-dimensional vector of vertices. This cloud can be represented by $N-1$ eigenmode vectors, where the first eigenmode is the largest variance in the population, the second eigenmode is the second largest variance perpendicular to the first, etc. This means that a new surface vector $\boldsymbol{y} \in \mathbb{R}^{3n}$ can be formed by adapting the SSM parameters as follows

$$\boldsymbol{y} = \bar{\boldsymbol{x}} + \boldsymbol{P}\boldsymbol{b}, \tag{1}$$

with $\boldsymbol{b} \in \mathbb{R}^{(N-1)}$ the vector which contains the SSM parameters.

3 Experiments and Results

In this section, the results of the framework are described.

3.1 Segmentation

In the dataset, none of the skulls were completely segmented, because the SPM12 package was constructed with a focus on brain mapping and works with a spatially limited skull template. The dataset was sufficient for our research, because we work on comfort of helmets and therefore focus on the upper part of the head. A slice of the head of a test subject and the resulting skull and scalp surfaces are shown in Fig. 2. Note that in some scans a bar is visible on the top of the head, because the heads of the subjects from the ICBM are fixated. This bar is not visible in the model, because a smooth template surface served as input for the elastic surface registration to reduce protrusions and other irregularities. Remaining irregularities were averaged out by calculating the SSM.

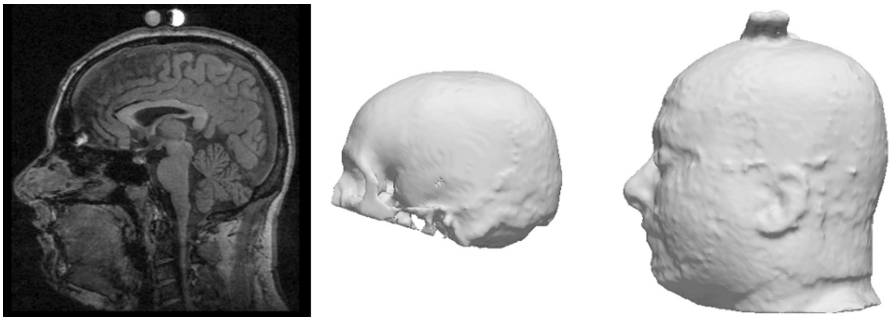

Fig. 2. Slice of a head scan and a segmented scalp and skull. Note that the skull is not fully segmented, because SPM12 focuses on the brain. A bar is noticeable on the top of the head.

3.2 Statistical Shape Model (SSM)

The scalp and the skull were separately segmented from each head scan, and were both registered by the same template surfaces. The skull template surface was uniformly resampled to 100041 vertices, the scalp template surface was uniformly resampled to 89389 vertices. After the surface registration, both scalp and skull of the same subject were merged to become a combined surface, as shown in Fig. 3.

In Fig. 4, the first three PC modes of the SSM, built from combined surfaces, are shown. These shape modes describe the shape variations inside the population. The first mode describes mainly the size of the head, the second mode describes the width-length ratio of the head, and the third mode describes mainly the curvedness of the skull.

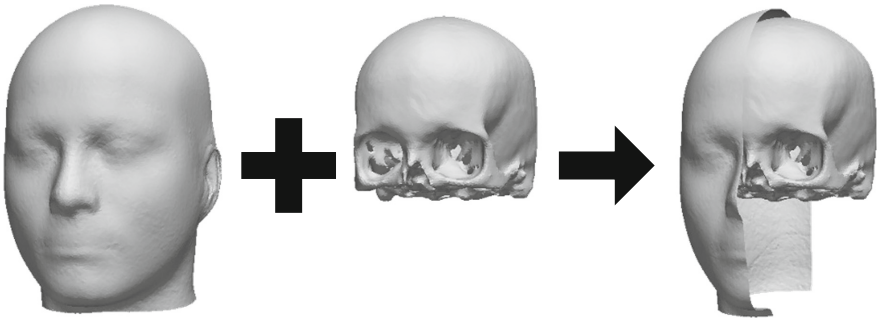

Fig. 3. Uniting the separate skull and scalp from Fig. 2 to result in a combined surface.

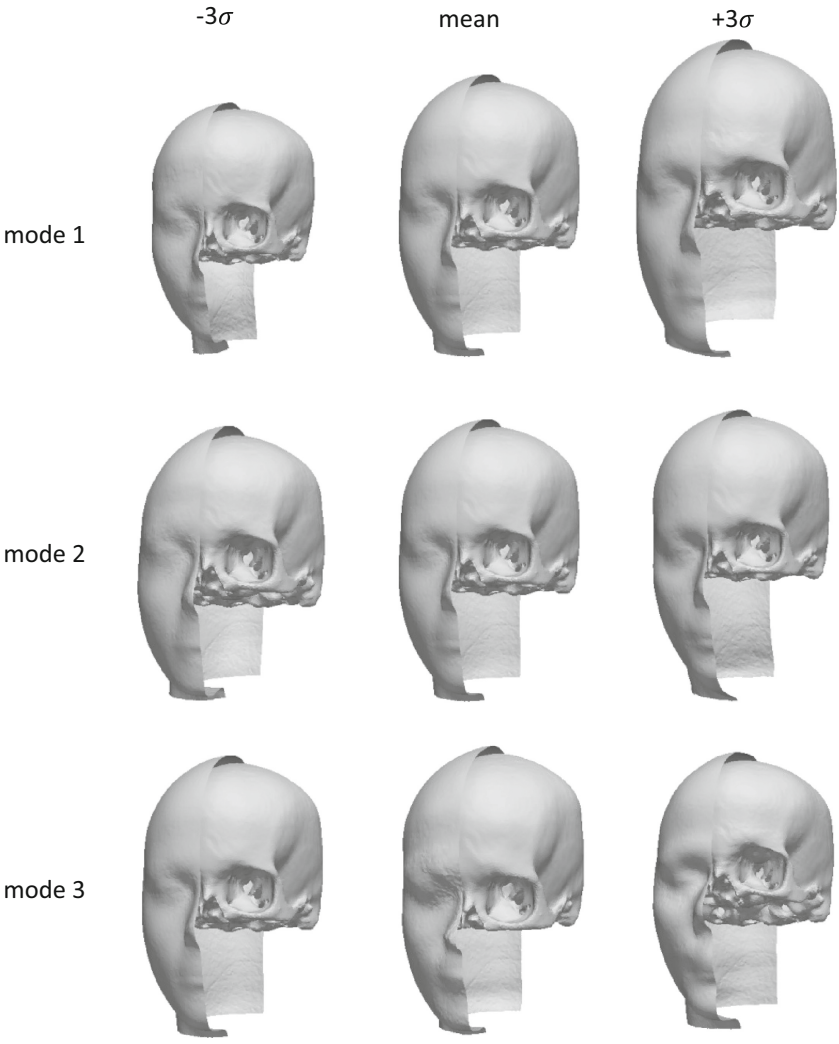

Fig. 4. First three eigenmodes of the combined SSM of the human scalp and skull.

3.3 Model Performance

Compactness, generalization ability, and specificity are widely used measures [20, 21] for quantifying the correspondence quality of an SSM. In this section, the different model performance measures were calculated for the combined SSM and the separate SSMs of the skull and the head.

Compactness. Compactness of a shape model is a measure how well a shape from the population is described by a limited amount of PC modes. Preferably, an SSM is approximated well with few modes. The compactness is expressed as the sum of variances of the SSM:

$$C(m) = \sum_{i=1}^{m} \lambda_i, \tag{2}$$

where λ_i is the variance on the vertex locations in shape mode i, and $C(m)$ is the compactness using m modes.

The results are shown in Fig. 5. To describe over 80% of the shape variation inside the population of combined head shapes, six shape modes were needed. Thirteen shape modes describe over 90% of the shape variation. Therefore, our combined SSM is a compact representation of the population.

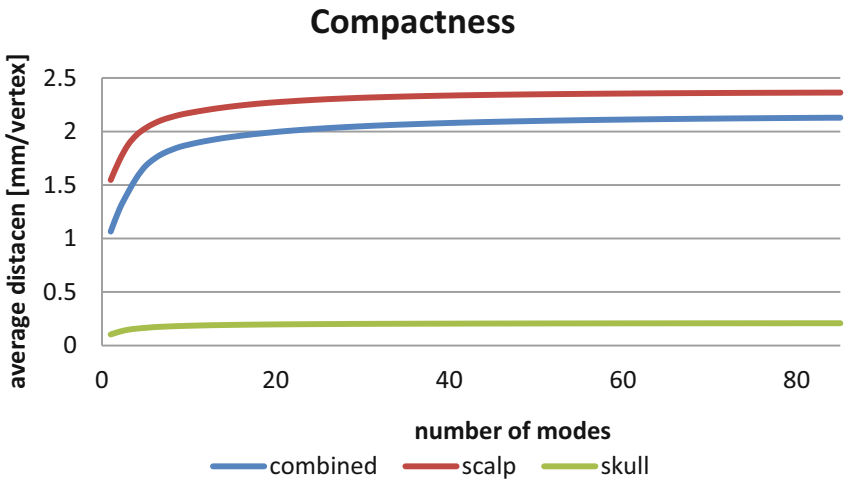

Fig. 5. Compactness graph. The average deviation from the mean shape to describe shapes with a specific number of shape modes is shown.

An example of a surface represented by different numbers of modes is shown in Fig. 6. Using more parameters led to a shape that looked more like the original shape. The more parameters that are used to reconstruct a shape, the less difference is noticeable.

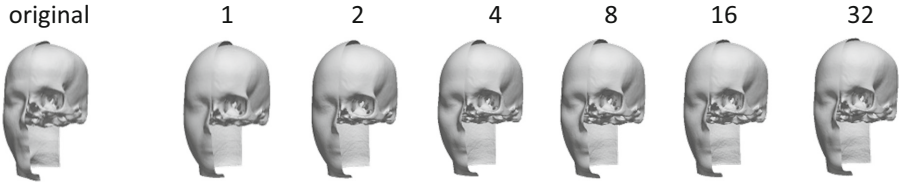

Fig. 6. Shape generated with a different number of shape modes. Note the difference in shape of the cheekbones and jaw. The difference between a surface reconstructed by 16 shape modes and 32 shape modes is minimal.

Generalizability. Generalizability relates to how well the SSM can generalize to a formerly unseen head shape. The SSM should be able to describe all head shapes, not only the head shapes of the training set. If an SSM is over-fitted to the training set, it will not be able to generalize to unseen samples.

Generalizability $G(m)$ was measured by performing leave-one-out tests, where an SSM was built by using all training shapes but one. Next, the left-out shape was described by adapting the shape parameters of the SSM. Generalizability was calculated as the mean error over all left out shapes,

$$G(m) = \frac{1}{N_m} \sum_{i=1}^{m} \|\boldsymbol{x}_i - \boldsymbol{x}_i'(m)\|^2, \tag{3}$$

where $\boldsymbol{x}_i$ is the left out shape and $\boldsymbol{x}_i'(m)$ is the attempted description using the SSM with m modes. The number of trials, or objects in the SSM, is represented by N_m.

In Fig. 7, the generalizability graph is shown. The generalizability error was calculated in mm per vertex. The error of fitting a scalp and skull to an unseen instance

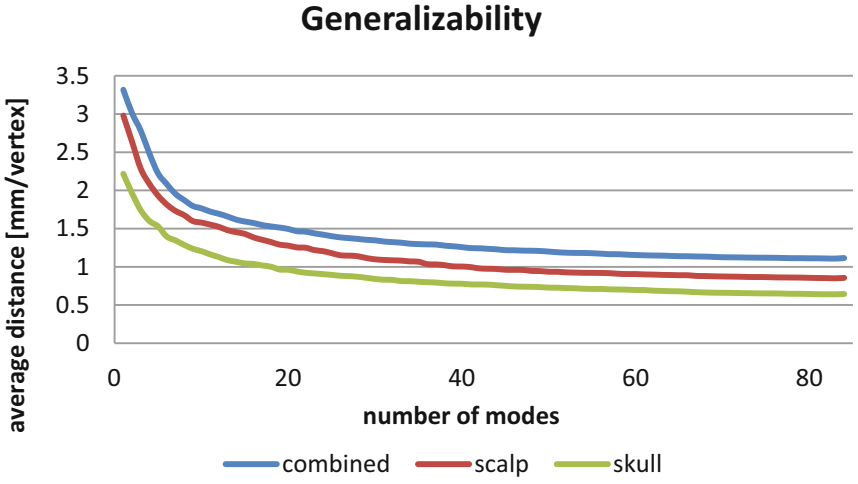

Fig. 7. The generalizability measure, in mm per vertex. The error flags represent the standard errors on the mean distance.

was 2.2 mm from five shape modes. Using 20 shape modes, the error was smaller than 1.5 mm. Note that the error for the scalp and skull separately was smaller than the error of the merged surface. This can be explained by the fact that the shape of both scalp and skull were dependent on each other. In future work, we will improve this by corresponding the scalp and skull together instead of corresponding them separately.

Specificity. A specific SSM can only represent instances of the object class that are similar to those in the training set. This was measured by generating an amount of shapes $(N_r = 1000)$ by generating a random parameter vector with m modes. Each sample was compared to the most similar shape in the training set. The specificity measure can be expressed as

$$G(m) = \frac{1}{N_m} \sum_{i=1}^{m} \|\boldsymbol{x}_i - \boldsymbol{x}_i'(m)\|^2, \tag{4}$$

with $\boldsymbol{x}_i'$ a shape example generated by the SSM and $\boldsymbol{x}_i$ the nearest member of the training set.

In Fig. 8, the specificity graph is shown. The specificity error was calculated in mm per vertex. The specificity test proved that our SSMs were able to generate shapes that resemble those in the training set, even though they differ from the shapes in the training set. The specificity error for the combined SSM is greater than the error for the separate SSMs. This means that the combined SSM represented more shape variation.

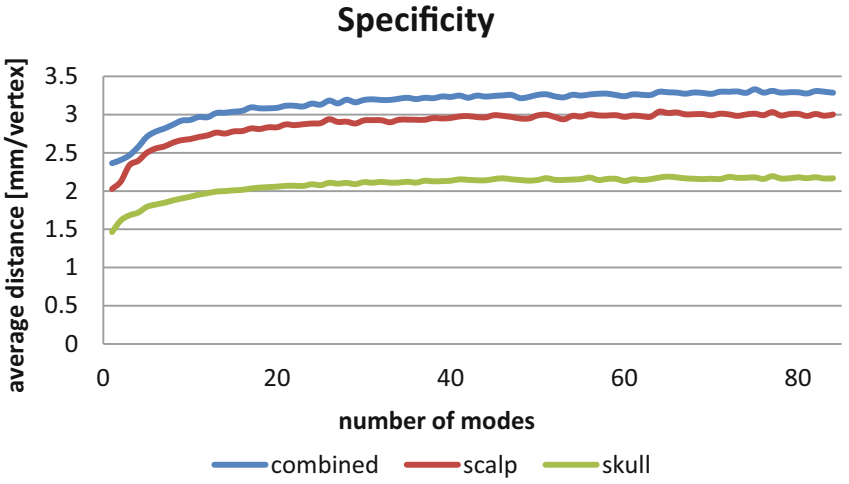

Fig. 8. The specificity measure, in mm per vertex. The error flags represent the standard errors on the mean distance.

4 Discussion

This combined SSM can be used as a virtual ergonomic 3D mannequin in Computer Aided Design (CAD) environments or as input for Finite Element (FE) and Computational Fluid Dynamics (CFD) simulations, when designing headgear. For example, it can be exploited in mass customization of all kinds of headgear systems that are built from FE models predicting local pressure. Another application is the development towards patient specific FE head impact models that may give more insight in brain damage due to accidents and can guide medical staff members during brain surgery.

The SSM is a compact representation of the population, because only six shape modes were needed to describe over 80% of the shape population. The model is able to generalize to an unseen instance, as six modes were sufficient to describe the instance with a mean error of 2.08 mm. A randomly generated shape using six shape modes is object specific, but differs from the dataset, since the average distance between a randomly generated object using six shape modes and the most similar object in the dataset was 2.77 mm. For helmet designing, a generalizability error of less than 1 mm is preferable. Our current model has a generalizability error of 1.1 mm when all shape modes are used to deform the model to an unseen head shape.

5 Conclusion and Further Work

In this work, we proposed a technique to perform statistical shape analysis on combined surfaces of the scalp and skull. Therefore, the relation between the scalp and skull can be analyzed. The constructed combined SSM is compact, so it can represent heads with a limited number of parameters with acceptable accuracy. Furthermore, we have proven that the combined SSM is able to generalize to unseen instances and is shape specific. Therefore, we can assure that by adjusting the shape parameters, a broad range of realistic head shapes can be formed. Our presented method is also applicable to other layered shapes.

The correspondences in the current SSM were split up in a skull part and a scalp part and merged for building a PCA model. For future work, we envision corresponding the combined surfaces, to assure a better correlation between skull and scalp.

Acknowledgements. This work was supported by the Agency for Innovation by Science and Technology in Flanders (IWT-SB 141520 and IWT 140881).

References

1. Lacko, D., et al.: Evaluation of an anthropometric shape model of the human scalp. Appl. Ergon. **48**, 70–85 (2015)
2. Bredbenner, T.L., Eliason, T.D., Francis, W.L., McFarland, J.M., Merkle, A.C., Nicolella, D.P.: Development and validation of a statistical shape modeling-based finite element model of the cervical spine under low-level multiple direction loading conditions. Front. Bioeng. Biotechnol. **2**(November), 58 (2014)

3. Jacob, A., et al.: Evaluation of helmet protection during impact of head to ground and impact of an object to head using finite element analysis. J. Saf. Eng. **5**(1), 8–16 (2016)
4. Mustafa, H., Pang, T.Y., Perret-Ellena, T., Subic, A.: Finite element bicycle helmet models development. Procedia Technol. **20**(July), 91–97 (2015)
5. Pintar, F.A., Philippens, M.M.G.M., Zhang, J., Yoganandan, N.: Methodology to determine skull bone and brain responses from ballistic helmet-to-head contact loading using experiments and finite element analysis. Med. Eng. Phys. **35**(11), 1682–1687 (2013)
6. Ponce, E., Ponce, D., Andresen, M.: Modeling heading in adult soccer players. IEEE Comput. Graph. Appl. **34**(5), 8–13 (2014)
7. Valdes-Hernandez, P.A., et al.: Approximate average head models for EEG source imaging. J. Neurosci. Methods **185**(1), 125–132 (2009)
8. Lei, Z., Yang, J.J., Zhuang, Z.: Headform and N95 filtering facepiece respirator interaction: contact pressure simulation and validation. J. Occup. Environ. Hyg. **9**(1), 46–58 (2012)
9. Asgharpour, Z., Baumgartner, D., Willinger, R., Graw, M., Peldschus, S.: The validation and application of a finite element human head model for frontal skull fracture analysis. J. Mech. Behav. Biomed. Mater. **33**, 16–23 (2014)
10. Tinard, V., Deck, C., Willinger, R.: New methodology for improvement of helmet performances during impacts with regards to biomechanical criteria. Mater. Des. **37**, 79–88 (2012)
11. Klein, K.F., Hu, J., Reed, M.P., Hoff, C.N., Rupp, J.D.: Development and validation of statistical models of femur geometry for use with parametric finite element models. Ann. Biomed. Eng. **43**(10), 2503–2514 (2015)
12. Zhang, L., Makwana, R., Sharma, S.: Brain response to primary blast wave using validated finite element models of human head and advanced combat helmet. Front. Neurol. **4**(August), 1–12 (2013)
13. Xi, P., Shu, C.: Consistent parameterization and statistical analysis of human head scans. Vis. Comput. **25**(9), 863–871 (2009)
14. Meunier, P., Shu, C., Xi, P.: Revealing the internal structure of human variability for design purposes. In: 17th World Congress on Ergonomics (2009)
15. Claes, P., Vandermeulen, D., De Greef, S., Willems, G., Suetens, P.: Craniofacial reconstruction using a combined statistical model of face shape and soft tissue depths: methodology and validation. Forensic Sci. Int. **159**, S147–S158 (2006)
16. Capetillo-Cunliffe, L.: Loni: Laboratory of Neuro Imaging (2007)
17. Kazemi, K., Noorizadeh, N.: Quantitative comparison of SPM, FSL, and brainsuite for brain MR image segmentation. J. Biomed. Phys. Eng. **4**, 13–26 (2014)
18. Danckaers, F., Huysmans, T., Lacko, D., Ledda, A., Verwulgen, S., Van Dongen, S., Sijbers, J.: Correspondence preserving elastic surface registration with shape model prior. In: Proceedings - International Conference on Pattern Recognition (2014)
19. Cootes, T.F., Taylor, C.J., Cooper, D.H., Graham, J.: Active shape models-their training and application. Comput. Vis. Image Underst. **61**(1), 38–59 (1995)
20. Davies, R.H., Twining, C.J., Cootes, T.F., Waterton, J.C., Taylor, C.J.: A minimum description length approach to statistical shape modeling. IEEE Trans. Med. Imaging **21**(5), 525–537 (2002)
21. Zihua, S.: Statistical Shape Modelling: Automatic Shape Model Building. University College London (2011)

Improved Motion Capture Processing for High-Fidelity Human Models Using Optimization-Based Prediction of Posture and Anthropometry

Anna Seydel[1], Kimberly Farrell[1(✉)], Ross Johnson[1], Timothy Marler[2], Salam Rahmatalla[1], Rajan Bhatt[1], and Karim Abdel-Malek[1]

[1] Virtual Soldier Research (VSR) Program, Center for Computer-Aided Design, The University of Iowa, Iowa City, IA 52242, USA
{anna-seydel, kimberly-farrell}@uiowa.edu
[2] RAND Corporation, Santa Monica, CA 90401, USA

Abstract. Improving motion capture processing onto a high-fidelity digital human model is an important research area. Although there has been significant research in this field, little work has been done to determine posture and anthropometry simultaneously with the intent of visualizing the data on high-fidelity human models. Many existing techniques are less accurate when applying processed data to a digital model for biomechanical analysis. This paper presents a novel approach that estimates posture and anthropometry using optimization-based posture prediction to determine joint angles and link-lengths of a digital human. By including anthropometric design variables, this approach introduces flexible handling of innate variance in subject-model measurements without need for pre- or post-processing. This produces a more realistic motion and exhibits anthropometric measurements closer to those of the original subject, resulting in a new level of biomechanical accuracy that allows for analysis of a processed motion with a higher degree of confidence.

Keywords: Posture prediction · Link-length · Motion capture · Inverse kinematics

1 Introduction

The increasing demand for accurate evaluation of biomechanical factors related to human motion on a digital model calls for improvement in the visualization of motion data. Specifically, there is a growing need to process motion capture (MoCap) data for high-fidelity (i.e. highly articulated) 3D human models capable of replicating complex human motion. Driven initially by the entertainment industry, MoCap technology has become a popular means for displaying motion in a virtual environment. To date, the primary use has been purely for visualizing motion or enhancing the animated motion of cinematic characters. Recently, MoCap technology has seen applications in the field of biomechanics. Mathematically describing movement provides a basis for the

D.N. Cassenti (ed.), *Advances in Human Factors in Simulation and Modeling*, Advances in Intelligent Systems and Computing 591, DOI 10.1007/978-3-319-60591-3_50

quantitative evaluation of human performance, and the processing of the retrieved motion data onto a digital human makes it possible to analyze attributes that are difficult to observe on real-world human subjects [1]. However, use in this capacity requires improved accuracy of methods for processing the raw data and translating it to biomechanically relevant parameters.

Current techniques are unable to adequately account for the variance in anthropometric measurements between the original subject from which the motion was captured and the high-fidelity digital human on which the data is processed. Consequently, it is difficult to visualize human motion on a high-fidelity model and perform accurate biomechanical analysis using the processed data. As discussed by Bonin et al., one method to overcome this obstacle is to utilize anthropometric databases in the generation of the digital human model. An advantage of this method includes the increased similarity between the anthropometric measurements of the original subject and the digital human. Adversely, there are certain obstacles, such as dealing with data for which the dimensions of the original subject are not available. Furthermore, it also requires reconstruction of the digital human model from three-dimensional scans, necessitating further tools and time [2].

Generally, a digital human is categorized as either an anthropometric model, used for analysis of human dimension and body shape, or a biomechanical model, used for analysis and simulation of motion [3]. Given the need for biomechanical analysis and the extreme variability of human body parameters, it is necessary to provide a flexible method that considers both anthropometric and kinematic factors—specifically, a method that is capable of handling the diverse anthropometric measurements of the human population, thus providing the means to analyze processed human motion with a higher degree of confidence. This paper presents a new approach to MoCap processing that estimates both posture and anthropometry simultaneously using optimization-based techniques. By including anthropometric design variables, this approach introduces a flexible method for handling innate variance in subject-model measurements without the need for pre/post-processing or digital model generation. Using this optimization-based approach, the need for an anthropometric human model and a biomechanical human model can be satisfied with a single representation. This produces a more realistic motion and exhibits anthropometric measurements closer to those of the original subject, resulting in a higher level of biomechanical accuracy.

2 Methods

2.1 Kinematic Human Model

A high-fidelity mathematical representation of the human body is necessary to simulate accurate human motion in a virtual environment. The human skeleton is modeled as a series of rigid links connected at vertices that are representative of joints. Each joint has between one and three degrees-of-freedom (DOF), dependent on the ability of the joint to rotate about the x-, y-, and z-axis [4]. The model in this study is a 55-DOF articulated kinematic chain as shown in Fig. 1. The location and orientation of each joint and link follows the Denavit-Hartenberg (DH) convention [5]. Although this method is

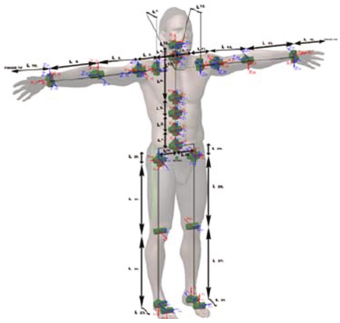

Fig. 1. 55-DOF kinematic human model used during posture prediction and motion simulation.

traditionally used in the robotics field, it has been used effectively for modeling human biomechanics in optimization-based posture prediction [6].

Optimization-Based Posture Prediction

The goal of posture prediction is to determine a conformation of kinematic joint angles that allows the digital human body to satisfy a particular requirement; for instance, touch a particular point in a workspace with a specified fingertip. Posture problems are often redundant with many possible solutions. To distinguish between these solutions, the optimization-based approach minimizes an objective function. Objective functions are mathematically representative of the driving factors of human posture, such as the desire to maintain neutral posture [7], reduce joint discomfort [8], or maintain visual contact with a given target [9]. The fundamental formulation is given as [10]:

$$\begin{aligned} &\text{Find: } \boldsymbol{q} \in R^{DOF} \\ &\text{Minimize: } f(\boldsymbol{x}(\boldsymbol{q}))(Discomfort,\ Effort,\ etc.) \\ &\text{Subject to: } \left\| \boldsymbol{x}(\boldsymbol{q})^{end-effector} - \boldsymbol{x}^{target\ point} \right\|^2 \leq \varepsilon \\ &\text{and} \quad q_i^L \leq q_i \leq q_i^U;\ i = 1, 2, \ldots, DOF \end{aligned} \tag{1}$$

In the above equation, $\boldsymbol{q}$ is a vector of joint angles, $\boldsymbol{x}$ is the position of an end-effector (i.e. marker on the digital human), ε is a small positive number that approximates zero, and DOF is the total number of degrees of freedom. The function $f(\boldsymbol{x}(\boldsymbol{q}))$ can be one of many objective functions, as discussed previously. The primary constraint, called the *distance* constraint, requires the marker(s) to contact a specified target point(s). Additionally, q_i^U represents the upper limit, and q_i^L represents the lower limit of a joint i as derived from kinematic data. In addition to these basic constraints, many others can be incorporated as boundary conditions to represent the virtual environment.

2.2 Motion Capture Processing

Most MoCap systems provide the three-dimensional Cartesian position of each marker placed on the subject at each frame of the motion, allowing the positions of the markers to be represented in a virtual environment at each frame [11]. For the purposes of this

paper, processing such MoCap data refers to using these marker positions as input to replicate the motion on a high-fidelity digital human model, represented as joint angles over time. Markers of this type will be referred to as MoCap markers. In Fig. 2c, the MoCap markers are depicted in blue. A mapping protocol is used to place virtual markers on the digital model (Fig. 2b), which correspond to the anatomical locations of the markers as they were placed on the subject (Fig. 2a). The protocol defines each of these virtual markers relative to a parent joint on the high-fidelity human model and maps each marker onto the model relative to a global coordinate system in three-dimensional space [12]. In Fig. 2c, the virtual markers are depicted in blue. To process an individual frame in the MoCap data, a *distance objective* is created for each virtual marker to minimize the distance to its mapped target obtained from the MoCap data. To replicate an entire motion, posture prediction is executed over all frames to determine joint angles using the formulation defined in Eq. 1.

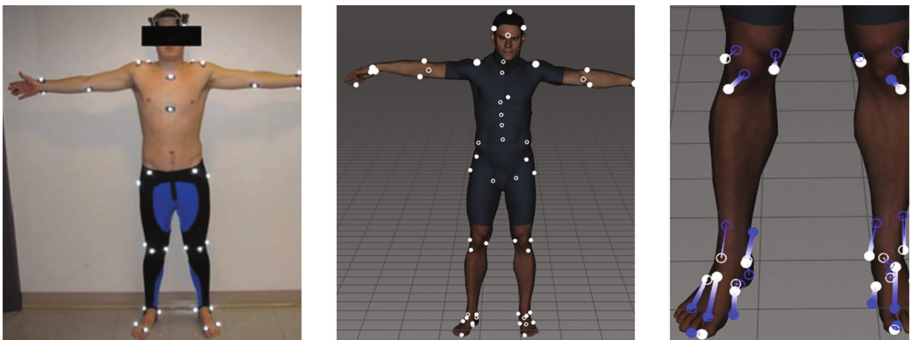

(a) (b) (c)

Fig. 2. Mapping MoCap markers on the human subject onto the digital human model: (a) MoCap markers [12] (b) virtual markers (c) distance between MoCap and virtual markers.

Because this formulation creates one distance objective for each of the virtual markers, a p-norm multi-objective optimization (MOO) representative of overall positional error is defined as [13]:

$$f(\boldsymbol{x}(\boldsymbol{q})) = \left[\sum_{i=1}^{n}\left(w_i \frac{\|\boldsymbol{x}_i(\boldsymbol{q}) - \boldsymbol{t}_i\|^2}{d_{max}^2}\right)^p\right]^{\frac{1}{p}}. \tag{2}$$

In the above equation, $\boldsymbol{p} = \boldsymbol{2}$ and $\boldsymbol{x_i}(\boldsymbol{q})$ refers to the position of each virtual marker, which is dependent on the vector of kinematic joint angles, $\boldsymbol{q}$. From this virtual marker, the MoCap marker position $\boldsymbol{t_i}$ is subtracted to find the positional error. Within this MOO approach, each distance objective is the square of the distance between the virtual marker and the MoCap marker position, normalized by a working maximum distance $\boldsymbol{d_{max}}$. Note that $\boldsymbol{w_i}$ has a value between 0 and 1 and refers to a weight corresponding to each virtual marker, as defined in the protocol—these weights ensure that markers with a critical role in a motion are evaluated as such (Eq. 2).

2.3 Link-Lengths as Design Variables

The initial approach to prediction of anthropometry involved optimizing additional anthropometric design variables known as link-lengths, the straight-line distances from one DH frame to the next that correspond to the anatomical distance between two joints. In posture prediction, link-lengths are traditionally given as input to the problem. However, in order to more accurately replicate the motion of subjects with body dimensions that differ from those of the digital model, the optimization problem can be set up with the intent of finding not only kinematic joint angles, but also the anthropometric link-lengths that satisfy the given constraints and minimize the positional error between the virtual markers and the MoCap markers. The modified optimization problem can be presented using the following formulation:

$$\begin{aligned}
&\text{Find: } \boldsymbol{q} \in R^{DOF},\ \boldsymbol{l} \in R^{LL} \\
&\text{Minimize: } f(\boldsymbol{x}(\boldsymbol{q},\boldsymbol{l}))\ (\textit{Distance objective}) \\
&\text{Subject to:} \\
&\quad a.\ q_i^L \le q_i \le q_i^U;\ i = 1,2,\ldots,DOF \\
&\quad b.\ l_j^L \le l_j \le l_j^U;\ j = 1,2,\ldots,LL \\
&\quad c.\ |l_{k^R} - l_{k^L}| < \varepsilon;\ \left\{k^R, k^L\right\} \in LL_{sym}.
\end{aligned} \tag{3}$$

Similar to Eq. 1, $\boldsymbol{q}$ represents the vector of kinematic joint angles. The additional variable $\boldsymbol{l}$ represents the vector of anthropometric link-lengths that will be determined in conjunction with the joint angles. Supplementary constraints ensure that the optimal solution remains within the boundary of feasible body dimensions. Equation 3b imposes limits on the anthropometric variability such that $\boldsymbol{l_j^L} \le \boldsymbol{l_j} \le \boldsymbol{l_j^U}$, where $\boldsymbol{l_j}$ represents the $\boldsymbol{j^{th}}$ link-length, $\boldsymbol{l_j^L}$ is its lower limit, and $\boldsymbol{l_j^U}$ is its upper limit. Additionally, Eq. 3c ensures that the right and left sides of the body remain symmetric, where $\boldsymbol{l_{k^R}}$ and $\boldsymbol{l_{k^L}}$ are corresponding link-lengths on the left and right sides of the body, respectively. The set of symmetric link-lengths, denoted as $\boldsymbol{LL_{sym}}$, includes the elbow-wrist, shoulder-elbow, clavicle-shoulder, sacrum-hip, hip-knee, knee-ankle, and ankle-toe distances. Using MOO, the combined objective function is defined as:

$$\boldsymbol{f}(\boldsymbol{x}(\boldsymbol{q},\boldsymbol{l})) = \left[\sum_{\boldsymbol{i}=1}^{\boldsymbol{n}} \left(\boldsymbol{w_i} \frac{\|\boldsymbol{x_i}(\boldsymbol{q},\boldsymbol{l}) - \boldsymbol{t_i}\|^2}{\boldsymbol{d_{max}}}\right)^{\boldsymbol{p}}\right]^{\frac{1}{\boldsymbol{p}}}. \tag{4}$$

Note that Eq. 4 is similar to Eq. 2, except that the virtual marker position $\boldsymbol{x_i}(\boldsymbol{q},\boldsymbol{l})$ is now a function of both kinematic joint angles $(\boldsymbol{q})$ and anthropometric link-lengths $(\boldsymbol{l})$.

2.4 Flexible Marker Positions

As the results will show, initial implementation of link-lengths as design variables using the formulation of Eq. 3 did not predict anthropometry as well as expected. Analysis

determined that the virtual markers on the digital human model became unrealistically far from anthropometric landmarks as the link-lengths were scaled during the optimization process. In Eq. 4, the virtual markers are represented with local positions rigidly attached to the parented joint, using the standard DH transformation [10]:

$$\boldsymbol{x}_i(\boldsymbol{q},\boldsymbol{l}) = \left(\prod_{j=1}^{n} {}^{j-1}\boldsymbol{T}_j(\boldsymbol{q},\boldsymbol{l})\right)\boldsymbol{x}_i^{local}. \tag{5}$$

The position of the digital human can be determined by successive multiplication of transformations [5]. The local position, denoted as $\boldsymbol{x}_i^{local}$, refers to the position of the virtual marker on the digital human, which is defined in the mapping protocol as a fixed value and is thus unaffected by the link-length design variables (Eq. 5).

Fig. 3. Fixed marker position (a) before and (b) after modifying link-length.

In Fig. 3a and b, the position of the marker $\left(\boldsymbol{x}^{marker}\right)$ represents the same anatomical landmark on the forearm. Figure 3a displays the position of the marker prior to running posture prediction using link-lengths as design variables. When a link-length is modified, represented in Fig. 3b, the virtual marker no longer represents the same anatomical position, since the coordinates of $\boldsymbol{x}^{marker}$ have not changed.

A new method was developed using *flexible marker positions*, which represent virtual markers relative to the link-lengths. Using flexible marker positions, the virtual marker moves proportionally as anthropometric measurements are modified, so that it

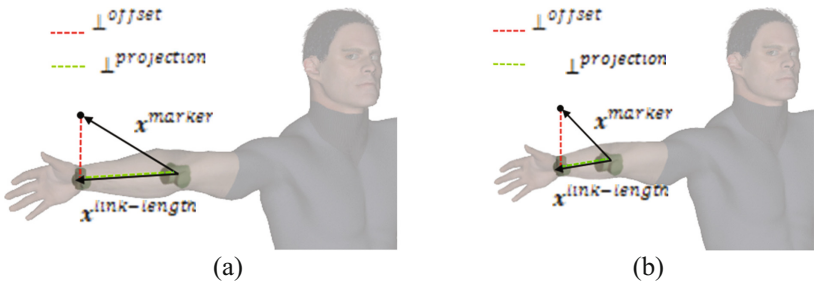

Fig. 4. Flexible marker position (a) before and (b) after modifying link-length.

stays relative to the same anatomical landmark, as shown in Fig. 4. The flexible marker position is implemented by describing the marker position $\left(\boldsymbol{x}^{marker}\right)$ relative to both of the link-length endpoints, rather than fixed to a parent joint.

First, $\boldsymbol{x}^{marker}$ is projected onto the centerline of the corresponding link-length, $\boldsymbol{x}^{link-length}$, as shown in Fig. 4 by the dashed yellow line long the limb, using Eq. 6.

$$\perp^{projection} = \left| \frac{\boldsymbol{x}^{marker} \bullet \boldsymbol{x}^{link-length}}{\boldsymbol{x}^{link-length} \bullet \boldsymbol{x}^{link-length}} \right|. \tag{6}$$

Next, the position of the marker along the centerline of the link-length is described using a percentage of its distance between the endpoints of the link-length, $\%^{link-length}$, as shown in Eq. 7.

$$\%^{link-length} = \left| \frac{\perp^{projection}}{\boldsymbol{x}^{link-length}} \right|. \tag{7}$$

The marker is translated from its position along the centerline of the link-length to the skin of the digital human model using an offset vector, $\perp^{offset}$, which is represented by the dashed red line in Fig. 3 (Eq. 8).

$$\perp^{offset} = \boldsymbol{x}^{marker} - \perp^{projection}. \tag{8}$$

The flexible position $\boldsymbol{x}_i^{local}(\boldsymbol{l})$ is defined in Eq. 9 and takes the place of the fixed position in the distance objective in Eq. 4. Thus, as the link-lengths change, the position of the marker will change proportionally, allowing it to represent more accurately the appropriate anatomical position.

$$\boldsymbol{x}_i^{local}(\boldsymbol{l}) = \%^{link-length} \cdot (\boldsymbol{x}^{next} - \boldsymbol{x}^{parent}) + \perp^{offset}. \tag{9}$$

$$\boldsymbol{x}_i(\boldsymbol{q}, \boldsymbol{l}) = \left(\prod_{j=1}^{n} {}^{j-1}\boldsymbol{T}_j(\boldsymbol{q}, \boldsymbol{l}) \right) \boldsymbol{x}_i^{local}(\boldsymbol{l}). \tag{10}$$

Note that in Eq. 9, the vector from the parent joint center $\boldsymbol{x}^{parent}$ to the next joint center $\boldsymbol{x}^{next}$ is dependent on the current values of the link-length design variables.

3 Results

3.1 Motion Capture Data

In order to test the prediction of anthropometry, MoCap data was used from variable subjects performing similar tasks. Three male subjects performed a walking motion consisting of four 180-degree turns, such that the subject was walking in either the left

or right direction relative to the viewport. From each motion, five key frames were selected for analysis. These key frames were selected based on the representative points of a single gait cycle while running. Specifically, these phases are described by Novacheck [14] as stance phase absorption, stance phase generation, swing phase generation, swing phase reversal, and swing phase absorption. Note that swing phase reversal was not used as a key frame in this paper; also, an additional neutral posture frame was included, during which the subject was instructed to stand in a comfortable position prior to any movement. In addition to the analysis of these key frames, the anthropometric dimensions of each subject over the entire motion were compared.

Prior to capturing the motion, body dimensions were measured in accordance with the MVN User Manual, developed by Xsens Technologies B.V. [15]. These measurements were later compared to the body segment dimensions of the digital human to evaluate the accuracy of the predicted link-lengths. The varying anthropometric dimensions of each subject, along with the default dimensions of the digital human model, are presented in Table 1.

Table 1. Anthropometric dimensions of subjects and default dimensions of digital model

Dimension (cm)	Subject 1	Subject 2	Subject 3	Model
Body height	166.0	174.0	193.0	182.0
Hip height	85.0	91.5	100.0	84.5
Knee height	48.9	51.0	60.0	53.3
Arm span	162.0	175.0	192.4	196.2
Hip width	27.5	25.0	28.0	28.4
Shoulder width	37.4	35.0	42.0	37.7

Corresponding body segments of the digital human were determined after optimization at each frame through the addition of link-lengths representing one of the above dimensions. However, the head and hands are not represented by link lengths; therefore, their anthropometry is not optimized, meaning their size is also equal across the various subjects' motions. To determine body height and arm span, the fixed values of the head and hands were added to the length of each corresponding segment. Additionally, because the body segments of the digital human only represent the distance between internal joint center locations, offsets were implemented to account for the length between the joint and the anatomical landmark at which the measurement was taken on the original subjects (Fig. 5).

The body height, hip height, and knee height are increased by the distance from the floor to the ankle joint center (D). Additionally, the hip height was decreased by the vertical distance from the hip joint center to the superficial prominence of the greater trochanter (C), and the hip width was increased by the horizontal distance from the left and right hip joint center to the anterior superior iliac spine (E).

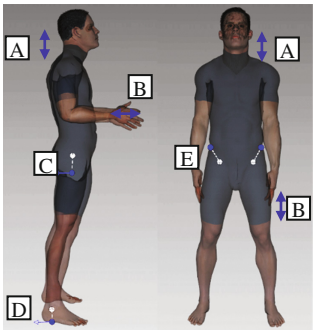

Fig. 5. Fixed offsets representing length of (A) head, (B) hand, (C) hip joint center to greater trochanter, (D) ankle joint center to floor, and (E) hip joint center to anterior superior iliac spine.

3.2 Implementation of Link-Lengths as Design Variables

Incorporating link-lengths as design variables using fixed marker positions yielded improved predicted postures in limited cases. However, in many cases, the resulting postures and anthropometries were unrealistic, due to the inaccuracies of fixed marker positions used to minimize the position error. Using the flexible marker positions visually improved the predicted postures and consistently resulted in predictions that are more accurate, as displayed in Fig. 6.

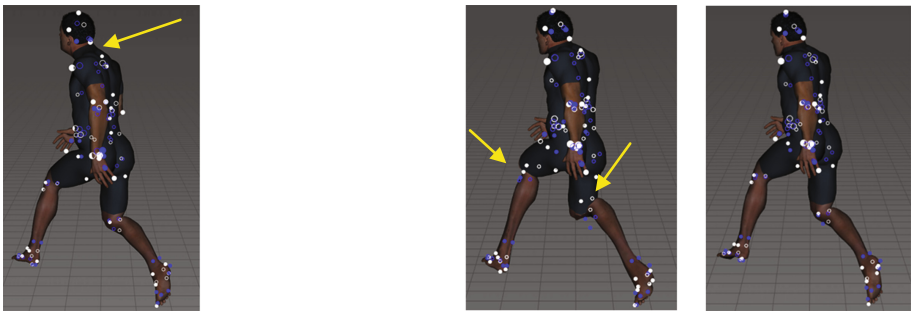

Fig. 6. Result of running posture prediction on a single frame of MoCap data (a) without anthropometric design variables, (b) with anthropometric design variables using fixed marker positions, and (c) with anthropometric design variables using flexible marker positions.

Markers associated with the MoCap data are depicted in blue, while the corresponding virtual markers are depicted in white. The motion data is of Subject 1, who is much smaller relative to the default measurements of the digital human (Fig. 6). Specific anthropometric measurements are documented in Table 1. Figure 6a depicts a posture obtained without the prediction of anthropometry. In this, the spine and neck are compressed, such that the neck must extend backward. Additionally, the shoulders are lowered such that the neck is more elongated. Both of these actions attempt to

compensate for the lower position of the MoCap markers due to the small stature of the Subject 1. Figure 6b depicts the use of fixed marker positions during prediction of both posture and anthropometry. To minimize the positional error between the virtual and MoCap markers, the link-lengths of the digital human should have decreased. However, the virtual markers were fixed, causing misrepresentation of the anatomical landmark. As a result, posture prediction produced a solution in which the knee is bent at an unrealistic angle in order to minimize the distance between then virtual and MoCap markers. This unrealistic angle is also in part due to the skinning of the high-fidelity model, which emphasizes discrepancies between the virtual and MoCap markers.

Comparison of the same frame in the motion data of Subject 1 highlights the improvements observed across all of the frames and subjects when using flexible marker positions. The flexible representation allowed the relative position of the virtual marker to scale proportionally as link-lengths were modified. Thus, the virtual markers stayed near their associated anthropometric landmarks throughout the optimization process (Fig. 6c). As such, the predicted posture was visually more plausible, which is particularly evident at the knee.

3.3 Comparison of Fixed and Flexible Marker Positions in Posture Prediction

Depicting the same frame using both the fixed and flexible marker positions provides a qualitative basis of support for the flexible method, which produced a visually more realistic posture. However, deeper analysis using quantitative comparison of the body dimensions of the digital human and original subject also suggests that the flexible method results in predicted anthropometry closer to that of the original subject.

Using the five key frames described in Sect. 3.1, percentage error in body dimension was calculated using the original subject's measurements as the expected values and the digital human's predicted measurements as the experimental values. The results in Fig. 7 are the sum of the percentage error at each body dimension, averaged

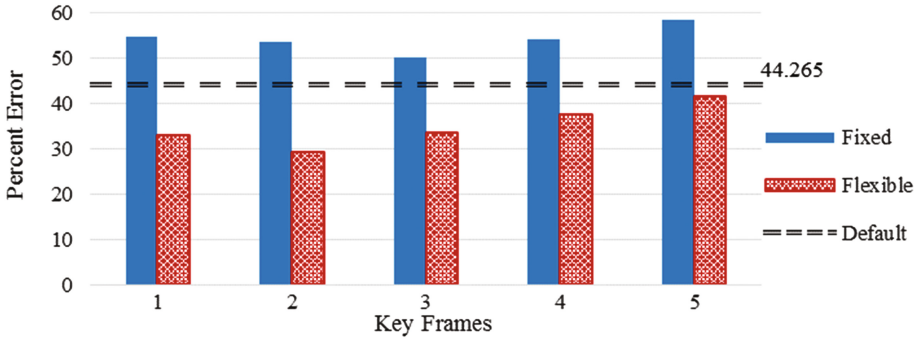

Fig. 7. Relative error in predicted anthropometry at five key frames averaged over subjects. Key frames include (1) neutral stance, (2) stance phase absorption, (3) stance phase generation, (4) swing phase generation, and (5) swing phase absorption [13].

across the three subjects. The default line corresponds to the absolute error in the digital human's default body dimensions. That is, it represents the error in body dimension when no anthropometric design variables are predicted. At the five frames selected, optimization using the flexible marker positions resulted in anthropometric measurements with a lower percentage of error across all of the subjects (Fig. 7).

The absolute error was calculated every five to ten frames over the entire motion and averaged across these frames. This process was repeated for all three subjects, and the average across the subjects is illustrated in Fig. 8. Visualization of the absolute error in the predicted anthropometry of the digital human, with regard to that of the original subject, suggests on a quantitative basis that the use of flexible marker positions during MoCap processing decreases the error between the anthropometry of the original subject and the digital human. Note that there is a large amount of error associated with the arm span dimension in all cases. This is in part because the body dimensions of the original subjects were measured while the subjects stood in a T-pose, as shown in Fig. 2a. In the motion analyzed for this work, the arms of the subject remained close to the body for most frames, and this affected the predicted arm span.

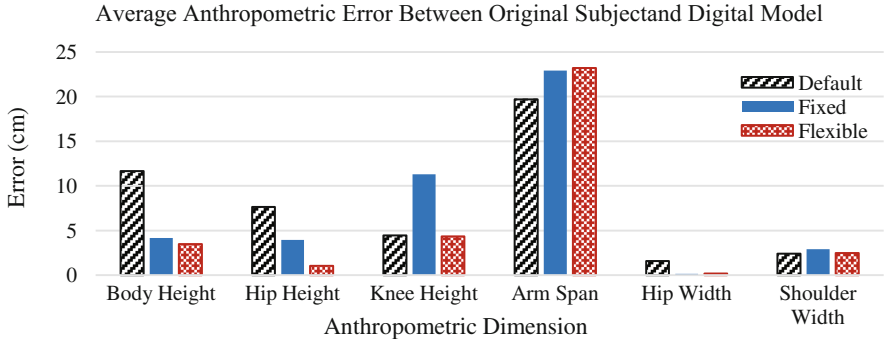

Fig. 8 Average of the absolute errors of each predicted body dimension calculated every 5–10 frames of motion.

4 Conclusion

In this paper, a new approach to improve MoCap processing using high-fidelity digital human models was presented. This approach incorporated both anthropometric and kinematic design variables to minimize the distance between MoCap markers and the corresponding virtual markers on the digital human. This optimization-based approach produced realistic motion with anthropometric measurements closer to those of the original subject and improved the overall appearance of the digital model. Because the anthropometry of the digital human model more closely replicates that of the original subject, the solution provides the basis for a more accurate biomechanical analysis. However, the effectiveness of the new approach needs further validation using a larger study in which the subjects have their motion captured and their anthropometry

measured while in the same pose. Additional validation should also include a focus on the accuracy of a biomechanical analysis by recording additional biomechanical factors (e.g. force plate data) on the original subject.

In addition to a need for further validation, a limitation to the presented approach is that it estimates only the link-lengths and does not consider the body shape parameters, such as the thickness of body segments. If the body shape of the subject is significantly different from the digital human used to process the corresponding MoCap data, the results will be less accurate. As such, integrating the thickness of each segment into this approach should be investigated as future work. Nonetheless, the use of flexible marker positions provides an effective framework for more accurate processing of MoCap data without the need for pre/post-processing, which can be extended to further improve the reliability of biomechanical analysis of the processed motion.

Acknowledgements. This work is funded by the US Office of Naval Research, under program W911QY-12-C-0009. The authors would like to thank the team at the University of Iowa's Virtual Soldier Research program. This work was completed at The University of Iowa, where the authors worked at the time.

References

1. Xiang, Y., Rahmatalla, S., Arora, J., K, Abdel-Malek: Enhanced optimization based inverse kinematics methodology considering joint discomfort. Int. J. Hum. Fact. Model. Simul. **2** (1/2), 111–126 (2011)
2. Bonin, D., Wischniewski, S., Wirsching, H.-J., Upmann, A., Rausch, J., Paul, G.: Exchanging data between Digital Human Modelling systems: a review of data formats. In: 3rd International Digital Human Modeling Symposium, Odaiba, Tokyo, Japan (2014)
3. Li, P., Carson, J., Parham, J., Paquette, S.: Digital human modeling pipeline with 3D anthropometry database. In: Duffy, V. (ed.) Advances in Applied Digital Human Modeling and Simulation, vol. 481. Springer, Cham (2017)
4. Yang, J., Rahmatalla, S., Marler, T., Abdel-Malek, K., Harrison, C.: Validation of predicted posture for the virtual human Santos®. In: Duffy, V. (ed.) Digital Human Modeling, vol. 4561, pp. 500–510 (2007)
5. Denavit, J., Hartenberg, R.S.: A kinematic notation for lower-pair mechanisms based on matrices. J. Appl. Mech. **77**, 215–221 (1955)
6. Farrell, K., Marler, R. T., Abdel-Malek, K.: Modeling duel-arm coordination for posture: an optimization-based approach. In: SAE Technical Paper, Digital Human Modeling for Design and Engineering Symposium, Iowa City, Iowa (2005)
7. Marler, R.T., Arora, J.S., Yang, J., Kim, H.-J., Abdel-Malek, K.: Use of multi-objective optimization for digital human posture prediction. Eng. Optim. **41**, 295–943 (2009)
8. Marler, R.T., Rahmatalla, S., Shanahan, M., Abdel-Malek, K.: A new discomfort function for optimization-based posture prediction. In: SAE Technical Paper, Digital Human modeling for Design and Engineering Symposium, Iowa City, Iowa (2005)
9. Marler, R.T., Farrell, K., Kim, J., Rahmatalla, S., Abdel-Malek, K.: Vision performance measures for optimization-based posture prediction. In: SAE Technical Paper, Digital Human Modeling for Design and Engineering Conference, Lyon, France (2006)

10. Abdel-Malek, K., Arora, J.: Human Motion Simulation: Predictive Dynamics. Academic Press, Cambridge (2013)
11. Inc, Motion Lab Systems: The C3D File Format: User Guide. Author, LA (2008)
12. Rahmatalla, S., Xiang, Y., Smith, R., Li, J., Muesch, J., Bhatt, R., Swan, C., Arora, J., Abdel-Malek, K.: A validation protocol for predictive human locomotion. In: SAE Technical Paper, Digital Human Modeling for Design and Engineering Conference, Pittsburgh, PA (2008)
13. Marler, R.T., Arora, J.: Survey of multi-objective optimization methods for engineering. Structrual Multi. Optim. **26**, 369–395 (2004)
14. Novacheck, T.F.: The biomechanics of running. In: Gait and Posture, vol. 7, pp. 77–95. Elsevier (1998)
15. XSens Technologies B.V.: MVN Motion Capture System: User Manual. CA: Author (2013)

Finding the Maximal Day-Time Dependent Component of a Subway System

Marian Sorin Nistor[1(✉)], Doina Bein[2], Horia Nicolai Teodorescu[3,4], and Stefan Wolfgang Pickl[1]

[1] Department of Computer Science, Universität der Bundeswehr München, 85577 Neubiberg, Germany
{sorin.nistor, stefan.pickl}@unibw.de
[2] Department of Computer Science, California State University, Fullerton, CA 92831, USA
dbein@fullerton.edu
[3] Institute of Computer Science of the Romanian Academy, Iaşi, Romania
[4] ETTI Department, "Gheorghe Asachi" Technical University of Iaşi, 700050 Iaşi, Romania
hteodor@etti.tuiasi.ro

Abstract. We analyze the properties of a transportation network with time-dependent flows with the aim of finding the maximal component along the duration of a period of the variation of the flow. We apply this analysis method to the subway network of Munich. The analysis is detailed and results are included. Beyond the theoretical interest in this type of network with periodically varying properties, the paper presents a well-structured analysis method that can be widely applied to numerous other networks of applicative interest.

Keywords: Subway network · Network analysis · Maximal component · Longest shortest path

1 Introduction

The subway systems in general are critical urban infrastructures, exposed to frequent disruptions. Various factors contribute towards serious schedule delays, including having the entire system shut down. A temporary shutdown of a means of public transport is relatively rare, but has a serious impact over the activity of a city. Moreover, if this unfortunate event was not due to natural hazards or temporary failures of the system, but purposely targeted attacks, it poses then security issues.

In this paper, we analyze the scenario where a threat propagates through the network using the subway system. For this, we tackle two research questions: 1. What is the longest ride one can have in a threat propagation, such as a flee attempt using the subway system within a limited travel time and at a specific time of the day? 2. What is the maximal number of stations one can reach in a flee attempt using the subway system within a limited travel time and at a specific time of the day?

We conducted the analysis on a subway system modeled as a mathematical network where the stations are nodes and the connection between pair of stations are edges [1].

D.N. Cassenti (ed.), *Advances in Human Factors in Simulation and Modeling*,
Advances in Intelligent Systems and Computing 591, DOI 10.1007/978-3-319-60591-3_51

The train frequency at each station, the corresponding subway line(s) of each station, and the travel time between adjacent stations are encoded as weights on edges. Hence, the research questions can be redefined as:

1. What is the longest day-dependent and time-dependent (i.e., day- and time dependent) shortest path of a subway network. (Recall that the shortest path is the path between two nodes in a network having the smallest edge-weight sum.)
2. What is the maximal day-time dependent sub-network (component) of a subway network? (Recall that the maximal component is a connected sub-network that starting from a root node of the network covers a range of nodes that satisfies a given maximal edge-weight sum.)

The first question is a particular application of the *weighted shortest path problem* [2] that can be solved efficiently using Dijkstra's algorithm [3]. The second question is a particular application of the *constrained maximum-weight connected graph problem* [4]. The latter is the focus of this paper. Here, the first problem is treated as a sub-problem of the second. Namely, a rooted day-time dependent component is a collection of the corresponding shortest paths starting from a root node to each node of a maximal edge-weight range of nodes. We consider the maximal day-time dependent component (MDTDC) to be the main problem, and the longest day-time dependent shortest path (LDTDSP) to be the sub-problem.

Various optimized solutions to this problem are available in [5–7]. The application range is very diversified and similar analyzes are applied to biological systems [8–10], wildlife corridors design [11, 12], forest planning [13], communication network design [4], computer vision [14], and few others.

Our main contribution is a well-defined analysis method that we apply to subway networks. The subway networks are special because of the variation of the edge weight value. Thus, we consider the weights to have two sets of values, depending on which case they fall into. One case is when two adjacent nodes are part of the same subway line; in that case the weight value on the edge represents the travel time between nodes. In the second case, when two adjacent nodes are not part of the same subway line, then the weight value on the edge represents the sum of waiting times at the starting node and the travel time between nodes.

A detailed description of the conducted analysis is given in Sect. 2. The Munich subway network proves to be a good candidate [15, 16] for our analysis due to its size, ridership [17], and train frequency variation over train time schedules [18]. More details on the data collection is given in Sect. 3. The results are presented and discussed in Sect. 4. The paper concludes with considerations on the application on this network and remarks for other subway networks.

2 The MDTDC Problem with the LDTDSP Sub-problem

2.1 Formulation

Let $G = (V, E)$ be a graph and $v_i \in V$ a random starting node. Knowing all edges e_{ij} of that node, the time of the day (or the hour of the schedule) t_D, the corresponding

frequencies $f(t_D, e_{ij})$, and their travel times along the edges $d(v_i, v_j)$, we define the component G_c of G of all nodes that can be reached in time t starting at $t = 0$ from v_i.

All the vertices v_h in G_c satisfy the condition that there is a shortest path from v_i to v_h such that it can be traveled along in time less than t:

$$P(v_i, v_h) = \min_{P(v_i, v_h)} \left(\sum\nolimits_{e_{ij} \in P(v_i, v_h)} \alpha \frac{60}{f(t_D, e_{ij})} + d(v_i, v_j) \right) \leq t \tag{1}$$

where $P(v_i, v_h)$ denotes the shortest paths from v_i to v_h, $\alpha = 0$ if v_i and v_j belong to the same subway line, else $\alpha = 1$.

From (1), for a given t_D and t, MDTDC is defined as $\sum P(v_i, v_h)$, and LDTDSP is defined as $P_{max}(v_i, v_h)$. In Fig. 1 (left) is an example of the MDTDC on a simple network. In this example, the MDTDC of the network starts from the red (center) node, and all the orange nodes represent the visiting range for a given maximal edge-weight of three. In Fig. 1 (right) is an example of the LDTDSP on the same simple network. Here, the LDTDSP of the network starts from the red (center) node, and all the orange nodes represent the visiting path for a given maximal edge-weight of three.

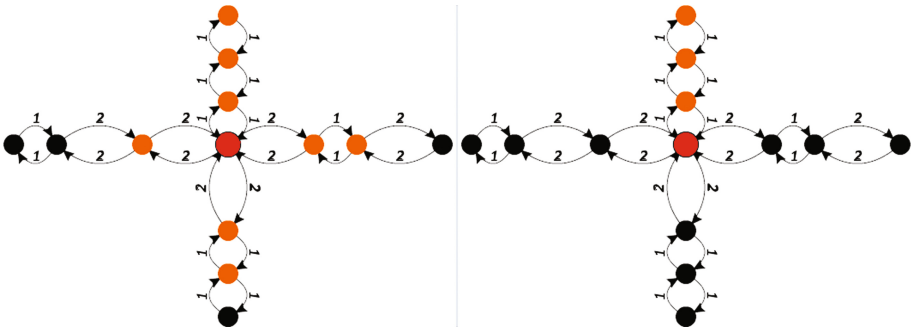

Fig. 1. A simplified version of the application for a given maximal edge-weight of three without considering subway lines or train frequencies. MDTDC is exemplified on a simple network to the left. LDTDSP is exemplified on a simple network to the right.

2.2 Algorithm

Input: An input file containing the adjacency list of the subway network for one schedule with multiple weights, and an array of the travel time limits. The input file has the following information on each column: col_1 = *station from*, col_2 = *station to*; col_3 to col_26 = *train frequency* on that edge by hour from *00* h *to 23* h (24 columns); col_27 = *subway line*; col_28 = *travel time* on edge in min. The array has the following elements: 5 min, 10 min, 15 min, 20 min.

Output: The results for MDTDC and LDTDSP for each travel time limit.

```
Begin
read master_list
read travel_limit
for each hour H do
    extract adjacency_list_H from master_list
    convert adjacency_list_H to graph_H
    for each node(graph_H) N do
        calculate visited_nodes with
                breadth_first_search(graph_H,from_node=N)
        order visited_nodes
        for each node(visited_nodes) V do
            calculate crnt_sp_V with
              shortest_path(graph_H,from_node=N,to_node=V)
            calculate crnt_travel_time for crnt_sp_V
            save crnt_travel_time to travel_time_nodes_V
            save crnt_sp_V to list_sp_V
        {end for}
        save list_sp_V & travel_time_nodes_V to LDTDSP_N
        save travel_time_nodes_V to travel_time_N
    {end for}
    calculate MDTDC_H with sum(LDTDSP_N)
    calculate LDTDSP_H with max(LDTDSP_N)
{end for}
for each travel_limit T do
    for each node(graph_H) N do
        save MDTDC_T from MDTDC_H with
                              travel_time_N < travel_limit_T
        save LDTDSP_T from LDTDSP_H with
                              travel_time_N < travel_limit_T
    {end for}
{end for}
```

3 Data Collection

The analysis described in the previous section was applied to the Munich subway network. The network ridership in average is above typical, with more than 398 million passengers per year [17] for a network with only 100 stations [17]. The train frequency of this network varies along the subway lines, and sometimes is different along the same line but in the opposite direction. Namely, the number of trains of a subway line entering a station in a day is not the same from both directions, because sometimes trains are redirected on other lines sharing the same destination station. This makes the Munich subway network a very good candidate for our analysis.

For this paper, the train frequency data for year 2017 was collected for every station of the network. This data is publicly available and it can be accessed from the website of the Munich's association of public transport authorities (MVV) [18].

The subway network has four main schedules, corresponding to *Monday-Thursday*, *Friday*, *Saturday*, and *Sunday/Holiday*. The latter one is the most relaxed schedule in terms of train frequency, while *Friday* schedule is the busiest. MVV provides few side schedules with a more relaxed train frequency during the children's vacation, or more intense during the carnival days, Christmas Eve and New Year's Eve [18]. In this paper, only the regular schedules are considered. This network has eight subway lines (U1–U8), but only six (U1–U6) have a daily schedule. The other two (U7–U8) reuse stations of other lines, with a limited train frequency, because these lines were created only to avoid overcrowding the central stations by supplementing the number of trains, e.g. during peak hours. Therefore, the train frequency of U7–U8 is assimilated by the lines having a regular schedule at the stations reused by these lines [19]. E.g. the line U7 only reuses stations of U1, U2, and U5, therefore in our analysis we do not treat this particularity, and the train frequency of U7 is attributed to the other three lines whose stations have been used.

For each edge, the train frequency starting or ending in one of the two corresponding stations is saved for each hour of the day. Along with the frequency on each edge, the travel time and the subway line are also stored. The train number handled by a station in an hour varies between 0–30 trains. The travel time between every two adjacent stations varies between 1–4 min. The lines are numbered between 1–6 for the stations corresponding to one line and 9 for shared stations by multiple subway lines. Figure 2 presents an example of cleaned input data for the analysis.

From station	To station	00:00	01:00	...	15:00	16:00	...	22:00	23:00	Line	Time
...	...	...	...	...	...	...	...	...	...	...	...
Maillingerstraße	Stiglmaierplatz	8	2	...	16	18	...	12	12	1	1
Moosfeld	Messestadt West	4	2	...	10	12	...	6	6	2	2
Scheidplatz	Bonner Platz	5	1	...	8	12	...	6	6	3	1
Prinzregentenplatz	Max-Weber-Platz	3	1	...	10	12	...	6	6	4	2
Neuperlach Zentrum	Therese-Giehse-Allee	5	1	...	12	12	...	6	6	5	2
Westpark	Partnachplatz	4	1	...	9	12	...	6	6	6	1
Münchner Freiheit	Giselastraße	10	2	...	23	24	...	12	12	9	1
...	...	...	...	...	...	...	...	...	...	...	...

Fig. 2. Example of cleaned input data for the analysis of the Munich subway network.

4 Results and Discussion

In this section, we present and discuss the results obtained after the data set was cleaned and we applied the analysis method from Sect. 2. MDTDC and LDTDSP are computed for the Munich subway network during the week days and weekend days. For the week days, two related schedules are analyzed: *Monday-Thursday* and *Friday*. For the weekend days, the other two schedules are analyzed: *Saturday* and *Sunday/Holiday*.

For our analysis, MDTDC and LDTDSP are calculated for a maximal given travel time corresponding to 5 min, 10 min, 15 min, and 20 min, in order to have a more diversified range of travel windows. For MDTDC, the results below 5 min travel time limit are flat, while for a travel time limit above 20 min, MDTDC covers more than half of the stations.

In Tables 1 and 2, the results show a linear growth of MDTDC from one travel time limit to another. One can observe that as the travel time limit increases, MDTDC varies from one hour to another. The results in Table 1 are more diversified than in Table 2 because the week days have a higher train frequency variation on the subway lines. For example, taking the 20 min travel limit, the difference between 4 am and 7 am on a *Monday-Thursday* schedule is more than double, while on a *Sunday/Holiday* schedule the difference is very small.

Table 1. MDTDC of the Munich subway network during week days, *Monday-Thursday* (M-T) and *Friday* (Fr) schedules, for a maximal given travel time of 5/10/15/20 min

Hour	5 min M-T	5 min Fr	10 min MT	10 min Fr	15 min MT	15 min Fr	20 min MT	20 min Fr
00:00	12	12	22	22	27	27	34	34
01:00	12	12	21	21	25	25	27	27
02:00	0	12	0	21	0	25	0	27
03:00	0	0	0	0	0	0	0	0
04:00	12	12	18	21	21	25	23	27
05:00	12	12	22	22	27	27	34	34
06:00	12	12	23	23	31	31	41	41
07:00	12	12	25	25	38	38	47	47
08:00	12	12	25	25	38	38	47	47
09:00	12	12	24	24	35	35	44	44
10:00	12	12	24	24	33	33	42	42
11:00	12	12	24	24	33	33	42	42
12:00	12	12	24	24	33	34	42	44
13:00	12	12	24	25	33	38	42	46
14:00	12	12	24	25	33	38	42	46
15:00	12	12	24	25	34	38	46	46
16:00	12	12	25	25	38	38	47	46
17:00	12	12	25	25	38	38	47	46
18:00	12	12	25	25	38	38	47	46
19:00	12	12	25	25	35	35	45	45
20:00	12	12	22	22	32	32	39	39
21:00	12	12	22	22	30	30	39	39
22:00	12	12	22	22	30	30	39	39
23:00	12	12	22	22	30	30	39	39

Notice that MDTDC formed in a 5 min travel time window is quite large for all train schedules except 2 am to 4 am. That is, if one finds the starting station that generated the size of this component, in only 5 min one can reach at any time of the week a range of up to 12 stations. This represents 12% of the size of the network. Furthermore, in up to 20 min time, one can reach up to 47 stations during the peak hours of the week days, which is almost half the size of the network.

This variation can be better explored in the two charts of Fig. 3. The left side chart corresponds to the MDTDC results from Table 1, while the right side chart corresponds to the MDTDC results from Table 2.

Table 2. MDTDC of the Munich subway network during weekend and holidays, *Saturday* (Sa) and *Sunday/Holiday* (S&H) schedules, for a given maximal travel time of 5/10/15/20 min.

Hour	5 min Sa	5 min S&H	10 min Sa	10 min S&H	15 min Sa	15 min S&H	20 min Sa	20 min S&H
00:00	12	12	22	22	27	27	34	34
01:00	12	12	21	21	25	25	27	27
02:00	12	0	21	0	25	0	27	0
03:00	0	0	0	0	0	0	0	0
04:00	12	12	21	21	25	25	27	27
05:00	12	12	21	21	25	25	29	29
06:00	12	12	21	21	25	25	29	29
07:00	12	12	21	21	26	25	34	29
08:00	12	12	22	21	30	25	39	30
09:00	12	12	22	22	30	30	39	39
10:00	12	12	23	22	30	30	39	39
11:00	12	12	24	22	31	30	39	39
12:00	12	12	24	22	31	30	40	39
13:00	12	12	24	22	31	30	40	39
14:00	12	12	24	22	31	30	40	39
15:00	12	12	24	22	31	30	40	39
16:00	12	12	24	22	31	30	40	39
17:00	12	12	24	22	31	30	40	39
18:00	12	12	24	22	31	30	40	39
19:00	12	12	23	22	30	30	39	39
20:00	12	12	22	22	30	30	39	39
21:00	12	12	22	22	30	30	39	39
22:00	12	12	22	22	30	30	39	39
23:00	12	12	22	22	30	30	39	39

Notice that, since the network has about 100 stations, 47 stations in the maximal component means about 47% of the network. Thus, the maximal component is between 12% for 5 min and 47% for 20 min., see Fig. 3.

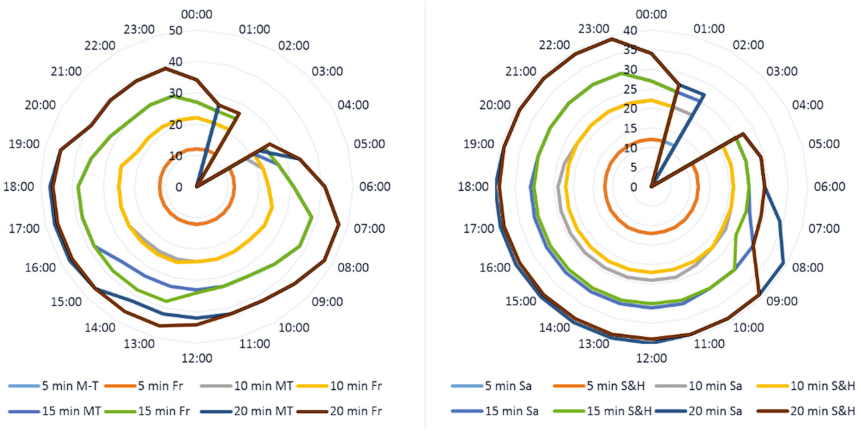

Fig. 3. Variation of MDTDC of the Munich subway network. The left side chart corresponds to week days (Table 1), and the right side chart corresponds to weekend and holidays (Table 2). The numbers along the radial axis represent the number of stations in the maximal component.

LDTDSP of the Munich subway network for each schedule is presented in Table 3. The results are the same for all the schedules. LDTDSP changes only from one time travel limit to another, but not from one schedule to another.

Table 3. LDTDSP of the Munich subway network of each schedule for a given maximal travel time of 5/10/15/20 min.

Schedule	5 min	10 min	15 min	20 min
Monday to Thursday	5	8	11	13
Friday	5	8	11	13
Saturday	5	8	11	13
Sunday/holiday	5	8	11	13

As mentioned before, there is a connection between LDTDSP and MDTDC. Thus, Table 3 can be read together with Tables 1 and 2. For example, if on *Friday* 8 o'clock MDTDC for a 20 min travel time is 47, then 13 ($\sim$28%) is given only by LDTDSP. The latter can be seen visual represented in Fig. 4.

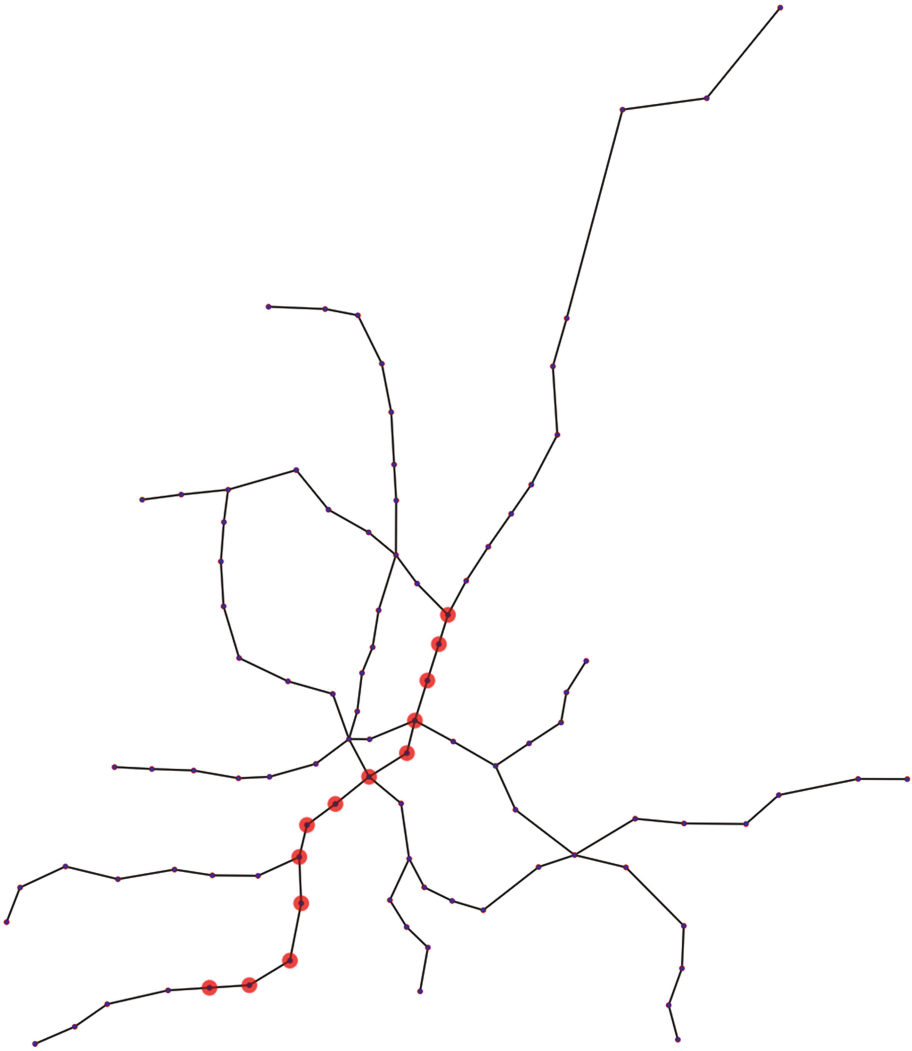

Fig. 4. The Munich subway network with the stations part of LDTDSP highlighted in red during the *Friday* schedule at 8 am for a 20 min travel time.

5 Conclusions

We analyzed the scenario where a human threat propagates through the network and we applied it on a subway system. We analyzed the properties of the system with propagation constrains in the attempt to find the maximal day-time dependent component and the longest day-time dependent shortest path for various schedules. The maximal component at the rush hours of the day, during the weekdays is very large, for a travel duration of 30 min; in fact, the maximal component is roughly half the total

network. Even for 15 min, the maximal component is almost 40%. This raises serious concerns and consequences for the security of people in the network. The application to the Munich subway system shows that the selected data samples and analysis criteria were sufficient for this application. The names of the starting stations creating the maximal components and the longest paths were removed on purpose, the results should be used only in scientific terms.

This paper is yet another example suggesting that the activity of a subway system is fragile and justifies its presence in the critical urban infrastructures category. Here, we established a well-defined analysis method that can be applied to other type of transportation systems or to other systems with similar properties.

Acknowledgments. MSN was supported by the German Federal Ministry of Education and Research (BMBF), project RE(H)STRAIN (Grant No. 13N13786). HNT was supported by a DAAD travel and exchange grant. Doina Bein acknowledges the support by Air Force Office of Scientific Research under award number FA9550-16-1-0257.

References

1. Teodorescu, H.-N.L.: Revisiting models of vulnerabilities of the networks. Stud. Inform. Control **25**(4), 469–478 (2016)
2. West, D.B.: Introduction to Graph Theory. Prentice Hall, Upper Saddle River (1996)
3. Dijkstra, E.W.: A note on two problems in connexion with graphs. Numer. Math. **1**(1), 269–271 (1959)
4. Lee, H.F., Dooly, D.R.: Algorithms for the constrained maximum-weight connected graph problem. Nav. Res. Logist. (NRL) **43**(7), 985–1008 (1996)
5. El-Kebir, M., Klau, G.W.: Solving the maximum-weight connected subgraph problem to optimality. arXiv preprint arXiv:1409.5308 (2014)
6. Álvarez-Miranda, E., Ljubić, I., Mutzel, P.: The rooted maximum node-weight connected subgraph problem. In: Gomes, C., Sellmann, M. (eds.) International Conference on AI and OR Techniques in Constraint Programming for Combinatorial Optimization Problems, pp. 300–315. Springer, Heidelberg (2013)
7. Li, Z., Zhang, S., Zhang, X.-S., Chen, L.: Exploring the constrained maximum edge-weight connected graph problem. Acta Math. Applicatae Sin. **25**(4), 697–708 (2009). English Series
8. Dittrich, M.T., Klau, G.W., Rosenwald, A., Dandekar, T., Müller, T.: Identifying functional modules in protein-protein interaction networks: an integrated exact approach. Bioinformatics **24**(13), i223–i231 (2008)
9. Guo, Z., Li, Y., Gong, X., Yao, C., Ma, W., Wang, D., Li, Y., Zhu, J., Zhang, M., Yang, D., et al.: Edge-based scoring and searching method for identifying condition-responsive protein-protein interaction sub-network. Bioinformatics **23**(16), 2121–2128 (2007)
10. Shannon, P., Markiel, A., Ozier, O., Baliga, N.S., Wang, J.T., Ramage, D., Amin, N., Schwikowski, B., Ideker, T.: Cytoscape: a software environment for integrated models of biomolecular interaction networks. Genome Res. **13**(11), 2498–2504 (2003)
11. Conrad, J.M., Gomes, C.P., van Hoeve, W.-J., Sabharwal, A., Suter, J.F.: Wildlife corridors as a connected subgraph problem. J. Environ. Econ. Manag. **63**(1), 1–18 (2012)
12. Dilkina, B., Gomes, C.P.: Solving connected subgraph problems in wildlife conservation. In: Lodi, A., Milano, M., Toth, P. (eds.) International Conference on Integration of Artificial Intelligence (AI) and Operations Research (OR) Techniques in Constraint Programming, pp. 102–116. Springer, Heidelberg (2010)

13. Carvajal, R., Constantino, M., Goycoolea, M., Vielma, J.P., Weintraub, A.: Imposing connectivity constraints in forest planning models. Oper. Res. **61**(4), 824–836 (2013)
14. Chen, C.-Y., Grauman, K.: Efficient activity detection with max-subgraph search. In: 2012 IEEE Conference on Computer Vision and Pattern Recognition (CVPR), pp. 1274–1281 (2012)
15. Nistor, M.S., Bein, D., Bein, W., Dehmer, M., Pickl, S.: Time-based estimation of vulnerable points in the munich subway network. In: Doerner, K., Ljubic, I., Pflug, G., Tragler, G. (eds.) Operations Research Proceedings 2015: Selected Papers of the International Conference of the German, Austrian and Swiss Operations Research Societies (GOR, ÖGOR, SVOR/ASRO), Vienna, Austria, 1–4 September 2015, pp. 355–360. Springer, Cham (2017)
16. Nistor, M.S., Pickl, S.W., Raap, M., Zsifkovits, M.: Network efficiency and vulnerability analysis using the flow-weighted efficiency measure. Int. Trans. Oper. Res. (2017). doi:10.1111/itor.12384
17. Münchner Verkehrsgesellschaft mbH (MVG): MVG in figures (2016). https://www.mvg.de/dam/mvg/ueber/unternehmensprofil/mvg-in-figures-s. Accessed 12 Mar 2017
18. MVV - Münchner Verkehrs- und Tarifverbund: MVV GmbH (2017). http://www.mvv-muenchen.de/. Accessed 12 Mar 2017
19. MVV - Münchner Verkehrs- und Tarifverbund: Alle Informationen zu den Bahnhöfen im MVV (2015). http://www.mvv-muenchen.de/de/netz-bahnhoefe/bahnhofsinformation/index.html. Accessed 12 Mar 2017

The Research of Maintainability Analysis Based on Immersive Virtual Maintenance Technology

Wei Wang, Wei Zhang(✉), and Weijia Feng

School of Reliability and Systems Engineering, Beihang Univesity, Beijing, China
{w.wei, zhangweil4, fengweijia}@buaa.edu.cn

Abstract. Maintainability as an intrinsic property should be designed and built into a product during the design phases to ensure service reliability. The virtual human can operate virtual prototype in virtual environment instead of the real person to analysis maintainability. This article introduces a method that use the Cave Automated Virtual Environment (CAVE), motion capture system (PHASESPACE MOTION CAPTURE) and virtual simulation software (DELMIA) to build immersive virtual maintenance simulation system, which not only can help analyze the maintenance data and products' maintainability, but also allows the users operate the virtual product in virtual environment. With the help of the simulation system, we can analyze the comfort of the user's action, and evaluate visibility, reachability and operation space of products for maintainability analysis to provide suggestions for the improvement of physical prototype design. At last, this paper will introduce a case study of this immersive virtual simulation system to implement maintainability analysis.

Keywords: Maintainability analysis · Immersive virtual maintenance environment · Ergonomic

1 Introduction

The traditional way to verify maintainability, how well a product can be maintained, relies on the physical prototype, which is timely lagged and time-consuming to modify the established design. The issue of lacking physical mock-up appears when verifying maintainability in the early design phase. The development of virtual reality (VR) technology provides an effective way to overcome the problem. Virtual maintenance (VM) is the application of virtual reality-based in the maintenance field that simulates the maintenance process in a virtual environment including digital prototypes, virtual humans and maintenance tools. For virtual maintenance, a considerable variety of studies have been conducted and a number of solutions have been proposed since the late 1990s. Caudell and Mizell proved the effectiveness of using a VR system to provide instructions for wiring harness assembly [1]. VM systems have been widely applied in maintenance process simulation [2], maintenance planning [3] and maintenance training [4]. In the recent years, the predominance of virtual maintenance allowed

D.N. Cassenti (ed.), *Advances in Human Factors in Simulation and Modeling*,
Advances in Intelligent Systems and Computing 591, DOI 10.1007/978-3-319-60591-3_52

more comprehensive applications, such as maintenance training [5], product design [6], process simulation, and analysis [7].

Compared to the non-immersive virtual maintenance, immersive virtual maintenance simulation is not only more realistic and natural, but also has a higher simulation efficiency and applicability, and is particularly important in the maintenance of the aero-space field. The rapid development of the virtual reality technology makes a big progress in immersive virtual simulation [8]. Real-time immersive virtual environments, such as the Workbench [9] and CAVE [10], have been used to assess the maintainability of virtual prototypes. Virtual humans have been used in many applications. The Human Modeling and Simulation Group at the University of Pennsylvania (2002) use virtual humans for task analysis and assembly validation. Based on the aforementioned observations, this study introduces the method to simulate and analyze the maintenance process to guide product design with virtual prototyping in immersive virtual maintenance environments. To achieve this goal, immersive virtual maintenance simulation process is introduced as shown in Fig. 1.

The rest of this paper is organized as follows: Sect. 2 introduces immersive virtual maintenance simulation system and maintainability evaluation method, Sect. 3 introduces maintainability analysis in immersive virtual maintenance environment combining case study. Section 4 is conclusion.

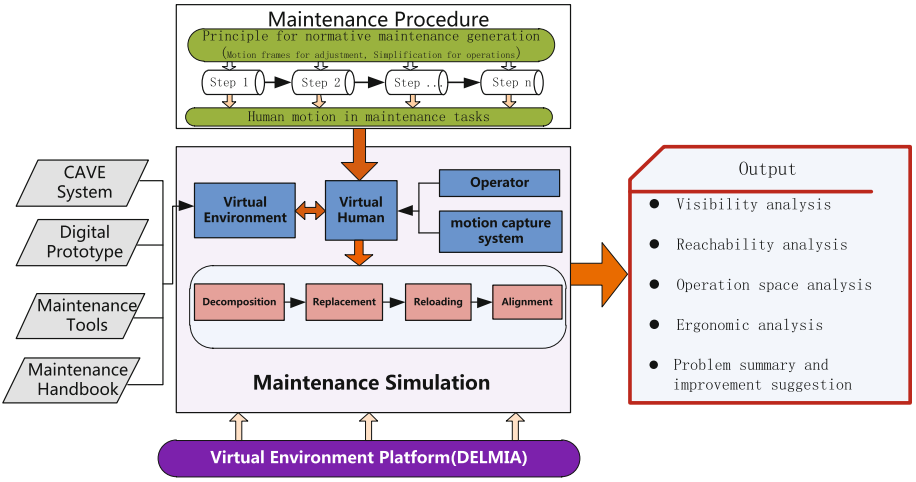

Fig. 1. Immersive virtual maintenance simulation process

2 Maintainability Simulation Environment and Maintainability Evaluation

2.1 Maintainability Simulation Environment

As shown in Fig. 1, the virtual environment consists of four parts: CAVE system, digital prototype, maintenance tools, maintenance handbook. The descriptions of the modules are as follows:

The CAVE system invented in 1992 by a group of researchers at the University of Illinois's Electronic Visualization Lab [10]. It was designed and implemented in response to a challenge of creating a one-to-many visualization tool that utilizes large projection screens as Fig. 5(a). Scenes displayed on the screens are reflected by mirrors positioned and rotated between high-resolution projectors and the screens. Projecting scenes in this particular setup guarantee a more immersive environment. Moreover, Fig. 5(b) shows how an operator of the CAVE sees a blurry, or overlapped, image inside the CAVE. This overlap is mathematically calculated to convey the third dimension to the participant, who, as shown in the figure, is wearing a special pair of goggles and head tracker device to see a stereoscopic view of the content inside the CAVE.

The digital prototype based on the CAX/DFX technology, is the digital description of the product, which not only reflects the geometric properties of the product, but also reflects the function and performance at least in a certain field. The appearance of digital prototype significantly reduces the dependence on the physical prototype and the money can be saved because of many maintenance activities being simulated by the digital prototype.

The commonly maintenance tools in maintenance tasks include fastener disassembling tools such as wrenches, pliers, knives, hammer, measuring tools such as caliper, barometer, etc. At present, a variety of commercial software has integrated complete standard parts library for direct call. Thus, according to the standard parts library developing the fastener disassembling tool library to implement maintenance simulation in immersive virtual maintenance environment is convenient and feasible.

Maintenance handbook is the reference book for operator to carry out maintenance tasks. In virtual maintenance environment, the operator can employ electronic maintenance book (EMB) to disassemble the broken-down parts from the digital prototype.

2.2 Maintainability Evaluation

Maintainability analysis as a vital part to evaluate how well a product can be designed, has a profound influence on the operation and maintenance of products. Maintainability analysis consists of two parts: namely accessibility evaluation and ergonomic evaluation.

Accessibility Evaluation. Accessibility, which is defined as a measure of the relative ease of admission to the various areas of an item for the purpose of operation or maintenance, is a key factor of maintainability. Accessibility design affects the range of maintenance personnel vision, the contact area of maintenance personnel, and the space of maintenance personnel operation. Therefore, accessibility is served as the key evaluation element for products' maintainability, which consists of three sub-elements: visibility, reachability, and operation space.

Visibility. Visibility design should guarantee maintenance personnel could see maintenance tools, object and himself directly by his eyes clearly during the maintenance process. Hence it plays a central role in a man–machine system while manipulation [11, 12]. Vision cone method obtained with an elliptical appearance in a computational way, which simulates human's view space, could give a vivid describe about if they are

visible [13–15]. In this paper, degree of visibility is divided into three levels. And here are the detailed describe about each level:

- Level I: All maintenance objects and action are located in the best vision area, and the maintenance personnel can clearly see the target and easily launch the work, as shown in Fig. 2(a).
- Level II: The maintenance objects and action are located in the widest vision area, while the eyes may feel tired in focusing the obscene scene for a long time.
- Level III: The maintenance objects and action are located in the invisible vision area even if the maintenance personnel adjusted the posture. Maintenance personnel could only finish his work all by sense of touch and experience.

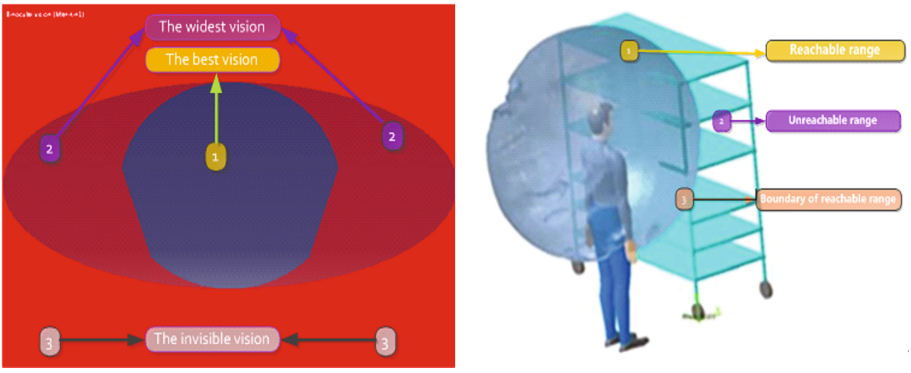

(a)Vision area of static eyes (b) Reach envelope of a limb

Fig. 2. Visibility and reachability analysis

Reachability. Reachability is a general term used to describe the degree, for maintenance personnel with different posture and tools, to get in touch with maintenance objects along predefined maintenance path. The envelope ball tool, shown in Fig. 2(b), is used to evaluate the degree of reachability. The spatial reach area for workplace design purposes relies on not only the length of forearm, but also the shoulder breadth, shoulder and torso rotation, spine bending, and hand operation characters. Considering finger and wrist bending in operation, we take the hand length 18 cm (50th percentile male data) as the quantitative consideration for reachability criteria. Here are the detailed describe of each reachability level.

- Level I: When maintenance personnel is in natural posture, maintenance objects are all located in the envelop ball. And for maintenance personnel, he could touch there objects easily.
- Level II: After changing to another posture, maintenance personnel could touch these objects. The maintenance objects are located in the envelop ball.
- Level III: After changing postures, maintenance personnel could hardly touch these objects. The maintenance objects could only be located at the edge of envelop ball.

Operation Space. Operation space design should provide enough space for human movement and operation. The assessment of maintenance space is key in evaluating maintainability and in ergonomic design. Existing methods of evaluating maintenance space are mainly based on expert knowledge and visual sense [16, 17]. A new way is introduced to verify the maintenance space in the design stage combining swept volumes and virtual environment [18]. Swept Volumes are applied represent the movement of the hand along the entire maintenance process. Maintenance operations are divided into three basic types, as shown in Table 1 and Fig. 3. Each type of basic operation refers to two quantitative indexes, namely, the surface area and the volume of the swept volume of the maintenance personnel. Data on the indexes are gathered and calculated to evaluate maintenance space.

Table 1. Three types of maintenance operations of the hand

Type	Description
Screw	Operation of the hand when the maintainer screws the screw bare-handed or uses the screwdriver
Twist	Operation of the hand when the maintainer uses a wrench and rotates the wrench from the center on the part to be maintained
Translate	Movement of the hand along a line without rotation

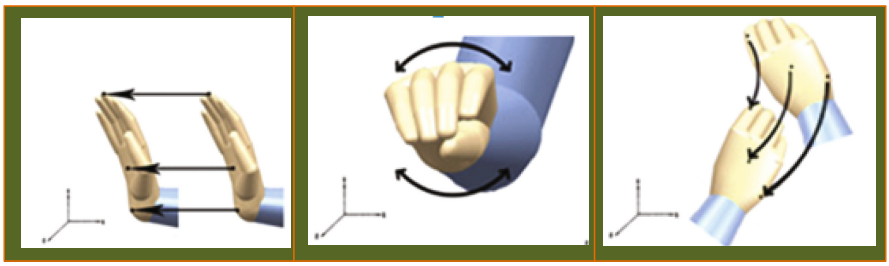

Fig. 3. Three types of maintenance operation unit of the hand

The free SV of the hand for each maintenance operation unit should be established to determine the space that the maintenance operation unit requires. The constrained SV of the hand for each maintenance operation unit can be obtained by using the tools in the Human Task Simulation module in DELMIA to determine the maintenance space based on the layout of machine parts. The SV of each maintenance operation unit constructed in DELMIA is shown in Fig. 4.

Evaluation criteria are constructed by considering the specific characteristics of maintenance work and by factoring in the maintainer's psychology. Given that both swept volumes are built, we can compare the two swept volumes to evaluate the maintenance space of the actual maintenance operation represented by the constraint swept volume. On the basis of the knowledge data, the larger the quantitative indicators of the constraint swept volume are, which the surface area and the volume, the better

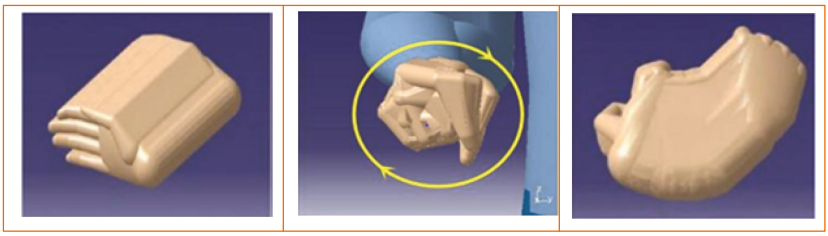

Fig. 4. Swept volumes of maintenance operation unit of the hand

the maintenance space is. Here, we define P_s and P_v as the ratio of the surface area of constraint swept volume to the surface area of free swept volume and the ratio of the volume of constraint swept volume to the volume of free swept volume, respectively:

$$P_s = S_{csv}/S_{fsv} \tag{1}$$

$$P_v = V_{csv}/V_{fsv}, \tag{2}$$

where S_{csv} and S_{fsv} are the surface area of the constraint swept volume and the free swept volume, respectively; V_{csv} and V_{fsv} are the volume of the constraint swept volume and the free swept volume, respectively.

Based on the discussion above, we divide the results of the maintenance space evaluation into three levels: good, normal, and bad. By using the ergonomics requirements of each maintenance operation unit, we can obtain the specific evaluation criteria for the different maintenance operations shown in Table 2.

Ergonomic Evaluation. Ergonomic designs focus on the man–machine interface to identify different defects in the design and provide suggestions to ensure the comfort for maintenance personnel during the maintenance process. Because of the defect of the existing digital human biomechanics model, ergonomic evaluation index is mainly evaluated by working posture. Working posture refers to the posture that an individual is required to adopt due to the layout of a workstation and/or the nature of the task. Poor working posture is a common ergonomic hazard in the course of maintenance and can cause fatigue, discomfort and injury risk. RULA (Rapid Upper Limb Assessment) is widely used because of the simple and feasible procedure without interruption. RULA launched the arm, wrist, neck trunk, and leg analysis, respectively. RULA followed the predefined maintenance procedure and dealt with two analysis results to obtain a final score [19]. Table 3 indicates the score range for each segment and the associated color. Here in this paper, we have concluded three levels for RULA classify:

- Level I: The final score is 1 or 2, the corresponding human limb will be green. For maintenance personnel, he is in a comfortable posture without tiredness.
- Level II: Both a final score of 3 or 4 with a yellow colored limb and a final score of 5 or 6 and an orange colored limb means that maintenance personnel is in a comfortable posture. For maintenance personnel, it will affect work efficiency and his health during the durative operation.

- Level III: The human limb turns red with a highest final score of 7 inevitably during the maintenance process. For maintenance personnel, his working rate may be obviously decreasing.

Table 2. The evaluation criteria of different maintenance operations

Operation type	Evaluation level	P_s	P_v
Screw	Good	>0.85	>0.8
	Normal	0.6–0.85	0.5–0.8
	Bad	<0.6	<0.5
Twist	Good	>0.8	>0.75
	Normal	0.4–0.8	0.25–0.75
	Bad	<0.4	<0.25
Translate	Good	>0.9	>0.9
	Normal	0.7–0.9	0.7–0.9
	Bad	<0.7	<0.7

Table 3. RULA score

Segment	Score range	Color associated with the score					
		1	2	3	4	5	6
Upper arm	1–6	Green	Green	Yellow	Yellow	Red	Red
Forearm	1–3	Green	Yellow	Red	Gray	Gray	Gray
Wrist	1–4	Green	Yellow	Orange	Red	Gray	Gray
Wrist rotation	1–2	Green	Red	Gray	Gray	Gray	Gray
Neck	1–6	Green	Green	Yellow	Yellow	Red	Red
Trunk	1–6	Green	Green	Yellow	Yellow	Red	Red

3 Maintainability Analysis of APU in Immersive Virtual Maintenance Environment

On the basis of the method presented above, we used part of the maintenance process for the auxiliary power unit (APU) of the Boeing 737 as an example. The operator wearing target sensor and head tracker sensor in the CAVE system and optical motion capture system drives the virtual human to unscrew six screws by using a wrench (Fig. 5(d), marked with a black circle). The virtual man used is a P50 person in the simulation.

In addition, the maintenance personnel can do maintainability analysis, such as visibility, reachability, maintenance space, and ergonomic evaluation in the virtual environment. Results of maintainability evaluation are shown as Fig. 6 and Table 4.

As shown in Fig. 6, during APU disassembling process, the APU is located in the best vision area, and the maintenance personnel can clearly see it. For reachability evaluation, it located in the envelop ball. And for maintenance personnel, he could touch there objects easily. The Table 4 indicates that the total evaluation result for

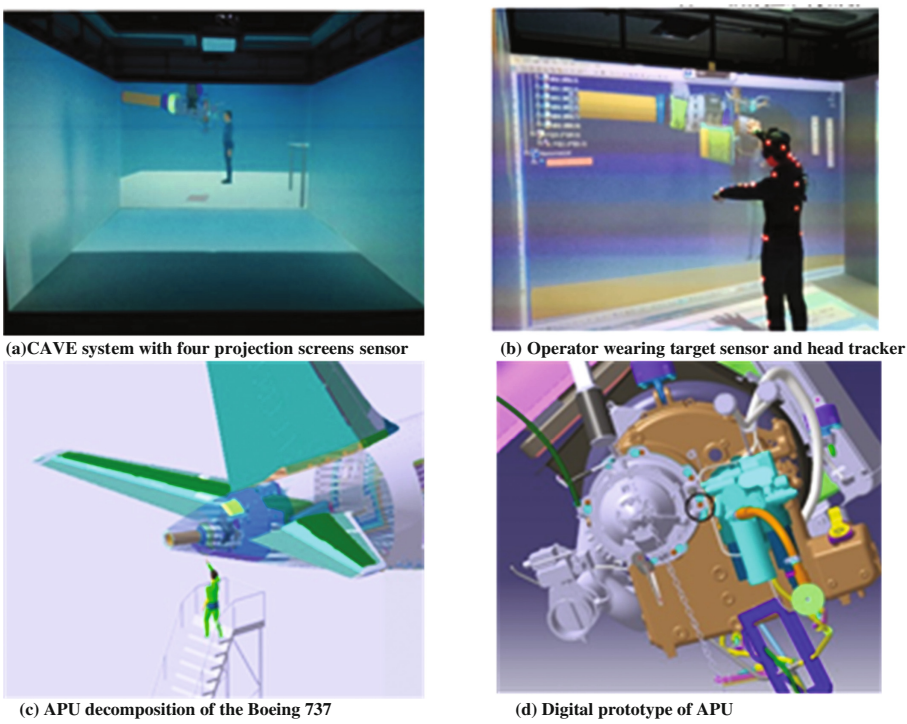

Fig. 5. Immersive virtual maintenance environment and digital prototype of APU

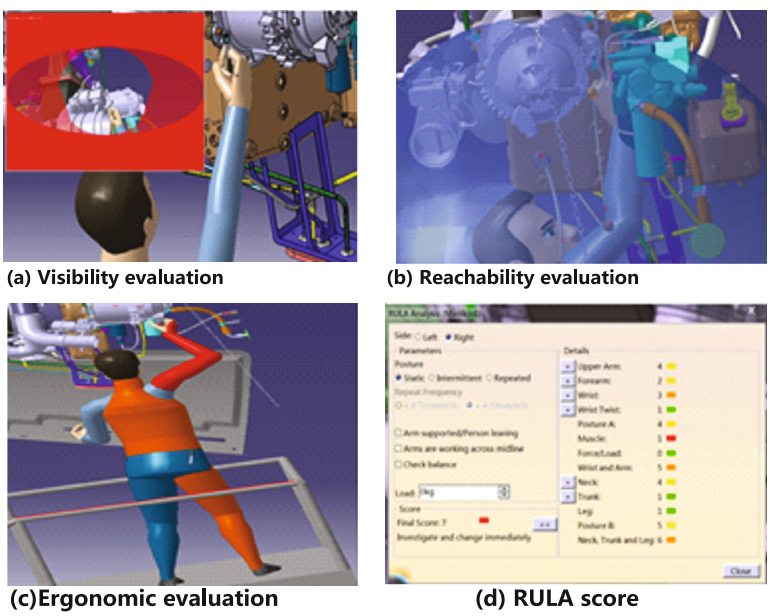

Fig. 6. The results of maintainability evaluation for APU decomposition of the Boeing 737

Table 4. Results of the studied maintenance space

Screw No.	1	2	3	4	5	6
Result level	Good	Normal	Bad	Good	Good	Good

Screw 3 is bad. Therefore, designers must adjust the design of Screw 3 to ensure that enough maintenance space is reserved to operate in it. The human limb turns red with a highest final score of 7 in Fig. 6(c), it indicates that operator' limb is uncomfortable during the durative operation, and his working rate may be obviously decreasing.

4 Conclusions

In virtual maintenance simulation environment, the maintenance personnel can operate the virtual product as like in the real scene. With the help of the simulation system, the maintainability analysis no longer totally relies on the physical prototype or equipment. When the maintenance factors are considered in product design, the possible maintenance design defects could be discovered and recommendations for design improvement could be indicated. Then it is possible to modify the original designation while designing to avoid troubles and economic loss caused by re-designation of the physical prototype or equipment. What's more, the maintenance personnel can avoid dangerous maintenance operate, and the money can be saved, and furthermore, developing a working platform to train and enhance the workers abilities in maintenance and supportability field will be taken into account.

References

1. Caudell, T. P, Mizell, D.W.: Augmented reality: an application of heads-up display technology to manual manufacturing processes. In: Hawaii International Conference on System Sciences, vol. 2, pp. 659–669. IEEE (1992)
2. De Sá, A.G., Zachmann, G.: Virtual reality as a tool for verification of assembly and maintenance processes. Comput. Graph. **23**(3), 389–403 (1999)
3. Van Houten, F.J.A.M., Kimura, F.: The virtual maintenance system: a computer-based support tool for robust design, product monitoring, fault diagnosis and maintenance planning. CIRP Ann. – Manuf. Technol. **49**(1), 91–94 (2000)
4. Leino, S.P., Lind, S., Poyade, M., Kiviranta, S., Multanen, P., Reyes-Lecuona, A., Makiranta, A., Muhammad, A.: Enhanced industrial maintenance work task planning by using virtual engineering tools and haptic user interfaces. In: Shumaker, R. (ed.) Third International Conference on Virtual and Mixed Reality, vol. 3, pp. 346–354. Springer, Heidelberg (2009)
5. Li, J.R., Khoo, L.P., Tor, S.B.: Desktop virtual reality for maintenance training: an object oriented prototype system (V-REALISM). Comput. Ind. **52**(2), 109–125 (2003)
6. Pouliquen, M., Bernard, A., Marsot, J., Chodorge, L.: Virtual hands and virtual reality multimodal platform to design safer industrial systems. Comput. Ind. **58**(1), 46–56 (2007)
7. Liu, X., Peng, G., Liu, X., Hou, Y.: Development of a collaborative virtual maintenance environment with agent technology. J. Manuf. Syst. **29**(4), 173–181 (2010)

8. Dureigne, M.: Collaborative large engineering: from IT dream to reality. In: Tichkiewitch, S., Brissaud, D. (eds.) Methods and Tools for Co-operative and Integrated Design, pp. 3–14. Springer, Netherlands (2004)
9. Cutler, L.D., Hanrahan, P.: Two-handed direct manipulation on the responsive workbench. In: Proceedings of the 1997 Symposium on Interactive 3d Graphics, pp. 107–114. ACM, New York (1997)
10. Cruz-Neira, C., Sandin, D.J., Defanti, T.A.: Surround-screen projection-based virtual reality: the design and implementation of the CAVE. In: Conference on Computer Graphics and Interactive Techniques, pp. 135–142. ACM (1993)
11. Anderson, J.R., Matessa, M., Lebiere, C.: Act-r: a theory of higher level cognition and its relation to visual attention. Hum. Comput. Interact. **12**(4), 439–462 (1997)
12. Itti, L., Koch, C.: Computational modelling of visual attention. Nat. Rev. Neurosci. **2**(3), 194–203 (2001)
13. Liu, H., Heynderickx, I.: A simplified human vision model applied to a blocking artifact metric. In: Kropatsch, W.G., Kampel, M., Hanbury, A. (eds.) Computer Analysis of Images and Patterns, pp. 334–341. Springer, Heidelberg (2007)
14. Neokleous, K.C., Schizas, C.N.: computational modeling of visual selective attention. Procedia Comput. Sci. **7**(29), 244–245 (2011)
15. Georgeson, M.A.: Edge-finding in human vision: a multi-stage model based on the perceived structure of plaids. Image Vis. Comput. **16**(6–7), 389–405 (1998)
16. Yu, H., Peng, G., Liu, W.: A practical method for measuring product maintainability in a virtual environment. Assembly Autom. **31**(1), 53–61 (2011)
17. Gaoliang, P., Yu, H., Xinhua, L., Yang, J., He, X.: A desktop virtual reality-based integrated system for complex product maintainability design and verification. Assembly Autom. **30**(4), 333–344 (2010)
18. Zhou, D., Jia, X., Lv, C., Kang, L.: Using the swept volume to verify maintenance space in virtual environment. Assembly Autom. **34**(2), 192–203 (2014)
19. Mcatamney, L., Nigel, C.E.: RULA: a survey method for the investigation of work-related upper limb disorders. Appl. Ergon. **24**(2), 91 (1993)

Biometric Identification Through Eye-Movement Patterns

Akram Bayat(✉) and Marc Pomplun

University of Massachusetts Boston, Boston, MA, USA
{akram,marc}@cs.umb.edu

Abstract. This paper describes how to identify unique individual readers using their eye-movement patterns. A case study including forty participants was conducted in order to measure eye movement during reading. The proposed biometric method is developed based on an informative and stable eye-movement feature set that gives rise to a high performance multi-class identification model. Multiple individual classifiers are trained and tested on our novel feature set consisting of 28 features that represent basic eye-movement, scan path and pupillary characteristics. We combine three high-accuracy classifiers, namely Multilayer Perceptron, Logistic, and Logistic Model Tree using the average of probabilities as the combination rule. We reach an overall accuracy of 95.31% and an average Equal Error Rate (EER) of 2.03%. Our approach dramatically outperforms previous methods, making it possible to build eye-movement biometric systems for user identification and personalized interfaces.

Keywords: Biometric identification · Eye movement · Equal error rate · Pattern recognition

1 Introduction

A biometric system is essentially a pattern recognition process that operates by acquiring biometric data from an individual, extracting a feature set from the acquired data, and comparing this feature set against the template set in the database [1].

In this work, we consider our biometric implementation to operate in the identification mode, which means that its task is to determine the user's identity or decide that the user is unknown.

Biometric systems based on physical or behavioral attributes of a person such as face, voice and fingerprint for personal recognition have been widely used over the last decade. Using eye movement in biometric systems is an important yet challenging research area with many applications in health care, smart environments, security and personalized interfaces. The eyes in particular offer a variety of physical (iris) and behavioral (eye movements) properties that make them ideal for the purposes of biometric identification, due to their high specificity and the complex mechanical logistics of reproduction [2]. For this reason, there is an increased tendency toward integration of eye movement biometrics into the standard identification methods in order to enhance the level of security. However, the error rates produced by current methods of eye movement analysis are higher than those of accepted biometric systems. For

D.N. Cassenti (ed.), *Advances in Human Factors in Simulation and Modeling*,
Advances in Intelligent Systems and Computing 591, DOI 10.1007/978-3-319-60591-3_53

example, the EER of 10.8% and Rank-1 identification rate of 51% by Rigas and Komogortsev [3] on a large database of 200 subjects yielded one of the best results among all existing eye movement-driven biometric methods. The work of Holland and Komogortsev [4] is one of the most successful studies in biometric identification via eye-movement tracking in reading. Scan path characteristics, representative of the observer's visual attention strategies during reading, were investigated. Eye movements were recorded for 32 subjects over four recording sessions. The best reported result yielded an EER of 27%.

In the context of biometric identification, we aim to develop a model that is capable of identifying a user by implementing various learning techniques to classify the user's eye movement patterns for the best match. Our identification task is formulated as a supervised classification problem, whose training data contains eye movements of forty human subjects that were recorded while they performed reading activities in laboratory conditions.

Our objective differs from earlier studies as follows: First, we provide an identification method by capturing normal user activity, yet are able to obtain significantly higher performance compared to previous studies. The reading process presents an instance of high usability, as it is a very common activity. However, the effects of learning and text content in reading tasks make it very challenging to achieve the same results by task repetition for the same person [5]. For this reason, many previous studies used designs for their eye-movement biometrics algorithms that require the display of specific stimuli and cannot be adapted to general task performance.

Second, our feature set consists of features that have not been widely studied in the context of reading experiments. The features allow us to reliably distinguish individuals based on differences in eye-movement patterns. The features have been evaluated and selected by considering two experiments to decrease the effect of the text content on the identification procedure.

Last but not least, we apply a multi-class classification methodology which constructs a decision threshold for each class.

The rest of the paper is organized as follows: Sect. 2 gives an overview over the experiment design and data collection. Section 3 describes the extracted features. The classification methods and performance evaluation are described in Sects. 4 and 5, respectively. Subsequently, we conclude the paper in Sect. 6.

2 Experimental Design

In this section, we describe an experimental design which provides our identification procedure with robustness against the content of the texts that are presented during experiments.

2.1 Design Criteria

In order to best capture an actual user's eye-movement behavior during a reading experiment, two important design criteria must be considered: first, if subjects read an identical set of passages, it is likely that the identification algorithm will be overfitted to

specific feature characteristics of texts used in the experiment. Second, if each subject reads a set of passages with different contents, it is possible that the identification algorithm captures differences in texts, rather than differences in subjects. Therefore, we need to consider the experiments in a way that the robustness of the identification procedure against the contents of the texts is guaranteed. For this, two different experiments are taken into account to investigate the effects of text content on identification performance. In the first experiment, different passages are used for different individuals, whereas in the second experiment, the same set of passages is presented to all subjects. We use two data sets (Dataset I and Dataset II), previously collected by Attar [6, 7], that are compatible with our experimental design. Datasets I and II meet the requirements of our first and second experimental design, respectively.

2.2 Experimental Setup

All screens were presented on a 22-inch View-Sonic LCD monitor with a refresh rate of 75 Hz and resolution of 1024 × 768 pixels. Eye movements were monitored with an SR Research EyeLink-2 k system with a sampling frequency of 1000 Hz.

The passages that were used for data collection contain general topics (food, science, health, history) taken from Washington Post News. Each passage has between 230 and 240 words. The passages are easily readable texts in order to decrease the influence of subjects' prior knowledge on the experiments.

Forty native English speakers (25 female) with an average age of 20.4 years (SD = 5.35) and with normal or corrected to normal vision participated in the experiments. For the first experiment with twenty participants (Dataset I), each subject read six passages which were different for each subject. In the second experiment that resulted in Dataset II, the other twenty subjects read six passages which were identical for all subjects. Every passage in both experiments was divided into 3 screens that added up to a total of 18 screens for six passages. The font color for the text was black and the background color was grey.

3 Feature Extraction

This section describes our feature extraction method, which consists of scan path and pupillary response analysis. We aim to discriminate individuals by their visual behavior during the reading task. The visual behavior is represented via a feature set reflecting the dynamics of eye movement patterns.

It is important to choose the candidate features that provide the highest level of specificity and noise tolerance. We attempt to choose features that represent the patterns of eye movements that are observed during reading. Most of the features used in this work are based on global processing, whereas word-by-word processing is not specifically analyzed.

By considering the properties of eye-movement patterns in the reading task, we extract features that hold promise as physiological and behavioral characteristics. Moreover, the designed features should be less influenced by the content of the particular texts used in the experiment. For instance, the frequency of the words

determines the likelihood that they are fixated. However, it is difficult to find features that are text independent since eye-movement patterns are reactions to the text stimulus. Besides, we use texts that require little prior knowledge in order to decrease the influence of this knowledge on the features. Furthermore, all subjects are at very similar age. For this reason, eye-movement patterns are not significantly influenced by the readers' age differences.

The raw data collected by the eye tracker system for each subject contains various activities during reading, including fixations, saccades and blinks. Each of these activities as well as the current gaze coordinates and pupil diameter were measured at a temporal resolution of one millisecond. A scan path is defined as the trajectory of eye movements over a screen, containing a number of fixations and saccades with the number, duration, order, and placement of the fixations and saccades varying among individuals [8]. Analyzing the scan path of each subject during reading can lead to measurable characteristics that are distinct for each subject. By analyzing a scan path, we compute features that can considerably support biometric characteristics. The extracted features are categorized into four groups: fixation features, saccadic features, pupillary response features and spatial reading features.

3.1 Fixation Features

Different types of fixation based features are defined as follows:

- **Scan path length** expresses the efficiency of reading which is computed as the sum of the Euclidean distances between all consecutive fixations in the scan path. Only fixations within the reading screen are considered for computing this length, so any fixation outside of the screen is discarded.
- **Spatial Fixation count average** is the number of fixations within the scan path divided by the number of lines of text being read. The line spacing, font size and formatting of text presentation are identical on all screens.
- **Fixation rate** is the average number of fixations per second. It is computed as the number of fixations over the sum of all fixation and saccade durations in a scan path.
- **Fixation Speed** is the number of fixations in a scan path over the total time needed for reading a screen.
- **Average fixation duration** is measured as the sum of fixation durations over the number of fixations.

3.2 Saccadic Features

We define basic and complex saccadic features, which are saccade related metrics. If a blink happens during any saccade, that saccade is removed from the computation of baseline and complex features.

Average saccade duration is computed as the sum of saccade durations over the total number of saccades.

Average horizontal (vertical) saccade amplitudes of at least 0.5° are measured as the sum of horizontal (vertical) saccade amplitudes greater than 0.5° over the total

number of saccades with horizontal (vertical) amplitudes greater than 0.5°. Horizontal and vertical saccade amplitudes indicate between-word and between-line saccades, respectively [4].

Average saccade horizontal (vertical) Euclidean length is the sum of horizontal (vertical) Euclidean distances between fixation locations over the total number of saccades.

Average saccade velocity is defined as the sum of Euclidean norm of the horizontal and vertical velocities over the total number of saccades in a scan path.

The horizontal (vertical) saccade velocity is defined as the velocity with which eyes move horizontally (vertically) from a fixation point to another. A very simple, fast and accurate way to compute saccade velocity is to use a two-point central difference. If these two points are considered as two adjacent fixation points (we discard all data points between two fixation points), the signal-to-noise ratio will significantly decrease. A more robust way to compute the horizontal saccade velocity (V_{HS}) and vertical saccade velocity (V_{VS}) is to use the following formulas which are designed for a 1000 Hz sampling rate of data collection:

$$V_{HS} = \frac{1}{n}\sum_{k=0}^{n} V_H(k). \tag{1}$$

$$V_{VS} = \frac{1}{n}\sum_{k=0}^{n} V_V(k). \tag{2}$$

where:

$$V_H(k) = \frac{x([k+3]T) - x([k-3]T)}{6T}. \tag{3}$$

$$V_V(k) = \frac{y([k+3]T) - y([k-3]T)}{6T}. \tag{4}$$

where x and y are the coordinates of a sample point within a saccade, T is the sampling interval (1 ms), and k is the index for discretized time, i.e. k = 0, 1, 2,…, n.

Average peak velocity is the sum of peak velocities over the total number of saccades in a scan path, where the peak velocity is defined as the highest velocity reached between any two consecutive samples during the saccade.

Average ratio of peak velocity over saccade velocity is the sum of all ratios of peak velocity over saccade velocity divided by the total number of saccades in a scan path.

Inflection count is the number of saccades in which the horizontal or vertical velocity has a different sign than the preceding saccade. This value can indicate direction of attention in progressing through the text [9].

3.3 Pupillary Response Features

Pupillary response features consist of features that reflect changes in pupil size during reading activity. The fact that the magnitude of pupil dilation is a function of processing load or mental effort has long been known in neurophysiology. The various changes in pupil diameters in different participants that result from their reactions to the

same reading task can be considered as dynamic features. In order to model these changes, the standard deviation, average rate of pupil size change, and difference between the minimum and maximum pupil size in a scan path are computed.

The standard deviation of pupil diameter is applied as follows:

$$\sigma = \sqrt{\frac{1}{\mathrm{N}} \sum_{\mathrm{i}=1}^{\mathrm{N}} \frac{\left(\mathrm{M}_{\mathrm{Fixation}}(\mathrm{i}) - \mathrm{M}_{\mathrm{ScanPath}}\right)^2}{\left(\mathrm{M}_{\mathrm{ScanPath}}\right)^2}}. \tag{5}$$

where $M_{Scan\ Path}$ and $M_{Fixation}$, respectively, are mean pupil diameters that are observed during one scan path and during each fixation in that scan path, and N is the number of fixations within the scan path.

The average rate of pupil size change, $\mathrm{V_P}$, is measured as follows:

$$\mathrm{V_P} = \frac{1}{\mathrm{n}-3} \sum_{\mathrm{k}=2}^{\mathrm{n}-2} \frac{\mathrm{P}([\mathrm{K}+2]\mathrm{T}) - \mathrm{P}([\mathrm{K}-2]\mathrm{T})}{4\mathrm{T}}. \tag{6}$$

where n is the number of fixations within a scan path, P is the pupil size, and T is the sampling interval (1 ms) of data collection.

The difference between minimal and maximal pupil diameter in each scan path is measured as another pupil feature.

3.4 Spatial Reading Features

Spatial reading features reveal eye movement behavior in terms of efficiency. For comprehending a sentence and a passage, readers must establish word order. It means that their gaze moves to upcoming words in the text when they become relevant for sentence comprehension. We define a progressive reading procedure as moving forward toward the next words on a line of text. We define a saccade as a progressive saccade if the saccade angle deviates from this direction by less than 20°. Saccades that move the eyes in other directions are not considered to belong to a progressive, efficient reading procedure. However, a saccade in opposite direction, landing on the next line of the text, is also counted as a progressive saccade. Then we define the following features in this reading space:

Average horizontal (vertical) forward saccade velocities are measured as the sum of progressive horizontal (vertical) saccade velocities over the total number of progressive saccades.

Average absolute forward saccade velocities are the sum of absolute values of progressive saccade velocities over the total number of progressive saccades.

4 Classification

Multi-class classification algorithms which consider each class label as a unique subject are implemented using several classifiers including the Multilayer Perceptron, Logistic, and decision tree based classifiers (Logistic Model Tree and Random Forest).

Table 1. Classification accuracies for different classifiers.

Dataset	Number of subjects	Classifier	Accuracy
Dataset I	20	Logistic	97.57%
		Multilayer perceptron	96.53%
		Logistic model tree	96.88%
		Random forest	96.87%
Dataset II	20	Logistic	92.76%
		Multilayer perceptron	92.50%
		Logistic model tree	93.03%
		Random forest	90.08%
Dataset I & II	40	Logistic	93.04%
		Multilayer perceptron	91.53%
		Logistic model tree	90.92%
		Random forest	89.26%

Classifiers are trained and tested using a 10-fold cross validation method on the set of extracted features. We primarily evaluate the performance of these classifiers using their accuracies. The summary results are presented in Table 1. Overall, the Logistic model outperforms the other classifiers. The Multilayer Perceptron is the second most accurate classifier; its good performance is in line with prior research on biometric identification [10]. Considering both datasets, the best performance is achieved with Dataset I as expected. Obtaining the highest accuracy when using Dataset I reflects higher recognition power due to the effects caused by differences in the texts that are used for that experiment.

Combining multiple good classifiers can improve accuracy, efficiency and robustness over single classifiers. The idea is that different classifiers may offer complementary and diverse information about patterns to be classified, allowing for potentially higher classification accuracy (e.g. [11]). We use the vote classifier to combine the optimal set of classifiers from the previous section by selecting a combination rule. The average of probabilities is considered as our combination rule that returns the mean of the probability distributions for each of the single classifiers. It is found that for our biometric identification model the average of probabilities yields a better result than other methods such as majority voting (94.40%). The combination consisting of the Logistic, Multilayer Perceptron and Logistic Model Tree classifiers yields the highest accuracy in all three datasets. The results of our combined classifiers are listed in Table 2. The accuracy decreases from 97.92% to 96.52% when considering data collected with the same set of passages for all subjects (Dataset II). The accuracy takes another drop to 95.31% when combining Dataset I and Dataset II. The reason for combining two datasets is to reduce the error rate exhibited by the content of the text that is used for identification. The small changes in accuracy rates for different datasets and the behavioral nature of our feature set suggest that our feature set and classifiers can well capture unique characteristics of different individuals by using their eye-movement patterns. For the remainder of this paper, the model constructed by using the combination of Datasets I and II will be used as our classifier.

Table 2. Classification accuracies for different combination rules.

Dataset	Number of subjects	Classifier	Accuracy
Dataset I	20	Average of probabilities	97.92%
		Majority voting	97.92%
Dataset II	20	Logistic	96.52%
		Multilayer perceptron	95.17%
Dataset I & II	40	Logistic	95.31%
		Random forest	94.40%

5 Identification Performance

Evaluating the predictive performance of models is a vital step in model development. Such evaluation assists in determining the suitability of a model for specific applications [12]. Simple classification accuracy is often a poor metric for measuring performance in biometric systems, which makes it necessary to assess the performance of the predictive model by other characteristics such as a receiver operating characteristic (ROC) and equal error rate (EER). An ROC curve is used to show proportions of correctly and incorrectly classified predictions over a wide and continuous range of decision threshold levels.

In biometric systems, from the user's point of view, an error of accuracy occurs when the system identifies an invalid user or when the system fails to identify a valid user. The associated error rates are called False Acceptance Rate (FAR) and False Rejection Rate (FRR), respectively, which are the most commonly used metrics for identification problems. EER is the rate at which both FAR and FRR are equal. The value of the EER can be easily obtained from the ROC curve. In general, lower EER indicates higher accuracy.

Our final combined classifier is a probabilistic multi-class classifier that yields an instance probability where an instance is a feature vector that represents a user's eye-movement scan path and its relevance probability is a value that represents the predicted degree to which an instance belongs to a given user. This probabilistic classifier uses a decision threshold with a probability of 0.5 for each class to produce a discrete classifier that reaches the accuracy value of 95.31%.

The general strategy in evaluating the FAR and FRR errors for multi-class classifiers is to reduce the problem of multiclass classification to multiple binary classifications in which each class has its own value of FAR and FRR errors. Figure 1 shows the values of FAR and FRR errors for all forty classes.

The combined multi-class classifier achieves 95.31% probability of identification at average 0.134% FAR and 6.051% FRR.

5.1 Optimizing the Performance of Identification

The combined classifier that obtains the accuracy of 95.31% uses a decision threshold with a probability of 0.5 to map from instances to predicted classes. However, it does not guarantee providing us with the optimal values of FAR and FRR errors. Figure 2

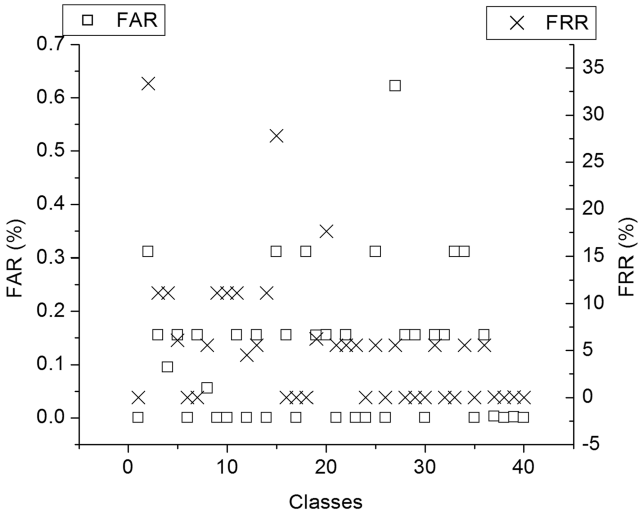

Fig. 1. FAR and FRR errors for the multi-class classifier with 95.31% accuracy and decision threshold with probability of 0.5. The maximum value of FAR and FRR over all classes is 0.62% and 33.33%, respectively.

shows the ROC graphs for two sample binary classes (two users) in which FAR and FRR are plotted on the vertical axis and decision threshold is plotted on the horizontal axis. Figure 2 (*left*) shows an EER value of 0.0015 for both FAR and FRR related to the decision threshold value of 0.49 for a sample binary class that guarantees 0.15% EER or less for this class.

Selecting the EER value as the decision threshold is often a good choice for identification applications. In Fig. 2 (*right*) the FAR and FRR errors are not optimal at a threshold value of 0.5, because the value of FAR (0.277) at a threshold of 0.5 is fairly high for an identification problem; it means that the classifier would fail at 27.7% of attempts to identify a valid user.

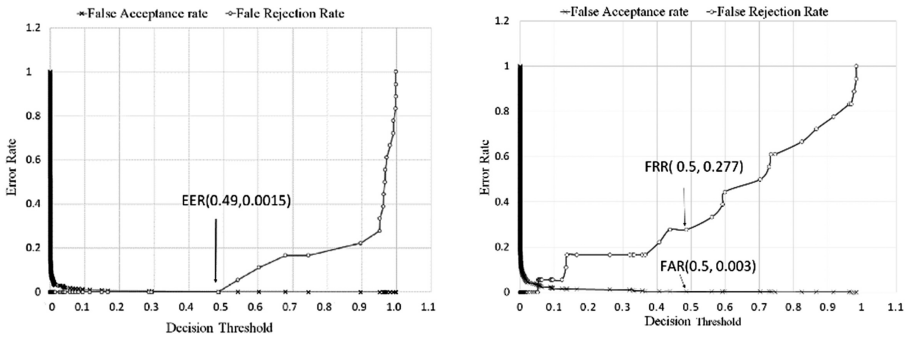

Fig. 2. FAR and FRR versus decision threshold for two-sample binary classes; the EER value serves as the decision threshold. FAR = FRR (*left figure*) and FAR $\neq$ FRR (*right figure*) in Threshold 0.5.

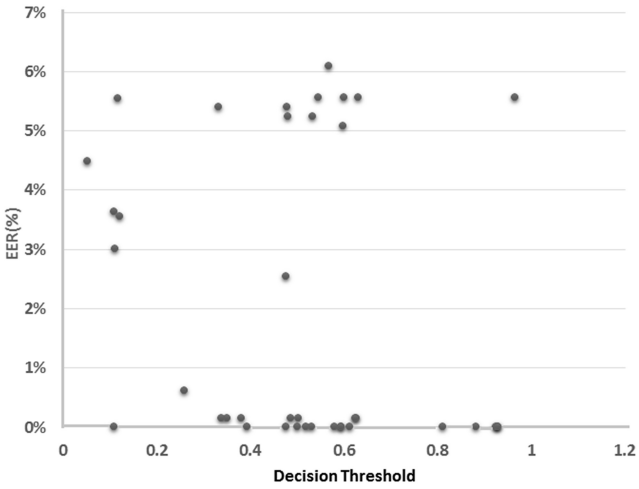

Fig. 3. EER vs. decision threshold for our proposed multi-class model.

ROC analysis and EER based decision making are commonly employed in two-class classification problems because they are easy to analyze and visualize. For our multi-class classifier we need to deal with more than one decision threshold and make multi-decisions for our multi-class predictive model. It is important to know that with more than two classes, ROC analysis becomes too complex to be managed. In our multi-class model, with 40 classes, the confusion matrix becomes a 40×40 matrix containing the 40 correct classifications (the major diagonal entries) and $(40^2 - 40)$ possible errors (the off-diagonal entries). Instead of managing trade-offs between FAR and FRR, we have 1560 errors [13].

One method for handling n classes is to consider each class as an independent binary problem and to produce n different ROC graphs, one for each class. It means that for any class in the set of all classes, the ROC graph plots classification performance only for that class as the positive class and all other classes as the negative class. In this way, we will have 40 decision thresholds and 40 EER values for our 40-class identification model that are represented in Fig. 3.

As a result, our classification model achieves an EER value no greater than 6.1% and an average EER rate of 2.03% for identifying users based on their eye-movement biometrics. As can be seen, by adjusting thresholds for having equal error rates of FAR and FRR, we obtain a lower average rate of FRR ($2.03 < 6.051(\%)$) but a greater rate of FAR ($2.03 > 0.134(\%)$).

6 Conclusion

In this paper, identification accuracy of up to 95.31% and an average EER rate of 2.03% were obtained from analyzing readers' eye movements. The data were acquired from 40 subjects under laboratory conditions. A new set of features was taken into

account and different performance metrics were used for evaluating identification performance. Combining the three best classifiers using the average of probabilities method turned out to be the best classifier for our biometric identification problem, outperforming all individual classifiers in terms of accuracy. We further showed that our multi-class probabilistic classifier can be improved in performance by selecting good decision thresholds that guarantee an average equal error rate of 2.03%, which is significantly lower than the EERs achieved by the best eye-movement classifiers in the literature. Our findings indicate that the incorporation of the proposed features and classification method can lead to a significant improvement in biometric accuracy and robustness in identification through reading tasks. The unique characteristics of eye movements and promising results of our identification method make this biometric an excellent approach for various applications such as personalized user interfaces or integration with other identification methods in order to enhance the level of security. While previous work already suggested that eye movements could be used for such purposes, the drastic increase in accuracy achieved by our technique makes this paradigm relevant for actual applications for the first time. For future work, we plan to extend our biometric identification task in several ways. First, we intend to collect data from more users of various ages. Second, we plan to consider eye-movement similarities among subjects and exploit interdependence among various classes. The goal of this line of research is to increase the robustness of our method for a wide range of users while requiring as few eye movements as possible for reliable identification.

References

1. Jain, A.K., Ross, A., Prabhakar, S.: An introduction to biometric recognition. IEEE Trans. Circ. Syst. Video Technol. **14**(1), 4–20 (2004)
2. Komogortsev, O.V., Khan, J.I.: Eye movement prediction by Kalman filter with integrated linear horizontal oculomotor plant mechanical model. In: Proceedings of the 2008 Symposium on Eye Tracking Research & Applications, pp. 229–236. ACM (2008)
3. Rigas, I., Komogortsev, O.V.: Biometric recognition via probabilistic spatial projection of eye movement trajectories in dynamic visual environments. IEEE Trans. Inf. Forensics Secur. **9**(10), 1743–1754 (2014)
4. Holland, C., Komogortsev, O.V.: Biometric identification via eye movement scanpaths in reading. In: 2011 International Joint Conference on Biometrics (IJCB), pp. 1–8. IEEE (2011)
5. Bayat, A. and Pomplun, M. The influence of text difficulty level and topic on eye-movement behavior and pupil size during reading. In: International Conference of Signal Processing and Intelligent Systems (ICSPIS), pp. 1–5. IEEE (2016)
6. Attar, N., Chien, C., Sia, D.E. and Pomplun, M.: A deeper understanding of optimal viewing position using eye fixations and character recognition on text-viewing and reading tasks. In Proceedings of the Ninth Biennial ACM Symposium on Eye Tracking Research & Applications, pp. 209–212. ACM (2016)
7. Attar, N., Fomenky, P., Ding, W. and Pomplun, M.: Improving cognitive load level measurement through preprocessing psychological data by random subspace method. In: IEEE 2nd International Conference on Human Computer Interactions, pp. 1–6. IEEE (2016)
8. Phillips, M.H., Edelman, J.A.: The dependence of visual scanning performance on saccade, fixation, and perceptual metrics. Vis. Res. **48**(7), 926–936 (2008)

9. Holland, C.D., Komogortsev, O.V.: Biometric verification via complex eye movements: The effects of environment and stimulus. In: 2012 IEEE Fifth International Conference on Biometrics: Theory, Applications and Systems (BTAS), pp. 39–46. IEEE (2012)
10. Rigas, I., Economou, G., Fotopoulos, S.: Biometric identification based on the eye movements and graph matching techniques. Pattern Recogn. Lett. **33**(6), 786–792 (2012)
11. Bayat, A., Pomplun, M., Tran, D.A.: A study on human activity recognition using accelerometer data from smartphones. Procedia Comput. Sci. **34**, 450–457 (2014)
12. Pearce, J., Ferrier, S.: Evaluating the predictive performance of habitat models developed using logistic regression. Ecol. Model. **133**(3), 225–245 (2000)
13. Fawcett, T.: An introduction to ROC analysis. Pattern Recogn. Lett. **27**(8), 861–874 (2006)

Author Index

D.N. Cassenti (ed.), *Advances in Human Factors in Simulation and Modeling*,
Advances in Intelligent Systems and Computing 591, DOI 10.1007/978-3-319-60591-3